The HKIE Geotechnical Division 37th Annual Seminar 2017

G-EVOLUTION

Geotechnical Practice in Hong Kong

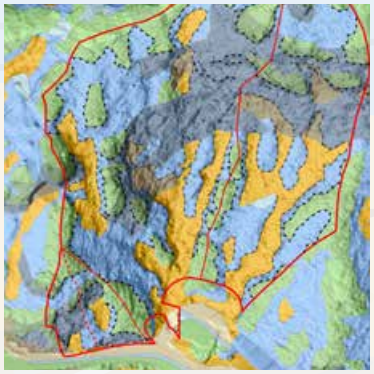

HKIE THE HONG KONG INSTITUTION OF ENGINEERS 香港工程師學會
Geotechnical Division 岩土分部

Co-organiser

HKGES 香港岩土工程學會 Since 2003

Supporting Organisations

HKIE THE HONG KONG INSTITUTION OF ENGINEERS 香港工程師學會 Civil Division 土木分部

HKIE THE HONG KONG INSTITUTION OF ENGINEERS 香港工程師學會 Structural Division 結構分部

AECOM

Embracing complexity, engaging technologies

We connect expertise across services, markets, and geographies to deliver transformative outcomes. Worldwide, we design, build, finance, operate and manage projects and programs that unlock opportunities, protect our environment and improve people's lives.

We are AECOM. Built to deliver a better world.

Tuen Mun – Chek Lap Lok Link

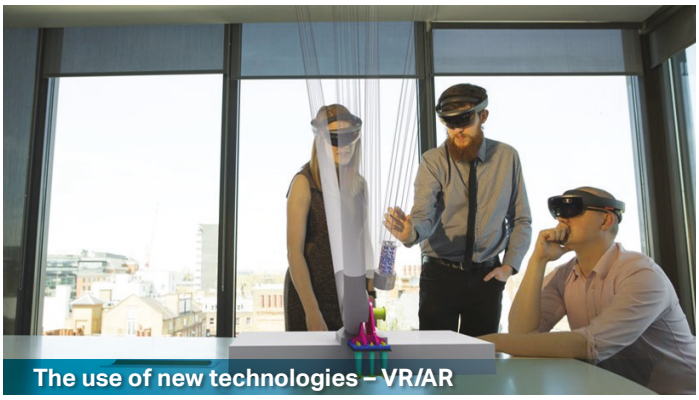
The use of new technologies – VR/AR

Natural Terrain Mitigation Works at Tung Chung North Lantau Expressway

Central – Wan Chai Bypass

aecom.com

歐美大地
EARTH PRODUCTS CHINA LTD

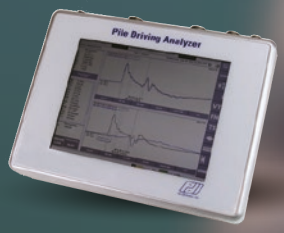

Pile Driving Analyzer

Corrosion Dectecter

The Ultimate Testing Instruments Provider

Infrared Camera

Concrete Test Hammer

Permeability System

Concrete In Situ Testing

Temperature & Maturity Sensor

(852) 2392 8698
info@epc.com.hk
www.epc.com.hk
12/F Asia Trade Ctr.,
79 Lei Muk Rd.,
Kwai Chung, N.T., H.K.

Reshaping our cities

As an acknowledged leader in geotechnics, Arup combines strategic thinking with technical expertise to help cities reconsider the way they use space, unlocking the potential for the future.

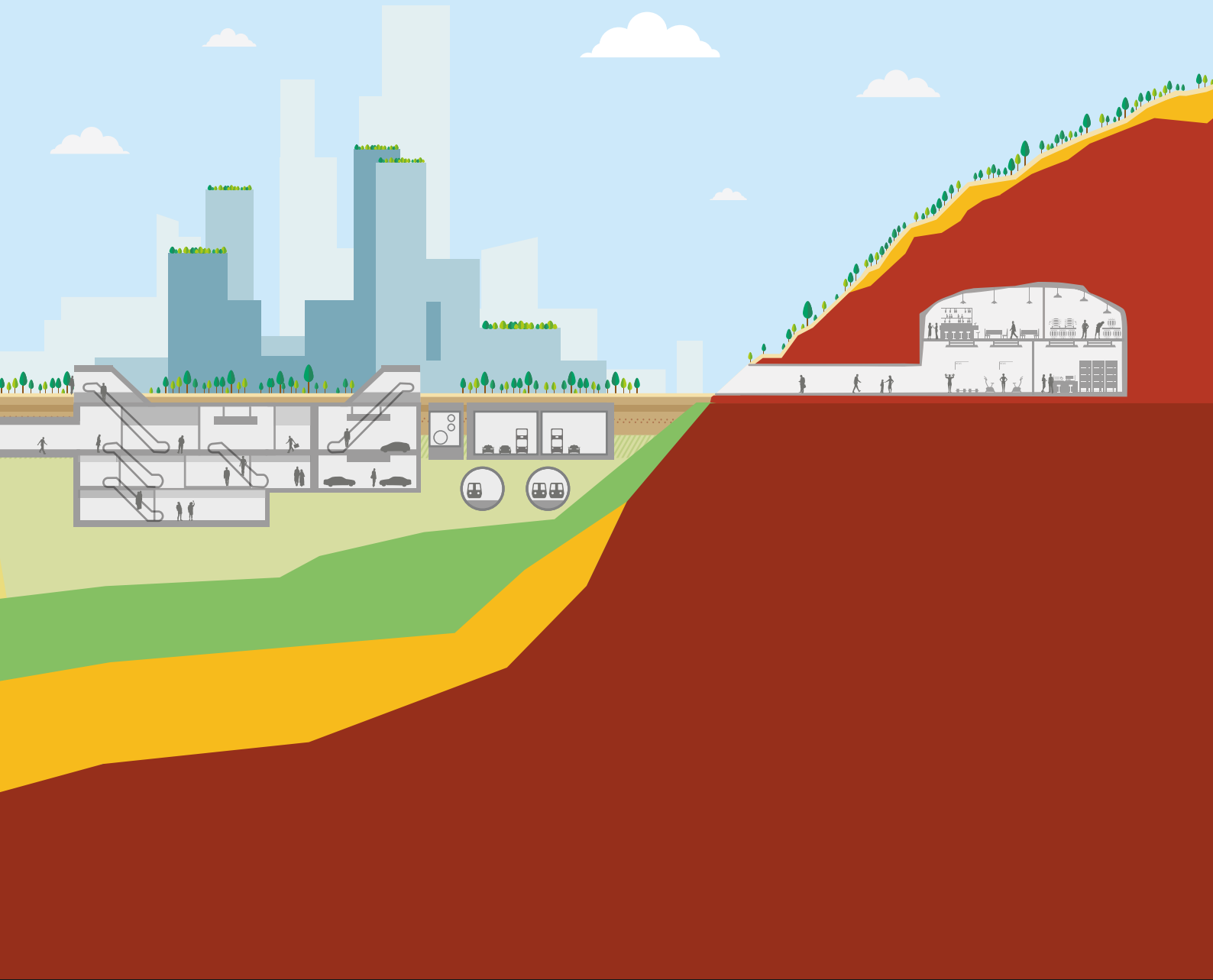

我們的主要業務包括：
Our Business includes:

- 基礎工程
  Foundation Works
- 斜坡及擋土牆長遠防治山泥傾瀉工程
  Construction of Landslip Preventive and Mitigation Works to Slopes and Retaining Walls
- 道路及渠務工程
  Roads and Drainage
- 水務工程
  Waterworks
- 地盤平整工程
  Site Formation

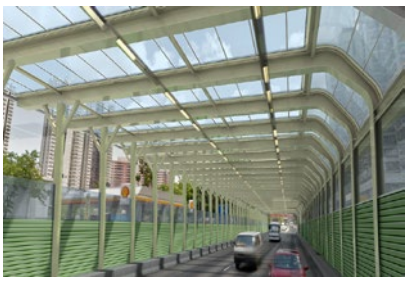

中国地质工程集团公司
CHINA GEO-ENGINEERING CORPORATION

香港灣仔港灣道 30 號新鴻基中心 24 樓 2421-25 室
Rm. 2421-25, 24/F., Sun Hung Kai Centre, 30 Harbour Road, Wanchai, Hong Kong
Tel: (852) 2511 9001 Fax: (852) 2580 0697

China Harbour Engineering Company Limited (CHEC) *founded its local representative, namely Zhen Hua Engineering Company Limited (ZHEC) and started its operation in Hong Kong in 1989. Over the past 20 years, CHEC has persisted in its pursuit of excellence and carved out for itself a solid market share in the local construction industry. Being one of the leading contractors in Hong Kong in the field of Road & Bridge, Marine Engineering, Infrastructures & Site Formation, and Environmental Protection & Waste Treatment, CHEC provides quality services in design, construction and project management for a variety of engineering projects in Hong Kong.*

CERTIFIED COMPANY HKQAA
ISO 9001 : 2008
Certificate No.: CC 624

CERTIFIED COMPANY HKQAA
ISO 14001 : 2004
Certificate No.: CC 2666

中國港灣工程有限責任公司
CHINA HARBOUR ENGINEERING COMPANY LTD.

China Harbour Engineering Company Limited
19/F, China Harbour Building, 370-374 King's Road, North Point, Hong Kong
Tel: (852) 2887 8118 (General Line) Fax: (852) 2512 0427
E-mail: chechk@chechk.com Websites: www.chec.bj.cn/ www.chechk.com

5 years+ 商界展關懷
caringcompany
Awarded by The Hong Kong Council of Social Service 香港社會服務聯會頒發

C M WONG & ASSOCIATES LTD
黃志明建築工程師有限公司

11/F Universal Trade Centre
3-5A Arbuthnot Road, Hong Kong
Tel: (852)2522-1068
Fax: (852)2526-3111
www.cmwal.com
cmwal@cmwal.com

C M Wong & Associates Ltd is a Hong Kong based consulting engineer in providing a full range of professional services including feasibility studies, planning, design and supervision in relation to building and infrastructure projects. Our clients include various Hong Kong Government departments, institutions and major developers.

We adopt a flexible approach to suit clients' needs. We are also renowned for providing innovative engineering solutions for challenging projects especially for those with difficult ground conditions.

ISO 9001 : 2008
Certificate No.: CC 801

ISO 14001 : 2004
Certificate No.: CC 5408

OHSAS 18001 : 2007
Certificate No.: CC 5409

Building on us

The leading geotechnical contractor in Hong Kong

www.bachy-soletanche.com.hk

bsg@soletanche-bachy.com

A subsidiary of SOLETANCHE BACHY

BACHY SOLETANCHE
法 國 地 基 建 築 公 司

ARCADIS | Design & Consultancy for natural and built assets

Facing the Challenge Exceeding Limits

Improving the quality of life

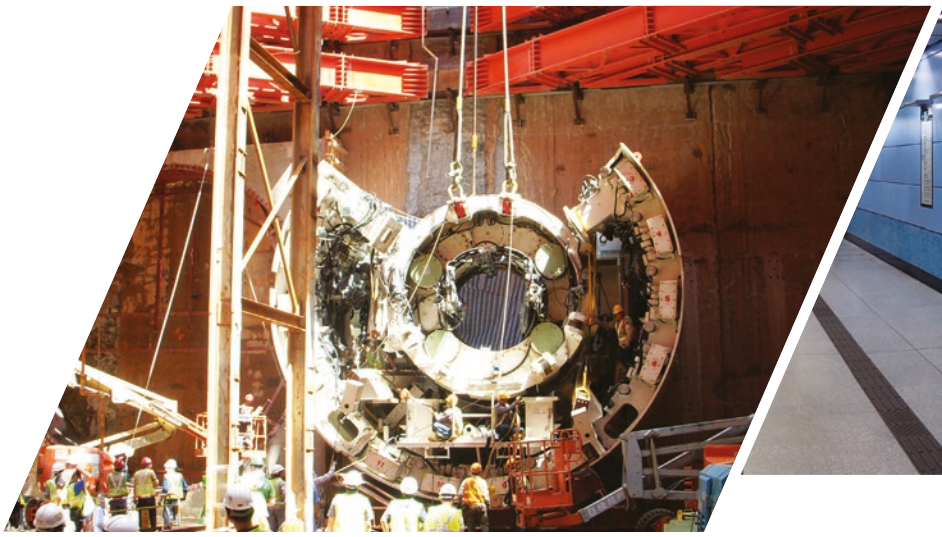

For over 80 years, Arcadis has contributed to Asia's natural and built asset environments by creating places of distinction and providing sustainable solutions.

We are one powerful Arcadis business incorporating brands such as Langdon & Seah, EC Harris, Hyder Consulting, Genesis, InProjects and SENES, delivering some of the most iconic projects in Asia such as Gardens by the Bay in Singapore, Television Cultural Centre in Beijing, International Finance Centre in Seoul and the newly opened MTR Whampoa Station in Hong Kong.

Applying our sector knowledge and collective design, consultancy, engineering, project and management services we deliver exceptional outcomes for our clients and continue to innovate in the fields of construction, design and architecture

Throughout the globe we employ 27,000 people and in Asia we have over 4,500 people across 50 offices delivering over $300m revenue (2016) . See how we live our passion at arcadis.com and follow us @Arcadis_Asia.

For more information please contact:
T: (852) 2911 2233
E: ArcadisDE-HK@arcadis.com
www.arcadis.com

FUGRO
CONSTANTLY EVOLVING

Fugro works with you, supporting each stage of your project, identifying and overcoming environmental, logistical and technical challenges.

Fugro are pleased to sponsor the HKIE Geotechnical Division 37th Annual Seminar.

www.fugro.com

GROUND ENGINEERING SPECIALIST

Intrafor performs a wide range of activities for buildings and civil infrastructure – including geotechnical investigation, ground improvement and the construction of special foundations such as deep diaphragm walls.

Intrafor Hong Kong Ltd.
20/F Eight Commercial Tower
8 Sun Yip Street, Chai Wan, Hong Kong
Tel. 2590 2288 - www.intrafor.com

INTRAFOR

TREVI

Foundation Specialists

Trevi Group is a worldwide leader in the field of ground engineering (special foundations, tunnel excavation, ground consolidation and the building and marketing of special rigs and equipment relevant to this engineering sector with its manufacturing division); the Group is also active in the drilling sector (oil, gas and water) both in the production of plant and the supply of services and in the construction of automated underground car parks.

The Group was established in Cesena (Italy) in 1957 and today has more than 50 subsidiary companies all over the world.

Its success is due to the vertical integration of the main divisions making up the Group:

- **Trevi**, the division that supplies special services in the field of ground engineering,
- **Petreven**, the oil drilling division of the Group,
- **Soilmec**, the division that produces and develops plant and machinery for ground engineering,
- **Drillmec,** the division that produces and develops drilling rigs (oil, gas and water).

The main activities of **Trevi Construction Co Ltd** in Hong Kong are:

1) Jet Grouting for ground improvement for basement excavation work and tunnelling work,
2) Ground Anchors, permanent and temporary,
3) Pipe Pile Installation,
4) Micro-piles (mini-piles),
5) All types of grouting including pressure, compensation, fissure, etc with cement and chemical based grout,
6) Ground freezing.

Contract No: HK/2012/08
Central – Wanchai Bypass
at Wanchai West
(Jet Grout Columns)

Contract No: CV/2012/08
Liantang / Heung Yuen Wai
Boundary Control Point
(Tie Back Soil Nails)

Trevi Construction Co Ltd
7/F, Sun Kwong Industrial Building, 1059 – 1061 Tung Chau West Street, Lai Chi Kok, Kowloon.
Tel : 2116 6966 Fax : 2117 0229 Email : info@trevihk.com Website : www.trevispa.com

QAS INTERNATIONAL
ISO 9001:2008
REGISTERED COMPANY

your FIRSTCHOICE

Innovative • High-quality • Value-added Solutions

A Leading Global Provider for the Ultimate Engineering Solution

Meinhardt has been providing engineering and planning excellence to the international construction industry for **60 years**. We provide engineering consulting capabilities in Infrastructure and Environment; Civil and Structures; Mechanical, Electrical and Plumbing (MEP); Project Management and Urban Development.

MEINHARDT

Consulting Engineers . Planners . Managers

Offices throughout
Asia, Australia, Middle East & UK
www.meinhardtgroup.com
www.meinhardt-china.com
mcehk@meinhardt.com.hk

HEESUNG GROUP
SAMBO E&C
삼보 E&C(주)

Address: Unit 1109-10, 11/F, Tower 2, Silvercord, 30 Canton Road, Kowloon
Tel : (852) 2735 3434 Fax : (852) 2735 9777
Website : www.samboenc.co.kr

No.1 Trust Builder

Sambo E&C to get trust from customers and give pride to members with best quality and service

MARINE FOUNDATION

HKIA C3203/3204/3205 (DCM)

LAND FOUNDATION

WAN CHAI (DIAPHRAGM WALL)

LOW HEAD ROOM WORK

SCL C1123

HONG KONG LINK ROAD

LAMBETH

Distinctly Different

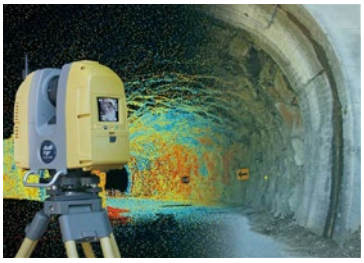
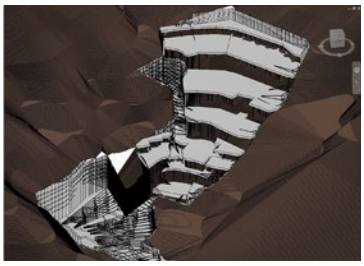

Lambeth brings together the diverse experience of operations, planning, commercial and design professionals – from within Gammon and Balfour Beatty – ensures it remains at the forefront of new techniques and new thinking. We set the standard for both innovation and technological advancement in building, civil, environmental, foundations, geotechnical and safety disciplines.

A member of the Gammon Group

28/F Devon House, Taikoo Place, 979 King's Road, Hong Kong Tel: 2516 8823 Fax: 2516 6352

香港國際機場 HONG KONG INTERNATIONAL AIRPORT

Hong Kong International Airport (HKIA) has a global network covering about 190 destinations worldwide, including 42 in the Mainland. HKIA is one of the busiest aviation hubs in the world which handled 70.5 million passenger trips and moved 4.52 million tonnes of cargo in 2016. HKIA is committed to sustainable growth and development, and aspires to be the finest in the world.

www.hongkongairport.com

康和建築工程有限公司
Konwall Construction & Engineering Co., Ltd

Buildings Department

- Registered General Building Contractor
- Registered Specialist Contractor in the Foundation Works Category
- Registered Specialist Contractor in the Demolition Works Category
- Registered Specialist Contractor in the Ground investigation Field Works Category

Development Bureau

- Approved Specialist Land Piling Contractor (Group II) for Public Works
- Approved Site Formation Contractor (Group B Probationary) for Public Works

Unit 1003, K. Wah Centre, 191 Java Road, North Point, Hong Kong 香港北角渣華道 191 號嘉華國際中心 1003 室 Tel: 2563 1233 Fax : 2561 7122

MOTT MACDONALD

Unlocking underground possibilities

We address ground condition uncertainties to manage risk and deliver long-lasting, cost effective and buildable solutions.

Opening opportunities with connected thinking.

Mott MacDonald
T +852 2828 5757
E marketing.mmhk@mottmac.com
W mottmac.hk

Proceedings of the 37th Annual Seminar
Geotechnical Division, The Hong Kong Institution of Engineers

G-EVOLUTION:
Geotechnical Practice in Hong Kong

19 May 2017
Hong Kong

Jointly organised by:
Geotechnical Division, The Hong Kong Institution of Engineers
The Hong Kong Geotechnical Society

Supported by:
Civil & Structural Divisions, The Hong Kong Institution of Engineers

Captions of Figures on the Front Cover

Top Left to Right:
1) Application of an Automated LiDAR-based Mapping System in Natural Terrain Hazard Studies in Hong Kong (By courtesy of CEDD of HKSAR and Fugro HK Ltd.)
2) Effect of Multiple Rainstorms on Landslides – A Case Study (By courtesy of AECOM)

Middle:
3) Central-Wan Chai Bypass Tunnel (By courtesy of HyD of HKSAR and AECOM)

Bottom Left to Right:
4) Large Scale Bored Pile Wall Supported by Permanent Tie Backs in Hong Kong (By courtesy of Sun Hung Kai Architects and Engineers Ltd. and Ove Arup & Partners Hong Kong Ltd.)
5) Design and Construction of a Rigid Steel Boulder-resisting Barrier in a Drainage Line, Lantau (By courtesy of CEDD of HKSAR and Jacobs China Ltd.)

Soft copy of the proceedings can be downloaded from the HKIE Geotechnical Division's website http://mobile.hkieged.org/download/as/AS2017.pdf

ORGANISING COMMITTEE

Chairman
Ir Barry Sum

Members
Ir Dr Tony Chen
Ir Dr Johnny Cheuk
Ir Sammy Cheung
Ir Warren Dou
Ir David Ho
Ir Derek Kwok
Ir David Lai
Ir Y C Lam
Ir Dr S W Lee
Ir Clifford Phung
Ir Jack Yiu
Ir Patrick Yong

Technical Sub-committee
Ir Dr Tony Chen
Ir Dr Johnny Cheuk
Ir Warren Dou
Ir Dr Julian Kwan
Ir Y C Lam
Ir Dr S W Lee
Dr Andy Leung
Dr Chao Li
Ir Jack Yiu
Ir Prof Limin Zhang

Any opinions, findings, conclusions or recommendations expressed in this material do not reflect the views of the Hong Kong Institution of Engineers or the Hong Kong Geotechnical Society

Published by:
Geotechnical Division
The Hong Kong Institution of Engineers
9/F., Island Beverley, 1 Great George Street, Causeway Bay, Hong Kong
Tel: 2895 4446 Fax: 2577 7791

Prepared in Hong Kong

FOREWORD

2017 is a special year. It marks the 30th anniversary of the HKIE Geotechnical Division as well as the 40th anniversary of the Geotechnical Engineering Office of the Civil Engineering and Development Department of HKSAR.

The importance and status of the geotechnical profession grew since 1970s after occurrence of several disastrous landslides as well as along with booming of the infrastructure and city developments in shaping the current Hong Kong territory.

In 2007, the Annual Seminar was themed "Geotechnical Advancements in Hong Kong since 1970s" to consolidate the then state-of-the-art and state-of-practice geotechnical engineering in Hong Kong. Over the last 10 years, significant underground and at-grade geotechnical works have been carried out for the new metro lines and railways, public and private housing developments and land reclamations. The geotechnical professions have gained valuable experience in the latest technology, standards and practices in multi-disciplinary working culture as well as built environment.

This Geotechnical Division Annual Seminar 2017 has chosen a theme of "G-EVOLUTION: Geotechnical Practice in Hong Kong" to consolidate the geotechnical advancement achieved in the past 10 years and more important to highlight challenges and new adventures ahead of us. There should be a drive to make use of these valuable geotechnical skills learnt in Hong Kong and export them overseas, in particular the developing countries, for sustainable development. The seminar is divided into four sessions on different subjects, each with an invited lecture and selected presentations from nearly 40 submitted technical papers.

On behalf of the Geotechnical Division, I would like to thank the Hong Kong Geotechnical Society (HKGES) for jointly organizing this seminar, and the HKIE Civil Division and Structural Division for their support. I would like to thank the generous financial support from the sponsors.

Last but not the least, I would also like to express my gratitude to the invited lecturers, authors and speakers contributing to this seminar and the dedicated effort of the Organising Committee, under the leadership of Ir Barry Sum, in revamping this seminar into more environmental friendly and technological advances.

Ir James Sze
Chairman, Geotechnical Division
Hong Kong Institution of Engineers (2016/17 session)
May 2017

ACKNOWLEDGEMENTS

The Organising Committee would like to acknowledge the support of the following sponsors for their generous support of the Seminar:-

AECOM Asia Co. Ltd.

Airport Authority

Arcadis Design & Engineering Limited

Arup

Bachy Soletanche Group Limited

C M Wong & Associates Ltd

China Geo-Engineering Corporation

China Harbour Engineering Co. Ltd.

Earth Products China

Fugro Geotechnical Services Ltd

Intrafor Hong Kong Limited

Konwall Construction & Engineering Co. Ltd.

Lambeth Associates Ltd

Meinhardt Consulting Engineers

Mott MacDonald Hong Kong Limited

Reinforced Earth Pacific Limited

Sambo E&C Co. Ltd.

Trevi Construction Co. Ltd.

TABLE OF CONTENTS

INVITED LECTURES		Page No.
1.	Forty Years of Slope Engineering in Hong Kong *H.N. Wong*	i – x
2.	Ground Engineering – Back to Basics *D. Lee*	xi
3.	Case Study: Design and Construction Challenges for Admiralty Station Expansion *M. Bezzano, S. Smith, J. Yiu, M. Wiltshire*	xii – xxvi
4.	Satellite CT Scanning for Urban Infrastructural Health Diagnosis *L. Hui & P. Ma*	xxvii – xxviii
PAPERS		
5.	Extensive use of I&M to Enable Safe TBM Drive in Urban Dense Area, a Focus on SCL1128 Eastern Downtrack Drive *S. Auvergne, J. Gauffre & A. Prost*	1 – 11
6.	Geophysical Investigations for Obstruction Detection and Subsequent Mitigation Works for Marsh Road TBM Crossing, SCL1128 *S. Auvergne, K. Yu, C. Mogenier & T. Barrett*	12 – 24
7.	Numerical Simulation of Cement-treated Soil Columns Used as Cantilever Earth Retaining Structure *L.S. Ay*	25 – 33
8.	Hong Kong's Hidden Aggregate Resource: The Potential for Underground Quarrying *H.K.K. Chan, S.W. Millis, M.I. Wallace & K.C. Hung*	34 – 44
9.	An Innovative Earth Supporting System for a Deep Excavation *R.K.S. Chan, C.W.C. Phung & C.W.C. Lau*	45 – 51
10.	An Overview of Deep Excavation Techniques in Hong Kong *R.K.S. Chan, C.W.C. Phung & K.C.L. Tse*	52 – 57

11. An Overview of Technological Advancements in Geotechnical Instrumentation and Monitoring 58 – 64
R.K.S. Chan, C. Phung, R. Lee & I. Lam

12. A Comparison of 2D and 3D Numerical Analyses of a Complex Tunnel Intersection Lining 65 – 71
L.T. Chen & J.W.Y. Yeung

13. 3D Numerical Analysis and Design of Flexible and Rigid Barriers 72 – 82
A.K.C. Cheung, J. Yiu & S.W. Millis

14. A Case Study of Temporary Support Design for Mined Adits in Highly Decomposed Granite 83 – 92
F. Desaintpaul, C. Hu, H. Ling, J. Rickard, E. Clech, R. Cho & C. Cacarié

15. Natural Terrain Hazard Studies in Hong Kong: Past, Present and Future 93 – 103
H.Y. Ho, K.J. Roberts & Y.K. Ho

16. SCL 1128 – Hong Kong's First Variable Density Tunnel Boring Machine 104 – 113
D. Jacques, H. Laverret, N. Ballu & J. Reilly

17. The Appropriate Use of the Coefficient of Secondary Compression in Settlement Analysis 114 – 120
D. Johnston

18. Economic Reclamation and Seawall Design and Temporary Stabilizing Berm 121 – 130
M.C.Y. Ko & H.C. Sze

19. Latest Developments of Hong Kong's Landslip Warning System 131 – 139
V.W.W. Kong, V.M. Tong, J.S.H. Kwan & H.W. Sun

20. Recent Technical Development of Natural Terrain Risk Mitigation Measures in Hong Kong 140 – 148
J.S.H. Kwan, H.W.K. Lam, C. Lam & E.H.Y. Sze

21. Hong Kong MTR Shatin to Central Link Contract 1128 (Eastern Approach) – Tunneling in Sensitive and Congested Urban Enivronment 149 – 161
K. Kwok, G. Bracq & T. Barrett

22. Mobile Application for Soil Nail Works Supervision 162 – 167
T.M.K. Lai, C.H.W. Chow, I.W.Y. Chan

23. Large Scale Bored Pile Wall Supported by Permanent Tie Backs in Hong Kong 168 – 176
A.K.M. Lam & K.P. Chan

24. Advances and Challenges of the Landslip Prevention and Mitigation Programme since 2007 177 – 187
T.T.M. Lam, C.Y.S. Wong, R.C.H. Koo, A.H.K. Wu & K.K.S. Ho

25. Recent Advances in Debris Mobility Modelling for Assessing Natural Terrain Landslide Hazards in Hong Kong 188 – 196
R.P.H. Law, F.W.Y. Ko, J.S.H. Kwan & H.W. Sun

26. Minimizing Traffic Impact Arising from Upgrading of a Roadside Man-made Slope: from Ideas to Implementation 197 – 207
K.P.W. Leung, A..C. Wong & R.K.Y. Leung

27. Adopting Advanced Technology for Terrain Evaluation 208 – 214
S.K.H. Leung & G.G. Pook

28. Overall strength evaluation of a soil-cement column under axial compression 215 – 220
Y. Liu & A.L. Saw

29. Evolution of Landslide Susceptibility Mapping for Natural Hillsides in Hong Kong 221 – 231
F.L.C. Lo & F.W.Y. Ko

30. Advancements in Ground Improvement Techniques for Non-dredged Reclamation Solutions in Hong Kong 232 – 239
A.D. Mackay

31. Artificial Ground Freezing Hong Kong Case Histories: Lessons Learnt 240 – 256
A.D. Mackay

32. Rock Mass In-Situ Stress in Hong Kong Determined by Hydraulic Fracturing Testing 257 – 268
A.D. Mackay, G. Klee & J. Wong

33. 4D Passive Seismic Imaging for soil monitoring during TBM excavation, Paris Metro 269 – 277
C. Mogenier & S. Robert

34. Effect of Multiple Rainstorms on Landslides – A Case Study 278 – 288
A.K.L. Ng

35. Design and Construction of a Rigid Steel Boulder-resisting Barrier in a Drainage Line, Lantau 289 – 298
L.H. Swann, M.J. Lorimer, S. Chung, P. Tsang & F. Cham

36. Finite Element Analysis of Deep Excavations in Soft Ground 299 – 308
L.H. Swann & Ci Wang

37. Application of an Automated LiDAR-based Mapping System in Natural Terrain Hazard Studies in Hong Kong 309 – 315
J.H.T. Tam, C.K.W. Yeung, J.P. Yu, R.S.L. Hu & K.A. Styles

38. Back analysis of temporary piles in alluvium using Plaxis 3D 316 – 325
M.R. Thompson, G.S.H. Toh

39. Machine Learning Study on Man-made Features in Hong Kong – A Data Driven Approach to Feature Classification 326 – 333
K.C.H. Tse, A.C.K. Chan & K.K.F. Yau

40. Practical Use of PLAXIS 2D for Tunnel Support in Variable Ground Conditions in Hong Kong 334 – 342
C.H.P. Wong, L.H. Swann & R.G. Hinchliffe

41. Numerical Analysis of Bored Piles in Sandstones 343 – 352
L.W. Wong

42. Design Suggestions on Flexible Debris-resisting Barriers 353 – 362
G. Yung & A.l Ng

Forty Years of Slope Engineering in Hong Kong

H.N. Wong

ABSTRACT

Slope engineering practice in Hong Kong has been evolving for the past 40 years, both in terms of the geotechnology involved and its scope of application. Several key areas of change, together with the context under which these took place, are highlighted in this paper. Here, 'slope engineering' refers to not only the applied science of geotechnical engineering and engineering geology, but also slope safety management in general. With concerted effort from the profession, the changes have brought about advances in slope engineering and improvement in slope safety, rendering Hong Kong a positive example in urban landslide risk management. These also prepare the profession to meet the future challenge and undertake expanded responsibility, particularly in coping with extreme rainfall events which may become more frequent and severe in the wake of climate change.

1 PREMISE

The vast majority of our contemporary engineering structures, such as buildings and bridges, are designed to ensure that the chance of collapse throughout their service life is negligibly low. In contrast, slopes typically have a finite and much higher failure rate, which is reflected by the occurrence of landslides at times. Many of these slope failures are tolerated, either willingly or unwillingly. The former may involve consideration of cost-effectiveness, resource constraints, priority, etc. The latter applies to cases where slope failure is not commensurate with the design intent but occurs in connection with deficiency in design, human error, inadequate technical understanding, etc.

Under this overall setting, with escalating public's expectation of slope safety, improving knowledge of slope performance and better system of landslide risk management, slope engineering practice in Hong Kong has notably evolved over the past 40 years. Its positive outcome is reflected in the drastic change in the landslide risk trend, with significant reduction in annual landslide fatalities since the late 1970s (Figure 1). The changes that stand as milestones in the evolution of slope engineering practice over the period, together with the context of the changes, are described below.

2 STARTING POINT – ENGINEERING SLOPES WITH GEOTECHNOLOGY

The landslide risk trend in Hong Kong based on 15-year rolling average annual landslide fatalities is shown in Figure 1. In the 1960s and 1970s, landslide risk was increasing significantly. This was mainly attributed to the extensive formation of man-made slopes as part of the rapid urban development in the period. The slopes were mostly formed according to empirical rule of thumb with little geotechnical input. They failed frequently, particularly during heavy rain.

The disastrous consequence of the Po Shan (Figure 2) and Sau Mau Ping landslides in 1972, followed by the occurrence of a similar failure in Sau Mau Ping in 1976 (Figure 3), revealed to all the serious deficiency of this rule-of-thumb approach of slope engineering. With the awareness that the level of slope safety in Hong Kong should be improved to meet the community's expectation, the Geotechnical Control Office (renamed Geotechnical Engineering Office, GEO, in 1992) was set up in 1977 to regulate slope

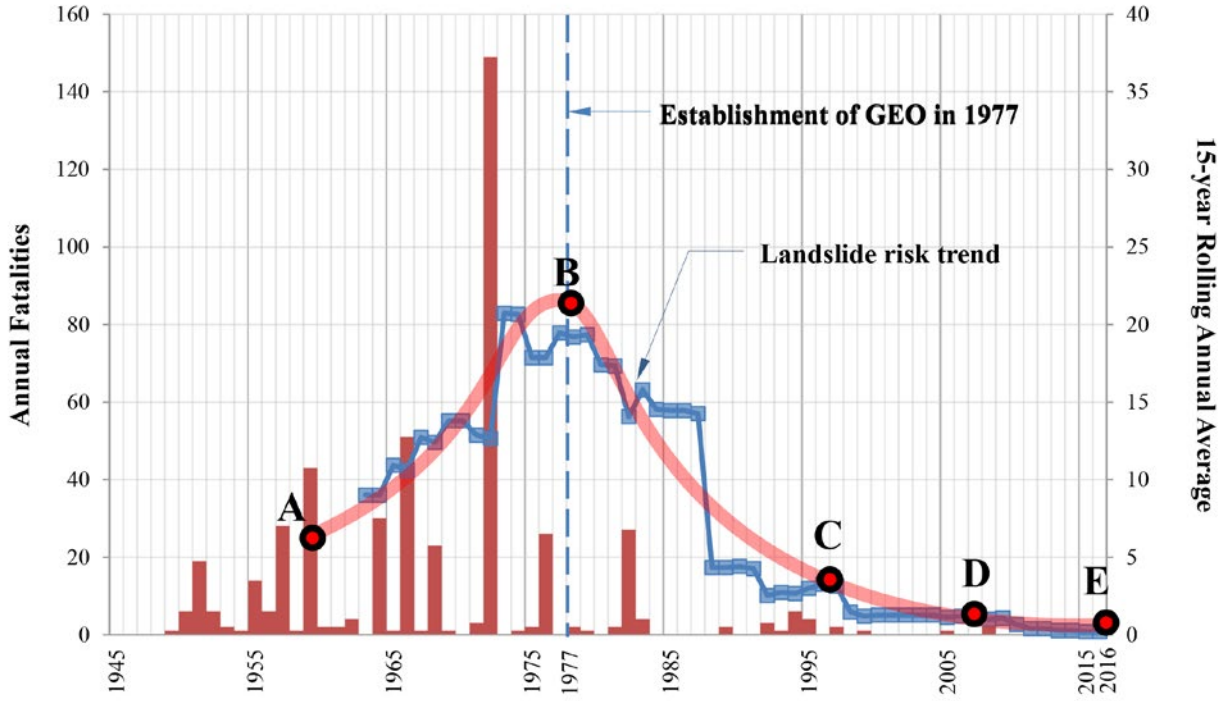

Figure 1: Landslide risk based on annual landslide fatalities in Hong Kong

Figure 2: Po Shan Landslide in 1972
(resulting in 67 fatalities)

engineering in Hong Kong. This marked the starting point of a complete revamp of the slope engineering practice in Hong Kong (Point B in Figure 1). It resulted in territory-wide application of state-of-the-art geotechnology to slope engineering and setting up of the Hong Kong Slope Safety System to regulate the application. Under the Slope Safety System, landslide risk is also being managed via other measures, e.g. retrofitting substandard slopes, landslide warning and emergency services, and public education on slope safety (Malone, 1998).

Figure 3: Sau Mau Ping Landslide in 1976
(resulting in 18 fatalities)

3 HIGHER LEVEL – ENHANCING ROBUSTNESS OF ENGINEERED SLOPES

Slope engineering with proper geotechnical input has enabled the practitioners to design new slopes according to geoscience principles, and to verify that the design meets the required geotechnical standards that are commensurate with international good practice. This, together with systematically retrofitting the existing, substandard slopes based on risk-based prioritization, has led to major reduction in the overall landslide risk (from Point B onward, Figure 1). It clearly demonstrates that slope stability is much improved by replacing the rule-of-thumb approach with application of geotechnology in slope engineering.

However, as time goes by when more engineered slopes have been formed and their actual performance in heavy rain tested, it becomes evident that even slopes engineered to the required design standards have a finite chance of failure (Wong & Ho, 2000). Many of these are small scale landslides, either washout failures caused by concentrated surface water flow (Figure 4) or slope instability controlled by localized geological weaknesses (Figure 5). Yet, sizeable failures of engineered slopes do also occur occasionally (e.g. see Figure 6), typically associated with adverse geological and hydrogeological setting that is not addressed in the design.

Through the landslip investigation programme launched as part of the follow-up actions of the 1994 Kwun Lung Lau landslide, the GEO has been systematically examining and studying all known

Figure 4: Concentrated flow of surface water commonly due to lack of slope maintenance or deficient drainage provisions

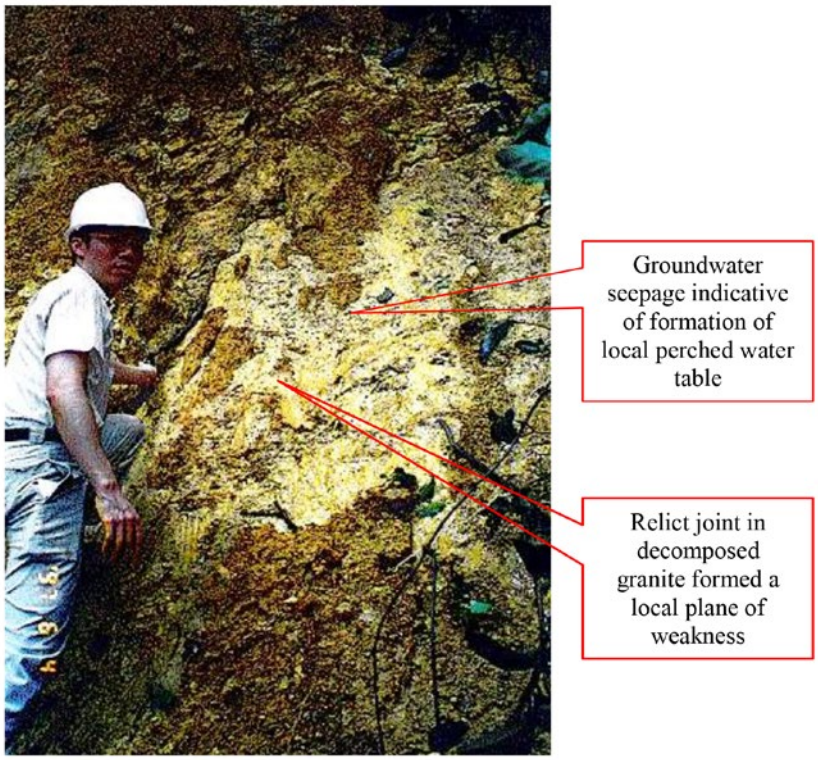

Figure 5: Small scale slope stability controlled by localized geological weakness

Figure 6: Ching Cheung Road Landslide in 1997 (~5,000m^3)

landslide incidents since 1997, including failure of engineered slopes. The investigation has provided comprehensive and rigorous data on the failure rates of different types of man-made slopes, together with useful findings on the causes of failure and areas for improvement.

The 5-year rolling average annual failure rates of engineered slopes and un-engineered slopes, based on the comprehensive data collated since 1997, are shown in Figure 7. The average annual failure rate of engineered slopes, which was 0.12% in the 5-year period from 1997 to 2001, was not negligible. Such a failure rate implies that over a notional design life of, say, 120 years, about 15% of the engineered slopes would fail at least once.

By the mid-1990s, although Hong Kong's slope engineering was on a par with international best practice and slope safety was greatly improved as compared with that in the 1970s, public's expectation of slope safety had further escalated as the quality of life continued to enhance. This is understandable

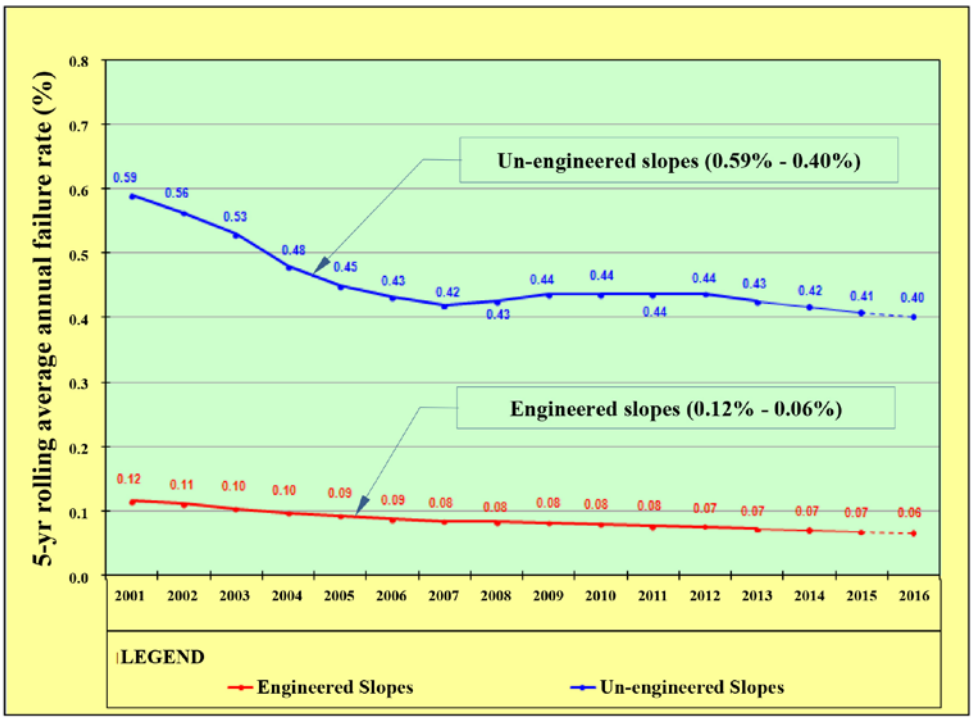

Figure 7: 5-year rolling average annual failure rates of engineered and un-engineered man-made slopes

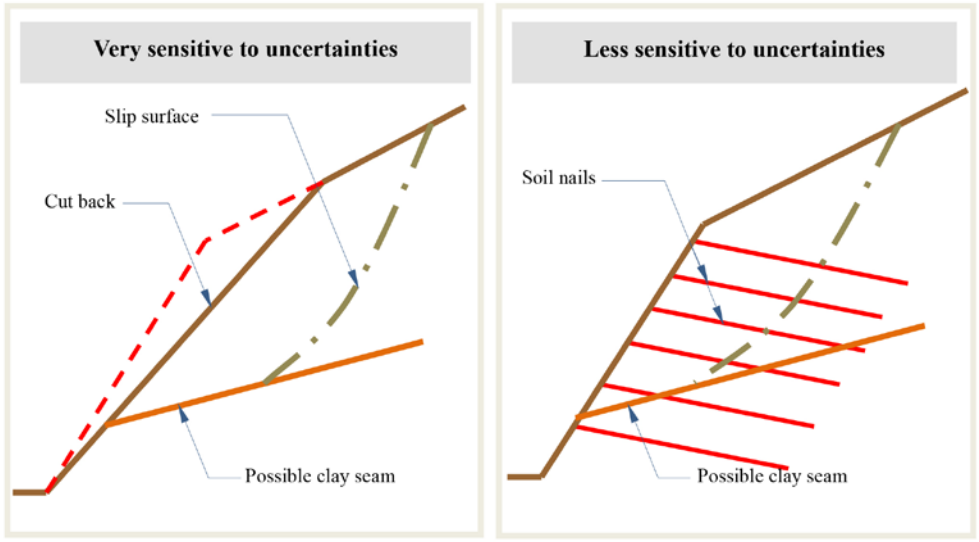

Figure 8: Enhancing the performance of engineered slopes with the use of robust design scheme (e.g. soil nailing)

given Hong Kong's setting as a major metropolitan with a high density of population and intense development on landslide-prone terrain. It was signified by the strong public reaction to a number of serious landslides occurred in the early to mid-1990s and the grave concern expressed in the failure of slopes subject to engineering input. In addition, the enhanced professional awareness of the actual performance and causes of failure of engineered slopes provided the essential technical insights and impetus for further improving the performance of engineered slopes. Consequently, Hong Kong's slope engineering underwent a new round of evolution in the late 1990s (Point C in Figure 1). The key changes included: (i) enhancing the robustness of engineered slopes through the use of design schemes that are less sensitive to uncertainties in geological and hydrogeological conditions (Figure 8), both in terms of the likelihood and consequence of failure, (ii) improving slope drainage and surface protection, and

thereby making the slopes less vulnerable to adverse effects from concentrated surface water flow and subsurface seepages, and (iii) maintaining slopes to minimize deterioration and upkeep their stability condition (Wong, 2001). These took the engineering of man-made slopes to a higher level of reliability and safety. The improvement achieved is reflected in the progressive reduction in the 5-year rolling average annual failure rate of engineered slopes, up to about 50% by 2016 (Figure 7).

It is note-worthy that the failure rate of un-engineered slopes (i.e. slopes formed before 1977 without proper geotechnical input and verification that the required geotechnical standards are met), which was within about one order of magnitude higher than that of engineered slopes (Figure 7), was not exceedingly high. This probably reflects the contribution of the priority ranking system adopted in selecting the more vulnerable un-engineered slopes for priority retrofitting and the effectiveness of maintaining all slopes (including the bulk of the existing, un-engineered slopes which have not been given the priority for retrofitting) in minimizing their chance of failure. It should also be considered under the context that the rule-of-thumb approach adopted in forming the un-engineered slopes in the old days, being empirically based, nevertheless serves some useful engineering purposes.

4 NEW FRONT – DEALING WITH NATURAL TERRAIN LANDSLIDES

Up to about mid-2000s, slope engineering in Hong Kong was primarily concerned about dealing with man-made slopes. Before better knowledge about natural terrain landslides became available, there had been some early suppositions that the natural hillsides in Hong Kong are old and mature landforms and thereby should have evolved into a relatively 'stable' condition. These early suppositions included the views that natural hillsides showed no signs of creep, all failures are first-time slips, and the concept of 'ripening' being dismissed in view of the long time needed for the degree of weathering to become significantly altered by chemical weathering.

Whilst acknowledging that 'natural slopes are frequently close to limiting equilibrium over very large areas', it is stipulated in the Geotechnical Manual for Slopes (GCO 1984) that natural slopes need not meet the factor of safety requirements for slope design provided that two conditions are met: (i) the slope is undisturbed; and (ii) a careful examination is made to determine that there is no evidence of instability or severe surface erosion. There was apparently a time in the past that these two conditions were presumed to have been met in many parts of the natural terrain in Hong Kong.

With ample data available from the systematic study of natural terrain landslides in the rainstorms of November 1993 (Figure 9) and April 2000, review of the historical records of failures in 1966 and 1982, and the comprehensive review of the available aerial photographs for compilation of the Enhanced Natural Terrain Landslide Inventory (ENTLI), it is now known that natural hillsides in Hong Kong are

Wide-spread failures in South Lantau Island | Debris flow in Tung Chung

Figure 9: Natural terrain landslides on Lantau Island in November 1993 rainstorm

indeed susceptible to rain-induced, shallow failures. Field investigations revealed that the failures typically occur within 1 to 2 m of the surface mantle, where erosion pipe holes, dilation and partial infilling of relict discontinuities, and localized tension cracks are often observed. The hillsides are subject to on-going degradation, and a large number of shallow landslides can be triggered under heavy rain (say, 24-hour rain exceeding 20% of the average annual rainfall) even though relatively few failures occur in less severe rainfall condition (Wong, 2009).

As Hong Kong is developing closer to the steep natural hillsides as a result of its continual urban growth, the overall risk of natural terrain landslides is increasing. In contrast, the risk of man-made slope failures has significantly reduced due to improved slope engineering practice and safety management. In the mid-2000s, the GEO estimated via Quantitative Risk Assessment (QRA) that the risk of landslides due to natural terrain failures would be comparable to that of man-made slope failures by the year 2010 (Wong et al, 2006). This sets the scene for an important change in the slope safety strategy (Point D in Figure 1) to: (i) step up the requirement of studying natural terrain landslide hazards and carrying out the necessary mitigation works as part of the new development in close proximity to natural hillsides, and (ii) commence systematic study and mitigation of natural terrain landslide hazards affecting existing development under Government's post-2010 Landslip Prevention and Mitigation Programme (LPMitP).

Consequently, the geotechnical profession is tasked to assess and mitigate natural terrain landslides, apart from engineering man-made slopes. This expanded responsibility calls for development of new areas of professional competence and further advances in our slope engineering practice. These include several important aspects, which are different from those conventionally involved in engineering man-made slopes: (i) natural terrain hazard study and related engineering geological assessment, (ii) modeling of the mobility of landslide debris (Figure 10), (iii) analysis of debris-barrier interaction and design of barriers, (iv) QRA for study and evaluation of natural terrain landslide risk.

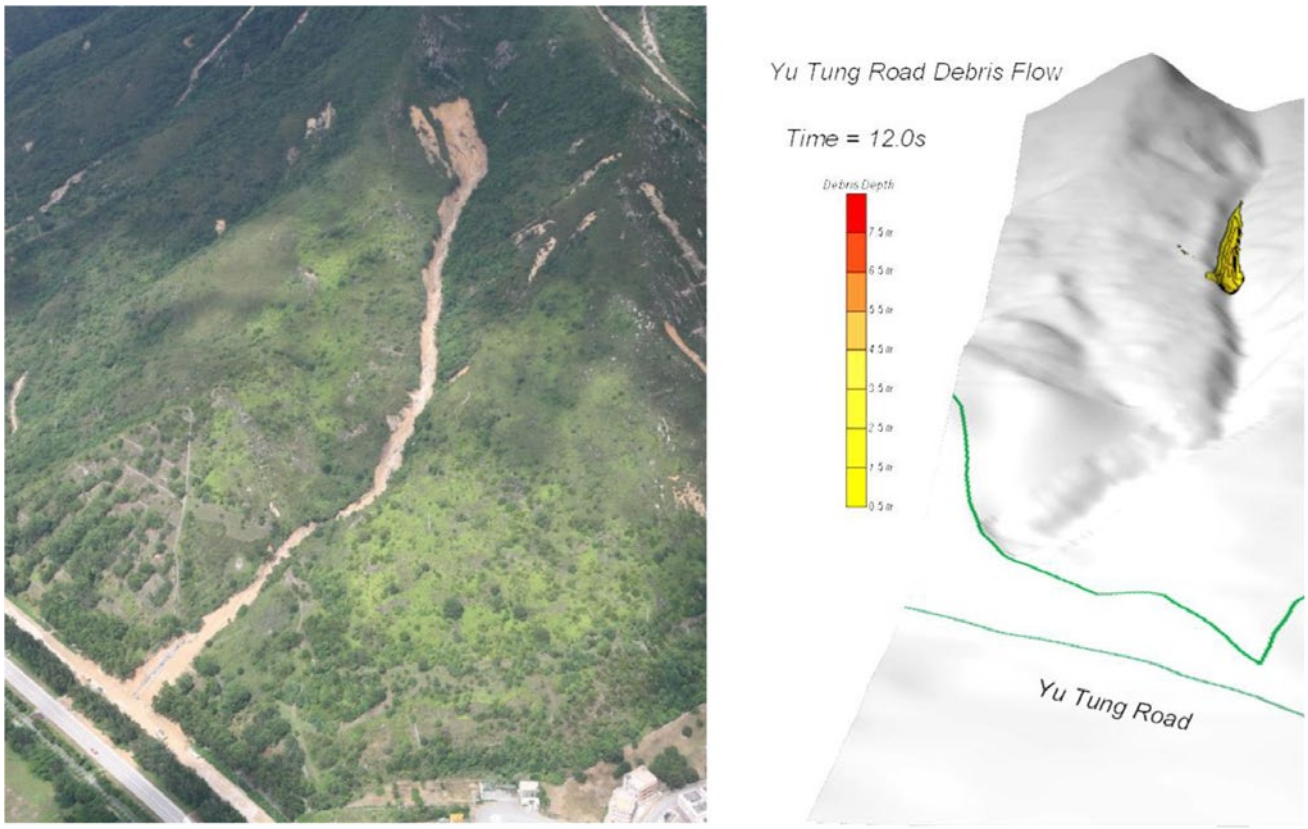

Figure 10: 3-D modeling of debris runout and mobility (The 2008 Yu Tung Road Debris Flow shown)

5 UNPRECEDENTED CHALLENGE – PREPARING FOR EXTREME WEATHER AND CLIMATE CHANGE

The concerted effort of the geotechnical profession has not only brought about continuous development in slope engineering practice, but also significant reduction of the landslide risk in Hong Kong. By 2016 (Point E, Figure 1), Hong Kong has experienced 8 consecutive years of zero landslide fatality, and 22 consecutive years with no multiple-fatality landslide. While the good slope safety performance provides an assurance of the effectiveness of our slope engineering practice in achieving the intended safety objectives, the profession is aware of the need to stay vigilant about the fact that our man-made slopes and natural hillsides still have a finite chance of failure, and that Hong Kong is still vulnerable to widespread and serious landslides particularly during extreme rainfall events. With the recognition that the global and local weather conditions are being affected by climate changes, meteorologists have assessed that this would not only increase the annual rainfall, but also escalate the frequency and severity of extreme rainfall events in Hong Kong (ENB, 2015). There are indications that the short-duration rainfall, e.g. 1-hr rainfall, in Hong Kong has already been significantly affected (Figure 11).

This poses an unprecedented challenge to slope safety in Hong Kong in the years to come, most notably in the following aspects: (i) the frequency and scale of failure of man-made slopes, including both un-engineered and engineered slopes, will increase as extreme rainfall events become more frequent and severe, (ii) washout failures will occur more frequently and seriously, due to increased short-duration rainfall intensity resulting in concentrated flow of surface water, which is difficult to control in an urbanized setting, (iii) widespread natural terrain landslides and debris flows will occur, with escalated frequency, scale and mobility, and (iv) concurrent occurrence of multiple hazards, such as landslides, flooding and storm surges, will lead to compounding effects and thereby aggravating the consequence and rendering landslide emergency more difficult to manage.

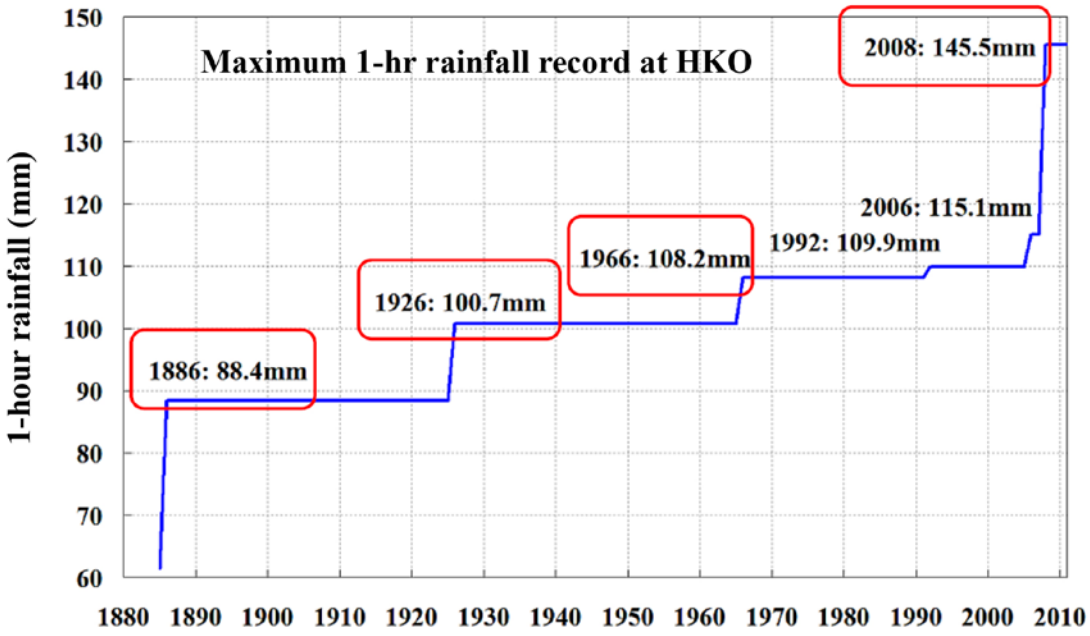

Figure 11: Record-breaking one-hour rainfall recorded by the Principal Raingauge in Hong Kong Observatory, Tsim Sha Tsui (Source: Hong Kong Observatory)

Since the 2010s, the GEO has been proactively undertaking studies on extreme rainfall events in collaboration with the Hong Kong Observatory and other research institutes. Scenario-based assessments of the territory-wide extent and consequence of landslides under extreme rainfall events have been conducted, together with evaluation of the capacity of the landslide emergency management system in coping with the events (Wong, 2013). It was found that natural terrain landslides and debris flows would overtake man-made slope failures as the principal slope safety concern in extreme rainfall

events (Figure 12). This is evident in the record-breaking rainstorm of June 2008, which resulted in over 2,400 natural terrain landslides on Lantau Island (Figure 13). The work also provided useful information and insights about improving our preparedness for meeting the challenge. This includes formulation of adaptation strategy, which involves further enhancement of the prevailing slope engineering practice to minimize failure and damage under extreme rainfall events. It also calls for enhancing our emergency preparedness and strengthening the resilience of the community in coping with extreme events. These are important areas for the geotechnical profession to address in the years to come, and will lead to further evolution of our slope engineering practice to meet the unprecedented challenge ahead.

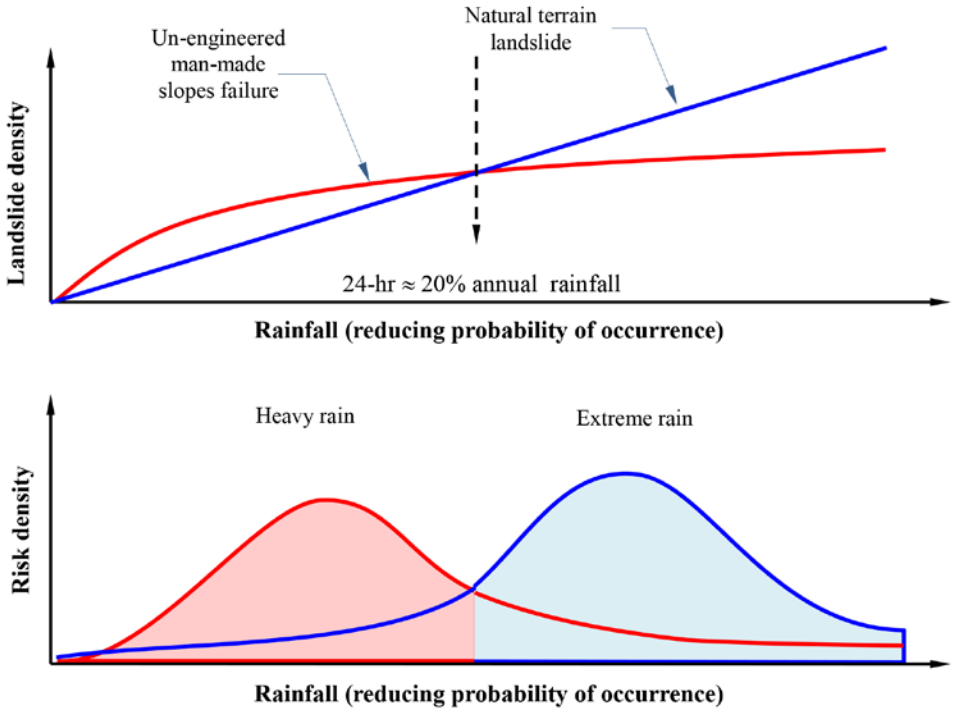

Figure 12: Diagrammatic illustration of change in principle landslide threat
From man-made slopes to natural terrain landslides in extreme rainfall events

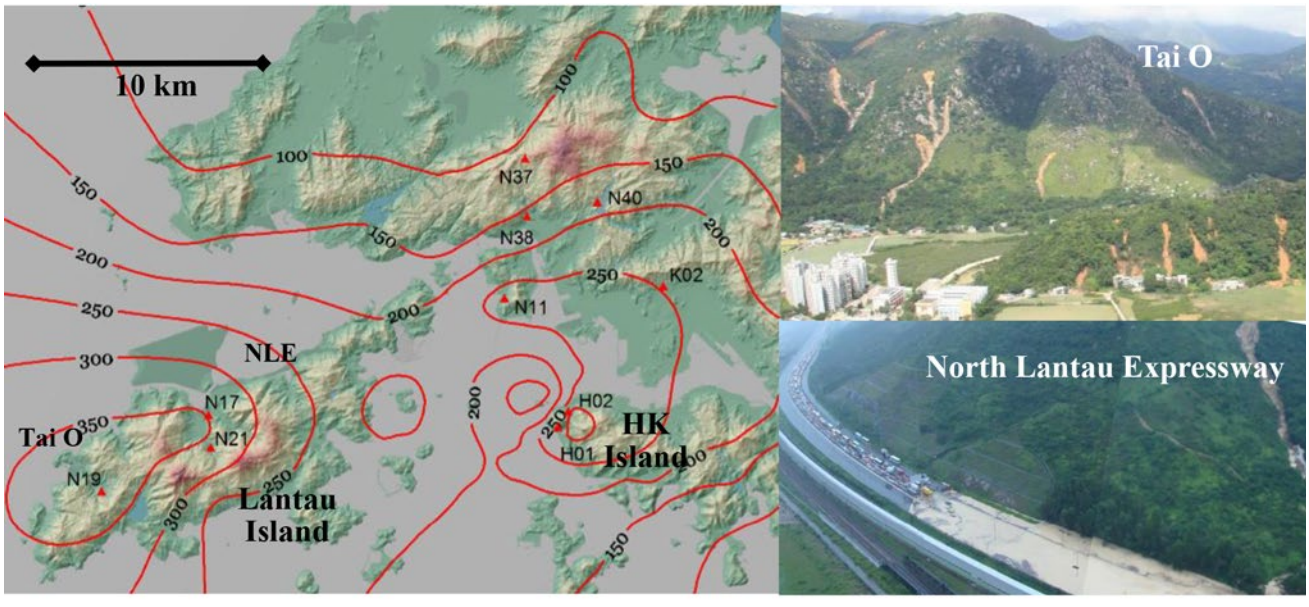

Figure 13: June 2008 rainstorm resulting in over 2,400 natural terrain landslides on Lantau Island

6 CLOSING REMARKS

Slope engineering practice in Hong Kong has been evolving for the past 40 years, in parallel with increasing public expectation of slope safety and improving professional knowledge and capability. The evolution has led to advances in slope engineering, and provided Hong Kong with the positive reputation for landslide risk management. Consequentially, the landslide risk in Hong Kong has been substantially reduced. This, instead of suggesting that the mission of combating landslides is accomplished and the job is done, places the geotechnical profession in a pivotal position to prepare Hong Kong to face the forthcoming, unprecedented challenge of extreme rainfall events in the wake of climate change. It calls for sustained effort from the profession, and will further reinforce our role in enabling Kong Kong's sustainable development and chartering international best practice in urban slope engineering and landslide risk management.

REFERENCES

Environment Bureau (2015). Hong Kong Climate Change Report 2015. Environment Bureau, Hong Kong, 122 p.

Geotechnical Control Office (1984). Geotechnical Manual for Slopes. (Second edition). Geotechnical Control Office, Hong Kong, 295 p.

Malone, A.W. (1998). Risk management and slope safety in Hong Kong. Proceedings of the Hong Kong Institution of Engineers Geotechnical Division Annual Seminar on Slope Engineering in Hong Kong, A.A. Balkema Publisher, Vol. 1, pp 3-17.

Wong, H.N. (2001). Recent advances in slope engineering in Hong Kong. Proceedings of the 14th Southeast Asian Geotechnical Conference, Hong Kong, Vol. 1, pp. 641-659.

Wong, H.N. (2009). Rising to the challenges of natural terrain landslides. Natural Hillsides: Study and Risk Management Measures; Proceedings of the 29th Annual Seminar of the HKIE Geotechnical Division, Hong Kong, pp15-53.

Wong, H.N. (2013). Enhancing the resilience of Slope Safety System against extreme events. The International Conference on Sichuan Reconstruction – The Review and Prospects of Sichuan (5.12) Post-disaster Reconstruction, Hong Kong, 11p.

Wong, H.N. & Ho, K.K.S. (2000). Learning from slope failures in Hong Kong. Proceedings of the 8th International Symposium on Landslides, Cardiff.

Wong, H.N., Ko, F.W.Y. & Hui, T.H.H. (2006). Assessment of landslide risk of natural hillsides in Hong Kong. GEO Report No. 191, Geotechnical Engineering Office, Hong Kong.

Ground Engineering – Back to Basics

Daman Lee
Hong Kong International Airport – Third Runway Division

ABSTRACT

Ground engineering in Hong Kong has long been taking a very conservative approach. It needed to be. There were times when developments and infrastructures were designed and constructed at astonishing pace and volume. The speed to complete the projects was taken to be much more important than taking the time for optimizations.

Increasing number of design tools are now available for more sophisticated analyses. For example, 3-D numerical models are becoming like a norm even for not so complicated designs. Outputs of the stresses, strains and movements in all directions could be produced at ease in numerous locations of interest. The analyses could be repeated to interrogate the sensitivities of the parameters and assumptions with little effort.

It is perhaps worth, or maybe even interesting, to trace back on how geotechnically complicated projects were designed in the past and reflect on how it is now being done. It is not an attempt to answer whether the design practice is evolving in the right way. Instead, a few work examples would be presented to stimulate thoughts on design trends, design approach, the standards being used and where are we seemingly heading in our own natural selection process.

Case Study: Design and Construction Challenges for Admiralty Station Expansion

Michael Bezzano
MTR Corporation Ltd, Hong Kong
Scott Smith
Aurecon Hong Kong Ltd, Hong Kong
Jack Yiu
Ove Arup and Partners Hong Kong Ltd, Hong Kong
Mark Wiltshire
Kier Laing O'Rourke Kaden Joint Venture, Hong Kong

ABSTRACT

Hong Kong's new South Island Line and Shatin to Central Link requires the expansion of Admiralty Station into Hong Kong's first 4 line interchange station. Already the busiest interchange station in Hong Kong, expanding this station without interrupting services involves major design, logistics and civil engineering challenges.

The new platforms are housed in a shallow cavern and platform tunnels immediately adjacent to the existing platforms and under major roads and high rise buildings. To facilitate connection with the existing station, the existing Island Line platform tunnel needed to be underpinned and up to 24m depth of rock below it removed, while safely keeping platforms and trains fully operational above.

Multi-party collaboration, interactive design and construction processes were adopted that allowed programme optimisation as the construction progressed.

1 INTRODUCTION

1.1 Background

The South Island Line is a medium capacity railway that connects the existing Island Line (ISL) and Tsuen Wan Line (TWL) from Admiralty to the Southern District of Hong Kong. It is approximately 7km long, with above ground stations at Ocean Park (OCP) and Wong Chuck Hang (WCH), cavern stations at Admiralty (ADM) and Lei Tung (LET) and a cut and cover station at South Horizons (SOH).

In May 2011, Contract 901 *Admiralty Integrated Station and SCL Enabling Works* was awarded to Kier-Laing O'Rourke-Kaden Joint Venture. Interfacing with the operating railway and the need to continue the full service of the existing lines without interruption, in what is one of the busiest interchange stations, were key aspects of the works.

Once the Shatin to Central Link (North South Corridor) is operational, the integrated ADM station will be the first four line interchange station in Hong Kong, providing a convenient interchange between SIL, the future Shatin to Central Link (North South Corridor), (SCL(NSC)), the existing TWL and the ISL. The Works included an extension east of the existing ADM station to accommodate an interchange concourse, circulation areas and plant rooms for SIL and SCL(NSC).

1.2 ADM Cavern, Associated Tunnels and ISL Underpinning

The new ADM Cavern is located to the south of the existing ADM station and immediately adjacent to the ISL Finger Platform tunnels (Figure 1). The cavern houses the new SIL platforms whilst the new SCL platforms are located within Platform Tunnels either side of the tunnel. The tunnels and cavern are connected through adits.

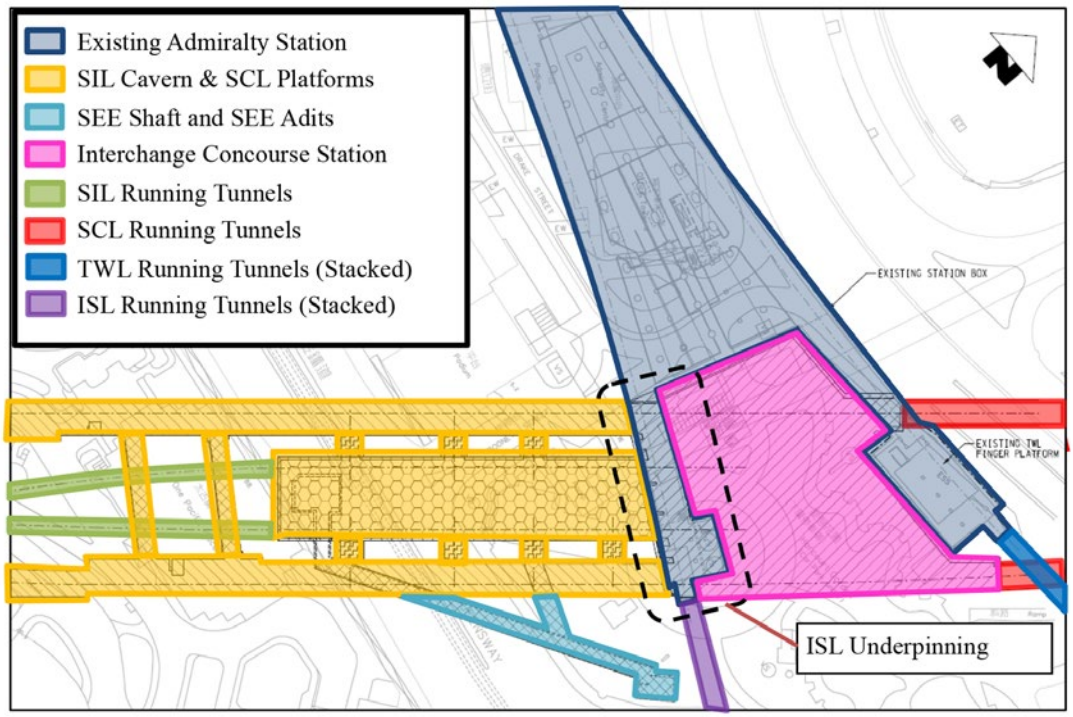

Figure 1: Layout of Existing and New Underground Structure of ADM Station

The cavern is 104 m long with a span of 25.4 m and a height of 15.9 m. The typically 7.5 m long, 7.8m span 6.7m high platform adits connect the platform to the concourse. The platform tunnels are 180 m long for the north bound and 170 m for the southbound, both are typically 11.2 m span and 10.2 m height. The northbound overrun tunnel is 120 m long and the southbound tunnel is 140 m long, both having variable span and height dimensions due to track bifurcations. The ISL finger platform underpinning included excavation immediately underneath the existing railway structures for a length of 58 m and depth of 24 m.

2 GEOLOGICAL SETTING

The project area is dominated by both granitic and volcanic rocks of the Jurassic-Cretaceous age. Kowloon Granite (Klk) of Lion Rock Suite is present at the northern fringe of the project area, where the ADM station is located; whereas volcanic rock of Ap Lei Chau Formation (Kra), which mainly consists of eutaxitic fine ash vitric tuff, is present to the south of the ADM station. The boundary between the two lithologies is not sharply constrained from the geological maps. Therefore, near the margin of the two lithologies, granite may occur locally within the area, which has been mapped / described as tuff, and vice versa.

From the published geological maps, there is no recorded fault identified in the vicinity of the tunnel alignment. NNW-SSE trending photolineaments were identified from the published 1:20,000 scale geological maps, intersecting the alignment of the station cavern and the associated tunnels. This suggested there may be potential weaker shear zones present in the project area. There is no recorded major dyke intrusion identified within or in the vicinity of the alignment. Intrusions of granite into the tuffs are anticipated near the lithological contact, where the granite veins can penetrate into the tuffs for several tens of metres. The granite intrusion is commonly associated with contact metamorphism

and hydrothermal alteration. The tuffs, which have been intruded by granites, are likely to be altered/ recrystallised by contact metamorphism. Complex geological and hydrogeological conditions are anticipated along the contact zone, where variable rock mass and material properties and more frequent intrusions of mineral veins and pegmatite dykes are encountered. They also constitute to sources with potentially high groundwater inflows.

Ground investigation drillholes were undertaken during different stages of the project to confirm the geological condition of the site. Additional information was also available from archival ground investigation data which were kept by the Geotechnical Information Unit of the government. These drillholes revealed that the rock head level ranges from +4 mPD in the southern portion of the site, descending to about -25 mPD in the northeast portion of the site. The rock was generally described as medium to coarse grained granite, locally altered and chloritised. The solid geology changed from granitic to volcanic nature beyond the south of Justice Drive.

Groundwater table was generally 2-4m below existing ground level in Admiralty and was influenced by a fixed head boundary at the coastline which was 250m north of the site, and the fluctuating intensity of groundwater inflow from the hillslopes to the south. Due to the large-scale excavations of the station box, access adits, platform tunnels and station cavern at the ADM site, groundwater drawdown was expected in the cavern area. Since large-scale dewatering has been carried out previously during earlier construction contracts in the Admiralty area, it was anticipated that any consolidation settlement due to groundwater drawdown had already occurred. Groundwater inflow was monitored during excavation works and ground treatment by grouting required where the inflow exceeded allowable limits. Groundwater levels are expected to recharge in the long-term case, affecting only the permanent lining design.

The NGI Tunneling Quality Index (Barton, 1994), otherwise known as the Q-System, was adopted to quantitatively describe the rock mass quality through assessing available drillholes in the general vicinity of the project area. It was shown that the Q values in general ranged between 1 – 10, with mean values of 4.5 and 8.0 on the northern and southern side of the ADM cavern respectively.

3 TEMPORARY SUPPORT DESIGN

3.1 Temporary Support Design Methodology

The cavern, narrow pillared platform tunnels, passenger adits and construction adits created a complex 3-dimensional underground excavation (Figure 2). This complex geometry required a robust temporary support design methodology that included significant analysis over and above the conventional use of the NGI Q-Chart (1994). The general methodology for the temporary support of the cavern and tunnels was:

1. Empirical support design using the NGI Q-Chart (1994).
2. Semi-empirical and numerical analysis using methodologies described by (Bischoff and Smart, 1975) plus embedded beam modelling.
3. Kinematic wedge analysis using UNWEDGE.
4. Finite element and finite difference analysis.

The Q-Chart was used to develop the preliminary temporary support design and the basis for further numerical analysis.

The Bischoff and Smart approach together with embedded beam modelling of the shotcrete allowed confirmation of the temporary support requirements (rock dowel spacing, shotcrete thickness) where arch action was considered the primary support mechanism (i.e. where lower Q values were considered).

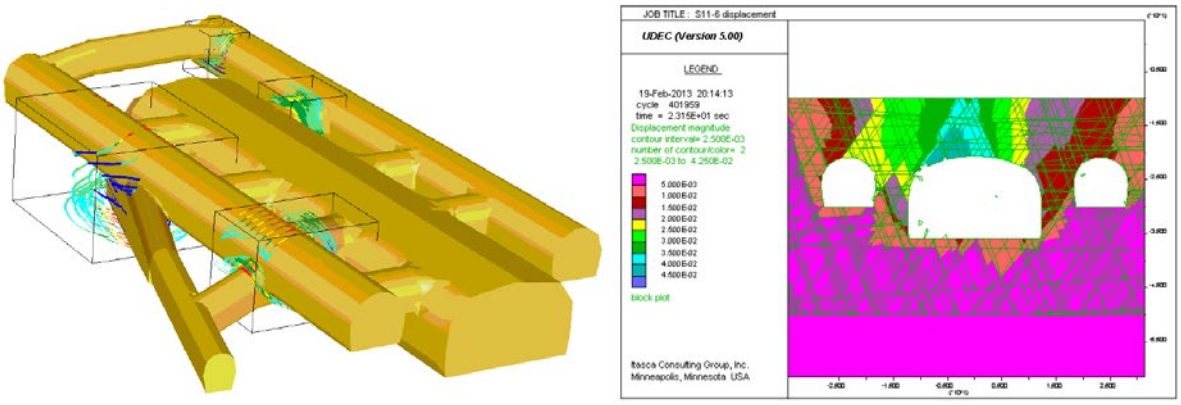

Figure 2: Numerical Modelling of the Cavern, Platform Tunnels and Adits

UNWEDGE was used to confirm that both the schematic rock dowel spacing and rock dowel length were appropriate for the possible rock wedges that could form with the given tunnel geometry and the geological model.

Given the complex geometry of the cavern, tunnels and adits, various forms of numerical modelling were used to finalise the temporary support design. The Universal Distinct Element Code (UDEC) was the primary numerical modelling tool adopted for the temporary supports. UDEC is a two-dimensional distinct element method for discontinuum modeling which simulates the response of discontinuous media (such as a jointed rock mass) subject to either static or dynamic loading.

The UDEC modelling was used to:

- Determine potential structural failure mechanisms of the rockmass around the excavation including the size of potential blocks that could form between the systematic rock dowels;
- Confirm suitability of the systematic rock dowel system including the size of the rock dowels (diameter and steel grade);
- Estimate ground movement during the various stages of excavation;
- Confirm the impacts from the Pacific Place caissons at the south of the cavern; and
- Test sensitivities of model inputs including:
  - Adoption of 10 different randomly generated rock mass models (within set boundaries)
  - Modification of the rock joint conditions
  - Increases and decreases of both horizontal stress and surcharges

Simplified 3DEC was also used to correlate any 3D impacts the junctions and adits had on the temporary support and overall tunnel stability.

Finally, elastic 3D finite element modelling using EXAMINE-3D was used to determine stresses within the various rock pillars around the excavation such that temporary pillar stability and rock support could be determined.

4 PERMANENT LINING DESIGN

4.1 Description of permanent works

The permanent works of the new integrated station comprise a cut and cover box forming the main connection to the existing station, a cavern housing the SCL platform level and SIL platform, and two finger tunnels with a series of interconnecting adits. The final lining consists of cast-in-place concrete with a PVC waterproofing membrane and protective geotextile fleece that is connected to the drainage layer at the invert and discharged via the station drainage system. Figure 3 shows a partial isometric view of the permanent works.

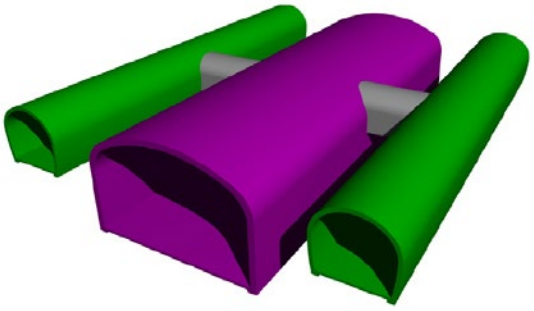

Figure 3: Isometric view of the permanent works (partial)

4.2 Permanent Lining Design methodology

The permanent lining was designed to provide adequate structural capacity and serviceability performance in accordance with the relevant MTR and statutory requirements. The adopted design methodology is summarized in the following steps:

1. Loads acting on the lining are determined based on the requirements of applicable standards and codes.
2. Structural analyses are performed to assess the lining response to the applied load combinations.
3. Member forces are extracted and lining thickness / reinforcement requirements are established.
4. Lining is checked against crack width, fire protection, and durability requirements.

The temporary shotcrete lining was assumed to completely degrade over time and have no structural contribution to the permanent works. It was also assumed that all ground movements stabilized prior to construction of the permanent lining.

4.3 Applied loads on permanent structures

Assessment of applied loads on the permanent structures was based on particular project specifications and applicable codes and standards. These loads included but were not limited to the dead weight of construction materials, rock and overhead caisson pressures, localized wedge loads and groundwater pressures due to potential blockage of the geotextile layer or conveyance pipe. The expected rock pressures were evaluated in accordance with the Q-System. As per Barton (1974), the pressures acting on the tunnel roof and sidewalls were determined from Equations 1 and 2. At junction locations, the joint set number was increased by a factor of three (3) to account for the greater effective spans and kinematic degrees of freedom. It is noted that Equation 2 is only applicable for the expected range of geologic conditions encountered at the cavern area.

$$P_{arch} = \frac{2J_n^{\frac{1}{2}} Q^{\frac{-1}{3}}}{3J_r} \quad (1)$$

$$P_{wall} = \frac{2J_n^{\frac{1}{2}} (2.5Q)^{\frac{-1}{3}}}{3J_r} \quad (2)$$

where P_{arch} = Rock Pressure at Roof (kg/cm^2), P_{wall} = Rock Pressure at Sidewalls (kg/cm^2), Q = Rock Mass Quality, J_n = Joint Set Number and J_r = Joint Roughness Number.

To assess the magnitude of the overhead caisson pressures, a 3D finite element model of the excavation and overhead foundation elements was developed with Midas, GTS. The geometry adopted in the model was similar to the subsequent beam spring analysis, while the rock mass properties were those identified during the geotechnical investigation and verified during excavation. The 3D finite element model was advantageous in that the unknown caisson loading could be removed since the model implicitly distributes the stress between the ground mass and lining. The construction sequence was simplified under the assumption that all ground movements were stabilized prior to permanent lining construction. As the load transfer process between temporary and permanent lining was difficult to model and validate, a 50% relaxation value was assumed, after which the permanent lining was considered constructed and the model solved for equilibrium. An overview of the Midas, GTS model is shown in Figure 4.

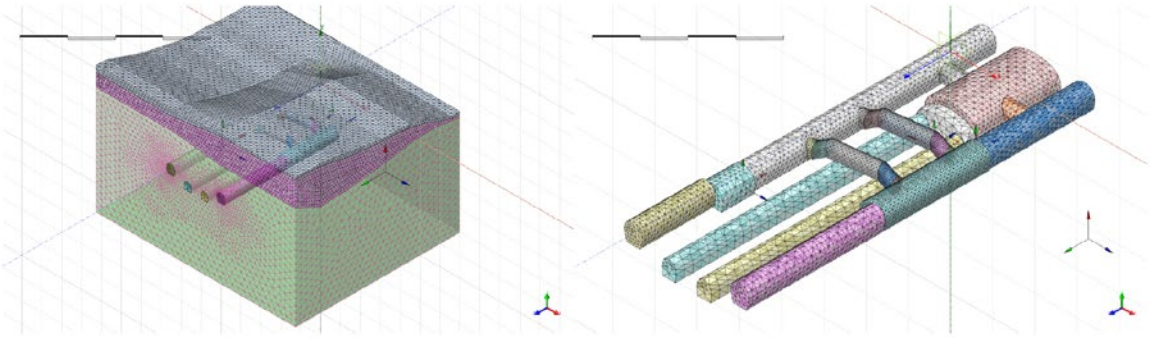

Figure 4: Midas 3D GTS Finite Element Model Mesh for the cavern area

4.4 Two and three dimensional structural analysis

To determine the structural requirements of the permanent lining (i.e. lining thickness, concrete grade and reinforcement schedule) a series of 2D and 3D structural models were generated. Specifically, 2D beam spring models were developed using Oasys, GSA in order to design the typical cavern sections. These sections exhibited plane strain behavior and were sited away from any boundary effects. Additional 3D non-linear elastic finite element models were developed with SAP2000 to simulate the permanent lining response at the cavern junctions. These models include two collars at either side of the passenger adits and utilized gap link elements to simulate construction and expansion joints. The finite element mesh comprised a series of thin shell elements with a maximum aspect ratio of 1.5, edge length of 0.75 meters, and angle between new faces of 110 degrees. As illustrated in Figure 5, the cavern and associated structures were divided in areas of similar structural requirements with coincident boundaries to locations of curvature changes.

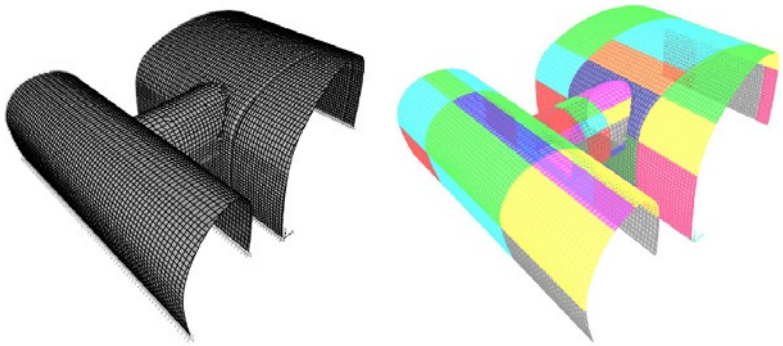

Figure 5: SAP2000 model mesh and areas of similar structural requirements

In general, the structural models included the cavern wall and arch above the concrete plinth footing. The connection between the lining and invert slab / plinth was assumed to be pinned, as was the connection between any internal structures and the permanent lining. The passive reaction provided by the rock surrounding the lining was simulated with a series of compression-only radial springs. The stiffness of these springs depends on the rock properties and curvature of the lining profile. The relationship proposed by Muir Wood (1975) as per Equation 3 was ultimately used for design. The tangential springs were assumed to have zero stiffness due to full slip conditions resulting from the PVC waterproofing membrane / lining interface not being able to transfer shear stresses.

$$K_r = \frac{3E_G}{r_o(1+v)(5-6v)} \quad (3)$$

where K_r = Radial Spring Stiffness (Force/Volume), E_G = Young's Modulus of Rock, r_o = Radius of Curvature of Lining, v = Poisson's Ratio of Rock.

The relevant combinations of moment / thrust interaction points for each model area and for all Ultimate Limit State (ULS) load combinations were extracted from the finite element models and checked for adequate capacity using the respective moment thrust (M-N) interaction diagrams. Outside the junction or portal influence zones, the results were compared to the 2D model sections, with the more conservative utilization result controlling the lining design. The region of junction behaviour / influence around each opening was determined by comparing stresses in the lining with those in a typical section. In addition to bending, the lining was checked for adequate shear capacity. Finally, deformation and maximum crack width were analyzed for all Serviceability Limit State (SLS) load combinations.

5 EXCAVATION OF CAVERN AND TUNNELS

5.1 Site Constraints

The Admiralty cavern and tunnels run under the existing structures of Pacific Place Shopping Mall, Harcourt Garden, Harcourt underground carpark, Pacific Place 3 Subway and Pacific Place Subway (Figure 6).

- Physical constraints: (existing sensitive receivers, such as MTR ISL platform tunnel and other station structures, utilities and services, geotechnical features and buildings)
- Non-physical constraints: (public holidays and weekend restrictions, timing of delivery of explosives to the site by the Mines Division, stakeholders management, blasting vibration controls, traffic restrictions, air and noise limitations).

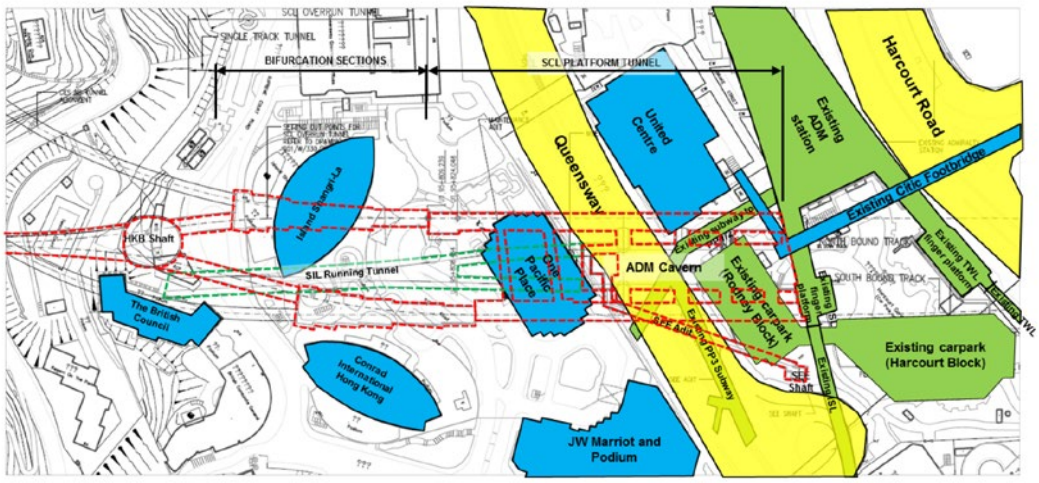

Figure 6: Existing Structures next to Admiralty Cavern

5.2 Drill and Blast Excavation Sequences

All tunneling excavation operations were carried out using the SEE shaft for access and egress. This enabled Tunneling works to be carried out independently from ISL Underpinning & Station Box works and thereby facilitated the latter to be constructed in a stiffly supported partial top-down sequence. A temporary, acoustically insulated, "Noise Enclosure" building, that housed a 55T SWL overhead gantry crane and two 400T storage / discharge hoppers, was constructed over the head of the shaft, for excavation plant delivery and rock spoil removal.

The contractor produced extensive blast assessment reports to identify vibration limits for each adjacent existing structure & infrastructure facility and to determine maximum charge weights for blasting.

Drill and blast techniques were subsequently used for all SEE Shaft and Cavern & Tunnel excavations in rock, except at a very small number of localized areas where railway exclusion zoning or the sensitivity of structures to predicted minimum charge weight blast vibration did not permit. In those areas, excavation was carried out by mechanical splitting / breaking.

Regression analysis of monitoring results during early blasts enabled refinement of rock parameters and a general increase in charge weight as excavation progressed.

The tunneling excavation sequence is shown in Figure 7a.

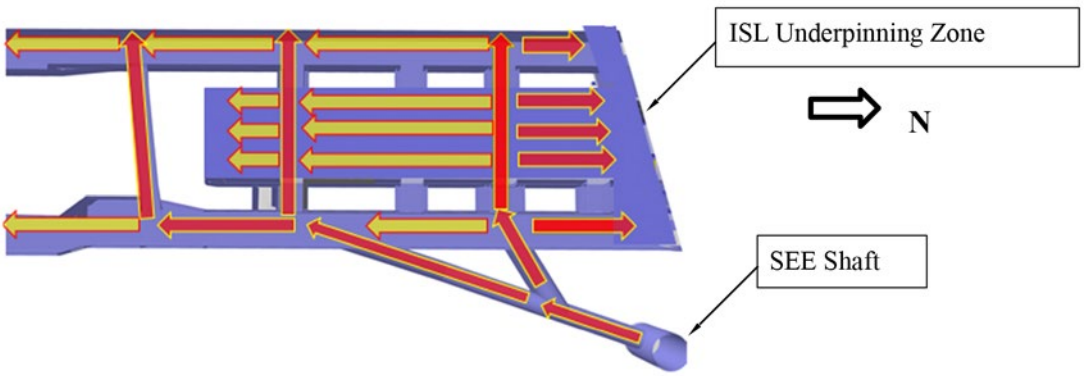

Figure 7a: Excavation Sequence for Cavern & Tunnels

The Cavern was excavated as shown in Figure 7b and Plates 1 & 2.

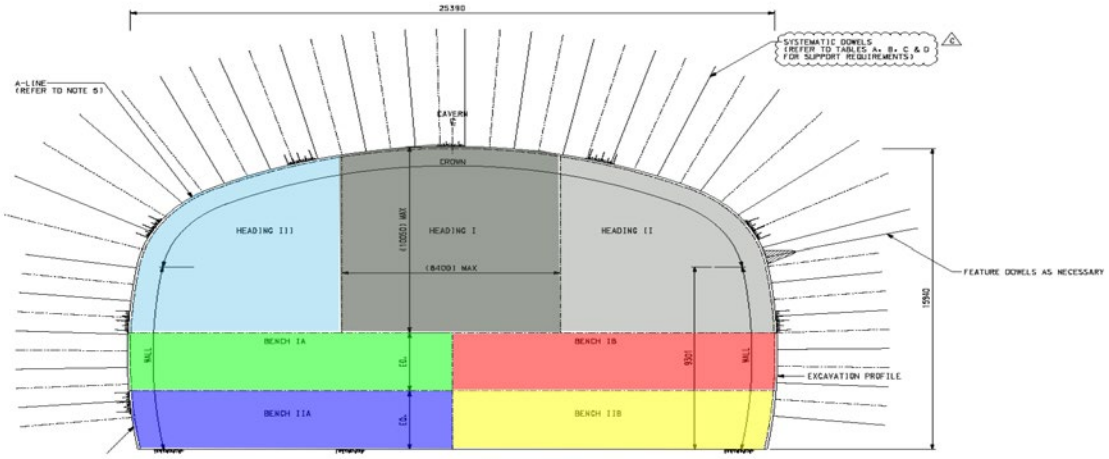

Figure 7b: Cavern Excavation Sequence

Plate 1: Excavation of Cavern Headings I, II and III

Plate 2: Cavern Excavation nearing completion

5.4 Process

To control safe access at recently blasted faces, for geological face mapping and rock bolt installation operations, a permitting process including four hold points was introduced. The following Permit forms were required to be signed-off by the respective delegated persons (Shift Supervisor, Shotfirer, Geologist or Tunnel Engineer) prior to commencement of the next work activity:

1. FORM 1 - Assess re-entry to the blasting area or excavation area
2. FORM 2 - Assess the excavated surface after scaling
3. FORM 3 - Confirm temporary support is installed as required
4. FORM 4 - Permit Tunnel Excavation to proceed

5.3 Rock Features Encountered

Geological mapping of blast faces showed that Q values, in general, ranged between 0.5 and 8.9, with a mean Q value of 4.2, slightly less than the interpreted prediction.

Probing was carried out from the blast faces, in 25m lengths with 10m overlaps. This probing identified the presence of two transmissive geological features in the ADM cavern. Excessive groundwater inflow was encountered at these features but pre-excavation grout injection (approx. 14000l) successfully sealed the fissures.

In addition, a sub-vertical shear zone with dip angle of 68 to 85 degrees and dip direction of 280 to 310 degrees was encountered intersecting the SCL North tunnel at an oblique angle. The width of the shear zone was initially 0.3m to 0.5m increasing to 2m to 3m moving southwards. Surface staining and chlorite coating (FeO/MnO + Chl) and sandy-clay were revealed from the joints at the shear zone. The mapped Q values of the face through the shear zone were low, between 0.5 and 0.75. As the shear zone was shown to be water bearing, pre-excavation grouting was carried out. An additional design review was also undertaken to validate the design assumption and parameters adopted for rock bolt supports. Based on the three pull out test results in the shear zone, the maximum working load of the dowel was limited to 60kN and additional shotcrete (total 390mm thick) was applied to compensate for the associated loss of rock support.

A comprehensive instrumentation system was installed to monitor existing structures and infrastructure around the construction site. In addition to traditional movement markers and convergence arrays (at 10m spacing), an Automatic Deformation Monitoring System (ADMS) was installed within the ISL and TWL tunnels to assess deflections and vibration in real time. The results of convergence monitoring indicated that the maximum deformation during the cavern and tunnels excavation was 7mm and the recorded above-ground settlement during the cavern and tunnel excavation was 3mm, both well within the design prediction.

6 ISL FINGER PLATFORM STRUCTURE UNDERPINNING

6.1 Description of the works and constraints

Underpinning a 58 m length of the existing ISL finger platform structure for a depth of 24m generally from its soffit level, whilst retaining full operational function throughout the works, presented a technically challenging and potentially high risk aspect of the project.

Site location, programme and overall sequence constraints demanded that access for this underpinning was possible only from the new Station Box side of the finger platform structure. In addition, the existing finger platform soffit slab, having originally been designed for transverse hogging between the side walls, was analyzed to be capable of spanning only 9m longitudinally without intermediate support.

Conventional full depth slot underpinning would have resulted in rock pillar supports with a height to width aspect ratio of approximately 5:1, and due to a multitude of constraints, only a very limited amount of advance geotechnical investigation was possible. Interpretation of this investigation data showed that extensive temporary rock pillar support would probably be required and, furthermore, that should the structure move outside of its operating parameters it would not be possible to move the structure back into its original position, thereby adversely affecting the railway.

An innovative staged support sequence was consequently devised, in which the pillar excavation and load from the finger platform would be transferred to alternating rock pillars with the use of temporary steel supports in 4.5m wide, 4.5m deep modules, as excavation progressed downwards (refer Figure 8). Rock pillar height to width aspect ratios could thereby be limited to 1:1 with associated reduction in temporary support and residual risk. This alternating sequence, necessitated an associated regime of finger platform load transfers between the steel support columns in slot A and B and then from B to A as the excavation continued downwards to the various intermediate levels. This required careful control and management, with a purpose built software system employed. In order to manage the risk to the lowest possible level the design was also based on a scenario whereby any one support could completely fail, shedding the load to adjacent supports whilst maintaining a minimum factor of safety for the railway to continue to operate.

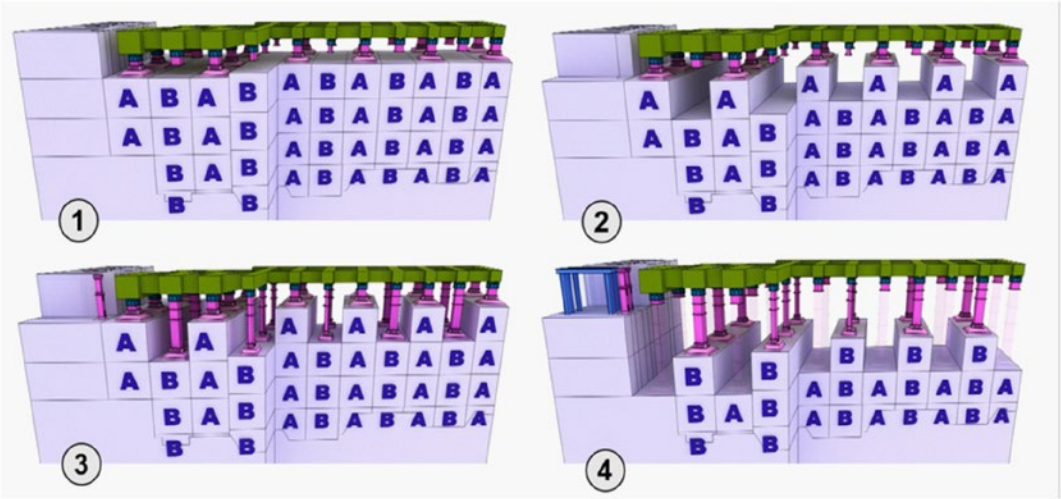

Figure 8: Staged Sequence to remove rock beneath ISL finger platform

6.2 Rock Pillar Design

The rock pillar support design was developed to allow an observational approach, consistent with a conservatively feasible set of pre-interpreted rock joint orientations and conditions. Based on laboratory testing of joint conditions from the boreholes in the vicinity and in consideration of limitations concerning the practicality of observational assessment, two friction angles were considered in the design, average (37 degrees) and poor joint conditions (27 degrees).

A matrix of rock-bolt support options was developed, to define bolt spacing based on the joint orientations and conditions actually encountered.

The design adopted the use of high strength through-pillar bolts, and traditional rock bolts drilled from both sides of the rock pillar designed with maximum overlapping. The through bolts were to be plated each side of the pillar, to fully mobilize bolt capacity, maximize bolt spacing and avoid the need for grouting. The adoption of un-grouted bolts would enable their re-use as the excavation progressed.

A simplified solution was developed to commence design. Assuming a worst-case joint (or combination of joints), the bolts were designed simply to apply a pressure in the horizontal direction. The increase in horizontal stress reduces the tendency for a pillar to slide along the joint plane.

Consider a pillar loaded vertically, with the worst joint in existence allowing the pillar to slide on the joint (see Figure 9).

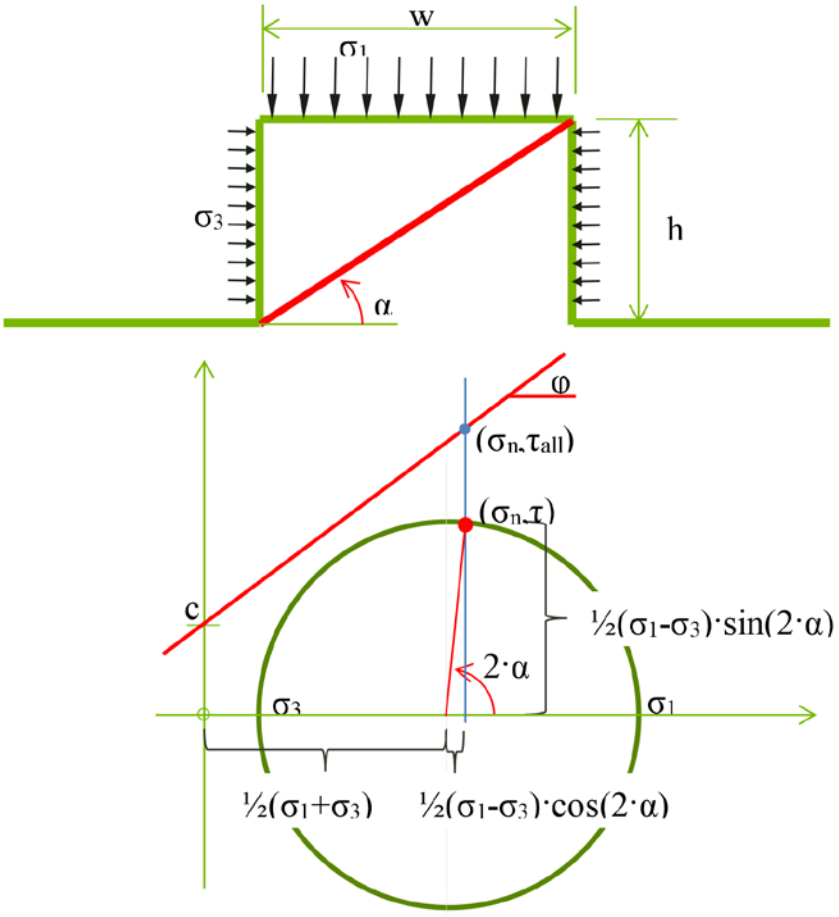

Figure 9: a) Geometry & b) Derivation of conditions across joint

Using Mohr's circle of stress, we get:

$$\sigma_n = \frac{1}{2} \cdot (\sigma_1 + \sigma_3) + \frac{1}{2} \cdot (\sigma_1 - \sigma_3) \cdot \cos(2 \cdot \alpha) \quad (4)$$

$$\tau = \frac{1}{2} \cdot (\sigma_1 - \sigma_3) \cdot \sin(2 \cdot \alpha) \quad (5)$$

The Mohr-Coulomb equation of equilibrium for the joint is

$$\tau_{all} = \sigma_n \cdot \tan(\varphi) + c \quad (6)$$

Where c and φ are the cohesion and friction angle parameters for the joint.

The FoS is based on the shear strength:

$$FoS_\tau = \frac{\tau_{all}}{\tau} = \frac{\frac{1}{2}\cdot(\sigma_1 - \sigma_3)\cdot\sin(2\cdot\alpha)\cdot\tan(\varphi) + c}{\frac{1}{2}\cdot(\sigma_1 + \sigma_3) + \frac{1}{2}\cdot(\sigma_1 - \sigma_3)\cdot\cos(2\cdot\alpha)} \quad (7)$$

In this analysis, the rockbolts contribute the horizontal stress, and also contribute the cohesion c.

The initial analysis was unrealistic in a number of ways; it conservatively assumed that the joints will exist in the worst orientation and that the weight of the pillar itself is treated simplistically as a uniform weight at the top.

The design methodology was subsequently updated to consider different joint orientations other than the worst case scenario. Figure 10 below describes the final through-bolt design.

LOCATION	JOINT QUALITY	MINIMUM TEMPORARY ROCK SUPPORT			MAXIMUM UNSUPPORTED ADVANCE LENGTH (X) /DEPTH (Y)
		JOINT DIP ANGLE (°)	ROCKBOLT GRID (Z)	SHOTCRETE	
UPPER SLOT OF ROCK PILLARS	AVERAGE CONDITIONS (φ = 37°)	27-52 52-61 61-67 67-70 >70	1.5m 1.6m 1.7m 1.9m 2.1m	-	3.4m
	POOR CONDITIONS (φ = 27°)	27-52 52-61 61-67 67-70 >70	1.1m 1.2m 1.3m 1.6m 1.8m	-	2.3m
ROCK PILLARS	AVERAGE CONDITIONS (φ = 37°)	27-52	1.1m	-	0.5m/2.8m*
		52-61 61-67 67-70 >70	1.1m 1.2m 1.4m 1.5m		1.3m/2.8m*
	POOR CONDITIONS (φ = 27°)	27-52	0.8m	-	0.5m/1.9m*
		52-61 61-67 67-70 >70	0.9m 1.0m 1.1m 1.3m		1.3m/1.9m*

Figure 10: Through bolt spacing requirements for the 4.5 x 4.5m pillars

Although this closed form solution was expected to be conservative it did not take into consideration the impact of jointing in the third dimension. 3DEC was used in a similar way to described above for the cavern to confirm the suitability of the calculated bolting density by the closed form solutions.

The 3D modelling proved to be an important step in the design process as it both confirmed the suitability of the through bolts and identified the need for end bolts to prevent a block sliding failure mechanism at the front face of the pillars. Figure 11, demonstrates larger displacements at the front of the pillar. Sensitivity runs with higher pillars showed this failure mechanism to be a controlling design case.

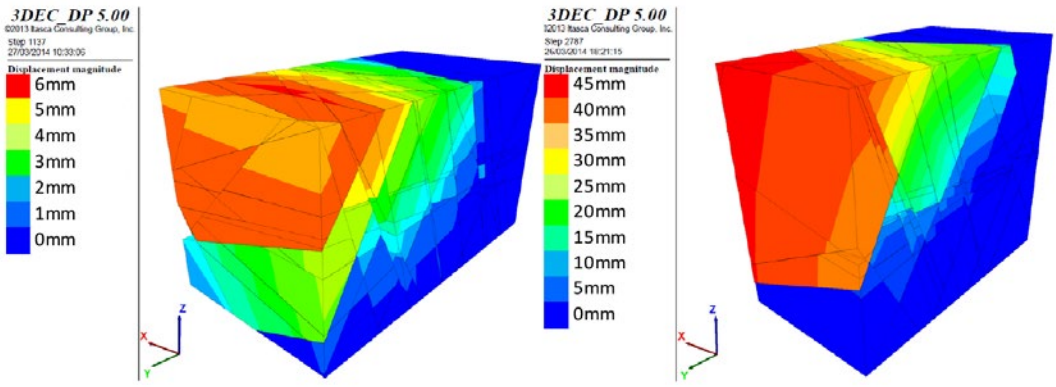

Figure 11: Large displacement at the nose of the pillars – 4.5m and 6.75m cases

6.3 ISL Underpinning Construction

Given the importance of maintaining safe continuous operations of the Island Line, a detailed instrumentation and monitoring regime was established to record the behavior of the existing Island Line finger platform and vent shaft structures, also the temporary underpinning structures and rock pillars. This regime included:

- Real time level and horizontal displacement monitoring inside the operational structure, using total stations and prisms (half hourly reporting)
- Real time level monitoring inside the operational structure, using a bespoke vibration wire water levelling system (2 minute interval reporting)
- Real time 3-D movement sensors on the key interface between the finger platform structure and the running tunnels and existing station structure (2 minute interval reporting)
- Real time level and horizontal displacement monitoring of the rock pillars and finger platform & vent shaft from outside the structures, using total stations and prisms (half hourly reporting)
- Real time Pressure/Load sensors and Stroke displacement monitoring within the hydraulic jacking system (daily reporting but instant reporting during load transfer operations)
- Precise levelling of the finger platform and vent shaft from outside the structures (daily reporting)
- Crack width monitoring at the top of the rock pillars (reporting on an as-required basis)

Alert, Alarm and Action levels were set for each of the monitoring systems at 50%, 75% and 100% of the expected movements and jack loads, with the real time monitoring systems raising automatic text and e-mail warning messages at each level. A comprehensive management plan was implemented to deal with each respective level of warning raised. In addition, a daily review of the data and forthcoming construction activity was held between responsible people, to determine any action that may have been required.

Monitoring of the existing structure was established 3 months prior to the commencement of construction to establish a credible baseline and understand any impacts caused by station box excavation, temperature and other factors.

The excavation followed the original plan to the letter with the initial 4.5m x 4.5m 'A' and 'B' slots (see Figure 8) being used to excavate the rock using excavators mounted with hydraulic hammers. The 150+MPa rock, although jointed, proved very difficult to remove. To help with progress, the rock in each of the slots was pattern drilled in advance to assist excavation.

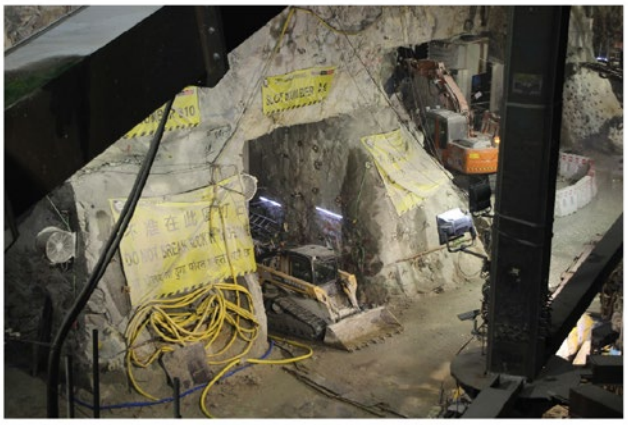

Plate 2: Initial slot excavation beneath the existing ISL Platform Tunnel

The through-pillar rock bolt concept led to downtime on those occasions when the rate of progress in adjacent slots varied. An alternative, "Grouted Bolt" solution was developed to overcome this constraint, although it followed that bolts could no longer be re-used. A reduction in bolt spacing was also necessary since capacity became reliant on permissible rock / grout bond stress rather than bolt strength.

It soon became evident that excavation rates could be significantly improved if, somehow, the excavation module sizes could be enlarged to facilitate the employment of heavier (physically larger) plant.

A thorough review of the design and sequencing was carried out. It became evident that the embedded design redundancy had room to accommodate an alternative "double width slot – double width pier" excavation sequence, once the finger platform & vent shaft soffit slab support grillage had been constructed. Slots & pillars could thereby be doubled in width whilst still maintaining the minimum factors of safety.

Furthermore, actual geological data feedback to the designers facilitated further 3DEC analysis of 6.75m and 9.0m deep slots, which justified the increase in excavation module depths by 50% to 100% (slot heights were constrained by the already fabricated 2.25m underpinning column module lengths).

The re-engineered excavation module enlargements, associated alternative construction sequence (refer Figure 12) and employment of larger plant led to a significant increase in excavation rates.

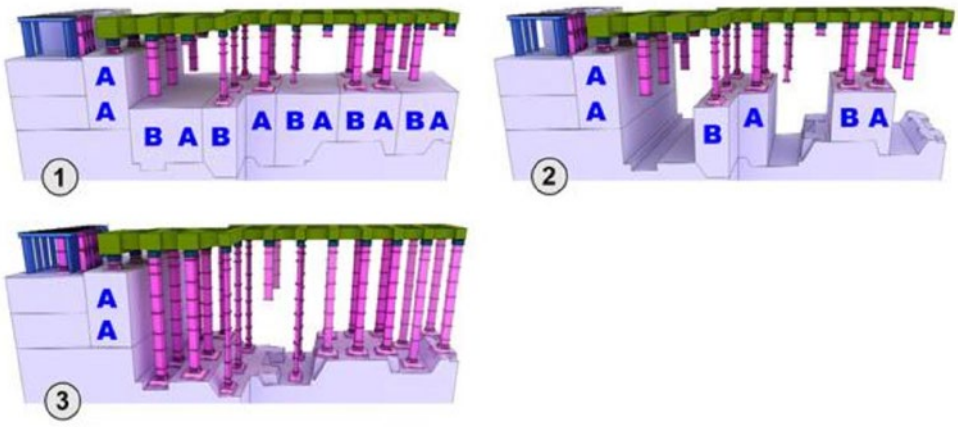

Figure 12: "Double Slot" Underpinning sequence

6.4 Blasting of the Slots

In parallel with the assessment and implementation of the wider and deeper slots, a detailed impact assessment and construction methodology was developed for rockmass removal using drill and blast methods. Blasting had already been highly successful in improving the rock excavation rates from the adjacent station box with no impact to the operating railway.

Detailed liaison was undertaken with MTR's Operations Division, Mines Division and the Buildings Department to enable approval for some limited blasting of the rock slots in the underpinning zone. It was decided to trial the blasting and 3 blasts were successfully undertaken. It was decided not to take this further forward as the excavation rates from the wider and deeper slots was now advancing at a rate that was faster than the limited blasting could achieve.

7 CONCLUSIONS

Despite the huge scale and complexity of the works undertaken, there has been zero disruption, and no impact on the safety on the Tsuen Wan Line or Island Line train service throughout the whole construction period. This was explicitly a result of the remarkable levels of collaboration between all the parties involved, with innovative design, excellent construction supervision, rigorous planning and attention to detail on work permits and safety procedures. The safe completion of the work marks an outstanding

achievement in completing work to customer satisfaction, and maintaining railway performance and the safest possible environment.

ACKNOWLEDGEMENTS

The authors acknowledge the contribution to the design, planning and construction of the many team members from MTR Corporation, Kier-Laing O'Rourke-Kaden Joint Venture, Arup, Benaim and Aurecon who were involved in the various stages of this work but are not recognized in this paper.

REFERENCES

Barton N. and Grimstad E., 1994. *The Q-system following twenty years of application in NMT support selection*. Felsbau, Vol. 12, No. 6, pp. 428-436.

Barton, N.R., Lien, R. and Lunde, 1974. *Engineering Classification of Rock Masses for the Design of Tunnel Support, Rock Mechanics, 6(4), pp. 189-239*.

Biscoff J.A. and Smart J.D. 1975. Proceedings of the 16th U.S Symposium on Rock Mechanics. *A method of computing a rock reinforcement system which is structurally equivalent to an internal support system*.

Geotechnical Engineering Office. 2006. *GEO Publication No. 1/2006: Foundation Design and Construction*.

Grimstad, E. & Barton, N. 1993. Proceedings of the International Symposium on Sprayed Concrete - Modern Use of Wet Mix Sprayed Concrete for Underground Support, Fagernes, (Eds Kompen, Opsahl and Berg. Norwegian Concrete Association). *Updating of the Q-System for NMT*.

Hoek, E., Kaiser, P.K. and Bawden, W.F. 2000. *Support of Underground Excavations in Hard Rock, Rotterdam, A.A. Balkema*.

Hong Kong Buildings Authority. 1996. *Hong Kong Code of Practice for Fire Resistant Construction: 1996 and amendments in PNAP199*.

Hong Kong Buildings Department. 2004. *Code of Practice for the Structural Use of Concrete 2004*.

Hong Kong Government. 1995. *CS2: Carbon Steel Bars for Reinforcement of Concrete 1995*.

MTR Corporation Limited. 2009. *New Works Design Standards Manual, Section 4 Civil Engineering – Revision A4 (NWDSM)*.

MTR Corporation Limited. 2009. *Materials and Workmanship Specification for Civil Engineering Works, Revision A3 (M&W Specification)*.

MTR Corporation Limited. 2011. *South Island Line (East), Contract 901, ADM Station and SCL Enabling Works, Particular Specification*s.

Muir Wood, A.M. 1975. Geotechnique 25, Issue 1. Thomas Telford, London. *The Circular Tunnel in Elastic Ground*, pp 115-127.

Satellite CT Scanning for Urban Infrastructural Health Diagnosis

Hui Lin & Peifeng Ma

Institute of Space and Earth Information Science, CUHK, Hong Kong

ABSTRACT

Global urbanization is creating a huge demand for civil infrastructure, such as buildings, bridges, tunnels, dams, highways, airports, and railroads. Unfortunately, their maintenance is usually not well coordinated. Under progressive natural and/or man-made stressors, such as structural aging, groundwater/gas extraction, underground construction, and design faults, civil infrastructure gradually deteriorates and can result in catastrophic failure if the early signs of disasters go unnoticed or are not properly managed. The building collapse at Ma Tau Wai Road of Hong Kong in 2010, which leads four people to death, is a vivid example. Ground subsidence has been reported in more than 50 cities in China, with aresulting economic loss of up to 315 billion RMB in the Yangtze River Delta alone. With the growing awareness of sustainability, emphasis has been placed not only on the efficient use of resources, but also on the proper management of existing infrastructural components to ensure that they remain in service throughout their designed lifespans. Obtaining early warning of such disasters is highly complex, mainly because of the extremely wide variety of causes, the hidden early signs, and the large areas and interdisciplinary knowledge involved. There is a need to address existing challenges and prepare for future ones by focusing on: monitoring, assessing and understanding disaster risks and sharing such information and how it is created.

Satellite interferometric synthetic aperture radar (InSAR) technology has the unique capability of monitoring large-scale and long-term movements of land surface, providing an excellent solution for urban infrastructural health monitoring compared with conventional point-based monitoring methods. The advanced persistent scatterer InSAR iscapable of achieving sub-meter accuracy in digital elevation model and millimetric motion detection. By analogy with X-ray computed tomography (CT) for human health diagnosis, satellite can screen civil infrastructures for "Urban CT Diagnosis". Today's SAR sensors have revisit times as short as a few days and improved spatial resolution down to one meter. For example, the German TerraSAR-X satellite is operational with an 11-day repeat cycle and a spatial resolution of up to 0.25 m. The Italian COSMO-SkyMed constellation comprises four satellites with the revisit time of 16 days each and a spatial resolution of up to 1 m. The most recent SAR satellites, Sentinel-1A/B operated by the ESA and ALOS-2 operated by JAXA, are designed specifically for land surface deformation monitoring. In particular, China launched the first C-band full-polarization Gaofen-3 SAR satellite in August 2016, and more are to come. As we look ahead, the multiplicity of SAR satellites, including multi-scale, multi-band, and multi-angular, will form an all-around and all-weather earth observation system for the near real-time monitoring of infrastructural dynamics over large scales. Fig. 1 presents the monitored reclamation settlement of Hong Kong International Airport and Fig. 2 presents the monitored sinkhole subsidence in Shenzhen.

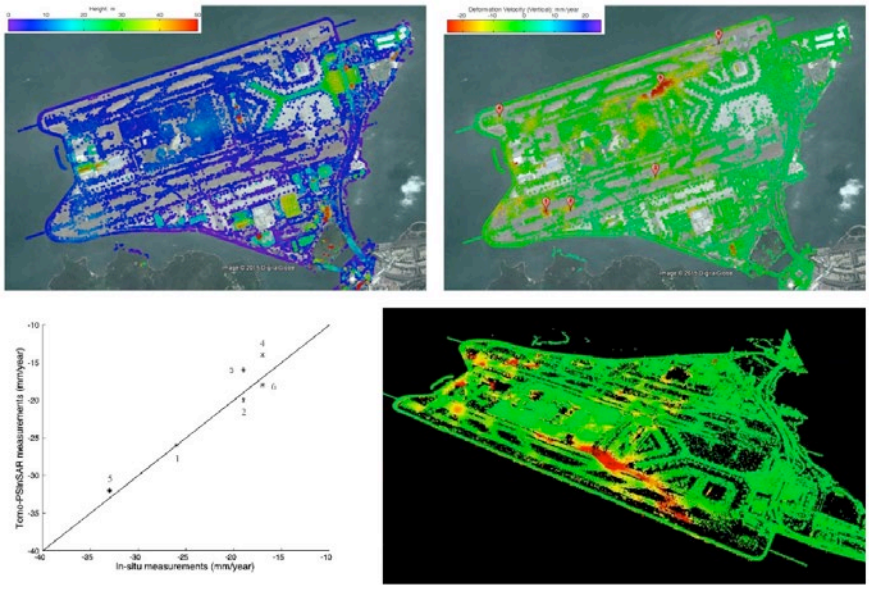

Figure 1: The reclamation settlement of Hong Kong International Airport

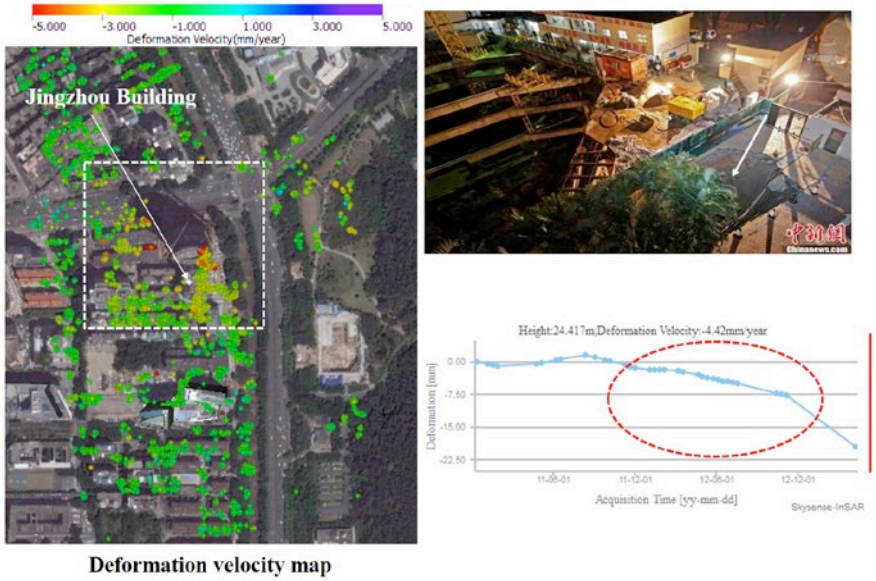

Figure 2: Sinkhole subsidence

REFERENCES

Assembly, U.G., 2015. The Sendai Framework for Disaster Risk Reduction 2015–2030.

Ferretti, A., Prati, C., Rocca, F., 2000. Nonlinear subsidence rate estimation using permanent scatterers in differential SAR interferometry. Geoscience and Remote Sensing, IEEE Transactions on 38, 2202-2212.

Forum, W.E., Global Risks 2015.

Liang, C., Yang, D., 2007. The China Environment Yearbook, Volume 1 (2005): Crisis and Breakthrough of China's Environment. Brill.

Ma, P., Lin, H., 2015. Robust Detection of Single and Double Persistent Scatterers in Urban Built Environments. Geoscience and Remote Sensing, IEEE Transactions on PP, 1-16.

Ramaswami, A., Russell, A.G., Culligan, P.J., Sharma, K.R., Kumar, E., 2016. Meta-principles for developing smart, sustainable, and healthy cities. Science 352, 940-943.

Extensive use of I&M to Enable Safe TBM Drive in Urban Dense Area, a Focus on SCL1128 Eastern Downtrack Drive

S. Auvergne & J. Gauffre
Dragages Bouygues Joint Venture (DBJV), Hong Kong SAR
A. Prost
Sixense Group Limited (ex-Soldata (Asia) Ltd.), Hong Kong SAR

ABSTRACT

The successful completion of the SCL1128 Downtrack TBM drive proved that the extensive use of instrumentation and monitoring has allowed a safe and quick TBM tunneling in urban dense area with minimal impact on all stakeholders. To attain this goal, extensive monitoring of sub surface, ground surface and existing structures was conducted using instrumented boreholes as well as manual and automatic techniques. The instrumentation and monitoring plan designed and implemented in this project will be discussed in this paper with an emphasis on describing the automatic monitoring techniques used.

A wide range of manual monitoring techniques and instruments has been used, such as instrumented boreholes monitoring with inclinometers, magnetic probe extensometers, standpipe and vibrating wire piezometers, ground and structure levelling, tilt plate monitoring, 3D fissurometers, vibration monitoring with seismographs as well as crack gauge monitoring on already deteriorated structures.

In addition to the manual monitoring systems, automatic optical systems, i.e. Automatic Deformation Monitoring System (ADMS) and its reflector-less variant commonly called "Centaur", were used. These systems consist of at least one automatic total station controlled by computers, which allowing continuous monitoring of critical structures with pre-installed optical prisms in three dimensions for ADMS and one dimension for Centaur targeting on inaccessible surfaces (such as settlement of road surface or the movement perpendicular to vertical walls).

All the data from monitoring were collected and presented in a web-based instrumentation database with instant messaging technologies to provide prompt response based on the real-time tunneling performance by the construction and emergency teams efficiently.

1 INTRODUCTION

This paper presents how the Contractor successfully completed a shallow cover variable density TBM drive in fill, marine deposits and alluvium under one of the busiest district of Hong Kong Island by using extensive manual and automatic monitoring techniques to ensure quick adaption of TBM excavation parameters based on ground and structure movements. Numerous sensitive structures are located above the TBM alignments; they therefore required specifically and adapted extensive instrumentation and monitoring plan.

1.1 Project Background and Description

Dragages Hong Kong Ltd. was awarded MTR Contract SCL1128 to construct two twin tunnels under one of the most congested and busiest areas of Hong Kong Island North from Causeway Typhoon Shelter to the integrated Admiralty Station with the existing Tsuen Wan Line, Island Line and recently opened South Island Line. The Eastern and Western Tunnels are connected on either side of the future Exhibition Centre Station (constructed under MTR Contract SCL1123).

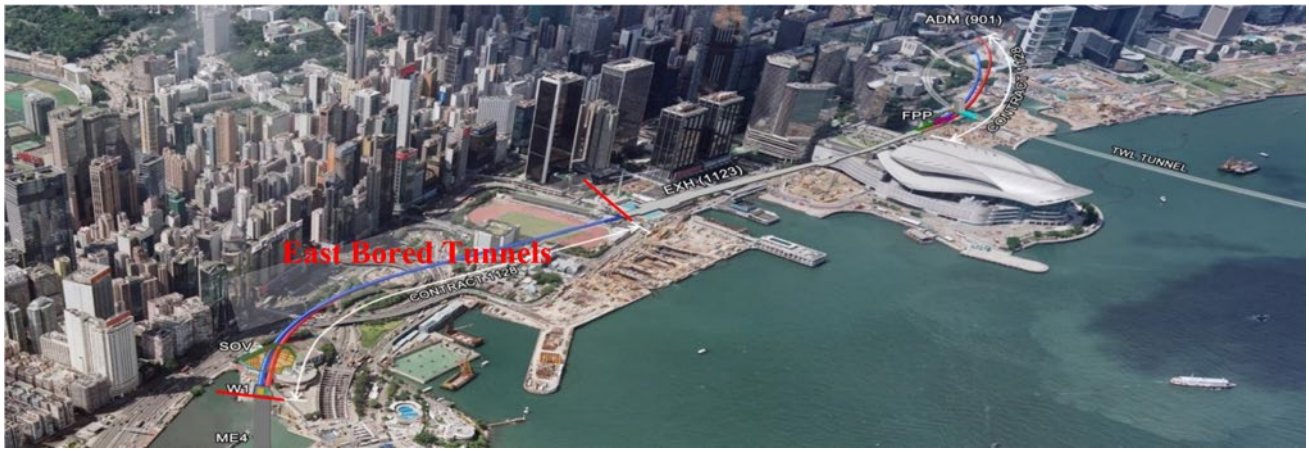

Figure 1: Location of East Bored Tunnels

The Eastern tunnels alignments cross several major and critical roads (Gloucester Road, Cross Harbour Tunnel Slip Roads, etc.), highway structures (Hung Hing, Causeway and Canal Road Flyovers, and Cross Harbour Tunnel Approach Road, Percival Street and Wan Shing Street footbridges), underground drainages (DN1800 trunk sewers, Canal Road Box Culvert, etc.), buildings (Hong Kong Electric Substation, LPG Filling Station, etc) and recreational facilities (Wan Chai Sport Ground).

Figure 2 below shows the location of those sensitive structures along the alignment of the east bored tunnels.

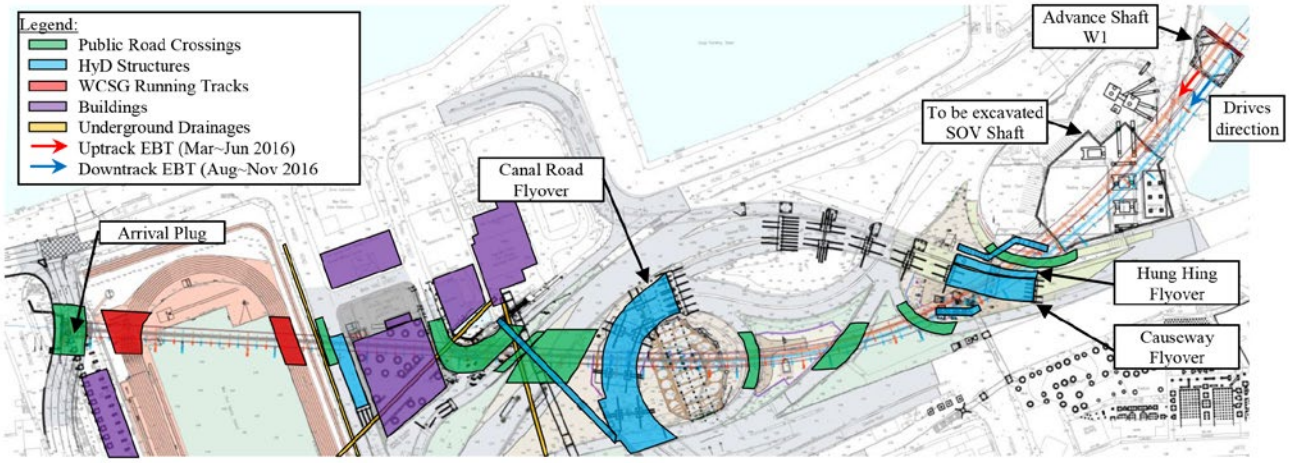

Figure 2: Sensitive Structure along the East Bored Tunnels

1.2 Brief Geological Description

The two Eastern Tunnels are stacked with the Uptrack Tunnel being in various grounds (rock, mix ground and soft ground in CDG and alluvium) with around 20 to 30m cover, while the Downtrack Tunnel being mostly in marine deposits and old reclaimed fill with much shallower cover (less than 3m cover under structures and mostly under one diameter of ground cover).

Figure 3 below show the longitudinal geological section along the eastern drives. Table 1 provides a brief description of the materials encountered while boring the eastern drives.

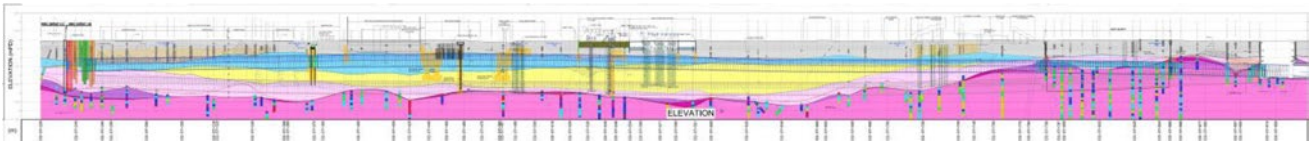

Figure 3: Longitudinal geological section along the eastern drives

Table 1: Brief description of the geological formations encountered through the eastern drives

Geological Formations	Brief Description	Eastern Drives	Color on Figure 3
FILL	Mostly composed of sand, gravels, clayey materials and man-made debris and structures	Downtrack	Grey
Marine Deposits	Mostly sandy/silty materials in upper part and more clayey soft materials in the lower part. Thicknesses varying along the alignment (up to full face).	Downtrack	Blue
Alluvium	Widespread stratum that comprises of mainly clayey to sandy materials with occasional gravels.	Downtrack and uptrack	Yellow
Kowloon Granite	Medium grained granite. Encountered in various stages of decompositions (from MDG to CDG)	Downtrack and uptrack	Pink (dark and light)
Mafic dykes	Dykes of mafic materials were encountered in the most eastern side of the drive.	Downtrack and uptrack	Not shown for clarity

Two tunnel boring machines (TBMs) were used for the tunneling works. One of them is a typical slurry type for the Uptrack Tunnel while the other one is the first variable density type TBM used in Hong Kong for the Downtrack Tunnel. The two TBM drives were successfully completed in July and November 2016 respectively.

2 PRESENTATION OF THE VARIABLE DENSITY TBM

2.1 The Machine

Numerous sensitive receivers above tunnel alignment with low cover and presence of marine deposits and highly permeable reclaimed ground lead to selecting a variable density tunnel boring machine. The 7.45m diameter Downtrack TBM was named “Zhi Nu” (Plate 1). She is a mix between a mix shield slurry and an EPB machine to produce the Variable Density system. As a results she can be used in Low Density mode (similar to slurry TBMs) and in High Density mode (similar to EPB machines but using a more fluid transportation medium). Break-in was on 23th Aug 2016 and “parking” on 28th Nov 2016 with an average of 8.3m per day. Table 2 provides the key figures for Zhi nu.

Table 2: Key figures for Zhi-Nu

Key Figures	Values
Best shift	9 rings
Best day	15 rings
Best week	72 rings

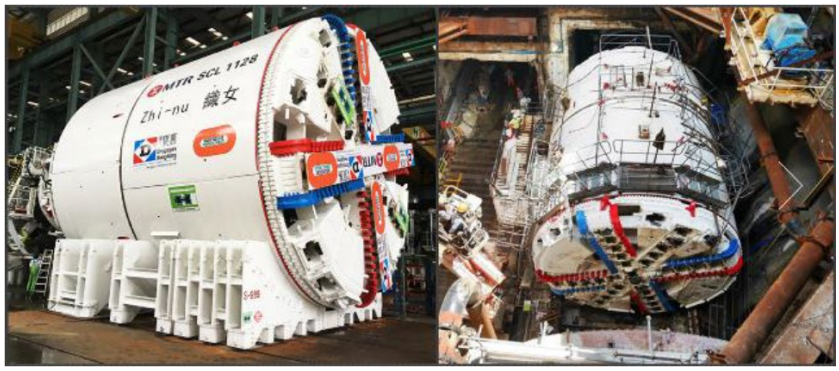

Plate 1: Zhi Nu in Factory and during assembly in W1 Advance Shaft

Zhi-nu is equipped with both an air bubble and a screw conveyor which is used for the mucking out of the excavation chamber (Figure 4). Similar to a slurry type TBM, the confinement is controlled using an air bubble in the working chamber. Should it be needed, high density slurry can be directly pumped to the cutting chamber, through a specific feed line, to increase the density of the confinement medium. Similarly to an EPB type confinement is partially controlled by regulating the screw speed and torque and TBM advance speed. At the back of the screw, the slurryfier box allows the dilution of excavated materials with fresh slurry and their transportation to the slurry treatment plant on surface (refer to Chapter 2.2 for working principle). Two working mode are available on this machine, they are summarized in Table 3 below.

Table 3: Summary of Zhi-nu working modes

Working Mode	Support Medium	Slurry Flow	Dilution of excavated materials in slurryfier box	Type of ground mined	Length of usage (m)
Low Density Mode	Typical slurry (d~1.0 to 1.2)	Mainly inside the excavation chamber	Low	CDG, HDG, MDG and alluvium	110
High Density Mode	High Density slurry (d~1.2 to 1.4)	Mainly inside the slurryfier box	High	Alluvium, marine deposits and fill.	570

2.2 Working Principle

The control of the materials density inside the excavation chamber allows maintaining the confinement even when the slurry pressures are reduced to prevent blowout in case of low cover as shown on Figure 5.

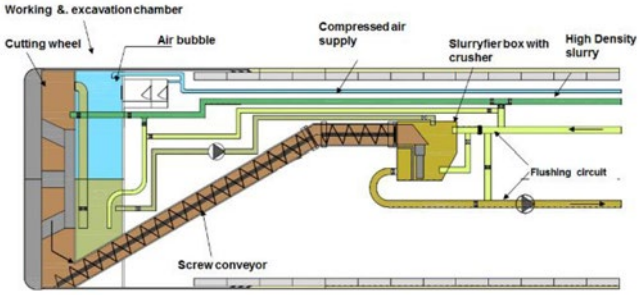

Figure 4: Simplified view of Variable Density TBM

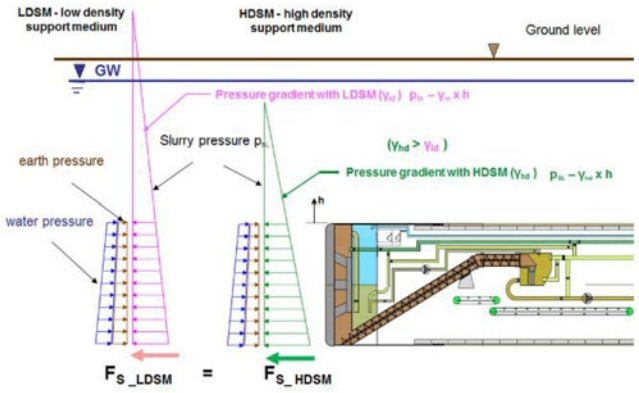

Figure 5: Difference between low and high density mode (face pressure)

3 PROPOSED INSTRUMENTATION AND MONITORING PLAN

3.1 Conforming and Alternative Instrumentation and Monitoring Plan

The conforming Instrumentation and Monitoring Plan was considered sufficient for the surface preparation works but found not suitable for TBM tunneling. An alternative proposal was made by the JV in which ADMS for critical HyD structures and additional volume loss sections were added. Table 4 below provides a high level comparison between the two I&M plan.

As part of the conforming scheme, all sensitive receivers and ground within 50m from the TBM alignments were monitored.

Table 4: High level comparison between conforming and alternative for TBM I&M Plans

I&M Plan	Public Road Crossings	Critical HyD Structures	Other HyD Structures	WCSG Running Tracks	Buildings	Underground Drainages
Conforming	N/A	BSM&TM	BSM&TM	GSM	BSM&TM	Deep GSM
Alternative	GSM	ADMS	BSM&TM	GSM&BSM	BSM&TM	Deep GSM, Deep UMP, EXT & INC

Another objective of the approved alternative scheme was to significantly reduce the number of borehole instruments by combining nearby instruments (two or three) into one single hole using inclinometer casings, extensometer magnets and piezometric probes. Combinations were: extensometer with inclinometer, extensometer with piezometer, inclinometer with piezometer and extensometer with inclinometer and piezometer. Plate 2 shows the INC casings with EXT spiders pre-installed on them prior to installation and installation process for combined I&M holes, in this case INC/EXT/PIZ(2).

Plate 2: Inclinometer casings with extensometer magnets installation in combined holes

Additional standpipes and piezometers were installed along the tunnel alignments to assess the effect of tidal variation at our preselected area for compressed air interventions and confirm the assumptions taken for the confinement pressure. The holes were equipped with levelloggers for continuous monitoring over long periods (Figure 6). It was found that levels in piezometers and standpipes vary of 0.1 to 0.4m with tides depending of the materials in which they are installed.

3.2 Review of Alternative I&M Plan and Needs of DBJV TBM Production and Management Teams

The Alternative I&M plan provided sufficient data and information to all parties in terms of structure and ground monitoring (movements, tilting, volume loss, etc.) for the EBT-UT TBM tunneling works. It was then proposed to adopt the same plan for the EBT-DT TBM tunneling works. However, the operation

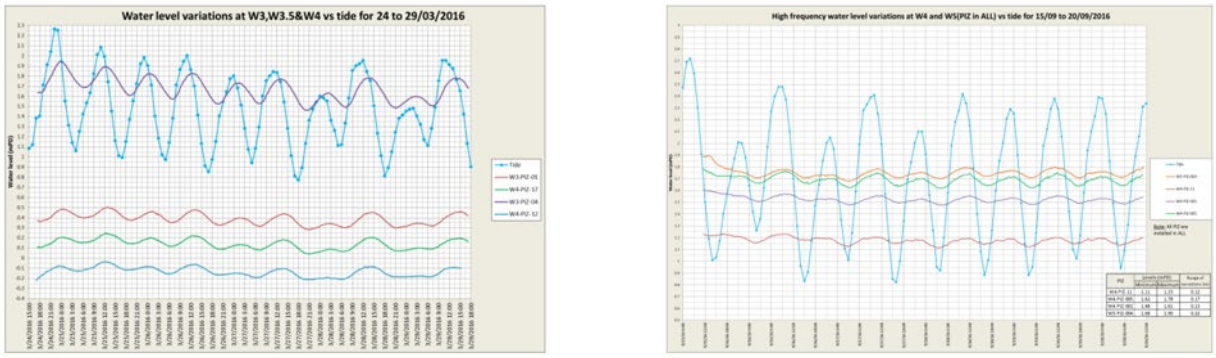

Figure 6: Effect of tidal variations on standpipes and piezometers along TBM alignments

complexity of the variable density machine and the low cover of the EBT-DT tunnel lead to a review of the approved I&M plan by the Contractor. DBJV TBM Production and Management Teams needed more data and quicker reporting to adapt the TBM settings based on ground movements. Zhi-nu being the first of its kind in Hong Kong, MTR management was worried about potential impact to public.

The Contractor decided to implement and conduct additional monitoring (the extensive I&M plan) to cover all the public road crossings and critical HyD Structures in near real-time. Frequency of manual monitoring was also increased to twice a day for critical points within 50m of the TBM cutterhead.

3.3 Extensive I&M Plan

As mentioned in 3.2 above, the alternative I&M plan was further enhanced with additional manual and automatic monitoring. Table 5 and Figure 7 Below provide a high level comparison and presentation of the extensive I&M Plan. The additional instrumentation and monitoring is presented in Chapter 4 below.

Table 5: High level comparison between alternative and extensive I&M Plans

I&M Plan	Public Road Crossings	Critical HyD Structures	Other HyD Structures	WCSG Running Tracks	Buildings	Underground Drainages
Alternative	GSM (daily)	ADMS	BSM&TM	GSM&BSM	BSM&TM	Deep GSM, Deep UMP, EXT & INC
Extensive for EBT-DT TBM tunneling works	Twice daily GSM and Centaur	ADMS	BSM&TM	GSM&BSM and Centaur	BSM&TM	Deep GSM, Deep UMP, EXT & INC

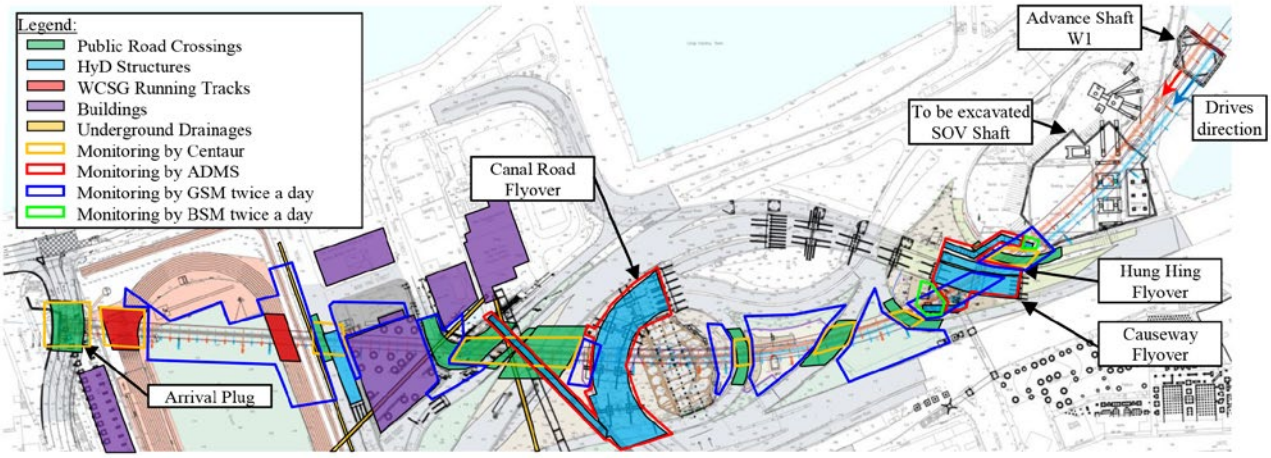

Figure 7: Extensive I&M Plan for EBT-DT TBM tunneling

4 PRESENTATION OF ADDITIONAL INSTRUMENTATION PROPOSED

Two problems in the conforming I&M plan were identified and needed to be addressed. Firstly, the instruments were located on the roads sides so their real movements were only estimated and secondly, the readings would be taken only once a day which would prevent any urgent reaction therefore, a solution combining manual and automatic instruments was selected.

4.1 Additional Manual Monitoring

In order to react quickly, accurate data would need to be provided to the production teams as early as possible with increased frequency to help them adjust depending on the movements of the roads. Therefore, a survey team was dedicated to follow the TBM and to monitor critical points on a twice daily basis before reporting right after each set of readings. However, with just manual monitoring, the two problems remained as the roads themselves were not monitored and the low frequencies of manual monitoring were not fast enough to significantly lower the risks to the vehicles on the road.

Last but not least, the additional GSM were also installed to cross-check the Centaur data (refer to Chap 4.2).

4.2 Additional Automatic Monitoring – Centaur System

With the traffic hindering the installation and monitoring of any instrument on the roads, an automatic solution without physical instruments was the only solution. The most adequate was Sixense's Centaur system, an optical automatic system based on the Automatic Deformation Monitoring System, also pioneered by Sixense. Both are used in several places in the world, but Centaur was only brought in recently for SCL. The ADMS uses magnetically motorized theodolites called total stations to monitor target prisms continuously in near real time. To do that, additional targets called reference prisms are installed on stable control stations to recalculate the position of the total stations after every cycle of readings which allows determining the positions of the monitoring prisms.

The main difference between the Centaur and a common ADMS is that it does not require any physical monitoring prism and only uses the reflection of its laser on the monitored surface to determine the distance of a pre-programmed point and to calculate its location.

The Centaur system permitted to obtain a very high frequency of readings, as high as 1 cycle every 15 minutes in some areas, as well as accurate data at the exact monitoring points. During the whole Downtrack drive, each road crossed by the TBM was monitored using Centaur which allowed getting a good knowledge of the ground movements and their relation to the TBM excavation parameters.

5 MONITORING DATA COLLECTION AND REPORTING SYSTEM – ROAD CROSSINGS

5.1 Database

All the recorded data from manual and automatic monitoring were afterwards stored in a database and displayed on the monitoring software from Sixense, Geoscope. Data would then be displayed with different information such as units or Alert, Action and Alarm values, usually using time graphs to better understand the movements and trends of the roads over time in order to interpret the readings (refer to Figure 12).

5.2 Reporting System in Place

The reporting system put in place was pre-defined in the Emergency Action Plans. "Alert-Action-Alarm" monitoring system was set up for monitoring ground and sensitive receivers movements during the excavation in accordance with relevant contractual requirement (M&W Specification cl. Section 23 Geotechnical Instrumentation). Three response Levels were clearly defined for instrument monitoring as "Alert", "Action" and "Alarm" Levels. They were determined accurately by both DBJV Designer and the Engineer and appropriate Response Actions are to be taken accordingly once a Level is reached.

"AAA" Monitoring and Response Team was responsible for routine monitoring as well as reviewing and discussing trigger values and determining and implementing relevant response actions at different response levels. The team was composed of DBJV Engineering, TBM Production and Geotechnical teams and MTR management teams.

Two experience DBJV geotechnical engineers were assigned on day and night shift to assist TBM Production Team in understanding the ground and structure movements during critical crossings. GEOSCOPE was made available to several teams (engineering, production and MTR) during critical crossings. The DBJV geotechnical engineers also had access to Bouygues Mobydic and BYDAS real time reporting for the Variable Density TBM drive. In addition of monitoring the data against the AAA, a general analysis of the ground movements was provided to TBM Production Team on regular basis through the shifts.

The high frequency of readings taken by the Centaur (up to every 15min) allowed quick review of ongoing ground movements induced by TBM as well as very high definition reporting (excavation, ring built, mortar injection, etc. could be seen in near real time). Two reporting methods were used:

1. Systematic reporting at each end of each shift along with reporting of ADMS data for critical HyD structures during crossing at two hours intervals
2. Ad Hoc reporting via a specifically created WhatsApp group between geotechnical and TBM teams using screenshot of either GEOSCOPE charts or more developed charts using software such as Excel and Surfer.

5 3 Example of Reports Provided to Production Teams

In this section we will present a report sent at the end of the last night shift during the Cross Harbour Tunnel Slip Road to Victoria Park (location shown in Figure 8) which uses available information from GEOSCOPE, Mobydic and Bydas. While under the slip road the TBM went through mixed ground conditions with 10 to 40% rock like materials with CDG and MD appeared in crown when cutterhead was at Ring 90 to 91. Cover to ground surface at this location is around 10.5m.

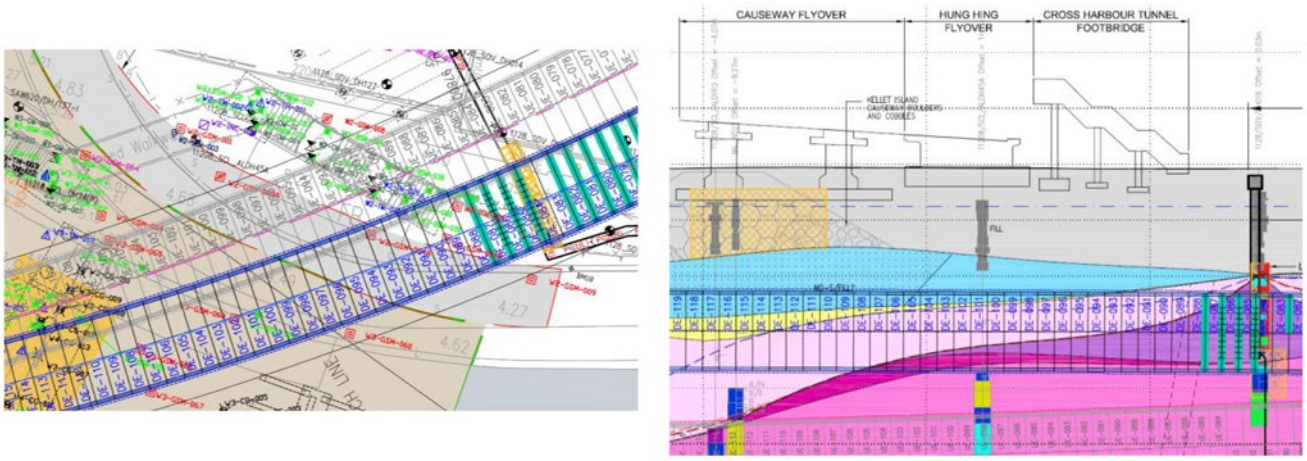

Figure 8: Location of Cross Harbour Tunnel Slip Road to Victoria Park

The maximum settlements recorded are around 25 to 30mm above the tunnel footprint. The settlement trough is relatively narrow (12 to 15m from TBM axis) due to the shallow cover (based on data collected at volume loss sections with GSMs on either side of the road crossing – Figure 9). Settlements recorded by Centaur are consistent with the values obtained by manual leveling on the GSMs on either side of the road. The spatial repartition of the settlements recorded by Centaur and manual leveling at 06/10/2016 5pm (cutterhead located at around 30 m from road crossing) is shown on Figure 11. Centaur could not be done on the left side of the TBM due to distance restriction to keep proper accuracy.

The chart below shows the movements of the road vs TBM advance (Figure 10). Most of the points start stabilizing when the ring 105 is being excavated (i.e. CH at DE112) or around 21m behind the cutterhead. Movements immediately started after the cutterhead enters the road section and acceleration is recorded once the cutterhead leaves the road. Following the annulus injection by cement grout mortar the settlements slowed down to completely stabilize between 20 and 25m behind the cutterhead. TBM team consistently adjusted the excavation parameters to limit the settlements. It was later found that the most of the settlements occurred due to vibration induced by mining through transition zone.

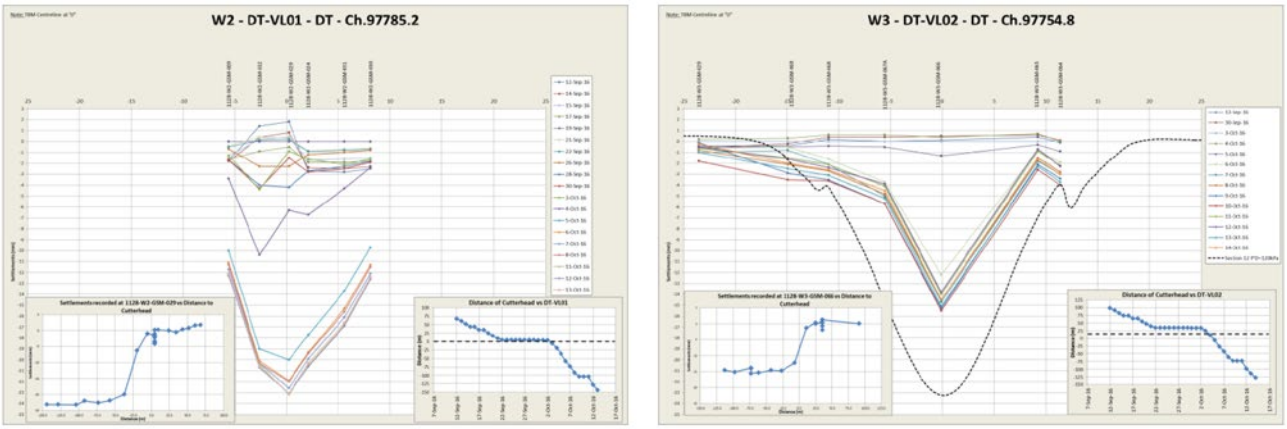

Figure 9: Volume Loss sections on either side of the crossing by DBJV

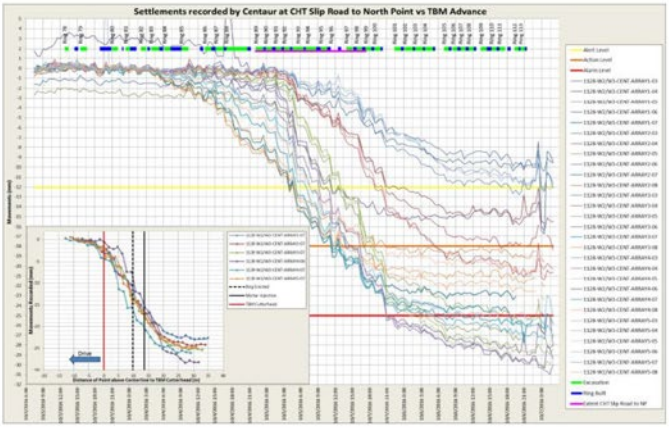

Figure 10: Movements Vs TBM Advance by DBJV

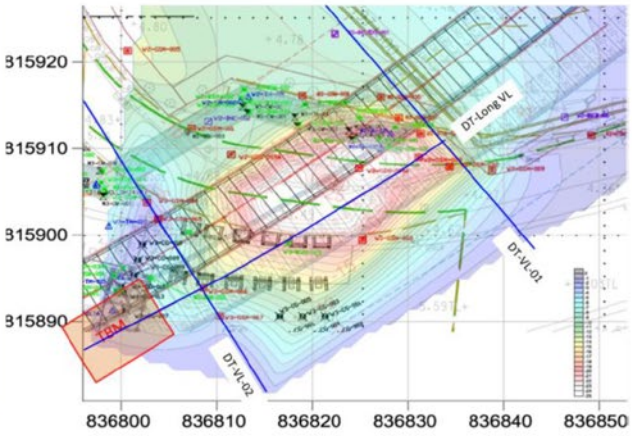

Figure 11: Geostatistical Plot of Settlement Recorded

5.4 Quick Adaptation of TBM Production Teams based on Monitoring Reporting

Based on monitoring feedback from the monitoring that were reported through WhatsApp and verbally through the phone or meetings, TBM production Team was able to adapt TBM excavation parameters and modify the target volumes for mortar injection in the annulus to limit the potential settlements. One of the most remarkable example of quick reactivity happened during the crossing of Gloucester Road West Bound Figure 12 below provides the centaur records of the points located directly above the centre line. Figure 13 shows that following reports from monitoring showing around 18mm of settlements at the start the road crossing, TBM production Team quickly reacted to minimize the settlements from 18 to 5mm by injection high density slurry prior to injecting the mortar in the annulus. TBM Production team also decided to increase the mortar maximum volumes for this section of the works. Settlements were stopped and ground was pushed upwards.

As previously recorded, settlements tend to stabilize after mortar injection around the newly installed lining.

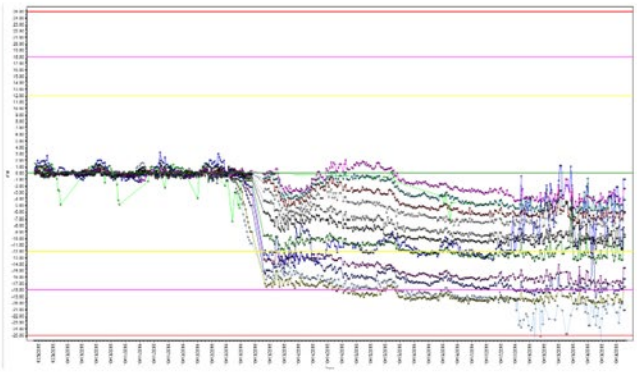

Figure 12: Screenshot of Centaur data from GEOSCOPE

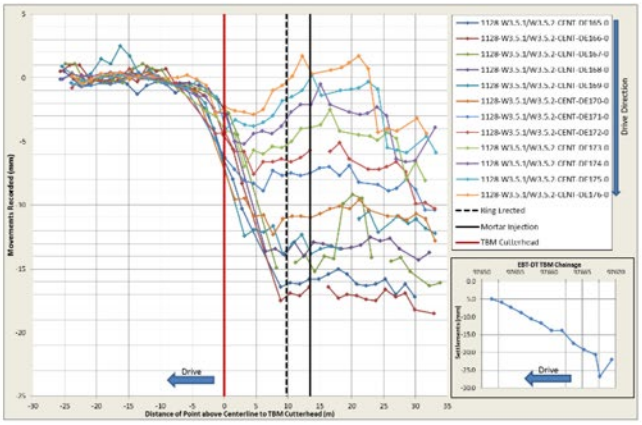

Figure 13: Reduction of TBM tunneling induced settlements while crossing the road by DBJV

6 LESSONS LEARNT AND RECOMMANDATIONS

6.1 Challenges faced

The major challenges faced were due to safety issues when monitoring of carriage way is required and due to the shear amount of data collected by both the monitoring and TBM and how to effectively analyse, interpret and report quickly the information to the proper teams.Table 6 below provides the main challenges face and how DBJV and Sixense coped with them.

Table 6: Main challenges and their solutions

Challenged Faced	Solution Found
No physical monitoring of carriage way due to heavy traffic on most of roads and implementation of 24h TTMS not possible	Reflector-less monitoring technique that does not require physical access on carriage way for either installation or monitoring.
Need for near continuous real-time monitoring to allow quick adaption of TBM excavation parameters	Use of automatic monitoring technique.
Shear number of data for manual and automatic monitoring to report	Use of GEOSCOPE to visualize the movements and export data quickly.
Interpretation and filtering of all monitoring data for better adaption of TBM Production Team	Experienced geotechnical team to provide quick monitoring reviews and end of shift reporting.
Quick reporting in case of newly found trend of movement	Use of WhatsApp group with TBM Teams to send screenshots of GEOSCOPE and observation.
Tight schedule for installation of Centaur at each road crossing due to excellent performance of TBM	Great synergy between the production and geotechnical teams from DBJV and Sixense.
Communication of data to third parties (government bodies and stakeholders)	MTR dedicated a team to liaise with third parties

6.2 Recommendations

One of the challenge that could not be solved was temporary obstruction of the Centaur points by the heavy traffic and heavy rain which lead to temporary loss of data and inaccurate readings and jumps. A better version of the Centaur can be designed by using the “Mesh Method” which consists in measuring several points evenly spaced around the wanted point to interpolate its location. This method has several benefits: It is more robust with a greatly improved accuracy and a better tolerance to obstructions. However, it is much slower and could be difficult to be setup when space is limited. In our case, this method could not be used because of the very high required frequency.

7 CONCLUSION

EBT-DT TBM drive was successfully completed without impact on the public thanks to close monitoring of the ground and structure responses in continuous near real time as well as the strong involvement of both DBJV and MTR geotechnical and TBM production Teams.

This automatic monitoring is a useful solution for tunneling through urban dense area and addressing stakeholder concerns. We will see more and more ADMS and Centaur systems over the coming years and those should be included in conforming instrumentation and monitoring plans for critical sensitive receivers.

REFERENCES

DBJV. *Emergency Action Plan for Excessive Ground Settlement, Slurry Egress, Sink Holes and Tunnel Collapse.*

Herrenknecht. *Basic Training on Variable Density TBM – A combination between mix and EPB TBM.*

Jacques, Laverret, Reilly 2017, *SCL1128 – Hong Kong's First Variable Density Tunnel Boring Machine, Proceedings of the HKIE Geotechnical Division Annual Seminar 2017, Hong Kong.*

MTR. M&W Specification cl. Section 23 Geotechnical Instrumentation.

Geophysical Investigations for Obstruction Detection and Subsequent Mitigation Works for Marsh Road TBM Crossing, SCL1128

S. Auvergne & K. Yu
Dragages Bouygues Joint-Venture, Hong Kong
C. Mogenier
SIXENSE Ltd., SIXENSE Group, Hong Kong
T. Barrett
MTR Corporation Limited, Hong Kong

ABSTRACT

The Dragages Hong Kong Ltd. Bouygues TP Joint Venture (DBJV) was awarded the Mass Transit Railway Corporation (MTRC) Shatin to Central Link (SCL) Contract SCL1128 in 2014. The contract includes the construction of the South Ventilation Building (SVB) to Admiralty Tunnels which form part of the Hong Kong Government's SCL Project. SCL1128 requires the construction of twin tunnels under one of the busiest and densely urban areas of Hong Kong Island. The Eastern and Western Tunnels are separated by the future Hong Kong Exhibition Center station. The Eastern tunnels alignments commence near the Causeway Bay Typhoon Shelter. These tunnels cross several critical roads termed 'Red Routes' which are of regional strategic importance to Hong Kong, significant underground drains, buildings and facilities. The two Eastern tunnels are stacked with the deeper Uptrack (UT) Tunnel excavated through varied geology with cover ranging from 20 to 30m. The shallower Downtrack (DT) tunnel is excavated with cover less than 3m under some structures and generally with less than one diameter to ground level. Two types of tunnel boring machine (TBMs) were used for the works; one typical slurry mix-shield and a new mark of TBM called a variable density shield for the shallow DT tunnel, the first of its kind to be used in Hong Kong. The two TBM drives were successfully completed in July and November 2016 respectively. These drives required an extensive geophysical investigation campaign; this paper presents the specific Marsh Road (Wan Chai District) case study.

1 INTRODUCTION

1.1 Site Geology Overview

The topography along the alignment of the SCL1128 tunnels is a relatively flat and low-lying plain of reclaimed land situated along the northern coastline of Hong Kong Island. The reclamation occurred in several phases over a period of time from the mid-1800s to the present day in order to satisfy land demands for development.

A review of historical maps and aerial photographs identified the development of the reclamation in five main stages: the first phase, constructed between 1842 and 1863, where the shoreline was extended from Queen's Road to Johnston Road in Wan Chai, as well as the Causeway Bay area; the second

phase, constructed between 1895 and 1930, where the shoreline was extended to Gloucester Road; the third phase, constructed between 1964 and 1970, which created the land under which the SCL would be constructed (Figure 1). A fourth phase of reclamation for the new wing of the Hong Kong Convention and Exhibition Centre to the north of Convention Avenue was constructed between 1993 and 2000 with a further fifth phase ongoing as part of the Central - Wan Chai Bypass and Island Eastern Corridor Link.

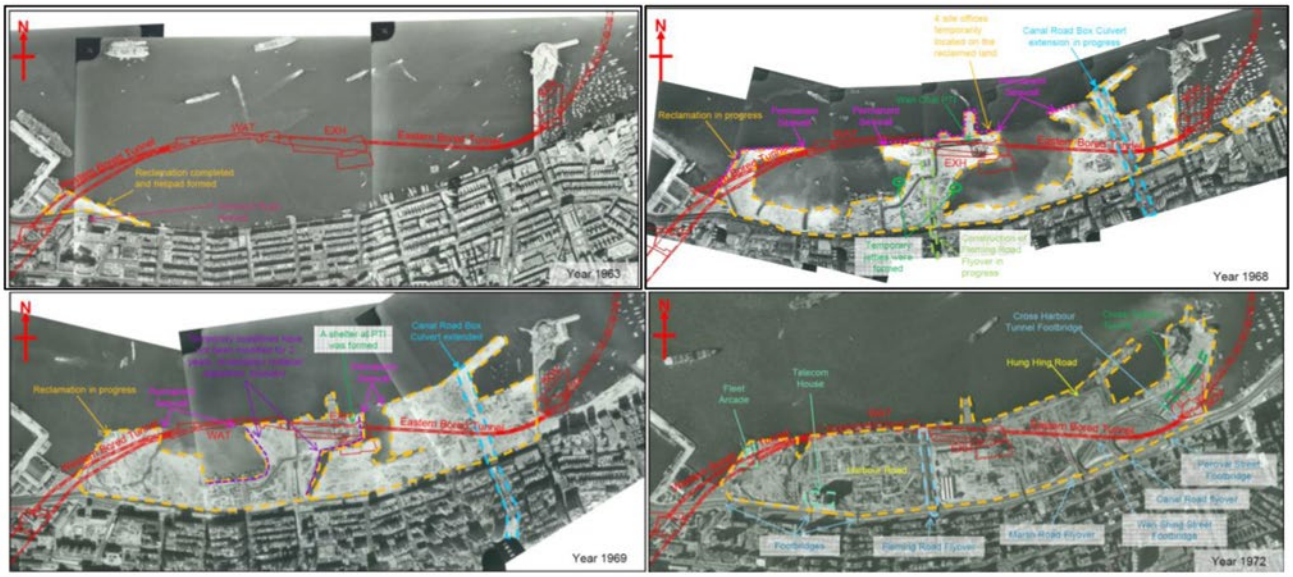

Figure 1: Aerial photos of the third phase of reclamation (timeline from 1963-1972)

Underlying the reclaimed land there is a layer of marine deposit (disturbed and mainly sandy on the upper part and soft clay on the lower part); beneath the marine deposit is an alluvium layer which in turn overlays the weathered granitic formations and granite rock. The thickness of fill, marine deposits and alluvium vary along the SCL tunnels alignment (Figure 2).

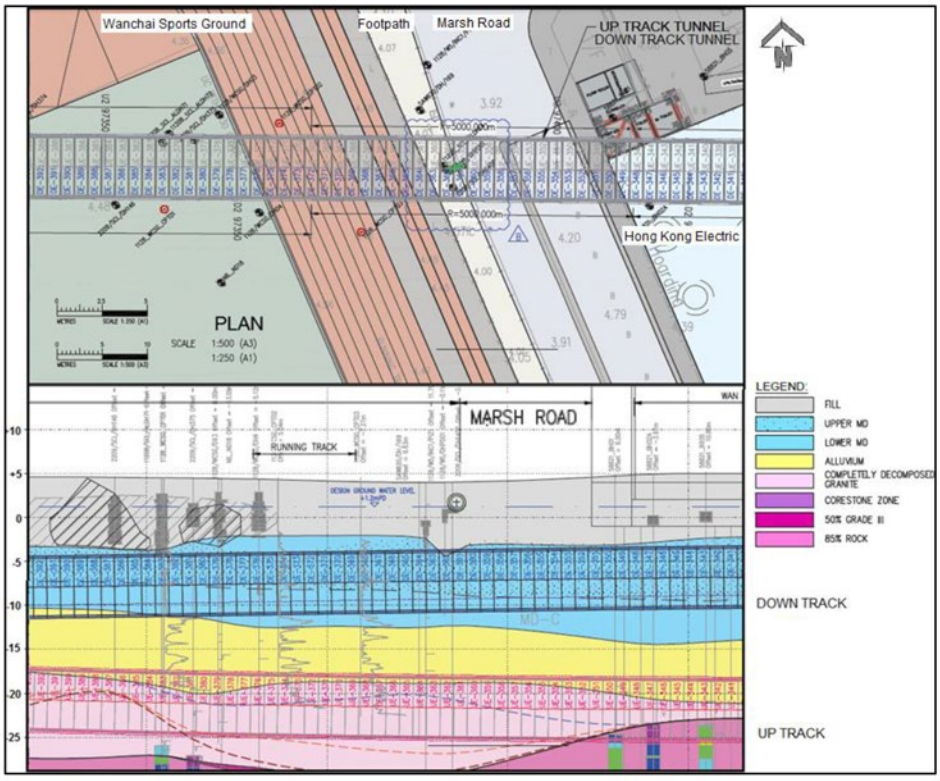

Figure 2: Extract of the SCL1128 Geological Section

Throughout the fill material it was expected that small steel obstructions would be encountered, at the interface between the marine deposit and the fill material there was again the possibility to intersect steel obstructions dropped into the sea along with World War II ordinance. Further to this historical left in place piles, temporary works and live piles supporting the highways structures needed to be located and removed, ahead of the SCL1128 TBM tunnelling, as such an extensive geophysical survey campaign was progressed.

1.2 Marsh Road 'Obstruction'

It was noted in the pre-contract investigations that there may be some sheet pile obstructions associated with a 1.5m diameter storm water drain along Marsh Road and that these may clash with the shallow Downtrack TBM drive. During the preliminary stage of the project, a geophysical survey was carried out from a single borehole at this location using magnetometry survey revealing the presence of magnetic targets. This characterized the presence of steel which brought the risk of damage and blockage to the TBM cutter head, which in turn could cause a collapse at shallow depths. As such a more detailed and targeted geophysical survey was required, especially as the magnetic targets were located in close proximity to Wan Chai Sports Ground a popular sporting facility with the public and local schools.

1.3 Site Context and Constraints

Marsh Road runs north south between Gloucester Road and Hung Hing Road, the western edge of Marsh Road is bounded by a 3.5m wide pedestrian footpath. The 1.5m dia. storm drain runs underneath the footpath with telecommunication cables and 11kVA cables to the west, a 450 dia. mm salt water main is located to the east under the road next to the kerb line. During discussions in the project Site Liaison Group with the Traffic and Police Departments it was stipulated that no road closures were allowed, with these constrains the allowable works area was limited. The storm drain collects surface run off water over a catchment area of circa 10ha of urban flat land located in Wan Chai District, this water is discharged into Victoria Harbour.

2 INVESTIGATION CAMPAIGN

2.1 Desktop Study and Preliminary Geophysical Survey

Based on the aerial photos, reclamation works and civil works were performed in parallel without sufficient time to allow sufficient ground consolidation to occur due to development demand. It should be noted that consolidation of reclamation can take many years. As such undocumented temporary works may have been adopted to control the impact of the settlement induced by the ground consolidation to structures in constructed at the reclaimed area which in turn could clash with the SCL TBM drives.

As discussed in Section 1.2, at Marsh Road shallow depth left-in temporary works associated with the construction of the 1.5m dia. storm pipe were expected. No as built information relating to the temporary works was available. In light of this a geophysical survey was carried out from a single borehole at the suspect location revealing the presence of magnetic targets (Figure 3). This characterized the presence of steel confirming the risk of steel clashing with the TBM drives.

To accurately define the extent of the steel, a further detailed geophysical survey was designed and implemented by DBJV and SIXENSE Ltd. As the nature, presence, orientation and extent of the possible obstruction(s) was unknown and partially within the fill formation which can contain odd bits of steel designing any such geophysical survey becomes a highly complex task. As such the investigations were progressed in several stages, the successive information obtained by following this approach allowed each phase of investigation to target the anomalies to a high degree of accuracy.

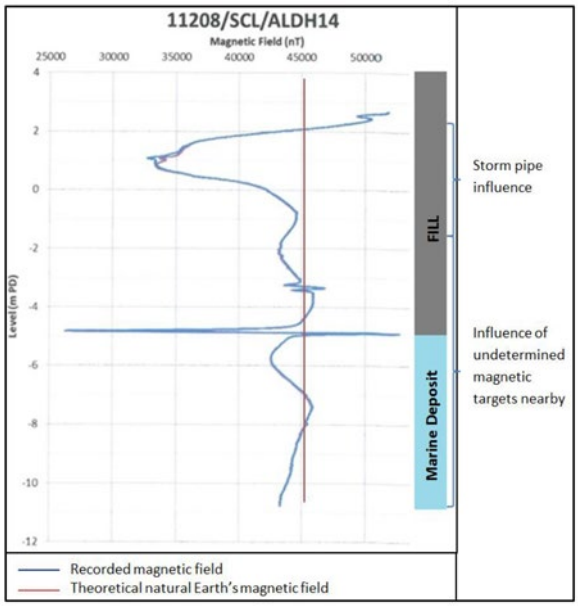

Figure 3: Borehole magnetic log recorded at preliminary stage

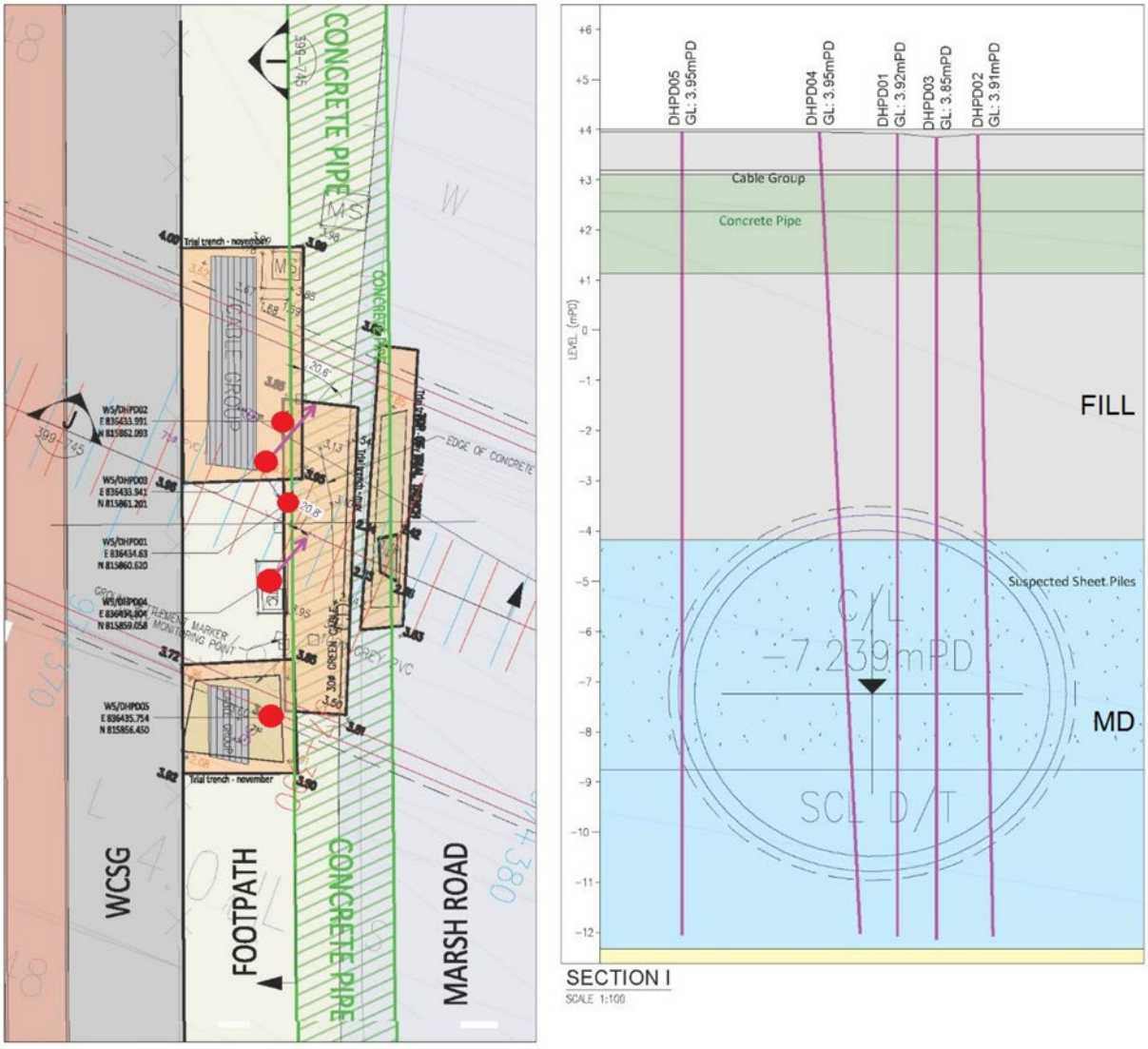

Figure 4: Stage 1, implementation layout and geological section

2.2 First stage of Geophysical Survey

2.2.1 Methodology:

The first geophysical investigation campaign consisted in drilling five nos. holes (DHPD01 to DHPD05) along the cut section of the East SCL down track tunnel to -12.08mPD (Figure 4).

Depending on the characteristics of the suspected obstruction(s) several geophysical methods can be implemented tailored to the specific case and physical characteristics expected. Marsh Road had no available information pertaining to the existing structures; therefore several methods were proposed to further investigate. Table 1 hereafter summarizes the methods implemented during this 1st stage, and their field of application.

Table 1: Geophysical techniques implemented at 1st stage

Implemented method	Measured parameter	Sensitive to	Limitations	Works well on
Borehole electromagnetism (Induction mode)	Works as a metal detector (induction field technique)	Any metal within a radius of 45cm around the probe	No information on the amount of metal or on the location around the hole	Reinforced structures or foundations, and localized metallic targets (small pieces)
Borehole magnetism	Magnetic field	Any magnetic target (steel, iron) in vicinity of the probe. Investigation radius depends on the size of the target and on its magnetization	Requires modelling software to better estimate the size and the location of the target(s). Not sensitive to non-ferrous objects	Reinforced structures and localized targets
Electric Cylinder™	Electrical resistivity of materials, in a cylinder volume around the borehole	Large and elongated metallic structures which easily conduct electrical current.	Less sensitive when used in saline water, or when steel is embedded into concrete.	Sheet piles, Casings, Sheet pile walls.
Cross Hole Electrical Resistivity Tomography	Electrical resistivity of materials, in a volume comprised between 2 or more boreholes	Large and elongated metallic structures like steel pipe piles or sheet piles.	Smaller resolution than Electric Cylinder™ but allows to cover larger areas between boreholes	Sheet piles, Casings, Sheet pile walls.

2.2.2 Methods Principles

1. Borehole magnetism (MAG):

   The borehole magnetic method was implemented to detect various buried metallic structures. This was based on the fact that reinforcement bars, steel casings, or embedded steel wires, are ferromagnetic and generate relatively strong induced magnetic fields. If the induced magnetic field measured within a borehole is assumed to be generated by steel embedded within the deep structure, estimates of the depth to the base of the structure can be generated. On the magnetic field curves (in Nanotesla) presented hereafter, variations of the curves indicate the presence of magnetic targets (steel). For instance, the presence of a known storm pipe at surface is revealed by the presence of a strong magnetic target. A flat signal indicates the absence of a magnetic target.

2. Electromagnetism using LITE probe (EM)

   The LITE uses the induction field method to evaluate the length of existing steel piles (Steel Sheet Piles, H-piles, Pipe piles, Cased Drilled Shafts, and highly reinforced Drilled Shafts), or to determine the existence of such targets in the vicinity of the surveyed borehole.

The operation of the LITE is straightforward: the LITE Probe is lowered into a PVC lined hole. If the LITE detects the proximity of steel or any metal, within 18 inches (450 mm) of the probe, the recorded Voltage would raise to a maximum. If there is no metal in its range of detection the LITE stays at the initial value set during the calibration stage of the probe.

On the electromagnetic induction field curves (in V) presented hereafter, the presence of metal is indicated by high values (5V), while a value remaining around 2.5V indicate the absence of metal within the detection range (45cm in radius).

3. Electric Cylinder™ (EC) and Cross Hole Electrical Resistivity Tomography (CHERT):

These two methods use the electrical properties of materials to image the electrical resistivity contrasts between the geological materials and potential conductive or resistive structures. The tests are carried out at a high resolution from a single borehole when implementing the Electric Cylinder™ (EC) technique, or at a relatively reduced resolution between several boreholes when implementing the Cross Hole Electrical Resistivity Tomography technique (CHERT).

During the CHERT technique current is applied to the ground between two electrodes, and the electric potential measured between another pair of electrodes set within a multi-electrode array located along the length of boreholes. Measured apparent resistivity values represent a volume of the ground located between the two boreholes. If several sets of boreholes are investigated within the same area, measurements can be merged into a 3D model including all available 2D sections.

In addition, Electric Cylinder™ measurements (EC) provide data which allows the imaging of the electrical resistivity contrasts in the vicinity of the boreholes. This method provides a resistivity pseudo section in the form of a 3 to 5 meter radius cylinder of ground (depending on ground resistivity) around the test hole The resistivity pseudo section depicts the depth and extent of hard and soft bedding, weathered and/or fractured zones, shear faults, buried structures, etc.

On the Electric Cylinders sections presented hereafter, blue colors and red colors respectively indicate the presence of conductive and resistive materials (in Ohm.m).

2.2.3 Results and Interpretation

At the end of the first stage, the following interpretation was proposed based on the observed results:

1. The two electrical methods (EC and CHERT) did not record a strong conductivity along the borehole alignment which would have been expected had a sheet pile or driven H pile been present. Thus the presence of such obstructions was ruled out by these electrical survey results.
2. The MAG survey clearly indicated the presence of magnetic structures beneath the existing storm water pipe close to two of the surveyed holes, DHPD04 and DHPD01. The modeling results adopting several mathematical solutions could explain the findings as several small targets located along the bore hole, or a single continuous one.
3. The EM results highlighted that a continuous target or a high density of targets (less than every 50cm) should be expected to be located in the vicinity of these two holes, as the curve obtained from DHPD04 indicated a continuous anomaly from -3 to -11mPD.

Figure 5 hereafter depicts the MAG, EM, and EC results obtained during the 1st stage.

The conclusion was that there were strong indications of numerous steel obstructions within the excavated profile of the East SCL down track tunnel at this location. The presence of steel obstructions underneath the fill within the in-situ ground underlined the possible presence of man-made obstructions. Due to this critical project risk a 2nd highly focused survey was proposed by the project team to fill in the gaps to our understanding and precisely identify the detail the obstructions.

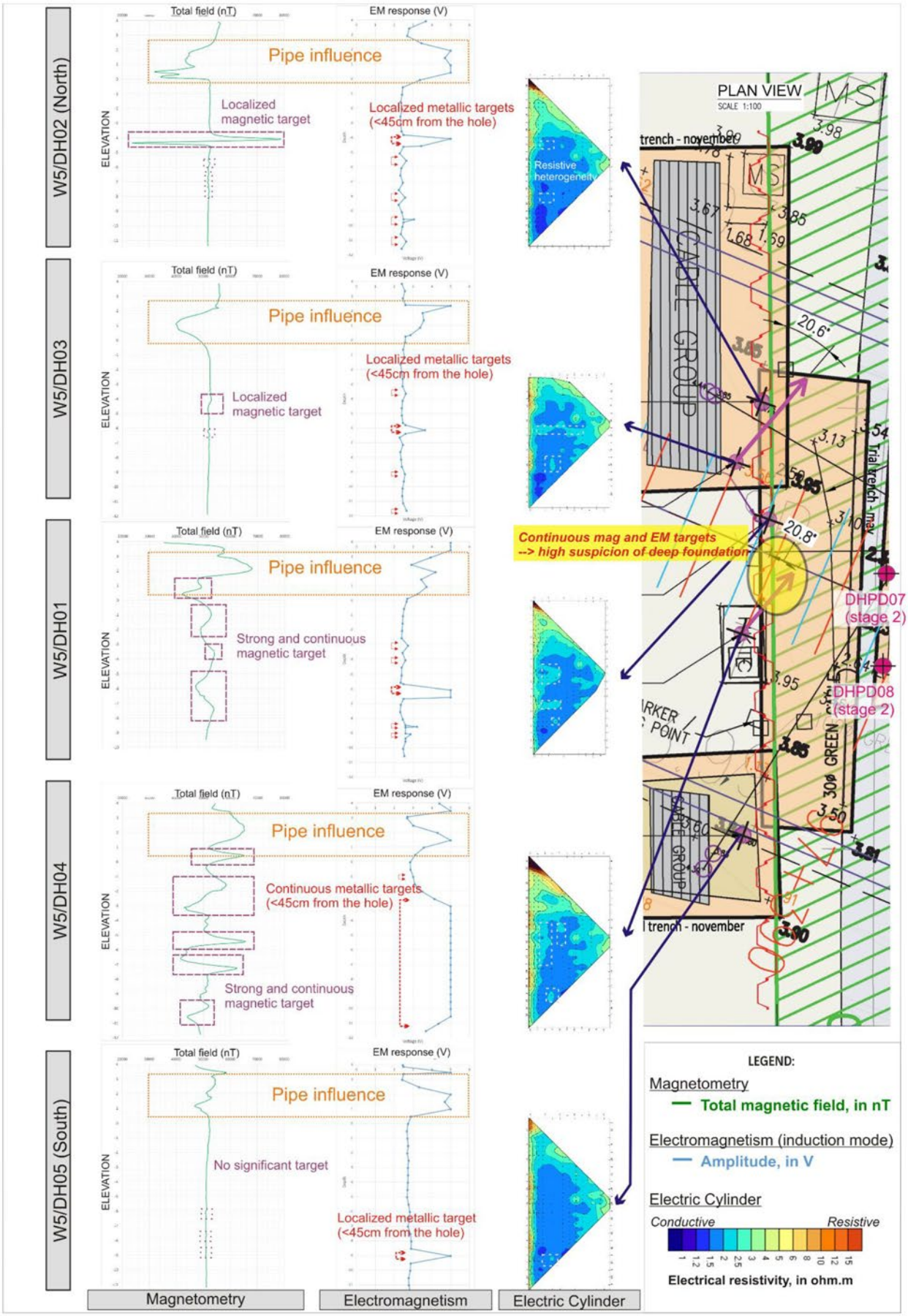

Figure 5: Results obtained during the 1st stage

2.3 Second stage of Geophysical Survey

2.3.1 Methodology

Two additional bore holes (DHPD07 and 08, Figure 5) were drilled to -20mPD to investigate deeper within the in-situ ground to ascertain if the potential obstruction affected the East SCL up track tunnel alignment.

EM and MAG test were progressed from these two new holes. It was also decided to employ an additional technique that considered a different physical property: the Parallel Seismic Method (PSM) (Table 2).

Table 2: Additional technique carried out at 2nd stage

Implemented method	Measured parameter	Sensitive to	Limitations	Works well on
Parallel Seismic Method	Seismic velocity and length of buried elongated structures, or just soil velocity in absence of structure	Stiff structures like concrete piles or steel made piles	Requires knowing the approximate location of the foundation top, otherwise it has to be carried out in "blind" mode with several seismic shot points at surface.	Reinforced structures.

During the first campaign it was difficult to conclude the nature of the target or targets, whether there was a single continuous target such as a wire or chain or a lot of steel pieces included in the fill material layer. The PSM seismic technique was proposed to resolve this issue. In the presence of several localized targets included in the fill layer the seismic velocity would correspond to that expected for fill material. By contrast, induced seismic velocities in the presence of a continuous foundation would be much higher, as reinforced concrete is stiffer than soil.

Published literature and past experience on the SCL1128 project provided well proven velocity ranges for both fill material and reinforced concrete structures meaning that we were confident the technique would work. PSM was also conducted in bore hole DHPD05, drilled during first campaign, as the tests did not show any metallic targets located nearby, thus we could record the velocity as a calibration within "natural" soil conditions.

2.3.2 Measurement

The Parallel Seismic Method (PSM), governed by a French Standard (NFP 94-160-3), is a borehole test method which can detect foundation depth as well as provide the surrounding soil velocity profile. PSM requires the installation of cased borehole close to the foundation being tested. Interestingly, PSM can be used when the foundation tops are not accessible or when the piles are too long and slender (such as H piles or driven piles) to be testable by sonic echo techniques.

In this case the existence, and by consequence, the top of the suspected foundations were not previously known. As a result of this the measurements were carried out in "blind" mode, with several shot points at the ground surface, but beneath the road and footpath structures, to enhance the chance of generating seismic waves into the searched structures.

Shot points were decided according the MAG & EM observations, i.e. above the magnetic and electromagnetic targets as they were suspected to correspond to existing foundations.

2.3.3 Results and interpretation:

An extract of the results obtained during the 2nd stage are presented in Figure 6. The magnetic and electromagnetic surveys from these two new boreholes (DHPD07 and 08) confirmed the presence of an unknown deep metallic structure located within a 45cm of radius around the borehole DHPD07. PSM showed high velocity structures nearby confirming the presence of a reinforced foundation system. As electromagnetism radius of detection was 45cm, two distinct structures with small cross sections

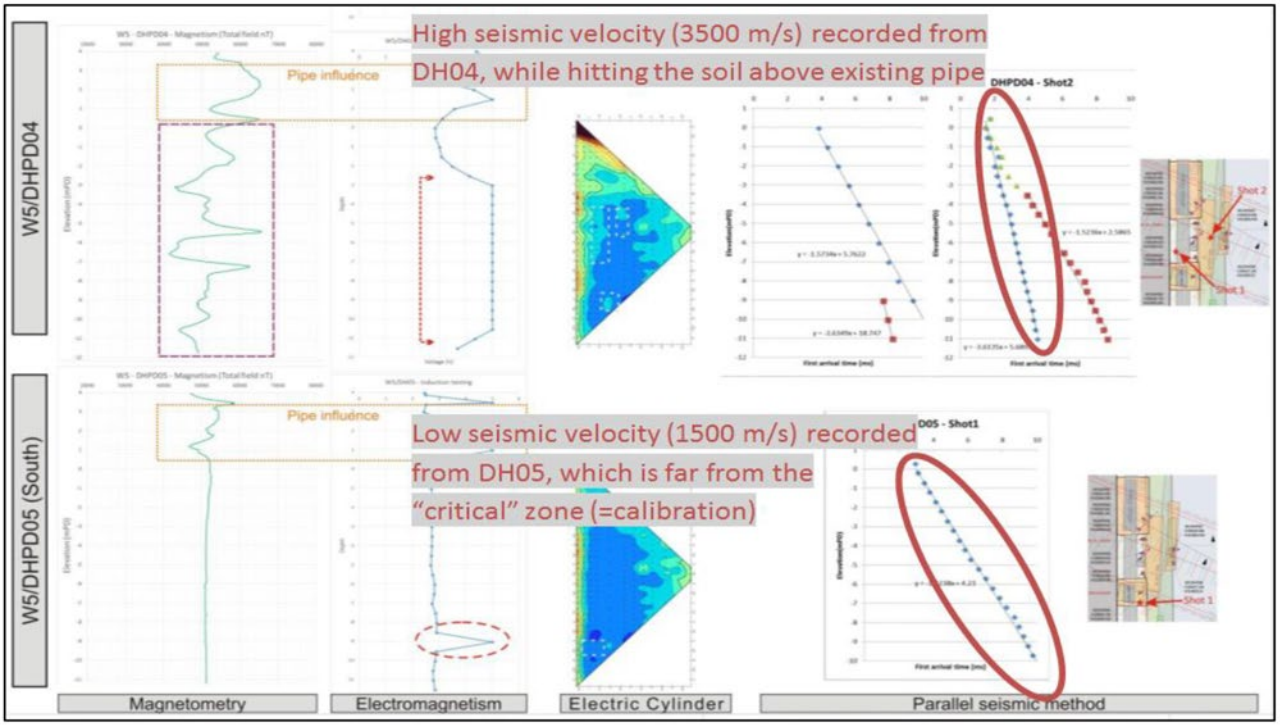

Figure 6: Results obtained during the 2nd stage

located at each side of the pipe were expected, as the spacing between DH04 and DH07 was greater than two times the radius of investigation of EM method. Otherwise a large section pile would have explained the anomaly observed from the two distant boreholes DHPD04 and DHPD07.

As can be seen these borehole geophysical methods demonstrated the existence of an unexpected foundation system as part of the large 1.5m dia. storm pipe located beneath Marsh Road clashing with both UT and DT tunnel alignments, from the results the base of this structure(s) is probably below the deepest measuring points surveyed. With reference to other contemporary structures (the nearby Canal Road Box Culvert), the pile toe was believed to be located between -21 to -25mPD which is the interface between the alluvium and the completely decomposed Granite formation. This interface corresponds to a SPT N value equal to 40. It could be safely assumed that the pile toe was within the UT TBM excavation profile, this informed the final drilling depth.

In addition, a nearby piezometer was investigated with Parallel Seismic Method, Magnetism and Electromagnetism, and indicated the presence of another pile supporting the existing storm pipe, about 10 meters South of the main survey area. This piezometer is located next to the storm pipe, and was drilled deep enough to observe the toe of this other pile. The figure here below presents the results obtained at this location.

Considering that the geology remained identical, the pile toe depth calculated for this neighboring pile was expected to be similar as the toe depth of the pile detected on the TBM alignment, around -21mPD.

2.4 Physical Investigation

With reference to the geophysical investigation results two unknown obstructing piles were indicated most likely to support the existing 1.5m dia. live storm drain pipe during the reclamations lengthy consolidation. To confirm the location and the nature of these foundations, a 7m long trench was excavated in the Marsh Road footpath to expose the storm water drain. At 4m below ground level, two concrete piles and a pile cap were found supporting the live storm drain pipe (Figure 8).

Site inspection indicated the pipe and its cradle were constructed in-situ, supported by a cross-beam (750mm wide x 500mm deep pile cap) and two precast square concrete piles (450mm x 450mm). No pipe joints were found in the upper part of the storm drain with one 70mm wide joint found at the

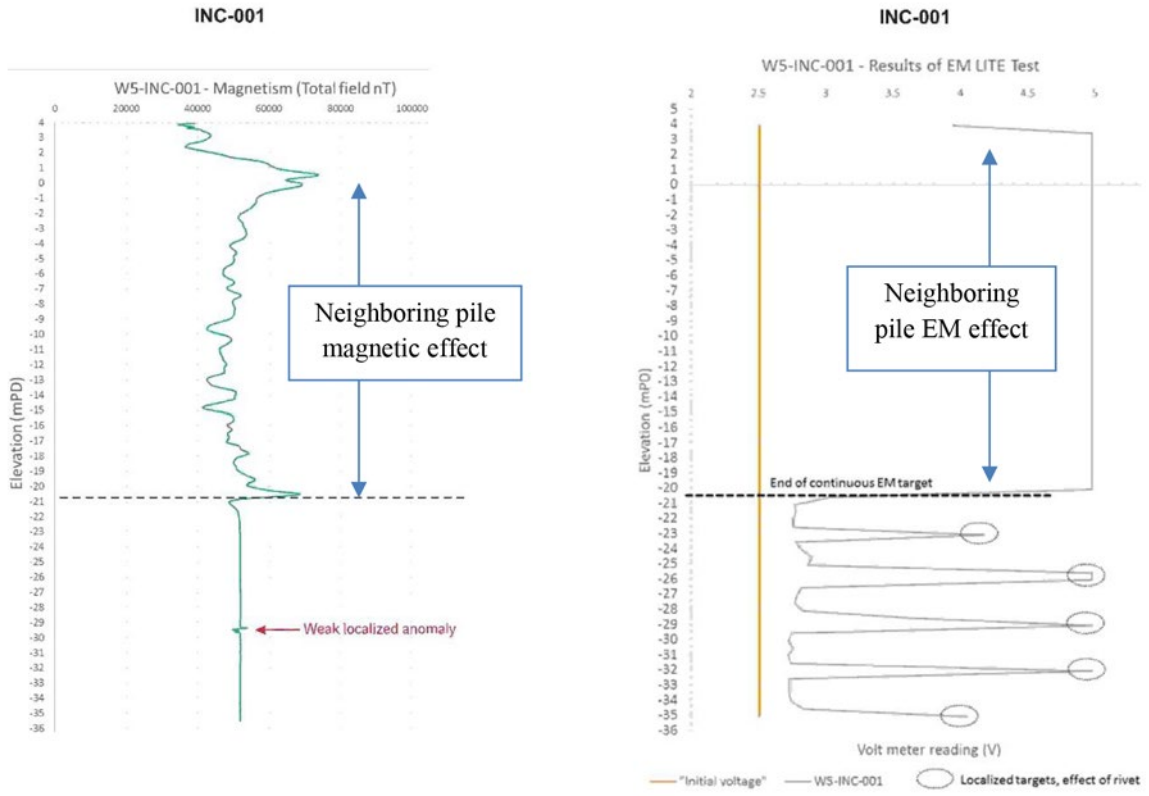

Figure 7: Pile length determination on a neighboring pile, using MAG and EM

Figure 8: Trench Excavation to expose 1500mm dia. Storm Drain

"cradle" of pipe at the location of pile cap. This indicated the storm drain foundations were constructed followed by a pre-cast lower section and a cast in-situ top section.

3 OVERCOME THE UNFORESEEN OBSTRUCTION PILES FOR TBM CROSSING

After completing the geophysical and physical investigations it was confirmed that two precast square concrete piles (450mm x 450mm) were found obstructing both up track and down track SCL 1128 TBM drives with another four in close proximity. A structural assessment confirmed that removal of the existing piles would not adversely affect the existing 1.5m dia. live storm drain.

Removal of the piles from the ground surface by rotator and wedge method was the preferred approach as it was a proven technology likely to succeed thus enabling a clear understanding of costs and programme. However, as the area was outside the Gazettal boundary a full road closure for Marsh Rd could not be obtained, this necessitated more complicated utilities diversions which extended the programme to the point that the rotator solution was unviable, as such innovative alternatives were agreed upon which are explained below.

3.1 Pile Mitigation for the UT TBM Drive:

The UT tunnel is excavated through a stiff CDG layer between level of -18mPD and -25mPD. DBJV proposed to disconnect the two piles from the pile cap and then drive through the piles with TBM. The two precast square concrete piles would be disconnected from the pile cap by coring a row of 100mm dia. holes at the top of the piles.

Tube-A Manchette (TAM) grouting around the concrete piles was performed from the UT tunnel crown level to the bottom of the storm pipe in order to fill the gaps between the soil and piles to mitigate the risk of slurry leaks along the piles during the TBM bore through. Therefore, ten TAM holes were progressed with approximately 97 cubic metres of cement grout injected.

In order to monitor the live storm drain pipe and surrounding ground movement during the tunnelling, additional geotechnical instrumentation was installed. In addition, CCTV was installed to record the internal condition of the pipe before and after the TBM crossing. The UT TBM drive was successfully completed in July 2016 with approximately 6~12mm settlement observed and no damage was recorded to the live storm drain. The UT TBM bored through both concrete piles, one pile shoe was recovered at the Slurry Treatment Plant (STP) in pieces and the other shoe was recovered as a whole from the TBM Cutter Head (Figure 9).

Figure 9: pile shoe recovered from the cutter head (right and middle) and other pile shoe recovered at STP (left)

3.2 Pile Mitigation for the DT TBM Drive:

The remaining part of the concrete piles within the DT excavation would move during own track TBM excavation if the bore through option was progressed due to the presence of a soft marine deposit layer within the tunnel alignment, between level of -4mPD and -11mPD. As the marine layer is relatively soft with an SPT N of circa 10, the forces exerted by the TBM would move the remaining pile sections likely resulting in ground collapse. Further to this sending workers into a compressed air environment at shallow cover in marine deposit to remove the piles is inherently unsafe. To remove this risk, ground treatment and pile removal schemes were studied with pile removal adopted as the preferred option.

An innovative pile removal method was introduced by DBJV to overcome the site constraints by using static hydraulic jacks to extract the obstructing piles at the road surface. In order to achieve this, the existing storm drain was widened with a temporary channel at the pile location. The concrete pile heads were exposed and a steel sleeve casing installed around each from 4m below ground level to above surface level, this was to prevent any muddy water flowing into this storm drain. A high tension bar was installed to the center of each concrete pile by coring a hole and grouting the bar in place. On top of this a jacking frame was constructed.

Prior to the jacking operation, approximately ten relief holes were drilled around each pile, in several of these holes water jetting was performed to reduce the friction between the concrete piles and the surrounding soil, noting care was required so as to not destabilise the surround strata. As the static jacking force was incrementally increased and reached 170~180 tons (around 1.7 times of the expected self-weight of these pre-stressed concrete piles), the concrete piles started to move significantly causing

the jacking force to drop sharply to circa 30 tons. The piles were extracted in 4m lifts, as each 4m section was pulled free it was cut and removed. During the pile extraction operation, the voids created below the two pile toes were backfilled by TAM grout installed in several of the relief holes, to control ground settlement. A total quantity of 8.6 cubic metres of grout was injected during this process. During the whole operation, geotechnical instrumentation was closely monitored with approximately 1~3mm settlement observed with no damage recorded to the live storm drain.

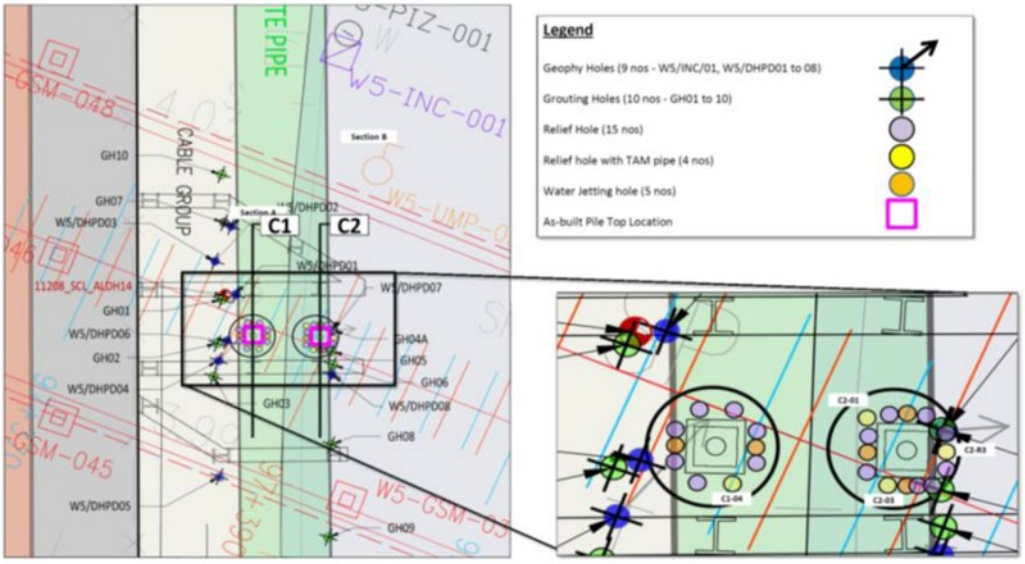

Figure 10: Layout of Marsh Road Removal Works

After successfully removing the 2 concrete piles, TAM grouting was implemented to strengthen the surrounding soil to prevent slurry or air leakage through the disturbed ground during DT TBM drive. Four number of TAM holes were completed and 25.5 cubic metres of cement grout was injected. The DT TBM drive was successfully completed in December 2016 with approximately 2~4mm settlement observed with no damage recorded to the live storm drain.

Figure 11: Site Photos of Marsh Road Removal Works

4 CONCLUSIONS

The lack of historical construction documents for the old structures increases the risk to new construction works being planned and progressed. Any metallic (steel) obstructions left in place underground may cause delay to a TBM project due to the associated risks of machine damage, slurry egress to surface, settlement and ground collapse. Left in obstructions also significantly increases safety risk to the TBM

compressed air workers during remedial works to remove or fix damage caused by said obstructions. In order to minimise these risks for the project, it is prerequisite to progress in depth investigations in order to ascertain the existence and location of any underground obstruction in the vicinity of the tunnel alignment.

As the nature, presence, orientation and extent of the possible obstructions is unknown and can fall within fill formations, often containing odd bits of steel, designing any such geophysical survey becomes a highly complex task. As such the investigations were progressed in several stages, the successive information obtained by following this approach allowed each phase of investigation to target the anomalies to a high degree of accuracy. This method clearly demonstrated the existence of an unexpected foundation system as part of the large sewer pipe located beneath Marsh Road. The depth, the location and the nature of these foundations being clearly identified within the tunnel alignments, DBJV and the client MTRC reviewed several options to mitigate the risks with the final outcome being to grout and drive through on the Uptrack and removal of the piles by static jacking method for the Downtrack.

The targeted geophysical campaign and subsequent innovative pile removal works allowed the two tunnels to be excavated safety without impact to the public, traffic or interruption of the water flow in the pipe in this small and confined works area. The two TBM drives were completed ahead of schedule with the removal completed just in advance of the DT TBM.

REFERENCE

Auvergne, Gauffre & Prost 2017a, *Extensive use of I&M to Enable Safe TBM Drive in Urban Dense Area, a Focus on SCL1128 Eastern Downtrack Drive, Proceedings of the HKIE Geotechnical Division Annual Seminar 2017, Hong Kong.*

Jacques, Laverret, Reilly 2017, *SCL1128 – Hong Kong's First Variable Density Tunnel Boring Machine, Proceedings of the HKIE Geotechnical Division Annual Seminar 2017, Hong Kong.*

Numerical Simulation of Cement-treated Soil Columns Used as Cantilever Earth Retaining Structure

Ay Lee Saw
Golder Associates (HK) Limited, Hong Kong

ABSTRACT

Design of cement-treated soil mass based on limit equilibrium approach for foundation system has been well documented but not for cantilever earth retaining system where the loading condition is different. CDIT (2002) proposed that finite element analysis should be conducted for case with more complicated improvement pattern. Nonetheless, the accuracy of prediction by finite element analyses highly depends on the ability of the selected constitutive model and approach to simulate the problem. So far, Tresca model has been widely used to describe the behavior of cement-treated soil due to minimum design parameters needed. Meanwhile, cement-treated soil mass is also often designed and analysed as a composite material with weighted average simulation (WAS) approach even though they are, in reality, not so. However, studies by Larsson (1999) and Kitazume and Maruyama (2007) both observed bending and tensile failure modes of individual cement-treated soil column in a treated mass, thus putting the aforementioned finite element simulation way in doubt whether it can capture the actual mechanism that they pretend. Therefore, this paper investigates the potential damage of cement-treated soil columns when they are used as cantilever earth retaining structure. All the analyses were performed using finite element (FE) software ABAQUS 6.10.

1 INTRODUCTION

1.1 Background

Cement-treated soil is a product of mixing cement to in-situ soil through different mechanical methods to increase the strength and stiffness by bonding the particles together. The most popular methods are the jet grouting method and the deep cement mixing method. The early application of cement-treated soil columns is mainly used in foundation system to increase bearing capacity and reduce settlement. In view of the effectiveness of this ground improvement method on dealing with weak ground, some have tried to explore the use of column-shaped cement-treated soil as a viable alternative to the conventional earth retaining system. It has been used to serve as a rigid gravity structure when constructed in continuous overlapping columns. Sometimes, different layouts of column installation are used to achieve the desired effect by utilizing space optimization purpose (Nicholson et al., 1998).

Owing to the short history of employing cement-treated soil columns as an earth retaining system, its basic design has yet to be firmly established. In the current design practice, focus has been placed on the shear failure of cement-treated soil columns using slip circle analysis. However, studies by Larsson (1999) and Kitazume and Maruyama (2007) both revealed that cement-treated soil columns could fail in bending and tensile modes. Namikawa and Koseki (2006) compared the shear fracture and tensile fracture for cement-treated sand. Their study showed that the ratio of average fracture energy for the shear failure, G_{fs}, to tensile failure, G_f, is approximately 15:1. This was due to the phenomena that the

breakage area of cementation in the shear failure is much larger than that in the tensile fracture. In other words, the tendency for cement-treated soil columns to fail in tension is much higher compared to shear mode. This is supported by Larsson (1999)'s finding where he found that even for a shear box test which purely aims to fail the material in shear, the individual lime-cement was failed in bending mode, and not by direct shearing across an imposed slip plane.

Finite element (FE) analysis tool has been well recognized to be a powerful tool in solving complicated geotechnical problems. Nonetheless, accuracy of the prediction highly depends on the selected constitutive soil model and how the assumptions being made to simulate the problem. Linear elastic-perfectly plastic Tresca model is often used by practicing engineers due to its simplicity and fewer parameters needed. However, it is generally too crude to capture the essential features of the treated soil behavior, i.e. brittleness (SAW, 2014). In general, the treated ground is generalized to a single material in the 2-D FE analysis for simplicity. The Weighted average simulation (WAS) approach is adopted to average the properties between the treated and untreated soils in term of volume ratio. However, averaging the properties for these two materials with very different behaviour indeed violates the underlying mechanism. In pace with the growth of computer technology, there is an increase in 3-D FE modeling prediction in the past decade. Yang (2009) conducted a series of 3-D finite element analyses using real allocation simulation (RAS) approach to examine the mobilized mass properties of an embedded treated soil columns. In RAS, the treated material properties are assigned to the mesh element corresponding to the treated soil columns zones; while the soil material properties are specified for the untreated zones. Yang's study shed the light into a deeper understanding of the underlying mechanism that cannot be addressed by the WAS approach.

In view of the above mentioned issues, this paper aims to evaluate the effects of the selected constitutive soil model and numerical (WAS and RAS) approaches in simulating the behavior of cement-treated soil mass in an open excavation. To do so, a 4-m deep vertical open excavation in weak soil with grid pattern cement-treated was taken as the hypothetical case study. The analyses were carried out using a 3-D finite element program, ABAQUS 6.10.

2 FINITE ELEMENT ANALYSES

2.1 Hypothetical Cases

Figure 1 shows the adopted hypothetical case geometry. The treated columns are arranged in grid pattern to form a block which is intended to act as a composite gravity wall. This treatment pattern intends to make use of the passive soil berm to facilitate a shallow excavation in weak soil. Typical modelling approach, WAS was used to simulate the treated zone in the hypothetical case. Two models for this grid pattern were considered in the WAS approach as presented in Figure 2. First, average property of treated soil columns and untreated soil were applied to the whole model, termed as the whole mass (WM) model. The second model in the WAS approach was referred as refined mass (RM) where the refined strips were assigned with treated properties. The geometry of grid pattern cement-treated soil columns was also modelled using the RAS approach where each cement-treated soil column was simulated according to their position. As such, a comparison between the WAS and RAS approaches can be made. Three constitutive models, namely classical Tresca, tension truncated Tresca and concrete damage plasticity (CDP) models were used to describe the behavior of the cement-treated columns. A total of five analyses were carried out as summarized in Table 1.

Table 1: Summary table of hypothetical cases

Case	Improvement Pattern	WAS/RAS	Soil Model for Treated Mass
La	Grid type	WAS-WM	Classical Tresca
Lb	Grid type	WAS-RM	Classical Tresca
L1-1	Grid type	RAS	Classical Tresca
L1-2	Grid type	RAS	Tension truncated Tresca
L1-3	Grid type	RAS	Concrete damage plasticity

2.2 Model Set-up

3-D finite element program, Abaqus/Explicit, was adopted to study the hypothetical cases. First-order tetrahedral elements (C3D4) were used to capture the geometry consisted of sharp curve between overlapping columns. This type of element has 4 nodes and 1 integration point. There is always an argument that this element type is stiffer and will underestimate the deformation of the analysed problem. However, this limitation can be overcome with very fine meshes.

In order to optimize the computational time, the problem was simplified as a plane strain condition by considering a 6 m wide from center of tangential row columns to center of another tangential row columns. The plane strain condition was simulated by restricting the movement of these two faces in y-direction. The lateral boundary was allowed for four times the depth of treated soil column, and was restricted from moving in x-direction. The bottom boundary was chosen to extend for at least two times the depth of treated column from the toe of column, and fixed from moving in any direction. The boundary condition and geometry for the hypothetical case is presented in Figure 1.

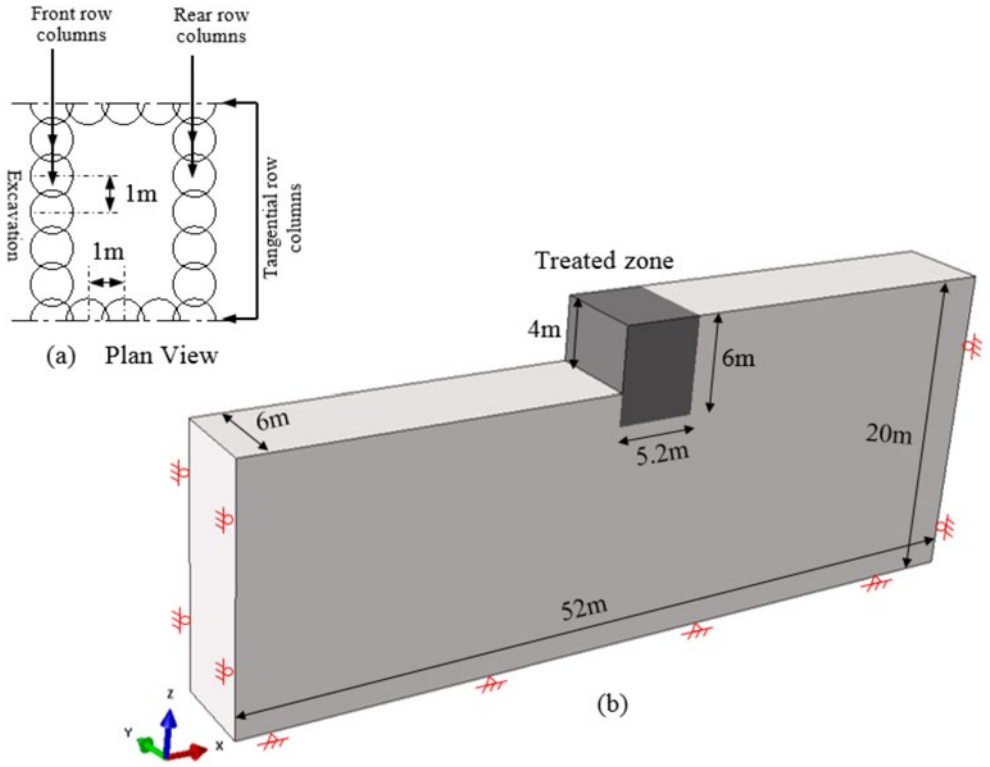

Figure 1: a) Plan view of grid improvement pattern; and
b) Geometry and boundary conditions for the hypothetical case

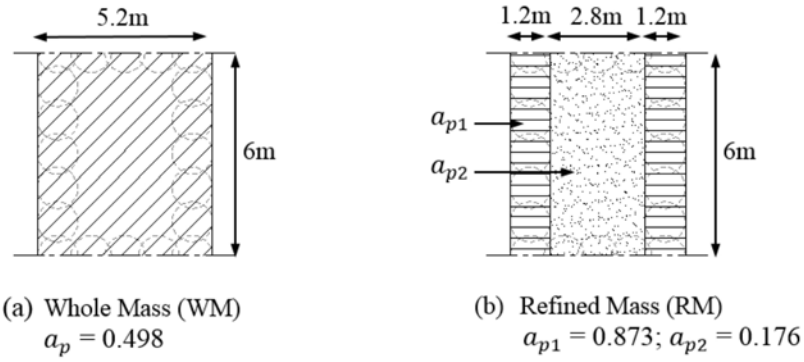

Figure 2: Two configurations of WAS approach for grid type ground improvement pattern

A total of three geometry models for five analyses were employed to simulate the problem, as summarized in Table 1. Two geometry models were adopted for WAS approach simulating the grid improvement pattern, see Figures 3 to 4. The adopted element size was 0.2 m within the treated zone and gradually increased to 1.5 m at the boundary. WM model was built from a total of 111,894 elements while RM model consisted of 195,939 elements. The remaining geometry model was used to simulate the grid ground improvement pattern with RAS approach as shown in Figure 5. Owing to the complex geometry of the columnar treated soil, the meshes within 5 m of the treated block were refined. The element size for columns was 0.2 m and gradually increased to 0.6 m within 5 m extended area and subsequently reached 1.5 m at boundary. As such, the total elements for grid type ground improvement RAS model were 256,758.

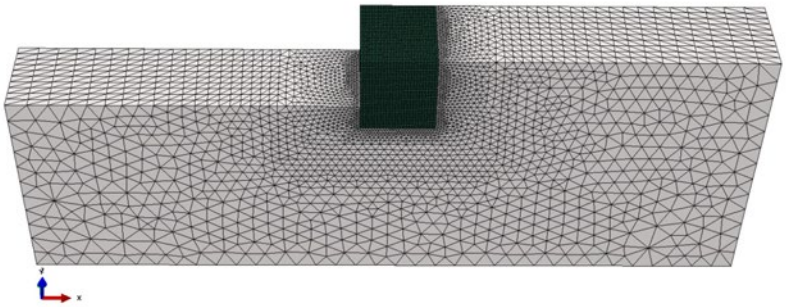

Figure 3: Finite element mesh for Whole Mass (WM) model in WAS approach, La

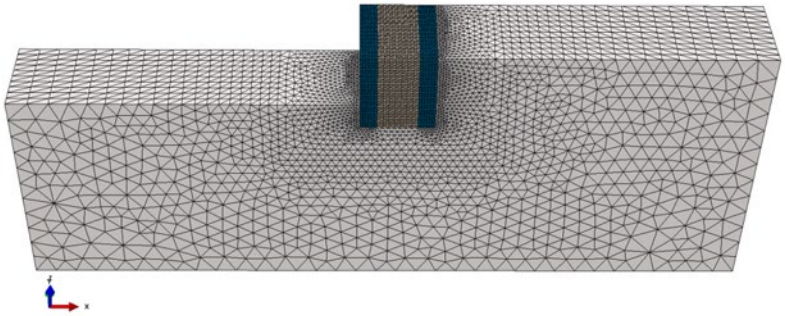

Figure 4: Finite element mesh for Refined Mass (RM) model in WAS approach, Lb

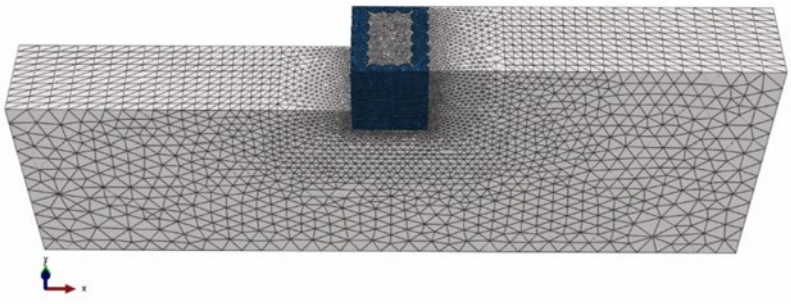

Figure 5: Finite element mesh for RAS approach, L1

2.3 Material Models

In these hypothetical cases, the ground material was assumed as homogenous weak soil. The bulk density (ρ) was taken as 1500 kg/m^3 while Young's modulus (E) and Poisson's ratio (ν) were taken as 20 MPa and 0.3, respectively. The yield criterion for this material was simulated by Mohr Coulomb model with c' = 2kPa and ϕ' = 22°. On the other hand, cement-treated soil columns were simulated by three types of

constitutive model, i.e. the classical Tresca model, tension truncated Tresca model and concrete damage plasticity (CDP) model for comparison between common practice and numerical criteria suggested by Saw (2014). The CDP has been widely used to simulate the crack development and strength degradation due to damage in concrete. The elastic region follows Hooke's laws. The CDP model assumes that the two main failure mechanisms are tensile cracking and compressive crushing. The design parameter for the cement-treated soil column referred to Saw (2014) with an unconfined compressive strength, q_u = 980kPa. In addition to the classical Tresca model, the cement-treated soil columns were also modeled with the tension truncated Tresca model for a better understanding of the simulation performance. The tensile strength, $\sigma_t = 0.11*q_u$ was adopted. The design parameters in these analyses are summarized in Tables 2-3. In common WAS approach, the classical Tresca model was adopted to average the properties of treated soil columns across the treated block and the untreated properties were not included.

In the WAS approach, a full contact between cement-treated soil columns and in-situ soil was assumed so no interface between surfaces was modeled. In the RAS model, the contact surfaces were distinguished in normal and tangential directions. The contact surfaces will separate if the contact pressure becomes zero (in tension condition). For the tangential direction, the frictional behavior was modeled with the classical Coulomb friction.

Table 2: Design parameters for Mohr Coulomb and Tresca models in hypothetical cases

Material	WAS configuration	σ_p	ρ (kg/m^3)	*c (kPa)	others	E (MPa)	ν
Silt	–	–	1500	#2	ϕ' = 22°	20	0.30
Treated columns	–	–	1500	490	σ_t = 107.8kPa	164	0.15
Composite Mass	WM	0.498	1500	244	–	81	0.30
	RM	0.176	1500	86	–	28	0.30
	RM	0.873	1500	427	–	143	0.30

Notes: *c = C_u unless otherwise stated; # denotes c'

Table 3: CDP design parameters for cement-treated soil columns used in hypothetical cases

Compression		Tension	
Compressive Yield Stress	**Inelastic Strain**	**Tensile Yield Stress**	**Fracture Energy**
640 kPa	0	107.8 kPa	5 N/m
900 kPa	0.0005		
980 kPa	0.002		
980 kPa	0.004		
850 kPa	0.0083		
410 kPa	0.0165		
150 kPa	0.0271		
60 kPa	0.035		

Compression		Tension	
d_c	**Inelastic Strain**	**d_t**	**crack displacement**
0	0	0	0
0	0.004	0.9	0.09 mm
0.95	0.035		

Plasticity parameters: ψ = 1°; eccentricity = 0.1; σ_{b0}/σ_{c0} = 1.16; Kc = 0.67

2.4 Numerical Procedures

In these analyses, sequential loading to simulate the installation of cement-treated soil columns and excavation was not considered. Since the main interest in the present study was to evaluate the failure mechanism, the analysis was simplified to one step. For the wish-in-place treated soil columns with final excavation profile model, the load-displacement-stress response of the system was investigated quantitatively by increasing the internal force due to the weight of soil with application of gravity loading (10 kN/m^3). In the beginning of this stage, the boundary conditions shown in Figure 1b were activated.

3 RESULTS AND DISCUSSION

3.1 WAS Approach

The analysed ground movements for the whole mass (WM) model, i.e. Case La and the refined mass (RM) model, i.e. Case Lb in WAS approach are presented in Figure 6. On the other hand, Figure 7 shows that the predicted plastic strains occur at the passive ground but not in the treated zone for these two models. In other words, WAS approach predicts a potential failure of insufficient passive resistance in this hypothetical case. Both analysis results reveal a rigid gravity wall behavior as assumed in the WAS modeling. No significant difference in ground response is observed between these two models.

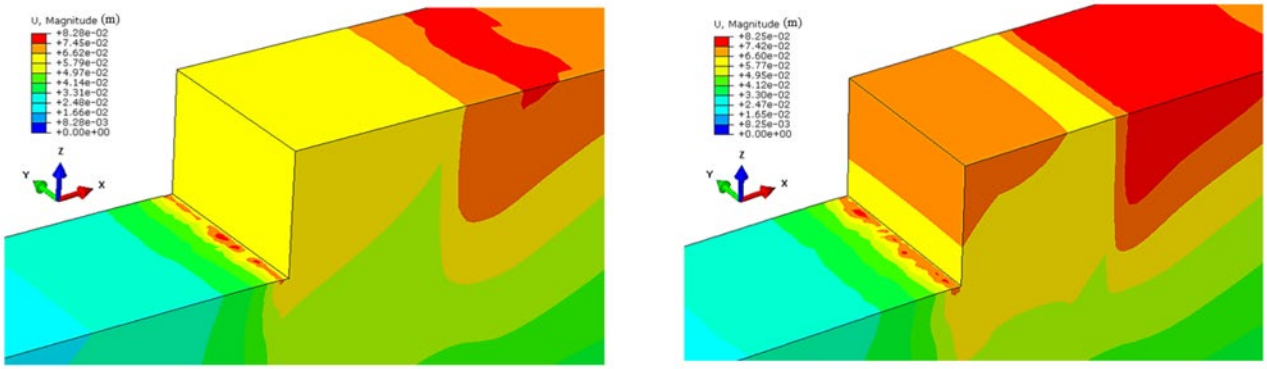

Figure 6: Ground responses for Case La (left) and Case Lb (right)

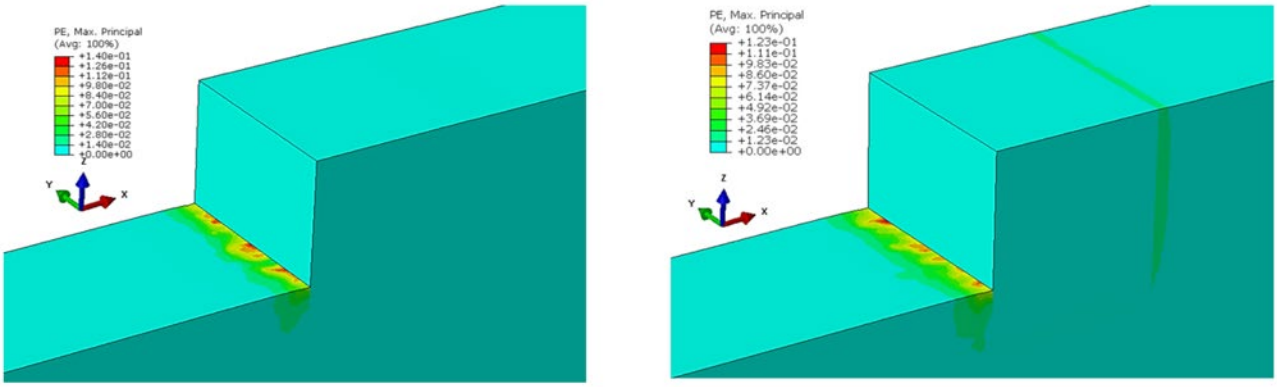

Figure 7: Plastic strains (PE) for Case La (left) and Case Lb (right)

3.2 RAS Approach

In the RAS approach, three constitutive models, namely classical Tresca, tension truncated Tresca and CDP models, were used to describe the behavior of cement-treated columns in Cases L1-1, L1-2 and L1-3, respectively. Figure 8 shows the ground response for Case L1-1 where non-uniform ground movement is observed within the grid block. Arching form of soil movement is observed where the maximum

movement appears at the center of the untreated zone and reduces towards the tangential row treated soil columns. In addition, some plastic strains are developed in the passive ground and some behind rear row columns, similar to that observed from the WAS approach. It is believed that the development of plastic strain is mainly due to the compressive pressure built-up when the ground moves towards the excavated side. No plastic strain is found in the treated soil columns. However, by limiting the tensile strength of the cement-treated columns in Case L1-2, the ground movement increases associated with plastic strain is observed in the overlap areas between the front row of columns and the tangential row of columns, as presented in Figure 9. The plastic strain appeared in the overlapping columns is believed to be caused by reaching the limiting tensile stress in contrary to that observed in Case L1-1. The plastic strain first occurred at the top of the overlap columns and propagated downward to half of the column length. This observation is supported by the concern raised by Broms (2004) where failures may occur due to separation of the columns. This will be further evaluated by the analysis result of Case L1-3.

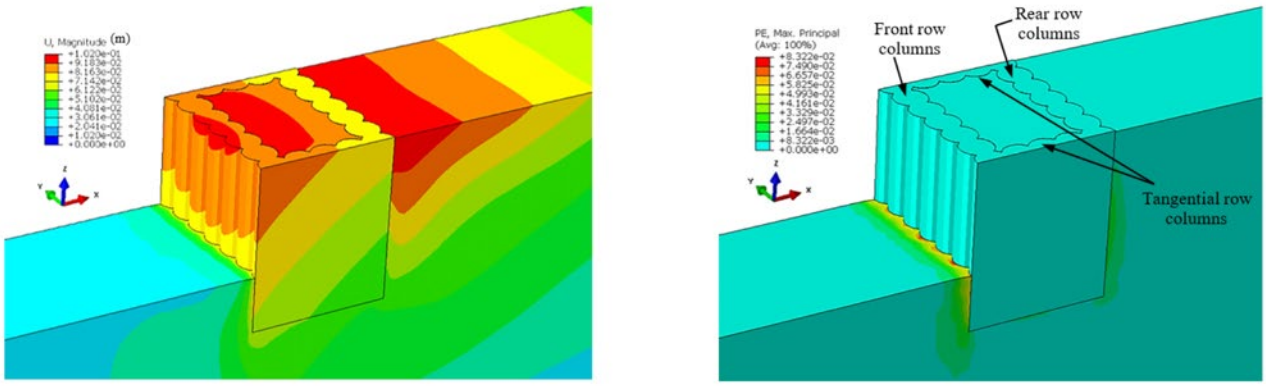

Figure 8: Ground response for RAS approach: Case L1-1

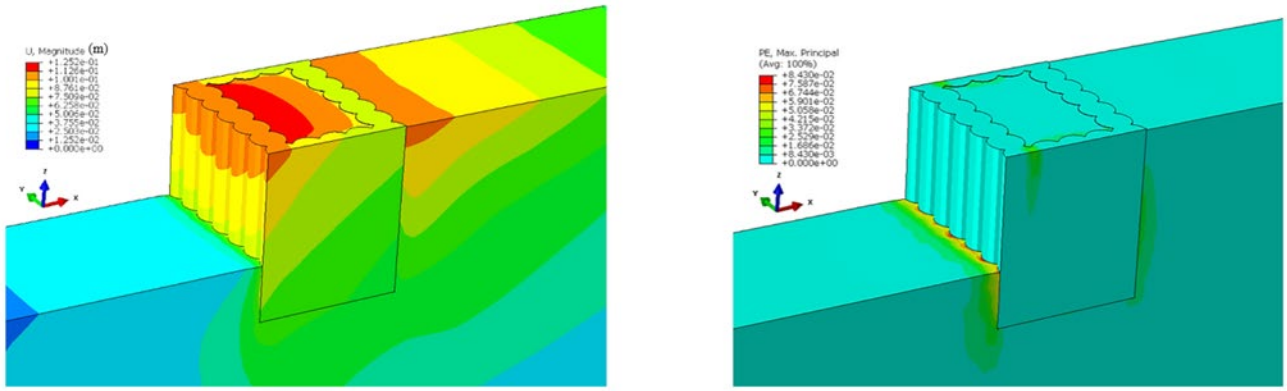

Figure 9: Ground response for RAS approach: Case L1-2

Case L1-3 adopted the CDP model to simulate the behavior of treated soil columns. Figure 10 shows the analysis results of ground movement and plastic strain developed in Case L1-3. The excessive movement observed at the top of the front row columns implies that the system is no longer stable according to Snitbhan and Chen (1978). It is shown that plastic strain is developed in a wedge envelope for the soil within the grid block while macro-cracks are observed in the tangential row columns and front row columns. The progressive crack development can be characterized by the damage variable, dt in the CDP model, as demonstrated in Figure 11. As expected, the soil pressure is acting against the front columns resulting in a “pulling away action” in the overlap areas between front row columns and tangential row columns. When the induced stress exceeds the tensile capacity, crack initiates at the top of the overlap areas and propagates downward along this overlap areas until the end of the cantilever part of the columns.

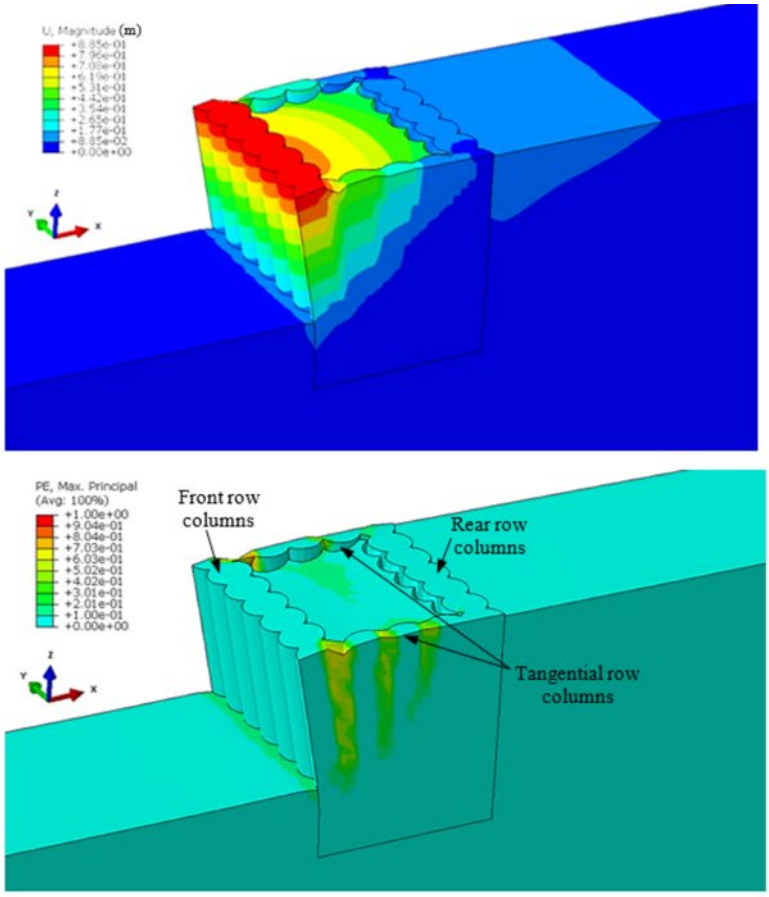

Figure 10: Ground response for RAS approach: Case L1-3

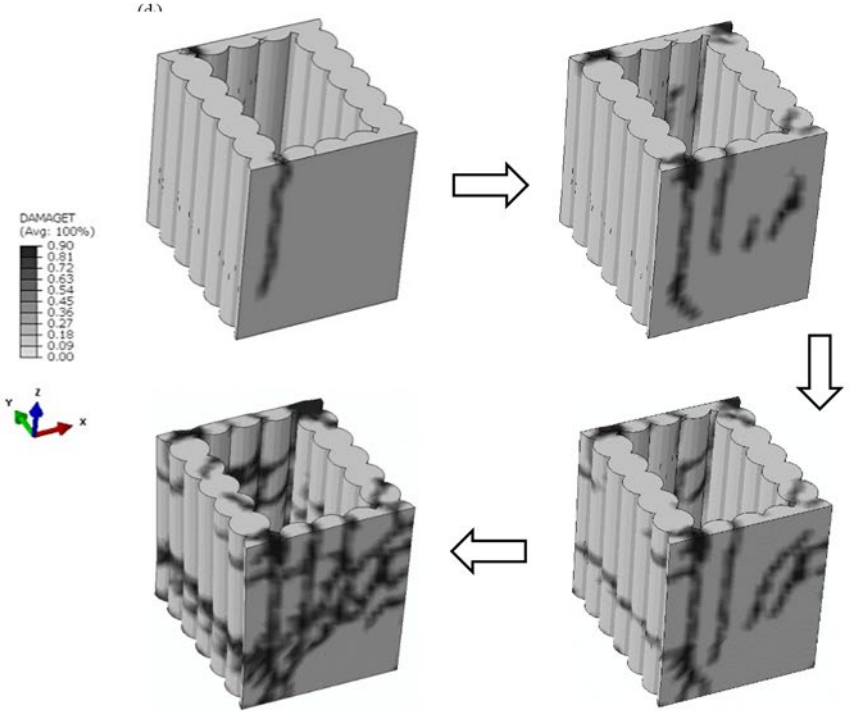

Figure 11: Progressive tensile crack development in treated columns for Case L1-3

Subsequent loading causes the columns in tangential rows to separate from one another forming new cracks in the overlap areas between columns. The grid type wall becomes vulnerable when the first crack at overlap area between the front row columns and tangential row columns continues to propagate into the embedded part till the toe of the columns. Separation of the front row columns from others results in a cantilever condition for the front columns which will then bend with maximum movement recorded at the top column. The failure is revealed when the horizontal crack propagating across the front columns from the back. Failure of the front columns induces a wedge envelope of soil sliding towards the excavated side, and also cracks on other remaining columns in the tangent row. The failure mechanism reported in Case L1-3 is thus more representative following to the observations made by Broms (2004) and Kitazume (2008).

In comparison, numerical simulation results using the WAS approach presented by Case La and Case Lb are unable to capture the right mechanism for this hypothetical case. The classical Treca model has its shortcoming of failing to address the tensile damage. Although the tension truncated Tresca model works better in capturing yielding in tensile but it tends to under-predict the damage occurred as it assumes no softening effect. Nevertheless, the aforementioned shortcomings can be addressed by the CDP model with the RAS approach.

3 CONCLUSION

This paper recommends the finite element simulation framework for the analysis of cement-treated soil used in an open excavation. The appropriateness of the WAS and RAS approaches in simulating cement-treated soil mass is evaluated. As demonstrated, it is revealed that tensile damage is the trigger for failure initiation in this retaining system. The damage process obtained with the RAS-CDP analysis is useful for understanding the failure mechanism. This phenomenological approach shows in detail the propagation of correct damage location, stress distribution and the interaction mechanism of cement-treated soil columns and untreated soil. In contrast, the numerical simulation results using the WAS approach or the Tresca model may fail to capture the possible failure happening within the treated mass.

REFERENCES

Broms, B. B. 2004. Lime and lime/cement columns. *Ground Improvement 2nd edition*: 252-330. M. P. M. a. K. Kirsch, Spon Press.

CDIT. 2002. *The Deep Mixing Method:Principle, Design and Construction*. The Netherlands, A.A. Balkema.

Kitazume, M. 2008. Stability of ground column type DM improved ground under embankment loading behavior of sheet pile quay wall. *Report of the Port and Airport Research Institute*. Nagase, Yokosuka, Japan, Port and Airport Research Institute.

Kitazume, M. and Maruyama, K. 2007. Internal stability of group column type deep mixing improved ground under embankment loading. *Soils and Foundations*, 47(3): 437-455.

Larsson, S. 1999. Shear box apparatus for modeling chemical stabilized soil - Introductory tests. *Proceedings of the International Conference on Deep Mixing, Best Practice and Recent Advances*, Stockholm,732-785.

Namikawa, T. and Koseki, J. 2006. Experimental determination of softening relations for cement-treated sand. *Soils and Foundations*, 46(4): 491-504.

Saw, A. L. 2014. Characterization and modeling of cement-treated soil column used as cantilever earth retaining structure. Ph.D, National University of Singapore.

Snitbhan, N. and Chen, W. F. 1978. Elastic-plastic large deformation analysis of soil slopes. *Computers and Structures*, 9:567-577.

Yang, H. B. 2009. Mobilised mass properties of embedded improved soil raft in an excavation. Ph.D, National University of Singapore

Hong Kong's Hidden Aggregate Resource: The Potential for Underground Quarrying

H.K.K. Chan, S.W. Millis & M.I. Wallace
Ove Arup & Partners Hong Kong Limited
K.C. Hung
Geotechnical Engineering Office,
The Government of Hong Kong Special Administrative Region

ABSTRACT

Local quarries have supported the development of Hong Kong for over 150-years through the provision of essential raw construction materials, specifically aggregates for the generation of concrete and asphalt. Although 26% of Hong Kong's landmass comprises granitic rock suitable for aggregate generation, access to about 83% of this is sterilised from surface quarrying due to a variety of socio-environmental constraints. With the majority of the existing quarries having closed in the last 20-years and no new sites established in almost 50-years, the local construction industry has grown increasingly reliant on the import of aggregate from outside of Hong Kong, with the associated issues this brings in terms of security of supply and cost control.

Although previously considered prohibitively expensive, recent increases in the cost of construction materials mean that underground quarrying could now form a technically and financially viable means of accessing rock reserves in areas hitherto considered unsuitable. Indeed, preliminary studies suggest this approach could yield sufficient resources to meet Hong Kong's aggregate requirements for well over half a century, whilst at the same time shielding the public from many of the unfavourable nuisance aspects of quarrying and also establishing a valuable land bank for underground space development.

1 INTRODUCTION

Hong Kong is often described as a 'concrete jungle (石屎森林)' and possesses one of the highest densities of skyscrapers in the world. The large volume of concrete used to achieve this means that crushed rock has become one of the fundamental materials used to build the impressive Hong Kong skyline. Apart from concrete, crushed rock forms an essential component in numerous other construction materials that make up the foundation and fabric of the city.

The crushed rock used in Hong Kong is typically obtained through surface quarrying in which blasting is used to loosen rock for excavation, which is then crushed and screened to form aggregate of varying sizes, most commonly 40 mm, 20 mm, 10 mm and 5 mm and crushed rock fines (CRF). The local rock quarry sites used to achieve this have played a significant role in the development of Hong Kong over the last 150 years, both directly through the extraction, processing and generation of aggregate and indirectly through the provision of temporary land to house NIMBY facilities such as concrete and asphalt batching plants and finally, upon quarry closure, providing a valuable land bank for residential and other development uses. However, with no new local quarries established for over 50-years, the majority of existing quarries having been progressively rehabilitated and closed over the past two

decades, and limited opportunity for the development of new surface quarry sites, the construction materials industry is in urgent need of new local supply sources for crushed rock such that it can meet Hong Kong's long-term projected aggregate demand and support the continued sustainable maintenance and development of the city.

2 SUPPLY AND DEMAND FOR AGGREGATE IN HONG KONG

2.1 Historic Supply and Demand

Quarrying is one of the oldest industries in Hong Kong, with several sites identified that date back to at least the Qing Dynasty. Although little is known about quarry operations before British colonisation in 1841, Poon (2011) reports that stone quarrying was highly active along the coastal areas of northern Hong Kong Island in the early to mid-nineteenth century and that a large proportion of the population was involved in quarrying works, with the well-known Quarry Bay area being named because of this trade. In the early days, these works were typically labour intensive permit based operations close to the areas of demand and by the 1950s numerous small-scale permit quarries had been established throughout the territory (PWD, 1966). These sites had little regulation on the way they were worked and, with the limited thought given to quarry restoration, numerous scars to the Hong Kong landscape from the works are still apparent to this day. However, increasing public concern on the impacts of quarry operations from the 1970s onwards led the Government to implement tighter control on the way they were worked and restored, first through a period of Contract Quarries and later through the use of Quarry Rehabilitation Contracts (Chan et al, 2007). These approaches focused on cleaning up the scars left by some of the more notable permit quarries through the use of large-scale modern operations that delivered a final restored landform aimed at merging the site with the surrounding environment and yielding platforms suitable for future development. The locations of notable quarry sites throughout Hong Kong, past and present, are shown in Figure 1 and good examples of the land supply benefits afforded by the quarry rehabilitation approach are shown by the on-going studies to develop the former quarry sites at Lamma and Anderson Road (Figure 2).

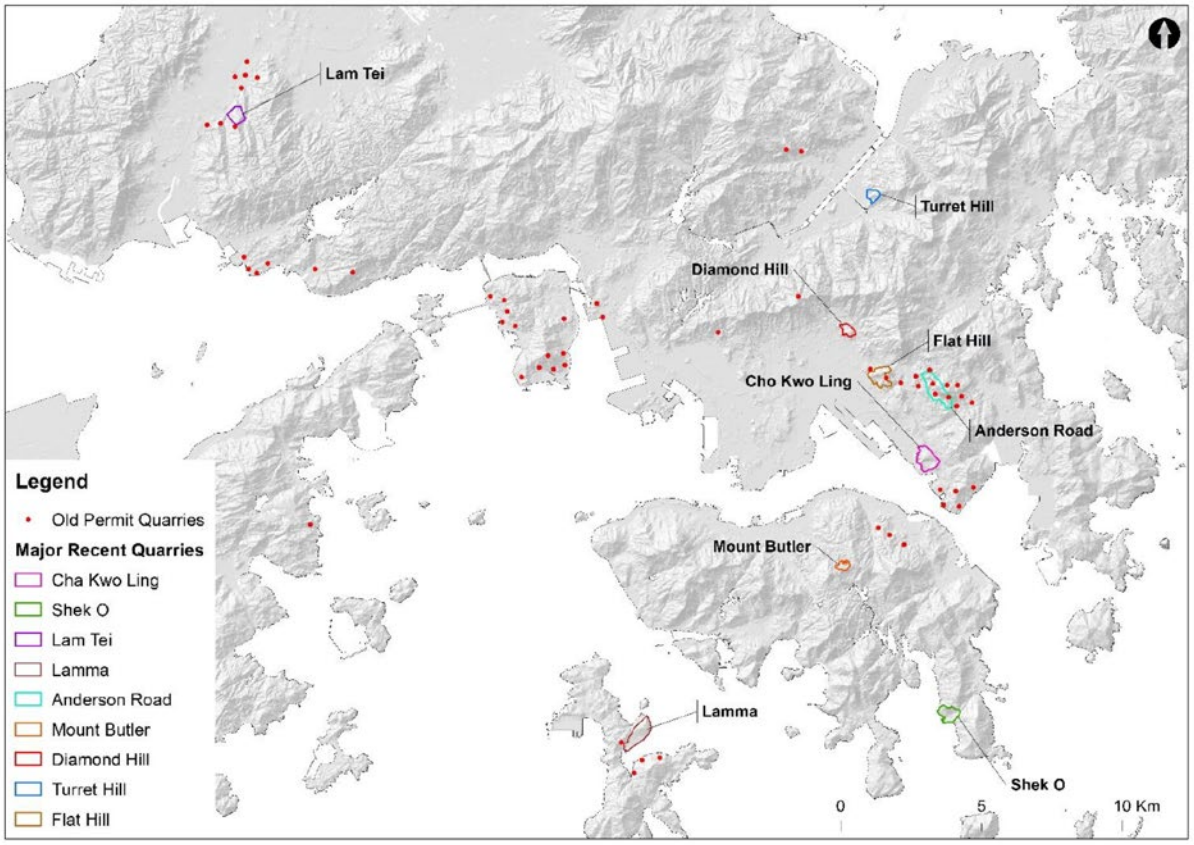

Figure 1: Location of Notable Quarry Sites in Hong Kong

Figure 2: Visualisations of the Proposed Developments at the former Anderson Road and Lamma Quarry Sites

Records maintained by the Government indicate that prior to the 1990s the demand for crushed rock in Hong Kong varied between 3Mt to 10Mt (Figure 3), virtually all of which was sourced locally either from the quarry sites or from site crushers processing and reusing/selling the material excavated from construction sites. However, the sustained period of urbanisation and development throughout the 1970s, 1980s and 1990s as a result of various reclamation projects, New Town developments and, most notably, the construction of Chek Lap Kok Airport and its associated infrastructure under the Airport Core Programme, resulted in a notable increase in the demand for crushed rock with annual consumption peaking at about 25Mt per year in the mid-1990s (Figure 3). Demand dropped significantly in the late-1990s following the completion of the Airport Core Programme and as a result of the Asian Financial Crisis and did not begin to bounce back until about 2010, when the Government began to implement the first of the 'Ten Major Infrastructure' projects outlined in the Chief Executive's 2007/08 Policy Address (CEO, 2007). These projects created a buoyant construction industry and the annual demand for crushed rock in recent years once again passed the 20Mt mark.

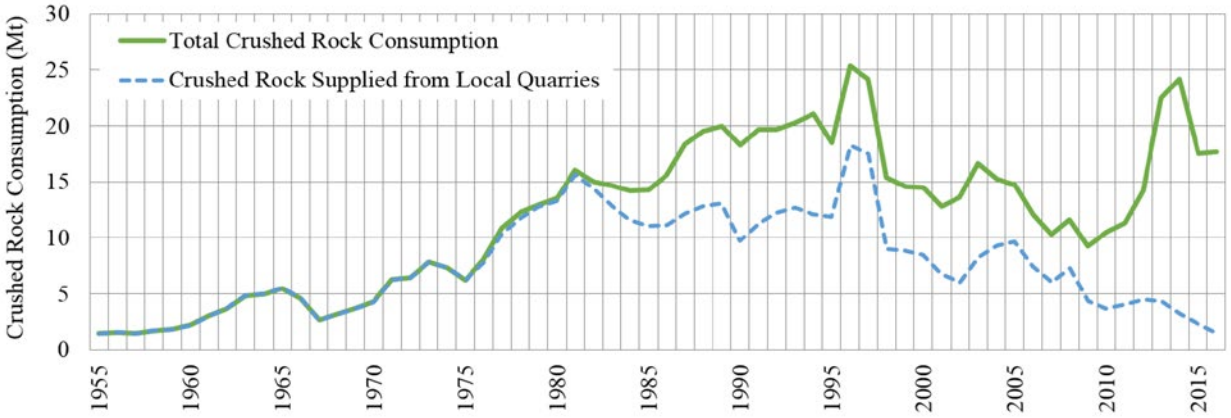

Figure 3: Historical Consumption of Crushed Rock in Hong Kong

2.2 Projected Demand

Periodic forecasts on the demand for crushed rock in Hong Kong have been conducted on a number of occasions, most notably in 1966 (PWD, 1966), 1974 (Jacobs, 1974), 1988 (GCO, 1988) and 2001 (GEO, 2001). However, the continually evolving social and political situations mean the strategies devised as part of these have seldom remained applicable in the long term. A new review was therefore initiated in late-2011 to determine both the short-term and long-term demand for crushed rock products, the existing supply situation and to establish whether there was a need for the development of new local quarry sites. This review identified a high projected annual demand for crushed rock of between 17Mt to 22Mt in the coming years (Figure 4). This demand arises from the general development and maintenance works in Hong Kong, together with the construction of the ten major infrastructure projects and the Government's commitments to provide at least 77,100 new public rental housing units over the period 2014/15 to 2018/19 (CEO, 2015). The forecast also indicates that the longer-term annual crushed rock demand would be in the order of 15Mt to 18Mt (Figure 4) once the spike arising from the above projects abates.

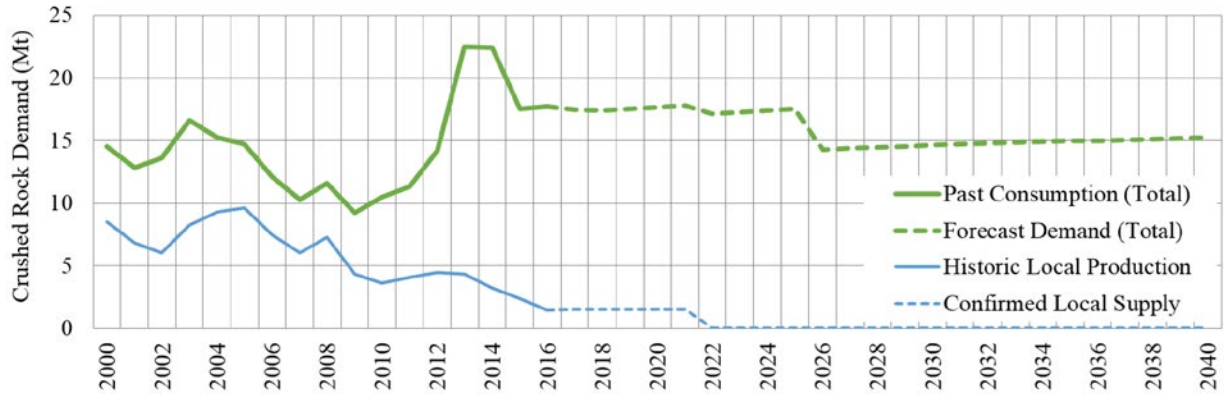

Figure 4: Projected Demand for Aggregate up to 2040

The closures of Lamma Quarry in 2002, Shek O Quarry in 2011 and Anderson Road Quarry in 2017 means that Lam Tei Quarry is now the only active site processing and supplying aggregate in Hong Kong. The production capacity of this quarry is relatively low at 1.5 to 2.0Mt per year, meaning that the amount of locally sourced aggregate has dropped to a historic low of <10% of total aggregate consumption. An increasing reliance on the import of aggregate from Mainland China arising from this situation has resulted in significant increases to the cost of aggregate over the past decade, during which time aggregate prices have almost doubled (Figure 5). The sustained high projected demand for aggregate together with the low degree of supply security currently provided by local quarry sites means that the trend of cost increase is likely to continue in the future unless measures are taken to enhance the local sources of aggregate supply.

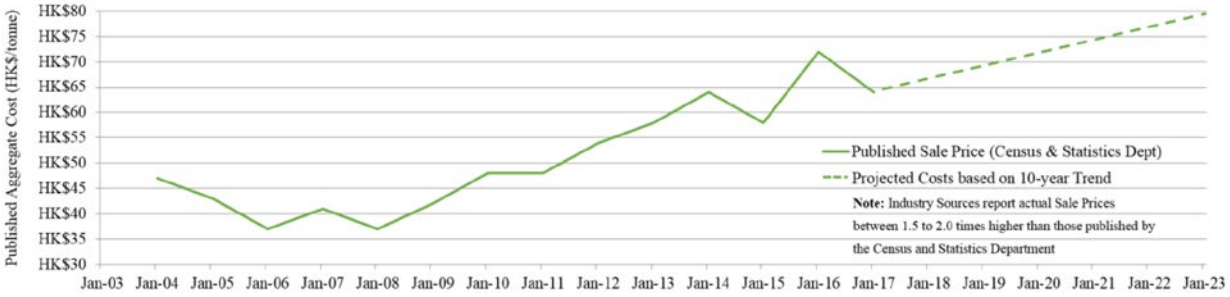

Figure 5: Aggregate Cost Trends

In order to combat any adverse impact to the construction industry arising from escalating costs, the Government determined that there was an immediate need to identify and develop new local quarry sites such that a reliable supply and stable price of crushed rock products in Hong Kong could be maintained. However, a detailed territory-wide site search for potential new surface quarry sites revealed that much of the granitic rock in Hong Kong is sterilised from surface quarry development due to various socio-environmental constraints (e.g. proximity to urban area, presence of Country Parks, etc.) and only three potentially suitable new surface quarry sites were identified (Figure 6). Preliminary feasibility assessments for these sites suggests that rock reserves in the order of 76Mt could be realised from them over the period 2022 to 2043, which would account for between 10% to 50% of the projected total aggregate demand. Although this could provide a reasonably robust supply of crushed rock to the local construction industry, a significant proportion of the market would still be dependent on material supply from the Mainland. As such, a number of alternative supply sources were also explored, including the continued and enhanced re-use of suitable construction spoil as well as the potential for underground quarry development.

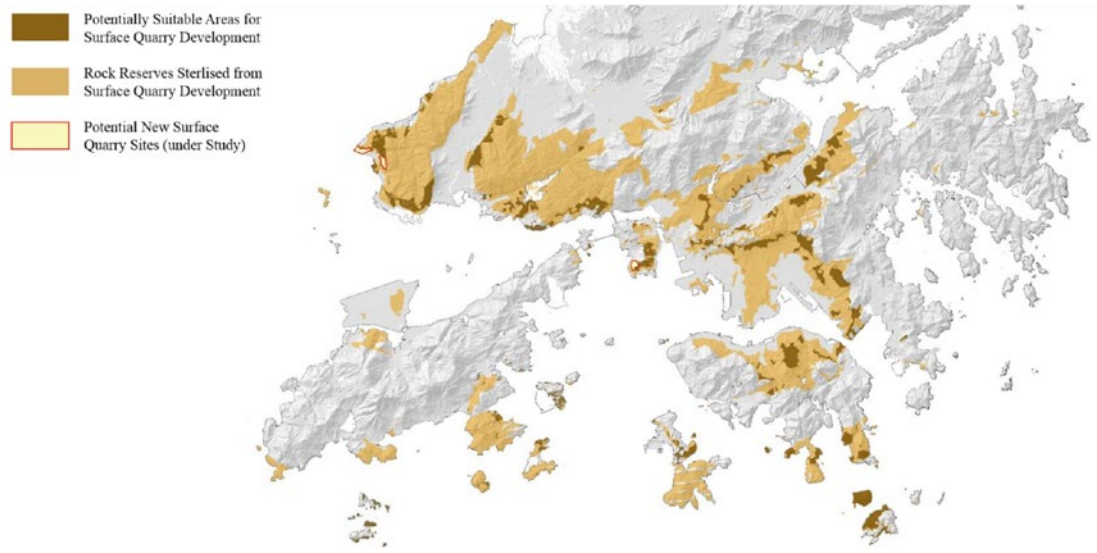

Figure 6: Hong Kong Rock Reserves and Potential New Quarry Sites under Investigation

3 UNDERGROUND QUARRYING

3.1 Concepts and Mechanisms

Approximately 26% of the landmass in Hong Kong comprises granitic rock that is suitable for use as aggregate, although about 83% of this is severely constrained from surface quarrying due to its proximity to the urban area or overlap with protected areas such as Country Parks (Figure 6). However, many of the adverse impacts precluding quarrying in these areas (i.e. noise, dust, landscape and visual impacts and direct ecological impacts) could be greatly reduced, if not all together eradicated, by moving the rock extraction underground. This suggests that underground quarrying could provide a mechanism of accessing the valuable rock reserves within the sterilised areas, forming a means to further support rock supply from surface quarry sites and thus enhancing the proportion of aggregate supply that could be sourced locally. In addition to the socio-environmental advantages of shifting quarry workings underground, well planned underground quarrying also has the potential to create a land bank of rock caverns ('Cavern Land') that could be retrofitted following the completion of quarrying and subsequently leased out to either public or private sector end users.

Underground quarrying essentially adopts techniques and approaches from the mining industry to facilitate the bulk extraction of rock in a systematic and cost-effective manner. In order to achieve this the works are undertaken in a highly mechanised manner using self-supported mining layouts such as Room and Pillar or Bord and Pillar excavations so that there is minimal need for the provision of additional roof support (Figure 7). The Room and Pillar method comprises the excavation of a rectangular grid of caverns separated by pillars of in-situ rock left in place to support the overburden above. Either square or rectangular pillars can be used depending on the characteristics of the rock mass, with past experience suggesting that pillar width to height ratios should not be less than 0.8 and a factor of safety of 1.8 should be adopted when checking pillar strength / stability. The Bord and Pillar mining method is similar to Room and Pillar in the longitudinal direction but does not include excavation between the longitudinal chambers, resulting in a series of parallel chambers separated by supporting walls. Each working section is essentially an autonomous system that is accessed via one or two adits. In order to gain the most benefit from this system, the cavern orientation should be parallel to the principal stress direction, thus keeping the lateral pressure on the chambers to a minimum. The efficiency of these types of mine workings are measured in terms of their areal exploitation ratio, which is the ratio between the excavation (cavern) area and the supporting area per pillar. In areas with good rock mass quality, spatial exploitation ratios in the order of 40% to 70% can be achieved. This can be further increased through the use of multi-level excavations, in particular when the Bord and Pillar approach is adopted.

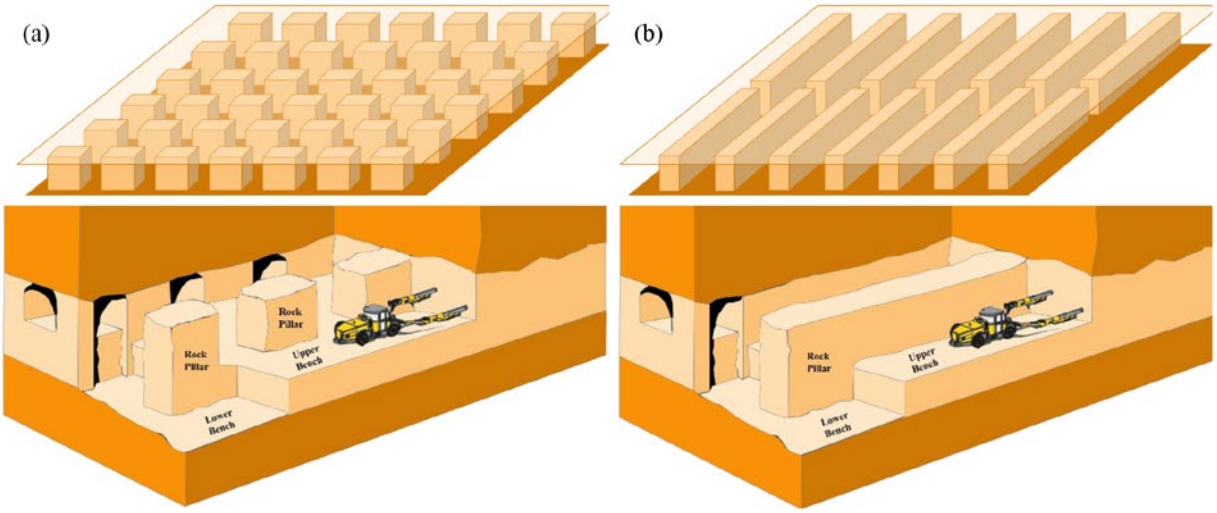

Figure 7: Schematic of (a) Typical Room and Pillar and (b) Pillar and Bord Mine Workings

3.2 Overseas Examples

Rock from tunnelling and cavern projects in Hong Kong has frequently been taken to quarry sites for processing into aggregate and the concept of local underground quarrying is not new, having first been considered in 1974 during the Investigation of Quarries (Jacobs, 1974). However, there are no previous examples of sites developed specifically for the purpose of underground quarrying in Hong Kong. In order to further investigate the feasibility of this approach a comprehensive literature search was therefore undertaken to identify overseas examples that could serve as reference cases on the drivers for underground quarry development as well as the technical and financial approaches adopted during the investigation, development, operation and, for those cases where quarrying has ceased, after-use of the sites. The review identified the presence of a number of notable active, or recently closed, underground quarries developed specifically for the extraction of aggregate or dimension stone at various locations worldwide, including the United States, the United Kingdom, Switzerland, Norway, Greece, Italy, and Japan (Figure 8).

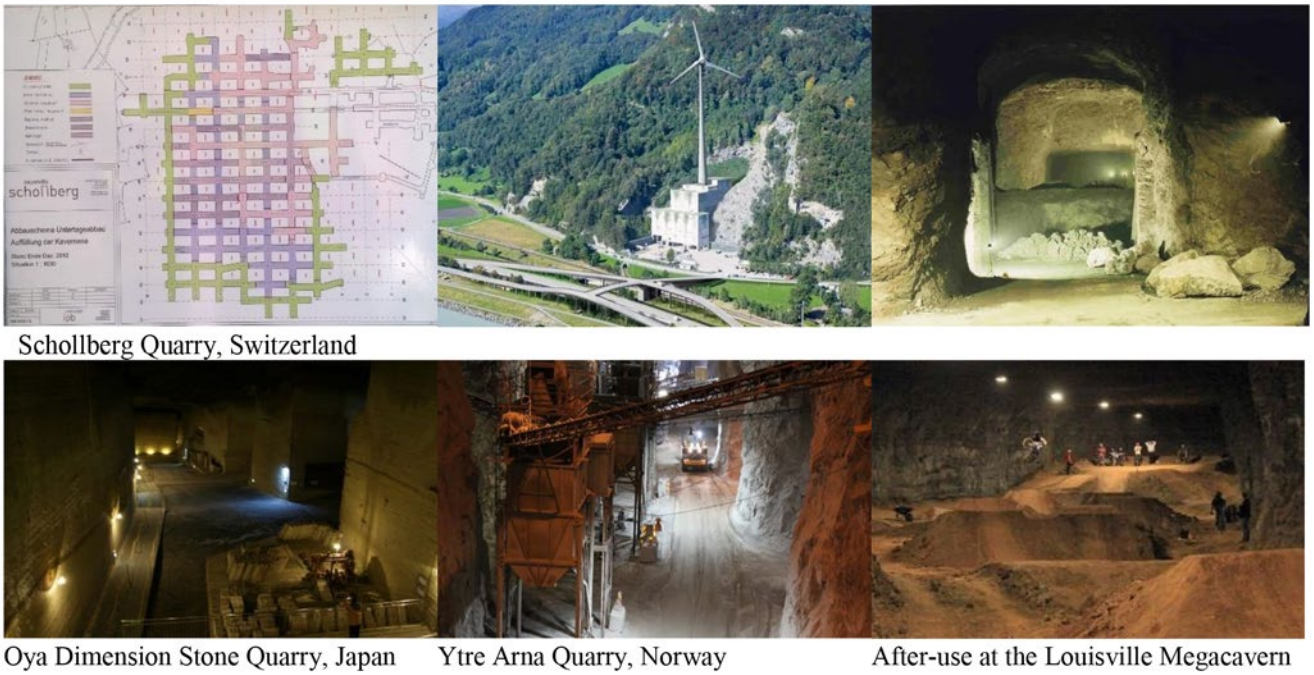

Figure 8: Examples of Selected Overseas Underground Quarry Sites

Similar to the situations now driving the investigation of underground quarrying opportunities in Hong Kong, the decision to take quarrying underground at these locations typically arose as a result of social and environmental constraints precluding the establishment of surface quarries. The sites identified have generally been worked following either a Room and Pillar or Pillar and Bord approach, with extraction rates in the order of 0.2 to 0.5 Mt depending on the specific demand from the region in which they are located. Rock processing has been undertaken by plant set up either within the underground excavation itself (i.e.Ytre Arna Quarry) or purpose built facilities at the excavation portal (i.e. Schollberg Quarry). A number of sites, in particular those located in the United States (e.g. Louisville Megacavern and Kansas Subtropolis), also provided good examples of how the space yielded by underground quarrying can be utilised for a variety of commercial, industrial and recreational land-uses.

3.3 Local Opportunities

Potentially suitable sites for underground quarrying in Hong Kong were identified through a systematic territory-wide site search of the potentially suitable granitic rock reserves presented in Figure 6. These reserve areas were further screened to identify the presence of potential portal areas located outside of constrained areas such as Country Parks (i.e. within those areas deemed suitable for surface quarry development) and to take due consideration of any geotechnical, environmental and traffic connectivity issues that would significantly impact and constrain the feasibility of underground quarry development. The screening exercise identified a total nineteen potential underground quarry sites, the locations of which are presented in Figure 9.

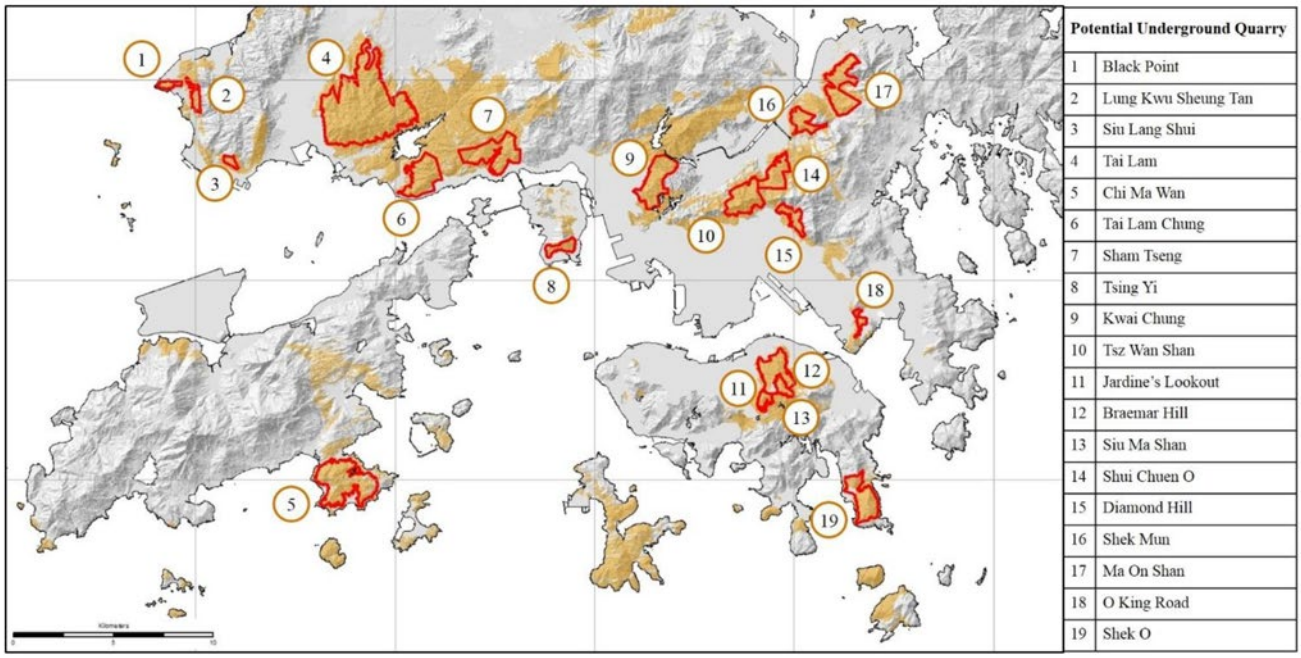

Potential Underground Quarry	
1	Black Point
2	Lung Kwu Sheung Tan
3	Siu Lang Shui
4	Tai Lam
5	Chi Ma Wan
6	Tai Lam Chung
7	Sham Tseng
8	Tsing Yi
9	Kwai Chung
10	Tsz Wan Shan
11	Jardine's Lookout
12	Braemar Hill
13	Siu Ma Shan
14	Shui Chuen O
15	Diamond Hill
16	Shek Mun
17	Ma On Shan
18	O King Road
19	Shek O

Figure 9: Location of Potential Underground Quarry Sites in Hong Kong

The suitability of these sites were further assessed through preliminary assessments of their reserve size, accessibility and connectivity, interface issues with existing infrastructure and utilities, and interface issues with other planned projects. Sites considered to warrant prioritised site-specific assessment were classified as High Suitability. Most favourable amongst these were sites with readily accessible reserves through existing rock/quarry faces. Sites warranting further consideration, provided that the specific constraints identified during the review could be resolved, were classified as Moderate Suitability, whilst sites with either significant constraints or low reserve volumes were classified as Low Suitability. The results of the site screening are presented in Table 1, which indicates that of the nineteen sites identified, six can be considered to have a high degree of suitability for underground quarry development whilst a further five sites were classified as having moderate suitability. The remaining

eight sites appear to offer limited potential for underground quarrying individually but could still yield rock reserves from any cavern developments in the area.

Table 1: Summary Underground Quarry Site Suitability Assessment

High Suitability Sites	Moderate Suitability Sites	Low Suitability Sites	
Tai Lam	Sham Tseng	Black Point	Jardines Lookout
Shek Mun	Kwai Chung	Lung Kwu Sheung Tan	Siu Ma Shan
Ma On Shan	Diamond Hill	Siu Lang Shui	O King Road
Tai Lam Chung	Chi Ma Wan *	Tsing Yi	Braemar Hill
Tsz Wan Shan	Shek O *		
Shui Chuen O	(* Denotes sites that are only feasible utilising marine access for material haulage)		

3.4 Feasibility of Underground Quarry Development

In order to further establish the feasibility of underground quarrying in Hong Kong, preliminary technical and financial assessments were conducted for the site identified at Tai Lam (Figure 10). This site was selected due to the large potential rock reserve present (>200 Mt) as well as the ease with which this could be accessed through the existing rock faces within the Lam Tei Quarry site. Quarry layouts were established following a room and pillar mining approach, with the initial geotechnical assessments indicating that 12m wide by 18m high caverns supported by 15m diameter pillars at 27m centre to centre spacing would provide adequate support (Figure 10). The final site layout covered an area of 550 hectares and would realise a rock reserve of approximately 165Mt with an excavation efficiency of about 65%. In view of the underground nature of the works, the assessment assumed that the quarry would operate around the clock six days per week, resulting in an annual production of about 1.5Mt of crushed rock on the basis of two blasts per day and a daily excavation rate of about 5,000 tonnes. This means that the site could support the local construction materials market for upwards of 100-years if necessary.

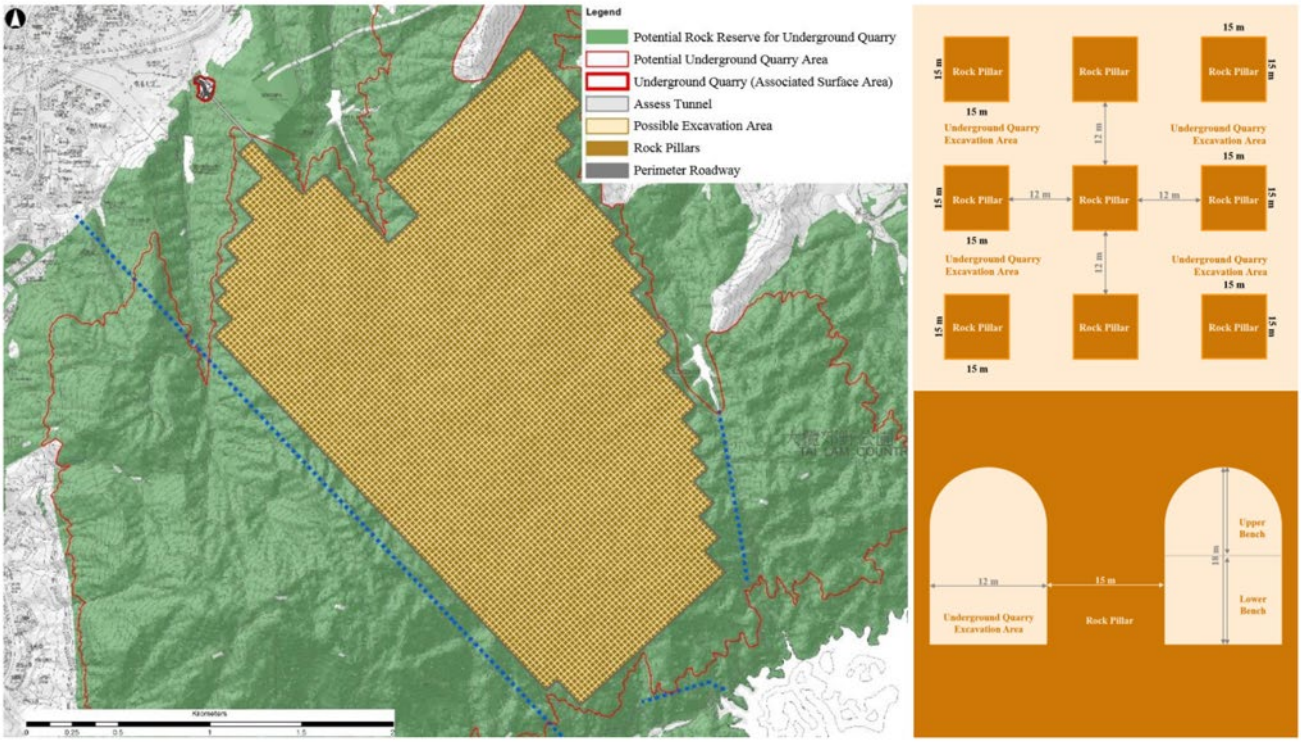

Figure 10: Conceptual Underground Quarry Layout for the Tai Lam Site

An initial business case for the quarry scheme was established following approaches similar to those developed by Brown et al (2010) during their investigations on the feasibility of underground quarrying in the U.K. This showed that although the costs associated with underground quarrying are likely to be almost double those within an equivalent surface quarry, the escalation of aggregate price over the last 10-years means that relatively large-scale underground quarries (i.e. > 20Mt reserve) could still constitute a financially viable approach to rock supply provided that operators are given the right to import and process rock from construction sites as well as the rights to generate and sell construction materials such as concrete and asphalt.

3.5 Synergy with Land Supply

In parallel with the search for underground quarry sites, the Government has also been developing strategic plans for the long-term development and use of rock caverns. This work has resulted in the delineation of a number of Strategic Cavern Areas (SCVAs) throughout Hong Kong (Ho et al, 2016), a number of which overlap with the potential underground quarry areas shown in Figure 9. This overlap presents notable opportunities for the cohabitation and development of sites for both underground quarrying and cavern development (Figure 11), with shallow portions excavated following predefined layouts that facilitate future cavern development and require minimal retrofitting, whilst deeper portions are excavated using mining approaches to yield the rock in the most cost effective manner, thus providing a win-win situation for both land and crushed rock supply.

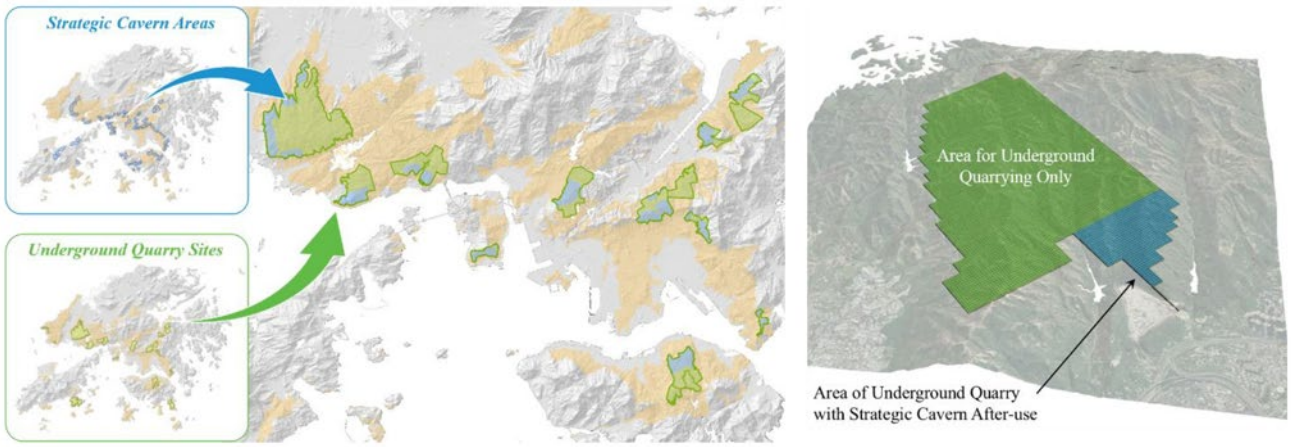

Figure 11: Opportunities for integrated underground quarry and rock cavern development

3.6 Potential Hurdles to Local Implementation

Whilst underground quarrying has been implemented in a number of parts of the world and research shows that numerous areas exist locally where this approach could be technically and financially viable, the unique conditions in Hong Kong mean that the feasibility of underground quarrying is still far from certain.

Although Hong Kong has a Mining Ordinance, this document was established in 1954 and primarily relates to the working of metalliferous ores and kaolin. Indeed, granite, porphyry and limestone are excluded from all parts of the Ordinance other than Section 3, which simply states that such minerals shall remain the property of the Government. This lack of specific legislation means that an underground quarry would currently need to be operated in the same manner as an underground construction site and would be subject to the same controls placed on these through ordinances and regulations such as the Factories and Industrial Undertakings Ordinance, Occupational Safety and Health Ordinance, etc. The ancillary facilities for the quarry (i.e. crushing and screening plant) would be classified as a building and subject to the controls of the Building Ordinance.

Although the majority of these controls still have direct relevance to an underground quarry, distinct differences exist in the way rock is extracted from an underground quarry as compared to an

underground construction site. Foremost amongst these is the fact that underground construction sites are designed with the final land-use and long-term safety of facility occupants in mind. This results in the use of notable ground support and waterproofing measures to ensure the space created is both safe and comfortably habitable. In contrast, an underground quarry will look to extract rock in the most cost-effective manner, without specific consideration to after-uses of the space created as this would typically remain vacant until completion of quarrying. To achieve this, the sites are operated in a highly mechanised manner with only a handful of staff present underground at any one time. These lower risk conditions, together with the use of self-supporting room and pillar / pillar and bord mining approaches, mean that limited importance is placed on the local stability of the excavation and the control of groundwater inflow. Adoption of such approaches in Hong Kong would likely require a notable change in the mind set of regulators before they could be widely implemented. Similarly, the strict fire safety, ventilation and evacuation controls imposed on underground facilities would also likely prove excessively restrictive if directly imposed upon an underground quarry, especially so given the low occupancy of the sites and the limited extent of areas that would be operational at any one time.

Despite providing some limitations and concerns to the future development of underground quarries in Hong Kong, the above matters are not considered insurmountable and could likely be addressed and resolved through further detailed assessment and, where necessary, development of new or updated standards specifically set out to control the operation and impacts of an underground quarry. To this end, it is noted that the Government is in the process of taking forward an initiative to further investigate and resolve the key issues influencing the feasibility of underground quarry development and operation in Hong Kong.

4 CONCLUSIONS

A steady and secure supply of construction materials is essential to the continued prosperity and sustainable development of Hong Kong. Traditionally construction materials, in particular crushed rock for use as aggregate, have been sourced from local surface quarry sites. However, as the urban area of Hong Kong has expanded and environmental controls and concerns have grown, our ability to continue sourcing aggregate from local surface quarry sites has diminished and Hong Kong has grown increasingly reliant on imports from Mainland China. This situation and a recent spike in the number of mega-infrastructure and development projects has resulted in notable competition for the limited resources available, with associated increases in the cost of construction materials. With only one local quarry site now operational, this situation is only likely to get worse in the years ahead unless measures to secure a consistent local supply of aggregate are found.

With recent territory-wide site searches revealing limited potential for the development of new surface quarry sites, the Government is now looking to more innovative and unconventional sources of aggregate supply. Foremost amongst these in terms of its ability to yield a consistent and long-term supply of crushed rock is the use of underground quarrying, with initial assessments suggesting this could provide a technically and financially viable mechanism of securing a long-term local supply of aggregate.

ACKNOWLEDGEMENTS

This paper is published with the kind permission of the Head of the Geotechnical Engineering Office and the Director of the Civil Engineering and Development Department of the Government of the Hong Kong Special Administrative Region.

REFERENCES

Brown, T.J., Coggan, J.S., Evans, D.J., Foster, P.J., Hewitt, J., Kruyswijk, J.B., Millar, D.L., Smith, N. & Steadman, E.J. 2010. *Underground Mining of Aggregate*. Mineral Industry Research Organisation. Department of Environment Food and Rural Affairs. United Kingdom, 322p.

Chan G, Pallot D, Hogan D. 2007. The Evolution of the Quarrying Industry in Hong Kong. Providing a Visionary Approach to the "Life Cycle of a Site". *Institute of Quarrying Australia Conference, Hobart, Australia, 2007.* Institute of Quarrying.

Chief Executive Office. 2007 & 2015. *Policy Address*. The Government of HKSAR, Hong Kong.

Geotechnical Control Office. 1988. *Quarry Policy Review. Administrative Report AR 3/88*, Geotechnical Control Office, Civil Engineering Services Department, Hong Kong, 52p.

Geotechnical Engineering Office. 2001 to 2011. *Natural Resources Report (2001-2011) Study on the Need for Future Quarrying in Hong Kong.* Geotechnical Engineering Office, Civil Engineering and Development Department, Hong Kong.

Ho, Y.K., Shum, K.W. & Wong, J.C.F. 2016. Strategic Use of Rock Caverns and Underground Space for Sustainable Urban Development of Hong Kong. *15th International scientific conference on Underground Urbanisation as a Prerequisite for Sustainable Development*. Procedia Engineering 165 (2016) pp. 705-716.

Jacobs Associates. 1974. *Investigation of Quarries*. Civil Engineering Office, Public Works Department, Hong Kong, 83p.

Poon SW, Ma KY, Man KF and Tsin TW. 2011. The Quarry Licensing System in Hong Kong 1841-1941. *Hong Kong Quarrying Conference 2011: Revelations of the Hong Kong Quarrying Industry, Yesterday, Today & Tomorrow.* Institute of Quarrying (Hong Kong Branch), Hong Kong.

Public Works Department. 1966. *Quarry Report*. Roads & Drainage Division, Civil Engineering Office, Public Works Department, Hong Kong, 23p.

An Innovative Earth Supporting System for a Deep Excavation

Raymond Chan Kin Sek, Clifford Phung Wing Cheung &
Carmen Lau Wan Chi
Meinhardt Infrastructure and Environment Ltd.

ABSTRACT

This paper discusses the development of an innovative and robust Excavation and Lateral Support System for the 21.5m deep excavation and the various measures taken to ensure that the existing hospital buildings and their facilities will be fully operational throughout the entire stage of the construction.

1 INTRODUCTION

The proposed Building Block A consists of two 18-storey towers, each with 3 levels of basements and the building will be founded on bored piles.

Conventional ELS consisting of struts and walings across the entire site would likely result in significant ground movement of some 50 mm which is well in excess of the generally acceptable limit of 25 mm. An innovative design would have to be developed, to limit ground movements due to excavation, provide adequate working space within the excavation and minimize construction cost and time.

2 SITE DESCRIPTION

The site area of the proposed Building Block A is approximately 13,000 sq.m and the existing ground level of the site is about +61.0mPD.

The site is currently occupied by four existing buildings and these buildings will be demolished prior to the excavation and lateral support works.

The existing SITE is generally built on a flat platform on the north at a level of about +61.0mPD and the ground level gradually reduces to +47.4mPD on the south. Along the eastern boundary there is a strip platform with a level of about +64.5mPD. The rockhead varies from about +55mPD near the northern site boundary to about +20mPD towards the southern boundary.

Around the SITE, there is a number of geotechnical features with a maximum height of 30m. The proposed Building Block A is located on a flat platform at around +61mPD and surrounded by a number of slopes. On three sides of the proposed building, the site is surrounded by existing fill slopes up to 16m high and retaining walls of 4m high maximum.

3 DEVELOPMENT OF SCHEME DESIGN FOR BASEMENT CONSTRUCTION

During the scheme design stage, consideration has been given to the merits of different options for the basement construction with respect to the client's requirements, existing ground conditions, statutory requirements, environmental consideration, site constraints, extent of ground movements and cost and construction time.

3.1 Statutory Consideration

The building proposal shall comply with the Buildings Ordinance and related Regulations and Practice Notes for Authorized Persons, Registered Structural Engineers and Registered Geotechnical Engineers (PNAP).

3.2 Environmental Consideration

As the site is located in a hospital area, noisy and dusty operations, such as pile driving or hard chiseling will have to be avoided. Water discharging from the site would be filtered to a high quality to fulfil the EPD's requirements. All these requirements needed to be incorporated in the specifications and implemented during the site works.

3.3 Site Constraints

The site is situated in a crowded area and surrounded by various sensitive structures. The distance of the sensitive receivers is generally 8m, which is found on bored piles and caissons. The basement construction shall be carried out in such manner that it will not cause significant ground movement and groundwater drawdown or vibration.

In addition, there are a number of utilities adjoining the site. Excessive movement or vibration may cause damage to these services. As the site which is about 100m by 100m is relatively large, the impact of the space constraints on various schemes would have to be carefully evaluated.

4 OPTIONS FOR BASEMENT CONSTRUCTION

4.1 Top-down Method

Top-down construction technique allowed a fast track construction programme which would allow basement construction concurrently with the superstructure construction, thereby shortening the construction programme of the whole project. However, as this method will involve excavation in the confined area, the amount of time savings would depend on the actual ground conditions and obstructions encountered.

Since the high rock head level could require longer excavation time and may involve higher cost for the rock excavation works under a confined working condition and localized removal of the existing foundation system and basement will be required before the construction of the footing for the new superstructure. These works will actually lengthen the construction period and may result in higher construction risk (i.e. unforeseen factors and unfavorable ground conditions) for the redevelopment.

4.2 Temporary Circular Cofferdams Method

Conventional excavation and lateral support system consisting of pipe pile/bored pile wall supported by struts (with preload) across the site was generally adopted. However, assessments indicated that the movements of the temporary wall and adjacent ground would be of the order of 50mm and would be unacceptable. To form a more robust supporting system, 4 temporary circular cofferdams formed by pipe piles would be constructed to support the struts for lateral earth pressure. Analyses showed that the movements would be significantly reduced to 22mm by adopting this scheme. Also, the cost and construction period of this scheme is lower than those of the conventional scheme.

5 OPTION FOR TYPE OF PERIMETER WALL

5.1 Contiguous Bored Pile Wall

Machine dug contiguous bored piles of diameter of 1.5m would be constructed with temporary steel casing down to the necessary cut off level. This method would involve smaller disturbance to the

surroundings and avoid dewatering problems. It can be constructed through the bouldery colluvium layer without any particular problems by using reverse circulation drilling technique. One additional advantage of the use of bored piles is its flexibility to fit the shape corner of the site, such that the usable floor area can be maximized. On the northern half of the site where the existing ground level is higher, a stiffer wall system would be needed to minimize ground movements due to excavation. Contiguous bored pile wall would be the preferred option in this area.

5.2 Pipe Pile Wall

On the other parts of the site where the depth of excavation is about 21.5m, a less stiff but more economical steel pipe pile wall would be installed. A grout curtain behind the wall is provided to ensure watertightness. This type of wall is fast to construct and the vibration and noise induced would be negligible. Although, the wall can only serve as a temporary structure and a permanent basement wall would be required, the watertightness of the pipe wall is easy to control. Long term maintenance cost would also be relatively low.

6 EXCAVATION AND LATERAL SUPPORT WORKS

Since the excavation is up to depth of 21.5m, the Excavation and Lateral Support (ELS) Works have to be sufficiently stiff and robust to provide safe ELS while at the same time, the deep excavation will not lead to undue movement of adjoining land and buildings, in particular, when the existing hospital buildings and their facilities will be fully operational throughout the entire construction stage.

After consideration of various temporary walling systems, a hybrid bored pile wall and pipe pile wall have been proposed at different edges of the site and supported by a strutting system.

6.1 Flotation for Both Temporary and Permanent Cases

To guard against flotation after demolition of the existing building and prior to completion of the superstructure, grout curtains would be installed along the existing basement wall with penetration into bedrock. The effectiveness of the grout curtain would be verified by pumping tests and the groundwater level under the existing basement slab would be drawn down to the likely lowest level during the basement and foundation construction. After construction of the proposed foundation system and during the basement excavation, groundwater monitoring would continue to be carried out inside the basement to ensure that no upthrust will be induced on the constructed foundation system. Water relief wells would also be provided for water pressure release against water uplift during foundation, basement and superstructure construction, if necessary. The full cut-off of the basement structure to the existing groundwater regime would be assessed at various stages of the basement and superstructure construction to ensure that the substructure/foundation system would possess adequate factor of safety of (1.5) against flotation. In view of the low permeability of the rock layer, the likelihood of developing upthrust loading on the foundation system would be low. Based on the above, there would be no uplift problem during the construction stage.

On completion of the superstructure, the water uplift force due to floatation would be resisted by the self-weight of superstructure plus tension piles to comply with the Building (Construction) Regulation.

7 Geotechnical Design

Results of the analyses of the soil/structure interaction of the basement excavation within the pipe pile wall and bored pile wall are described in this section. The analyses have been carried out using the BD approved programs “PLAXIS”.

7.1 Geotechnical Model

Geotechnical model has been developed based on the site investigation results and design requirements. In this project, the major geotechnical design parameters include shear strength parameters, earth pressure coefficients, stiffness of soil matrix, inferred rockhead level and groundwater conditions.

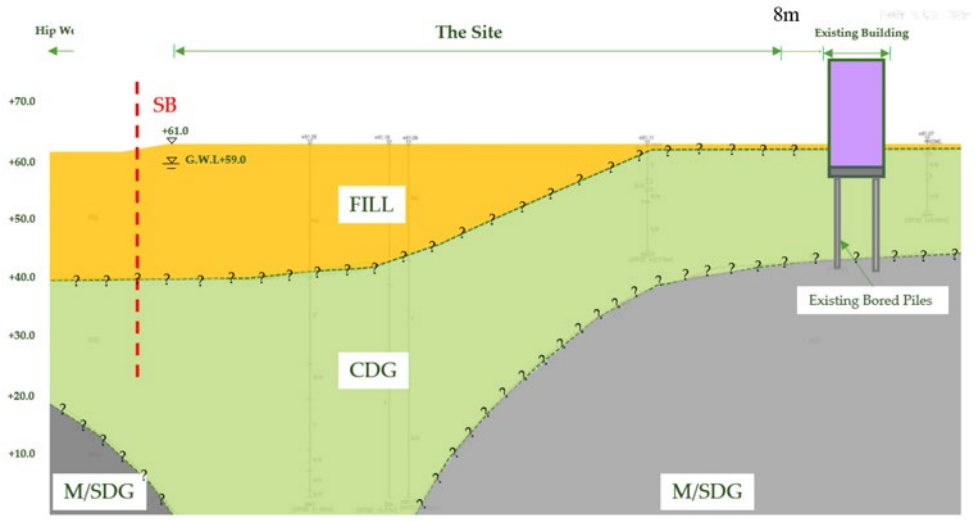

Figure 1: Ground Profile

7.2 Geotechnical Design Parameters

Shear strength parameters of soils are important in various geotechnical designs, e.g. assessing earth pressure on the pipe pile/bored pile wall. As revealed in the ground investigation, the ground mainly composes decomposed granitic rocks. Therefore, conventional single stage consolidated undrained triaxial tests with pore pressure measurements were conducted on undisturbed mazier samples saturated with back pressure. The laboratory test results were plotted on s'-t plot for each type of soil and the c' and ϕ' were obtained for the appropriate stress ranges

Lateral earth pressure coefficients were estimated based on the shear strength parameters for various types of soils and are summarized in Table 1.

Table 1: Summary of Soil Parameters & Earth Pressure Coefficients

Type of material	Unit weight, r' (kN/m^3)	Cohesion, c' (kPa)	Friction angle, Ø'	Active earth pressure coefficient, Ka	Passive earth pressure coefficient, Kp
Existing Fill	19	0	35	0.25	6.23
CDG	19	6	37	0.23	7.57
HDG	19	10	40	0.21	9.45

The SPT N-values taken from the existing boreholes were used to estimate the stiffness of the soils. For correlation between SPT N-values and effective stiffness of soils, E' = 1 x 'N' MPa as recommended in Stroud has been used. The adopted Young's Modulus for various types of soils are summarized in Table 2.

Table 2: Summary of Young's Modulus of soil

Soil Stratum	SPT-N	Soil Young's Modulus, E (kPa)
Fill (Above 40mPD)	10	10000
Fill (Below 40mPD)	15	15000
CDG (Above 35mPD)	25	37500
CDG (Below 35mPD)	200	300000

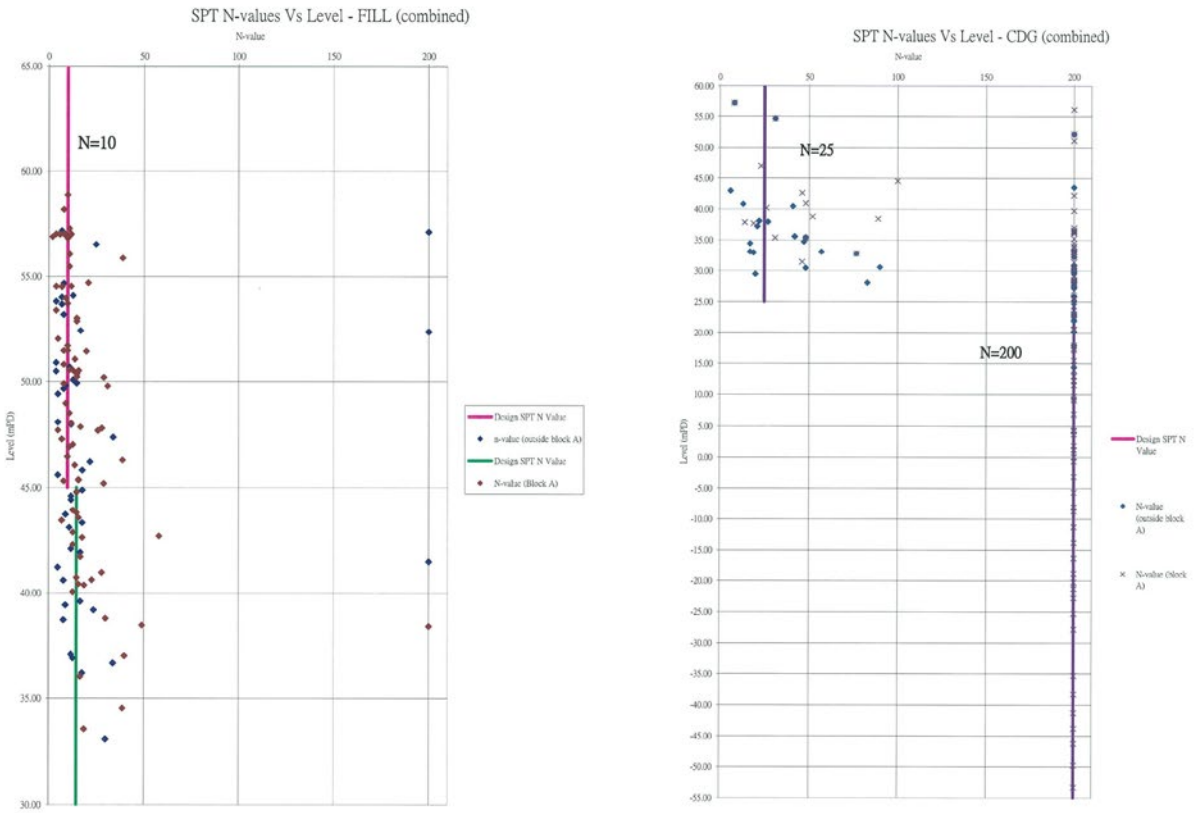

Figure 2&3: SPT N-values for Fill and CDG

7.3 PLAXIS Analysis

The BD approved computer programme "PLAXIS 2011" (B.D. ref. G0169) has been used to analyse the overall serviceability and the structural analysis of the lateral support system. Based on the varying soil profiles and excavation need, critical sections are designed to represent the worst case scenario for the pipe pile wall and bored pile wall design.

To form a robust supporting system, the temporary wall would consist a combination of pipe piles and bored piles. As contrast to the conventional strut and waling system across the entire site, the struts would be supported by 4 temporary circular cofferdams (18 m diameter) formed by pipe piles at 3m centres with concrete ring beams at each strutting level. To cater for possible variations in forces

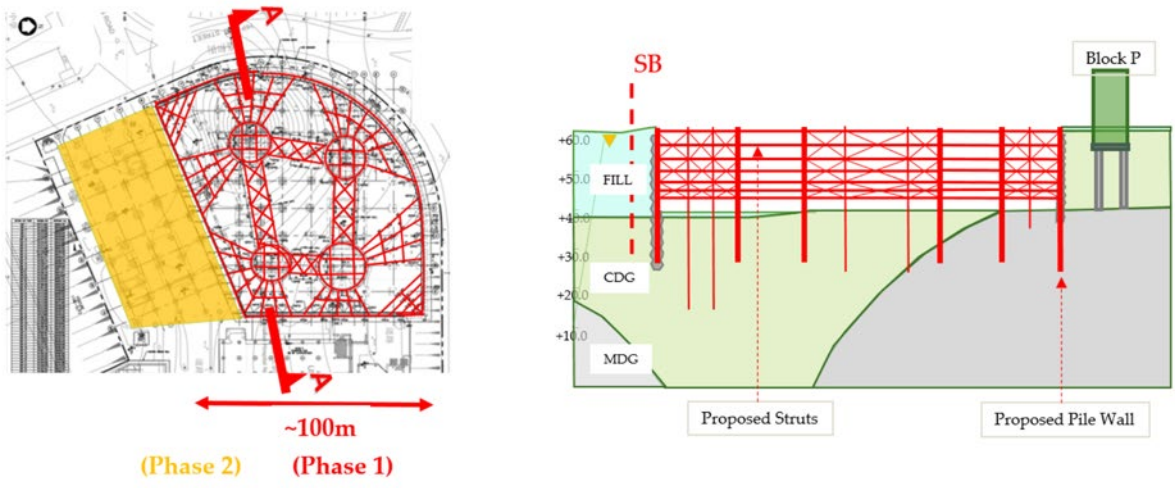

Figure 4: Plan and section of the temporary circular shafts ELS scheme

transmitted from the struts, adequate cross-bracings would be provided across the ring beams of the cofferdams. A PLAXIS model has been developed based on the geological and groundwater conditions of the site. PLAXIS analyses indicate ground movements to be significantly reduced to 22 mm. In assessing the cost-effectiveness of the Scheme, our estimates indicate that the cost is much lower than the conventional scheme. There were also bracings within each ring structure to enhance the rigidity. These 4 ring structures would be tied together by structural steel works, thus forming a single stiff structure. Form the structural analysis, the maximum movement of circular cofferdams is 3.8mm. (Figure 8 & 9)

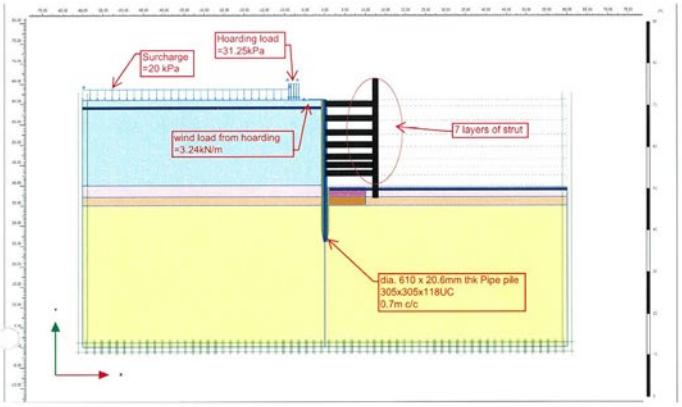

Figure 5: Design Assumption for PLAXIS Model

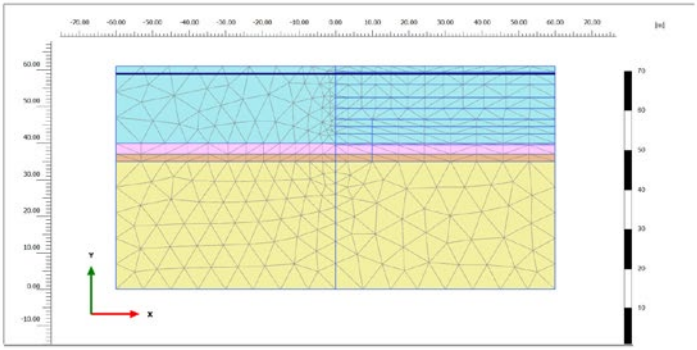

Figure 6: The PLAXIS Finite Element Grid for the Ground before Excavation

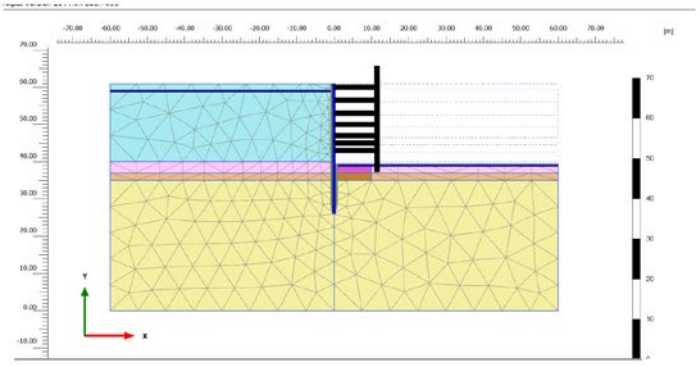

Figure 7: The PLAXIS Finite Element Grid for the Excavated Ground with Strutted Support

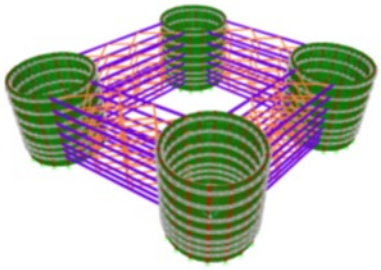

Figure 8: Structural Model of the temporary circular

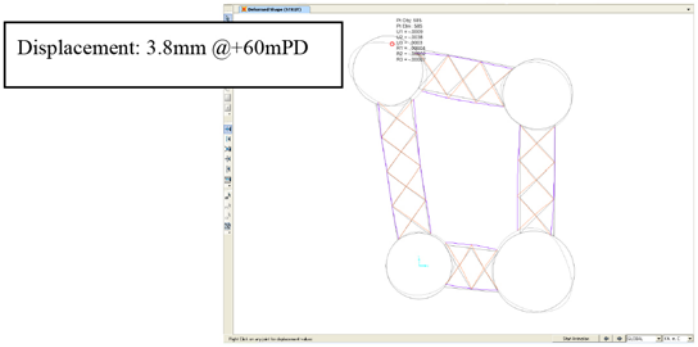

Figure 9: Deformed shape for the temporary circular temporary structure

8 CONCLUSIONS AND RECOMMENDATIONS

In Hong Kong, due to the scarcity of land, there is a trend of increasing depth of excavation to accommodate deep basements and foundations in densely developed areas. Ground movements will inevitably take place and the engineering design team of geotechnical engineers and structural engineers will have to work together to develop innovative excavation and lateral support (ELS) system to ensure that the construction will not cause undue/unacceptable ground movements which could adversely affect adjoining land, buildings and structures. For the 21.5m (max) deep excavation, it is necessary to think out of the box to arrive at an ELS system. The use of 4 temporary cofferdams within the excavation will reduce the number and lengths of struts required and, at the same time, provide a stiff and robust supporting system, which will minimize ground movements due to excavation and deformation of the strutting system.

Detailed assessments of ground movements at various stages of construction have been made based on the best engineering solution available with various geotechnical design assumptions and the commonly adopted computer software PLAXIS. It is recommended that adequate regular monitoring be carried out during the construction stages to verify these assumptions and to make suitable changes to the design to cater for differences in design and actual soil/structure interaction.

REFERENCES

GEO 1990. Review of Design Methods for Excavations (1990). GCO Publication No. 1/90, Geotechnical Engineer Office, Civil Engineering and Development Department, Hong Kong SAR Government, Hong Kong.

Knappett, J.A. & Craig R.F. 2012. Craig's soil mechanics. 8th Edition, Spon Press, New York.

Code of Practice for Foundation, p.11, Buildings Department.

An Overview of Deep Excavation Techniques in Hong Kong

Raymond K.S. Chan, Clifford W.C. Phung & Kelvin C.L. Tse
Meinhardt Infrastructure and Environment Limited, Hong Kong

ABSTRACT

Owing to the limitation of land supply, deep excavation has been a significant part of construction in Hong Kong to strive for more space in various kinds of developments, which include basement car parks, plant rooms and malls etc. Deep excavation has become more challenging as the urban area in Hong Kong has been densely developed. Different techniques and construction methods have to be adopted to ensure safety, to minimize impact and nuisance to the neighborhoods and to suit the actual site conditions.

This paper gives an overview and presents two interesting and innovative cases of deep excavation in the last decade in Hong Kong. Possible ways to enhance practice in deep excavation is also discussed.

1 INTRODUCTION

In many developments in Hong Kong, deep excavation has to be carried out to accommodate basement structures and underground facilities, and excavation depth of more than 20m is not uncommon. For general sites with regular-shaped excavation areas on level ground, the deep excavation is often "typically" supported by layers of horizontal / sub-horizontal structural steel shorings between temporary pile walls, such as pipe pile walls and sheet pile walls (Plate 1). Engineers are accustomed to this kind of excavation and lateral support (ELS) system from both design and construction point of view.

Plate 1: "Typical" ELS Systems in Hong Kong

Nevertheless, for sites with irregular excavation area, such as those at the hillside, or with some special site constraints, such as sites with significant ground level difference across the site, the above-mentioned "typical" ELS system may not be cost-effective or may even technically unacceptable. In

these cases, some "non-typical" design / construction lateral support systems (Plate 2) would have to be developed. These include tie-back walls and inclined shorings supported by partially constructed structures.

In the following sections, 2 interesting and innovative ELS system, which were developed in the last decade in Hong Kong, will be presented.

Plate 2: "Non-typical" ELS Systems in Hong Kong

2 CASE 1: MTR VIADUCT SECTION AT HOLY SPIRIT SEMINARY, WONG CHUK HANG

From the Wong Chuk Hang MTR Station westward just before crossing the Aberdeen Channel, a viaduct section with reinforced concrete retaining walls of about 80m long had to be built on a natural hillside. The natural slope was originally about 26m high (from about +4mPD to +30mPD) and stood at an average slope angle of 40 degrees, with heavy vegetation on it. At the crest of the slope, it is generally a flat area where the Holy Spirit Seminary (HSS) is situated. The site location and condition of the natural slope is shown in Figure 1 and Plate 3 respectively.

Figure 1: Site Location Plan

Plate 3: Conditions of the Natural Slope

The solid geology of the area is fine ash vitric tuff with subordinate eutaxite and coarse ash tuff of the Ap Lei Chau Formation. At the viaduct section which was to be constructed, the bedrock level is generally at +13mPD to +23mPD, with a layer of highly / moderately decomposed tuff above and a local fill / colluvium layer at the top. The highest groundwater level measured is about +23mPD.

The viaduct would encroach into the existing natural hillside. To construct the viaduct, a maximum of 14m deep excavation had to be carried out in the vicinity of the HSS below the crest of the natural slope. To achieve this, several challenges had to be overcome:

1) It would be difficult for sizeable construction plants to be deployed on the top of the natural slope as the natural slope is fairly steep. In addition, construction plants were not allowed to be transported through HSS.
2) There is only limited working space between the site boundary and the natural slope crest, which posed constraints on the excavation design / method.
3) The excavation had to be carried out in the open hillside and the ground level difference between the upslope side and downslope side of the excavation is more than 13m, which makes the "typical" ELS system not applicable.

To overcome the challenges, an ELS system comprising a row of 273mm diameter pipe piles @ 500mm c/c and supported by rows of removable pre-stressed ground anchors at 2m c/c horizontal spacing and fixed anchor length of up to 10m in rock was adopted. Each ground anchor comprised 6 steel strands of 15.7mm diameter and was pre-stressed to a maximum load of 600kN. The pipe piles were first installed by piling rigs which can be manoeuvred on a temporary haul road through a small cutting into the natural slope. Excavation and installation of ground anchors were then progressively constructed layer by layer below the slope crest until the final excavation level was reached. As the construction of the viaduct structure proceeded, the ground anchors were de-stressed and removed in turn from the bottommost layer until the entire permanent structures were completed. The design, testing and monitoring of the anchors were made reference to BSI (1989) and GEO (1989). A typical section of the ELS works is illustrated in Figure 2. A few photos of the ELS system are shown in Plate 4 and Plate 5.

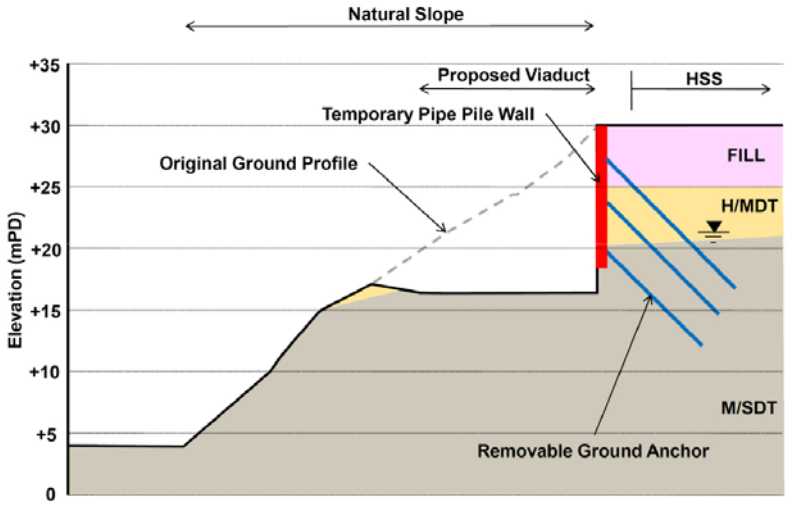

Figure 2: Typical Section of ELS Works

Plate 4: General View of the ELS Works with Removable Ground Anchor

Plate 5: Free Working Space in front of the ELS Works

With the above ELS system, the issues on access for construction plants and working space were solved. The application of removable pre-stressed ground anchors provided sufficient working space within the excavation area which facilitated the construction works. Although the fixed anchor length of the installed ground anchors were outside the site boundary during excavation, they can be removed upon the completion of the works (except a tiny component which would be buried in the ground as agreed with the Client and relevant lot owners) and thus would not hinder future development of land at the slope crest. Unlike soil nails, these pre-stressed anchors are "active" in nature and therefore ground movements of the adjacent ground were well controlled within the allowable limits of 25mm during the course of the excavation. The excavation and viaduct construction was completed successfully.

3 CASE 2: BUILDING WORKS WITH DEEP BASEMENT IN EAST KOWLOON

The ELS works in this case has undergone the detailed design stage and is being constructed. The site is located in East Kowloon and the land on which the building is to be built is generally flat with a ground level of +61mPD. The footprint of the proposed building is about 120m (north-south direction) x 90m (east-west direction). On three sides of the proposed building, the site is surrounded by existing fill slopes of up to 16m high and retaining walls of 4m high maximum. The excavation area, which is about 75m x 90m, is fan-shaped, with the east and south side being straight (Figure 3). The excavation depth required is generally 21.5m, with a maximum depth of 26.5m for a local area at the northern corner due to higher existing ground level.

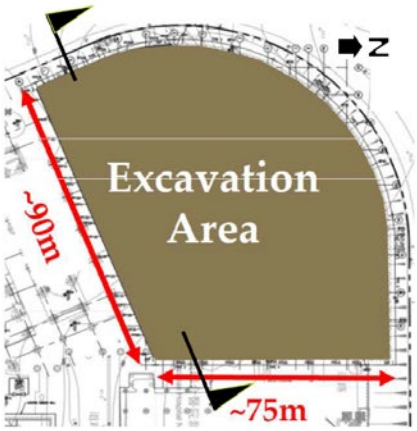

Figure 3: Approximate Dimension and Shape of Excavation Area

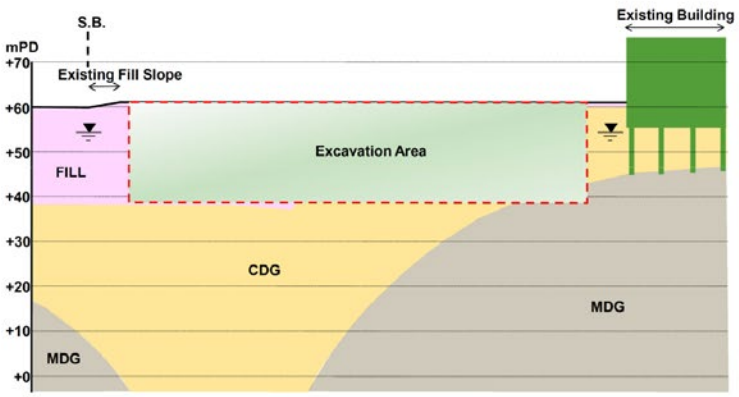

Figure 4: Typical Geological Section

Based on the available information from desk study and site-specific ground investigation for the development, the geology of the site comprises a thick layer of fill materials at the top (maximum ~30m thick), underlain by completely to highly decomposed granite with corestones. The bedrock level is generally at +55mPD at the north dipping southward to about +25mPD at the south. A local depression of bedrock level due to the presence of a fault zone below -45mPD was found at the west of site. The highest groundwater level measured is about +55mPD. A typical geological section of the site is shown in Figure 4.

Due to contractual requirements of this project, the option of adopting top-down excavation method and diaphragm wall as vertical elements was opted out. Bottom-up construction was the only method that could be considered. Sensitive receivers, including underground utilities and existing buildings founded on both shallow and piled foundations, are also present immediately adjacent to the excavation area and thus stringent control on ground movements is required.

"Typical" horizontal / sub-horizontal shoring arrangements were considered as an initial option for the ELS works. However, this ELS scheme was later opted out due to the following reasons:

1) The main struts would be of a minimum span of 75m across the excavation area which is structurally not effective.
2) Pre-loaded struts are required to control the adjacent ground movement. As the struts would be long, the temperature effect on the struts would be significant, making it difficult to maintain the strut pre-load to minimize the ground movements during construction.
3) Due to the fan-shaped excavation area, struts would be closely spaced on a side, which poses constraints to the excavation works and may delay the overall construction programme.

As a result, an innovative ELS scheme was designed to overcome the above constraints. For the peripheral vertical elements, a combination of large diameter bored pile wall (1.5m diameter at 2.0-3.0m spacing) and 610mm diameter pipe pile wall strengthened with structural steel H-sections at 0.7m-1.0m spacing was proposed to withstand the large internal stresses due to deep excavation. To minimize the span of struts, a temporary core structure was designed at the centre of the excavation area. This temporary core structure would be composed of 4 large ring structures, each of which would be made of layers of reinforced concrete ring beams with a maximum external diameter of 20m, supported by pipe piles. There were also bracings within each ring structure to enhance the rigidity. These 4 ring structures would be tied together by structural steel works, thus forming a single stiff structure (Figure 5 and Figure 6). All the strut loads from the peripheral vertical elements would be supported by this stiff temporary core structure. The location and configuration of the stiff temporary core structure was carefully studied such that it would not clash with the proposed pile foundations and core walls of the future building. The stiff core structure was designed to be constructed from the top, layer by layer, as the excavation proceeds, similar to the sequence of shoring installation. A plan view of the schematic ELS works is shown in Figure 7.

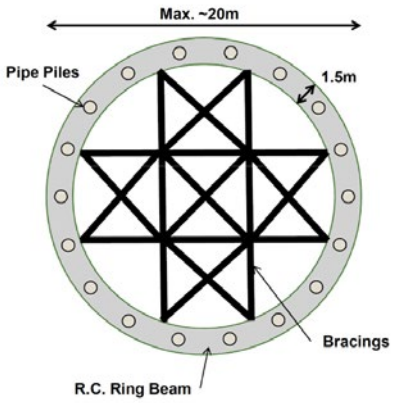

Figure 5: Typical Section of Ring Beam (Plan View)

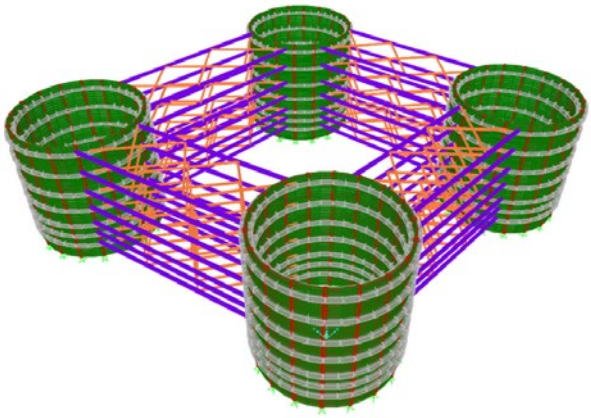

Figure 6: Structural Model of the Temporary Core Structure

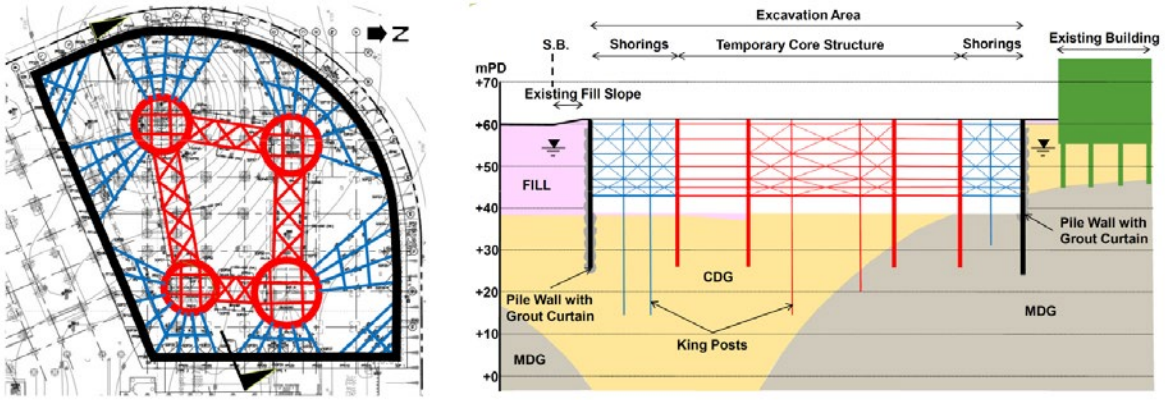

Figure 7: Schematic ELS Works (Red - Temporary Core Structure; Blue - Struts)

By adopting the innovative temporary core structure, the whole ELS system became structurally more robust and effective as the span of the struts would be limited to around 30m maximum only. The adjacent ground movement estimated could also be controlled within the limits of 25mm. In addition, comparing to the "typical" shoring arrangement, more working space would be provided for transporting plants and materials from / to the excavation area as fewer struts were needed. Finally, all the contractual requirements would also be satisfied.

4 DISCUSSIONS

There would not be only a single solution for supporting a deep excavation. Professional engineers can always make use of their technical knowledge to work out different solutions for an engineering problem. Nevertheless, the most challenging part of designing an deep ELS system is how to work out the most cost-effective solution.

In Case 1, the ELS system has made use of the favourable side of the geological conditions and geotechnical properties of the ground on the site. The high bedrock level allows the rock socket for the ground anchors to be formed without too much drilling. Despite the numerous site constraints, the design engineer understands both the engineering properties of the ground and the characteristics of the specialized engineering product, i.e. removable ground anchors, and works out the solution for supporting the excavation works, which has proved to be not only technically feasible, but also cost-effective.

In Case 2, the ELS system cannot be similar to that in Case 1 due to different site conditions and constraints. However, the design engineer applied another concept and made use of structural knowledge to design the temporary core structure, which is the core element of the ELS system. With the presence of this core structure, the whole ELS system was formulated to tackle all the constraints.

5 CONCLUSIONS

From the 2 cases presented in this paper, it can be seen that an ELS system is in fact a product of combined geotechnical and structural engineering. To enhance the cost-effectiveness of a deep ELS system, the design engineer should equip himself / herself with both geotechnical and structural capability so that he / she can fully understand and have a holistic view of the engineering problem. In addition, the mindset of the engineer shall not be bounded by his / her own or other's experience. One should always be reminded that there is always room for being innovative and creative and the engineer shall think out of the box whenever and wherever.

REFERENCES

BSI (The British Standards Institution) 1989. *BS8081:1989 – Code of Practice for Ground Anchorages*. The British Standards Institution, the United Kingdom.

GEO (Geotechnical Engineering Office) 1989. *GEOSPEC 1 – Model Specification for Prestressed Ground Anchors*. Geotechnical Engineering Office, Civil Engineering Department, Hong Kong Government.

An Overview of Technological Advancements in Geotechnical Instrumentation and Monitoring

Raymond K.S. Chan, Clifford Phung, Roger Lee & Ivan Lam
Meinhardt Infrastructure and Environment Ltd.

ABSTRACT

Geotechnical works in Hong Kong over the past decades are continuously becoming more complex, are larger in scale, and involve higher risks and consequences. The demand for innovative and creative solutions in geotechnical instrumentation to monitor the performance of such complex works is also increasing; with a view to overcome the constraints and problems associated with manual and wired monitoring methods, such as difficult access for installations & readings, susceptibility for site damage, data coverage, consistency, frequency & reliability, as well as the efficiency of record keeping and reporting.

The Tilt and Vibration (T&V) sensor is an example of a dual monitoring system that is easy to install and miniature in size, can be remotely and wirelessly managed at long distances, provides data security, and requires low power for reliable data acquisition & transfer. This paper discusses the innovative application of T&V technology that may ease some challenges in today's geotechnical instrumentation; and ultimately enable engineers and scientists to enhance complacency with the quality and reliability of remote sensing monitoring.

1 INTRODUCTION

1.1 Instrumentation and Monitoring for Geotechnical Works

Despite the profound aspects of geotechnical engineering, a seasoned practitioner may acknowledge that "To improve is to change; to be perfect is to change often." (Winston S. Churchill). Although the degree of complexity puts us far from perfection, we should strive to enhance our predictions of ground response due to geotechnical works. In which, a key component is the use of trenchant verification of the ground response versus design prediction by means of geodetic monitoring.

1.2 Wireless Technology

Current manual and wired monitoring remains the mellifluous method to reliably and consistently monitor the performance of geotechnical works. Wireless technology is often perceived as a method fraught with risk of data inconsistency and adverse quality with exhortations on the industry to subsist to wired and manual technology. However, current advances along with field verification in trial studies have further evolved the acceptance of automated remote sensing technology. Wireless technology has currently been applied to precision monitoring systems such as in-place inclinometers, remote groundwater monitoring with vibrating wire, extensometers, blast event data (vibration, noise, and air overpressure) and total stations. The tilt and vibration sensor system (T&V) is currently spawning a new branch of successful wireless monitoring solutions.

2 Remote Sensing Technology

2.1 The Success of the Automated Deformation Monitoring System

Engineers and scientists have a penchant to continuously drive innovative and creative solutions in the instrumentation and monitoring field. The Automated Deformation Monitoring System (ADMS) has in recent years been widely adopted in large infrastructure projects in Hong Kong to measure vertical and horizontal movements at a designated target point over time. Deployment of ADMS provides reading consistency with use of motorized total stations with predetermined point positioning of targets, thus negating any parallax and human effects succumbed by manual surveying. Continuous monitoring with high measurements rates provides real time alert, action, alarm triggers and enables instant notification to subsequently prescribe remedial measures. The efficacy of ADMS technology relies on correct and efficient logging of large amounts of data, and subsequent data distribution via an online database readily accessible by interpretors. With the use of ADMS, technological improvements have steadily reduced the industry's propensity to adopt manual monitoring methods and therefore many archaic obstacles have now been overcome. Such automation technology provides a precedent which spearheads the use of other geodetic monitoring systems such as the Tilt and Vibration Sensors.

2.2 The Wireless Tilt and Vibration Monitoring System

Tiltmeters and vibration sensors are regularly used for monitoring the structural health and vibration sensitive structures and such sensor technology has been widely applied in the automotive, aviation, and electronics industries. Tiltmeters are sensitive inclinometers that measure the change of position from the vertical axis (ie. angle of rotation) and are typically attached on the surface of sensitive structures or utilities. In terms of geotechnical works, the tilt of the surface provides an indication to assess the structural stability or potential risk of deterioration during construction works within the influence. Vibration monitoring (also known as portable seismographs) is the measure of cyclic or an oscillating motion of a point from its mean position. Vibration sensors are typically installed on affected structures, slopes, retaining walls and utilities that are within the influence of vibratory works such as piling or blasting. Examples of facilities that may be sensitive to vibration include hospitals and testing laboratories. To provide an overall picture of the ground and construction works interaction, the tilting and vibration data may be read in conjunction with other major modes of monitoring such as surface movement, settlement, groundwater monitoring, and subsurface movement including extensometers and inclinometers.

Due to the automation process of T&V monitoring, many drawbacks of manual reading are negated by enhancing the consistency of routine data reading. Each manual reading is nuanced by the technician, the tiltmeter / vibration sensor, the placement of the tiltmeter / vibration sensor, and temperature corrections. T&V may be programmed to take readings at different frequencies and intervals so that movement responses are easily correlated to the activity. Advantages of real-time monitoring includes easy filtering of noise, timely alert of response and in-depth interpretation of grouping effects of multiple vibration sources. Albeit, the wealth of data requires efficient organization and processing to ease the user's management and interpretation of results. Built-in data loggers buffers data in the sensor and data is transferred to management consoles by a reliable hand-shaking protocol. Record keeping and reporting is then processed by standard software and predetermined formats to ease knowledge sharing. Similar to the ADMS, tilt and vibration alert limits or impact alerts may be setup for instant notification of responsible parties.

Miniature sensor with wireless transmission has overall cost and time benefits. The risk of wire damage due to construction works is reduced with improved safety during installation and readings, and reduced maintenance and setup time with less logistics planning. The tiltmeter reference to the gravity vector and the vibration reference to a static position have no optical path limitations which provides added wireless freedom. Multiple sensor arrays may be remotely managed from a single management node as each sensor in the network acts as a repeater providing added data coverage. T&V's wireless benefits the monitoring of slopes, of locations of dense vegetation, at inaccessible locations, on remote flexible barriers within natural terrain, within restricted areas, and at offshore locations. Technology

has also replaced the battery with solar energy which provides added flexibility and with minimal maintenance.

Plate 1 indicates a photograph of Engineers reading the T&V's during piling works. The site is located at a remote location and testing time was constrained to a single work shift. The miniature size and relatively low cost of the T&V enabled Engineers and Technicians to carry multiple units to site and install in an array setup providing large monitoring coverage coupled with fast setup and dismantling.

Plate 1: Site B Photograph of Vibration Sensor Reading

2.3 An Overview of Tilt and Monitoring System Site Trials

For illustrative purposes, two examples of T&V application at trial sites are described in this section: Site A - excavation and lateral support works at a site in Hong Kong, and Site B - demolition works, enabling works and retaining wall construction works on a site in Hong Kong. The T&V monitoring data are read in conjunction with wired and manual tiltmeters and vibration monitoring equipment for comparison and calibration purposes for each study.

At Site A, the proposed structure consists of a basement structure 5m deep with area 20m by 30m. A strutted sheet pile excavation and lateral support system is proposed for temporary works to enable the bottom-up construction of the permanent structure. The site is bounded by existing high-rise structures immediately to the north and east, a road to the south, and a sensitive structure to the west. In this ongoing study, the T&V are used to measure the tilt of the existing structures during the excavation works. Figure 1 indicates Site A's the general site layout plan of the T&V, along with manual stand-alone vibration sensors and tiltmeters.

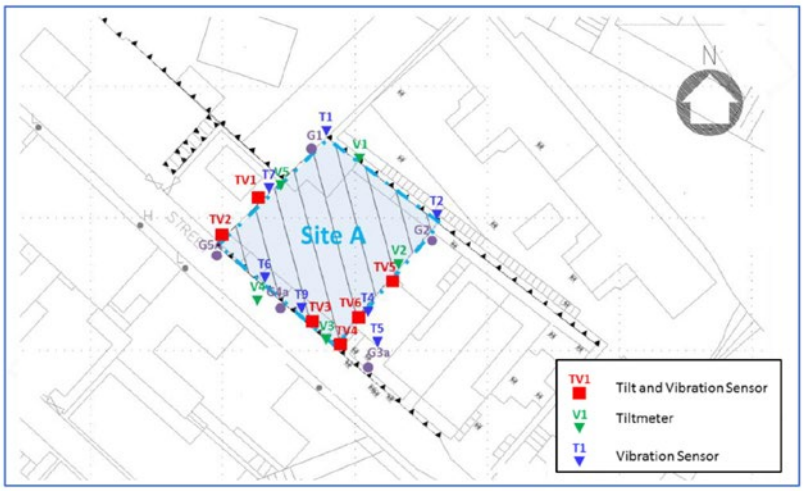

Figure 1: Site A Layout Plan

Plate 2 indicates a photograph of the excavation works highlighting the T&V sensor location. The T&V is attached to the existing structure at a high level on the existing wall providing minimal disturbance to workers, without wiring, and without the need for service access which enhances the safety of workers.

Plate 2: Site A Photograph of Site Activities

Plate 3 indicates the miniature size of the T&V sensor which is easily attached to the wall surface, is mobile and is encased in a protective box to resist minor impacts from construction works or vandalism.

Plate 3: Wireless Tilt and Vibration Sensor at Site A

Figure 2 indicates a snapshot of the T&V readings which shows correlation between the wireless and manual tilt readings along with site activities demonstrating the reliability of the wireless T&V system.

Site B is located in Hong Kong with proposed demolition works, enabling works and retaining wall construction works. The site is bounded by two roads to the east and west and adjacent structures to the north and south which are sensitive to excessive vibrations. At time of reporting, negligible vibrations were indicated although a comprehensive study will be carried out when more information is made available.

Figure 3 indicates the instrumentation and monitoring plan for Site B and positions of attached vibration monitoring points on adjacent structures. Plate 4 indicates the partial demolition works immediate adjacent to an existing structure and Plate 5 indicates the T&V securely attached to the adjacent wall.

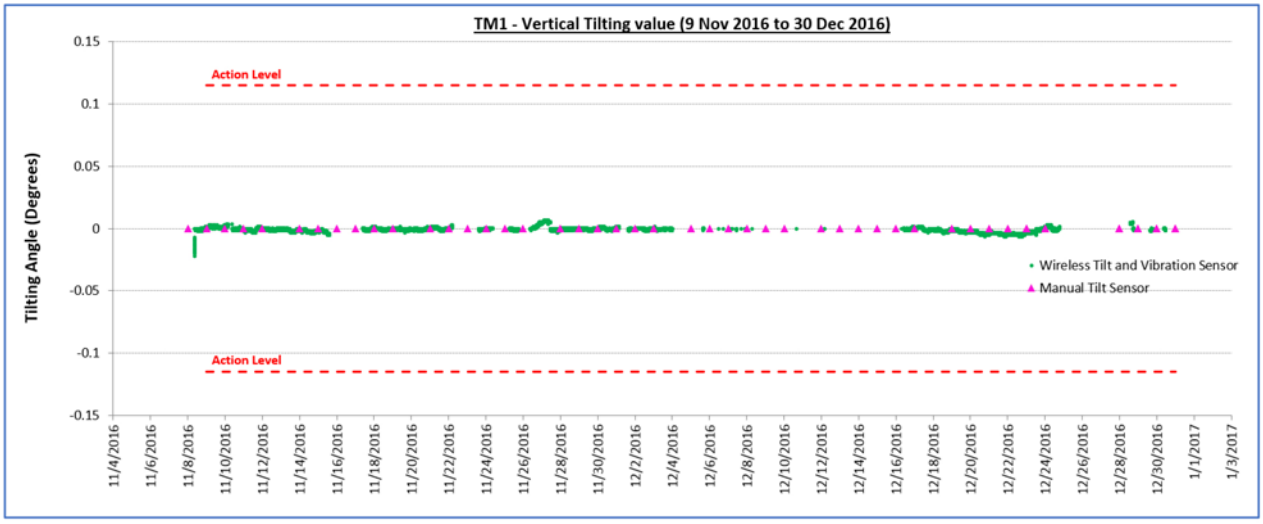

Figure 2: Site A Template of Data Reading Output

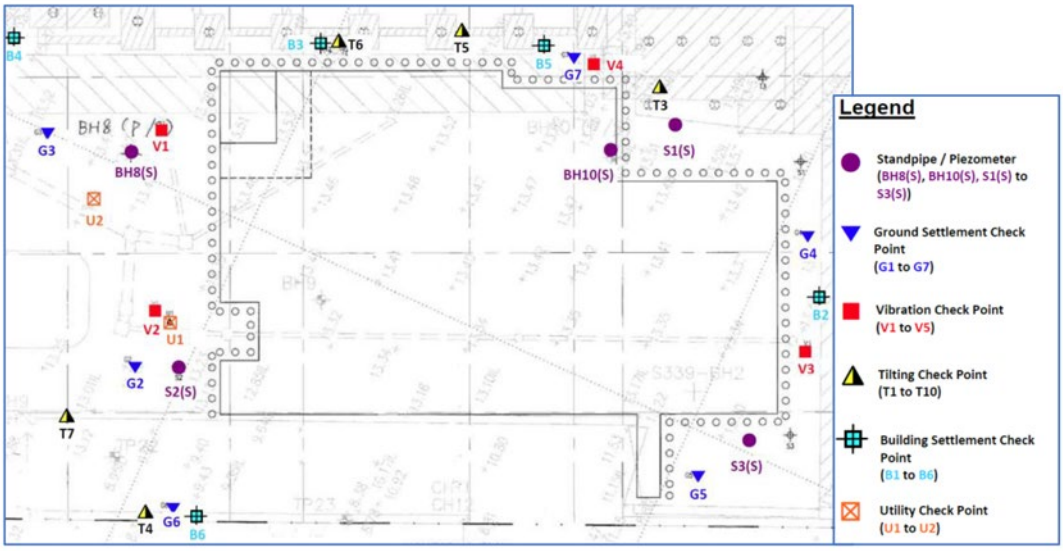

Figure 3: Instrumentation and Monitoring Plan at Site B

Plate 4: Photograph of Demolition Works at Site B

Plate 5: Wireless Tilt and Vibration Sensor Securely Attached to the Adjacent Wall

2.4 Instrumentation and Monitoring Data Management Systems

As infrastructure works become more complex and are increasingly situated within dense urban settings with higher consequences, engineers endeavor to seek automation and innovative wireless monitoring solutions. The flourishing of ADMS and T&V technology is envisaged to cross pollinate and increase the wireless application in drillhole inclinometers, groundwater monitoring, extensometers, and material testing. Upon merging all monitoring modes into a standard instrumentation format, monitoring data may be further projected onto 3D models and virtual reality for easy visualization of the ground response as a whole.

A standard management system of all monitoring data, along with the proposed works, construction activity, ground model, topography and existing facilities will provide a holistic approach for Engineers to efficiently identify geotechnical issues and unexpected geological variations. Comprehensive web-based platforms compiles, organizes and securely stores for blasting works monitoring data on the internet thus enabling engineers to efficiently propose remedial measures. The management interface provides functions for presenting, evaluating, and analyzing data for blast events including survey mapping, vibration, noise, air overpressure, crack width, water-shock, pore pressure, temperature, humidity, wind and dust. Figure 4 indicates a typical platform setup diagram with blast event data sharing capabilities to relevant stakeholders. Figure 5 indicates an easy-to-use web interface with an active monitoring point location plan.

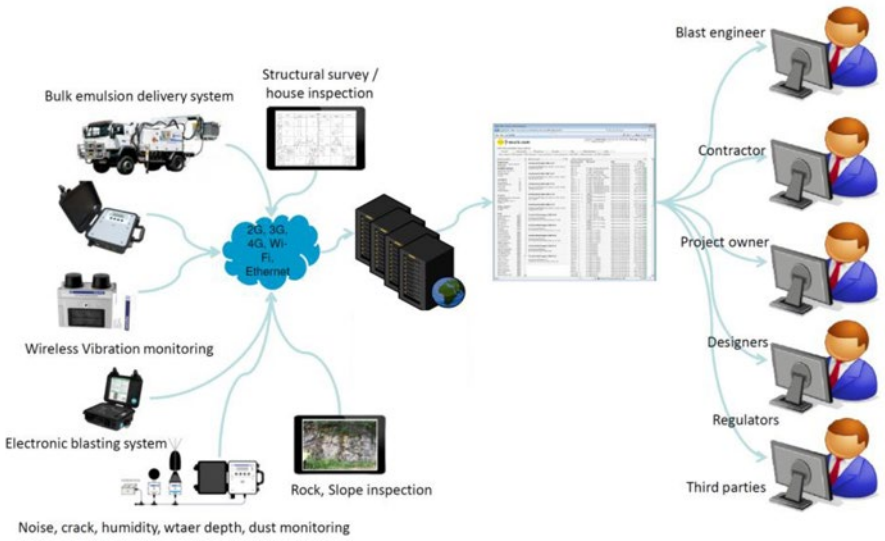

Figure 4: Data Management Platform Setup Diagram

Figure 5: Web Application Interface

3 CONCLUSIONS

With the recent trends of the wireless monitoring, Tilt and Vibration Sensors have made a strong foothold in the instrumentation and monitoring field. The multi-function, wireless and miniature sized sensor has myriads of merits over manual sensors which suits difficult access for installations & readings, reduces susceptibility for site damage, increases data coverage, maintains reading consistency, frequency & reliability, and provides efficient record keeping and reporting. Site trials have been carried out to assess the efficacy of the T&V sensors with proven success and correlation with manual monitoring techniques. Comprehensive web-based platforms allow users to review all available monitoring and spatial data compiled in a single database via the internet. The T&V and management platforms provide an innovative and value-added solution to the geotechnical instrumentation and monitoring field Engineers and Scientists may reliably depend on, and ultimately allocate more time for interpretation of data and prediction of the ground response.

ACKNOWLEDGEMENTS

Global Sensing Solutions, Orica and Nitro-Consult is gratefully acknowledged for their assistance and support provided to the authors when they were working on this paper and associated projects. The views expressed in this paper are those of the authors only.

REFERENCES

CEDD (Civil Engineering and Development Department) – Mines Division. 2015. Vibration Monitoring. Civil Engineering and Development Department, Hong Kong.

A Comparison of 2D and 3D Numerical Analyses of a Complex Tunnel Intersection Lining

L. Tony Chen & John W.Y. Yeung
Arcadis Design & Engineering Limited

ABSTRACT

This paper presents a comparison between 2D and 3D numerical modeling carried out to analyze a tunnel intersection lining located in Hong Kong. The tunnel intersection involves a main tunnel and an adit tunnel joining from different directions and elevations. The purpose of the paper is twofold: firstly to compare the results of the two modeling methods in order to gain a better understanding of the limitations of the 2D modeling; and secondly, to introduce a modeling technique which can be used to improve 2D modelling accuracy. It is shown that, where the stress state is close to a 2D condition, the analysis results from both the 2D and 3D modeling are similar. However, the calculated stresses by the 2D modeling are seen to be markedly different from, and larger than, those by the 3D modeling, where the stress state is significantly influenced by 3D effects. An internal lining is then introduced to account for the 3D effects and the stresses calculated from the revised 2D modeling are seen to be very close to those by the 3D modeling. With this modeling technique, the complicated and time-consuming 3D modeling may be replaced, to a certain extent, by the simpler and more efficient 2D modeling.

1 INTRODUCTION

Two or more tunnels running from different directions may intersect and form an intersection for drill & blast tunnels. The intersection so formed may be complex in geometry and massive in size, posing great challenges to design. The intersection may be constructed of plain concrete or reinforced concrete. The former is better for corrosion resistance, while the latter is advantageous in reducing intersection size, hence minimizing both excavation and concrete volume. It is challenging to analyze and design such a tunnel intersection due to its complex and often irregular geometry. Reinforced concrete lining design is even more challenging as it is not intuitive how to dimension steel reinforcement to carry the developed stresses. Chen & Yeung (2015) have discussed the design and analysis of such a tunnel intersection, focusing on 3D numerical modeling and steel reinforcement design.

Application of 3D numerical modeling to design of complex tunnel intersections is considered necessary but its process is generally time-consuming. Due to time and budget constraints, 2D numerical modeling is often preferred by practicing engineers, especially for preliminary design. A good understanding of the limitations associated with 2D modeling therefore becomes necessary.

In this paper, both 2D and 3D numerical modelling will be carried out to re-analyze the tunnel intersection as discussed in Chen & Yeung (2015) with the following two main objectives:

(1) To compare the analysis results of the two numerical methods in order to gain a better understanding of the limitations of 2D modeling; and

(2) To introduce a modeling technique which can be used to improve 2D modelling accuracy.

2 THE TUNNEL INTERSECTION AND ROCK CONDITIONS

The tunnel intersection consists of a main tunnel and an adit tunnel approaching from different directions and elevations, the former comprising two oval shaped conduits of different sizes, while the latter comprising two circular shaped conduits of the same diameter, as shown in Figure 1. Located at over 100m below the ground surface and within weathered granitic rocks, the tunnel intersection was excavated by the drill-and-blast method.

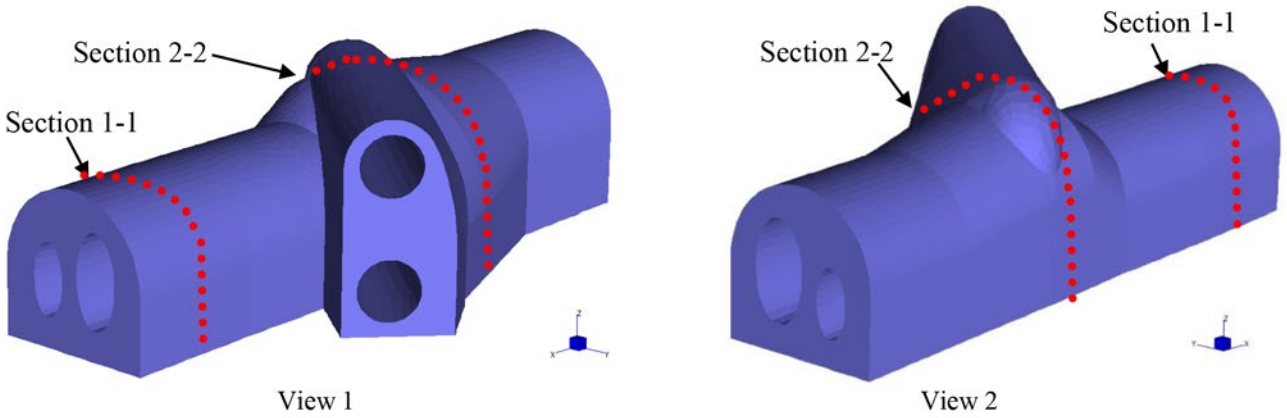

Figure 1: 3D views of tunnel intersection

The solid geology at the tunnel intersection consists of medium grained granite, predominantly Kowloon Pluton type (Klk). The quality of the rock masses around the tunnels is classified based on the Q–system developed at the Norwegian Geotechnical Institution (NGI, 1997 & 2003). The Q value is assessed to be about 5 based on the available ground investigation and mapping results.

The measured groundwater levels range from 3.0m (highest groundwater level) to 5.96m (lowest groundwater level) below the ground surface.

3 LOADINGS

The design loadings include dead loads, external groundwater pressure, internal sewage pressure, surcharges, rock load and seismic load. For simplicity, only one load combination consisting of tunnel dead load, groundwater pressure, sewage pressure and rock load is considered in this paper.

The rock load is calculated using NGI Q-system (NGI, 1997 & 2003) as per Equations 1(a) and (b):

$$P_{roof} = \frac{2J_n^{1/2} Q_r^{-1/3}}{3J_r} \quad (1a)$$

$$P_{wall} = \frac{2J_n^{1/2} Q_w^{-1/3}}{3J_r} \quad (1b)$$

where P_{roof} is rock load acting at tunnel roof, P_{wall} is rock load acting at tunnel walls, Q_r is Q value at tunnel roof, Q_w is Q value at tunnel walls, $Q_w = 2.5\ Q_r$, J_n is number of joint sets and J_r is joint roughness parameter.

In considering the sewage pressure, the case scenario where the upper adit conduit and the smaller tunnel conduit are empty while the lower adit conduit and the larger tunnel conduit are full is considered, as illustrated in Figure 2.

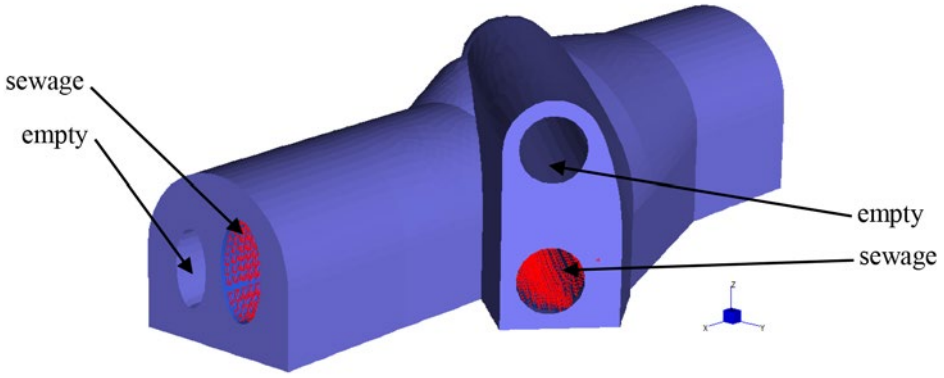

Figure 2: Adopted sewage load combination

4 ANALYSIS METHODS

4.1 Numerical model

The 2D and 3D analyses of the rock – lining interaction are carried out using the commercial software Phase^2 and Strand 7, respectively. Phase^2 is a 2 dimensional elasto-plastic finite element program for calculating stresses and displacements around underground openings. Strand 7 is a 3 dimensional finite element program for calculating stresses and displacements for general engineering applications. It provides a design tool to model and analyze structures using 3D brick elements.

The rock is modelled as a plastic material following the Hoek-Brown failure criterion. Elastic Young's modulus of rock (E_r) is determined by Equation 2 according to Bieniawski (1978):

$$E_r = 2\,RMR - 100 \qquad \text{for } RMR > 55 \tag{2}$$

where RMR = 9 ln Q + 44, is the rock mass rating according to Bieniawski (1976).

The adopted geotechnical parameters are shown in Table 1.

Table 1: Adopted geotechnical design parameters for rock

Q	RMR	Er (GPa)	Poisson's ratio, ν	Unit weight (kN/m^3)
5	58	17	0.23	27

Phase^2 modeling is carried out at two cross sections, namely Section 1-1 and Section 2-2, at the locations shown in Figure 1. Section 1-1 cuts through the main tunnel only and is a bit distant from the interaction, representing a stress state which is close to a 2D condition. Section 2-2 cuts through the upper adit and the tunnel, at which location the adit and the smaller tunnel conduit are not separated by any internal lining, representing the most critical stress condition. The adopted numerical models for the two sections are presented in Figure 3.

The adopted numerical model for Strand 7 analysis is shown in Figure 4. In the model, the rock-lining interface is represented by both radial and tangential springs whose stiffness coefficients are estimated based on the recommendations given in USACE (1997). Allowing only compression but no tension to develop, the radial and tangential spring stiffness coefficients can be estimated using Equations 3a and 3b, respectively.

$$K_r = \frac{E_r\, b\phi}{1 + \upsilon_r} \tag{3a}$$

$$k_t = \frac{k_r}{2(1 + \upsilon_r)} \tag{3b}$$

where b = breadth represented by the frame, ϕ = angle subtended by the spring.

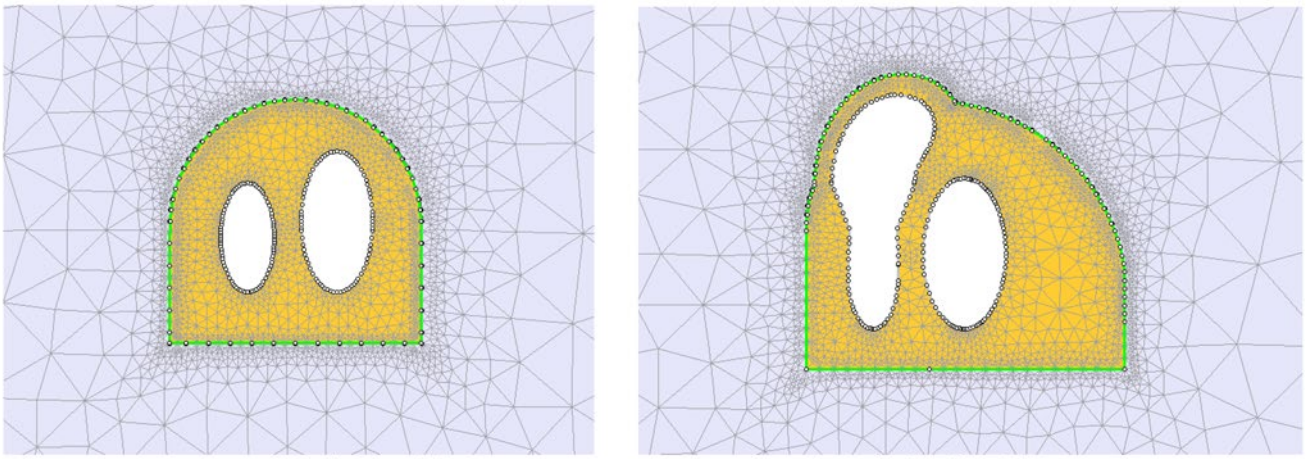

Figure 3: Adopted numerical models for Phase^2 analyses

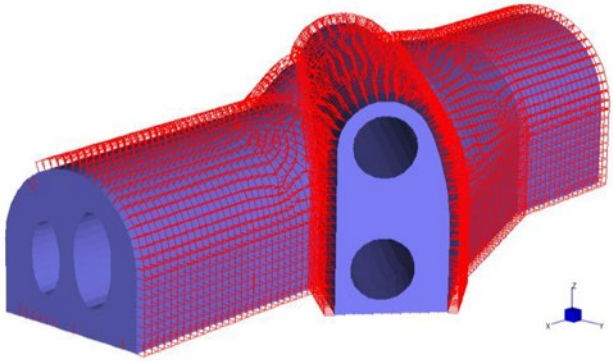

Figure 4: Adopted numerical model for Strand 7 analysis

4.2 Cases analyzed

A series of 2D and 3D analyses have been undertaken to determine the concrete grade and lining thickness. Since the focus of this paper is on the comparison of 2D and 3D analyses, all the analyses discussed in this paper are based on concrete Grade 60 and the lining geometry shown in Figure 1.

The calculated stresses from Phase^2 will be compared with those from Strand 7. Since Section 1-1 is close to a 2D condition, the calculated stresses from both 2D and 3D analyses are expected to be similar.

For Section 2-2, the following two cases are analyzed:

- Case 1: the geometry shown in Figure 3 is adopted as is;
- Case 2: the upper adit and the lower smaller tunnel conduit is assumed to be separated by an internal concrete lining to account for the effects of the adjacent lining which is not modelled (because not being cut through), as shown in Figure 5.

5 ANALYSIS RESULTS

5.1 Section 1-1

The computed stresses from both the Strand 7 and Phase^2 analyses for Section 1-1are shown graphically in Figures 6 and 7, respectively, while their maximum values are summarized in Table 2 for easy comparison.

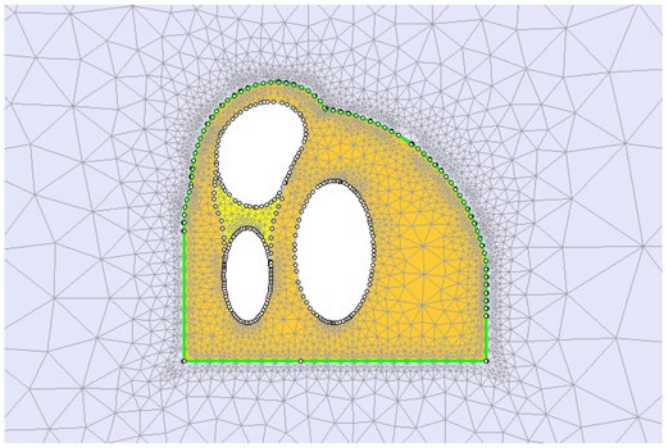

Figure 5: Adopted Phase2 model at Section 2-2 with an assumed internal lining

As can be seen, the stress distributions from the two methods are similar. The calculated maximum tensile and shear stresses from the two methods are very close, while there is about 20% difference in the maximum compressive stress. The difference is expected to diminish should Section 1-1 is located farther away from the intersection so that it can truly represent a 2D stress condition.

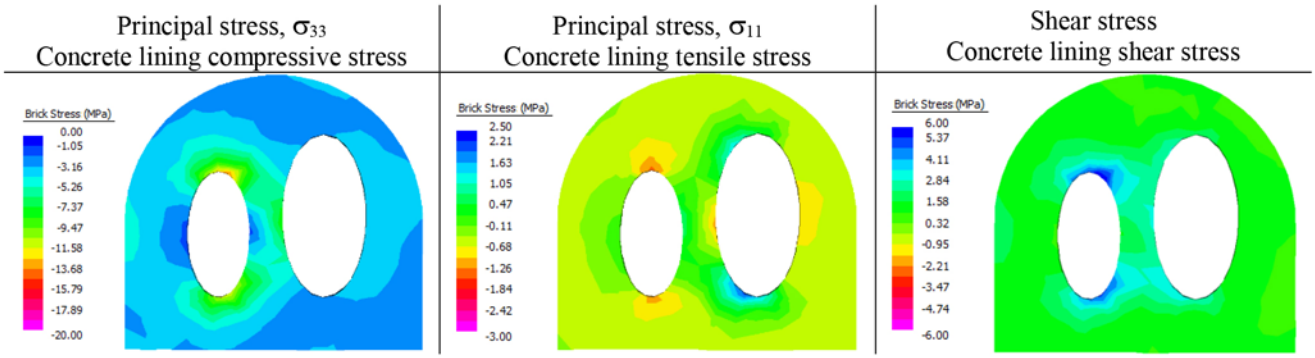

Figure 6: Outputs from Strand 7 at Section 1-1

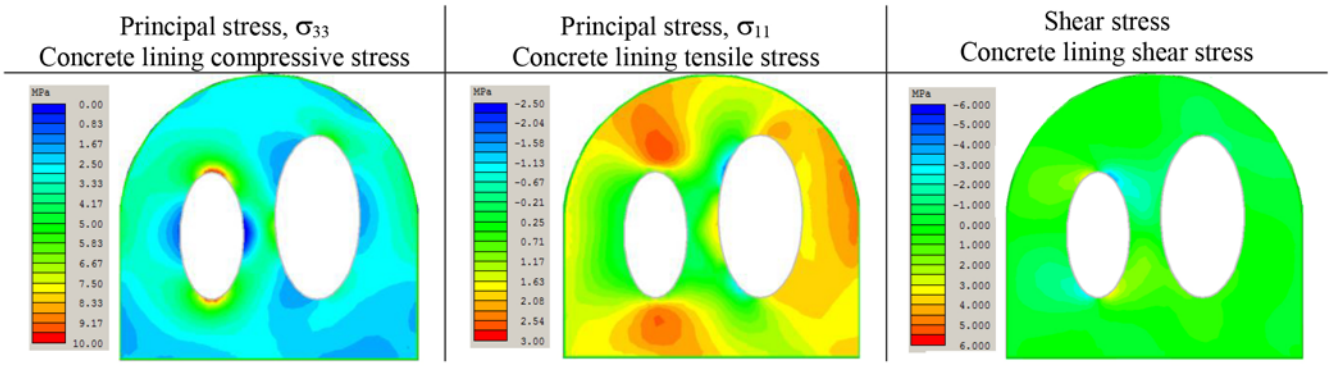

Figure 7: Outputs from Phase2 at Section 1-1

Table 2: Summary of calculated maximum stresses at Section 1-1

Analysis model	Calculated maximum stresses (MPa)		
	compressive	tensile	shear
3D Strand 7	7.0	2.0	5.8
2D Phase[2]	10.0	2.1	5.4

5.2 Section 2-2

The computed stresses from both the Phase^2 (Case 1 and Case 2) and Strand 7 analyses for Section 2-2 are shown graphically in Figures 8, 9 and 10, respectively, while their maximum values are summarized in Table 3 for easy comparison.

As can be seen, the calculated stresses from Phase^2 for Case 1 are markedly different from, and larger than, those from Strand 7. Due to the significant 3D effects which are not modeled, a 2D analysis clearly cannot accurately capture the stress condition at this location, and is very conservative.

On the other hand, the calculated stress distributions and their maximum values from Phase^2 for Case 2 are seen to be very similar to those from Strand 7, indicating that the assumed internal lining is able to allow the 3D effects to be accounted for in the 2D analysis. In this case, the Young's modulus of the added lining is adopted to be one third of that for Grade 60 concrete, based on a trial and error selection process. With this modeling technique, the complicated and time-consuming 3D modeling can be replaced, to a certain extent, by the simpler and more efficient 2D modeling.

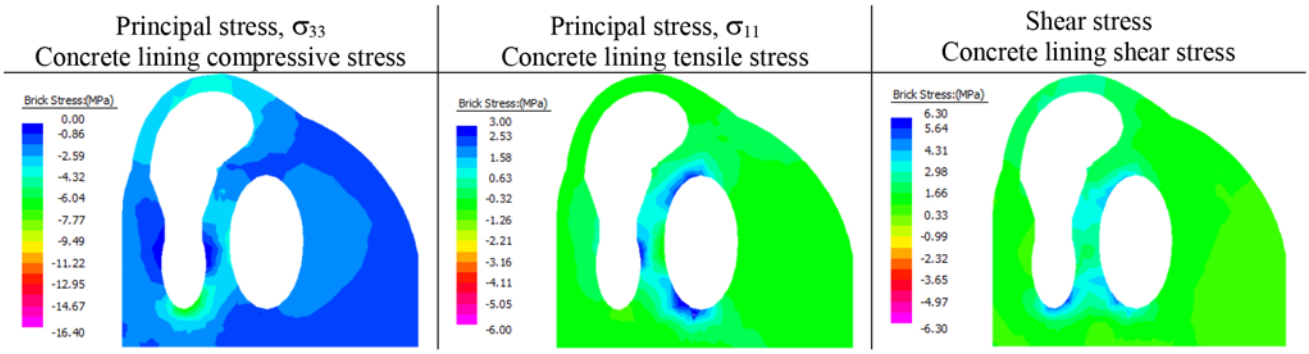

Figure 8: Outputs from Strand 7 at Section 2-2

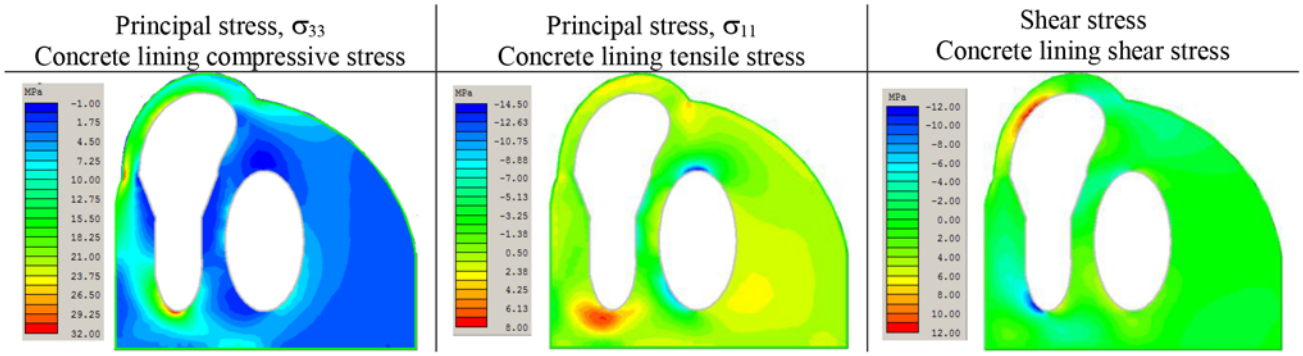

Figure 9: Outputs from Phase^2 at Section 2-2: Case 1

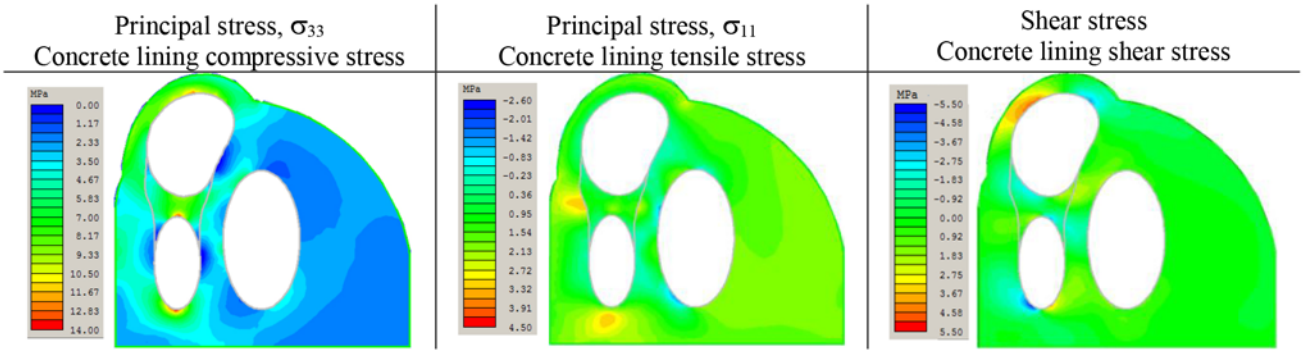

Figure 10: Outputs from Phase^2 at Section 2-2: Case 2

Table 3: Summary of calculated maximum stresses at Section 2-2

Analysis model		Calculated maximum stresses (MPa)		
		compressive	tensile	shear
3D Strand 7		16.4	3.0	6.3
2D Phase^2	Case 1: without an assumed internal lining	32.0	14.5	12.0
	Case 2: with an assumed internal lining	14.0	2.6	5.5

6 CONCLUSION

Applications of both 2D and 3D numerical analyses to the design of a tunnel intersection lining located in Hong Kong, via the software Phase2 and Strand 7, respectively, have been discussed in this paper. The tunnel intersection involves a main tunnel and an adit tunnel joining from different directions and elevations.

It is shown that, where the stress state is close to a 2D condition, the analysis results from both the 2D and 3D analyses are similar. However, the calculated stresses by the 2D modeling are seen to be markedly different from, and larger than, those by the 3D modeling, where the stress state is significantly influenced by 3D effects.

A modeling technique has been introduced to improve the accuracy of the 2D modeling. This is done by adding an internal lining between the upper adit and the lower tunnel to account for the presence of the adjacent lining which is not modeled in the 2D analysis. The stresses thus calculated are seen to be very close to those by the 3D modeling, indicating that this modeling technique is able to allow the 3D effects to be accounted for in the 2D analysis. With this modeling technique, the complicated and time-consuming 3D modeling may be replaced, to a certain extent, by the simpler and more efficient 2D modeling

REFERENCES

Bieniawski, Z. T.. 1976. Rock mass classification in rock engineering. *Proceedings of the Symposium on Exploration for Rock Engineering*, Johannesburg, Vol. 1: 97-106.

Bieniawski, Z. T.. 1978. Determining rock mass deformability – experiences from case histories. *International Journal of Rock Mechanics and Mining Sciences*, 15: 237-247.

Chen, L. T. & Yeung, J.W.Y.. 2015. 3D numerical analysis and design of a complex tunnel intersection. *Proceedings of the Underground Design and Construction. Conference 2015*, IOM3, Hong Kong Branch, pp. 121 – 130.

Hoek, E. and Brown, E.T. 1997. Practical estimates of rock mass strength. *International Journal of Rock Mechanics and Mining Sciences & Geomechanics Abstracts*, 34 (8): 1165-1186.

NGI. 1997. *Engineering Geology, Practical Use of the Q-method*. Oslo, Norwegian Geotechnical Institute.

NGI. 2003. *Handbook: Using the Q System*. Oslo, Norwegian Geotechnical Institute.

Strand 7. 2010. *Strand 7- Using Strand 7 – User Manual Release 2.4.4.* G+D Computing Pty Ltd., Sydney.

USACE. 1997. *Engineering and Design – Tunnel and Shaft in Rock. EM-1110-2-2901.* Washington, DC. U.S. Army Corps of Engineers.

3D Numerical Analysis and Design of Flexible and Rigid Barriers

A.K.C. Cheung, J. Yiu & S.W. Millis
Ove Arup & Partners Hong Kong Limited, Hong Kong

ABSTRACT

The mitigation of natural terrain hazards through the use of flexible and rigid barriers has become an increasingly common aspect of geotechnical works in Hong Kong in recent years. However, the design of these measures typically follows a relatively simplified process based on the use of two-dimensional debris flow models and spreadsheet calculations. This paper discusses the recent advances made in the use of coupled three-dimensional analysis for both debris flow run-out and barrier interaction using LS-DYNA. The findings of various studies to critically review and evaluate the energy balance associated with debris impact on flexible barriers were presented. These studies found that the energy loading obtained from 3D analysis was noticeably less than that typically determined under the current conventional design approaches, highlighting the potential for significant cost savings for hazard mitigation if this approach is adopted. Further discussion and examples on the use of LS-DYNA for the design and assessment of rigid debris resisting barriers is also provided, making reference to two case studies from recent sites under the LPMit Programme and international peer reviews of the effectiveness of the barriers provided at Mount Umyeon in Seoul, South Korea following the devastating and fatal landslides in 2011.

1 INTRODUCTION

1.1 Background

Hong Kong has a high proportion of land area that comprises relatively steep natural terrain. Due to the scarcity of land for both commercial and residential developments, this has resulted in the need to construct more facilities in close proximity to natural terrain areas. In order to protect these facilities, landslide mitigation measures in the form of flexible barriers and rigid barriers have become widely adopted in Hong Kong, with rigid barriers commonly built at the mouth of drainage lines for the mitigation of channelised debris flows while flexible barriers are commonly built along the toe of open hillslope to mitigate open hillslope hazards. In general, flexible barriers have been considered an attractive option for hazard mitigation as they require only light weight plant and materials for construction, have relatively versatile layouts and are more aesthetically pleasing and easy to install within hilly terrain. However, there is no comprehensive and internationally recognized method for the design of flexible barriers for debris flows. A better understanding of the interaction between debris and flexible barrier structures is therefore needed for these measures to be implemented in a cost-effective and reliable manner. As an initiative of the Hong Kong SAR Government, the Geotechnical Engineering Office commissioned Arup to conduct a study of the interaction between landslide debris and flexible barriers using an advanced three-dimensional numerical methods since 2011.

1.2 The LS-DYNA software

LS-DYNA is a multi-purpose finite element program for linear and non-linear mechanics. Its automated contact algorithm and wide range of material models support the solution of complex real world problems such as automotive crash analysis, rail, civil, structural, wind and vibration engineering, etc. It is considered capable of simulating highly dynamic and large deformation problems. In addition, new program codes can be introduced to suit particular geotechnical problems. As the numerical analysis for soil-structure interaction of flexible barriers is complex, LS-DYNA has been chosen for the numerical investigation.

1.3 Previous studies

A number of simulations of well published field tests / landslide events were carried out between 2011 and 2014 to test the capability of LS-DYNA and provide benchmarks on use of LS-DYNA for predictive analysis. These simulations included: (1) the USGS laboratory flume tests (Iverson et al., 2004); (2) rockfall tests on a flexible barrier structure (Volkwein, 2004); (3) various well documented debris flow incidents in Hong Kong; and (4) Illgraben flexible barrier field test (Wendeler et al., 2008). This pilot study (Arup, 2014) demonstrated the capability of LS-DYNA for the modelling of large deformation and movement of debris masses, rockfall as well as the simulation of the interaction between flexible barriers and the debris mass. Output from the analysis included, but was not limited to, the debris velocity, cable forces, debris pressure on the flexible barrier, and the energy balance. Moreover, the simulations proved that numerical code within LS-DYNA can be adjusted for a specific model to take account of both frictional and Voellmy rheologies.

2 OPTIMISATION TO THE DESIGN OF FLEXIBLE BARRIER

2.1 The Ap Lei Chau barrier case study

The Ap Lei Chau flexible barrier (the ALC barrier) was designed as part of the LPMit Programme. Unlike other previously constructed barriers in Hong Kong, the ALC barrier was the first barrier designed using the force approach, as detailed in Kwan & Cheung (2012). The ALC barrier was considered as a tailor-made barrier since the design was modified from a standard prescriptive rock-fall barriers typically installed, with additional cables and energy dissipaters as well as strengthened ring nets specified. The anticipated maximum impact velocity and retained volume of the debris mass were considered substantial and representative of a relatively large-scale debris flow event. The original design consultant adopted LS-DYNA for the calculation of structural forces developed in the barrier, although no debris-structure interaction was taken into account in their analysis. In view of the design background discussed above, the ALC barrier was considered one of the most appropriate cases for the study of coupled debris impact and flexible barrier capacity assessment. It was anticipated that the modelling for the ALC barrier, with the consideration of debris-structure interaction and non-linear behaviour in LS-DYNA, would allow the comparison against the currently available design methodologies and therefore enable the investigation in possible design optimisation for flexible barriers. It would also provide insights in the use of advanced numerical tools for future design of barriers by local practitioners.

2.2 Model setup

The designed ALC barrier consists of the interconnected circular steel ring nets, 7 layers of horizontal cables, 5 layers of upslope cables, energy dissipaters and steel posts. These structural components were modelled explicitly as much as possible to avoid over-simplification of the complex non-linear behaviour of the flexible barrier system, except when such explicit modelling was deemed impossible or impractical in terms of computation efficiency. The ALC flexible barrier model was placed in a numerical flume, in which the debris source was located 10 m away from the barrier. The debris was then injected into the flume at the controlled thickness and velocity required for each simulation case. The duration of the debris injection was also controlled in order to give the correct moving debris volume. Barrier

deformation and the structural forces developed in the system were then measured and recorded with respect to time throughout the course of the simulation. Figure 1 provides an example of one of the LS-DYNA simulations undertaken.

The Drucker-Prager constitutive model was adopted for Arbitrary Lagrangian-Eulerian (ALE) material representing the debris mass. The density of the material was assumed to be 2,200 kg/m^3. The most important parameters that control the energy dissipation of the debris mass during the landslide event were found to be the internal friction angle of the debris and the basal friction between the debris and the topography. However, as the debris source was placed in close proximity to the barrier, the anticipated energy dissipation would be small. In fact, it was found preferable to lower the energy dissipation due to frictional loss between the debris and the ground. It would also be conservative to ignore the possible energy dissipation due to turbulence effect within the debris, which would be described by the Voellmy resistance term in CDF cases. In view of the above, a relatively small internal friction angle of 15° and basal friction of 12° were adopted.

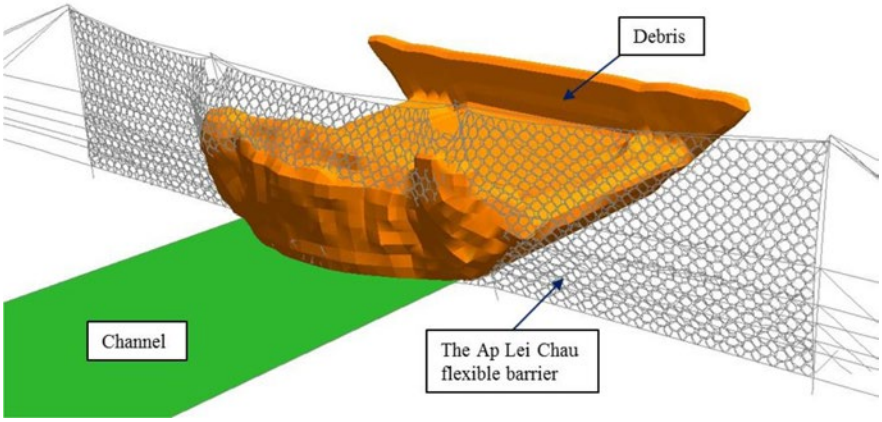

Figure 1: Snapshot of the LS-DYNA simulation in this Study

2.3 Simulation strategy

In order to provide findings and commentaries on the accuracy of the design and simulation approach adopted in the original design of the ALC Barrier; and to provide findings and possible optimisation to the original design of the ALC Barrier, if any, the following simulation cases were developed:

1. Base case – debris volume of 230 m^3 with a constant inflowing velocity of 11 m/s impacting the original design of ALC Type A flexible barrier consisting 7 nos. layers of horizontal cables;
2. Sensitivity check of the base case – simulations carried out based on the base case model, but varying the volume of debris from 230 m^3 to overflow, as well as velocity between 5 m/s and 15 m/s; and
3. Parametric study – simulations carried out on ALC Type A flexible barrier but with reduced layers of horizontal cables, as well as specifying different velocity and different volume of the moving debris.

To evaluate whether a flexible barrier could retain all debris without excessive bulging or deformation, a set of acceptance criteria was predefined when analysing the simulation results. The flexible barrier would be considered as capable of retaining the debris without excessive deformation if it satisfied the following criteria. First, for barrier deformation, the bulging distance should not be more than the height (H) of the barrier (6 m), and the residual height should be > 0.6H. Second, all cable force / energy dissipater axial force should not be more than 80% of the specified maximum load of 300 kN per energy dissipater.

2.4 Results

The LS-DYNA simulation results demonstrated that the barrier deformation of the original "7-layer" barrier in terms of bulging, residual height, forces of all cables and energy dissipaters were well within the design capacity for cases where the barrier was subject to impacts from debris volumes up to 230 m^3 and 11 m/s velocity. Indeed, the analysis showed that the original "7-layer" flexible barrier could be considered underused based on the low utilisation percentage of the energy dissipaters in both the horizontal cables and upslope cables.

The capacity of the barrier was subsequently tested by varying the debris volume from 230 m^3 to 460 m^3 and to continuously inflow from debris source, i.e. overflow case; and by varying the debris velocity to 5 m/s and 15 m/s. This sensitivity analysis found that the barrier can sustain continuous and overtopping flows with velocities up to 11 m/s and still maintain a bulge and residual height within the acceptance criteria. The analysis further showed that barrier deformation only exceeded its design capacity after the debris velocity was increased to 15 m/s with overflow. The results of the utilisation percentages of the cable energy dissipator forces indicated that all horizontal cable energy dissipaters had not been fully utilised in all models, with only the upslope cable energy dissipaters in the overflow cases having been fully utilised.

The findings of this test case confirmed that further optimisation on the design of the flexible barrier is feasible, if not essential. In the parametric study, the number of horizontal cable layers gradually decreased from seven to five, five to three, and three to two. With the same design debris volume of 230 m^3 and debris velocity of 11 m/s, the maximum bulge and residual height of all barriers, except the "2-layer" scenario, satisfied the acceptance criteria. In other words, with the consideration of structure-debris interaction, the number of layers of cables could have been reduced down to three only. Furthermore, it was noted that the utilisation percentage of the horizontal energy dissipaters were all less than 55% for all models, indicating that the number of cables at all horizontal layers can be reduced.

2.6 Energy balance of the ALC barrier

The energy balance of the impact process of the ALC barrier model is presented in Figure 2 below.

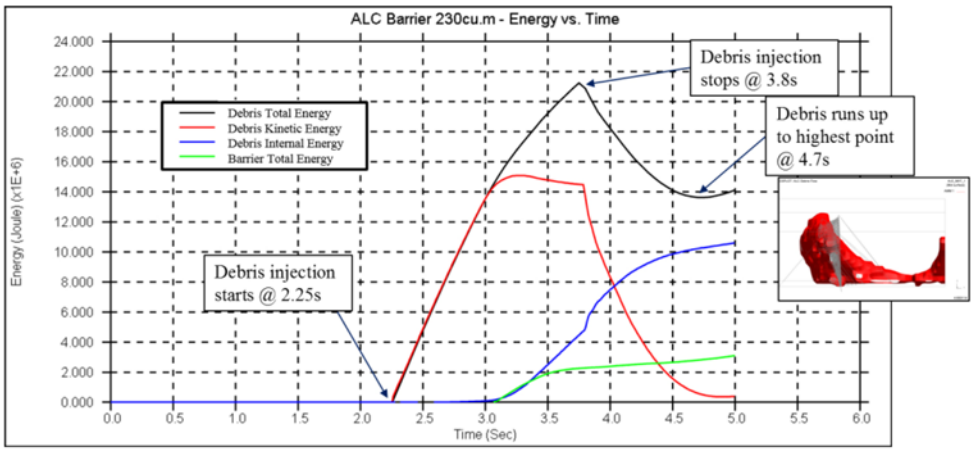

Figure 2: Energy Balance of the ALC barrier base case model

This shows that the kinetic energy of the debris, represented by the red line, increased after debris injection at 2.25 s. At 3 s, the debris impacted on the barrier and a portion of kinetic energy was dissipated by the energy dissipaters and ring net deformation of the barrier. Therefore, the total energy absorbed by the barrier, represented by the green line, increased after impact at 3 s. The debris internal energy, which was defined as the energy produced due to plastic deformation of debris, started to increase at 3 s. It was evident that the maximum energy absorbed by the barrier was approximately 3000 kJ, while the kinetic energy of the debris at impact was approximately 15000 kJ. In other words, the impact

energy absorbed by the ALC barrier could be up to five times less than the energy loading established using the Energy Approach proposed by Kwan & Cheung (2012), which neglects the debris-barrier interaction. Further study to review and evaluate the energy balance involved in the impact process based on simulation using LS-DYNA on some documented cases was therefore deemed necessary.

3 KEY FACTORS GOVERNING THE ENERGY BALANCE

3.1 The Maccaferri 3000 kJ flexible barrier

In order to further investigate the key factors governing the energy balance of a flexible barrier system, a standard type of flexible barrier was chosen to be simulated by varying the selected key factors. The Maccaferri 3000 kJ flexible barrier was chosen in this task as it has been used extensively for landslide mitigation design in Hong Kong and has a detailed product specification. In addition, the ALC barrier was modified from the Maccaferri 3000 kJ flexible barrier and the results could therefore be used as a baseline for comparison in the parametric study.

A 30 m length of Maccaferri 3000 kJ flexible barrier was modelled in LS-DYNA (see Figure 3). This represented a typical flexible barrier module with one centre and two side ring net panels. All structural components were modelled as 1D beam elements. Similar to the modelling technique adopted in the ALC barrier, structural components such as steel rings were modelled explicitly to allow for accurate simulation of the relative movement among the rings, thus the flexibility of the barrier system. A relatively small internal friction angle of 15° and basal friction of 12° were adopted.

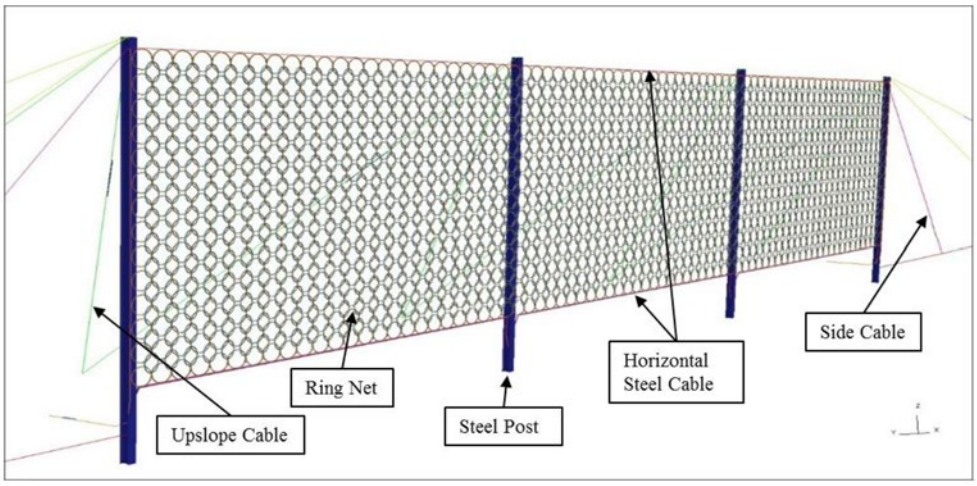

Figure 3: A perspective view of the Maccaferri 3000 kJ LS-DYNA model

3.2 Simulation strategy

Although the energy balance during impact can be influenced by many factors, only debris impact velocity, slope inclination and debris volume were studied in detail. Debris velocity and volume were chosen because they are standard output values from other debris mobility analysis packages used in flexible barrier design such as DAN-W or 2D-DMM. Slope inclination was chosen because it was believed that the higher the slope angle, the higher the static pressure that would build up behind the barrier, which might contribute to higher energy absorption of the barrier. The following simulation cases were developed:

1. Base case: debris volume of 100 m^3 with impact velocity of 6.9 m/s along a 0° inclined slope;
2. Increasing impact velocity from 6.9 m/s to 15.6 m/s, keeping debris volume at 100 m^3 along a 0° inclined slope;
3. Increasing inclination from 0° to 30°, keeping impact velocity at around 10 m/s and debris volume at 100 m^3; and

4. Increasing debris volume from 100 m^3 to 260 m^3, keeping impact velocity of 6.9 m/s along a 0° slope.

The acceptance criteria was kept the same as the ALC barrier in order to assess whether the barrier is capable of retaining the debris without excessive deformation.

3.3 Effect of increasing debris velocity

The results of the models with different debris velocities before impact and their associated energy balances are presented in Table 1. Both slope inclination and debris volume were kept constant for these cases. All energy dissipaters within Models F and N did not exceed 80% utilisation. However, when the debris velocity before impact increased from 9 m/s to 11.1 m/s, the energy dissipaters in the upslope cables exceeded 80% utilisation.

The BE to KE ratio in the four models ranged approximately between 11% and 22%, indicating the barriers were absorbing only less than 22% of the debris kinetic energy at impact. The result suggested that an increase in debris velocity would only slightly increase the amount of energy absorbed by the barrier, but would lead to >80% utilisation of the upslope dissipaters. After yielding of the energy dissipater (>80% utilisation), the BE to KE ratio did not increase with the velocity before impact.

Table 1: Summary of energy balance of models with increasing debris impact velocity

Model ID	Slope (°)	Initial velocity (m/s)	Velocity before impact (m/s)	Debris volume (m^3)	Energy Dissipater >80% Utilisation (Yes / No)	Debris Internal Energy at impact (IE)(kJ)	Debris Kinetic Energy at impact (KE) (kJ)	Max. Barrier Total Energy (BE) (kJ)	BE to KE Ratio (%)
F (Base Case)	0	5.0	6.9	100	No	1100	1060	120	11
N	0	7.5	9	100	No	1550	2700	460	17
O	0	10.0	11.1	100	Yes (Upslope)	2100	4900	1080	22
G	0	15.0	15.6	100	Yes (Upslope and Horizontal)	2700	11700	2240	19

3.4 Effect of increasing slope inclination

The results for models with different slope inclinations and their associated energy balances are tabulated in Table 2 below. Debris volume and velocity before impact were kept as close as possible. At least one of the energy dissipaters in Models Q, K and R exceed 80% utilisation.

The BE to KE ratio in Models N, Q and K increased from 17% to 36% gradually, with respect to an increase in slope inclination from 0° to 15°. The BE to KE ratio increased significantly from 36% to 83% with an increase in slope inclination from 15° to 30°. The result suggested that an increase in slope inclination would increase the amount of energy absorbed by the barrier. Although at least one of the energy dissipaters exceed 80% utilisation in Models Q, K and R, the results showed that the barrier still absorb less than 83% of the debris kinetic energy during impact.

Table 2: Summary of energy balance of models with increasing slope inclination

Model ID	Slope (°)	Initial velocity (m/s)	Velocity before impact (m/s)	Debris volume (m^3)	Energy Dissipater >80% Utilisation (Yes / No)	Debris Internal Energy at impact (IE)(kJ)	Debris Kinetic Energy at impact (KE) (kJ)	Max. Barrier Total Energy (BE) (kJ)	BE to KE Ratio (%)
N	0	7.5	9	100	No	1550	2700	460	17
Q	10	7.5	10	100	Yes (Upslope)	1480	3900	1140	29
K	15	5.0	9.1	100	Yes (Upslope)	850	2850	1030	36
R	30	3.0	10.1	108	Yes (Upslope and Horizontal)	400	2450	2040	83

3.5 Effect of debris volume

The results for models with different debris volumes and their associated energy balances are tabulated in Table 3. Slope inclination and debris velocity before impact were kept constant. All energy dissipaters within all models did not exceed 80% utilisation. The BE to KE ratio ranged approximately between 5% and 11%. The result suggested that an increase in the debris volume would have no significant effect on the energy absorbed by the barrier and the energy dissipater utilisation ratio, athough it still showed trend of decreasing BE to KE ratio with increasing debris volume.

Table 3: Summary of energy balance of models with increasing debris volume

Model ID	Slope (°)	Initial velocity (m/s)	Velocity before impact (m/s)	Debris volume (m^3)	Energy Dissipater >80% Utilisation (Yes / No)	Debris Internal Energy at impact (IE)(kJ)	Debris Kinetic Energy at impact (KE) (kJ)	Max. Barrier Total Energy (BE) (kJ)	BE to KE Ratio (%)
F (Base Case)	0	5.0	6.9	100	No	1100	1060	120	11
U	0	5.0	6.9	180	No	1200	3528*	214	6
V	0	5.0	6.9	260	No	1200	5096*	260	5
*Remarks: Due to the short flume distance, the debris in Models U and V were not fully released at the moment of impact. The kinetic energy value was deduced by assuming the debris were fully released and impacted the barrier at the moment when all debris has just been released.									

3.6 Insight for design optimization

The effect of velocity before impact to the BE to KE ratio appeared to be not significant. One possible explanation was that an increase in velocity would also lead to an increase in kinetic energy, which in turn lead to the increase in the energy absorbed by the barrier. Since BE and KE both increased with velocity, the BE to KE ratio would remain similar.

The effect of slope inclination to the BE to KE ratio was considered significant. One possible explanation was that an increase in slope inclination would suppress jet-up and internal turbulence of the debris, which was reflected in the decrease in debris internal energy. Due to the lower debris internal energy, more energy would be transferred to the barrier and therefore BE increased.

The effect of debris volume to the BE to KE ratio appeared to be not significant, though it still showed trend of decreasing BE to KE ratio with increasing debris volume. One possible explanation was that once the dead load of debris was formed in front of the barrier, further impact of debris along a horizontal

slope would not contribute significantly to the energy absorbed by the barrier. However, it should be qualified that this result was only applicable to the 0° slope and with approximately 10 m wide channel.

The findings of the sensitivity analysis for the ALC barrier and the Maccaferri 3000 kJ barrier indicate that there is likely to be some rooms for design optimization of debris-resisting flexible barriers. In this respect it is noted that the upslope cables of proprietary rockfall barriers designed for resisting debris impact might constitute a weak link that requires further study. Further parametric study using LS-DYNA to explore the energy dissipation capacity of barriers under debris impact is therefore suggested. This could be validated by means of physical tests.

4 CASE STUDIES ON RIGID BARRIER DESIGN

4.1 Multiple rigid barrier design in Fo Tan study area

Following on from the analysis for flexible barriers, LS-DYNA was subsequently used as a design tool for rigid barrier design under an LPMit Agreement for Study Area 7SW-B/SA1 in Fo Tan (Arup, 2016a). The Study Area included three catchments (FT01-03) and previous hazard assessments had indicated that mitigation works for channelised debris flow (CDF) hazards were required at the mouth of a drainage line within Catchment FT03. An internal friction angle of 15° and a basal friction angle of 11° with a turbulence coefficient of 500 m/s^2 were adopted in LS-DYNA as recommended by GEO for CDF hazards. Debris mobility modelling for this catchment using LS-DYNA indicated that 445.5 m^3 of debris would pass through the proposed barrier location and hence a mitigation design volume of 450 m^3 was adopted.

Various combinations of single barrier and multiple rigid barrier options were evaluated by LS-DYNA, with different dimensions, configurations and locations assessed in order to optimise and balance the construction cost, construction period, visual impact, complexity and impact from temporary works. The multiple rigid barriers option, as shown in Figure 4, was subsequently adopted as the preferred approach for the detailed design. This configuration comprises three rigid barriers with heights and lengths of 2.5 m by 26.0 m, 2.5 m by 21.0 m and 2.5 m by 14.0 m respectively placed at 8 m horizontal intervals. Openings of 1 m height and 5 m length were explicitly designed in the middle of the two upper barriers in order to control the manner of overtopping and enhance the retention capacity at the terminal barrier.

Figure 4: Multiple barriers option designed by LS-DYNA

Unlike traditional 2D-DMM and spreadsheet calculations, LS-DYNA is capable of modelling the debris flow characteristics, such as the overtopping of debris at the two upper barriers. In addition, the barriers can be designed to fit the topography using LiDAR dataset, which helped the designer to determine the best configurations, dimensions and locations for the barriers and thus minimise construction cost and impacts. This example demonstrated the significant benefits afforded by the use of three-dimensional analytical tools such as LS-DYNA in the design process.

4.2 International peer reviews for landslide restoration works at Mount Umyeon in Seoul

4.2.1 Background

On 27 July 2011, a total of thirty three (33) debris flows occurred in Umyeonsan, Seoul. At least seventeen (17) fatalities were reported as a result of these debris flows and a comprehensive landslide restoration works programme was initiated following the event. This included the fast-track design and construction of numerous erosion control dams (e.g. check dams) within the various catchments at Umyeonsan.

Following the completion of the works a stability check was requested by the Seoul Metropolitan Government (SMG) for the existing erosion control dams located within the four selected basins. LS-DYNA was adopted as the numerical tool to check both the debris mobility and barrier stability against Hong Kong standards, with both static and dynamic impact forces considered. Some of the key findings from the stability check of the erosion control dams in the Raemian Basin, in which four (4) landslides and three (3) fatalities occurred, are briefly described.

4.2.2 Debris mobility back analysis in Raemian basin

In the Raemian basin, the initial landslide volume from the 2011 event of 1,839 m^3 was modelled. The LS-DYNA input parameters were calibrated based on the video clips of the landslide, site photos and the records of on-site examinations carried out by the SMG. By trial and error, an internal friction angle of 18° and a basal friction angle of 11° with a turbulence coefficient of 500 m/s^2 were adopted in LS-DYNA. The final shape and extent of debris deposition, debris flow velocity and thickness at Raemian Apartment were extracted from LS-DYNA and compared with site data. Figure 5 illustrates the graphical output of the LS-DYNA simulation at specific timesteps.

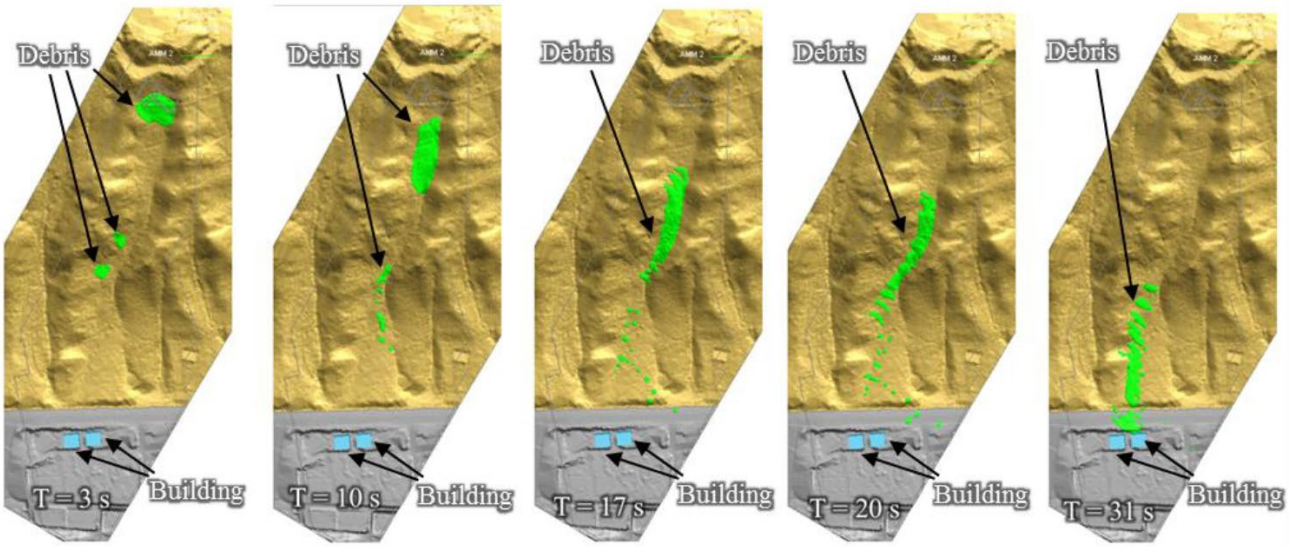

Figure 5: Graphical output of the LS-DYNA simulation at specific timesteps

4.2.3 Stability check

Following the LS-DYNA back analysis, a stability check of the barriers constructed following the 2011 landslide events was carried out. The four barriers located within the Raemian Basin were modelled based on the details presented in as-constructed drawings, the accuracy of which was verified during site inspections in late-2016. Figure 6 shows the initial debris source location and the final debris deposition profile after reaching the barriers.

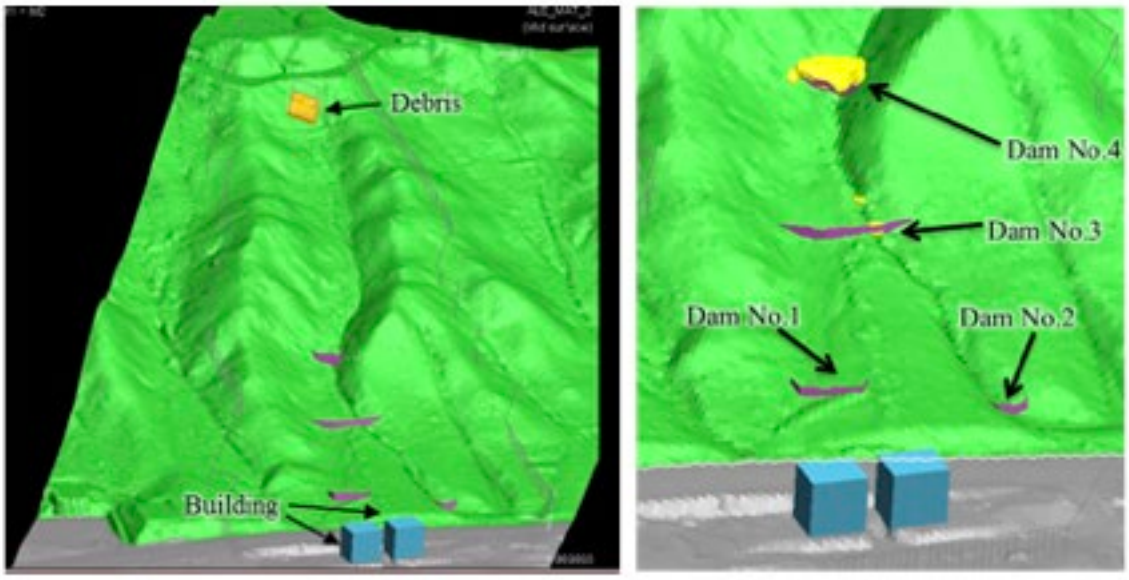

Figure 6: Initial debris source location (left) and final deposition (right)

LS-DYNA output includes dynamic impact pressure and static impact pressure. The pressure output from the analysis was extracted for checking of the barriers' bearing capacity and factor of safety against sliding and overturning. In the event that the barriers failed to satisfy the local code requirements for stability, possible mitigation measures would be provided. A similar checking process was also implemented for the other three basins selected for study. This example indicates how tools such as LS-DYNA can also be utilised for design review and checking purposes to provide an additional layer of confidence in the measures provided.

5 CONCLUSIONS

The findings from the Ap Lei Chau flexible barrier LS-DYNA model provided insight on the potential for optimisation in the design of flexible barriers. The analysis showed that the total energy absorbed by the barrier could be significantly less than the kinetic energy of debris during impact. However, it highlighted that the upslope cables might be a weak link in the barrier systems that requires further study. Additional parametric studies using a standard prescriptive flexible barrier indicated that the amount of energy absorbed by the barrier was significantly influenced by the upslope inclination, yet less dependent on the debris impact velocity and debris volume. The software package was also trialled for several cases of design and design validation for rigid barriers and has also proven it usefulness and benefit in this regard, showing significant benefits to the pseudo-three dimensional approaches typically adopted for such works.

ACKNOWLEDGEMENTS

This paper is based on the reports produced for the pilot numerical investigation of the debris-resisting capacity of flexible barriers, computer services of numerical investigation of the debris-resisting capacity of flexible barriers from the energy perspective, design option assessment report for Study Area No. 7SW-B/SA1 behind Fo Tan Cottage Area, Fo Tan, Shatin and the stability analysis of restored area of landslide in Mt. Umyeon. This paper is published with permission of the Head of the Geotechnical Engineering Office, and the Director of Civil Engineering and Development Department of the Hong Kong Special Administrative Region. The authors would like to thank all of the staff associated with the projects for their valuable contributions.

REFERENCES

Arup 2014. *Pilot Numerical Investigation of the Interactions between Landslide Debris and Flexible Debris-resisting Barriers (under Agreement No. CE10/2009 (GE) Study of Landslides Occurring in Kowloon and the New Territories in 2010 and 2011 – Feasibility Study)*. Final report prepared for the Geotechnical Engineering Office, Civil Engineering and Development Department, Hong Kong, 143 p.

Arup 2016a. *Design Option Assessment Report, Study Area No. 7SW-B/SA1 behind Fo Tan Cottage Area, Fo Tan, Shatin (under Agreement No. CE31/2013 (GE) Landslip Prevention and Mitigation Programme (LPMit), 2013, Package E, Landslip Prevention and Mitigation Works – Investigation, Design and Construction)*. Final report prepared for the Geotechnical Engineering Office, Civil Engineering and Development Department, Hong Kong, 11 p.

Arup 2016b. *Pilot Numerical Investigation of the Debris-resisting Capacity of Flexible Barriers. Phase 1 Final Report – Ap Lei Chau Flexible Barrier Simulation*. Final report prepared for the Geotechnical Engineering Office, Civil Engineering and Development Department, Hong Kong, 98 p.

Arup 2016c. *Stability Analysis of Restored Area of Landslide in Mt. Umyeon*. Final report prepared for the Green Seoul Bureau, Seoul Metropolitan Government, Seoul, 116 p.

Arup 2017. Computer Services of Numerical Investigation of the Debris-resisting Capacity of Flexible Barriers from the Energy Perspective. Final report no.2 prepared for the Geotechnical Engineering Office, Civil Engineering and Development Department, Hong Kong, 73 p.

Iverson, R.M., Logan, M. & Denlinger, R.P. 2004. Granular avalanches across irregular three-dimensional terrain: 2. Experimental tests, *Journal of Geophysical Research*, VOL. 109, F01015.

Kwan, J.S.H. & Cheung, R.W.M. 2012. *Suggestions on Design Approaches for Flexible Debris-resisting Barriers, incl. Appendix C Comments and Responses*. Discussion Note DN1/2012, Geotechnical Engineering Office, Civil Engineering and Development Department, Hong Kong.

Wendeler, C., McArdell, B.W., Volkwein, A., Denk, M. & Groener, E. 2008. Debris Flow Mitigation with Flexible Ring Net Barriers – Field Tests and Case Studies. *Proceedings of Second International Conference on Monitoring Simulation, Prevention and Remediation of Dense and Debris Flows II, Wessex Institute of Technology, UK*, 21-31.

Volkwein, A.K.H. 2004. Numerical simulation of flexible rockfall protection systems. *Thesis for Doctor of Technical Sciences of the Swiss Federal Institute of Technology Zurich*.

A Case Study of Temporary Support Design for Mined Adits in Highly Decomposed Granite

F. Desaintpaul, C. Hu, H. Ling & J. Rickard
Arup, Hong Kong
E. Clech, R. Cho & C. Cacarié
Vinci Construction Grands Projets, Hong Kong

ABSTRACT

MTRC SCL Contract 1103 includes the construction of four short adit connections between segmentally-lined tunnels and a deep excavation. The ground conditions at the level of the Ma Chai Hang Ventilation (MCV) Building Connection Adits consist of Highly Decomposed Granite (HDG). The adits were mined in free air while dewatering was being carried out during construction for groundwater control.

This paper presents the temporary adit support techniques used and the construction sequence developed to enhance the effectiveness and robustness of the design. Temporary support included pre-support pipe roofs or spiles, shotcrete lining and precautionary face stabilization measures. The design employed a combination of prescriptive and analytical design methods supplemented by PLAXIS two-dimensional finite-element analysis. The temporary support design principles are presented, with particular emphasis on the pre-support design in terms of design loading calculation, structural capacity checking and three-dimensional arrangement. The deformation of the temporary linings was monitored during adit construction and the main findings are presented.

1 INTRODUCTION

The Shatin to Central Link (SCL) is to provide a new strategic link to cater for the growing passenger demand between the North-East New Territories and the urban areas of Hong Kong. SCL Contract 1103 (Hin Keng to Diamond Hill Tunnels) was awarded to Vinci Construction Grands Projets (VCGP) in 2012, with Ove Arup & Partners Hong Kong Ltd (ARUP) being VCGP's Designer.

The contract comprises the construction of a range of tunnels and structures using a variety of construction methods. The works include the Ma Chai Hang Ventilation Building (MCV) and two running tunnels (Figure 1), between Ma Chai Hang and the new Diamond Hill Station (constructed by others).

This paper presents the temporary support design of four adits providing part of the connections between the running tunnels and the MCV Shaft, namely the MCV "Backup Access Vehicle" (BAV) and "Emergency Egress Passage" (EEP) adits.

2 SITE DESCRIPTION AND ADIT GENERAL ARRANGEMENT

2.1 Site location

A portion of the running tunnels under Contract 1103 is of twin bore single-track segmental lining type constructed by a slurry Tunnel Boring Machine (TBM). The tunnels interface with the MCV Shaft, which

is located in the north-west corner of Ma Chai Hang Recreation Ground at the junction of Chuk Yuen Road and Ma Chai Hang Road, as shown in Figure 1.

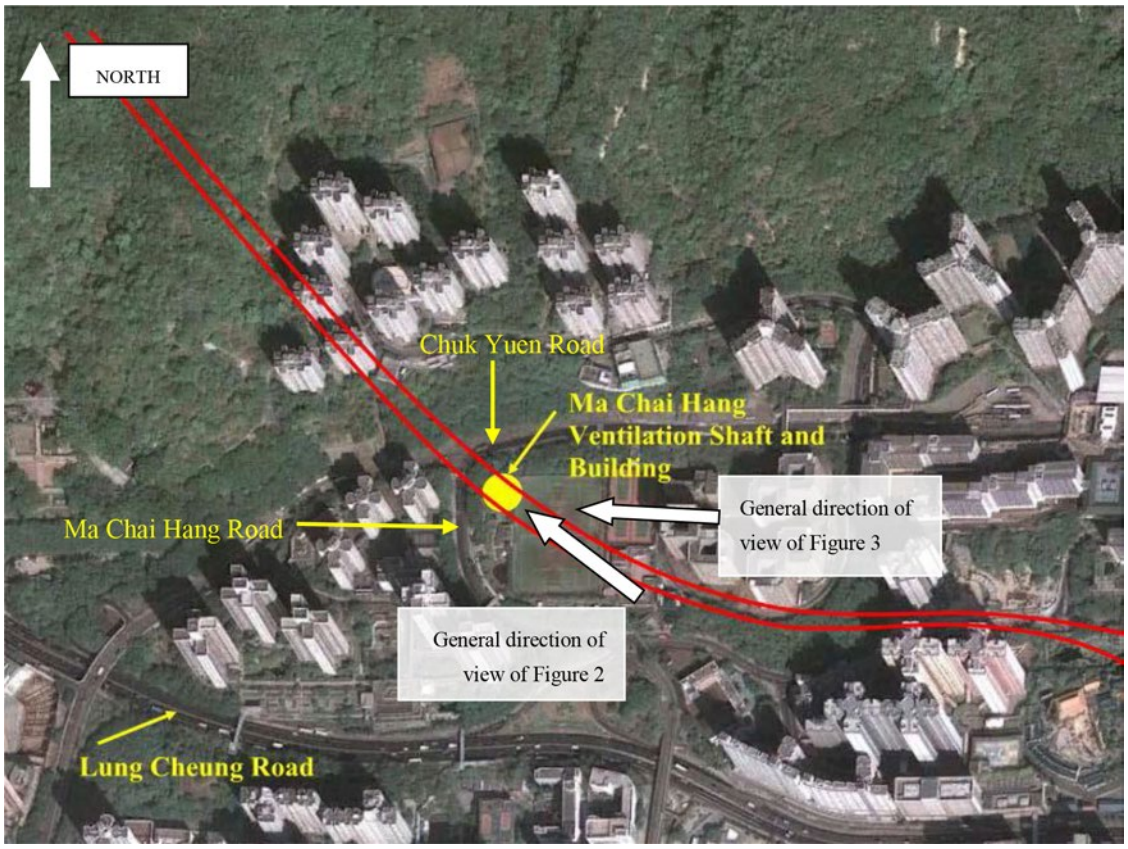

Figure 1: Location plan of the Ma Chai Hang Ventilation (MCV) Building

The site is relatively flat at an elevation of approximately +45.5mPD and was used as a recreation ground prior to construction. Both existing roads are at a higher elevation than the site and the general topography falls from the steep terrain of the Lion Rock Country Park in the north to Kowloon Bay in the south.

2.2 General description

The MCV Building/ Shaft is a reinforced concrete structure built within the shaft. Its lower central portion is called the Central Accommodation of the MCV Internal Structure (MCV-CA) and is shown in Figures 2 and 3. The MCV Shaft is a circular diaphragm wall structure with an inner diameter of 40.6m. The MCV-CA was constructed within a 16m (approx.) deep pipe pile strutted cofferdam, located in the middle of the shaft, below the general site formation platform of the shaft base.

The BAV adits are located at the lowest level (L8) of the MCV-CA. They provide an access to the running tunnels for a rubber tyres-mounted rescue vehicle in the event of an emergency (the vehicle would access the permanent rails by means of a level crossing). The EEP serves as an emergency egress point for the running tunnels, connecting to the L7 level of the MCV-CA. The adits also contain services for the running tunnels. A layout plan and 3D model of the MCV are shown in Figures 2 and 3. Figure 4 shows the BAV Adits excavation plan, and typical adit sections are shown in Figures 5 to 7. The BAV Adits are approximately circular, with an inner diameter of 5.8m, with a power cable trough at the invert of the Up Track (UT) Adit. The EEP Adits are horse-shaped with approximately outer dimensions of 3.6m (span) x 3.9m (height). The BAV final works will provide a passageway in each tunnel of 3m min. width at the running tunnel segmental lining, at the centre of a group of 3 tunnel segments. Likewise, the EEP will provide a 1.5m wide passageway at the running tunnel openings. The centre line of the adits was aligned with a circumferential joint of the segmental lining, so that the opening is at the centre of 2 segments. The adits final alignment was adapted to the as-built location of the two running tunnel

segmental lining. All adits were constructed using a similar sequence similar, with the permanent structural concrete cast after installation of the two steel lintel beams above and beneath the running tunnel lining openings.

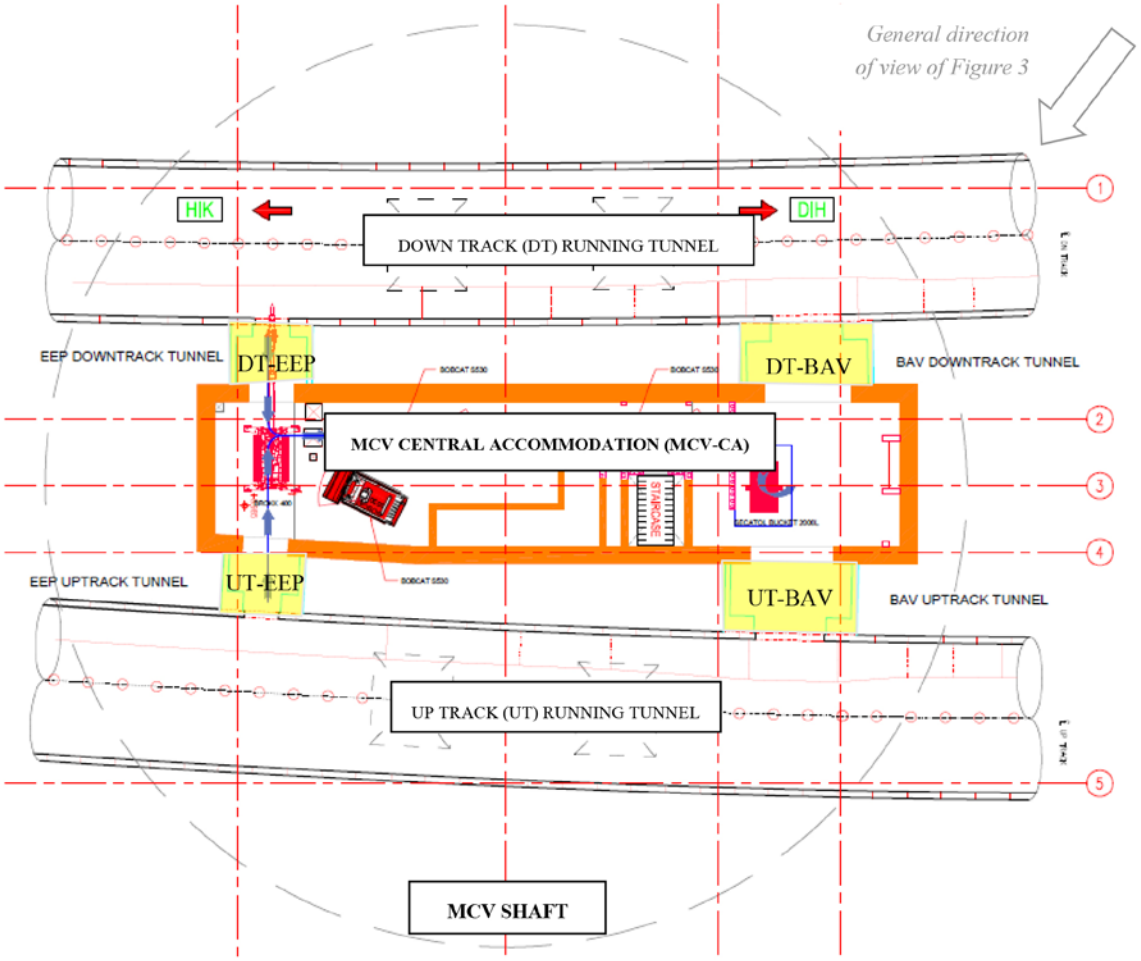

Figure 2: MCV layout plan (the adits are shaded in yellow)

3 GROUND AND GROUNDWATER CONDITIONS

3.1 Ground investigation

Ground investigation (GI) data within the immediate area of the MCV Shaft comprise 7 vertical boreholes and 7 inclined boreholes. The majority of these were project-specific, with only one archival borehole in the area. Two piezometers had been installed. Further GI data from the surrounding area were considered when building the site ground model, particularly for the rockhead model. This included the predrillings records for each of the diaphragm wall panels and for the excavation required for construction of the MCV-CA.

3.2 Geological characterization

The MCV site is underlain by Kowloon Granite, locally overlain by Colluvium. GI data revealed a layer of Fill up to 6m thick overlying Granite of various decomposition grades. The Engineering Rockhead or Category 1(c) rockhead is defined as the level below which 5m or more Grade III or better rock with 85% or greater total core recovery is proven. Predrilling revealed extremely variable, rockhead, with

elevation differences of up to 50m over lateral distances of less than 5m, with a conspicuous north west – south east trending trough of low rockhead crossing the centre of the MCV Shaft footprint, as illustrated in Figure 3.

Generally, the running tunnels were driven through mixed ground ranging from Highly Decomposed Granite (HDG) to Moderately Decomposed Granite (MDG).

Within the MCV Shaft area, the upper portion of the ground profile was excavated, leaving material expected to be HDG (or less decomposed material) below the shaft final excavation level. This was the ground conditions of relevance to the connection adits. This assumption was verified against construction records of the works previously completed, namely the MCV Shaft and the MCV-CA excavation and lateral support (ELS) works. This confirmed that the adits would be located in HDG, with about 7m ground cover between the adit crown and the MCV Shaft general site formation level of about +19mPD.

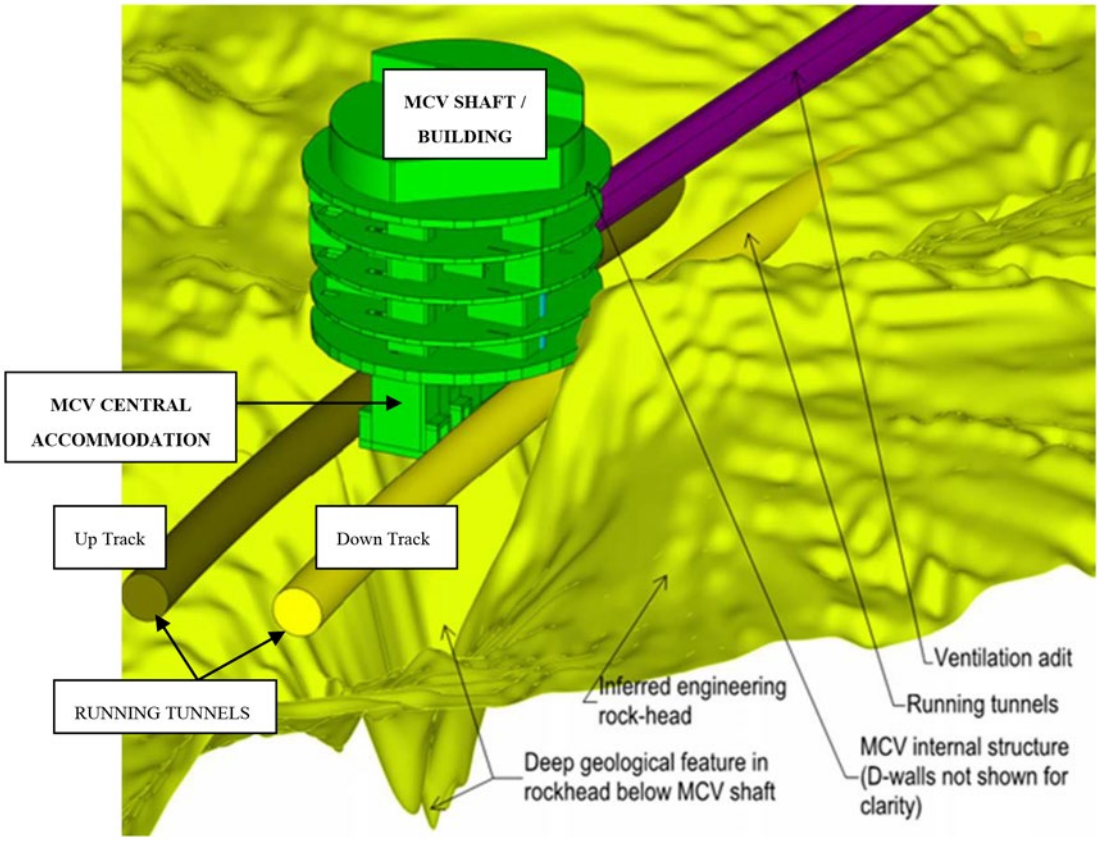

Figure 3: 3D model of MCV Shaft/Building, running tunnels and inferred rockhead
(Note: the MCV Adits are not visible on this figure)

3.3 Groundwater

Prior to construction of the MCV shaft, the groundwater level was measured to be at a depth of up to about 2m below ground surface. However this did not have a significant effect on the design of the connecting adits, due to the MCV Shaft dewatering being carried out during the course of these temporary works (the rationale for and general benefits of that dewatering scheme are described by Lee et al. (2015)).

3.4 Geotechnical design parameters

The HDG design parameters, given in Table 1, were derived based on field and laboratory testing results.

Table 1: HDG design parameters at MCV

Bulk Unit Weight (kN/m^3)	Cohesion c' (kPa)	Angle of Shearing Resistance φ' (°)	SPT-N Design Line	Poisson's Ratio ν	In-situ Stress Ratio k	Elastic Modulus (MPa)
20.5	15	40	N = 667	0.3	0.36	E = 2 N

This considered data from triaxial testing of HDG borehole samples collected within the vicinity of the MCV Shaft. The adopted parameters are on the conservative side, compared to the upper bound parameters quoted in Geoguide 1 for Completely Decomposed Granite (CDG), i.e. c' = 15kPa and φ' = 45°, and to values reported in Costello et al. (1986), i.e. c' = 20kPa and φ' = 42°.

4 TEMPORARY WORKS DESIGN

4.1 Overall construction sequence and challenges

The adit construction was carried out from the MCV-CA area, while bottom–up construction of both the MCV-CA structure and the MCV Building Structure was in progress. This staging was adopted due to programme requirements for TBM tunnelling and MCV structure construction. The design was also closely coordinated with the Construction Team to ensure that the design was fully aligned with the construction programme, methodology and plant to be deployed for the works, with detailed consideration of all necessary construction tolerances and working space. A site-specific risk assessment was also carried out.

The excavation of the UT Adits was scheduled to be completed after the first floor of the MCV-CA was built, therefore imposing a surcharge on the temporary support of the adit under construction. To suit the programme of the second running tunnel drive, the excavation of the Down Track (DT) Adits would commence after completion of the MCV-CA structure, resulting in an even larger surcharge onto the DT adit temporary support.

At the two UT adit portals, a temporary box-out of the MCV-CA walls was used. This enabled to subsequently expose the MCV-CA temporary pipe pile cofferdam wall, so that pipe piles may be removed before installation of the first round of adit pre-support, and subsequent adit excavation works. At the two DT adit portals, a reinforced concrete bulkhead had to be removed at the MCV-CA permanent cast external walls, prior to proceeding with the adit (this bulkhead was necessary to resist to the slurry and grouting TBM pressures arising from the DT TBM drive, in close proximity to the MCV-CA structure). Advance probing was carried out prior to excavation to verify that groundwater conditions were as per design assumption.

Adit excavation was carried our using a Brokk 400 excavator, in typical advance lengths of 0.8m and 0.5m in the BAV Adits and EEP Adits respectively. A sprayed concrete lining was applied sequentially on the adit excavation perimeter and face (as a precautionary measure). Figure 4 illustrates some of the adit works.

The adit excavation resulted in an unbalanced horizontal earth pressure acting onto the tunnel segmental linings. This had been considered in the design of the segments (and their bicones) to be installed at the tunnel/adit junctions. Due to their relatively small size, the permanent openings could be formed in the segmental lining without the need for a temporary strengthening structure. A permanent external steel lintel beam was then installed around the tunnel opening, to be later encased in the final adit concrete lining.

It should be noted that no temporary adit steel supports (e.g. lattice girders or steel arches) were used, as the temporary shotcrete lining provided sufficient support (this lining was not mesh reinforced).

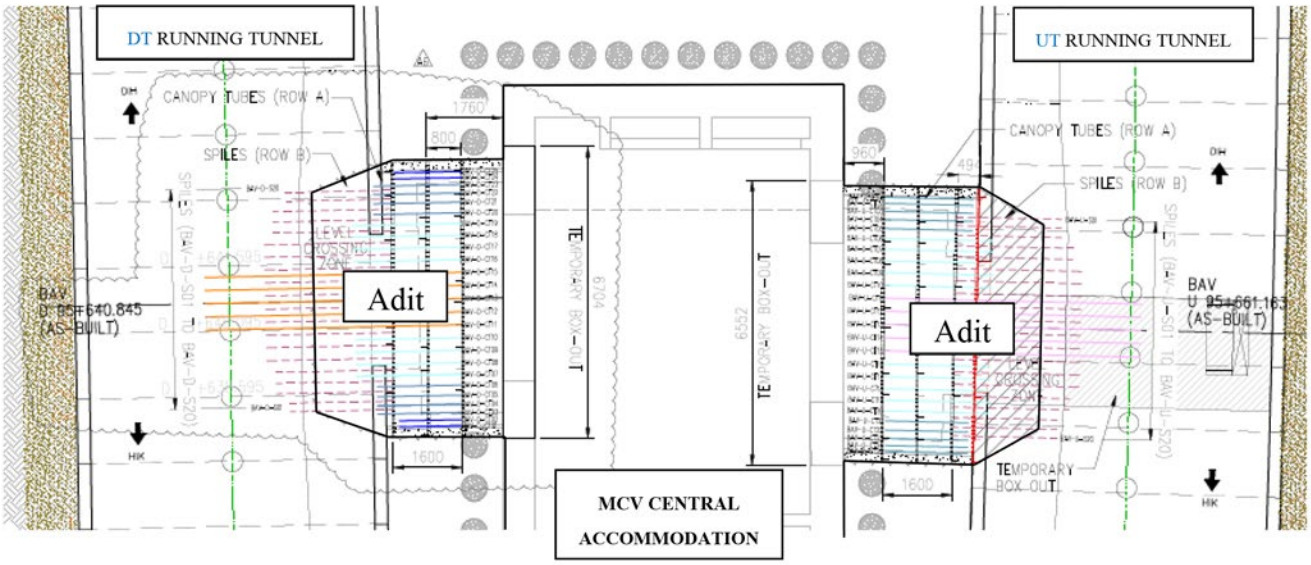

Figure 4: MCV-CA – BAV Adits excavation layout plan (Down Track & Up Track)

4.2 Overall approach to temporary works design

The design employed a combination of prescriptive design, analytical design methods and PLAXIS finite-element analyses. The key design aspects include face stability analysis and support, design of pre-support system for the selected advance round length, and determination of the temporary shotcrete lining requirements, and associated instrumentation and monitoring.

4.3 Face support analysis

The adits were proposed to be excavated full face. Due to the proximity of the running tunnel, face bolting was not a viable option for face support. Therefore face stability had to be maintained by selecting the appropriate staging (i.e. full face or divided face excavation) and adit face angle.

From engineering judgment, considering the relatively small adit face area, the prevailing ground conditions (HDG) and the favourable effect of MCV Shaft dewatering on face stability, the adit faces were expected to be self-supporting.

However, to verify the effect of the surcharge imposed by the MCV-CA structure under construction, a face stability analysis was carried out. This used the approach described by Mayer et al. (2003). This method enables to determine the face support required to prevent an active wedge failure condition from developing. It is assumed the wedge formed is in accordance with Rankine active earth pressure theory. This was also verified using the approach proposed by Leca & Dormieux (1990).

The analysis indicated that no face support was required for the proposed vertical face excavation. Notwithstanding this, as a precautionary measure, the application of a thin shotcrete layer on the adit face was specified (min. 50mm thick steel fibre reinforced, of MTRC Type "S1", with a strength of 40MPa).

4.4 Pre-support design (canopy tubes and spiles)

In conventional soft ground tunnelling, pre-support is generally used to provide advance support at the face and limit any potential over-excavation or ground fallout from the crown. This provides an adequately safe working environment while the temporary sprayed concrete lining is being applied. A challenge was the close proximity of the segmental lining of the running tunnels. In a conventional pre-support arrangement, the tubes or spiles are overlapped between successive rounds of excavation. For the MCV Adits, a more complex arrangement was required due to the proximity of the tunnels, which ran approximately perpendicular to the adits. This included an initial round of pre-support elements, installed from the adit portals, supplemented by an array of spiles installed at another stage of excavation. The orientation and length of the canopy tubes and spiles were adjusted to suit the individual adit configuration, as illustrated in Figures 5 to 7.

The design loading was estimated using the approach proposed by John & Mattle (2002). Canopy tubes are designed as a beam carrying a factored uniformed dead load to bridge the unsupported ground during advancement, with a design beam length chosen as 1.5 times the unsupported length, with a fixed end ahead of the face, the other end being simply-supported. However, some of the pre-support elements had to be relatively short, to avoid clashing with the tunnel segmental lining. The structural capacity of these shorter elements were therefore checked assuming a cantilevered beam condition.

While the pre-support design principles for the BAV and EEP adits were similar, details varied to suit the different adit profiles and lengths. For the BAV adits, with an excavated span of 6.4m, the design used a combination of canopy tubes (of type AT-89, with a steel yield strength of 355 MPa, and nipple coupling) and 38mm dia. self-drilling spiles (of type R38, DSI DYHI® Drill Hollow Bar System, with a steel yield strength of 560 MPa). For the EEP adits (of 4.1m excavated span), R38 self-drilling spiles were found to be sufficient, with an installation angle of between 30° and 40° to the horizontal, due to the adit-running tunnel configuration. All pre-support elements were grouted (20MPa min. strength at 28 days).

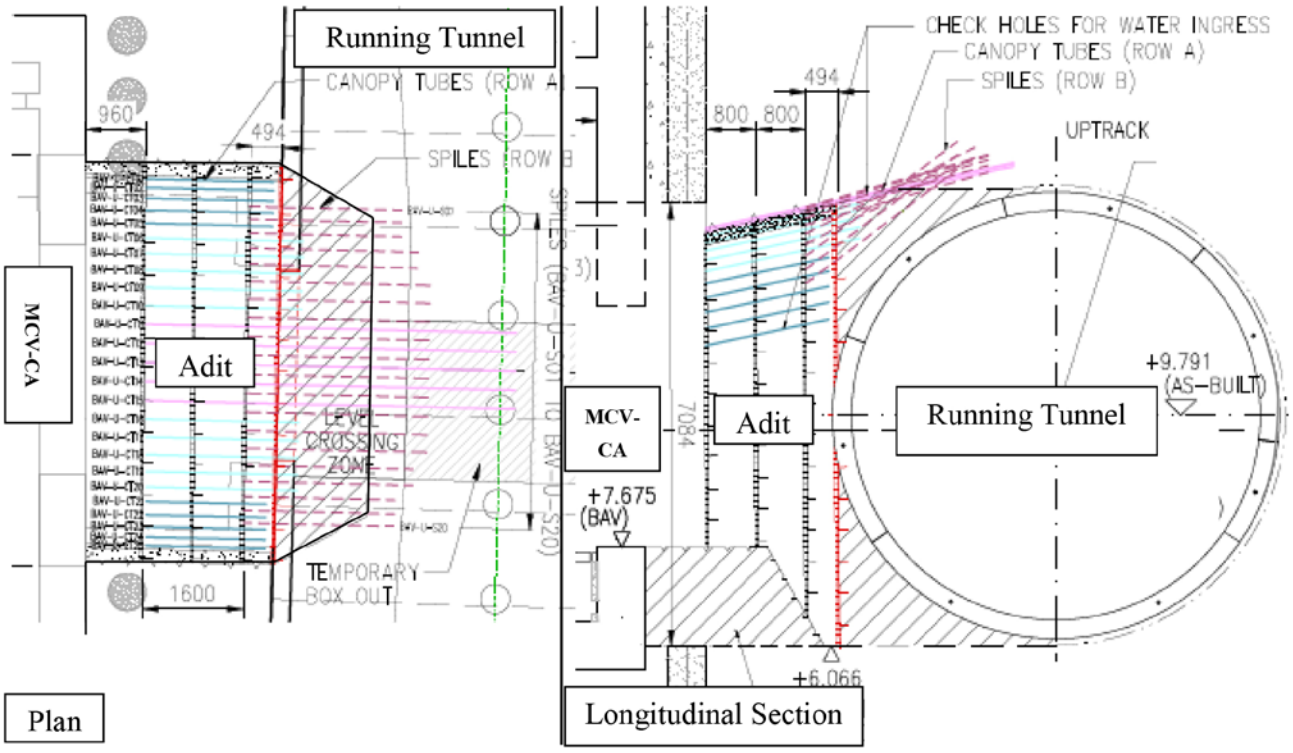

Figure 5: BAV UT Adit plan and longitudinal section (similar arrangement for BAV DT Adit)

For the BAV Adits, canopy tubes of 88.9mm outer diameter and 6.3mm tube thickness were installed from the portal at a maximum inclination of 12° to the horizontal. Design spacing was at 400mm c/c for the UT Adit, reduced to 300mm c/c for the DT Adit, due to the effect of the larger surcharge acting above that adit (see Section 4.1). A few 6m long tubes could be used at the crown of the adit, while tube length had to be gradually reduced to approx. 3m towards the base of the pre-support zone. A localised enlargement to the adit excavation profile was required for the installation of a permanent lintel beam along the running tunnel lining opening. To provide additional support to this excavation pocket, which had a flat roof, another row of spiles was specified to be installed before the final excavation step. This was based on a prescriptive design approach, in conjunction with visual inspections to be carried out during the works, to confirm the adequate performance of the support.

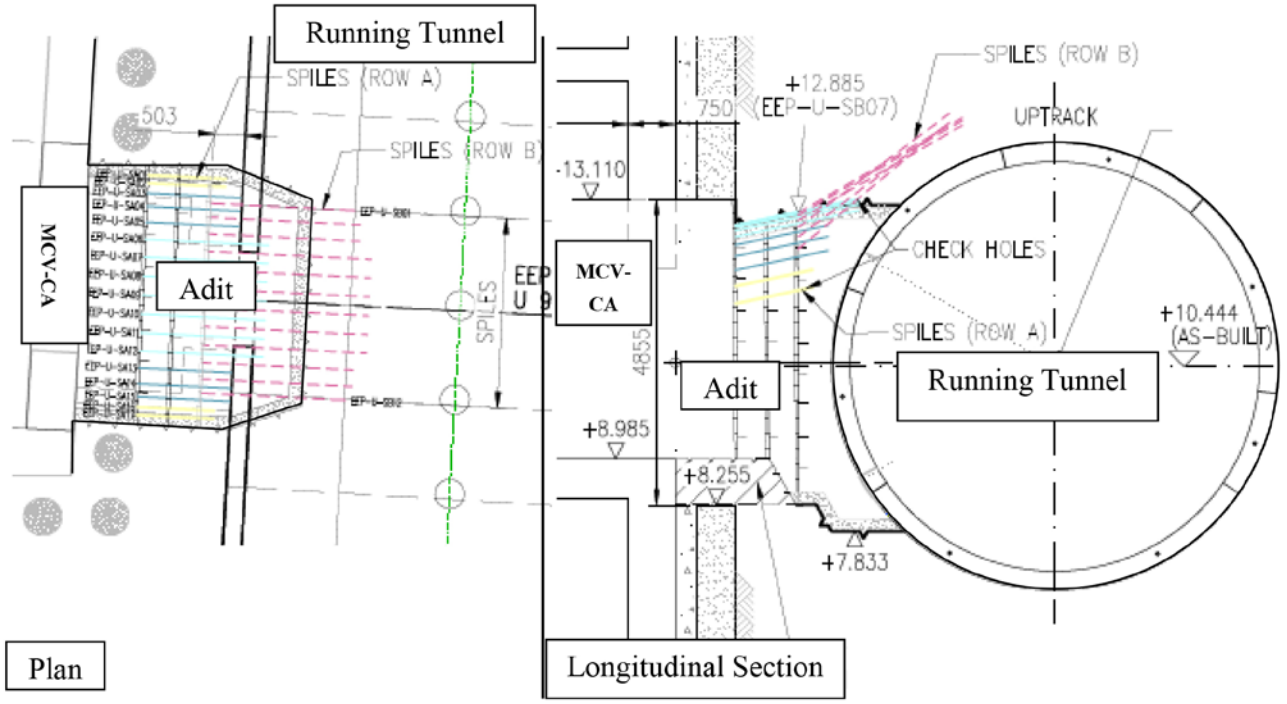

Figure 6: EEP UT Adit plan and longitudinal section (similar arrangement for EEP DT Adit)

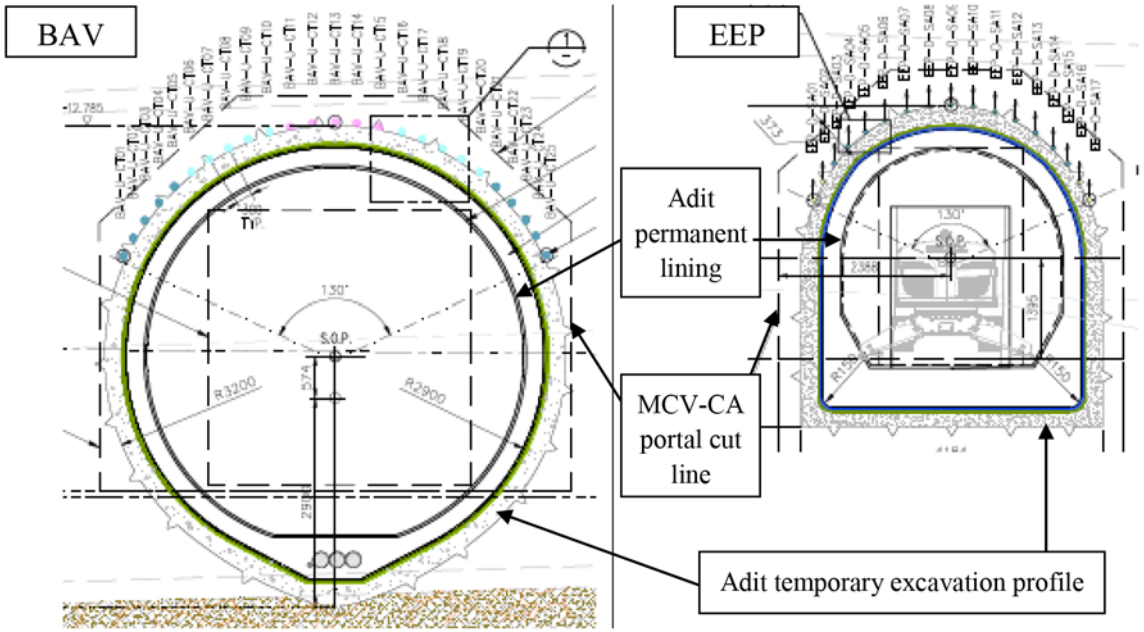

Figure 7: Adit typical cross sections at portals (UT BAV and EEP Adits)

4.5 Shotcrete lining design

A numerical analysis was carried using the 2-dimensional finite-element (FE) programme PLAXIS. This provided the loading on the shotcrete lining in terms of hoop force (thrust), bending moment and shear force.

Type S1 steel fibre reinforced shotcrete was adopted for both BAV and EEP Adits. The lining thickness was 200mm for all adits (including the initial 50mm thick sealing layer), in layers up to 100mm thick.

In soft ground tunnelling, the time-dependent hardening and strength gain of the early-age shotcrete is particularly important. As this aspect is not covered by the local design structural code, reference was

made to Chang & Stille (1993). The shotcrete ages of 1 day, 3 days and 7 days were then subsequently utilized to determine shotcrete strength, for used in the finite-element analysis, in accordance with the relevant adit construction stage. The design of the shotcrete lining took into consideration the ground relaxation, and hence the adit wall radial displacement, that takes place prior to installation of the temporary shotcrete lining. This was estimated based on principles of the convergence-confinement method (CCM – after Panet & Guenot (1982), using the shotcrete time-dependent material properties. The stage construction was performed using the total multiplier ($\sum$ Mstage) in PLAXIS to stimulate the stress relaxation of the ground and the installation of the shotcrete lining. Due to the short length of the adit excavation, it was assumed that 30% of the ground load was applied to the then 1-day shotcrete lining, and subsequently loading was distributed to the 3-day old shotcrete lining. With a relative stiff shotcrete lining of 3 days age, the remaining ground load was largely transferred to the temporary shotcrete lining.

As the Hong Kong Code of Practice for Structural Use of Concrete does not recognize steel fibre reinforcement in concrete, and its resulting tensile strength, the design did not take into account this potential benefit, but this was not critical for this particular design.

5 CONSTRUCTION DATA

5.1 Construction key dates and site photographs

Excavation and temporary support works for the UT BAV and EEP adits commenced in July 2016 after completion of the TBM Tunnel drives within the MCV shaft area, and the completion of MCV-CA external walls. This was followed by the DT adits works. All adit excavation and support was completed in October 2016. Typical site photographs are shown in Plate 1.

Plate 1: BAV Adit excavation and support (left) and exposed TBM segment opening at EEP Adit (right)

5.2 Instrumentation and monitoring

The movements of the adit temporary support lining were anticipated to be minimal. Conventional convergence monitoring was carried out daily basis following the excavation. The recorded convergence was in the range of 1mm to 3mm, less than the design estimates.

6 CONCLUSION

The challenging excavation of the four SCL 1103 MCV Adits in soft ground (Highly Decomposed Granite) was successfully completed. The adits were mined in free air without ground treatment, due to the implementation of temporary groundwater drawdown below the adit invert level, within the MCV Shaft area. The temporary works design included a risk assessment and measures to optimize constructability and staging of the works.

Adit temporary works included pre-support (pipe roofs or spiles), shotcrete lining, and precautionary adit face support. These were designed with the aid of finite element analysis, closed-form solutions, and a prescriptive approach for spiles. No temporary adit steel supports (e.g. lattice girders or steel arches) were used, as the steel fibre reinforced shotcrete lining provided sufficient support capacity. As expected, no significant adit convergence was observed during excavation.

ACKNOWLEDGEMENTS

This paper is published with the kind permission of the Mass Transit Railway Corporation. The views expressed herewith are those of the authors and not necessary those of the Mass Transit Railway Corporation.

REFERENCES

Chang, Y. & Stille, H. 1993. Influence of early-age properties of shotcrete on tunnel construction sequences. In D.F. Wood & D.R. Morgan (ed.), *Proc of Shotcrete for Underground Support VI, Engineering Foundation Conference. Niagara-on-the-Lake, 2-6 May 1993*. American Society of Civil Engineers.

Costello J., Mak L. M., Chan M.T.S. (1986). Geotechnical designs for the construction of Fortress Hill Station, Island Line, Hong Kong. In L. Richards (ed.), *Proc of Conference on Rock Engineering and Excavation in an Urban Environment, Hong Kong, 24-27 Feb 1986*. Institution of Mining and Metallurgy.

John, M. & Mattle, B. 2002. Design of Tube Umbrellas, *Magazine of the Czech Tunnelling Committee and the Slovak Tunnelling Association ITA/AITES*, TUNNEL 3/2002, 11. Ročník:4-11.

Leca, E. & Dormieux, L. (1990). Upper and lower bound solutions for the face stability of shallow circular tunnels in frictional material, *Géotechnique* 40, No. 4:581-606.

Lee, T.H., Cheng, W.C. & Rickard, J. 2015. Evaluation of the Pumping Test Data for the Water Pressure Relief System of an Underground Ventilation Building, in G. Bridges, W.L. Siu & A. Dias (ed.), *Proc* Hong Kong, *Underground Design and Construction Conference 2015*, Hong Kong, 11-12 September 2015. IOM^3 Hong Kong Branch.

Mayer P-M., Hartwig U. & Schwab, C. 2003. Face stability analysis by means of an analytical failure mass model and FEM (Standsicherheitsuntersuchungen der Ortsbrust mittels Bruchkörpermodell und FEM), *Bautechnik* 80 (2003), Heft 7:452-467 (in German).

Panet, M. & Guenot, A. 1982. Analysis of convergence behind the face of a tunnel. In M.J. Jones Editor, *Proc of International Symposium on Tunnelling '82*, London. Institute of Mining and Metallurgy.

Natural Terrain Hazard Studies in Hong Kong: Past, Present and Future

H.Y. Ho, K.J. Roberts & Y.K. Ho

Geotechnical Engineering Office, Civil Engineering and Development Department, The Government of Hong Kong Special Administrative Region

ABSTRACT

Urban expansion in Hong Kong is gradually encroaching further upon the steeper natural hillsides that fringe the urban area. Landsliding on these hillsides during intense rainfall is not uncommon and can be widespread. This calls for the implementation of systematic studies and mitigation of natural terrain landslide risk, which has become a core component of the Landslip Prevention and Mitigation Programme (LPMitP) in Hong Kong.

The recommended practice and procedures for studying natural terrain hazards in Hong Kong was initially documented in the First Edition of GEO Report No. 138 "Guidelines for Natural Terrain Hazard Studies" in 2003. This paper presents the enhancement of the natural terrain hazard assessment strategy in the last decade, which led to the publication of the Second Edition of GEO Report No. 138 in 2016. Some technical areas that merit further development are also discussed.

1 INTRODUCTION

Natural terrain covers over 60% of the land area of Hong Kong. Historically, the main population centres were located on the coastal fringe of Hong Kong Island and on the Kowloon Peninsula. With the continual population growth over the past few decades, there has been a growing number of developments encroaching on the steep natural hillsides thereby resulting in a consequential increase in exposure to landslide risk.

With increasing awareness of potential hazards from natural terrain failures, the Geotechnical Engineering Office (GEO), in collaboration with geotechnical practitioners, has been undertaking technical development work on the subject since the early 1990s (Ng *et al*., 2014). This has led to an improved understanding of the nature and characteristics of natural terrain landslides and the potential hazards and approaches for risk management (e.g. Wong, 2009; Ho & Lau, 2010; Martin & Ng, 2011). This paper gives an overview of the development of natural terrain hazard studies (NTHS), with particular focus on the work in the last decade and recommends areas for future development.

2 NATURAL TERRAIN HAZARD STUDIES IN THE PAST

2.1 Background

Prior to 2000, there was no statutory requirement for conducting NTHS for new developments and no systematic programme to deal with natural terrain hazards affecting existing developments. Administrative measures were introduced in January 2000 through the issuance of an Advice Note for Planning Application under Town Planning Ordinance (Chapter 131) (Ng *et al*., 2000) to control undue risk increase from new development, through avoidance of development in hazardous areas as far as

possible, and study and mitigation of hazards as part of the development where necessary.

From 2001 onwards, discrete packages of NTHS with associated mitigation actions were introduced in the Landslip Preventive Measures (LPM) Programme, following the 'react-to-known-hazard' principle to deal with landslide risk posed to existing developments that were affected by very recent natural terrain failures (i.e. occurred in the preceding few years). Since 2010, the systematic natural terrain landslide risk management phase started with the launching of the LPMitP.

2.2 Guidelines for Natural Terrain Hazard Studies

Interim NTHS guidelines were published in August 2000 (Ng *et al*., 2000) to recommend appropriate practice and procedures, in particular for application of the Design Event Approach (DEA). A revision of the guidelines was carried out in 2002 with updates on (i) the criteria for screening of sites subject to natural terrain hazards, (ii) explanation of the differences between DEA and Quantitative Risk Assessment (QRA), (iii) requirement of a detailed Aerial Photograph Interpretation (API) at an early stage of the study, (iv) review of notable NTHS, (v) relevance of geomorphology to NTHS, and (vi) environmental considerations and maintenance requirements of mitigation measures. The revised guidelines were produced as GEO Special Project Report (SPR) No. 1/2002, which was later converted into the First Edition of GEO Report No. 138 (Ng *et al*., 2003). In 2004, Technical Guidance Note (TGN) No. 22 (GEO, 2004) was issued to supplement GEO Report No. 138. It provides some selected examples of geomorphological mapping that could be considered for undertaking NTHS.

In Hong Kong, three different approaches, viz., Factor of Safety, DEA and QRA, may be used, either individually or in combination, to evaluate natural terrain hazards (Ng *et al*., 2003). The majority of NTHS since the early 2000s have been carried out following the DEA, which is based on a qualitative risk framework, with account taken of both the potential hazards and failure consequence. The methodology is generally based on the landslide susceptibility of the terrain, type of facility and proximity of the facility to the terrain (Ng *et al*., 2003).

3 ENHANCED APPROACH FOR NATURAL TERRAIN HAZARD STUDIES SINCE 2013

3.1 Background

Since the publication of GEO Report No. 138 (Ng *et al*., 2003), much experience has been gained in the study and mitigation of natural terrain hazards in Hong Kong, particularly under the LPMitP since 2010. By consolidating the experience gained and incorporating the findings from technical development work, and following extensive consultation with practitioners, key areas for enhancement to the approach for dealing with natural terrain hazards in Hong Kong were identified. The improvements are aimed at pitching hazard mitigation at a level that is more practicably achievable, and serve to provide more cost-effective solutions. The enhanced approach was firstly documented in GEO TGN No. 36 in 2013 and subsequently superseded by publication of the Second Edition of GEO Report No. 138 (Ho & Roberts, 2016). The enhancement mainly covers the following aspects:

(a) introduction of Topographic Depression (TD) catchments,

(b) rationalisation of Design Event assessment,

(c) application of the 'react-to-known-hazard' principle with regard to undertaking detailed NTHS and mitigation works, and

(d) revision of the DEA framework and design requirements.

3.2 Introduction of TD Catchments

In the past, natural hillside catchments were normally classified as either Channelized (CD) catchments or Open Hillslope (OH) catchments in an NTHS. In landslide studies and field mapping, it is observed that some hillside catchments have a topographic depression where convergence of surface water and debris may occur, and that debris flows or avalanches may develop, with possible entrainment in the process.

On the one hand, a failure involving a TD catchment is different from that in an OH catchment in terms of the mechanism and mobility of debris movement as well as in terms of the cost-effectiveness aspect of hazard mitigation. On the other hand, a TD catchment is also different from a CD catchment, in that there will be a lesser degree of drainage and debris concentration, and that failure within a TD catchment will tend to result in less watery and hence less mobile debris. Examples of different types of hillside catchments and the characteristics of TD catchments are given in Figure 1 and Table 1 respectively.

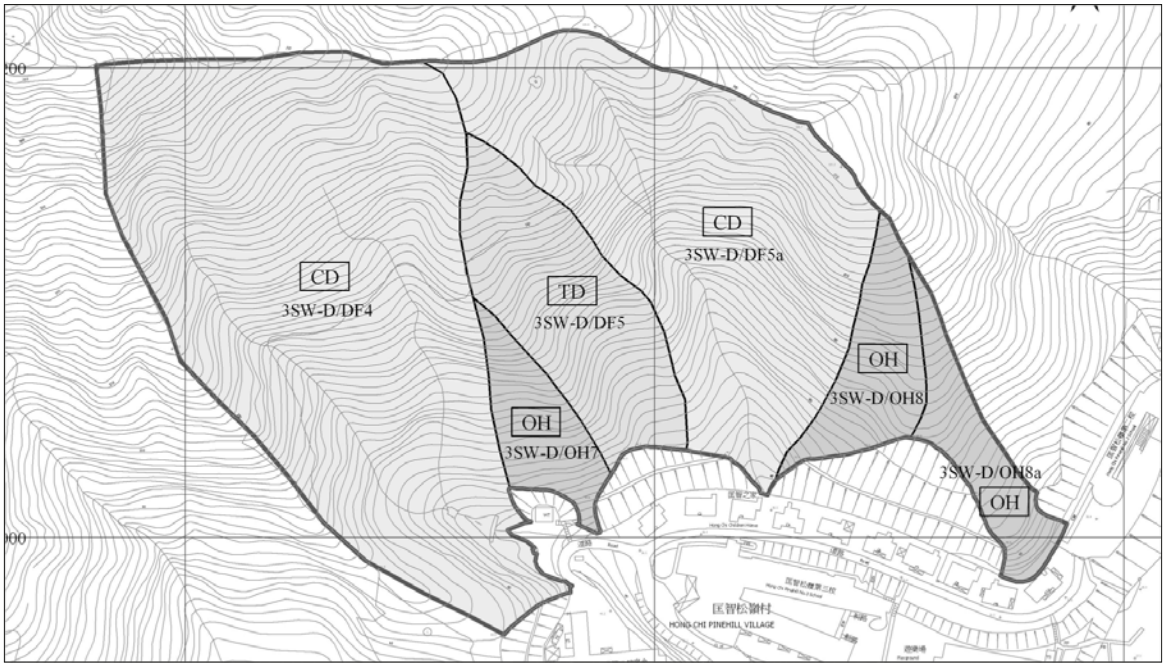

Figure 1: Examples of different types of hillside catchments (Ho & Roberts, 2016)

Table 1: Characteristics of TD catchments

Catchment Characteristics	Descriptions
Topography	Presence of a pronounced topographic depression
Drainage concentration	Some drainage concentration
Discharge outlet	Preferential pathway until exiting the topographic depression
Debris path	Somewhat confined by topography
Potential hazard to consider	Debris flows

The turbulent action involved in the debris motion within TD catchments is expected to be somewhere between that of Open Hillslope Landslides (OHL) and Channelised Debris Flows (CDF). Details of the numerical modelling and rheological parameters considered, together with the results of the back analyses, are presented in TGN 38 (GEO, 2013).

3.3 Rationalization of Design Event Assessment

The DEA was stated in the First Edition of GEO Report No. 138 (Ng *et al*., 2003) as an acceptable approach for design of natural terrain hazard mitigation works, with 'Worst Credible Event' and 'Conservative Event' adopted as the design requirements, which correspond to a notional return period of 1,000 years and 100 years respectively. Except for recent landslides with known years of failure, there is

lack of reliable 'age' information for relict landslides that occurred before aerial photographs were available. This uncertainty poses difficulties in judging the scale of the hazard to be mitigated, including determination of both the failure volume and debris mobility. There is a concern that a combination of very conservatively assessed failure volume and mobile runout scenario could result in overly conservative design, which exceeds the intended notional return period.

Given the current state of knowledge and limited available data, it is more realistic to assess a credible failure volume without excessive extrapolation as compared to the failure volume of an 'extreme' event. The design principle is that the mitigation measures to be provided are aimed at dealing with a sufficiently realistic estimate of the credible failure volume (e.g. based on recent landslides as well as relict landslides with a high degree of certainty). As the term 'Worst Credible Event' may lead to a misunderstanding that it should be interpreted as pertaining to an 'extreme' event, the term 'Design Event' is now used. When it is used in combination with a conservative assessment of debris mobility, the Design Event is considered to be adequately robust for the purpose of mitigating natural terrain landslide hazard based on analytical design.

3.4 Application of React-to-Known-Hazard Principle

Under the LPMitP, an area-based approach for NTHS is adopted, whereby hillside catchments of similar geological and geomorphological settings and affecting the same unit of development are studied in one go. A Study Area typically includes a Historical Landslide Catchment (HLC) (i.e. hillside catchments with historical natural terrain landslides that have occurred close to existing buildings and important transport corridors) and other adjoining hillside catchments (referred to as Related Catchments, RC). The original practice makes no distinction between HLC and RC, in respect of undertaking mitigation works, despite the former generally meeting the 'react-to-known-hazard' principle whereas the latter does not. Also, it has not taken into consideration that the risk from a Debris Flow (DF) catchment is generally about an order of magnitude higher than that from an OH catchment (Wong *et al*., 2006).

In the NTHS, it is noted that some of the catchments, especially the RC, may not meet the 'react-to-known-hazard' principle based on the updated information obtained from the site-specific assessment. Such catchments may be excluded from the LPMit works after sufficient confirmatory work has been carried out in the assessment. As such, further guidelines are provided in deliberating whether or not a hillside catchment, or part of the catchment, assessed under LPMitP meets the 'react-to-known-hazard' principle. Consideration should be given to the following factors:

(a) past persistent landslides indicating an active catchment,

(b) strong geological/geomorphological evidence of a hazardous catchment, and

(c) newly emerged hazardous situation as a result of occurrence of new landslide(s), development of new signs of distress and hazardous movement, or exacerbation of existing signs of distress and hazardous movement.

Where any of the above factors are evident and where a significant consequence to life or serious damage to property may occur in the event of future landsliding, the 'react-to-known-hazard' principle is deemed to have been met. Further elaborations on the above are given in the Second Edition of GEO Report No. 138 (Ho & Roberts, 2016).

3.5 Revised DEA Framework and Design Requirements

The revised framework allows for the use of both analytical design and empirical design as appropriate. Two different levels of hazard mitigation, viz. Primary Protection and Enhanced Protection, are denoted. In essence, for CDF affecting Group 1 and 2 facilities (Ho & Roberts, 2016), analytical design is called for which is denoted as Level 2 hazard mitigation, i.e. Enhanced Protection. Failure within TD catchment is to be dealt with in a similar manner to CDF, except that the recommended rheological parameters given in TGN 38 should be adopted in the assessment of debris mobility for analytical design. For OHL, empirical design is adopted to provide Level 1 hazard mitigation, i.e. Primary Protection.

4 OTHER RECENT ENHANCEMENTS

4.1 Clarification and Rationalization of Boulder Policy

'Boulder fall' is one of the main hazard types that needs to be assessed in the NTHS. However, the approach in assessing boulder fall hazard varies amongst practitioners and detailed survey on individual boulders was sometimes conducted unnecessarily for the entire hillside. The cost and manpower resources required for systematic inspection and consequent preventive works to the boulder-strewn terrain could be completely out of proportion to the risk that boulders pose, judging from the records of boulder falls over the last 50 years. Furthermore, detailed investigation of boulders very often necessitates partial removal of vegetation which can in itself aggravate the risk of boulder falls, and the execution of preventive works in such areas may require extensive deforestation of the hillsides thereby creating a severely adverse environmental impact.

a. Boulder-strewn terrain in Hong Kong b. Boulder fall c. Presence of precarious boulders

Figure 2: Boulder Fall Hazard in Hong Kong

Further guidelines on mapping of boulders were provided by the GEO (Ho & Roberts, 2016). In general, follow-up action for boulders affecting existing development, including evaluation of boulder stability and implementation of preventive and mitigation measures, is only required where there have been persistent boulder falls or there is reason to believe that a dangerous situation could develop. For boulders affecting new developments, it is necessary to establish that there would be a significant risk before any further action is taken to deal with boulders. The mere presence of a cluster of boulders should not be considered sufficient grounds for requiring boulder mapping.

4.2 Revised NTHS Alert Criteria for Dealing with Planar Hillside Catchments

The Alert Criteria have been adopted by the GEO since the early 2000s to screen new development proposals in respect of the requirement to undertake NTHS. The Alert Criteria are defined as "where there is natural terrain at an angular elevation of ≥ 20° (1st Criterion) and where there is ground sloping at > 15° within 50 m horizontally upslope of the site (2nd Criterion)".

In a recent review of the Alert Criteria (Ko, 2013), it was noted that natural terrain at an angular elevation of 20° or more from the site encompasses 98.4 % of all the OHL and 99.6% of the large recent natural terrain landslides (source width >15 m) in the Enhanced Natural Terrain Landslide Inventory (ENTLI) (i.e. the 1st Criterion regarding angular elevation). The review concluded that this was still applicable as a global criterion. The review also showed that natural terrain at an angular elevation of 25° or more from the site encompassed 92.5 % of all the OHL and 92.9% of the large recent natural terrain landslides in the ENTLI. The corresponding figures significantly reduce to 71.7% and 67.2% respectively at an angular elevation of 30° or more. It therefore appears that there is a significant break at an angular elevation of about 25°.

A review of the ENTLI showed that the majority of OHL (i.e. landslides that occurred on planar hillsides) have source areas < 100 m^2. This translates to landslide volumes of 25 to 50 m^3 (assuming average depths of 0.5 to 1.0 m). Also, the runout path of OHL is generally not confined and their runout distances are generally less than that of debris flows for a similar landslide volume.

Given the above background, the requirement for NTHS would not be imposed on new development sites if all the following principles are met:

(a) the hillside catchment(s) directly overlooking the site is planar in nature, i.e. devoid of topographic depressions or drainage lines;

(b) the natural hillside overlooking the subject site has an angular elevation of < 25° (i.e. relaxation of the 1st Criterion);

(c) there are no recent ENTLI records and reported landslide incidents within and in the immediate vicinity of the hillside catchment(s);

(d) there are no Class A and B relict ENTLI records within and in the immediate vicinity of the hillside catchment(s);

(e) there are no obvious signs of distress (e.g. tension crack) within and in the immediate vicinity of the hillside catchment(s) from API or vantage point observations; and

(f) there are no obvious signs of boulder fall hazard or evidence of severe surface erosion within and in the immediate vicinity of the hillside from a review of aerial photographs.

4.3 Known Tension Crack Inventory

The GEO has recently compiled an inventory on known tension cracks in Hong Kong. Sources of information included photographic records, topographical plans from API studies, sketch plans from natural terrain landslide mapping records and engineering geomorphological maps from various NTHS. The Known Tension Crack Inventory (KTCI) contains information on about 600 known tension cracks (at the time of compilation in 2016) identify on the natural terrain throughout Hong Kong. The inventory provides additional information for reference in natural terrain risk management. The data are presented in a Geographical Information System (GIS) format that enables easy query, analysis and updating.

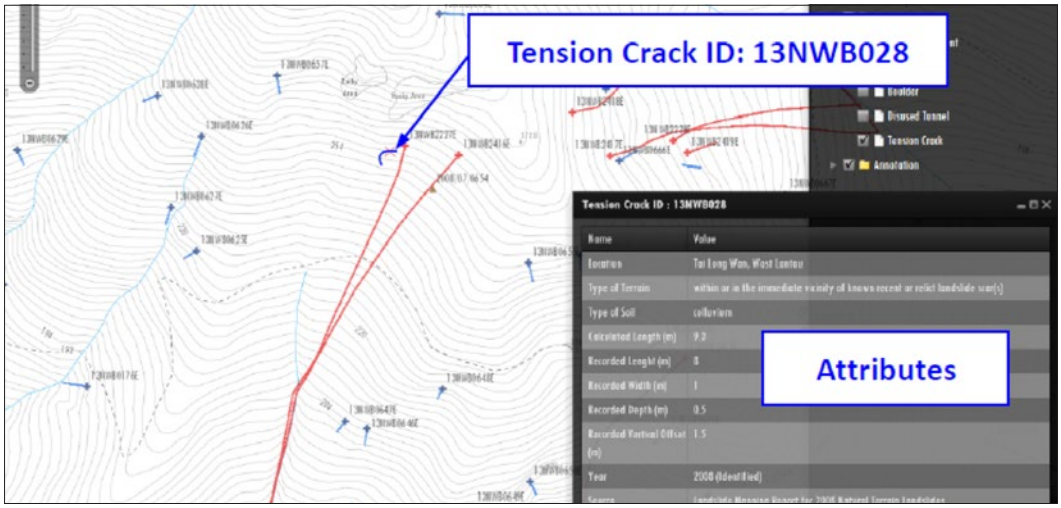

Figure 3: A Known Tension Crack Inventory on GIS Platform

4.4 Guidelines on Study of Hillside Pockets

Hillside Pockets (HP) are small tracts of natural hillsides within developed areas, which are affected by human disturbance to varying degrees (e.g. construction of roads or building platforms) (Figure 4).

In view of the difference between natural terrain and HP, supplementary guidelines for undertaking hazard assessment and additional guidance on mitigation strategy for HP are provided in TGN 46 (GEO, 2016). In particular, the following hazard factors associated with HP settings should be duly considered:

(a) presence of recognizable fill bodies (plan area > 10 m^2) with adverse site setting (e.g. a fill body located at the upper portion of a catchment on steep terrain with a slope gradient > 30°, and with a credible flow path reaching the facility at risk);

(b) adequacy of drainage provisions at the crest and within the HP, specifically the likelihood of any possible concentration of surface water onto the HP; and

(c) condition of surface protection (e.g. cracks on the hard surfacing).

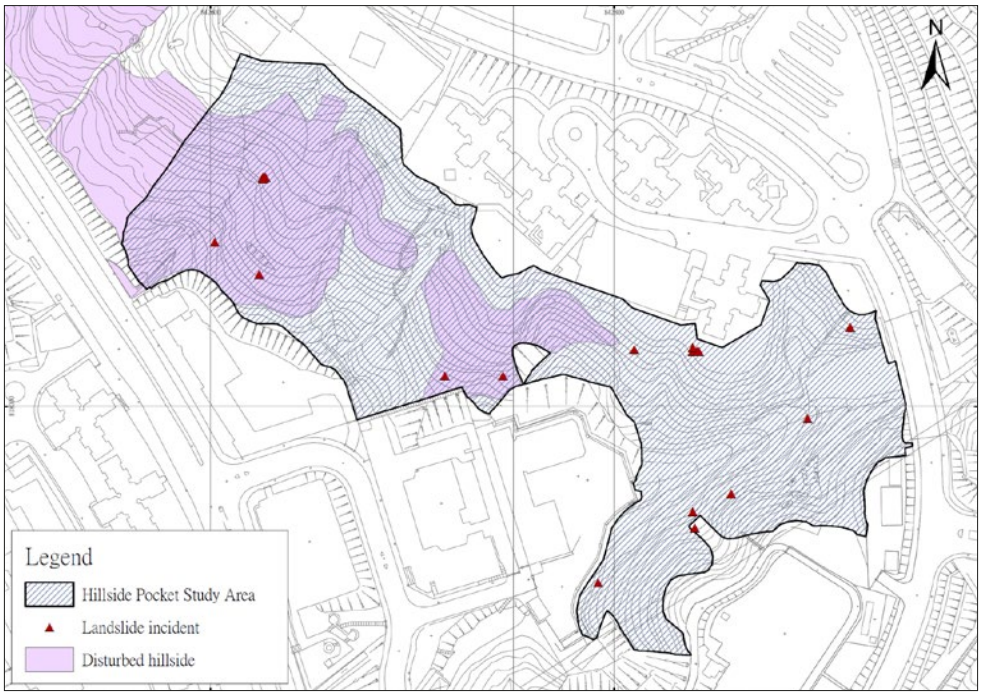

Figure 4: Example of Vulnerable Hillside Catchments with Hillside Pocket-Type Settings

5 RECENT TECHNICAL DEVELOPMENT WORK

5.1 Review of Entrainment Potential

The GEO has recently undertaken a review on the entrainment rates for a number of large debris flows that occurred during the 7 June 2008 rainstorm (Figure 5). Review of the mapping records and the 1963 aerial photos suggests that majority of entrainment tends to involve materials perching on the drainage line, instead of eroding into the side slopes and stream bed of the drainage line. Significant amounts of materials perching on the drainage lines, if present, could generally be identified from the 1963 low-flight aerial photos (Figure 6). From the review, it is noted that a high entrainment rate would usually be attributed to the following factors:

(i) debris flow having large landslide source;

(ii) multiple sources along the landslide trail contributing to the active volume;

(iii) presence of previous failures with significant debris retained on the drainage line;

(iv) presence of steep rock steps where the debris flow energy would increase;

(v) loose material accumulating where drainage line becomes gentler; and

(vi) presence of man-made sources of material, e.g. loose fill.

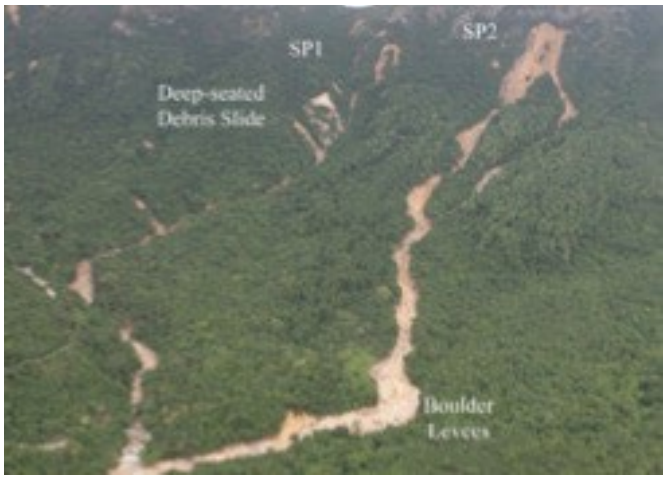

Figure 5: Large debris flow in West Lantau during the 7 June 2008 rainstorm

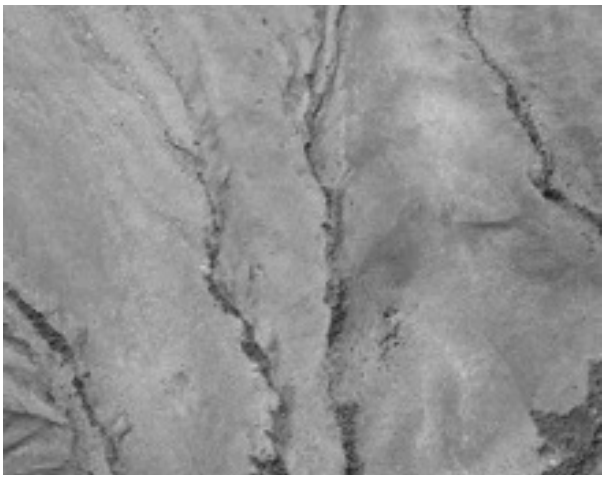

Figure 6: Factors attributed to high entrainment as evidenced in the 1963 aerial photos

At present, knowledge of the entrainment potential and characteristics of the drainage network's life-cycle is rather limited. There is a need to further improve the understanding of the drainage catchment behaviour and debris transport mechanisms.

5.2 Remote Sensing Techniques

Significant advances have been made in the application of digital and remote sensing technologies to enhance the capability and efficiency of NTHS in the last decade. A recent example is to pilot the use of Unmanned Aerial Vehicle (UAV) equipped with Global Navigation Satellite System (GNSS), Inertial Measurement Unit and high resolution digital camera, to generate digital elevation models (DEM) and orthomosaics to facilitate landside mapping. A detailed landslide source mapping exercise by coupling UAV photogrammetry and LiDAR technology has been carried out for a deep-seated slide that occurred above Sai Wan Road during the 20 May 2016 rainstorm. Due to the steepness of the hillside, it was very difficult to safely access the landslide scarp for detailed landslide mapping. Close-up photos (Figure 7) were taken by the UAV to provide detailed information on the failure without physically accessing the landslide source.

Figure 7: Photos taken by UAV after the landslide

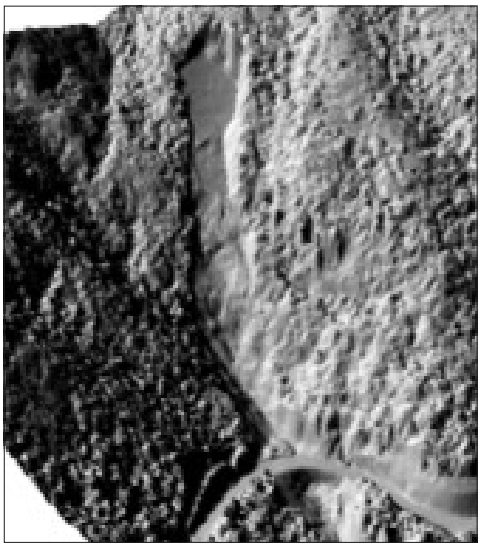

Figure 8: DEM generated from UAV photos

By processing the captured UAV photographs, an after-landslide DEM was constructed using a photogrammetry technique known as "Structure from Motion" (Figure 8). Compared to field

measurement, this provided more accurate after-landslide topography for estimating the dimensions of the landslide scar as well as the general orientation of the failure plane. Coupled with the pre-landslide topography generated from the 2011 territory-wide airborne LiDAR data, the landslide source volume was obtained by comparing the two DEMs (estimated to be 2,000 m^3). This figure correlated well with the information obtained from detailed mapping by the landslide investigation consultants after access was provided. This case has shown the potential use of UAV for obtaining basic information for landslides in difficult terrain. Keeping abreast of different technological advances may help to develop new approaches to undertaking NTHS.

5.3 Field Instrumentation Works

In 2005, GEO commissioned a geotechnical instrumentation project to carry out real-time monitoring at four selected natural hillsides in Tsing Shan, Pa Mei, Tung Chung and Ching Cheung Road to assess the responses of the hillslopes to rainfall with respect to ground movements and hydrogeological conditions. This project was a pilot scheme to evaluate the geotechnical instrumentation, data acquisition and communication technologies for long-term performance monitoring of landslide development at individual sites.

In 2014, GEO commissioned another field instrumentation project in West Lantau. Conventional instrumentation and emerging slope monitoring techniques were installed on a distressed natural terrain in Tai O Cemetery to monitor slope movements and variations of groundwater pressure in real time. A high-density network of raingauges was also installed at different locations of West Lantau to provide high-resolution regional rainfall distribution data for better understanding of orographic effects on rainfall and the correlation between rainfall and other monitoring data. The monitoring started in late 2015 and is still on-going. The performance of the instruments installed will be reviewed and analysed at the end of the monitoring period.

6 FURTHER DEVELOPMENT AREAS

6.1 Background

Given the observed trend of climate change, the challenges that the geotechnical profession will face in the study of natural terrain should not be overlooked. The behaviour of natural hillsides is affected by geomorphological processes and anthropogenic influences, which are still not fully understood given the current state of knowledge. The uncertainties involved need to be properly addressed in risk assessment and mitigation. A few technical areas on this subject that merit further studies are given below.

6.2 QRA Benchmarking Exercise

The GEO has initiated a QRA exercise on selected HLC which have been subject to NTHS and implementation of mitigation measures using the enhanced approach. The analyses will be carried out using the established QRA procedures developed by the GEO. The results of this exercise will be useful for assessing whether the hazard assessment and mitigation programme is adequate to maintain residual risks at the As Low As Reasonably Practicable (ALARP) level and, also, that it is cost-effective.

6.3 Enhancement of Large Landslide Study (LLS) Dataset

The Large Landslide Study (LLS) Dataset was compiled between 1998 and 1999 (Scott Wilson, 1999) by a team of aerial photograph interpreters. It was at that time simply a landslide mapping exercise without due consideration of their associated terrain characteristics. The LLS Dataset has therefore always been treated as having marginal value in the current NTHS.

With mounting concerns regarding the occurrence of large magnitude events in respect of extreme rainfall events resulting from climate change, a better understanding of large relict landslides could provide insight into likely geomorphological settings for developing large magnitude events. Therefore,

the GEO has recently commenced a review of the LLS Dataset with a view to identifying geomorphological settings that are conducive to large-scale slope movement.

6.4 Review of Landslide Clusters

It is noted from the ENTLI that there are clusters of relict landslides at many locations. Clusters of relict landslides in an area may be a proxy to the presence of adverse geological and/or morphological features that have been affecting slope movement in the area. The rainfall-based landslide susceptibility model was updated in 2016 to include clusters of relict landslides as an additional predictor parameter and examine how they relate to recent landslides statistically (Lo & Ko, 2017). The study shows that clusters of relict landslides and recent landslide activities are statistically correlated. The GEO will investigate the underlying geological and geomorphological factors that may potentially control the mass wasting process in selected areas in order to explore the relevance of the geomorphological features to rainfall-based landslide susceptibility.

7 CONCLUSIONS

With collaborative efforts and technological advances made over the years by the geotechnical and geological professions, the assessment strategy and associated technical development work for dealing with natural terrain hazards in Hong Kong has gradually developed. Nevertheless, judgment by experienced and competent professionals remains a key aspect in assessing hazards and in formulating appropriate mitigation strategies, as our understanding about the complex interaction between various attributes contributing to natural terrain failures is still evolving. Despite NTHS apparently becoming routine work under the LPMitP, much effort is still needed to enhance the current state of knowledge and practice for assessing natural terrain hazards, in order to implement more cost effective and appropriate mitigation works.

ACKNOWLEDGEMENTS

This paper is published with the permission of the Head of the Geotechnical Engineering Office and the Director of Civil Engineering and Development of the Government of the HKSAR. The authors would like to thank Dr K C Ng for reviewing the paper and Mr W L Shum for providing information on the Sai Wan Road landslide.

REFERENCES

GEO, 2004. Guidelines on geomorphological mapping for natural terrain hazard studies. Technical Guidance Note (TGN) No. 22. Geotechnical Engineering Office, Hong Kong.

GEO, 2013. Guidelines on the assessment of debris mobility for failures with topographic depression catchments. Technical Guidance Note (TGN) No. 38. Geotechnical Engineering Office, Hong Kong.

GEO, 2016. Supplementary guidelines on natural terrain hazard studies for hillside pockets. Technical Guidance Note (TGN) No. 46. Geotechnical Engineering Office, Hong Kong.

Ho, H.Y. & Roberts, K.J. 2016. Guidelines for natural terrain hazard studies. GEO Report No. 138 (Second Edition). Geotechnical Engineering Office, Hong Kong.

Ho, K.K.S. & Lau, J.W.C. 2010. Learning from slope failures to enhance landslide risk management. *Quarterly Journal of Engineering Geology and Hydrogeology*, 43: 33-68.

Lo, F.L.C. & Ko, F.W.Y. 2017. Rainfall-based correlation of recent landslides with clusters of relict landslides. Discussion Note (DN) No. 2/2017. Geotechnical Engineering Office, Hong Kong.

Martin, R.P. & Ng, K.C. 2011. Geological Input to the LPM and LPMit Programmes 1972 to 2011. *The Hong Kong Institution of Engineers Geotechnical Division Annual Seminar, 20 May 2011*. p. 29-44.

Ng, K. C., Ho, H. Y. & Roberts, K. J. 2014. Evolution of natural terrain hazard assessment strategy in Hong Kong. *Proceedings of the Conference on 'Advances in Terrain Mapping and Analysis for Landslide Hazard Assessment'.* Geological Society of London, Hong Kong Regional Group, pp 17-35.

Ng, K.C., King, J.P., Franks, C.A.M. & Shaw, R. 2000. Natural terrain hazard study: interim guidelines. Special Project Report (SPR) 5/2000. Geotechnical Engineering Office, Hong Kong.

Ng, K.C., Parry, S., King, J.P., Franks, C.A.M. & Shaw, R. 2003. Guidelines for natural terrain hazard studies. GEO Report No. 138 (First Edition). Geotechnical Engineering Office, Hong Kong.

Scott Wilson, 1999. Specialist API Services for the Natural Terrain Landslide Study – Task B Factual Report. Report to Geotechnical Engineering Office, Hong Kong, 9 p. plus 4 Appendices.

Wong, H.N. 2009. Rising to the Challenges of Natural Terrain Landslides. *Proceedings of the HKIE Geotechnical Division Annual Seminar on Natural Hillsides: Study and Risk Management Measures,* Hong Kong Institution of Engineers, p. 15-53.

SCL 1128 – Hong Kong's First Variable Density Tunnel Boring Machine

D. Jacques, H. Laverret, N. Ballu & J. Reilly
Dragages Bouygues Joint-Venture (DBJV), Hong Kong SAR

ABSTRACT

The MTR Shatin Central link (SCL) is a new strategic rail corridor, providing a direct link between the New Territories and Central, Hong Kong. Contract 1128 involves the construction of two sets of twin tunnels between Causeway Bay Typhoon Shelter and Admiralty MTR station; boring underneath the densely urbanized district of Wan Chai.

Challenging and variable ground conditions were specifically expected throughout the alignment of the Eastern Down Track tunnel. The geology ranges from hard rock to marine deposits and fill requiring a machine that could cope with such a heterogeneous environment. The main constraint was the shallow ground cover of less than one tunnel boring machine (TBM) diameter giving high risks of settlements and slurry blow outs on the surface. A Mix-shield and Earth Pressure Balance (EPB) TBM individually were deemed not suitable, rather requiring a combination of the two. As a result, the implementation of Hong Kong's first Variable Density (VaD) TBM - able to use both low and high density slurries - was chosen to control the above concerns.

In partnership with Herrenknecht, the project team refined and improved the concept used during the construction of the Klang Valley MRT project in Kuala Lumpur; where the first Variable Density TBM was used. As a result, the processes and equipment have been developed to suit the needs of the anticipated geological conditions for the 1128 project.

1 INTRODUCTION

The Sha Tin Central link comprises of two sections; the Tai Wai to Hung Hom section and the cross harbor section. The cross harbor section is an approximate 6km extension of the East Rail Line from Hung Hom station - crossing the Victoria Harbor with a new station at the Exhibition Centre - to an interchange at Admiralty Station.

The 1128 works contract – South Ventilation Building (SOV) to Admiralty tunnel was awarded to the Dragages Hong Kong and Bouygues Travaux Public joint venture (DBJV). It involves the construction of 2.3km of twin tunnels (ø 7.45m excavated diameter with lengths between 470m and 678m), ventilation buildings and ancillary works. The stacked eastern bored tunnels run between the South Ventilation building (SOV) and future Exhibition station; with the western bored tunnels running from the Fenwick Pier Emergency Egress Point (opposite side of the Exhibition Centre) to Admiralty station. During the tender stage, it was understood that the eastern down track tunnel would present a significant challenge to the project team. Thus, DBJV proposed an alternative solution to the client, MTR, to limit the risks due to shallow ground cover and complex geological conditions by making use of a Variable Density TBM.

2 ALIGNMENT AND GEOLOGY

2.1 Alignment

The alignment of the eastern down track tunnel passes through the urban district of Wan Chai on Hong Kong Island in the east to west direction. The tunnel excavation path is exclusively within a reclamation area, constructed in various stages during the 1960's and 1970's. Figure 1 below shows the progression of reclaimed land from 1945 to 2009, with the red line indicating the future SCL alignment and Exhibition station.

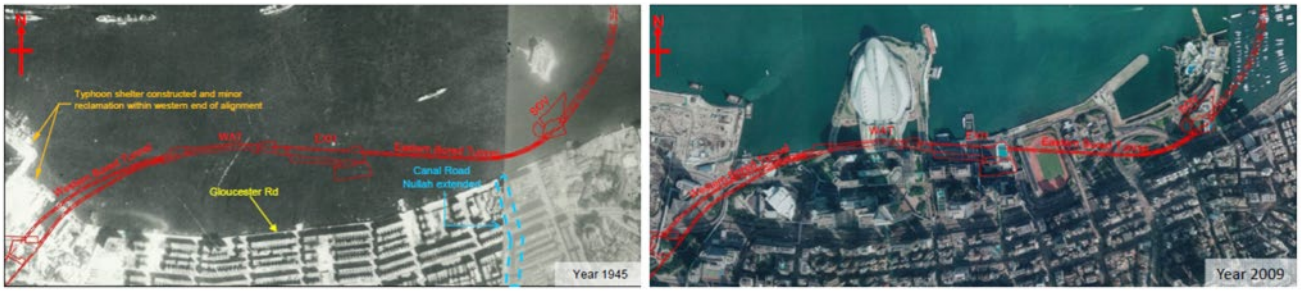

Figure 1: Reclaimed land along the SCL alignment from 1945 to 2009

Due to the MTR program of development requiring space for the future North Island Line, the two eastern SCL 1128 tunnels are staggered requiring the down track tunnel to mine through the fully reclaimed area.

The excavated tunnel passes underneath critical road structures, services and sensitive areas which could not be disturbed during construction. These include Gloucester road, Cross Harbor Tunnel slip roads, various highway flyovers and foot bridges, the Wan Chai Sports Ground (under normal operation), sewers and drains. With a number of structures supported on piles that conflicted with the TBM alignment, advance works were required to remove these obstructions. These works prevented interruption to TBM operations and avoided the need to undertake a number of dangerous compressed air interventions (CAI).

Temporary steel structures and new piles were constructed to redefine the foundation support, allowing the exiting piles to be removed. Potential settlements during TBM excavation were counteracted with hydraulic jacks installed on temporary steel supports. Such arrangements limited movements that would otherwise affect the permanent structure. More detail regarding obstruction removal and re-provision can be found in the paper by Kwok (2017).

Figure 2: Alignment of the Eastern tunnels

2.2 Geology

From site investigation conducted, the eastern down track alignment was found to have a complex geological profile. The solid geology consists of Kowloon Granite/CDG, comprising of fine, fine-medium and medium grained varieties, found roughly 20 to 30m below surface level. Above this stratum, sandy to clayey alluviums and sedimentary marine deposits of varying thicknesses can be found before reaching the top layer of fill. The fill layer was expected to contain reinforced concrete, bricks, plastics, woods and steel bars as well as rubble mound that had previously formed as parts of temporary or permanent sea walls. Figure 3 illustrates the various geological layers.

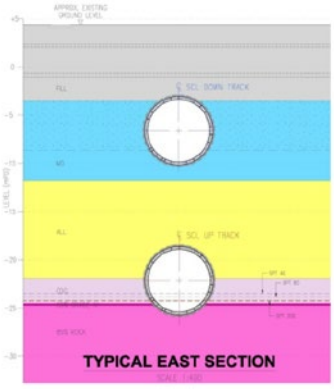

Figure 3: Typical cross section of the Eastern tunnels

The alignment itself can be roughly divided into 3 general geological sections. First, 120m was excavated mainly in a rock and completely decomposed granite (CDG) mix, followed by a 90m section of transition from rock through to alluviums and marine deposits. The remaining 470m of the drive was completed in soft open ground conditions, containing alluviums, clayey and sandy marine deposits and reclaimed areas of fill. The last 90m of the excavation contained boulder sized rubble (as part of the reclaimed land in the Wan Chai Sports Ground area) embedded in silty fine coarse sands. This area was expected to cause difficulties for TBM operation with the decision made to perform void filling and ground treatment, avoiding slurry losses and larger settlements.

At the shallowest point, the excavation took place with cover of less than one TBM diameter and at some locations, the TBM passed closed to existing live structures with less than 1m of very soft soil in between. Figure 3 highlights one of the significantly more challenging areas in terms of ground cover and potential obstructions.

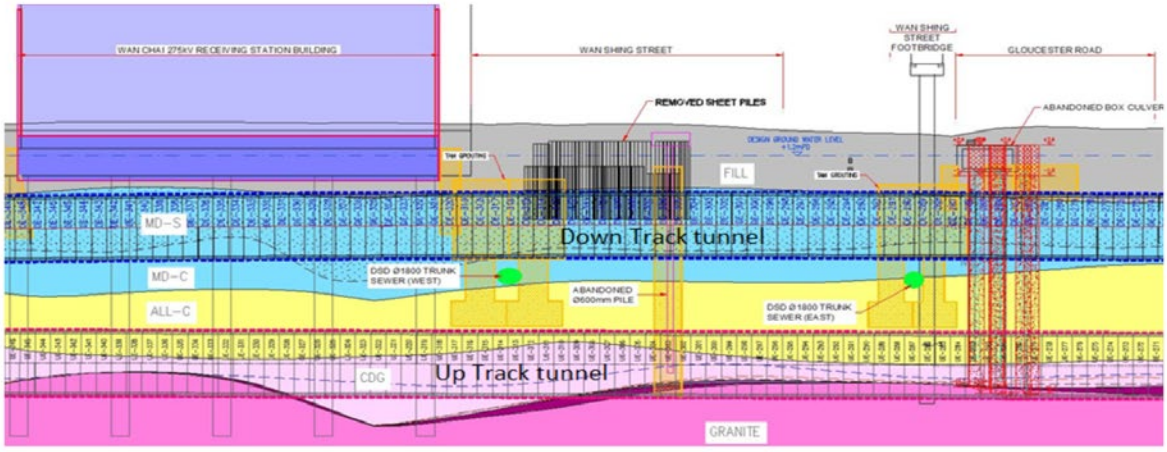

Figure 3: Section of down track TBM drive displaying an area with a number of obstructions, varying geology, close proximity to existing ground structures and shallow cover

3 TBM SELECTION AND EXPLANATION

3.1 Choice of TBM

During the tender stage of this project, an EPB TBM was initially specified by the client to complete the eastern down track tunnel drive. This was due to the potential risk of blowouts that a Mix-shield TBM would cause as a result of the limited cover and type of soil above. Slurry losses through the ground or potential old opened boreholes and areas of removed obstructions would have impacted the support of the excavated face leading to settlements underneath various structures and services.

However, DBJV had considered these concerns and proposed the use of a Variable Density TBM. DBJV believed that the EPB option could not deliver the correct support because of the complex geology and limited cover. With the open ground conditions, transitions present throughout the alignment, and sections containing boulders and rubble, there were very high chances that sink holes could form while boring with an EPB TBM. A further risk using this type of TBM were foam blowouts caused by the conditioning of the excavated material. Given the geology, there was another concern of the moisture content for spoil disposal (below 25%) not being reached using an EPB TBM. An additional interest was the possibility of accessing the cutter head quickly and safely, should compressed air interventions being required to remove unforeseen obstructions. Completing the process for these CAI's would be much simpler operating in a Mix-shield mode rather than EPB, giving DBJV the option to re-launch the machine faster.

The project team was aware of the experience from the Klang Valley MRT project in Kuala Lumpur, where a Variable Density TBM was used for the first time. The reason for using such a machine there was based on the extreme karstification of the Kuala Lumpur limestone which resulted in a large number of cavities and voids to be encountered within the geology. From prior projects in KL using mix-shield TBM's, slurry losses would occur away from the excavated face, due to the connection between the voids, creating face instability and ground collapse. The Variable Density TBM was designed and used to solve these issues in KL by using a thicker and denser slurry inside the excavation chamber to provide improved face support. These improvements, using a higher density at the excavated face than a normal Mix-shield mode, made this TBM more suited to the eastern down track tunnel.

As a result, the VaD TBM appeared to offer the flexibility of both a Mix-shield and EPB TBM which the client accepted.

3.2 Variable Density Concept

The applied concept of this Variable Density TBM is the ability to work with a range of slurry densities to support and stabilise the excavated face while preventing surface blow-outs. Similar to a mix shield TBM, a designed confinement pressure is regulated through a pressurised air bubble to support the excavated face accurately.

With a standard Mix-shield using low density slurry at the designed confinement pressure, combined with the shallow cover found along the alignment, there was an increased risk of blowouts. The slurry is of a low viscosity (very fluid) and can be forced to the surface with such a confinement pressure more easily. Alternatively, having higher density slurry with a higher viscosity in the excavation chamber can minimize these risks due to the heavier particles in the mud not being able to reach the surface at the designed confinement pressure. Figure 4 below illustrates a simplified description of the concept, indicating the difference between using low and high density slurries at the excavated face. For the same pressure applied at the axis of the TBM in the excavation chamber, given the difference in density and viscosity, the blowout risk is reduced by applying a higher density medium.

On this project, the Variable Density TBM used two different modes of excavation; a Low Density mode where slurry is supplied similarly to a mix-shield TBM (roughly 1.05-1.20T/m^3) through the slurry circuit, and a High Density mode that took the TBM to the lower boundary of an EPB TBM where the density in the excavation chamber was limited to 1.50T/m3. Above this density, a full switch to EPB mode is required including foam conditioning to prevent plugging inside the cutter head and installation of a conveyor belt for spoil mucking out.

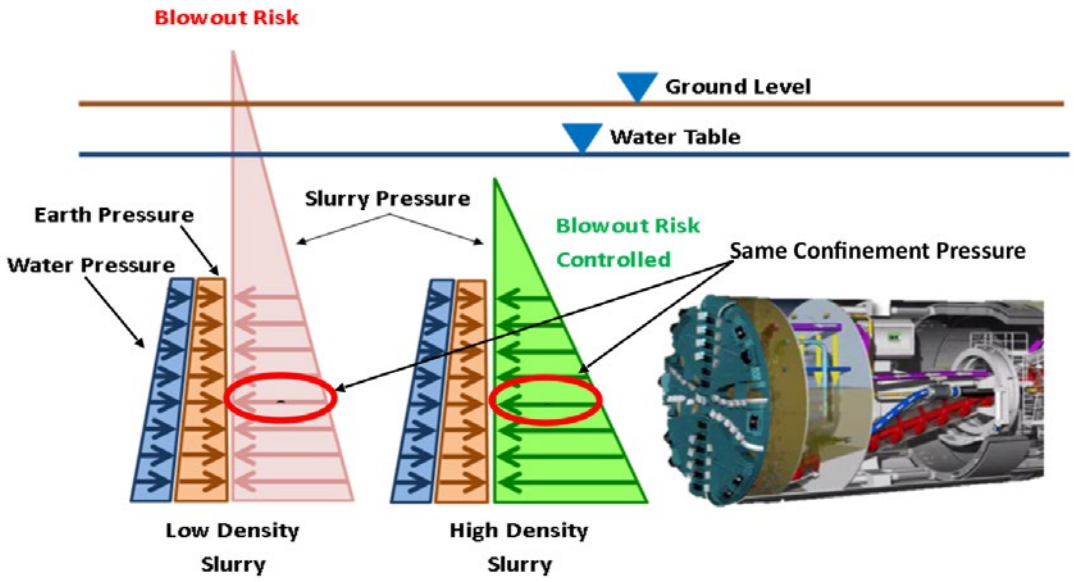

Figure 4: Difference between a low density slurry and high density slurry used to support the face at the same confinement pressure at crown

3.3 Recommended Density

To provide a recommend density for the TBM operators to follow and limit risk of slurry blowouts, a basic calculation was computed based on an open path between the crown of the TBM and the surface.

The calculation assumed the design confinement pressure that would be applied at the TBM axis for relevant sections across the drive. The value then provided a height that would be reached by the slurry, at various densities inside the open void. This dimension was compared to the depth of TBM excavation. The design confinement pressure would, as a result, not have enough force to counter act the weight of the slurry/soil mix column at such a recommended density, avoiding the risk of blowouts. The calculation is provided below with 9.81 representing the effect of gravity on the slurry/soil column. Safety factors were considered in the calculation such as increasing the confinement pressure and reducing the depth to ensure the recommended density limited the risk of a blowout.

$$\textit{Recommended Density} = \frac{\textit{design confinement pressure at axis}}{\textit{depth from surface to TBM axis x 9.81}} \quad (1)$$

3.4 Variable Density Specific Components

The diagram below (figure 5) identifies the key components of the variable density system. The Variable Density type shares similarities between a Mix-shield and EPB TBM and a number of major components are common. However, some additional new components are required to enable the high and low density modes of operation. The following are identified as the key features of this machine.

On a VaD TBM, material is removed from the pressurised excavation chamber through a screw conveyor. For operation, the screw was not required to reduce the support pressure from the front like a regular EPB TBM as the slurryfier box remained pressurised with the slurry circuit.

The slurryfier box's primary function is to dilute material removed from screw to a suitable density allowing hydraulic transportation to the Slurry Treatment Plant (STP) and separation. This 6m3 box was constantly fed with four slurry feed lines mounted at different locations on the box, providing adequate flushing and preventing clogging. The stone crusher inside the slurryfier box is a ø500mm "jaw" type, permitting the machine to pass through the initial granite geology.

Due to the presence of the screw conveyor, supply of pressure to the excavation chamber is not possible through a submerge wall, as found in mix-shield TBM's. Instead, pressure is transmitted via a communication pipe, joining the working and excavation chambers at the crown. The air bubble is

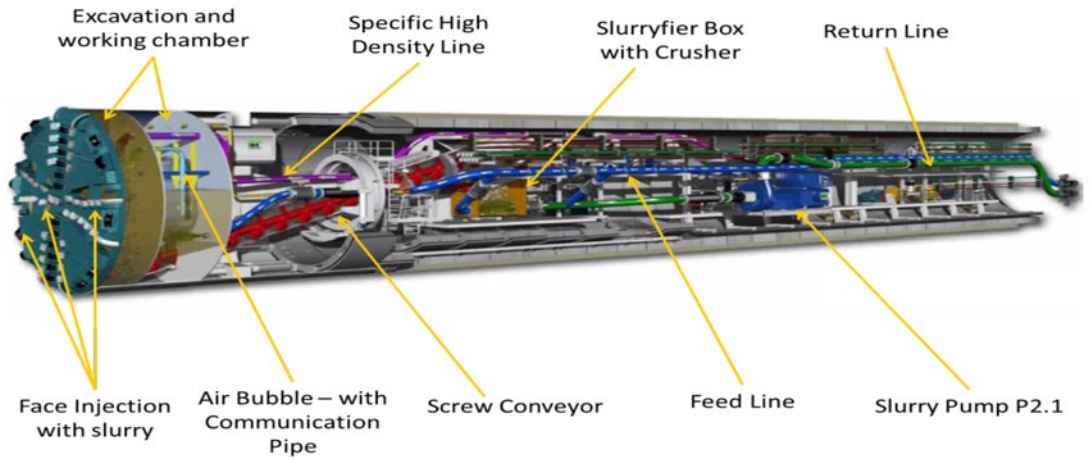

Figure 5: VaD TBM system and components

regulated by a Samson system, forcing slurry up through the pipe, maintaining the design confinement pressure at the face. Figure 6 explains its function, comparing the pressure delivery at the crown instead of through the submerged wall. To ensure the pipe remains active during mining, a minimum flow of slurry must be injected inside the bubble so there is constant through the pipe. A hydraulic propeller is present at the top of the pipe to reduce backflow of large particles into the working chamber.

The VaD TBM has the option of injecting a high density mix (HDM) directly to the excavation chamber. Its main purpose for this project was to fill voids encountered at the excavated face temporarily, refill the chamber after compressed air interventions and to inject around the shield to help minimize settlement, rather than being used to regulate the density. The circuit on the TBM was made up of a 5m3 tank with a pump delivering HDM. The mix itself was manufactured on the site surface from base materials in a high density mix batching plant and pumped directly to the tank located on the TBM.

To measure density inside excavation chamber, sampling of slurry from the crown is completed via a small pump, where it is recorded by a gamma density meter. This information is provided to the TBM operator, who can adjust TBM parameters to reach the recommended density.

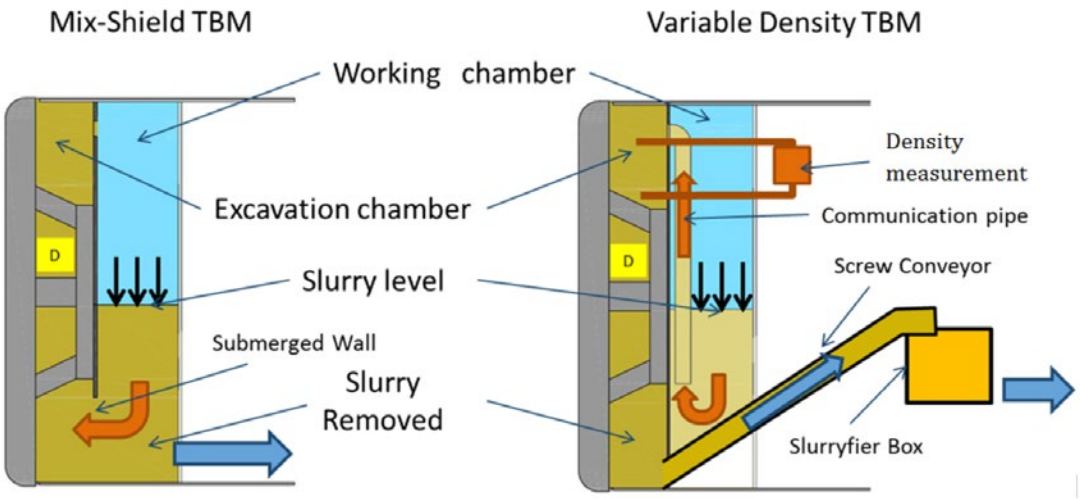

Figure 6: Explanation of pressure application in the excavation chamber

3.5 Bentonite Injection Ratio

To enable the higher density slurry mode in the excavation chamber, regulation of slurry injected to the excavated face was necessary. The bentonite injection ratio (BIR) controlled this injection. The BIR is the flow of slurry sent to the excavation chamber divided by the flow of material physically excavated with basic formula shown below.

$$BIR\ (\%) = \frac{Flow\ of\ slurry}{Flow\ of\ excavated\ material} \quad (2)$$

The ratio is adjusted by operator depending on the density of slurry measured in the excavation chamber. When the density is too low in the excavation chamber, the flow of slurry must be reduced and vice versa if the density it too high, the flow of slurry must be increased.

Flow entering excavation chamber is divided into two parts. One part is sent to the working chamber where slurry is sent through the communication pipe by the pressurised air bubble. The second part is a controlled quantity directed through the face injection lines located on the cutterhead. These work the same as the foam injection lines found on an EPB TBM, however, it is only slurry that is pumped and not foam. A $2m^3$ tank supplies slurry to the 6 individually controlled pumps with the facility to add a polymer to aid dispersion in the excavation chamber if necessary. In semi-automatic mode, the PLC system manipulates the flow through the face injection lines to make up the total slurry directed to the excavation chamber, reaching the set BIR selected by the operator. In manual mode, the operator has control of the pumps which can be adjusted as required.

4 TBM OPTIMISATION

From the original Kuala Lumpur VaD concept, several changes have been developed with Herrenknecht during the design stage to upgrade the TBM processes for working in Hong Kong ground conditions. These were mainly with regard to the transition from hard rock (granite) to full face marine deposits and areas with rubble mount and boulders. Below a list of some item specifically redesigned for the S989 VaD TBM:

- The main drive size and power was increased from 8 motors on a Mix-shield TBM to 12 motors on the VaD TBM.
- The crusher needed to operate in hard rock conditions requiring a “jaw” type crusher, impacting the size and shape of the slurryfier while still providing easy access to the front shield. Regular maintenance of the crusher was also required.
- The slurryfier box was increased to 6m3. Most of the interfaces between the slurryfier box and the working chamber have been redesigned to ensure pressures changes do not interfere with the set bubble pressure.
- Direct and independent injection lines to the cutterhead were adequately designed to face clayey ground conditions and regulate the BIR to maintain the face density.
- Creating several automatic and semi-automatic functions to implement for the slurry circuit operation, simplifying the interfaces on a touch screen for the operators.

5 EXCAVATION ANALYSIS

5.1 TBM Operation

The VaD TBM requires more active manipulation than a Mix-shield TBM due to the increased number of parameters the operator must be aware of when excavating.

In Low Density mode, the machine operates similar to a Mix-shield, mainly having to control the flow of slurry to the excavated face and monitoring level changes in the bubble chamber as well as general

excavation values. No focus is placed on the density inside the excavation chamber due to the ground conditions with which this mode is being used. There is roughly a 50-50 split between the flow sent to the excavated face and the slurryfier box, to aid dilution of the material removed. The main change in operation is the use of the screw conveyor to remove material from the excavation chamber, adjusting the revolution speed as the geology changes. The operator must also be aware of pressure changes inside the slurryfier box, with an increase in pressure indicating the crusher may be full of material. Otherwise advancing and operating procedures are the same.

The concept behind the High Density mode is controlling the supply of slurry to produce a higher density mud in front using the excavated ground in the excavation chamber without plugging the cutter head. The operator has the parameter of excavation chamber density that must be maintained at the recommended density to reduce the risks of blowouts. To sustain the higher density, the screw speed and BIR must be manipulated while also ensuring pressures in the excavation chamber are stable. In general, if a higher density is required, the screw speed will be reduced to retain more material inside the excavation chamber together with a reduction in the BIR, limiting the slurry directed to the face. If a lower density is required, the opposite is enacted, increasing the screw speed, removing more material while also increasing the total slurry sent to the face by changing the BIR.

5.2 Other Advantages

With a hydraulic flap located on the communication pipe between the excavation and working chamber, the team had the option of closing it to access the bubble chamber at atmospheric pressure while maintaining the confinement pressure at the excavated face. This allowed for maintenance inside the working chamber and the ability to prepare materials for compressed air interventions. Pressure was maintained in the excavation chamber via injections of HD mix or bentonite slurry.

The crusher, located inside the slurryfier box, could also be accessed under non-hyperbaric conditions. The screw gate prevented any loss of pressure from the front. This option became useful when needing complete maintenance.

5.3 Drive Analysis

Despite the fact the drives were very short (~677m each) and learning curves considered, the down track drive, mined with the VaD TBM, was completed in 81 days with an average excavation of 8.3m/day. In comparison, the up track tunnel mined with a Mix-shield TBM completed the drive in 86 days, excavating an average of 7.9m/day. The difference is largely a result of the softer ground conditions found along the down track alignment with 35m of rock and 122m of transition, compared to the up track having 172m of rock and 261m of transition. This is due to the up track tunnel excavating at a deeper depth compared to the down track, which is stacked above it. Table 1 provides a comparison of average excavation rates for the various types of geology encountered.

An aspect that did impact the progress of the Variable Density TBM was the processing time of the excess slurry treatment as the softer ground contained up to a 60% fine content. As a result, the process time of the filter presses was slower than what the STP could store. This was anticipated during the tender stage but due to the limited space available, increasing size of the STP set-up was not possible. This kind of geology (with high content of fine) was not encountered during Mix-shield TBM drive with the STP coping well in the mixed face conditions of mainly CDG, allowing for continuous excavation.

As the VaD TBM went through an initial long transition of rock/CDG and mixed face soil with boulders, several CAI's were required to maintain and replace cutters. Due to the shallow cover and very unstable ground conditions along the east down track drive, most of the CAI's were anticipated and carried out in defined, treated areas (ground treatment from the surface). This minimized risks for the public on the surface and the workers working in compressed air.

Table 1: Comparison of average excavation rates between the mix-shield and variable density TBM drives

	Up Track Tunnel (Mix-Shield TBM)		Down Track Tunnel (VaD TBM)	
	Length	Average Progress Rate	Length	Average Progress Rate
Rock	172m	4.0m/day	35m	3.2m/day
Mixed	261m	10.4m/day	122m	5.7m/day
CDG	240m	12.6m/day	–	–
Soft (All, MD)	–	–	165m	7.8m/day
MD (Marine Deposits)	–	–	215m	10.4m/day
Seawall (Rubble Mount)	–	–	140m	12.0m/day
Total Length	**673m**	**7.9m/day**	**677m**	**8.3m/day**

Table 2: General comparison between the two TBM's

	Mix-Shield TBM	VaD TBM
Tunnel Length	673m	677m
Duration of Drive	86 days	81 days
Machine Length	72m	102m
Weight	375T	418T

When working in the high density mode, the recommended densities calculated were reached with TBM operators manipulating the BIR and screw rotation speed to maintain the set value. Areas where quick changes of operation were required occurred when excavating back filled concrete piles and jet grouted ground. The developed BIR concept gave the TBM operator the means to react swiftly to control and regulate the face density to avoid clogging the cutter head.

The TBM performed within the expected settlement values, with the following paper providing more detail by Auvergne (2017a). Throughout the alignment, a number of monitoring sensors were installed to follow the changes as the TBM progress, with no point during the excavation requiring a stop as a result of effects on the surface settlements and safety of the public.

As the TBM excavated through the reclamation area, the team encountered many unexpected object ranging from pieces of steel to blocks of wood. The specific cutter head and "jaw" type crusher design allowed the TBM to pass these objects with approximately 5Tons of steel removed from the slurry circuit by the magnet at the STP. Due to the risk of encountering unexploded ordinances, specific training was conducted with the workers, with stoppages necessary to clearly identify and check objects found on the magnet before removing and restarting TBM excavations.

6 CONCLUSION

Overall, the application of the Variable Density TBM for the eastern down track drive in these very shallow conditions was deemed a success, with no effects to existing structures and the highly dense and congested roads on the surface, which continued to run as normal during excavation. With an initial learning curve, the TBM operated smoothly, having no significant breakdowns during operation. By using the Variable Density TBM, it provides the contractor and the client the flexibility to operate in challenging and changing ground conditions, with the ability to switch modes when necessary.

Although the full EPB mode was not used for this tunnel, it is clear that this new development of High Density mode can tackle such a challenging geological environment that would otherwise not be possible with more conventional machines.

REFERENCES

Straesser, M. 2012. *Klang Valley Mass Rail Transit Kuala Lumpur, Malaysia, Final Report of the Predesign for the Variable Density TBM* Herrenknecht AG, Schwanau

Auvergne, Gauffre & Prost 2017a, *Extensive use of I&M to Enable Safe TBM Drive in Urban Dense Area, a Focus on SCL1128 Eastern Downtrack Drive, Proceedings of the HKIE Geotechnical Division Annual Seminar 2017, Hong Kong*

Auvergne, Yu, Mogenier & Barrett 2017b, *Geophysical Investigations for Obstruction Detection and Mitigation for Marsh Road TBM Crossing, SCL1128, Proceedings of the HKIE Geotechnical Division Annual Seminar 2017, Hong Kong*

Kwok, Bracq & Barrett 2017, *Hong Kong MTR Shatin to Central Link Contract1128 (Eastern Approach) – Tunneling in Sensitive and Congested Urban Environment, Proceedings of the HKIE Geotechnical Division Annual Seminar 2017, Hong Kong*

The Appropriate Use of the Coefficient of Secondary Compression in Settlement Analysis

D. Johnston
Arup, Edinburgh

ABSTRACT

There are several methods to estimate the rate and magnitude of secondary compression settlement in cohesive soils, however one of the most common methods incorporates the 'coefficient of secondary compression'. In order to avoid erroneous calculations, it is important that this parameter is not misconstrued with the 'secondary compression index', which although related to the coefficient, is derived in terms of changes in void ratio as opposed to strain.

Misunderstandings with regard to these parameters occur due to a number of reasons, with the main cause being the inconsistent and incorrect terminology often used in publications. In addition, the index and the coefficient can be described by a multitude of terms and can be expressed by different, yet similar, symbols. Many engineers also have a lack of understanding of this subject, with granular creep terminology often described and erroneous hybrid terminology used.

Therefore, whether based on laboratory testing or established empirical relationships, it is key that engineers understand the source derivation of their settlement parameters and use the correct terminology in their work. This, together with a knowledge of the relationship between the index and the coefficient, will increase confidence in the reporting of settlement values and result in more reliable estimations of settlement.

1 INTRODUCTION

There are several philosophies surrounding the settlement behaviour of cohesive soil, all of which have resulted in various theories, mathematical approaches and rheological models, but for the practicalities of design it is generally accepted that this settlement is attributable to three consecutive processes. These being; immediate settlement, primary consolidation and secondary compression. Immediate settlement is the elastic compression that arises as a result of the application of load, occurring without the dissipation of porewater pressure or volume change, and as its name suggests is almost instantaneous. As load is applied, the total stress increase will initially result in an increase of porewater pressure within the soil and primary consolidation will then occur as this excess porewater pressure dissipates; thereby increasing the effective stress and transferring stress to the soil skeleton. The subsequent time-dependent settlement following primary consolidation is the secondary compression stage, often referred to as secondary consolidation, and arises due to the ensuring re-arrangement and deformation of particles within the soil structure.

To estimate the rate and magnitude of secondary compression, engineers typically adopt a common calculation approach, which will be referred to hereafter as the 'standard method'. This method considers the rate of secondary compression settlement as a function of the logarithm of time, with the magnitude a function of the initial undeformed height, time and the coefficient of secondary compression. Although most engineers would acknowledge that a degree of secondary compression occurs during the primary

consolidation stage, particularly as the excess porewater pressure at the strata boundaries will dissipate at a faster rate than that in the middle of the layer, for the purposes of settlement analysis it is generally assumed that the onset of secondary compression commences following the substantial completion of primary consolidation. Therefore, a time corresponding to 90% or 95% of the completion of primary consolidation is adopted for calculation.

However, despite common usage of the standard method, the coefficient of secondary compression is often misconstrued with the secondary compression index and engineers inadvertently adopt the incorrect parameter in analysis. Therefore, for the appropriate use of the coefficient of secondary compression in design, it is important to understand its relationship with the secondary compression index and the correct terminology.

2 DEFINITION OF TERMS

The characteristic settlement curve is presented in Figure 1 and illustrates the subject both in terms of changes of strata height or void ratio with the logarithm of time. As shown, the initial settlement is attributable to the 'primary consolidation' stage, whereby the settlement occurs due to the dissipation of excess porewater pressures and subsequent compression of the soil skeleton with the increase in effective stress. The latter stage of the settlement curve, where the gradient becomes relatively linear with the logarithm with time, is attributed to the 'secondary compression' stage where soil particle re-arrangement and deformation results in continued settlement.

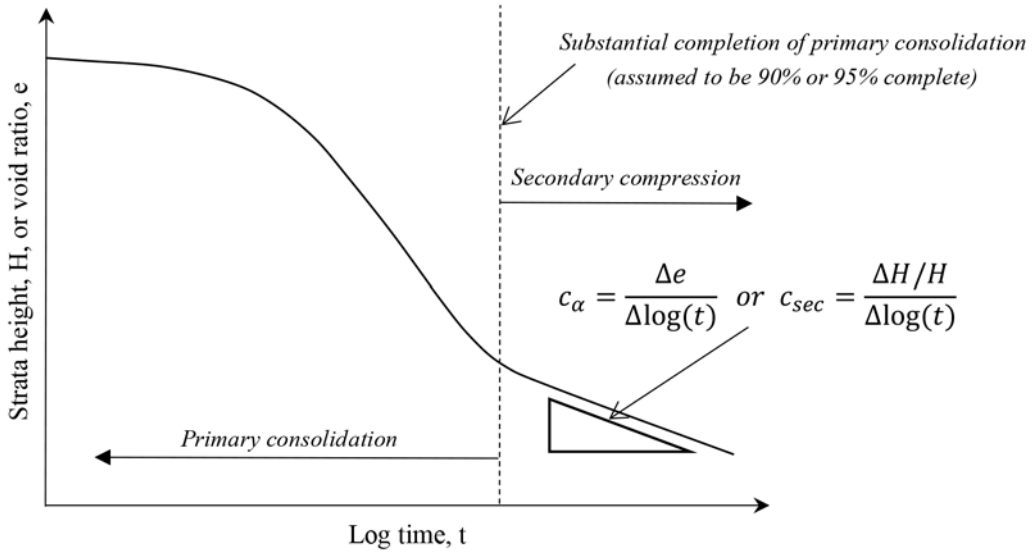

Figure 1: Characteristic settlement curve

If the settlement curve as illustrated in Figure 1 is expressed in terms of void ratio with the logarithm of time on an e-log(t) plot, then the gradient of the primary consolidation stage is termed the 'compression index', or the 'primary consolidation index', and denoted by C_c. The approximately linear gradient of the secondary compression stage is then termed the 'secondary compression index', denoted by the term c_α and defined by Equation 1. This parameter is most derived from conventional laboratory one-dimensional consolidation tests, commonly known as oedometers, with the loading period extended without any additional stress increase following primary consolidation (GEO, 2001).

$$c_\alpha = \frac{-de}{d\log(t)} = \frac{\Delta e}{\Delta \log(t)} \quad (1)$$

where, Δe = change in void ratio over time interval and t = time

If the settlement curve is considered as a function of changes in strata thickness with the logarithm of time on an H-log(t) plot, then the gradient of the primary consolidation curve is termed the 'compression

ratio' and denoted by CR. The approximately linear gradient of the secondary compression stage is termed the 'coefficient of secondary compression' and is most commonly denoted by either c_{sec} or $c_{\alpha\varepsilon}$ and defined by Equation 2. This can also be derived from laboratory oedometer testing or from the monitoring results of field instrumentation.

$$c_{sec} = \frac{-dH}{d\log(t)} = \frac{\Delta H/H}{\Delta\log(t)} \quad (2)$$

where, ΔH = change in strata thickness over time interval, H = strata thickness and t = time

Research has established that the both the secondary compression index and the coefficient of secondary compression vary as a function of time and applied vertical stress. Work undertaken by Mesri (1973) and Mesri & Godlewski (1977) indicate notably lower secondary compression indices when the applied stress is less than the pre-consolidation pressure, but increases significantly during the re-compression stage and reaches a maximum at a stress between 1.5 and 2.0 times the pre-consolidation pressure (Lo, 2002; Balasubramaniam, 1981; Takeda et. al, 2012). However for the purposes of calculation using the standard method, it is assumed that both these parameters are independent of time, strata thickness and oedometer test load increment ratio.

In light of the various terminology discussed, Table 1 attempts to summarise these terms in a clear and concise manner; in terms of void ratio and strain and for both the primary consolidation and secondary compression stages. It should be noted that in the case of the secondary compression in terms of strain, the terms in Table 1 do not necessarily correspond directly with the symbol in the adjacent column.

Table 1: Summary of settlement parameter terminology

	Considered in terms of void ratio e-log(t)		Considered in terms of strain H-log(t)		
	Term	Symbol	Term	Symbol	Relationship between e-log(t) and H-log(t)
Primary consolidation: gradient of e-log(t) plot	Compression Index or Primary Compression Index	C_c	Compression ratio	CR	$CR = \frac{C_c}{1 + e_o}$
Secondary compression: gradient of H-log(t) plot	Secondary Compression Index	c_α or $c_{\alpha e}$	Coefficient of Secondary Compression or Coefficient of Secondary Consolidation or Modified Secondary Compression Index or Rate of Secondary Compression or Rate of Secondary Consolidation	c_{sec} or $c_{\alpha\varepsilon}$ or ε_α	$c_{\alpha\varepsilon} = \frac{C_\alpha}{1 + e_p}$

where, e_p = void ratio at the start of the linear section of the e-log(t) plot.

As shown in Table 1, the secondary compression index can be denoted as either c_α or $c_{\alpha e}$. However, the secondary compression stage on the H-log(t) plot is often described by many terms and denoted by different symbols; most commonly as c_{sec} or $c_{\alpha\varepsilon}$, but in rare cases is sometimes denoted as ε_α (Mesri, 1973).

3 CALCULATION OF SECONDARY COMPRESSION

The standard method of calculating secondary compression settlement is considered to be most applicable to small strain situations and works on the principle of linear strain, thereby considering the initial undeformed condition of the soil. Given this, the calculation of secondary compression settlement using the secondary compression index, c_α, with parameters derived in terms of change of void ratio, is presented in Equation 3.

$$\Delta H = H_o\left(\frac{c_\alpha}{1 + e_p}\right)\log\left(\frac{t_1}{t_o}\right) \quad (3)$$

where, ΔH = settlement between time t_1 and t_o, H_o = initial layer thickness, e_p = void ratio at start of the linear section of the e-log(t) plot, t_1 = design time and t_o = time when primary consolidation is substantially complete.

The relationship between the coefficient of secondary compression, c_{sec}, and the secondary compression index, c_α, is shown by Equation 4.

$$c_{sec} = \frac{c_\alpha}{1 + e_p} \quad (4)$$

Substitution of Equation 4 into Equation 3 thereby allows secondary compression to be calculated using parameters derived on the basis of strain; see Equation 5.

$$\Delta H = H_o c_{sec}\log\left(\frac{t_1}{t_o}\right) \quad (5)$$

where, ΔH = settlement between time t_1 and t_o, H_o = initial layer thickness, t_1 = design time and t_o = time when primary consolidation is substantially complete.

4 METHODS TO DERIVE SECONDARY COMPRESSION PARAMETERS

4.1 The secondary compression index

The secondary compression index can be derived from the results of conventional laboratory oedometer tests undertaken on intact soil samples recovered from the site ground investigation. The tests are undertaken as standard, with the addition of an extended loading period at constant stress once it is observed that primary consolidation is complete. It is important to note that the applied stress of the oedometer test should exceed the pre-consolidation pressure of the soil sample and that the duration of extended load is held for at least one logarithmic time cycle.

In the absence of oedometer testing to determine the secondary compression properties, or for parameter comparison purposes, engineers often refer to the established correlation between the compression index and the secondary compression index; where the c_α/C_c ratio falls within a narrow range and is found to be constant for any one soil type. Mesri & Godlewski (1977) established a series of constants for varying cohesive soils and concluded that this range is typically 0.04 ± 0.01 for soft inorganic soils, in the region of 0.05 ± 0.01 for highly organic plastic clay (Holtz, 1991) and typically 0.07 ± 0.02 for peat (Ladd, 1977). For the purposes of this correlation the research concluded that both these parameters should be determined at similar stress ranges and a minimum of three sets of measurements undertaken at varying levels of applied stress. To further assist engineers, subsequent research has been undertaken to supplement the catalogue of c_α/C_c constants, which include; Mesri & Castro (1987), Mesri & Shahien (1992), Feng (1993) and Mesri et al. (1994).

The ratio between the compression index and the secondary compression index is the most commonly used and published correlation, however, there are several less established correlations have been researched. These include the relationship between the secondary compression index and liquidity index by Walker (1969) and Yasuhara et al. (1983), whereby the index is shown to increase with increasing liquidity index, and the relationship between the secondary compression index and void ratio by Wahls (1962) and Kapp et al. (1966).

4.2 The coefficient of secondary compression

Engineers can also derive secondary compression parameters from sources derived in terms of strain. As with the method for assessing the secondary compression index, the coefficient of secondary compression can also be determined from conventional laboratory oedometer tests and assessment of the resulting H-log(t) plot.

In the absence of oedometer testing, the Mesri (1973) chart can be consulted. This illustrates the relationship between the natural moisture content and the coefficient of secondary compression, both on a logarithmic scale, for different soil types. Usually such classification data is easily obtainable from ground investigations, where a limited volume of soil sample is required for the relatively inexpensive moisture content test.

During and following construction, in-situ monitoring of settlement instrumentation can be used to assess the coefficient secondary compression, in which the H-log(t) data from magnetic extensometers, settlement plates or surface movement markers can be interpreted. However if doing so, it is critical to also understand the corresponding primary consolidation behaviour. This may require the use of vibrating wire piezometers or cone penetration testing with porewater measurement. Not only will this information provide the engineer with primary consolidation and secondary compression data, it will allow the accurate time of substantial completion of primary consolidation to be determined. However, in practice the use of field instrumentation to assess the coefficient of secondary compression is rarely undertaken. This is because the settlement analysis is undertaken in advance of construction and, as the rate of secondary compression occurs on a logarithmic time scale, there is generally an insufficient period of monitoring to allow a reliable assessment to be made.

5 REASONS FOR MISUNDERSTANDING

5.1 Introduction

Given the various methods available to derive secondary compression parameters, engineers often misinterpret the secondary compression index (derived in terms of void ratio) with the coefficient of secondary compression (derived in terms of strain). Although these parameters are related to one another, they are not equivalent and each should be used within their appropriate expressions. There are various reasons for this misinterpretation, most of which are discussed as follows.

5.2 Incorrect and inconsistent terminology

One of the main reasons for this misunderstanding is due to the widespread use of inconsistent and incorrect terminology in published literature and within the engineering profession. In the preparation of this study, fourteen sources of published literature were reviewed for consistency and accuracy of reporting. This found that eight of the sources reported incorrect terminology or were ambiguous in their use of symbols. For example, most of these cases referred to the secondary compression index as the coefficient of secondary compression or designated the coefficient of secondary compression as ‘cα’ (which is the index, unless denoted otherwise). Erroneous hybrid terminology was also used, such as reference to the ‘coefficient of secondary compression in terms of void ratio’ (with the coefficient only applicable in terms of strain) and the ‘modified coefficient of secondary compression’ (rather than the modified secondary compression index).

5.3 Diverse use of terminology and symbols

Even with the correct use of terminology there is still the potential for confusion. As shown in Table 1, the same parameter can be described by various means and expressed by different symbols. Many of these terms and symbols appear similar and are often only differentiated by the use of subscripts. For example, the secondary compression index can be denoted as cαe and the coefficient of secondary compression denoted as cαε. Not only is this confusing, the use of subscripts can be difficult to read in printed form.

5.4 Unknown sources of derivation

As the scheduling of laboratory oedometers to derive secondary compression parameters is not standard practice, as intact samples can be difficult to recover and extended period of oedometer testing can be expensive, many engineers then have to rely on the established correlations from published sources. However, it is common for these sources to not report the method of parameter derivation or identify whether the correlation is in relation to the secondary compression index or the coefficient of secondary compression. As such it is common for the parameters to be simply denoted as cα. As both the secondary compression index and the coefficient of secondary compression are unitless, engineers cannot make this differentiation.

5.5 Engineers' lack of understanding

Engineers generally consider a range of sources before concluding the parameters to adopt in design. However, many engineers do not fully understand the relationship between the secondary compression index and the coefficient of secondary compression. In their review of sources to derive parameters they often incorrectly mix the index and the coefficient. For example, the Mesri (1973) correlation between the coefficient of secondary compression and the natural moisture content is frequently compared directly with the Mesri & Godlewski (1977) relationship between the c_α/C_c ratio. As the magnitude of the secondary compression index is larger than the coefficient, then in the interest of being conservative, engineers often incorrectly adopt the index into the expression intended for the coefficient.

5.6 Comparison with granular creep terminology

In the case of granular soil settlement terminology, there is no differentiation of parameters being derived in terms of either strain or void ratio. Instead, the creep settlement of granular soil is estimated using a method similar to Equation 5, with the coefficient of secondary compression replaced by the 'logarithmic rate of creep', otherwise referred to as the 'coefficient of creep', which is denoted as c_α. It is unfortunate that the granular coefficient of creep is denoted by the same symbol as that of the secondary compression index. Consequently, engineers have a tendency to interchange granular and cohesive terminology and often incorrectly refer to both the coefficient of creep and the coefficient of secondary compression as c_α.

6 CONCLUSION

For the calculation of secondary compression settlement, most engineers employ a standard method which uses the 'secondary compression index'. This parameter is not to be misconstrued with the 'coefficient of secondary compression', which although related, is derived in terms of changes to void ratio rather than strain.

Engineers can derive both the coefficient and the index by the results of conventional laboratory one-dimensional consolidation testing, consulting established empirical relationships or by the assessment of field settlement instrumentation. However despite their differences, it is common for both these parameters to be misinterpreted with one another and the index used in place of the coefficient.

This misunderstanding arises due to a number of reasons, but is primarily due to the inconsistent and incorrect publishing of terminology, which is further compounded by the same parameters being described differently and denoted by different symbols. In addition, published information does not always report the source of parameter derivation and many engineers do not fully understand the difference between the secondary compression index and the coefficient of secondary compression. To complicate matters, further confusion can arise from the interchanging of granular and cohesive settlement terminology.

As a result, it is clear that engineers undertaking settlement analysis must have an appreciation of the differences between the secondary compression index and the coefficient of secondary compression. Whether they intend to derive parameters based on laboratory testing or from established empirical relationships, engineers need to understand the source of derivation in order that the appropriate

expression is used. In doing so, engineers can become more confident in their settlement predictions and more realistic estimations of settlement can be reported.

REFERENCES

Balasubramaniam, A.S. & Brenner, R. P. 1981. Chapter 7. Edited by Brand, E.W. & Brenner, R.P. Brenner. *Soft clay engineering. Developments in geotechnical engineering*. pp481-594. Elsevier Scientific Publishing Company.

Bowles, J. E. 1997. *Foundation Analysis and Design*. Pp335-336. Fifth Edition. McGraw-Hill Companies Inc.

Carter, M. & Bentley, S.P. 1991. *Correlations of Soil Properties*. pp68-70. Pentech Press Limited.

Feng, T.W. 1993. Consolidation properties of a lacustrine clay in Taipei. *Proceedings of the Eleventh Southeast Asian Geotechnical Conference*, Singapore, pp117-120.

Geotechnical Engineering Office, 2001. *Geospec 3 Model Specification for Soil Testing*. Civil Engineering Department, The Government of the Hong Kong Special Administrative Region.

Holtz, R.D. 1991. Chapter 5. Edited by Fang, H. *Foundation Engineering Handbook*. pp209-212. Second Edition. Chapman & Hall.

Kapp, M.S., York, D.L., Arnowitz, A. & Sitomer, H. 1966. Construction on marshland deposits: treatments and results. *Highway Research Board*, Record no.133, pp1-22.

Ladd, C.C., Foot, R., Ishihara, K., Schlosser, F. & Poulos, H.G. 1977. Stress-Deformation and Strength Characteristics. 9th *International Conference on Soil Mechanics and Foundation Engineering*, Tokyo, Vol.2, pp421-494.

Lo, D.O.K & Premchitt, J. *Long-term consolidation tests on clays from the Chek Lap Kok Formation*. 2002. GEO Report No. 72. The Government of the Hong Kong Special Administrative Region. Geotechnical Engineering Office, Civil Engineering Department.

Mesri. G. 1973. Coefficient of Secondary Compression. *Journal of Soil Mechanics and Foundation Division*, *American Society of Civil Engineers* 99: 123-137.

Mesri, G. & Godlewski, P. M. 1977. Time and stress compressibility interrelationships. *Proceedings ASCE Journal of Geotechnical Engineering Division*, 103: 417-430.

Mesri, G. & Choi, Y.K. 1984. Discussion on time effects on the stress-strain behavior of natural soft clays by J. Graham, J.H.A Crook & A.L. Bell. *Géotechnique*, vol. 34, no.3, pp439-442.

Mesri, G. & Castro, A. 1987. Cα/Cc concept and Ko during secondary compression. *Journal of the Geotechnical Engineering Division*, *American Society of Civil Engineers*, vol. 113, no.3m pp230-247.

Mesri, G. & Shahien, M. 1992. Discussion on long-term consolidation characteristics of diluvial clay in Osaka Bay by K. Akai, M. Kamon, I. Sano and K. Soga. *Soils and Foundations*, vol.33, no.1, pp 213-215.

Mesri, G, Lo, D.O.K & Feng, T.W. 1994. Settlements of embankments on soft clays. *Proceedings of Settlement'94, Vertical and Horizontal Deformations of Foundations and Embankments*, American Society of Civil Engineers, Geotechnical Special Publication No.40, vol.1, pp8-56.

Simons, N.E. 1974. Normally consolidated and lightly over-consolidated cohesive materials. *Review paper: Session II. Proceedings of the BGS Conference on Settlement of Structures*. Cambridge, pp500-530.

Takeda, T., Sugiyama, M., Akaishi, M. & Chang, H. 2012. Secondary compression behavior in one-dimensional consolidation tests. *Journal of GeoEngineering*, Vol.7, No.2, pp53-58.

Wahls, H.E. 1962. Analysis of primary and secondary consolidation. *Journal of the Soil Mechanics and Foundations Division, American Society of Civil Engineers*, vol.88, no.SM6, pp107-231.

Walker, L.K. 1969. Secondary settlement in sensitive clays. *Canadian Geotechnical Journal*, vol. 6, no.2, pp219-222.

Yasuhara, K., Yamanouchi, T., Ue, S. & Hirao, K. 1983. Secondary compression of clay in consolidation and undrained shear tests. *Proceedings of the Symposium on Recent Developments in Laboratory and Field Tests and Analysis of Geotechnical Problems*, Thailand, pp230-255.

Economic Reclamation and Seawall Design and Temporary Stabilizing Berm

M.C.Y. Ko & H.C. Sze
Ove Arup & Partners (H.K.) Ltd

ABSTRACT

Similar to non-dredged reclamation method that maintains the existing superficial deposit in place, there is a trend of constructing a seawall foundation without dredging. In this paper, a case history of failure in a Hong Kong reclamation project that adopted no-dredging works at seawall foundation has been discussed to demonstrate the consequence of unforeseen ground condition at non-dredged seawall. Limit equilibrium analyses of a series of hypothetical non-dredged seawall models have been carried out and show that a portion of strengthening measure required during surcharge preloading might become abundant after surcharge removal. As such, a pilot study on reducing the amount of abundance by the application of temporary stabilizing berms has also been carried out. Based on the analysis results, the extent of strengthening works could be reduced with the provision of temporary stabilizing berms.

1 INTRODUCTION

Reclamation will play an important role on land supply of Hong Kong in the coming future. In order to meet the fast track construction programme of a reclamation project, drained reclamation that accelerates the consolidation of insitu superficial deposit with the application of surcharge preloading and vertical drains becomes one of the common reclamation methods in Hong Kong. On the other hand, although seawall foundation formed by dredging and replacing the insitu weak superficial deposit with better engineering properties materials (e.g. rockfill) were commonly adopted in the reclamation project of Hong Kong (e.g. Tuen Mun New Town Development) in 19th Century, forming a seawall foundation that requires disposal of marine deposit is generally discouraged, unless strong justifications on the need of removal of the marine deposit have been satisfactorily demonstrated, since the enforcement the Technical Circular No. 34/2002 of the Management of Dredged/Excavated Sediment in 2002. As such, there is a demand to construct the seawall foundation without dredging of existing seabed (hereinafter refers as non-dredged seawall foundation).

However, non-dredged seawall foundation might expose to risk inherent from the highly variant of stratigraphy and properties of the existing superficial deposit. The consequence of any unforeseen weak layer within the non-dredged seawall foundation could be and had been recorded as catastrophic. In this paper, a case history of non-dredged seawall foundation failure of a reclamation project in Hong Kong has been discussed to demonstrate the risk and consequence of unforeseen ground condition. In addition, non-dredged seawall foundation usually involves more sophisticated strengthening measures to either strengthen or retain the insitu superficial deposit, and thus higher construction cost and time would be induced.

Due to the fact that a portion of strengthening measures required to resist the substantial temporary unbalanced earth pressure from surcharge preloading would be abundant after removal of surcharge, a series of hypothetical non-dredged seawall models have been formulated to 1) estimate the portion

of abundance by comparing the difference between the extent of strengthening measures required for "operating case" (i.e. up to final formation level of a reclamation project) and "surcharge case" (i.e. up to surcharge top level) and 2) study the effect of applying additional temporary stabilization measures before and during placing of surcharge to reduce the amount of abundance required during surcharge preloading stage.

2 CASE HISTORY AND LESSON LEARNT

2.1 General

Among the reclamation failure cases that detailed in Fred et. al, 2007, the controlled tip in the Junk Bay of Tsuen Kwan O development was a reclamation project that formed the temporary seawalls foundations by displacing the insitu marine deposit and with no dredging works been carried out for forming seawall foundation. Unfortunately, a major failure that involved 500,000m^3 was happened in March 1984. The details of this failure are described below.

2.2 Junk Bay (Tseung Kwan O) Controlled Tip

A controlled tip had being constructed in the Junk Bay area since 1977 for disposal of waste. The tip was developed in stages, which involved adding cells of lagoons that enclosed by enclosing bunds for filling up the lagoons subsequently. The tip advanced away from the shoreline as further enclosing bunds were added to form lagoons for receiving the waste. The sequence is illustrated in Figure 1. The enclosing bunds were created by dumping construction waste (e.g. soft fill and building rubbles) to displace the marine mud and found the bunds on firm layer without any dredging works nor treatment to strengthen the existing marine mud been carried out.

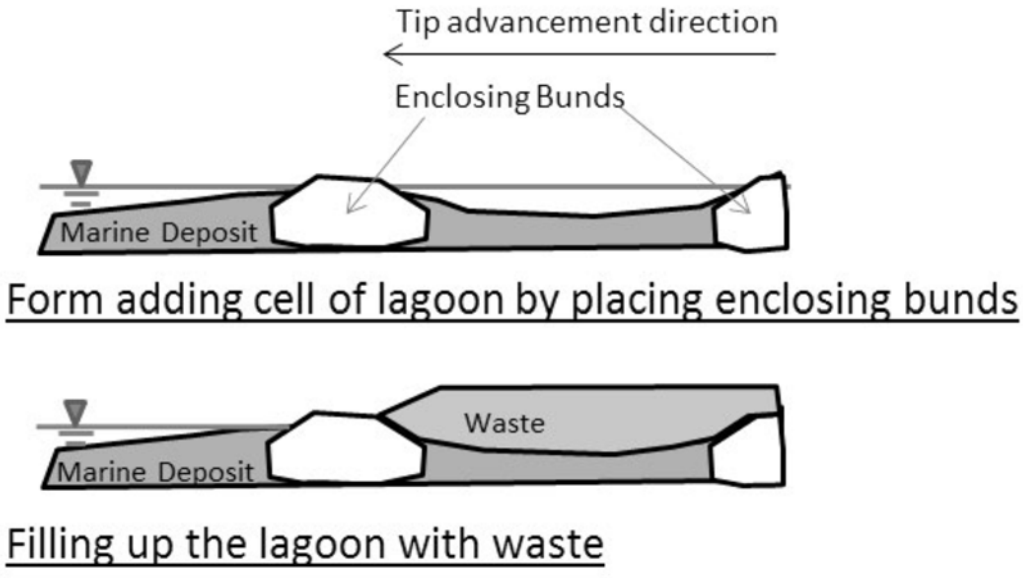

Figure 1: Schematic Sequence of Junk Bay (Tseung Kwan O) Controlled Tip

2.3 Case History of Junk Bay (Tseung Kwan O) Controlled Tip Failure

Waste was being tipped behind the enclosing bunds and the failure was reported to have developed rapidly in March 1984, which involved an estimated 500,000m^3 of materials and a horizontal displacement of about 20m of the edge of the reclamation site (Fred. et. al., 2007). The failure had been thoroughly investigated by the Geotechnical Engineering Office and detailed in GCO, 1984. The failure was deducted to have a slip surface located in the very soft marine mud that passed beneath the enclosing bunds (L.J.Endicott, 2001). It was concluded that 1) the bunds did not make full contact with underlying firm soils of alluvium; 2) the entrapped marine mud underneath the bunds was insufficiently strong to carry

the load from the waste; and thus failure occurred through the entrapped soft marine mud beneath the bunds.

2.4 Insight for Reclamation Projects with Non-dredged Seawall Foundation

As shown in the case history above, unforeseen ground condition at non-dredged seawall foundation could cause a great influence to the overall stability of a reclamation project and the result was catastrophic. The inherent risk of insitu superficial deposit could be mitigated by carrying out extensive ground investigation works to increase the level of confidence on the geology of the reclamation site; to adopt higher factor of safety against instability; intercept the weak layer by installation of structural elements or strengthening the insitu superficial deposit by construction method like Deep Cement Mixing (DCM) or jet grouting etc.

3 PILOT STUDY OF APPLYING TEMPORARY STABILIZATION TO NON-DREDGED SEAWALL FOUNDATION

3.1 Overview

Depends on the anticipated mode of failures of a seawall design, a minimum Factor of Safety (FoS) under Normal Loading Conditions against slip failure is 1.3 (CED,2003). In addition, attentions should also be paid to the particular modes of failure for the type of strengthening measures being considered, for example bulging of sand/stone columns, flexural failure of individual deep cement mixed piles or shearing on vertical planes within a deep cement mixed block etc.

The commercially available computer programme of PLAXIS 2D that commonly used for geotechnical engineering analysis in Hong Kong has been employed for carrying out limit equilibrium analysis of the hypothetical non-dredged seawall models. The geology of the models is based on the offshore soil strata that commonly encountered in Hong Kong and detailed in Section 3.2.

Two loading conditions representing the operating case (i.e. up to final formation level) and surcharge case (i.e. up to surcharge top level) have been modelled to estimate the amount of abundance by comparing the difference on the extent of strengthening measures required in both cases. Moreover, additional temporary stabilization measures have been modelled in the surcharge case to study the effectiveness on reducing the amount of abundance on strengthening measures during surcharge preloading stage. Relevant details are discussed in Section 3.3 and 3.4

3.2 The Geological Model

The offshore soil strata of Hong Kong comprise marine deposit and alluvial deposit to a considerable thickness, and they are underlain with residual soil and weathered rock. The marine deposit is typically 10m to 20m thick and is usually soft to very soft normal consolidated clay and the alluvial deposit is typically 5m to 10m thick (GEO Report No. 63, 1996). With reference to the R.J.Sewell & P.A. Kirk 2002, the undrained shear strength of the Marine Deposit from the youngest offshore Quaternary stratigraphic unit in the Hong Kong varies from less than 3 to 20kPa, while the undrained shear strength of the clay layer underneath varies between 30 and 90kPa.

The final formation level of the hypothetical models have been assumed as +5mPD (i.e. higher than the extreme sea level of +4.6mPD at Hong Kong region). The hypothetical geological model and input parameters the analyses illustrated and listed in Figure 2 and Table 1 respectively.

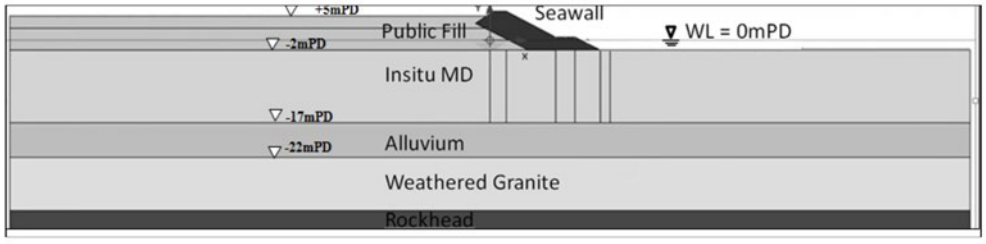

Figure 2: The Hypothetical Geological Model

Table 1: Input Parameters for the Hypothetical Model

Material	Drainage Type	γ_{sat} (kN/m^3)	c' (kPa)	ϕ' (deg)	c_u (kPa)	ν'	E' (kPa)
Public Fill	Drained	19	0	35	–	0.25	20000
Seawall	Drained	19	0	40	–	0.25	50000
Insitu MD	Undrained (B)	16	–	–	3+1.5D Where D is the depth from the assumed seabed of -2mPD	0.33	400c_u
Alluvium	Undrained (B)	19	–	–	50+5D Where D is the depth from the assumed insitu MD base of -17mPD	0.3	30000
Weathered Granite	Drained	19	3	33	–	0.25	50000

* All the materials are modelled as Mohr-Coulomb material model.

3.3 Implication of Surcharge Towards Extent of Strengthening Measures

Deep Cement Mixing (DCM) has been adopted as the strengthening measure in this study. Continuous DCM in block installation pattern (Figure 3) has been adopted at seawall toe area to prevent overall reclamation stability failure. As mentioned in Section 3.1, particular modes of failure for the type of strengthening measures being considered should also be checked. Based on the minimum FoS against typical modes of failure of DCM work as recommended in FHWA, 2013 (Table 2a), the minimum FoS for slope stability failure of DCM should be 1.5, which therefore overrides the value of 1.3 against slip failure as required in CED, 2003.

Table 2a: Typical Modes of Failure of DCM Block and Corresponding FoS

Mode of Failure of DCM Block*	Minimum FoS
Slope stability failure, including global stability and shearing through the DCM block	1.5
Combined overturning and bearing capacity failure of the DCM block	1.3
Crushing of the deep mixed ground at the toe of the DCM block	1.3
Shearing on vertical planes through the DCM block	1.3

* Only modes of failure relevant to DCM block have been extracted from FHWA, 2013.

As detailed design of DCM is out of the scope of this paper, the area replacement ratio of DCM and overlaps along the chord length of each adjacent DCM columns have also been assumed to be sufficient to prevent crushing of the toe of DCM block and shearing on vertical planes in DCM respectively.

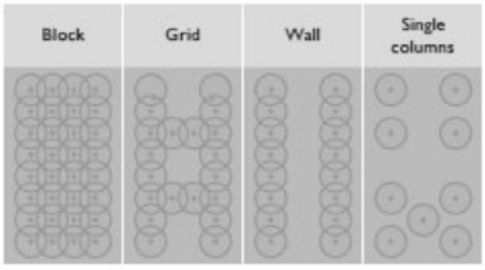

Figure 3: Examples of DCM Installation Patterns

The input parameters of the soil-cement for DCM block are summarized in Table 2b below:-

Table 2b: Input Parameter for Soil-Cement Mix

Model	Drainage Type	γ_{sat} (kN/m^3)	q_u* (kPa)	c_u (kPa)	ν'	E' (kPa)
Mohr-Coulomb	Undrained (B)	18	600	0.5 x q_u	0.33	150 x q_u

*A water cement ratio of approximately 4% has been assumed for obtaining the unconfined compressive strength of soil-cement mix from the laboratory results of 28 days unconfined compressive strength on various water cement ratios (FHWA, 2013).

3.3.2 Results of Operating and Surcharge Case

Band drains would be installed at the early stability of reclamation, and with surcharge preloading, to accelerate the consolidation of insitu marine deposit. As the distribution of the surcharge load between the DCM block and insitu soil varies with time (i.e. degree of consolidation at the time of placing surcharge), sensitivity checks using two degrees of consolidation (i.e. 50% and 70%) of the insitu superficial deposit underneath the footprint of reclamation and seawall have been carried out. The gain in undrained shear strength of the superficial deposits due to consolidation have been calculated in accordance with the correlation in Equation 1 that given by Skempton 1957.

$$\frac{C_u}{\sigma_v'} = 0.11 + 0.0037(PI) \qquad (1)$$

where PI = Plastic Index in % and an average PI of 45% has been estimated based on previous reclamation projects at Chek Lap Kok and Tung Chung Area (GEO Report No. 63, 1996).

It is noted from the case histories non-dredged seawalls in Singapore (C.F. Leung, 2016), Hong Kong (A.D. Mackay and N.R. Wightman) and Macau (De Silva A., Fong L.T.T., 2013) that the extent and configuration of strengthening measures varied with design assumptions, for instance, insitu soil in front of seawall toe had been strengthened in some of the above case histories. As it was commented that geotechnical instability at the seawall toe could be triggered and generally lead to overall failure of the seawall (R.S. Thomas, 1992), strengthening measure (i.e. DCM block) in front of seawall toe has been adopted in the surcharge case models.

Sensitivity checks on the widths of DCM block against various degree of consolidation of insitu soil have first been carried out. The widths of DCM block for the surcharge case have been optimized to achieve a minimum FoS of 1.50 (tolerance up to +0.04) against slope failure. It is noted from Figure 4 that the critical slip surfaces for each case of the sensitivity checks are non-circular and subhorizontally along the bottom of DCM block and are similar to the potential sliding surface across a Deep mixed shear wall as discussed in FHWA, 2013 (Figure 4). The results on the sensitivity checks on the widths of DCM block are summarized in Table 3.

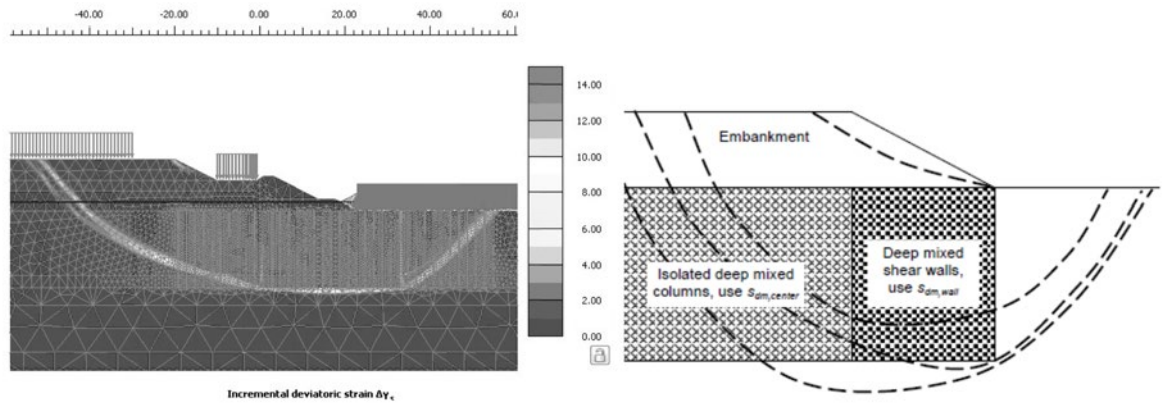

Figure 4: Incremental Deviatoric Strain Plot for Surcharge Case and Potential Slip Surface (after FHWA, 2013)

Table 3: Result on Sensitivity Checks

Loading Condition	U (%)	Width of DCM (landward side from seawall toe)	Width of DCM (seaward side from seawall toe)	Total width of DCM block for obtaining FoS = 1.50 (tolerance = +0.04) against slope failure
With Surcharge	70	22.4	10.0m	32.4m
With Surcharge	50	36.4m	13.6m	50.0m

To estimate the amount of abundance of strengthening measures after surcharge removal, an analysis model for the operating case (i.e. up to final formation level) with assumption of 90% consolidation of insitu superficial deposit to represent the condition after commissioning has been formulated.

The width of DCM block of the model has also been optimized to 8.7m for satisfying the requirement on a minimum FoS of 1.50 (tolerance up to +0.04) against slope failure. However, based on Figure 5 that shows relatively large shear strain along both sides and , especially, at the toe of the DCM block, the 8.7m wide DCM block is likely subject to the mode of combined overturning and bearing capacity failure. As discussed in FHWA, 2013, the combined overturning and bearing capacity failure would typically be resolved by increasing the width or depth of the DCM block, the width of DCM has then been widened until the mode of failure is changed to slip failure. The width of DCM block for operating case has then been widened from 8.7m to 16.4m. For a more precise calculation of DCM works in detailed design of DCM works (i.e. out of the scope of this paper), the width of DCM block should be further widened to satisfy the required FoS of combined overturning and bearing capacity failure.

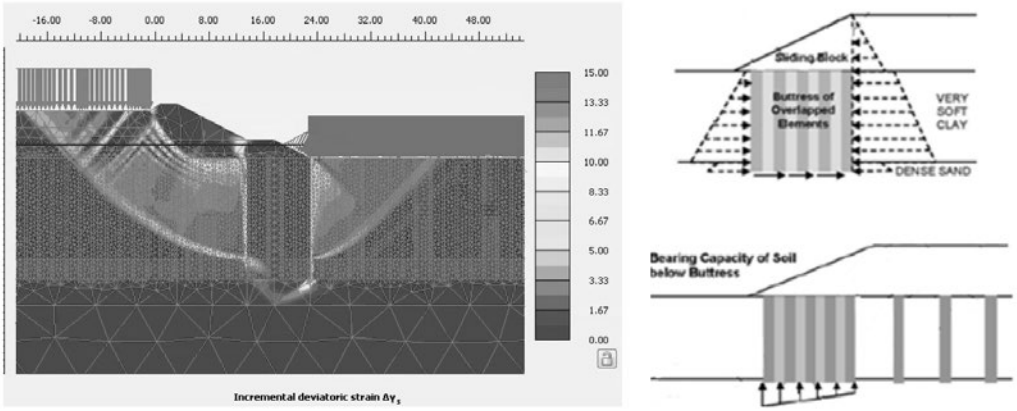

Figure 5: Incremental Deviatoric Strain Plot for Operating Case and Mode of Failure for Overturning and Bearing Capacity (after FHWA, 2013)

As demonstrated above that substantial amount of strengthening measures (i.e. the width of DCM block in this study) becomes abundant after removal of surcharge. In order to reduce the amount of abundance, analyses on the effect of applying temporary stabilizing berm as temporary stabilization measures before and during placing of surcharge have been carried out.

3.4 Parametric Study on Temporary Stabilizing Berm

Based on a survey on embankment slope remediation technologies of Iowa country that conducted in 2001, the design and construction of stabilizing berms has been considered as a simple and effective option for slope stabilization (Mark and David 2005). With the prohibition of premature removal of temporary stabilizing berm (V. R. Raju et. al. 2016), application of temporary stabilizing berm could be an alternative to replace the need of providing the substantial amount of strengthening measures during surcharge preloading stage.

To carry out a parametric study on the effectiveness of stabilizing berm on reducing the extent of strengthening measures for a non-dredged, various widths (i.e. measuring the from crest of seawall toe to crest of temporary stabilizing berm = 8m, 18m, 28m, and 38m) of stabilizing berm (i.e. assumed to be

rockfill with c' = 0; ϕ' =35°) have been applied to the surcharge case models with degrees of consolidation of 50% and 70%. A 2.65m high temporary stabilizing berm with leading edge gradient of 1 in 8 has been adopted in the model. Typical configuration is illustrated in Figure 6.

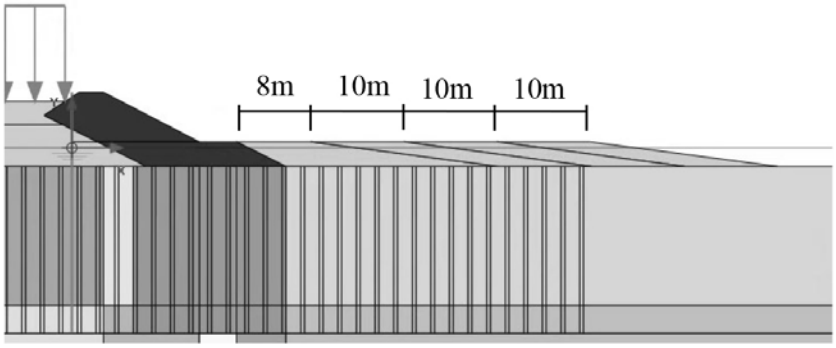

Figure 6: Configuration of Parametric Study

Stabilizing berm is a layer of earth material at the toe of the slope of embankment or seawall that provides a counterweight to resist deep, rotational failure (FHWA 1998). With the concept of utilizing the weight of stabilizing berms to reduce the net driving force along the critical slip surface and increasing the length and depth of all potential slip surfaces (analysis results of the parametric study and conceptual illustrations are shown in Figure 7), the effect of applying of temporary stabilizing berms to reclamation for counterbalancing the unbalanced earth load, especially during surcharge preloading stage, is also been analyzed and studied.

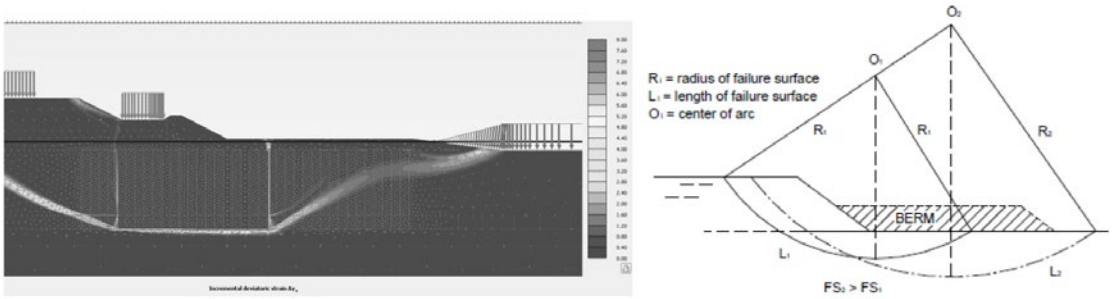

Figure 7: Effect of Stabilizing Berm for Slope Stabilization (Abramson et. al. 2002)

The results with corresponding volume of DCM required for 0m, 8m, 18m and 28m wide temporary stabilizing berms are summarized in Tables 4 and 5 and are graphically presented in Figures 8 and 9 below.

Table 4: Strengthening Works for Different Stabilizing Berms (U=50% Surcharge Stage Model)

Width of Temporary Stabilizing Berm (m)	Width of DCM (landward side from seawall toe)	Width of DCM (seaward side from seawall toe)	Total width of DCM block for obtaining FoS = 1.50 (tolerance = +0.04) against slope failure	Estimated DCM Volume (m^3/m)
Base Case = 0m	36.4m	13.6m	50m	900
8	36m	12m	48m	864
18	34.4m	8m	42.4m	763
28	34m	3.6m	37.6m	677
38	34m	0m	34m	612

Table 5: Strengthening Works for Different Stabilizing Berms (U=70% Surcharge Stage Model)

Width of Temporary Stabilizing Berm (m)	Width of DCM (landward side from seawall toe)	Width of DCM (seaward side from seawall toe)	Total width of DCM block for obtaining FoS = 1.50 (tolerance = +0.04) against slope failure	Estimated DCM Volume (m^3/m)
Base Case = 0m	22.4m	10m	32.4m	583
8	22.4m	7.6m	30m	540
18	22.4m	1.6m	24m	432
28	19m	0m	19m	342
38	16.4m	0m	16.4m	295

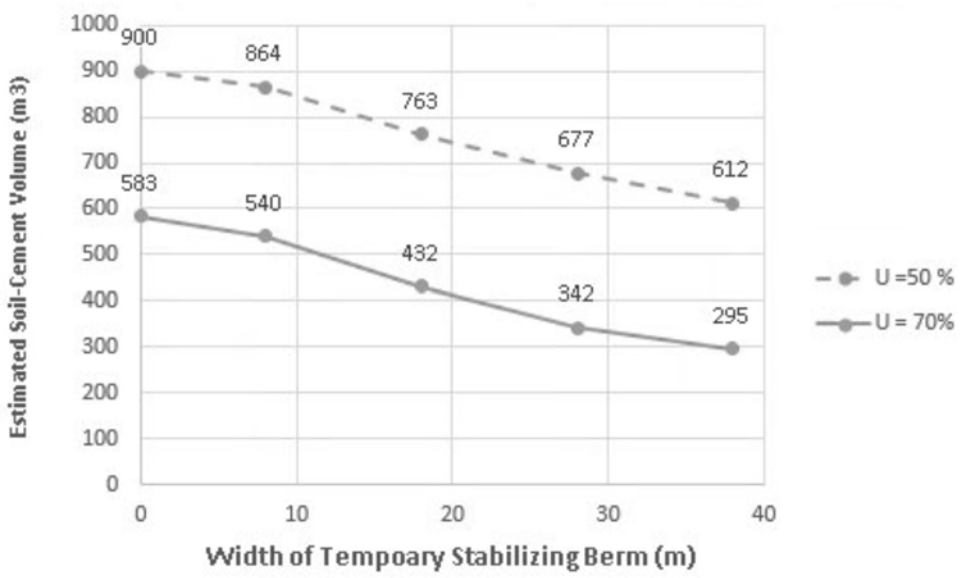

Figure 8: Soil-Cement Volume Vs Provision of Temporary Stabilizing Berm Plot

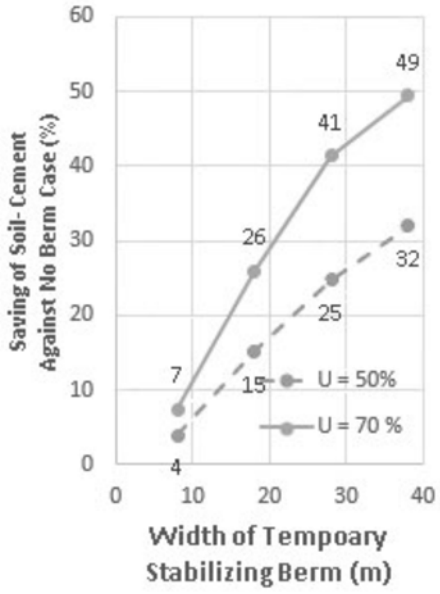

Figure 9: Saving on the Amount of DCM by Provision of Temporary Stabilizing Berm

As indicated in the above and depends on the degree of consolidation/average shear strength achieved by the insitu soil, a considerable amount of strengthening measures of a non-dredged seawall foundation (i.e. width of DCM block determined by the hypothetical analysis model of this paper) could be offset by the provision of temporary stabilizing term (i.e. as high as 49% as determined in the hypothetical models of this paper). As such, with detailed calculation during detailed design stage of a reclamation project, temporary stabilizing berm can be an economical alternative to provide temporary counterweight and reduce the amount of abundance of the strengthening measure at surcharge preloading stage.

3.5 Point to Note and Way Forward

As the analyses were carried out in limit equilibrium assumption, stress and strain history of the soil during reclamation construction activities had not been considered. In addition, the settlement of temporary stabilizing berm had been ignored based on an assumption that maintenance of the profile would be carried out in regular basis. As such, a detailed model modelling the entire reclamation construction sequence with consideration of the effect consolidation is recommended during detailed geotechnical design for seawall foundation.

Although the temporary stabilizing berm effectively provided counterweight to resist the unbalanced earth pressure and substantially reduce the demand on strengthening work required at the non-dredged seawall foundation, the local instability at the temporary stabilizing berm should also be considered. For reclamation at very soft soil, where the surface cohesion is virtually zone, it is concluded in Davis and Booker (1973) and Fred et al. (2007) that the leading edge can have maximum gradient of 1 in 8 and 1 in 10, respectively, for avoidance of causing mud wave in front of the leading edge. As such, the practitioner is recommended to strike the balance between local stability of leading edge of a temporary stabilizing berm and environmental concern.

4 CONCLUSIONS

The study described in this paper demonstrated substantial amount of strengthening measures (i.e. the width of DCM block in this study) becomes abundant after removal of surcharge. As such, an alternative temporary stabilization measure (i.e. stabilizing berm) to reduce the amount of abundance has been studied. The result shows that a considerable amount of strengthening measures of a non-dredged seawall foundation (i.e. width of DCM block determined by the hypothetical analysis model of this paper) could be reduced by the provision of temporary stabilizing berms. Point to note and way forward when considering adopting temporary stabilizing berm have also been discussed in this paper.

REFERENCES

Abramson, L., Lee, T., Sharma, S. and G. Boyce. 2002. *Slope Stability and Stabilization Methods*, 2nd Ed., John Wiley & Sons, Inc., New York.

A.D. Mackay, N.R. Wightman, 2016. Design and Construction Considerations for Reclamations and the Use of Vibro-Floatation to Accelerate Settlement, *The HKIE Geotechnical Division Annual Seminar 2016.*

Civil Engineering Office (CEO), 2003. *Port Works Design Manual Part 4*. Civil Engineering Department, Hong Kong.

Civil Engineering Office (CEO), 2002. *Port Works Design Manual Part 1 and 3*. Civil Engineering Department, Hong Kong.

C.F. Leung, 2016. Land Reclamation and Ground Improvement: Singapore Experience. *The HKIE Geotechnical Division Annual Seminar 2016.*

De Silva A., Fong L.T.T., 2013. Design and Construction of a Landfill Containment Bund cum Seawall Support on Stone Columns Installed in Very Soft Marine Mud in Cotai, Macau, *Proceedings of the 18th International Conference on Soil Mechanics and Geotechnical Engineering, Paris 2013*.

E.H. Davis and J.R. Booker, 1973. The effect of increasing strength with depth on the bearing capacity of clays. *Geotechnique 23.*

Fred. H. Y. Ng & Suraj De Silva, 2007. Geotechnical Practice of Reclamation in Hong Kong. In *Geotechnical Advancements in Hong Kong since 1970s*. The Hong Kong Institution of Engineers Geotechnical Division.

Federal Highway Administration (FHWA). 1988. *Highway Slope Maintenance and Slide Restoration Workshop Participant Manual*. Report No. FHWA-RT-88-040.

Federal Highway Administration (FHWA). 2013. *Deep Mixing for Embankment and Foundation Support*. Report No. FHWA-HRT-13-046.

Geotechnical Control Office (GCO), 1984. Investigation of a Failure at Junk Ray Controlled Tip. Advisory Report ADR 17/84. Engineering Development Department, Hong Kong.

GEO Report No. 63, 1996. A Review of Some Drained Reclamation Works in Hong Kong, Geotechnical Engineering Office, Hong Kong.

L.J.Endicott, 2001. Drained Reclamation in Hong Kong. In C.F.Lee, C.K.Lau, C.W.W. Ng, A.K.Kong, P.L.R. Pang, J.-H. Yin & Z.Q.Yue, Proc of The Third International Conference on Soft Soil Engineering, 6-8 December 2001. A.A. BALKEMA PUBLISHERS.

Mark J. Thompson and David J, White. 2005. Review of Stability Berm Alternative for Environmentally Sensitive Areas. Center for Transportation Research and Eduction.

N.H.Minh and D.T. Dergado, 2006. Numerical Modelling of A Full Scaled Reinforced Embankment on Deep Mixing Cement Piles, *Australian Geomechanics Vol 41 No.2 June 2006*.

N J O'Riordan and J W Seaman, 1994. Chapter 5, *Highway Embankments Over Soft Compressible Alluvial Deposits: Guidelines for Design and Construction*, Bridges and Ground Engineering Resource Centre Transport Research Laboratory.

R.J.Sewell & P.A. Kirk, 2002. Chapter 8 in Geology of Tung Chung and Northshore Lantau Island. Geotechnical Engineering Office Civil Engineering Department Hong Kong.

R.S. Thomas, B. Hall, 1992. *Seawall Design*. Construction Industry Research and Information Association.

Skempton, A.W. 1954. Discussion: Sensitivity of clays and the c/p ratio in normally consolidated clays. Proceedings of the American Society of Civil Engineers.

Skempton, A.W. 1957. Discussion: Further data on the c/p ratio in normally consolidated clays. Proceedings of the Institution of Civil Engineers.

V.R. Raju, Y.W.Yee, J. Daramalinggam, Vibro, 2016. Stone Columns: Proper Construction Practices, *The HKIE Geotechnical Division Annual Seminar 2016.*

Latest Developments of Hong Kong's Landslip Warning System

V.W.W. Kong, V.M. Tong, J.S.H. Kwan & H.W. Sun
Geotechnical Engineering Office, Civil Engineering and Development Department
The Government of the Hong Kong Special Administrative Region

ABSTRACT

Most landslides in Hong Kong are caused by heavy rainfall. The Geotechnical Engineering Office (GEO) has been operating, in conjunction with the Hong Kong Observatory (HKO), a territory-wide Landslip Warning System for nearly 40 years. The purpose of the Landslip Warning is to alert the public to the risks of landslides during heavy rainstorm situations. The GEO operates an extensive network of automatic raingauges which provides real-time rainfall information for use in the Landslip Warning System.

Over the years, the Landslip Warning System has been continuously enhanced and upgraded since it commenced operation. The landslip frequency-rainfall correlation model has recently been updated and a new Natural Terrain Landslip Alert framework has been incorporated to enhance landslide emergency preparedness and response during widespread natural terrain landslide events. This paper presents the key element of the Landslip Warning System together with recent improvement measures by leveraging the recent development in mobile networks and information technology. The technical development work currently being undertaken to enhance the system resilience and raingauge network coverage is also presented.

1 INTRODUCTION

Landslides in Hong Kong generally occur during periods of heavy rainfall. The GEO has been operating a territory-wide Landslip Warning System, in conjunction with the HKO, since 1977. The purpose is to alert the general public of possible landslide risks during periods of heavy rainfall.

The Landslip Warning System consists of four key components: (a) information on real-time rainfall, (b) sufficiently reliable short-term forecast of rainfall, (c) rainfall-landslide correlation, and (d) decision-making processes.

An extensive network of automatic raingauges has been installed to provide real-time rainfall over Hong Kong. Over the years, various measures and initiatives have been taken to enhance the efficiency and reliability of the Raingauge System. This system provides real-time information on measured and forecasted rainfall.

The measured and forecast rainfall information is the key input for prediction of number of landslides, which facilitates effective decision-making on whether and when to issue a landslip warning. Various improvements in the rainfall-landslide correlation models have been made over the years. These have led to more reliable prediction of landslides and hence better performance of the Landslip Warning System. The recent development of susceptibility-based rainfall-natural terrain landslide correlations has resulted in the formulation of a new Natural Terrain Landslip Alert framework for enhancing landslide emergency preparedness.

This paper gives an overview of the major components of the Landslip Warning System and consolidates the extensive experience in using the system as a risk management tool. The key elements of the GEO Raingauge System, together with recent improvement measures, are described. The development work undertaken to establish the prevailing rainfall-landslide correlations for man-made slope failures and the Natural Terrain Landslip Alert framework is summarised.

2 GEO RAINGAUGE SYSTEM

The GEO has been operating an extensive automatic raingauge network to provide real-time rainfall information for use in the Landslip Warning System since 1984. The efficiency and reliability of the raingauge network has been enhanced by various measures including the improvement of network coverage, system robustness, information dissemination and system architecture.

2.1 Real-time rainfall data

The current network (Figure 1) comprises 90 automatic raingauge field stations that are installed and maintained by the GEO, together with another 31 owned by other government departments, giving an average raingauge density of 9 km2/gauge. Real-time rainfall data of the GEO raingauges are transmitted via 3G mobile network and metro ethernet network services at 1-minute intervals to the GEO Control Centre which is equipped with a number of server computers (i.e. the GEO computer system) for receiving and processing the data. Data transmission and data sharing between the HKO and the GEO is carried out by means of dedicated fixed networks.

Each field raingauge station consists of a tipping bucket rainfall measuring unit and a data-logger with an internal modem powered by solar energy with a back-up rechargeable battery capable to provide power for 14 cloudy days (Figure 2). To ensure reliable rainfall data acquisition by the field raingauge stations, each raingauge is calibrated and tested before the onset of the wet season each year.

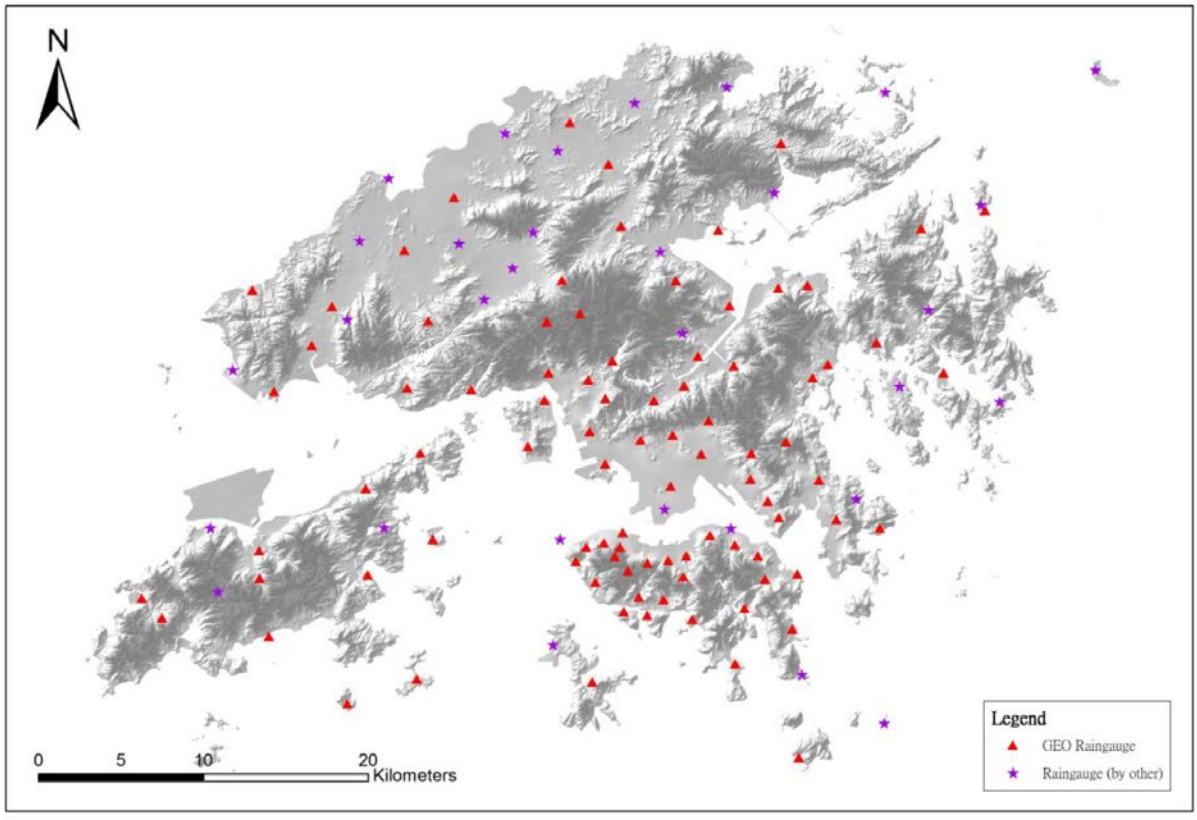

Figure 1: Locations of field raingauge stations maintained by the GEO and others

Figure 2: GEO field raingauge station

In addition to the real-time rainfall data collected from raingauge field stations, the GEO Raingauge System also incorporates HKO's real-time rainfall data generated by the radar-raingauge co-Kriging technique (Yeung et al. 2010). This advanced quantitative precipitation estimate technique could help to produce a realistic rainfall distribution pattern, in particular in areas where the raingauge density is low, e.g. along the coastline. In the event of low data availability from raingauge field stations, the GEO Raingauge System will adopt HKO's radar-raingauge co-Kriging data to maintain the functionality of the system.

2.2 Rainfall forecasting data

The short-term rainfall forecasting data (1-hour to 3-hour) are provided by HKO's Short-Range Warning of Intense Rainstorms in Localized Systems (SWIRLS) (Li et al. 2000). SWIRLS operates based on real-time correlation between radar echo intensity and rainfall amount recorded by raingauges, and consideration of predicted rain cloud movements.

2.3 Information technologies

Computer programs are developed for the operation of the GEO computer system. They are implemented, together with other proprietary software packages, to acquire and analyse real-time rainfall data from the raingauges, display situation of rainfall development (such as rainfall contour maps, cumulative rainfall curves, etc.), and predict the number of landslides (based on 24-hour recorded rainfall, 21-hour recorded rainfall + 3-hour forecast rainfall, 22-hour recorded rainfall + 2-hour forecast rainfall and 23-hour recorded rainfall + 1-hour forecast rainfall respectively) using a rainfall-landslide correlation model. The predicted landslide numbers are computed at 5-minute interval and checked automatically against the pre-defined criteria for issuing Landslip Warning. Rainfall and landslip warning-related information are disseminated through internet websites and mobile app. Authorized users can access the information using desktop computers, notebook computers, tablets or smart phones. Figure 3 shows the diagrammatic structure of the GEO Raingauge System.

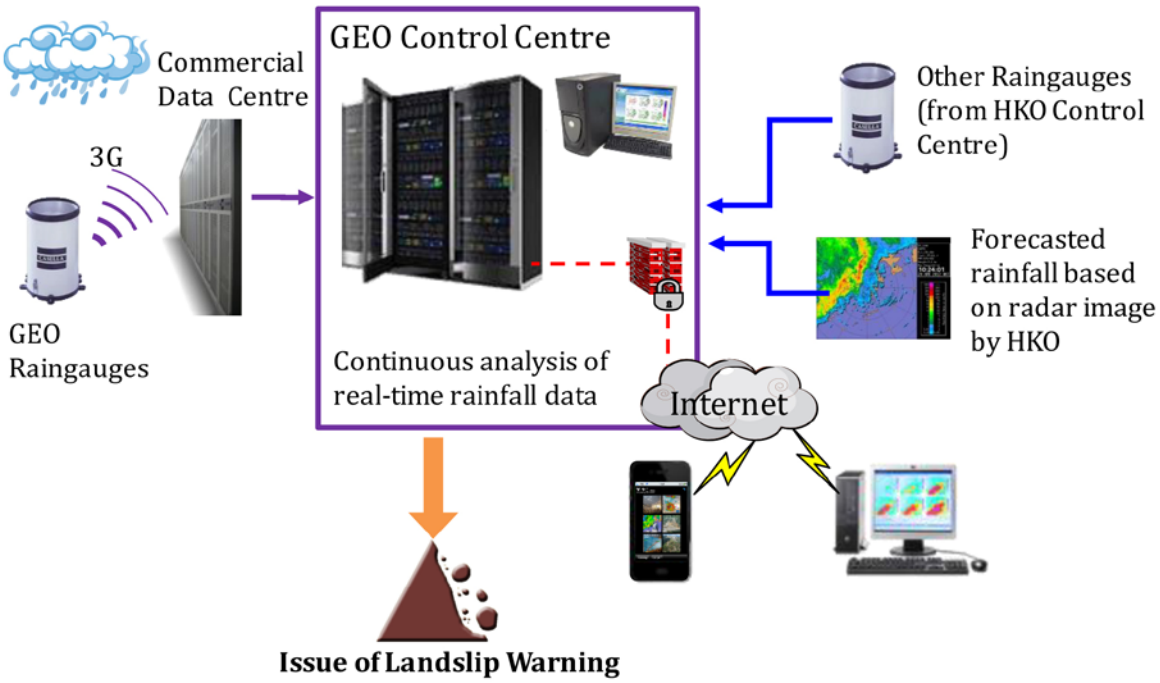

Figure 3: GEO Raingauge System

3 RAINFALL-LANDSLIDE CORRELATION MODELS

Most of landslides in Hong Kong are triggered by heavy rainfall. GEO's rainfall-landslide correlation model adopts empirical methods based on statistical relationships between historic rainfall parameters and landslide occurrence. The model has been continually updated and improved over the years.

3.1 Evolution of rainfall-landslide correlations for man-made slopes

From 1977 to 1984, the Landslip Warning System was operated based on the first generation of landslide-triggering rainfall threshold model proposed by Lumb (1975). Landslip warnings would be issued when the rainfall measured from the principal raingauge at HKO headquarter in Tsim Sha Tsui exceeded the threshold value.

Brand et al. (1984) and Premchitt (1985) reviewed the landslide and rainfall data covering a period of 20 years or longer and developed threshold values for the on-set of widespread landslides associated with 1-hour rainfall and 24-hour rainfall respectively. These second generation models were used in the 1980's and 1990's. Premchitt & Massey (1988) considered 24-hour rainfall from network of raingauges (rather than just the principal raingauge at the HKO) to cater for the geographical variation of rainfall. All these models were largely based on the rainfall threshold concept, i.e. the rainfall intensity above which a large number of landslides would occur, as observed in the past rainstorms.

The rainfall-landslide correlations were completely revamped in the late 1990's. At that time, the focus of the development work on rainfall-landslide correlations turned to statistical analyses of the relationship between rainfall intensity and landslide density/probability. Such analyses became possible because of the availability of a complete catalogue of slopes, and the availability of systematic landslide record since early 1980's. The landslide record contains the time of occurrence, spatial and temporal distribution of landslides. The third generation rainfall-landslide correlation model was established based on the work of Pun et al. (1999). The model predicted the number of landslides based on rolling 24-hour rainfall (21-hour recorded plus 3-hour forecast rainfall) over 'vulnerable areas'. It was used for Landslip Warning operation in the late 1990's until 2003. It was subsequently replaced by the prevailing fourth generation correlation, a landslide frequency approach (and a grid-based approach) developed by Yu et al. (2003).

3.2 Prevailing rainfall-landslide correlations for man-made slopes

The fourth generation rainfall-landslide correlation model developed by the GEO form the basis of the prevailing Landslip Warning algorithm. It adopts a probability-based framework, which can be integrated with the spatial distribution of the registered man-made slopes and the spatial and temporal variation of rainfall for the prediction of number and distribution of landslides. The correlation was developed based on the rainfall and landslide data obtained from 1996 to 2010. The model allows a projection of the number of landslide and landslide pattern in real time as the rainfall pattern develops, which is essential for the effective operation of the Landslip Warning system. The model also allows consideration of both recorded rainfall and short-term rainfall forecasts (1-hour, 2-hour and 3-hour).

In addition to rainfall intensities, the probability of slope failure is also correlated with the slope type. Rainfall-landslide frequency correlation has been developed for each of the four main types of man-made slopes in Hong Kong, namely soil cut slopes, rock cut slopes, fill slopes and retaining walls (Figure 4). For all of the four correlation models, the correlation lines correspond to a bi-linear relationship between landslide frequency and rainfall intensity. The gradients of the lines (in semi-log scale) are significantly greater for rainfall with lower intensity than those for rainfall with higher intensity. The workflow of the prevailing Landslip Warning algorithm is shown in Figure 5.

The performance of the model is constantly being reviewed and the statistical correlation may be enhanced as more rainfall and landslide data become available.

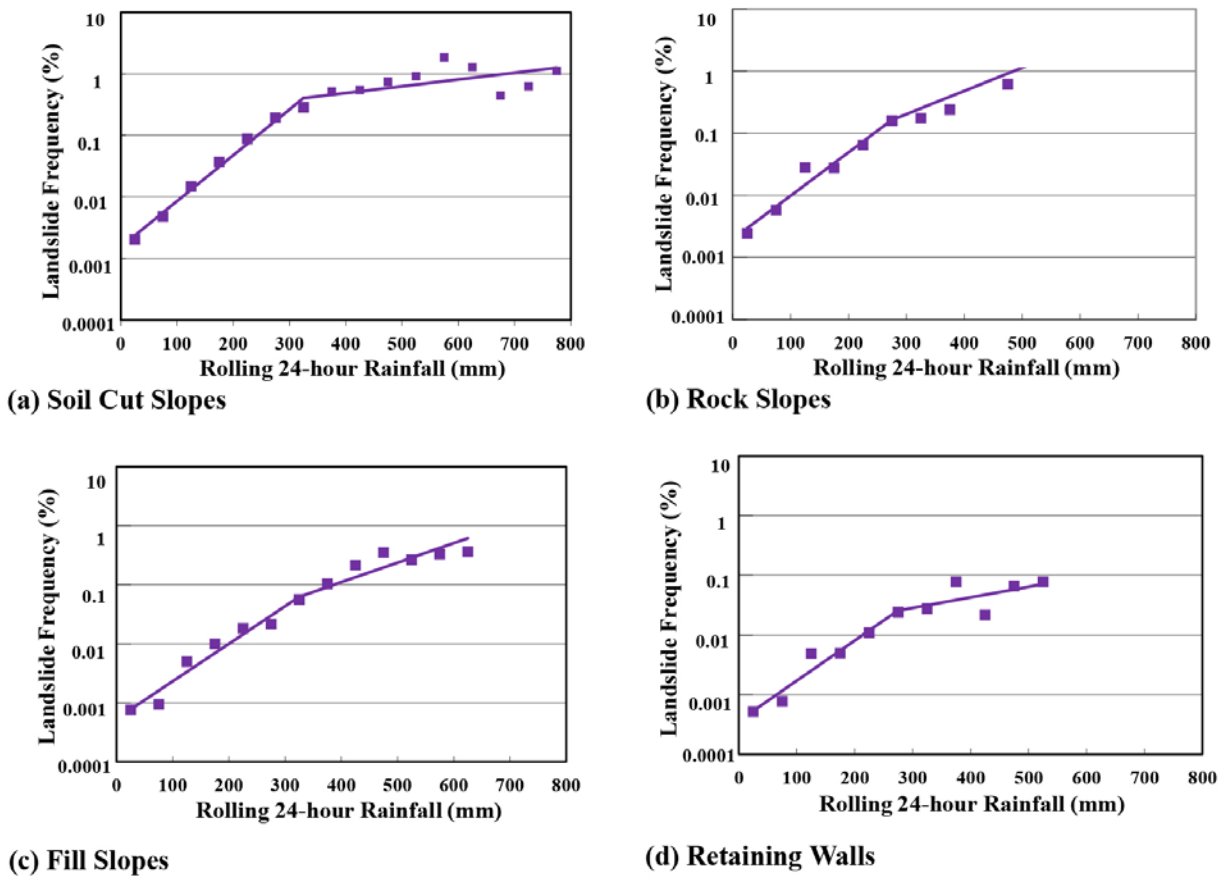

Figure 4: Correlations between landslide frequency and rolling 24-hour rainfall

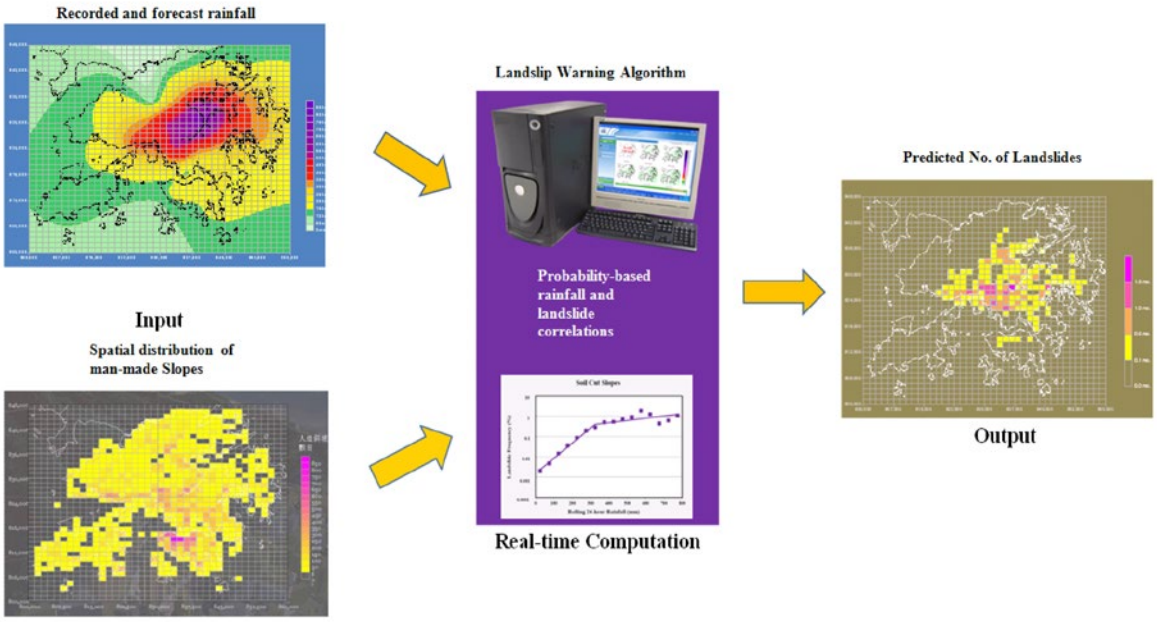

Figure 5: Workflow of the prevailing Landslip Warning algorithm

3.3 Issue of Landslip Warnings

The prevailing Landslip Warning Trigger Level is at a point when the predicted landslide number over the territory equals or exceeds 15. This generally corresponds to a situation where a large part of the territory is subject to a rolling 24-hour rainfall in the range between 150 and 250 mm. Based on the experience gained over the past 20 years, one out of every 15 landsides, on average, is a major incident (defined as a landslide incident with a failure volume of 50km3 or more). The Landslip Warning aims to alert the public risk of landslides with possible impact. Setting the Landslip Warning Trigger Level at 15 predicted landslides could achieve satisfying results in terms of landslide emergency preparedness (e.g. mobilisation of emergency control centre and emergency teams on stand-by for inspection of landslides and provision of advice on emergency actions or measures to reduce landslide risk) and warning to the public.

Decision-making on the issue of Landslip Warning is not a straightward process. It usually involves a lot of expert judgement. When deciding on whether a Landslip Warning is to be issued and its timing of issue, factors such as the real-time predicted landslide number, the actual reported landslide number at the time, and the uncertainty of rainfall forecast, etc., need to be considered. Close communication has to be maintained between the GEO and the HKO.

When a Landslip Warning is issued, GEO Emergency Control Centre (ECC) will come into operation. Local radio and television stations are notified and requested to broadcast the warning to the public at regular intervals, together with advice on the precautionary measures that should be taken by the general public. The issuing of the Landslip Warning also triggers an emergency system within government departments (e.g. the Buildings Department, the Lands Department and the Highways Department), which mobilizes staff and other resources to deal with landslide incidents. The Home Affairs Department opens temporary shelters for the public including anyone whose dwelling is endangered by unstable slopes or boulders.

3.4 Landslide Potential Index

The GEO has developed an index, called the Landslide Potential Index (LPI), to describe and compare rainstorm severity with respect to landslide occurrence potential (GEO 2014). The LPI of a rainstorm is determined based on the probable number of landslides that could be caused by a given storm. The disastrous rainstorm in July 1994 that caused the Kwun Lung Lau landslide with five fatalities and three serious injuries is set with an LPI of 10. A rainstorm with an LPI of 5 could be considered to be half as severe as the Kwun Lung Lau rainstorm in terms of the predicted number of landslides. To enable the

public to better understand the severity of a rainstorm with the issue of the Landslip Warning, the LPI of the rainstorm will be uploaded onto the Hong Kong Slope Safety Website (http://hkss.cedd.gov.hk/hkss) within a week after the cancellation of a Landslip Warning.

4 NATURAL TERRAIN LANDSLIP ALERT

Past experience shows that in extreme rainstorm events like the June 2008 rainstorm which resulted in about 2,400 natural terrain landslides, very different hazard scenarios and landslide patterns would result as compared to a moderately heavy rainstorm event (i.e. 24-hour rainfall at about 200 to 300 mm). Prediction of the spatial distribution and number of natural terrain landslides during a storm is therefore essential for emergency preparedness and response planning.

4.1 Establishment of storm-based rainfall-natural terrain landslide correlations

With the use of the 1985 to 2006 natural terrain landslide data from the Enhanced Natural Terrain Landslide Inventory (MFJV 2007) and inspections for natural terrain landslides of the June 2008 rainstorm, Chan et al. (2012) developed two sets of storm-based rainfall-natural terrain landslide correlations using statistical methods: one based on normalized maximum rolling 24-hour rainfall and the other on combination of normalized maximum rolling 4-hour and 24-hour rainfalls. The correlations were further refined in 2014 which took into account various slope angle classes and solid geology in a territory-wide rainfall-based landslide susceptibility analysis for natural terrain in Hong Kong (Lo et al. 2015). The updated storm-based rainfall-natural terrain landslide correlations are shown in Figures 6(a) and 6(b).

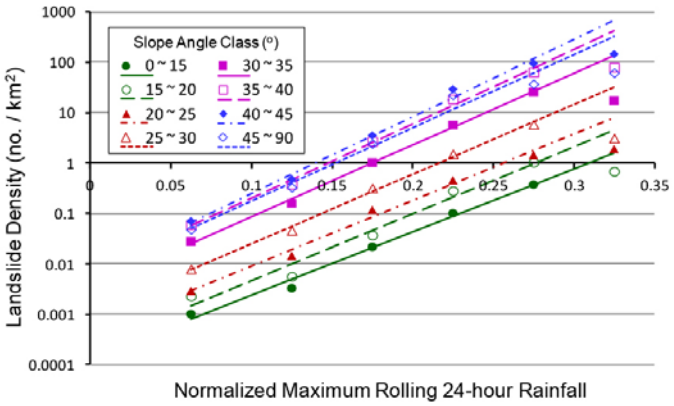

(a) Correlation based on normalized maximum rolling 24-hour rainfall

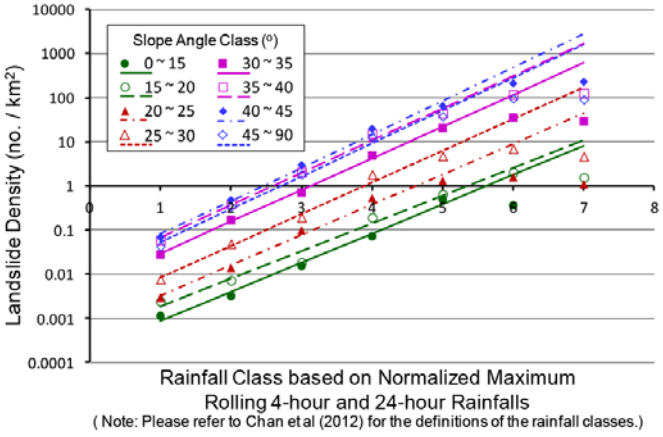

(b) Correlation based on normalized maximum rolling 4-hour and 24-hour rainfalls

Figure 6: Storm-based rainfall-natural terrain landslide correlations

The calibration exercise adopted 10 previous severe rainstorms which caused several hundreds to over 2,000 natural terrain landslides since 1985 indicating that a better fit could be obtained using the mean of the predicted number of landslides from both correlations. The number of natural terrain landslides is predicted using the mean of the two correlations.

Natural terrain landslides occurring in different regions of Hong Kong pose different risk level due to variation in the development settings. The relative risk levels for different regions are incorporated by scaling up the predicted number of natural terrain landslides in more developed areas to account for the higher consequence to landslide. Based on the broad development settings, the whole territory is divided into five regions and a scaling factor is assigned to each region.

4.2 Three-tier natural terrain landslip alert criteria

The Natural Terrain Landslip Alert Criteria are a three-tier alert system (Table 1). The alert levels are determined on the basis of the actual recorded rainfall and an equivalent number of predicted natural terrain landslides, which accounts for the relative landslide risks of different regions.

Table 1: Natural Terrain Landslip Alert Criteria framework

Equivalent number of predicted natural terrain landslides	Alert level	Scenarios
> 500 to < 1,000	1	Alert of possible widespread natural terrain landslides
> 1,000 to < 2,000	2	Warning of widespread natural terrain landslides
> 2,000	3	Warning of very widespread natural terrain landslides

4.3 Implementation

The new alert criteria for natural terrain landslides are being operated as internal alerts in the GEO in conjunction with the Landslip Warning System for reference by Government emergency managers. For example, when widespread natural terrain landslides are predicted, the arrangement within the GEO is to mobilize special standby emergency teams comprising professionals with requisite engineering geological expertise to inspect the natural terrain landslides and assess the residual risks.

5 FURTHER DEVELOPMENT

In line with GEO's strategy of continuous improvement for effective delivery of services, the GEO is currently exploring the opportunities to further enhance the efficiency and resilience of the Landslip Warning System by leveraging the latest advance in mobile network and information technology. The application of cloud computing technology is being explored to build a more resilient system under a high availability environment. A pilot study for proof-of-concept is being undertaken to test the performance of real-time rainfall information collection, storage, analyses and dissemination on cloud platform. Besides, a novel smart mobile data-logger has been developed for deployment in remote area with marginal and unstable mobile network coverage. It enhances data transmission reliability by employing dual active mobile networks with fully redundant connections, transparent data buffering and automatic resend mechanism, equipped with self-diagnosis and correction algorithm.

6 CONCLUSIONS

Significant efforts have been made to continuously improve the Landslip Warning System in Hong Kong over the years. The GEO Raingauge System collects, processes and analyses predicted number of landslides in real-time at 5-minute interval. The rainfall and landslip warning-related information are being disseminated through websites and mobile app to better support decision-making on issue

of Landslip Warning. The probabilistic-based rainfall-landslide correlation model for man-made slopes established based on the most recent landslide and rainfall data is being used in the current Landslip Warning algorithm. A new set of Natural Terrain Landslip Alert Criteria has been formulated in recent years for internal use for enhanced landslide emergency preparedness in respect of widespread natural terrain landslide events. By leveraging the recent advances in mobile and information technology, the GEO is exploring further enhancements in the Landslip Warning System as before with an aim to improving its reliability in serving the community.

ACKNOWLEDGEMENTS

This paper is published with the permission of the Head of the Geotechnical Engineering Office and the Director of Civil Engineering and Development, Government of the Hong Kong Special Administrative Region.

REFERENCES

Brand, E.W., Premchitt, J. & Phillipson, H.B. 1984. Relationship between rainfall and landslides in Hong Kong. *Proceedings of the 4th International Symposium on Landslides,* Toronto. Vol. 1, 377-384.

Chan, C.H.W., Ting, S.M. & Wong, A.C.W. 2012. *Development of Natural Terrain Landslip Alert Criteria,* Special Project Report SPR 1/2012. Geotechnical Engineering Office, Hong Kong, 68p.

GEO 2014. *GEO Information Note 8/2014 – Landslide Potential Index*. Geotechnical Engineering Office, Hong Kong, 3p.

Li, P.W., Wong, W.K., Chan, K.Y. & Lai, E.S.T. 2000. *SWIRLS – An Evolving Nowcasting System,* Hong Kong Observatory Technical Note No. 100. Hong Kong Observatory, Hong Kong, 33p.

Lo, F.L.C., Law, R.P.H. & Ko, F.W.Y. 2015. *Territory-wide Rainfall-based Landslide Susceptibility Analysis,* Special Project Report SPR 1/2015. Geotechnical Engineering Office, Hong Kong, 27p.

Lumb, P. 1975. Slope failures in Hong Kong. *Quarterly Journal of Engineering Geology*. Vol. 8, 31-65.

MFJV 2007. *Natural Terrain Landslide Identification – Feasibility, Final Report on Compilation of the Enhanced Natural Terrain Landslide Inventory (ENTLI),* Agreement No. CE 15/2005 (GE). Geotechnical Engineering Office, Hong Kong, 113p.

Premchitt, J. 1985. *Proposal for New Landslip Warning Criteria,* Special Project Report SPR 4/85. Geotechnical Control Office, Hong Kong, 36p.

Premchitt J. & Massey, J.B. 1988. *Revision of Landslip Warning Criteria 1988*. Special Project Report SPR 2/88). Geotechnical Control Office, Hong Kong, 30p.

Pun, W.K., Wong, A.C.W. & Pang, P.L.R. 1999. *Review of Landslip Warning Criteria 1998/1999,* Special Project Report SPR 4/99. Geotechnical Engineering Office, Hong Kong, 77p.

Yeung, H.Y., Man, C., Seed, A. & Chan, S.T. 2010. Development of a Localized Radar-Rain Gauge Co-Kriging QPE Scheme for potential use in quality control of real-time rainfall data. *The Third WMO International Conference on Quantitative Precipitation Estimation and Quantitative Precipitation Forecasting and Hydrology,* 12-18 Oct 2010, Nanjing, China.

Yu, Y.F., Lam, J.S. & Siu, C.K. 2003. *Interim Report on Review of Landslip Warning Criteria 2003,* Special Project Report SPR 4/2003. Geotechnical Engineering Office, Hong Kong, 19p.

Recent Technical Development of Natural Terrain Risk Mitigation Measures in Hong Kong

J.S.H. Kwan, H.W.K. Lam, C. Lam & E.H.Y. Sze

Geotechnical Engineering Office, Civil Engineering and Development Department, The Government of Hong Kong Special Administrative Region

ABSTRACT

Vulnerable natural hillside catchments in Hong Kong are systematically dealt with under the Landslip Prevention and Mitigation Programme (LPMitP) managed by the Geotechnical Engineering Office (GEO). Based on both international and local experiences, the use of landslide debris-resisting structures has been a practical means for mitigating natural terrain landslide risk. For many years, the GEO has been directing continuous efforts in the technical development work to enhance understanding of the debris-structure interaction as well as the performance of these structures for optimisation of the design approach. This paper highlights the key technological development of the landslide risk management measures, including: 1) physical modelling of baffles as flow-impeding structures, 2) centrifuge modelling of debris-barrier interaction, 3) advanced numerical modelling of debris-barrier interaction, 4) staged debris mobility analysis for the design of multiple barriers, and 5) the use of cushioning materials to reduce bouldery debris impact load on rigid barriers.

1 INTRODUCTION

The Geotechnical Engineering Office (GEO) launched the Landslip Prevention and Mitigation Programme (LPMitP) since 2010 to deal with both man-made slope and vulnerable natural hillside catchments in Hong Kong. Unlike man-made slope features, natural hillside catchments are usually sizeable rendering the application of conventional slope stabilisation measures less sustainable and less cost-effective. A more pragmatic approach to manage the natural terrain landslide risk is thus called for. At present, natural terrain hazards are commonly mitigated by providing defence measures, such as rigid barriers or steel flexible barriers, to arrest the landslide debris and to protect the downslope facilities.

In essence, rigid barriers take advantage of their high structural stiffness to resist impact pressures resulting from landslide debris. On the other hand, flexible barriers resist the landslide debris by absorbing the impact energy by means of mobilisation of the energy-dissipating elements and deformation of the rope-net structure. Flexible barriers bear a slimmer structure, which is relatively easier for installation on remote hillsides and less visually intrusive.

Despite the popularity on the use of these defence measures in the international practice, there appear no well established design guidance around the world. Since early 2000s, the GEO has been developing technical guidance on the design of debris-resisting structures. Local design practice mainly relies on prescriptive or conservative design approach.

In view of the need to improve understanding of the problems and optimise the current design approach, the GEO has been directing continuous efforts in the technical development work in collaboration with geotechnical profession and experts in other engineering disciplines. In this paper, five notable areas of recent technological development of the landslide risk management measures are

presented. These subjects involve study of debris dynamics and structural response of barriers through physical tests and numerical analyses. They include: 1) physical modelling of baffles as flow-impeding structures, 2) centrifuge modelling of debris-barrier interaction, 3) advanced numerical modelling of debris-barrier interaction, 4) staged debris mobility analysis for the design of multiple barriers, and 5) the use of cushioning materials to reduce bouldery debris impact load on rigid barriers.

2 TECHNOLOGICAL DEVELOPMENT WORKS ON LANDSLIDE RISK MANAGEMENT

2.1 Physical modelling of baffles as flow-impeding structures

In hydraulic engineering, baffle blocks may be used as energy dissipaters to perturb the pattern of fluid flow (Peterka 1978). Similarly, these flow-impeding structures may also be used to attenuate the debris flow energy and reduce the impact induced on barriers. Since debris flow baffles occupy only a small area, they are considered compact for constructability on steep natural hillside. However, interaction between flowing debris and obstacles entails complex mechanisms, such as deposition and run-up of material behind an obstacle and the deflection of jets between obstacles. Teufelsbauer et al. (2011), for example, studied the interactions between granular flows and rigid obstacles, but the degree of flow impedance is still not well understood. As a result, baffles are currently designed in Hong Kong on an empirical and prescriptive basis.

To enhance understanding of the effect of baffle configuration on flow impedance, the GEO commissioned a series of flume experiments to investigate the influence of baffle height, row number, and spacing between rows on the reduction of debris frontal velocity (Choi et al. 2013, 2014). Dry uniform sand was used for the experiments as it represented the simplest flow case for understanding of the complex yet fundamental impact flow mechanisms. That facilitated back-analysis using numerical models. Instrumentation of the tests included photoconductive sensors for measurement of frontal flow velocity, laser sensors for measurement of flow depth, and high-speed cameras to capture the flow kinematics.

Figure 1 shows the flume and the baffle arrangement used for one of the tests. Froude similitude was adopted to characterise the flow front impacting the baffles. A Froude number of about 3 was taken for this study. It represents a prototype channelised debris flow with, approximately, a velocity of 10 m/s and a flow depth of 1 m.

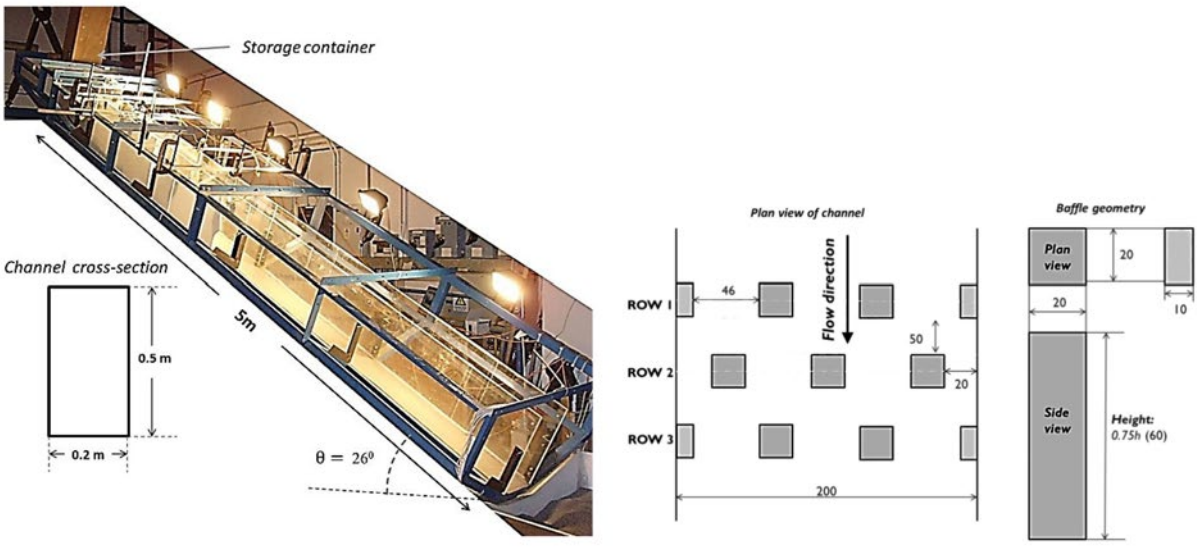

Figure 1: Flume and baffle arrangement used in the physical model (Choi et al. 2013)

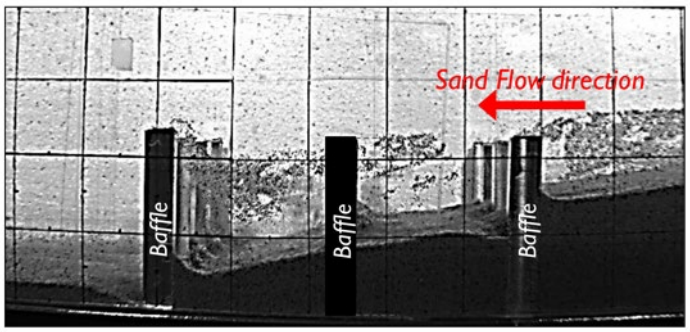

Figure 2: Interaction between baffles and sand flow

Figure 2 shows an image captured by a high-speed camera during one of the tests. The flume tests showed that interaction between sand flow and baffles could be characterised with respect to the approach flow depth (h) and the baffle height. It was found that increasing the baffle height could lead to a more effective development of subcritical conditions, which promote additional energy losses upstream of baffles through the formation of a granular jump. Increasing the baffle height from 0.75h to 1.5h could result in a 40% increase in upstream flow depth due to backwater effects. It was also found that increasing the number of rows of 1.5h baffles from a single row to a three-row staggered array could result in up to 72% additional energy loss. The energy loss was attributed to the deflection of granular jets and additional backwater effects. Increasing the row spacing from 50 to 100 mm could result in up to a 14% increase in energy loss. These findings provided insights for design of baffles.

2.2 Centrifuge modelling of debris-barrier interaction

Geotechnical centrifuge modelling is capable of reproducing the field-scale stress conditions using models of a reduced scale. This can be done by imposing the physical model to an increased body force generated by a centripetal acceleration of magnitude appropriate for the model scale. Hence, a geotechnical centrifuge is suitable for modelling gravity and time dependent problems (Schofield 1980; Taylor 1995; Ng et al. 2006). Since 2012, the GEO had initiated a pioneering project by commissioning the Hong Kong University of Science and Technology to conduct a series of centrifuge tests to model landslide debris impacting on both rigid and flexible barriers. Details of the setup and results of single-phase debris material, i.e. dry sand and viscous liquid, were reported by Ng et al. (2016).

Recently, a series of centrifuge tests has been carried out to investigate the impact mechanisms of debris flow with hard inclusions on a rigid barrier. The model rigid barrier (Figure 3) was made of magnesium alloy with similar stiffness as that of reinforced concrete. A load cell was mounted on the barrier to measure the impact load. The debris materials were made up of mixing Leighton Buzzard sand with glass beads of different diameters ranging from 3 to 39 mm in model scale. The tests were spinned up to a g-level of 22.4 g. Hence, the glass beads represented hard inclusions of size up to about 0.9 m in prototype scale. During the tests, debris materials were released on to a ramp inclined at 25° and impacted on the model barriers.

The centrifuge model was fully instrumented and equipped with a high-speed camera. It allowed the entire process of debris flows and debris-barrier interaction to be captured and fully interpreted. Figure 4 shows a snap-shot of the instant of impact and the impact force – time history for the test of 39 mm glass beads mixed with sand. The results indicated that the presence of hard inclusions induced force spikes, the magnitude of which could be many times higher than the maximum static force imposed by the deposited debris on the barrier. Larger glass beads appeared to induce higher impact force on the barrier. Nevertheless, the force spikes generated were found to be highly transient compared with the overall impact duration.

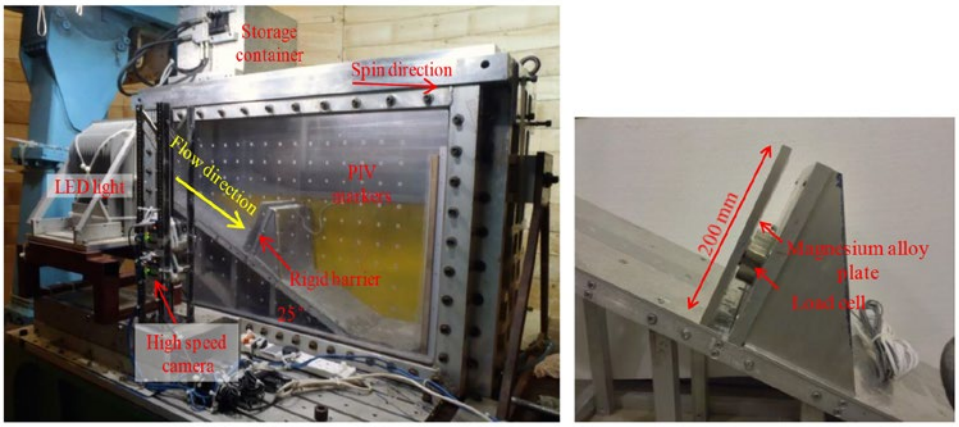

Figure 3: Model rigid barrier used in the centrifuge tests

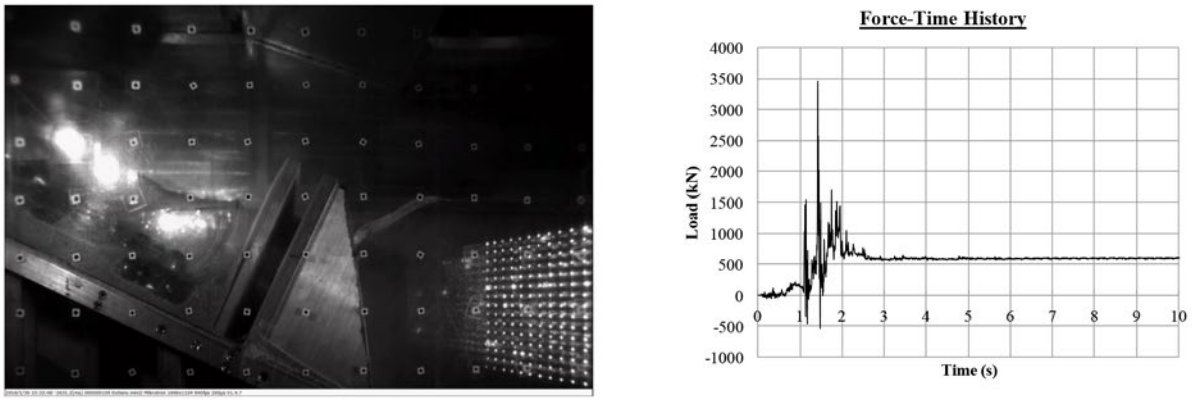

Figure 4: Snapshot of glass bead (39 mm) - sand mixture impacting on the model rigid barrier and the measured force-time history

2.3 Advanced numerical modelling of debris-barrier interaction

Over the last few years, the GEO has been developing capability in numerical modelling to supplement field observations and physical tests in the technological development work related to landslide mitigation measures. For example, Kwan et al. (2014) used a finite element program NIDA-MNN (Chan et al. 2012) to back analyse a landslide case in Jordan Valley, Hong Kong, which involved a volume of 110 m3 debris impacting on a flexible rockfall barrier. The numerical analysis successfully reproduced the key salient field observations and provided useful insights into the conditions of major barrier components.

Recently, the GEO, in collaboration with Arup, developed the numerical technique in simulating the dynamics of debris-barrier interaction using a three-dimensional finite-element package "Livermore Software - Dial-a-yield Nonlinear Analysis" (LS-DYNA). Huang et al. (2014) and Kwan et al. (2015) demonstrated that the use of the Arbitrary Lagrangian-Eulerian (ALE) method in LS-DYNA is a promising tool for modelling debris flow. Such modelling had been benchmarked against laboratory flume tests and actual landslide cases. Yiu et al. (2012), using LS-DYNA, explicitly modelled all structural elements (e.g. steel ring nets, shackles, energy-dissipating devices) of a flexible net structure subject to concrete block impact and successfully replicated a full-scale rockfall test by Volkwein (2004).

In the conventional approach, landslide motion analysis and structural analysis of the barrier are carried out separately. The landslide motion is first simulated to obtain design parameters such as the flow velocity and depth, which are then converted into a pseudo-static impact force as an input to a separate structural model. This approach neglects the dynamics of debris-barrier interaction and may not represent the actual barrier behaviour. By coupling the ALE debris flow model with the structural

flexible barrier model using LS-DYNA, the technique of coupled analysis to simulate the dynamic interaction between landslide debris and a flexible barrier structure was developed. The numerical flume model, as shown in Figure 5, was successfully verified against the large-scale instrumented field test in Illgraben, Switzerland (Wendeler et al. 2008a). In this study, the numerical model was capable of simulating the impact of debris flow on the flexible barrier, and successfully reproduced the subsequent deformations of the barrier. It also reasonably replicated the forces developed in various structural components and gave the maximum debris impact pressure exerted on the barrier netting. Table 1 summarises the calculated and measured maximum debris pressure and axial forces in the top and bottom ropes.

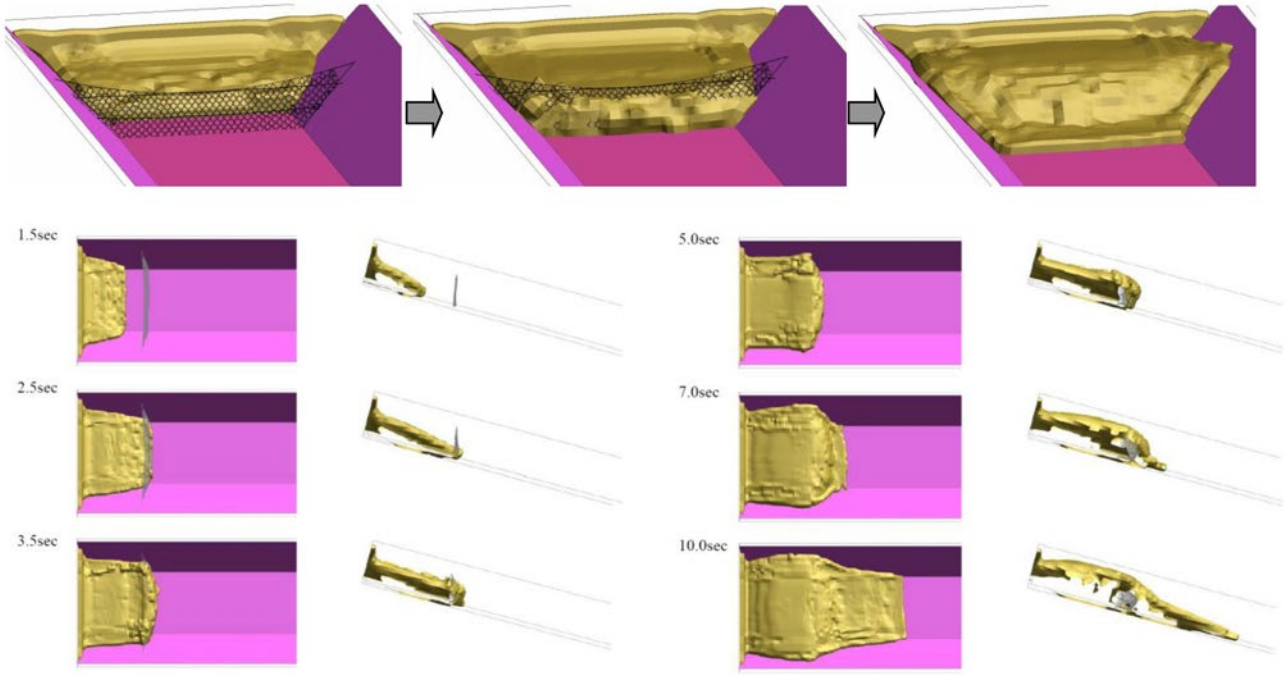

Figure 5: Coupled analysis of debris flow impacting on flexible barrier using LS-DYNA

Table 1: Calculated and measured maximum pressure and rope forces for a documented debris-barrier interaction case history in Illgraben, Switzerland

Parameter	LS-DYNA	Wendeler et al. (2008a)
Maximum debris pressure (kPa)	69	60 *
aximum top rope force (kN)	200	150
Maximum bottom rope force (kN)	261	248

* Back-calculated from measured rope force

The LS-DYNA model together with the coupled analysis technique developed appears to provide an effective tool to simulate the debris-structure interaction in addition to the landslide debris mobility, hence providing insights on the actual behavioural mechanism. This greatly facilitates the engineering design of the landslide mitigation measures.

2.4 Staged debris mobility analysis for the design of multiple barriers

Multiple barriers have been used to mitigate landslide hazards such as debris flow in many places, such as Switzerland, Japan, Mainland China and Taiwan (Shum & Lam 2011). They comprise rows of single

barrier installed at different strategic positions along the predicted runout path of the debris flow. Each of these rows of single barrier is designed to retain a portion of the debris of the design landslide event. As a result, the scale of each individual barrier, in terms of structural requirements and retaining height, could be optimised. Overseas experience suggests that multiple barriers can potentially be a practicable means to mitigate reasonably large debris flows, possibly including low-frequency, large magnitude events in catchments with major drainage lines in Hong Kong. Multiple barriers have been used in countries such as Switzerland to resist debris flows along natural drainage lines (Wendeler et al. 2008b). Despite their usefulness in resisting debris flows, no established methods are available for the assessment of debris mobility with consideration of flow obstruction because of the presence of the barriers. Hence, a study was initiated by the GEO to formulate a preliminary design methodology of the use of multiple barriers for mitigation of debris flows.

When a landslide impacts on a barrier, a portion of the debris is trapped and retained behind the barrier, which results in a kinetic energy loss of the debris flow. Once the barrier is being filled up, the remaining debris would probably launch into a ballistic flight from the crest of the barrier, carrying the kinetic energy of the remaining landslide debris. Speerli et al. (2010), based on several flume tests, observed similar ballistic projectile path when debris overtopped from a barrier. The debris was retarded upon impacting the flume bed at the landing position and then accelerated when it propagated downstream along the inclined flume. Such process cannot be simulated by some commonly used computer programs such as those adopting a depth-averaged scheme. Hence, a staged analysis method that adopts the solutions of a depth-averaged Lagrangian model was proposed by Kwan et al. (2015). This method comprises the following five key steps:

i. Carry out debris mobility analysis using a suitable program (e.g. DAN or 2d-DMM) to simulate the dynamics of the debris that travels from the landslide source to the first barrier.

ii. Use the results of the mobility analysis to determine the velocity at which the debris will launch into a ballistic flight from the crest of the barrier.

iii. Calculate the geometry of the ballistic trajectory path and debris velocity after landing.

iv. Carry out another debris mobility analysis to simulate the dynamics of the debris travelling from the landing position to the next barrier.

v. Repeat Steps (ii) to (iv) until the debris reaches the terminal barrier.

Figure 6 is a schematic drawing showing the process of landslide debris overflowing an intermediate barrier and the corresponding stages in the proposed analysis method. The proposed design framework would serve as a starting point to examine the potential use of multiple barriers to mitigate natural terrain landslides in Hong Kong. Further work would be needed to improve the proposed design framework, e.g. in the subject of energy dissipation of debris interacting with barriers.

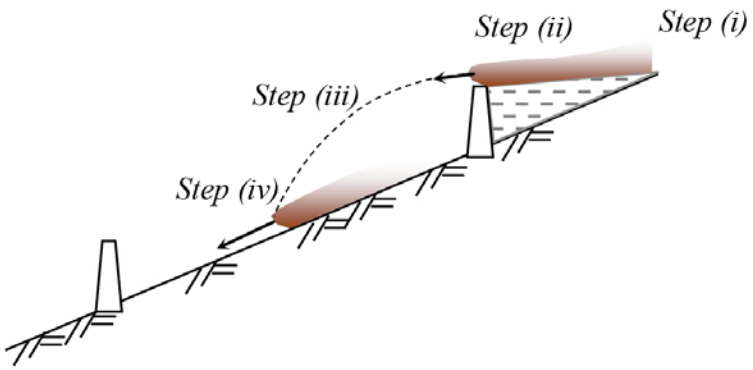

Figure 6: Dynamic motion of landslide debris overflowing an intermediate barrier (modified after Kwan et al. 2015)

2.5 Use of cushioning materials to reduce boulder impact load on rigid barriers

Rigid barriers are commonly used to resist the impact of landslide debris which may include large boulders especially near the debris front. In Hong Kong, the Hertz equation with a load reduction factor is commonly used to estimate boulder impact forces (Kwan 2012). The calculated impact force could be very high for large boulders travelling at high velocities. To effectively reduce boulder and debris impact forces acting on a rigid barrier, cushioning materials could be used. These materials are characterised by large deformations when they are subjected to a dynamic impact load, and through the deformations, the associated impact energy is absorbed.

The performance of cushioning materials for rockfall protection galleries has been studied by researchers in Switzerland. For example, Schellenberg et al. (2007) carried out large-scale drop tests on cushioning materials placed above reinforced concrete slabs. Both gravel and cellular glass aggregates were used as cushioning materials. Chikatamarla (2007) also studied the effect of cushioning materials by laboratory experiments and numerical modelling. Materials considered included, among others, sand, rubber tyre chips, and sand-rubber mixtures. These previous studies showed that boulder impact forces can be significantly reduced by the use of cushioning materials.

To further advance our knowledge of the performance of cushioning materials and to enhance the design of rigid debris-resisting barriers in Hong Kong, the GEO commissioned a study to identify suitable cushioning materials that could reduce the impact load from bouldery debris. A large-scale pendulum impact test facility was constructed for this study. Figure 7 shows the test facility, which comprised a concrete ball to simulate a natural boulder, and a 1-m thick and 3-m high reinforced concrete wall. The concrete ball weighted about 2 tonnes and was suspended from a steel frame. The ball was lifted up by a mobile crane to a height of up to 5 m. Upon release, the concrete ball could achieve an impact energy of up to 70 kJ. During the tests, the acceleration of the concrete ball was measured by an accelerometer attached to the ball. The impact loads on the wall were also measured by load cells.

Figure 7: A large-scale physical impact test on a concrete barrier with a gabion cushioning layer

Impact tests on potential cushioning materials such as cellular glass aggregates, foam rubber and rock-filled gabions had been carried out using the test facility. Figure 8 shows the maximum impact forces for a boulder impacting on a 1-m thick gabion cushion layer at three impact energy levels (20, 40 and 70 kJ). The results show that the cushion layer could effectively reduce the maximum impact forces although it would become less effective after successive impacts. The data collected had been used to calibrate numerical models for parametric studies. The results helped establish technical guidance for

the estimation of boulder impact loads on rigid barriers with consideration of the load-reduction effect provided by cushioning materials.

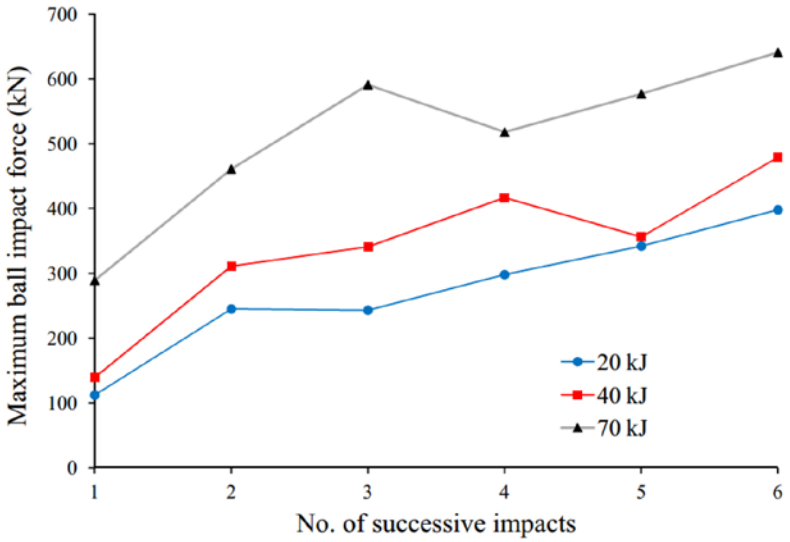

Figure 8: Maximum boulder impact forces on rock-filled gabions impacted by a spherical boulder at three different energy levels.

3 CONCLUSIONS

This paper presents some of the recent advances in landslide risk management measures in Hong Kong. These advances are driven by the need to provide more cost-effective and robust solutions to mitigate landslide risks. For projects involving the use of multiple barriers, a staged analysis method has been developed to consider the effects of debris overtopping and volume retention. On the other hand, findings from centrifuge modelling of flexible barriers and numerical modelling using LS-DYNA have provided useful insights into the interaction between debris and barriers during the impacting process. The results have been used to optimise the design of barriers in Hong Kong. New initiatives such as the use of baffles and cushioning materials also offer an opportunity to effectively reduce the flow energy of landslide debris and their impact forces on barriers. Together, these measures will significantly improve the risk mitigation measures in Hong Kong.

ACKNOWLEDGEMENTS

This paper is published with the permission of the Head of Geotechnical Engineering Office and the Director of Civil Engineering and Development of the Government of the Hong Kong Special Administrative Region.

REFERENCES

Chan, S.L., Zhou, Z.H. & Liu, Y.P. 2012. Numerical analysis and design of flexible barriers allowing for sliding nodes and large deflection effects. *Proceedings of Seminar on Natural Terrain Hazard Mitigation Measures, Hong Kong.*

Chikatamarla, R. 2007. *Optimisation of cushion materials for rockfall protection galleries*. PhD thesis, ETH Zürich, Switzerland.

Choi, C.E., Ng, C.W.W., Kwan, J.S.H., Shiu, H.Y.K., Ho, K.K.S. & Koo, R.C.H. 2013. Downstream frontal velocity reduction resulting from baffles. In *Proceedings of the 18th International Conference on Soil Mechanics and Geotechnical Engineering, Paris, 2-6 September 2015*. Paris: Presses des Ponts.

Choi, C.E., Ng, C.W.W., Song, D., Kwan, J.S.H., Shiu, H.Y.K., Ho, K.K.S. & Koo, R.C.H. 2014. Flume investigation of landslide debris–resisting baffles. *Canadian Geotechnical Journal,* 51(5): 540-553.

Huang, Y., Yiu, J., Pappin, J., Sturt, R., Kwan, J.S.H. & Ho, K.K.S. 2014. Numerical investigation of landslide mobility and debris-resistant flexible barrier with LS-DYNA. In *Proceedings of the 13th International LS-DYNA Users Conference, Dearborn, 8-10 June 2014*. Livermore: Livermore Software Technology Corporation.

Kwan, J.S.H. 2012. *Supplementary technical guidance on design of rigid debris-resisting barriers,* GEO Report 270. Geotechnical Engineering Office, Civil Engineering and Development Department, Hong Kong.

Kwan, J.S.H., Chan, S.L., Cheuk, J.C.Y. & Koo, R.C.H. 2014. A case study on an open hillside landslide impacting on a flexible rockfall barrier at Jordan Valley, Hong Kong. *Landslides,* 11(6): 1037-1050.

Kwan, J.S.H., Koo, R.C.H., & Ng, C.W.W. 2015. Landslide mobility analysis for design of multiple debris-resisting barriers. *Canadian Geotechnical Journal,* 52(9): 1345-1359.

Ng, C.W.W, Zhang, L.M. & Wang, Y.H. (2006). Co-editors of the *Proceedings of 6th International Conference on Physical Modelling in Geotechnics (TC2).* Publisher: Taylor & Francis. Vols 1 and 2. ISBN: 978-0-415-41587-3 and 978-0-415-41588-0. 1608p.

Ng, C.W.W., Choi, C.E., Su, A.Y., Kwan, J.S.H. & Lam, C. 2016. Large-scale successive boulder impacts on a rigid barrier shielded by gabions. *Canadian Geotechnical Journal,* 53(10): 1688-1699.

Peterka, A.J. 1978. Hydraulic design of stilling basins and energy dissipaters. *Engineering Monograph No. 25*. Washington, D.C.: Bureau of Reclamation, United States Department of the Interior.

Schofield, A.N. 1980. Cambridge Geotechnical Centrifuge Operations. *Géotechnique,* 30(3): 227-268.

Schellenberg, K., Volkwein, A., Roth, A. & Vogel, T. 2007. Large-scale impact tests on rock fall galleries. In *Proceedings of 7th International Conference on Shock and Impact Loads on Structures, Beijing, 17-19 October 2007*. Singapore: CI-Premier.

Shum, L.K.W. & Lam, A.Y.T. 2011. *Review of natural terrain landslide risk management practice and mitigation measures,* GEO Technical Note TN 3/2011. Geotechnical Engineering Office, Civil Engineering and Development Department, Hong Kong, 168p.

Speerli, J., Hersperger, R., Wendeler, C. & Roth, A. 2010. Physical modeling of debris flows over flexible ring net barriers. In *Proceedings of the 7th International Conference on Physical Modelling in Geotechnics, Zurich, 28 June - 1 July 2010*. Leiden: CRC Press/Balkema.

Taylor, R.N. 1995. *Centrifuge modelling: principles and scale effects*. Geotechnical Centrifuge Technology, Ed. R.N.Taylor, Blackie Academic & Professional, 19-33.

Teufelsbauer, H., Wang, Y., Pudasaini, S.P., Borja, R.I. & Wu, W. 2011. DEM simulation of impact force exerted by granular flow on rigid structures. *Acta Geotechnica,* 6(3): 119-133.

Volkwein, A.K.H. 2004. *Numerical simulation of flexible rockfall protection systems*. Thesis for Doctor of Technical Sciences of the Swiss Federal Institute of Technology Zurich.

Wendeler, C., McArdell, B.W., Volkwein, A., Denk, M. & Gröner, E. 2008a. Debris flow mitigation with flexible ring net barriers–field tests and case studies. *WIT Transactions on Engineering Sciences,* 60: 23-31.

Wendeler, C., Volkwein, A., Roth, A., Herzog, B., Hählen, N. & Wenger, M. 2008b. Hazard prevention using flexible multi-level debris flow barriers. In *Proceedings of 11th Interpraevent Congress, Dornbirn, 26-30 May 2008*. Klagenfurt: Interpraevent.

Yiu, J., Pappin, J., Stuart, R., Kwan, J.S.H. & Ho, K.K.S. 2012. Landslide mobility and flexible barrier modelling using LS-DYNA. In *Proceedings of AGS Seminar on Natural Terrain Hazards Mitigation Measures, 16 October 2012, Hong Kong* (eds C.K. Lau, E. Chan and J. Kwan), 67-77. The Association of Geotechnical and Geoenvironmental Specialists.

Hong Kong MTR Shatin to Central Link Contract 1128 (Eastern Approach) – Tunneling in Sensitive and Congested Urban Enivronment

Ken Kwok
Dragages-Bouygues JV, Hong Kong
Gonzague Bracq
Bouygues Travaux Publics, Paris, France
Thomas Barrett
MTR Corporation Limited, Hong Kong

ABSTRACT

MTR Shatin to Central Link (SCL) Works Contract 1128 (SCL1128) – South Ventilation Building to Admiralty Tunnels forms part of the new strategic rail corridor from Shatin to Central District. It comprises twin rail tunnels constructed by Tunnel Boring Machine (TBM) from Causeway Bay Typhoon Shelter to Admiralty Station, under the most congested urban setting of the northern shore of Hong Kong Island, specifically the Eastern Approach Section (EAS) between Causeway Bay and Wanchai Sports Ground. The TBMs had to excavate under and in close proximity to major existing utilities and live bridge structures. 3D finite element modeling techniques were used to provide accurate estimations of the works impact in order to define suitable mitigation measures.

Moreover, the Tunnel Boring Machine (TBM) confinement pressures were carefully designed to include the critical constraint of shallow ground cover, less than one tunnel diameter, experienced by the Variable Density TBM (VDM). The SCL1128 VDM is the first of its kind to be used in Hong Kong to minimize the risks of settlement, compressed air blow out and slurry egress. This paper demonstrates the detailed planning and engineering applied to the eastern approach tunnels of the SCL1128, from Causeway Bay Typhoon Shelter to Wanchai Sports Ground, in order to achieve zero disruption to the public, and complete both TBM drives in a safe and timely manner.

1 INTRODUCTION

1. Background and scope

MTR Shatin to Central Link (SCL) Works Contract 1128 (SCL1128) – South Ventilation Building to Admiralty Tunnels is part of the new strategic rail corridor from Shatin to Central awarded to the Dragages-Bouygues JV on the 18 August 2015. The EAS twin tunnels were constructed using two different Tunnel Boring Machines. A Mixed-Slurry Shield named Athena (雅典娜) constructed the deeper Up Track Tunnel Drive (UT) with a Variable Density TBM (VDM) called Zhi-nu (織女), discussed in detail by Jacques (2017), the first of its kind to be used in Hong Kong and only one of a handful used globally to date, constructing the Down Track Tunnel Drive (DT). Both tunnels were excavated beneath public roads including strategically important 'red routes' with the DT VDM excavating an alignment

with very shallow ground cover less than the diameter of the excavation profile of 7.45m at circa 6.5m, this alignment included excavating underneath a temporarily diverted box culvert with less than 2m of separation.

After completing the EAS UT Athena (雅典娜) will be dismantled and reassembled several times in order to excavate the two Western Approach Section (WAS) tunnel drives at approximately 35m below the ground surface. The WAS include four critical crossing underneath the existing and operational MTR Tsuen Wan Line, a separate paper for the technical aspects of the WAS tunnels may be issued once the drives are completed by Athena (雅典娜) in late 2017 or early 2018.

A key risk associated with excavating in shallow cover to the TBM is uncontrolled ground collapse mainly due to compressed air blow out during maintenance or excessive confinement pressure or hitting unforeseen obstruction which can cause over-excavation as the cutter head attempts to pass through, at shallow depths there is less soil above the TBM as such any over-excavation is critical. The key mitigations for these risks involve ensuring that the confinement study has taken cognisance of the available geological data with any blanks being filled in with additional investigation, making sure the confinement is robustly checked and amended based on observation as required and to ensure that there are no obstructions to prevent the TBM excavation along the alignment. Further to this, early launching of the TBM to create programme buffer in case TBM stoppages are required due to obstructions, should be encouraged where possible.

Associated with the confinement and potential to over excavate is another major risk, excessive movement, caused by the TBM to the existing Highway Bridges, Roads and nearby structures. Based on the 3D study these structures can require underpinning with complex jacking systems or extensive ground treatment.

This paper will present the technical aspects applied and the preparation works undertaken prior to commencing the TBM excavations including: alternative alignment, launching shaft and method, obstruction removal, bridge underpinning & load transfer, the adopted design approach for assessing the confinement pressure and an example of check the effect to the nearby structures. Finally the paper will discuss the overall performance of the TBM drives and the associated mitigation measures for the EAS of SCL1128. The EAS arrangement is presented in Plate 1.

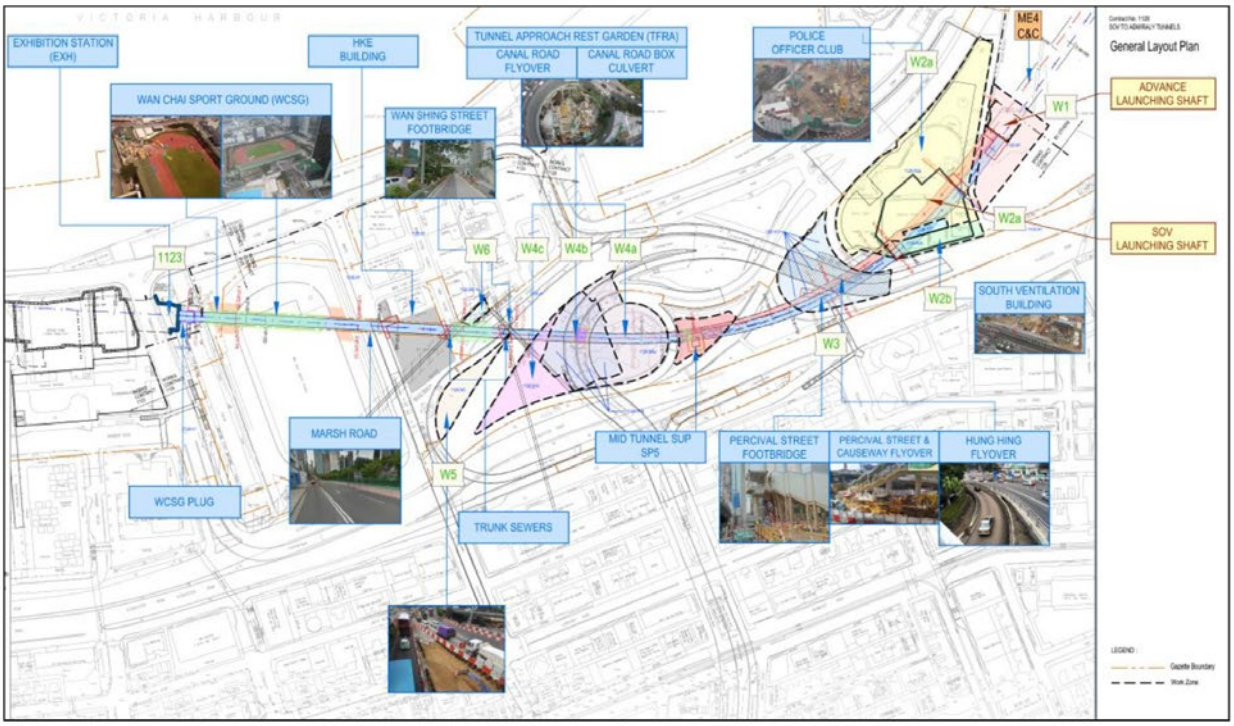

Plate 1: East Tunnels (left hand side) from former Police Officer Club (W2a) to Wan Chai Sports Ground

1.2 Geology

The topography along the alignment of the SCL1128 tunnels is a relatively flat low lying plain of reclaimed land situated along the northern coastline of Hong Kong Island. The reclamation occurred in several phases over a period of time from the mid-1800s to the present day in order to satisfy land demands for development. Underlying the reclaimed land there is a layer of marine deposit (disturbed and mainly sandy on the upper part and soft clay on the lower part); beneath the marine deposit is an alluvium layer which in turn overlays the Completely Decomposed Granitic (CDG) formations and granite rock. The thickness of fill, marine deposits and alluvium vary along the SCL tunnels alignment with the higher DT tunnel alignment passing through the interface between the marine deposits and the fill material; as such old seawalls, junk dumped into the sea and fill material were unavoidable. The lower UT tunnel alignment most of the time encounter mixed face rock, CDG and Alluvium at crown. A geological section between Canal Road and Wan Shing Street is shown in Plate 2.

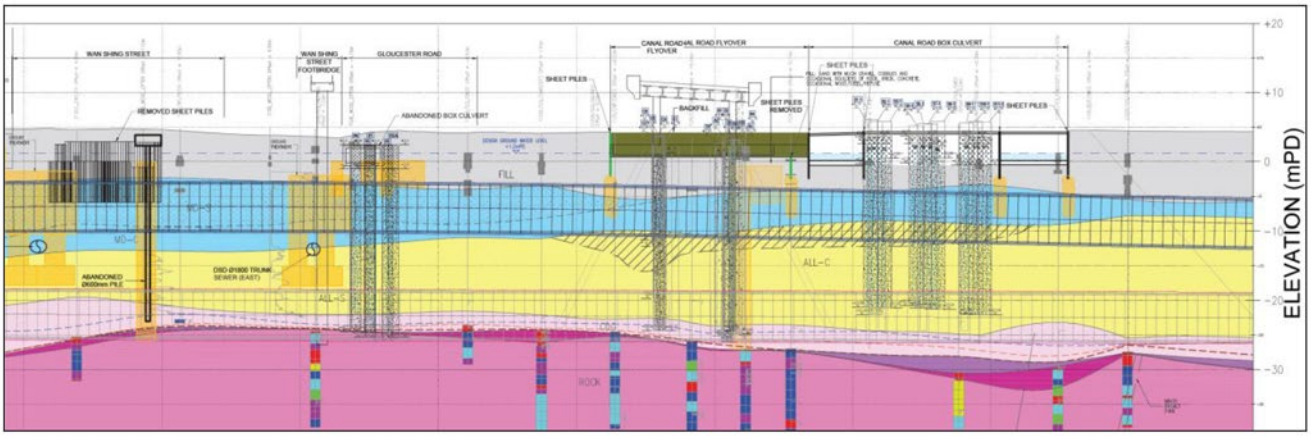

Plate 2: Geological Section at Canal Road Box Culvert/Flyover, Gloucester Road and Wan Shing Street

1.3 Base case tunnel alignment, TBM launching and retrieval

The eastern launch shaft was planned in the old Police Officers Club (POC) with the tunnel vertical alignments side by side with the DT some 7.5m higher than the UT. As the alignments progress from the launch shaft to Wan Chai Sports Ground (WCSG) the DT continues to rise to within 6m of the surface with the UT dropping to 27m below the surface such that the two tunnels become stacked DT on top of the UT. The POC was demolished to facilitate the SCL construction and will be reinstated in its original location by DBJV combined with the new SOV building. The tunnels are in a stacked alignment for all the major structures east to west, i.e. the Cross Habour Tunnel Footbridge, the Cross Habour Tunnel Slip Road, Hung Hing Flyover, Causeway Flyover, Percival Street Footbridge, Canal Road Flyover, Canal Road Box Culvert, Gloucester Road, Wan Shing Footbridge, Wan Shing Street, Trunk Sewers, a Hong Kong Electric Building, Marsh Road before reaching WCSG. Due to the existing twin trunk sewers at circa -12mPD the shallowest ground cover to the TBM crown was approximately 6.5m based on the original alignment to the north of Gloucester Road and south of Wan Shing Street.

Regarding TBM Launching, the Shaft in W2 was supposed to be constructed after the demolition of the Police Officer Club (POC) with the rest of tunnels between W2 and W1 constructed by by Cut and Cover Method, this also required the construction of a vertical wall and the removal of the existing seawall. It was a logical and reasonable scheme as it is preferred to launch the TBM in a relatively long shaft to aid commissioning logistics.

2 TUNNEL ALTERNATIVES

Several alternatives were proposed which brought significant benefits to the project, these are outlined below.

2.1 Tunnel Alignment Level

One alternative proposed involved changing both the UT and DT alignments using the following principles:

- The deeper UT tunnel alignment was raised to higher level so that the transition zone between the CDG and granite rock was minimized. This was progressed as this type of interface will cause more wear and damage to the cutter head tools (Discs, Scrapers and Picks) which in turn would result in an increase of Compressed Air Intervention (CAI), a high risk activity, which should be minimized and avoided where possible. In addition to the safety concerns reducing the duration of CAI required has a direct relationship with the risk of excessive ground movement; minimizing the CAI works minimizes the settlement.
- The shallower DT tunnel was lowered in level in order to avoid an old seawall/rubble mound during excavation. The maximum change in level was 2.5m lower than the original alignment located at the Causeway Flyover, the footing of which is partly supported by said seawall. Overall the DT tunnel alignment was lowered 0.5m than the original alignment in order to provide an increased margin to the confinement pressure design, this was critical due to the fact that the hydraulic gradient is affected by the Victoria Harbour tidal influences. The lower the alignment brought the TBM excavation closer to the existing trunk sewer with a reduced clearance of 900mm, stringent monitoring was required.

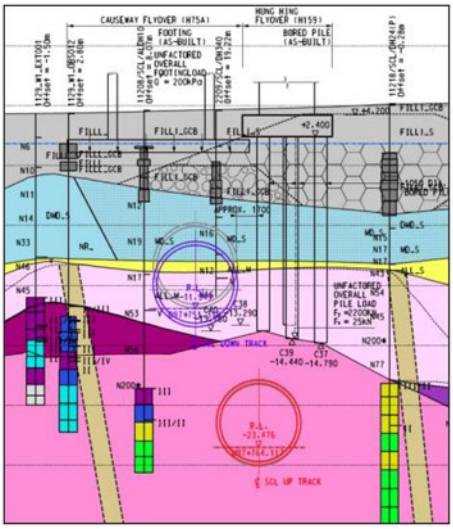

Plate 3: Geological section and alternative tunnel alignment at Hung Hing Flyover

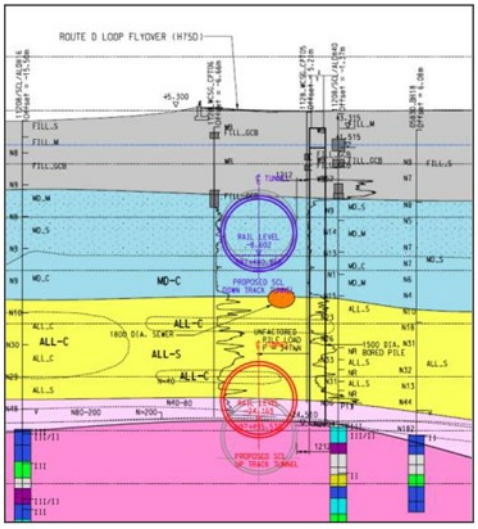

Plate 4: Geological section and alternative tunnel alignment at Wan Shing Street

2.2 TBM Launching

A second alternative changed the location of the TBM launching shaft from the W2 area to an area of reclaimed land (W1), originally between W2 and W1 it was intended to use the 'cut and cover' method to construct the tunnels. The W2 shaft was to be constructed after demolition of the POC as such the demolition was critical path to the TBM launch. Moving the launch shaft to W1 took the POC demolition off the TBM launch critical path accelerating the launch by approximately 1 year creating float in case of unforeseen obstructions.

As this launch shaft at W1 was only 17m in length the existing and adjoining ME4 SCL rail tunnels, constructed by Central Wan Chai Bypass as entrusted works for SCL, were used to facilitate the TBM assembly, launch and logistics. This took careful planning as the two tunnels were approximately 1.5m different in level with the DT being higher; also the backup gantries had to be installed inside ME4 prior to the TBM shields along with enough segments to allow the gantries to pass the first mid wall opening thereby providing segmental lining logistic access from surface.

Plate 5: W1 Advance Shaft TBM assembly in process on the right and W2 Shaft Diaphragm Wall Construction in process on the left

As the TBM was 1 year ahead of the W2 shaft construction, there were a few technical reviews to be completed prior to excavating through the W2 shaft:

- The minimum number Diaphragm Wall Panels to be completed before TBM crossing i.e. the ones the TBM mined through or under
- The W2 Excavation and Lateral Support (ELS) impact to the erected tunnel lining
- The sequence required to dismantle the erected tunnel lining and support to the erected permanent rings to ensure no damage or deformation occurred

As planned, no retrieval shaft could be constructed in time for removal of TBM at the Exhibition Centre Station, instead, the front shield, middle shield and the tail shield steel skins are left in-situ underground with a cast in-situ tunnel lining constructed inside these in line with the constructed segmental lining. The backup units, erector, main drive and all flanges are all removed, requiring extensive hot works, back down the tunnel to the W1 shaft for retrieval. In order to ensure face stability at the TBM parking area a 2.8m thick lean concrete plug with slurry walls were constructed to surround the TBM shield isolating it from the local hydrology and ensuring ingress of ground or excessive settlement occurred.

3 OBSTRUCTIONS

Overcoming Steel H or reinforced concrete pile obstructions during TBM excavation is possible but is very complex, time-consuming and high risk due to repetitive CAI being required for said removal or cutter head repair. In most cases CAI works would not be progressed for extended obstruction removal without an extensive ground treatment scheme in place. This is compounded when in shallow ground cover and in close proximity to major utilities and/or structures such as highway bridges, box culvert, trunk sewers etc. due to the increased settlement caused.

The Contract Geotechnical Baseline Report identifies the known obstructions clashing with the tunnel alignment, all of which are pile foundation, either abandoned or supporting the existing nearby structures. The ‘live’ piles were required to be altered or underpinned such that they no longer impeded the TBM progress, Table 1 shows the pile foundation to be removed and the replacement support provided when TBM crossings.

Location	Obstruction to be removed	Support provided when TBM crossing	Site Constraints
Percival Street Footbridge	9 nos. of Dia. 600mm Bored Piles with 8mm casing	Pre-bored Socket H piles, pilecap and steel support frame	Limited Space / Underground Utilities
Canal Road Box culvert	21 nos. of 18" Square Driven Concrete Pre-stressed Pile	Sheetpile cofferdam with concrete base slab	Limited Space / Underground Utilities / Dry Season Limited
Canal Road Flyover	6 nos. of 18" Square Driven Concrete Pre-stressed Pile (raking)	Pre-bored Socket H piles, Pilecaps, crossing beams, steel support frame and hydraulic jacks	Limited Space / Height Restriction
Wan Shing Street Footbridge	1 nos. of Dia. 600mm in-situ concrete bored pile (abandoned)	Abandoned structure	Limited Space / Underground Utilities
Wan Chai West Treatment Plant	24 nos. of Driven steel H-Pile	Abandoned structure	Limited Space
Fleet Arcade	3 nos. of Dia. 500mm Driven Concrete Piles with 19mm thick Casing	Abandoned structure	Limited Space / Underground Utilities

Table 1: Locations of the piles obstructing the tunneling work

Numerous foundation were removed during the construction of the MTR Express Rail Link projects, various methods were adopted and good practical experience for such works are now available within the Hong Kong Construction Industry. The Rotary-All-Casing (RAC) and Hydraulic-Jacking (HJ) methods were used to remove the piles on the EAS. The decision to utilize the HJ method depends on the sensitivity of the works area, geology, pile type and depth. Lean concrete or grout is used to fill the void left by the pile either during or after removal.

The most challenging pile removal on the EAS was associated with the Canal Road Flyover. A specialised plant setup was utilised to overcome the 4m headroom restriction as shown in Plate 6.

The pile removal associated with the Canal Road Box Culvert required a full diversion of the existing culvert flow based upon the Hydraulic Analysis for both Wet and Dry Seasons conditions. This was to define the work sequence required to construct the pile removal platform and reinstate Box Culvert as shown in Plate 7.

The known obstructions were removed according to the sequence, on time prior to the TBM arrival. Additional obstructions not identified in the Contract, were discovered at Marsh Road and Wan Shing Street.

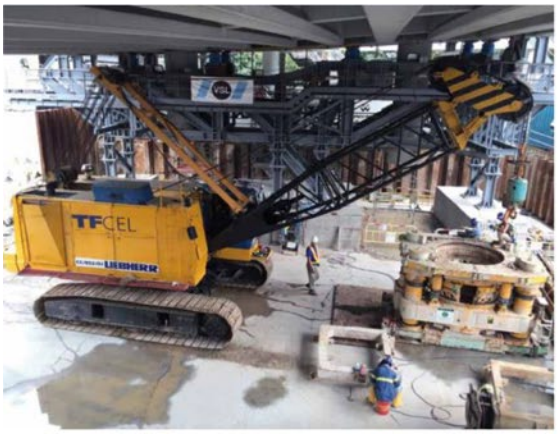

Plate 6: Obstruction Removal by Rotator Method at Canal Road Flyover

Plate 7: Temporary flow diversion at Canal Road Box Culvert for obstruction removal by rotator method

3.1 Marsh Road Storm Drain Piles

MTR undertook an extensive obstruction detection campaign using desktop studies, trial pits and Geophysical Surveys. This campaign found a suspect signal at Marsh Road adjacent to Wanchai Sports Ground at -5 mPD, near a 1.8m diameter storm drain. Multiple geophysical survey methods, namely Borehole Magnetism (MAG), Electromagnetism (EM), Electric Cylinder™ (EC) and Cross Hole Electrical Resistivity Tomography (CHERT), were undertaken reconfirming a metallic signal between -3 to -11mPD. The signal indicated that the metallic content was low and intermittent over 8m presenting scenarios of a metallic chain/cable rather than the initially expected left-in sheetpile. The team agreed to carry out additional investigations to further define the obstruction and its depth to see if it affected the DT only as originally assumed or both the UT and DT. The Geophysical Survey for Marsh Road is described in Auvergne (2017a).

These additional results confirmed that there were two obstructions presenting as concrete with strong metallic signals at a depth between -21 to -25mPD within the TBM excavation profile. At this point the UT TBM drive was due to arrive at the location within two weeks with the later DT TBM arriving within two months. A trial pit was opened and the storm drain was diverted locally upon which it was confirmed that a series of square concrete precast piles with steel shoes, identified by the metallic signals at depth, were in place beneath the storm drain. No record of these files could be found however it has been hypothesised that there were installed to avoid excessive settlement to the storm drain during the long process of consolidation in the reclamation as the drains were installed shortly after its completion. This is commonly seen for old reclamation where a surcharge cannot be applied but facilities need to be constructed before consolidation.

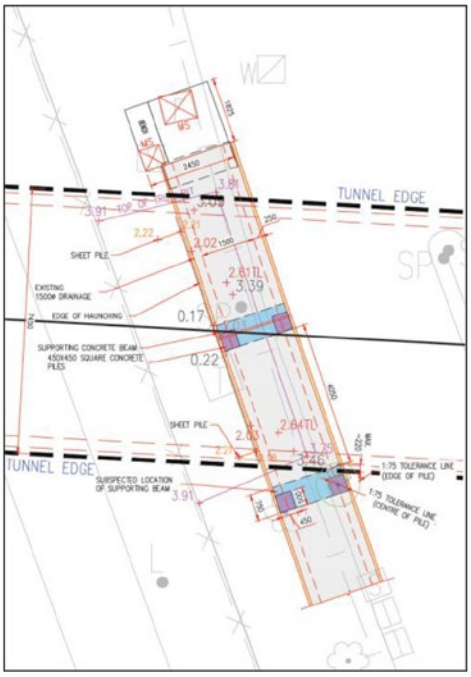

Plate 8: Plan view of Tunnel crossing 1.5m drain pipe at Marsh Road

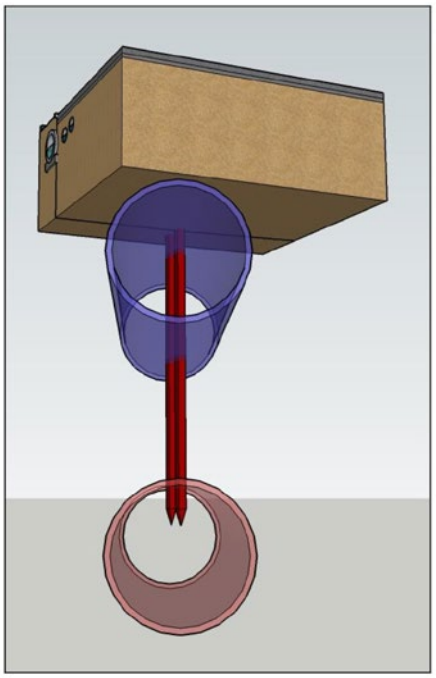

Plate 9: 3D view of 1.5m drain pipe (top), its piles, and two tunnels at Marsh Road

The UT tunnel was excavated through a stiff CDG layer between level of -18mPD and -25mPD. DBJV proposed to disconnect the two piles from the pile cap and then drive through the piles with TBM. The two precast square concrete piles would be disconnected from the pile cap by coring a row of 100mm dia. holes at the top of the piles. The UT TBM bored through both concrete piles recovered at the Slurry Treatment Plant in pieces and the shoe recovered whole from the TBM Cutter Head.

The bore through option was not viable for the shallow DT drive due to the presence of marine deposit and fill material, these would destabilize due to the TBM forces on the piles with a high probability of collapse. Due to the tight site constraints a novel Hydraulic Jack method (HJ) was carried out to remove

the remaining pile sections prior to the DT TBM arrival, the piles were removed and the TBM passed without incident and with minimal settlement.

Plate 10: Square Precast Pile removed by crane lorry after removal by Hydraulic Jack at Marsh Road

Plate 11: Temporary Traffic Arrangement for Obstruction Removal at Wan Shing Street

3.2 Wan Shing Street Sheet Piles

Wan Shing Street was the most critical tunnel section at it had the shallowest ground cover at circa 6.5m with the adoption of the alternative alignment. Any obstruction encountered under Wan Shing Street had a great potential to cause slurry egress, excessive settlement or collapse compounded by the undesirable geology making CAI impossible without significant ground treatment. On top of this twin trunk sewers sit approximately 900mm below the TBM alignment, although the design check proved there would be no adverse impact to the sewer pipe we wanted to minimize the duration the TBM was loading these sewers.

Although no foundations were expected in this area it had been noted that another project had previously undertaken works in the area and that the excavations used sheetpiles for temporary support. With the co-operation of utilities companies, contractors and consultants, old site progress photo indicated that not all the sheetpiles were removed. Wan Shing Street could not be closed for the necessary site investigation and geophysical survey to identify the locations of the left-in sheetpiles, as such a night time one-lane/two-way Temporary Traffic Arrangement (TTA) was adopted.

As a result of the geophysics deep trial trenches were excavated locating more than 100 sheetpiles and steel obstructions found clashing with the DT Tunnel Alignment all along and within the tunnel crown. With the approval of a two-lane/two-way TTA, all left-in sheetpiles were removed just prior to the DT TBM arrival.

4 BRIDGE UNDERPINNING AND TBM CROSSING

Within the EAS there are three vehicular bridges, classified as trunk roads that required underpinning or temporary support by hydraulic jacks in order to allow compensation for TBM induced movement. They are:

- Canal Road Flyover (CRF), supporting 4 traffic lanes, is the main trunk to connect Island North and South. The TBM excavated between Gridline 18 and 19 of the Flyover, DT at a depth of -3.8mPD in fill and the UT at a depth of -18.8mPD in alluvium referenced to TBM crown.
- Hung Hing Flyover (HHF) and Causeway Flyover (CF), two separate bridges supporting 1 and 3 traffic lanes respectively but at same level with a longitudinal movement joint between them. The TBM excavated under Gridline A6 footing of CF at a skewed angle, DT at a depth of -6.5mPD in fill and the UT at a depth of -17.5mPD in rock referenced to TBM crown. The deck of HHF was essentially a pre-stressed concrete hollow box structure sitting at grade.

4.1 Canal Road Flyover

The six supporting piles had to be removed, thus the bridge required underpinning with new pre-bored H piles, a pilecap and robust temporary steel supporting frame with an adjustable hydraulic jacking system. The jacks were used to adjust the level of the bridge deck as necessary during the pier disconnection, load transfer, TBM crossing and final reinstatement. Throughout these works the traffic flow was agreed to remain constant based upon the estimated movement falling well within the structures serviceability.

Due to the low headroom under the flyover, roughly 4m, the ground level was lowered using a sheet pile cofferdam increasing the working headroom to 6.5m. A special low-height plant setup was adopted to overcome the low headroom restriction as shown in Plate 6.

An Automatic Deformation Monitoring System (ADMS) monitored the structures movement both inside and outside the TBMs zone of influence in order to verify and back analyse our assumptions and design studies during all work stages. The Bridge Decks, Cross Beams, Movement Joints, Steel Supporting Frames and Pilecap structures were all monitored. In additional to the ADMS, manual optical survey was carried out to verify the ADMS results and as a backup in case of ADMS system failure. More discussion on extensive use of ADMS is described by Auvergne (2017b).

The HJ system provided control in three directions: vertical, longitudinal and transverse effectively confining the structure during all work stages. This required a sufficiently stiff steel frame structure for the jacks to react off between the piles and the deck. After the load transfer and TBM excavation, the jacks adjust the structure, once satisfactory all jacks are mechanically locked to eliminate the risk of movement caused by failure of hydraulic system.

Very minor movements were observed during all work stages which were well within design estimation and structures serviceability. The entire HJ set up has been removed and the CRF piers are reinstated without any impact to the traffic flow at all stages.

Plate 12: Canal Road Flyover on steel supporting frame and hydraulic jacks

Plate 13: Hung Hing (with hydraulic jacks) and Causeway Flyover

4.2 Hung Hing Flyover and Causeway Flyover

The support arrangement for HHF and CF are shown in Plate 14, and they are separate bridge structures with a longitudinal movement joint without barrier between the traffic lanes.

HHF is supported at-grade connecting to an abutment at one end with the other end supported by a piled foundation. Located next to the HHF piled foundation are the two CF piers supported on a pad footing. At the other end CF is supported by friction piles, next to the connection between the HHF and its abutment. To conclude, the two bridges are supported by piled foundations and one at grade foundation spanning the alignment; as such no piles associated with these flyovers obstructed the TBM excavations.

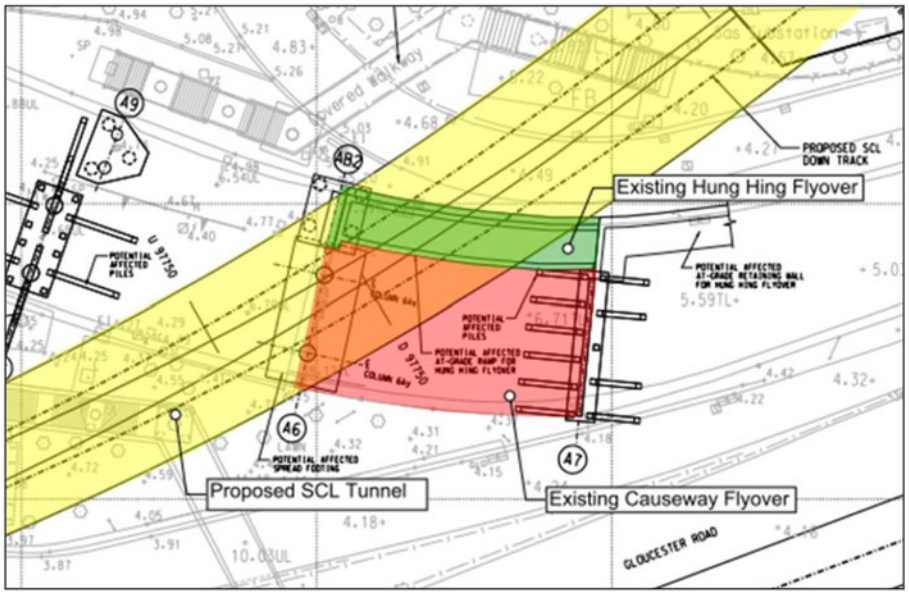

Plate 14: Foundation system of Hung Hing and Causeway Flyover

The crossing of Hung Hing Flyover, as long as keeping no significant movement at transverse movement joint, it is not a high concern operation as one side is piled support and the whole bridge is at grade together with abutment. The TBM cross, in skew direction, underneath the footing A6, any vertical movement will create step joint between in longitudinal joint between Hung Hing and Causeway Flyover in which it will affect the driving safety for the road users. As an effective mitigation, the double line road marking to the longitudinal joint were extended along with anchored traffic posts.

Unlike the CRF founded on rock the HHF and CF sit at-grade, therefore, extensive ground treatment was completed to improve the stiffness of the ground at the footing A6 in order to limit movement. The structural capacity and serviceability limit of the flyovers, as usual, set the criteria for the allowable movement. As the foundation of the jacking system is affected by the TBM excavation and was expected to move and additional precaution was adopted above the ADMS and manual survey monitoring used on the CRF, the hydraulic pressure was agreed to be kept at a safety margin as defined by the Designer to ensure the loading of the bridges are evenly distributed to the ground.

Better than expected settlement results due to the Variable Density TBM, high quality ground treatment and stringent control of the jacking system limited the movement to the CF to approximately 5mm or 8% of the movement predicted by the structural analysis.

5 CONFINEMENT PRESSURE DESIGN

The Ultimate Limit State (ULS) verifications require the application of a confinement pressure at tunnel face in order to maintain the stability of soil column from excavation front to the surface which is discussed in paper by Tsang, Salisbury & Yeung 2012, which is fully in line with GEO Report 249, GEO (2009). This ULS confinement pressure defines the minimum face pressure. For the Service Limit State (SLS), the ground and building settlements at surface are verified with the 2D finite element models, to define the recommended pressure.

To define the confinement pressures to be applied, a set of 2D (plain strain) Finite Element models were developed along the tunnel alignment. Slurry pressure to support the excavation and grout pressure injected by TBM behind the segmental lining are considered in the models to account for their interaction and the associate effect on the surface settlement. PLAXIS 2D revision 2015 is used to model the excavation. The approach used to model the soil - structure Interaction during a TBM excavation consist in modelling the excavation as two steps:

1. Excavation of the section with a confinement pressure applied on the soil. A proportion λ of the loads are applied (λ=90% in our approach)
2. Installation of the lining. The remaining proportion (1-λ) of the loads are applied.

The complexity of the DT geology in conjunction with the shallow ground cover, circa 6.5m, made up of fill material used in the reclamation 50 years previously required specialist design and technology. As such a new mark of TBM was used called a Variable Density TBM (VDM) allowing the TBM to be operated as a standard slurry mix shield or in high density mode. In addition, to avoid slurry blow out, specific verifications were made limiting the slurry pressure ($P<P_{max}$). Conservatively, a pipe connecting the TBM to the surface was considered, with this hypothetic pipe a blowout occurs only when the pressure is higher than the weight of slurry in the pipe $P_{max} = \gamma_s \times d$ (with γ_s, the slurry density and d, the distance between the TBM and surface).

Figure 1 below depicts that with a higher slurry density ($\gamma 1<\gamma 2$), the maximal value of slurry pressure Pmax is higher ($Pmax1<Pmax2$). Thus you can have a better front confinement with a higher slurry density (for the same criteria on the blowout).

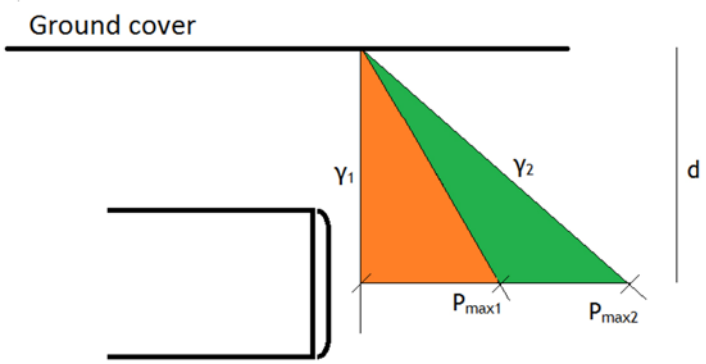

Figure 1: Relationship between density and pressure

Thus, in utilising the VDM, the high density slurry becomes an additional parameter to control in conjunction with the confinement pressure. This check is particularly important for shallow cover such as Canal Road Box Culvert which the difference between minimum and recommended pressure is about 0.2Bars which does not include the water variation.

The shallow cover implies a low effective stress at TBM crown and a relatively high variation of this effective stress depending on the water level variations. As a consequence, specific monitoring of the water table was undertaken around the box culvert to understand the tidal influences on the ground table. In addition, compressed air intervention is avoided in this area.

Apart from this factor the confinement pressure definition is the same for a slurry TBM and a VDM.

Upon completion of the TBM drives, the measured volume loss of the two tunnels are found in between 0.1 – 1.0% which is well within the predicted volume loss of 0.5 – 1.5% from the confinement pressure analysis. Reasons for this excellent performance could be due to conservative soil parameters and good ground treatment implemented on site. A detail analysis of the TBM performance will be completed and submitted to the Client MTR and GEO in due course.

6 3D ANALYSIS AND PRECAUTIONARY MEASURES – TRUNK SEWERS

Two trunk sewers were in close proximity to the 1128 EAS tunnels, approximately 900mm beneath the DT tunnel. Specific studies were needed to forecast the impact of the TBM excavation on this structure between the two tunnels. The 1.8m internal diameter sewer pipe is made of 16cm thick reinforced concrete. After several preliminary studies with 2D FEM models on the tunnel excavation impacts, it was considered necessary to realise a complete model of both tunnels excavation in a 3D model including the sewer structure.

This model, carried out with the software César 3D V5, had several requirements and outputs:

- take into account the crossing between the sewer and the tunnel boring machines,
- take into account the excavation in more detail (with modeling of the confinement pressure at the front, around the shield as well as the mortar pressure and the weight of the TBM),

- determine the deformations and stresses in the sewer,
- analyse the effect of several key parameters (stiffness of soil, stiffness of the sewer, the confinement pressures, and the geometry).

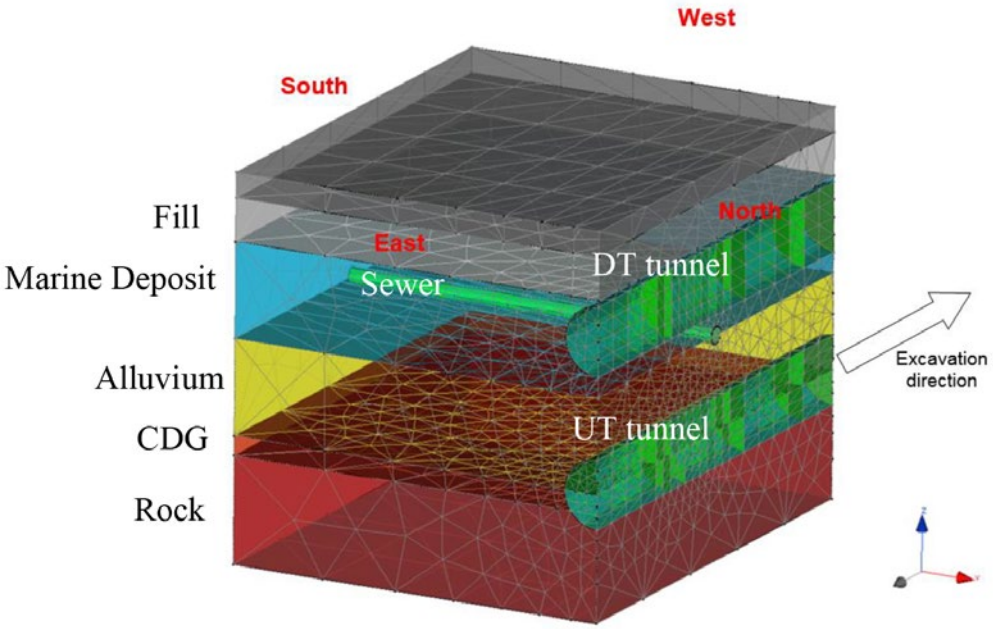

Figure 2: Graphical output of the 3D model

The model indicated a 15mm settlement to the sewer after the UT tunnel passed beneath it, after the DT passed above the sewer it was expected to rise with a final settlement of 2-6mm as seen in Figure 3 below;

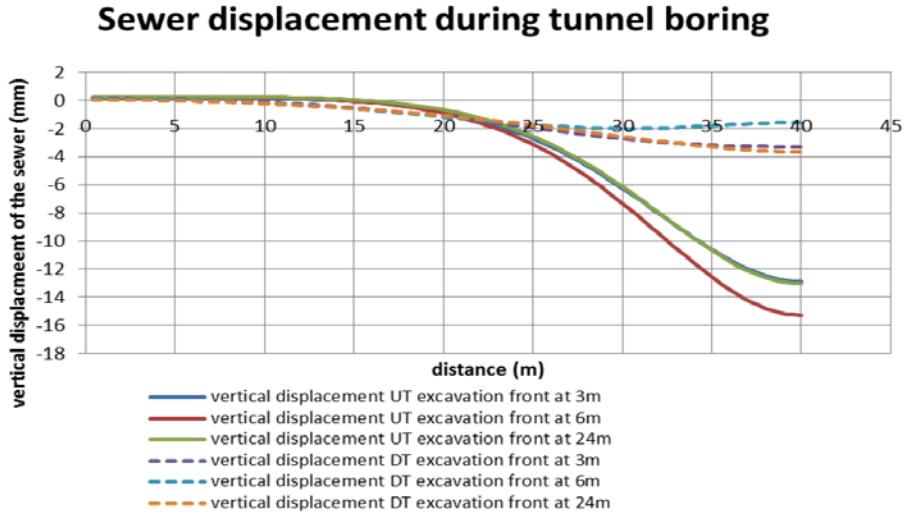

Figure: 3 Modelled Sewer Displacements

The model also estimated the ovalisation caused to the pipe and found this to be greater than the longitudinal bending of the pipe.

This study demonstrated that the excavation of the EAS tunnels could be completed without detrimentally affecting the sewer. In addition, the sewer pipe jacking construction was suspected to weaken the soil around the sewer. In order to be compliant with the modelling hypothesis of a homogeneous soil and to guarantee a good found of the sewer in soil, a cement and bentonite mix was used to fill the void around the sewer and improve the ground conditions.

7 CONCLUSION

In conclusion it can be seen that several key activities must be taken when tunnelling, especially in a densely urbanised environment:

- Detailed desk top study including latest data from all possible construction activities in the arrears taking cognisance as to the tender packs information cutoff date.
- Exhaustive investigation including trial pits and geophysical surveys to locate known piles, left in temporary works, checks to structures constructed on reclaimed before consolidation can completed land irrespective or the owners records.
- Detailed modelling of known structures based on recent site inspection, structures can deteriorate from the assumed tender condition, in order to define the necessary remedial actions if any.
- Detailed confinement studies.
- The observance and adoption of new technologies as they become available.
- Removal of all known obstructions either from surface or with the TBM dependent on location, geology and foundation type in order to minimize the amount of CAI required, thus reducing the safety risk to the workers, along with the risk of excessive settlement and/or collapse.
- Underpinning of structures as required, todays hydraulic jacking systems can effectively confine and correct movements to existing structures, if planned properly, without disruption to the users.
- The ability to look at a project and come up with ideas that can add value such as early commencement of critical activities like tunnelling or even scope reduction.

If these best practices are followed it can be seen that not only can a project be progressed safely and to a high standard of quality to the satisfaction of the Client, it can also be constructed ahead of programme thereby generating financial benefit.

REFERENCES

GEO 2009, *Ground Control for Slurry TBM Tunnelling, GEO Report No. 249, Geotechnical Engineer Office, Civil Engineering and Development Department, Government of Hong Kong SAR.*

Tsang, Salisbury & Yeung 2012, *Confinement Pressure for Face Stability of Tunnel Boring Machine (TBM) Tunnel Excavation Under Hong Kong's Western District, Proceedings of the HKIE Geotechnical Division Annual Seminar 2012, Hong Kong.*

Auvergne, Gauffre & Prost 2017a, *Extensive use of I&M to Enable Safe TBM Drive in Urban Dense Area, a Focus on SCL1128 Eastern Downtrack Drive, Proceedings of the HKIE Geotechnical Division Annual Seminar 2017, Hong Kong.*

Auvergne, Yu, Mogenier & Barrett 2017b, *Geophysical Investigations for Obstruction Detection and Mitigation for Marsh Road TBM Crossing, SCL1128, Proceedings of the HKIE Geotechnical Division Annual Seminar 2017, Hong Kong.*

Jacques, Laverret, Reilly 2017, *SCL1128 – Hong Kong's First Variable Density Tunnel Boring Machine, Proceedings of the HKIE Geotechnical Division Annual Seminar 2017, Hong Kong*.

Mobile Application for Soil Nail Works Supervision

Thomson M.K. Lai, Cliff H.W. Chow, Ivy W.Y. Chan
AECOM Asia Company Limited, Shatin, Hong Kong
Email: thomson.lai@aecom.com, cliff.chow@aecom.com, ivy.chan@aecom.com

ABSTRACT

The construction industry is constantly evolving, and now that most construction professionals have smartphones with them at all times, there is a great opportunity to improve efficiency, reduce costs and speed up project timelines with mobile solutions. Soil nailing is a construction technique that are often used as a remedial measure to upgrade existing soil slopes or stablise newly formed soil slopes. However, it is necessary that the soil nailing works are properly carried out and much emphasis has been placed on the supervision of the works at different critical stages. Mobile technology allows real-time information to be collected on field and synchronized with the office system simultaneously and it has significant potential on improving the practice of the construction industry. This technology is being used to track daily activities and collect critical information, and streamline collaboration between teams in the field and at the office. To facilitate the supervision works, the Innovative Solutions Department (ISD) of AECOM has developed a mobile application that integrates the workflow for soil nailing works supervision with engineer friendly interface for instant recording of data electronically during different stages of soil nail construction.

1 INTRODUCTION

Conventionally, standard inspection forms have to be filled and numerous photographic records have to be taken with digital camera by resident site staff (RSS) at different stages of soil nail construction. After the inspection, much time is spent by the RSS on manual data input, which is tedious and unexpected errors may be made. Furthermore, paper is not only an environmental unfriendly recording media but it is also not durable under the rain.

AECOM is continually improving and adopting innovative solutions that lead to more sustainable and efficient operations. In this regard, an all-in-one mobile application for the RSS is developed, so as to modernize their workflow on supervising soil nailing works and allow them to view job information, update checklists, and perform inspections in a faster and more effective way.

2 APPROACH FOR DATA COLLECTION & MANAGEMENT

The mobile application improves the quality and efficiency on field inspection of data collection. Standard templates and previous relevant record data have been downloaded to mobile device. Field data and photos taken on site could be synchronized to server and filed systematically, which can eliminate the risk of losing records and avoid abortive works. The field inspection sheets with photos are generated automatically and hence the submission quality is ensured. The inspection process can now be conducted in a paperless mode and more environmental friendly manner.

With the handy mobile application, RSSs only need to bring along with a mobile device, e.g. their contract phone, for site inspection. They are able to import soil nail schedule of a slope and choose

a slope feature from the list, input actual soil nail details on site, modify details and take site photo using the mobile device with the mobile application. All the field records are delivered and stored in the centralized database without further post inspection processing so that resident engineer (RE) and resident inspector of works (RIOW) can monitor the quality and progress instantly after the site inspection. After reviewing, a "Soil Nail Record Form" is ready to be generated for endorsement by the Director's representative.

The whole process is streamlined with this paperless and weather proof tool. Consistency across inspections are also maintained even if inspections are carried out by different RSSs as the paper-based inspection forms has been transformed into pre-defined pick list to standardize the entry. With standard forms and guided steps, data integrity problem is significantly reduced and data checking process can be shortened, RSSs can now spend less time on data entry from paper records but focus more on field works. The following figure illustrates the entire soil nail construction process simulated in the mobile device.

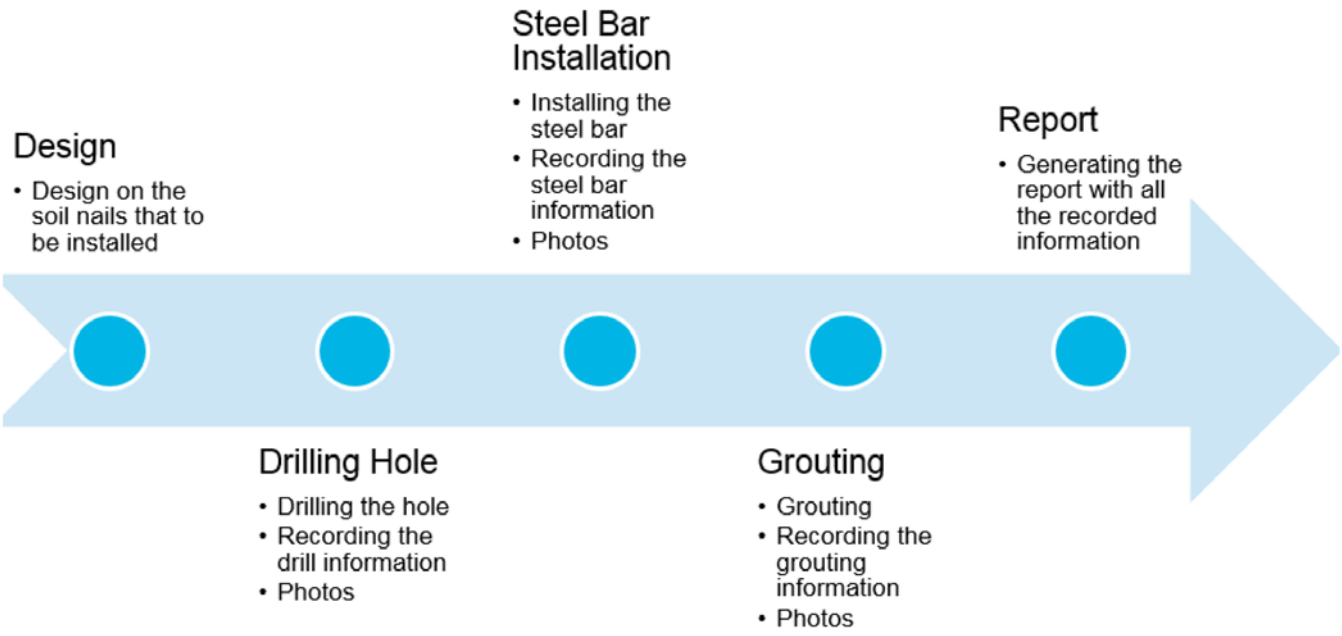

Figure 1: Workflow for Soil Nail Construction

3 IMPLEMENTATION OF THE MOBILE APPLICATION

The design and application implementation starts from getting the user requirements from the engineers. The data to captured and report formats have to be well defined in the beginning in order to minimize abortive programming works. In order to develop the application meeting with the conceptual requirements, process map with key input are proposed when the project started.

Before using the application for recording the activities to be inspected, the RSS needs to prepare an import template for importing the details of the soil nails that to be installed to the mobile application. The template is structured in Microsoft Excel form for inserting all the predefined soil nails installation details, such as the diameter of the drill hole, inclination and steel bar dimension.

The essential information on the import template include the Contract Number, Works Order Number, Feature Number and Feature Location. For each row in the Excel template, it represents one soil nail to be installed on site. The soil nail number is taken as the unique reference. If there is any duplicated soil nail number, the record will not be imported into the application.

When the template is ready, it can be copied to the mobile device for application installation. Specific folder is designed to store data to be captured. The import summary will show all the imported works order with the summary of progress. Once completed, the application is ready for use in the field.

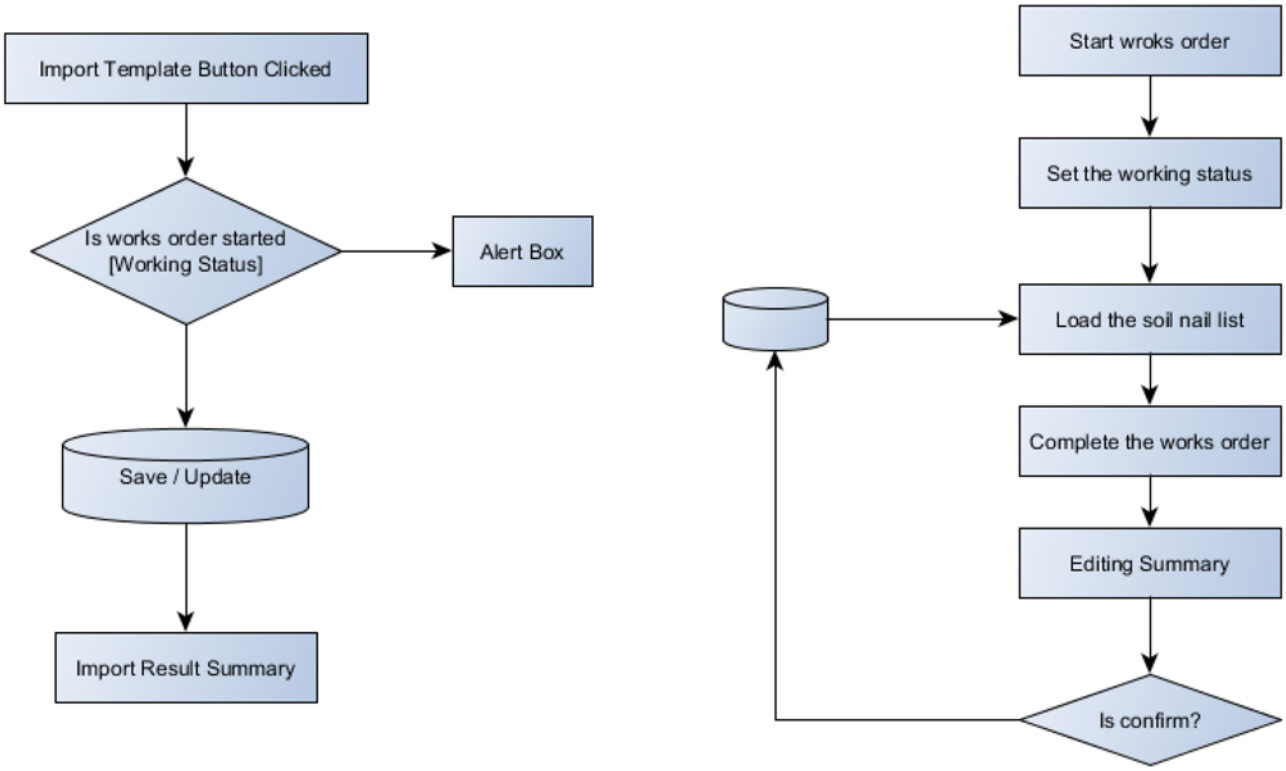

Figure 2: Workflow for Data Import (Left) and Mobile Application (Right)

1	***ContractNum***	GE/2015/02				
2	***WorksOrderNur***	LPM201502/24/BC675				
3	***FeatureNum***	7NW-B/C675				
4	***FeatureLocatio***	BEHIND HOUSE NO.43E KAM SHAN,TAI				
5	***SoilNailNum***	***DrillHole_Diamet***	***DrillHole_Inclinati***	***SteelBar_Diamet***	***SteelBar_Lengt***	***GroutVol***
6	A1	150	20	25	9	
7	A2	150	20	25	9	
8	A3	150	20	25	9	
9	A4	150	20	25	10	
10	A5	150	20	25	10	
11	A6	150	20	25	10	
12	A7	150	20	25	10	
13	A8	150	20	25	10	
14	A9	150	20	25	10	
15	A10	150	20	25	11	
16	A11	150	20	25	11	
17	A12	150	20	25	11	
18	A13	150	20	25	9	

Figure 3: Sample Template for Data Import

There are 4 different working phases of the soil nail installation which are considered as critical steps and the works must be inspected and witnessed by the RSS. These include drilling hole, installing steel bar, grouting and after grouting.

For each works order, several photos should be taken to record the quality of the soil nailing works. The “Photo” function allows engineer to take photos for respective works. A photo summary will be listed for the engineer to review the photo taken on site. All the photos are saved under a designated directory with the feature number as a folder. It is structured for the application to transfer the photos to the servers automatically.

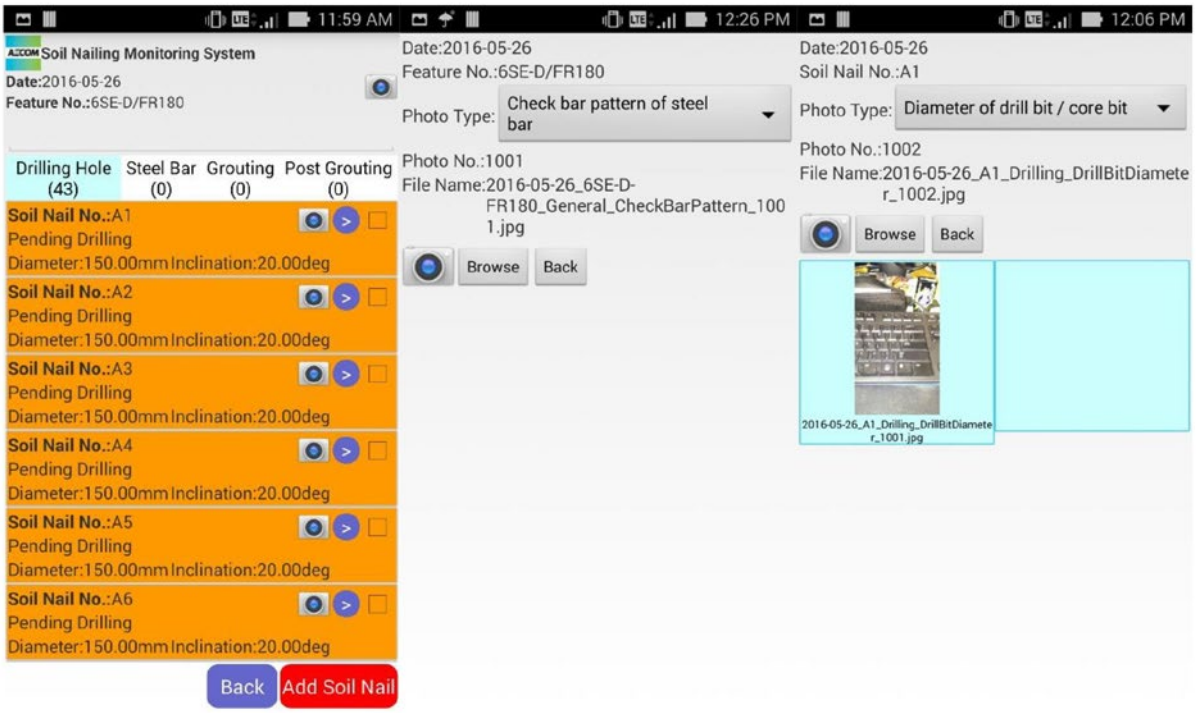

Figure 4: Soil Nail Orders in the Mobile Application

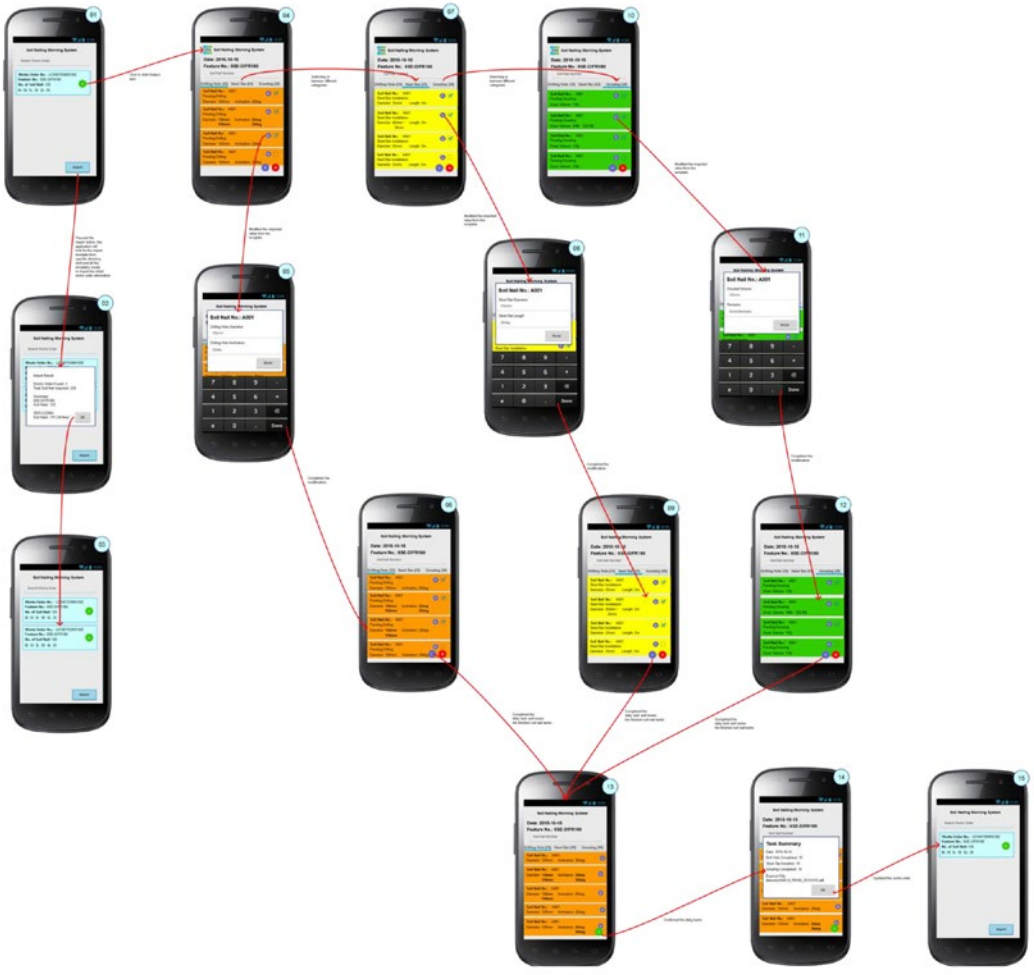

Figure 5: Step by Step Interface for Soil Nail Information Capture

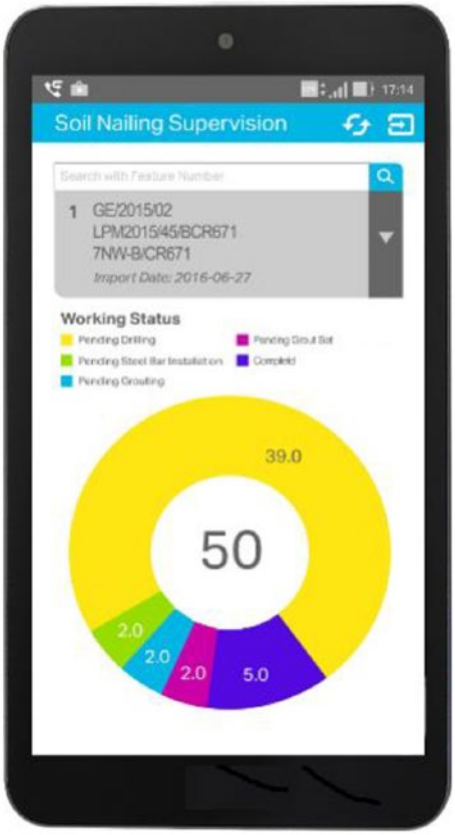

Figure 6: Work Status Summary

Engineer can make use of the design interface below to input the soil nail details. To facilitate the input procedures, the data is loaded from the pre-defined template as mentioned above. Engineer can edit the detail if there are changes due to the site condition. Similar procedures are applied to all critical phases including drilling hole, installing steel bar, grouting and after grouting.

After inspection, the RSS is required to click "Submit" to complete the submission and save process. If there is any soil nails completed with the grouting works, a report will be generated to record all the completed soil nails. All the generated files are stored within the application.

A work status summary lists out all the work status of the soil nail procedures and allows the engineers to have a clear picture of the progress and quality of the soil nailing works.

4 CONCLUSIONS & BENEFITS

In conclusion, the ease of use and the ability to increase productivity by the mobile application for geotechnical site supervision works has brought much benefits to both the engineering consultants and the clients. We foresees more benefits can be brought to the design and construction industry in the future. The benefits of this project are as below:

1. Improved communication with owners and project stakeholders – Completing daily reports at the job site on mobile devices and sending automated emails can strengthen the communication loop with project stakeholders. When all parties involved in the project have access to the same information at the same time, errors can be minimised and issues requiring attention can be addressed faster.
2. Increased back-office efficiency – By eliminating the use of paper records, design and construction companies can save hundreds of hours spent on entering data, collating information for reporting, or looking for paperwork that could be easily lost or misplaced. Increasing back-office efficiency allows projects to be run leaner, and completed on time and on budget.

3. More accurate project documentation – Using mobile apps to capture information at the site improves accuracy and reduces issues that arise from illegible handwriting, inconsistent data, and information gaps. Photos, GPS, time stamps and signatures captured on-site provide accurate and indisputable audit trail for the project;and delivering accountability to clients or evidence in legal disputes.
4. Better equipment management – A database-driven mobile solution can maximize the use of equipment through better management and tracking. Real-time information about maintenance schedules, availability, and equipment locations help to improve investigation and resource planning and use.
5. Real-time mobile access – With mobile application that provide two-way access to information, field staff can file electronic versions of drawings and plans for quick offline access by teams in the field. This improves productivity and reduces the need for post processing of data.

Upon adoption of the mobile soil nail system, the entire soil nail information recording process has been significantly shortened and the following figure summarizes the efficiency gain from the current manual process to the mobile system process.

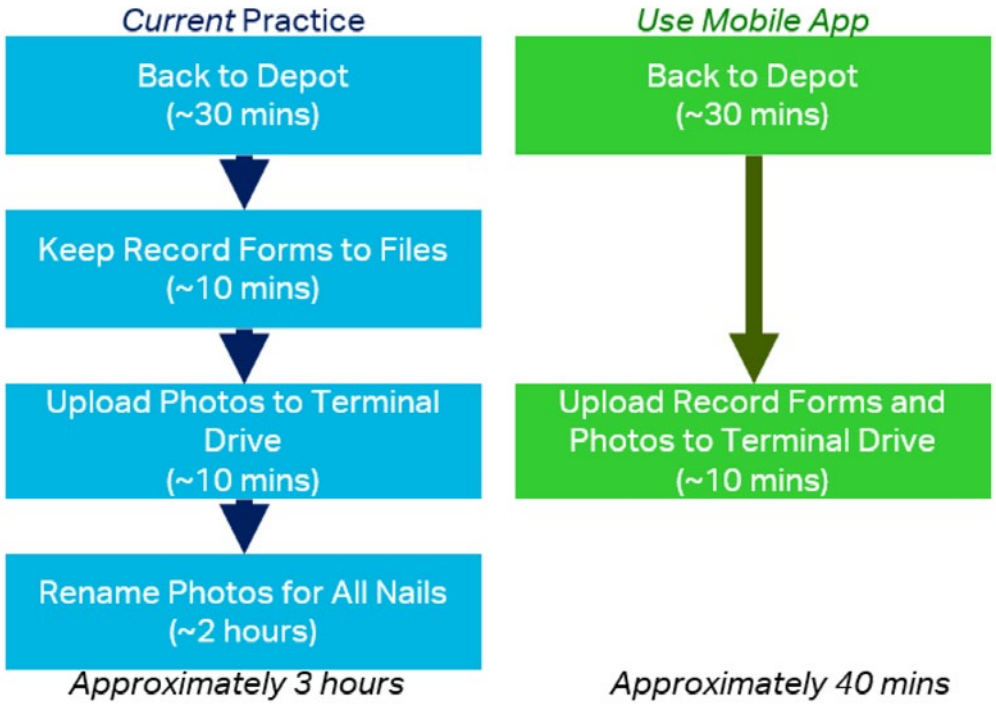

ACKNOWLEDGEMENTS

This paper is published with the permission of the Head of Geotechnical Engineering Office and the Director of Civil Engineering & Development, Government of Hong Kong Special Administrative Region.

Large Scale Bored Pile Wall Supported by Permanent Tie Backs in Hong Kong

A.K.M. Lam & K.P. Chan
Ove Arup & Partners Hong Kong Limited, Hong Kong

ABSTRACT

In order to provide enough supply of lands to meet the growing demand by the community, some of these lands encroach into existing hillslopes or even natural terrain with exceptional constraints such as limited site access, lack of suitable working platforms or flat grounds, high exposure to natural terrain hazards, highly unbalanced excavation, etc. These constraints result in extensive temporary platforms and temporary site formation with complex construction sequence to facilitate the construction. The permanent site formation would also be highly complicated with various platforms, slope and wall features being created. This gives a big challenge to the geotechnical engineers and the private developers to guesstimate the amount of site works to be required at the time of land purchase and to compromise the architectural design with the amount of the site formation works involved during the detailed design stage. This paper showcases an example of a large scale site formation work with the use of a 3m diameter permanent contiguous bored pile wall supported by permanent tie backs to facilitate a 38m deep excavation against a sloping terrain to minimize the movements of the adjacent ground and maximize the development potential of the site. The paper will also discuss the construction challenges in this project.

1 INTRODUCTION

The site was located between Stubbs Road and Bowen Road to the southwest of the Happy Valley Racecourse. The ground level within the site varied from +70mPD at Stubbs Road to +123mPD close to Bowen Road with man-made and natural slopes in various geological settings including soil and rock. The elevation along the site boundary at the upper hillside varied from +95mPD to +115mPD. The site location and topography are shown in Figures 1 & 2 respectively.

The slopes along the western boundary were steep with slope angle generally over 35 to 40 degrees while those along the southern boundary were gentler with slope angle of around 30 degrees. The proposed residential development comprises five 7-storey residential blocks, thirteen 3-storey, six 2-storey houses and a clubhouse with a total GFA amounting to 16,800m^2. A two-storey car park basement and a vehicular access were provided generally across the site, making the final formation level generally varying from +70.0mPD at the entrance level at Stubbs Road to +85.0mPD at the level immediately above the Drainage Tunnel Reserve Zone (DTRZ), and descending to +83.0mPD at the western end of the site.

2 GROUND CONDITIONS

The site comprised occasional Fill and Colluvial materials near the surface and mainly granite of various degrees of weathering from completely decomposed to slightly decomposed. The levels of SPT 'N' ≥ 200, Category 1(c) and Category 1(b) rockhead classified in Table 2.1, BD (2004) were identified at

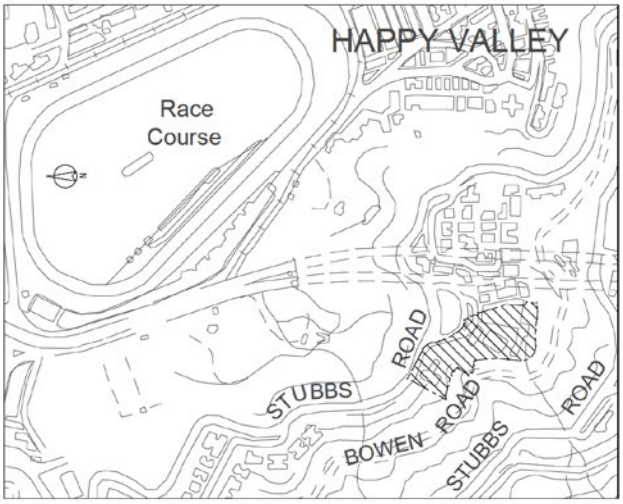

Figure 1: Site Location

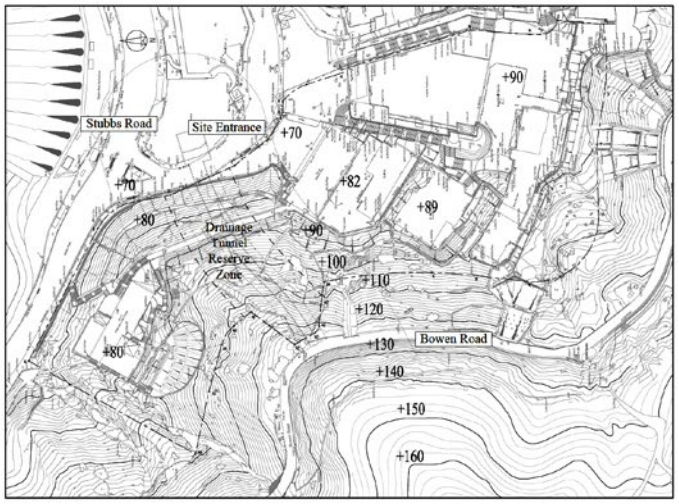

Figure 2: Site Topography

each borehole as relevant. The weathering profile was found to be deeper on the northern side of the site comparing to that on the southern side. At the southern portion, the rockhead was located from 4m to 15m below existing ground level (i.e. about +60mPD to +107mPD). At the northern portion, the rockhead varied from 20m to 45m below the existing ground (i.e. about +40mPD to +80mPD). The rockhead level within the DTRZ varied from +60mPD to +95mPD. The rockhead levels rose towards the hillside with the levels near the Bowen Road level varying from +95mPD to +110mPD. Deep weathering profile with thick corestones was identified at the northern portion of the site, while the rockhead profile was more distinctive at the southern portion without significant thickness of corestones.

3 CONSIDERATIONS AND EVOLUTION OF THE BORED PILE WALL WITH TIE BACKS

The design of the site formation works for this project was governed by the following factors: -

- **Vehicular access** – Based on the topographic survey, starting from site entrance and going clockwise, the ground level along the site boundary varied from +70mPD at Stubbs Road gradually rose to +105mPD at the south-eastern corner of the site. The ground level maintained at this level with local variations along the western perimeter and climbed up to +115mPD above the DTRZ. The ground then dropped gradually to +95mPD at the western corner and returned to Stubbs Road level at +64mPD. Vehicular access needed to be provided linking the different portions of the site.
- **Development height limit** – The development of the site was subjected to a height limit at +120mPD, which was slightly lower than the level of Bowen Road at about +123mPD such that the view at Bowen Road would not be affected.
- **The Hong Kong West Drainage Tunnel (HKWDT) within the DTRZ** – The existing HKWDT was located below the rockhead with crown and invert levels at +44mPD and +40mPD respectively. The DTRZ was defined at +30mPD to +55mPD in elevation and 25m away from the centerline of the drainage tunnel on plan. The stress change and movement of the drainage tunnel due to the excavation effect and the imposition of the foundation load needed to be considered.
- **Car park basement** – A two-storey car park basement were provided generally across the site. In view of the site topography and the height limit, the car park basement needed to be housed below the existing topography.
- **Existing tree** – A tree located towards the southwest of the site was required to be protected under the Lease by maintaining the existing ground level between +90mPD to +99mPD in a circular area of 7.5m radius from the center of the tree.

With the above considerations, multiple building platforms were proposed across the site and raised towards the south and west from the entrance at Stubbs Road. The final excavation level for the majority of the eastern portion of the site maintained at +70mPD and raised to +85mPD close to the southern perimeter for the provision of building platform of Towers 1 to 3. In this area, the retained ground within the circular area of the existing tree would be approximately 10m to 20m above the proposed formation level. Towards the western portion of the site, the proposed formation level raised from Stubbs Road entrance level at +70mPD to +75mPD above the DTRZ. The building platform further raised to +83mPD where Towers 5 and 6 were situated. These building platforms were mainly formed by cutting into the existing hillside/sloping ground. Various earth retaining structures in the form of permanent bored pile walls or L-shaped retaining walls were considered depending on the height of the vertical cutting. The proposed developments were founded on piles or shallow foundation bearing directly on rock. The master layout plan and the approximate excavation levels of the building platform are shown in Figure 3.

Figure 3: Site Development Plan

Along the western site boundary, it was proposed to form a platform at +75mPD to +83mPD and the retaining height varied from 23m to 38m. In order to maintain such a substantial level difference, large diameter bored pile wall was proposed. Based on the available GI information, about 1/3 to 4/5 of the retaining height was within bedrock. The rock profile was generally shallower at the southern end of the site but deepened towards the western end. The biggest challenge for the bored pile wall design was to control the ground movement within a reasonable limit in order not to cause any substantial damage or instability to the surrounding structures, geotechnical features and underground utilities, particularly under long-term condition.

Behind the western site boundary was an undeveloped greenbelt area, which was relatively insensitivity to ground movements. At approximately 30m uphill behind the site was the existing Bowen Road, which was a rural path mainly used by hikers and served as an access to nearby services. Bridged crossing, water pipes and conduits were constructed along certain sections of Bowen Road. Therefore, there was a concern on ground movement at Bowen Road in order not to jeopardize the safety of the general public. In order to demonstrate the feasibility of using the bored pile wall system, preliminary analyzes using finite element computer program were carried out to check the internal stresses and the deformation of the bored pile wall system and the ground movements behind the wall.

Two different schemes, which included the multiple rows of cantilever bored pile walls and a single row of cantilever bored pile wall together with extensive upslope stabilization by soil nails, were first considered. However, the former scheme caused excessive upslope movement although it was proven by the finite element analysis that it would not trigger any upslope instability and the latter scheme would extensively limit the development potential of the upslope areas due to the extensive installation

of soil nails. In order to better control the ground movement at Bowen Road with public safety concern and to reduce the extent and number of nails, a third scheme using a single row of 22 numbers of 3m diameter bored pile at 5m centers supported by 229 numbers of permanent tie-backs was developed. The advantages of this scheme are discussed as follows: -

- The development potential within the upslope area outside the western site boundary was substantially improved as the tie backs were installed in front of the bored pile wall commencing at deeper level resulting in shorter lengths compared with the use of upslope stabilization by soil nails. The spacing of tie-back followed the spacing of the bored pile which was about 3 times wider than the conventional spacing of soil nails;
- The permanent tie backs scheme offered another advantage in terms of the provision of permanent steel casing to prevent the soil collapse during the course of installation while only temporary casing would be used for conventional soil nails. This greatly reduced the risk of soil collapse and loss of grout during installation;
- The construction of the tie back would be carried out commencing at levels well below the existing ground and within the lot boundary. Therefore, the disturbance to the trees outside the western site boundary was very much minimized;
- The permanent tie backs were designed to be bonded into bedrock, which was considered to be a robust design comparing with the soil nails to be bonded into in-situ soil; and
- The tie backs were installed below ground. The existing hillside appearance and vegetation would remain unaffected.

Based on these advantages, the scheme of bored pile wall supported by permanent tie backs was finally adopted for this project. In order to reduce the embedment depth of the bored piles, a number of shear pins consisting of 4T50 deformed bars were designed to provide the necessary shear resistance against the kick out stability of the bored piles. The permanent tie backs consisted of 4T50 deformed bars in a 240mm diameter drillhole bonded into Category 1(c) rock or better. The working capacity of the tie-backs was 2,067kN with 8m rock socket length. They were installed in front of the bored pile wall with typical vertical spacing of 2m and 4m and dipping at 30 degrees when the excavation progressed downwards. The elevation of the bored pile wall is shown in Figure 4.

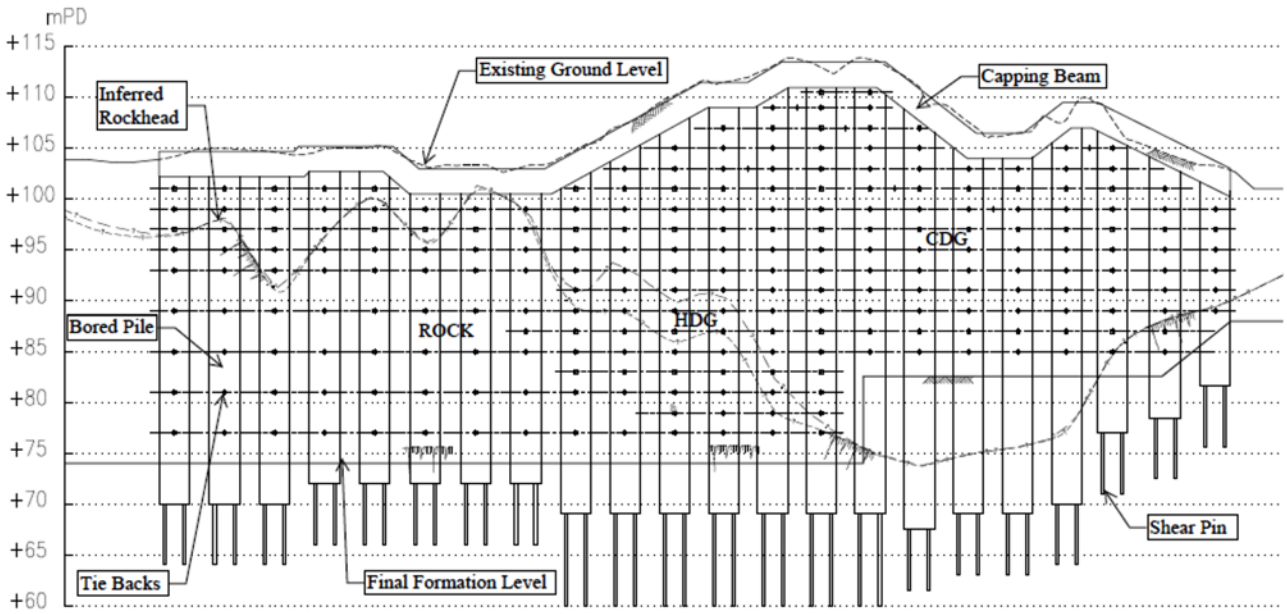

Figure 4: Bored Pile Wall Elevation

The site was also subjected to natural terrain hazards, which were mitigated by three rigid barriers positioned at the existing main stream courses below Bowen Road to capture the channelized debris flow and a continuous upstand wall behind the western and southern site boundary to capture any boulder falls and minor open hillside landslides. A portion of the upstand wall was integrated into the capping beam of the bored pile wall so as to minimize the construction impact to the natural terrain and the existing trees. The general view of the constructed bored pile wall and the integrated upstand wall is illustrated in Plate 1.

Plate 1: General view of the bored pile wall

4 DESIGN OF THE BORED PILE WALL SUPPORTED BY TIE BACKS

The design of the bored pile wall supported by permanent tie backs was carried out by using the finite element model 2D PLAXIS. The Mohr Coulomb constitutive model was adopted for the geological stratum. The wall was modelled as a plate element while the free and bond lengths of the tie backs were modelled as node to node element and geogrid respectively. The shear strength parameters of the soil stratum were based on the triaxial test results from the laboratory and the ground stiffness was derived based on the empirical correlation of 2N after Chan (2003) where N is the mean SPT N-values of the respectively stratum. The rock mass shear strength parameters were made reference to Hoek (1990). Based on the televiewer results, although discrete daylighting joints behind the bored pile wall were found to be kinematically feasible on the active side of the bored pile wall, the installed tie backs were served as dowel bars, which effectively stabilized any persistent daylighting joints on the active side of the wall if they exists and reduced the active pressure. In this connection, the rock mass properties were considered appropriate on both the active and passive sides of the bored pile wall. The adopted design parameters for the PLAXIS analysis is summarized in Table 1.

Table 1: Design parameters

Stratum	γ' (mm)	ϕ_{peak}' (kN)	c_{peak}' (kN/m²)	ψ' (°)	E' (MPa)*	k (m/s)
CDG	19	38	10	5	20+5z	1e-5
HDG	19	40	10	5	800	1e-5
Rock	24	45	100	5	10,000	1e-7

* E'= 2N (MPa) for CDG/HDG. "z" refer to the depth below ground in meter.

Majority of the standpipes indicated that the measured groundwater levels were only 2m slightly above or below the rockhead along the western site boundary. Using the wetting band analysis, a 3m high perched water table above the rockhead was assumed in the PLAXIS model. Considering that the amount of groundwater within the rockmass can be readily drained away by the drainage layer and the weepholes installed behind and at the lagging panels between the bored piles, no groundwater pressure was allowed beneath 3m of the rockhead. The design of the bored pile wall was generally governed by the ground settlement at Bowen Road. The displacement output from PLAXIS is presented in Figure 5.

The wall deflection was estimated to be about 22mm while the ground movement at Bowen Road was in similar order. The maximum load in the tie back was well within the design capacity but was close to the limit with consideration of the impact load on the upstand wall integrated to the top of the capping beam. Prestressing of the tie backs was not required as the tie backs could provide enough axial stiffness to control the wall deflection as well as the upslope ground movement during the course of excavation. The design of the tie backs generally complied with Geoguide 7 published by GEO (2008). Pull out tests and Time Domain Reflectometry (TDR) tests were performed to verify the capacity and the length of the tie backs respectively.

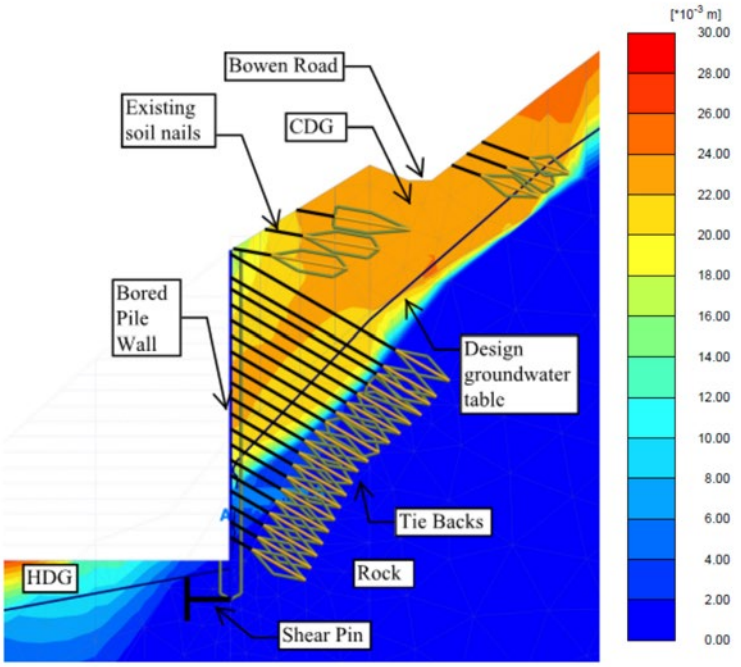

Figure 5: Displacement contour in PLAXIS

5 PERFORMANCE OF THE BORED PILE WALL

The performance of the bored pile wall was monitored by a total of three numbers of inclinometers embedded into three designated bored piles, 40 numbers of strain gauges installed near the head of the tie backs, 4 numbers of ground settlement markers along Bowen Road and 3 numbers of standpipe and piezometers between the Bowen Road and the bored pile wall. After completion of the excavation

work, the inclinometers recorded that the maximum wall deflection was about 4mm and the ground settlement of Bowen Road was about similar order. The maximum load of tie backs measured by the strain gauges was found to be about 660kN. The piezometeric head immediately behind the bored pile wall was generally below the design prediction. A comparison between the design prediction and the actual measurement of the wall deflection and the tie back load are presented in Figures 6 and 7 respectively.

It is not unusual that the actual ground movement is less than the predicted movement. In the PLAXIS model, the bored pile wall was modelled as a plate element having no physical dimension. In reality, the 3m diameter bored pile wall had a finite dimension which could provide additional restoring moment due to the shaft friction developed between the front and the back face of the bored pile wall in opposite direction. This effect was particularly prominent at shallow depth of excavation. In addition, the Mohr-Coulomb constitutive model overestimated the ground deformation under a small strain condition. The use of HS small model in PLAXIS was considered to be more appropriate to take into account very-small strain stiffness and its non-linear dependency on strain level.

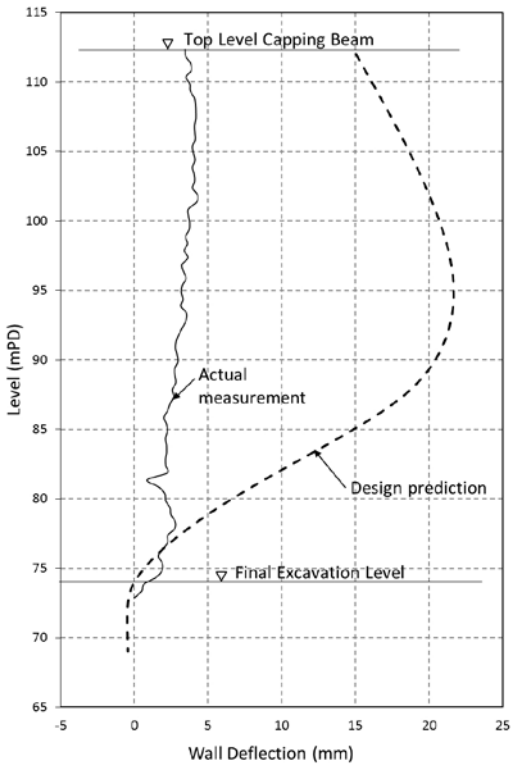

Figure 6: Wall Deflection

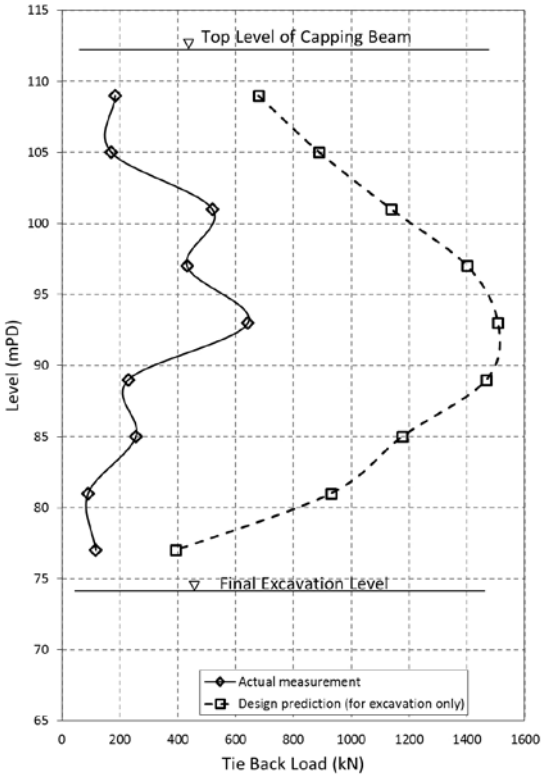

Figure 7: Tie Back Load

6 CONSTRUCTION CHALLENGES

In view of the site topography as illustrated in Figure 2, one of the construction challenges was to form a site haul road linking the southern and western parts of the site over the steep terrain and the terraced platforms in order to enable the delivery of equipment, plants and materials from Stubbs Road. Temporary access ramps with gradient as steep as 1V:4.5H were therefore formed using stacked concrete blocks and temporary fill slopes from the entrance at +70mPD all the way up to the highest platform level to the south at about +100mPD. To the western end, the existing slope was cut back and supported by additional soil nails in order to widen the existing walkway to about 3m and reaching the western platform at about +80mPD. Safety measures including limiting the loading condition of trucks, sufficient wheel wedges, and look out men are straightly controlled on site.

In order to facilitate the bored pile wall construction, a 15m wide and over 100m long temporary steel platform supported by vertical and raking mini-piles was built on the sloping terrain within the site, which could accommodate a total of 6 numbers of bored pile oscillators and reverse circulation

drilling rigs with 4 numbers of service crawler cranes to be operated simultaneously. This temporary platform indeed fell into the critical path of the construction of the project. In order to expedite the construction process, the platform was split into three parts and the stability of the individual part was designed to be independent from one another such that when one-third of the platform was built, the bored pile works could be commenced right away. The independent platform could also allow faster dismantle. The general view of the temporary steel platform for the construction of the bored pile wall is illustrated in Plate 2.

Plate 2: General view of the temporary working platform

In this project, a 500mm thick concrete lagging with weepholes was placed at the front face of the bored pile wall. Behind the concrete lagging was the drainage blanket, which consisted of a layer of miradrain and a 200mm thick no-fine concrete for the exposed soil and rock faces respectively from the top of the capping beam to the final formation level. Construction of the concrete lagging between the bored piles (see Plate 3) and the preparation of the tie back head (see Plate 4) were indeed labor intensive and repetitive. In order to expedite the work sequence, a temporary lagging constructed by sprayed concrete was introduced such that the progress of the excavation could be expedite and the permanent lagging could be constructed afterwards.

Plate 3: Concrete lagging between bored piles

Plate 4: Tie back head detail

7 CONCLUSIONS

Due to the proposed formation of multi-level building platforms within the site and the significant depression of the proposed formation below the surrounding topographic profile, a 38m high bored pile wall reinforced by tie back system was proposed to satisfy the structural and serviceability performances of the surrounding structures and slopes, which set a precedent case for the new developments over a hilly terrain.

ACKNOWLEDGEMENT

The authors would like to express their sincere gratuity to Sun Hung Kai Architects and Engineers Ltd. for their permission in publishing this Paper.

REFERENCES

BD 2004. *Code of Practice on Foundations*, Buildings Department, Hong Kong,

Chan, K.C. 2003. Observations from excavations – A reflection. Case Histories in Geotechnical Engineering in Hong Kong. *Proceedings of the Hong Kong Institution of Engineers Seminar*, pp. 83-102.

GEO 2008. Guide to Soil Nail Design and Construction (Geoguide 7). Geotechnical Engineering Office, Civil Engineering Department, Hong Kong.

Hoek, E. 1990, Estimating Mohr-Coulomb friction and cohesion values from the Hoek-Brown failure criterion, *Int. J. Rock Mech. Min. Sci. & Geomech. Abstr.,* Vol. 27, No. 3, pp. 227-229.

Advances and Challenges of the Landslip Prevention and Mitigation Programme since 2007

T.T.M. Lam, C.Y.S. Wong, R.C.H. Koo, A.H.K. Wu & K.K.S. Ho

Geotechnical Engineering Office, Civil Engineering and Development Department, The Government of Hong Kong Special Administrative Region

ABSTRACT

The dense urban development on a hilly terrain, together with high seasonal rainfall, gives rise to acute slope safety problems in Hong Kong, as reflected by a death toll of over 470 people due to landslides since the 1940s. In 1977, the Hong Kong Government embarked on a slope retrofitting programme, known as the Landslip Preventive Measures Programme (LPMP), to systematically reduce landslide risk by upgrading substandard man-made slopes to modern safety standards. By 2010, some 4,500 high-risk government man-made slopes have been upgraded through engineering works and the overall landslide risk arising from man-made slopes has been reduced to less than 25% of the 1977 risk level. In 2007, the Legislative Council endorsed the Government's proposal to launch the Landslip Prevention and Mitigation Programme (LPMitP) in 2010 to dovetail with the LPMP. The rolling LPMitP aims to contain the overall landslide risk to an 'as low as reasonably practicable' (ALARP) level by upgrading the remaining substandard man-made slopes and systematically mitigating natural terrain landslide risk. This paper presents the advances and challenges of the LPMitP since 2007.

1 INTRODUCTION

Hong Kong has a hilly terrain with a scarcity of flat land. Of the total land area of about 1,100 km^2, about 63% and 30% of the land is steeper than 15° and 30° respectively. It has a high concentration of urban development in close proximity to steep man-made slopes or natural hillsides, many of which can be susceptible to landsliding during periods of high seasonal rainfall. The situation was exacerbated by the absence of proper geotechnical engineering standards and lack of geotechnical input in the design and construction of man-made slopes before the late 1970s. Rain-induced landslides have occurred extensively in Hong Kong, causing significant socio-economic damage and loss of life. The severity of the landslide problem is reflected by a death toll of over 470 people since 1947.

Following a series of disastrous landslides with multiple fatalities, the Geotechnical Engineering Office (GEO) (formerly known as the Geotechnical Control Office) was established in 1977 as a central body to regulate slope safety in Hong Kong. Although serious landslides still occurred subsequently from time to time, the scale and severity of the landslide problem have been reduced considerably as a result of the implementation of a comprehensive slope safety system to manage landslide risk (Wong, 2009).

Apart from substandard man-made slopes, Hong Kong is also subjected to natural terrain landslide hazards posed by the steep terrain, much of which is only marginally stable. A review of aerial photographs taken from 1924 to 2006 has identified more than 100,000 historical landslides on natural terrain. In the severe rainstorm of November 1993, over 800 landslides occurred on natural terrain in Lantau Island. Some 2,400 natural terrain landslides occurred in West Lantau during another severe

rainstorm on 7 June 2008. Whilst most of these natural terrain landslides occurred in relatively remote areas, some of them had affected existing development including buildings and roads. Since 1980, natural terrain landslides have caused 16 fatalities.

2 LANDSLIP PREVENTION AND MITIGATION PROGRAMME

2.1 Landslip Preventive Measures Programme (1977–2010)

In 1977, the GEO launched the LPMP to systematically retrofit substandard government man-made slopes and undertake safety-screening studies of private man-made slopes.

The LPMP has evolved progressively over the years to cope with the growing public expectations for enhanced slope safety and aesthetics. Following the fatal Kwun Lung Lau landslide in 1994 (Wong and Ho, 1997), the LPMP was accelerated with the injection of additional resources. Typically, over 150 sites scattered over different places were active at any one time under different works contracts. The LPMP has brought about many technical advances and system improvements, as summarized by Tang et al. (2007).

By 2010, the overall risk to life posed by substandard man-made slopes had been reduced to less than 25% of the 1977 level, as demonstrated by quantitative risk assessment techniques (Wong, 2005).

2.2 Landslip Prevention and Mitigation Programme (2010–present)

In 2007, the Legislative Council endorsed the Government's proposal to launch a new rolling Landslip Prevention and Mitigation Programme (LPMitP) in 2010 to dovetail with the LPMP. The LPMitP has an expanded scope that covers natural hillside catchments in addition to man-made slopes. The strategy of the LPMitP is to contain the remaining landslide risk to within the 'as low as reasonably practicable' (ALARP) region. This is done through enhancement of the remaining substandard man-made slopes and systematic mitigation of landslide risk posed by vulnerable natural hillside catchments, in accordance with the 'react-to-known-hazard' principle (i.e. to carry out studies and mitigation actions where significant hazards become evident). This systematic programme is the first of its kind to comprehensively deal with landslide risk posed by both man-made slopes and natural terrain.

Two separate risk-based priority ranking systems have been developed to prioritize actions for man-made slopes and natural hillside catchments respectively. The priority ranking system for man-made slopes is an update of the one adopted in the past, with due refinement of the resolution of the ranking system for those slopes with moderate risk given that the high-risk man-made slopes had been largely dealt with under the LPMP (Cheng, 2013). The prioritization also takes into account the risk posed by "old technology" slopes whereby robustness was not explicitly considered in the design (for example, soil cut slopes improved by trimming back without structural support). With regard to the landslide risk posed to squatter dwellings where non-development clearance of the occupants of such dwellings by means of persuasion proves unsuccessful, engineering works in accordance with the risk-based priority ranking system are to be implemented under the LPMitP.

The pledged annual target outputs of the LPMitP are: (a) to upgrade 150 substandard government man-made slopes, (b) to complete safety-screening studies on 100 private man-made slopes, and (c) to undertake landslide risk mitigation works for 30 vulnerable natural hillside catchments. The annual expenditure is approximately HK$1 billion.

3 ADVANCES UNDER THE LANDSLIP PREVENTION AND MITIGATION PROGRAMME

3.1 Enhanced approach for natural terrain hazard studies

Since the publication of technical guidelines for natural terrain hazard studies by the GEO in 2003 (Ng et al., 2003), much experience has been gained in the study and mitigation of natural terrain hazards in Hong Kong, particularly from systematically dealing with Historical Landslide Catchments (HLC) under the LPMitP since 2010. By drawing on the experience gained and incorporating the findings from technical development work and following extensive consultation with practitioners, an enhanced

approach for dealing with natural terrain hazards in Hong Kong were developed. The enhancement serves to provide a more cost effective and practical approach to project delivery, and to better denote the level of hazard mitigation that can be practicably achieved under the current state of knowledge and technology. The enhanced approach has been promulgated through the update of existing technical guidelines (Ho and Roberts, 2016) and publication of new technical guidance notes (GEO, 2013; GEO, 2014). The key issues pertinent to the enhanced approach are summarized as follows:

- Differentiation of three types of catchments for mitigation actions - Ng et al. (2003) described two types of natural terrain landslide hazards in Hong Kong, viz. channelised debris flow (CDF) and open hillslope landslide (OHL). As observed from landslide studies and field mapping, landslides that occur at some hillside catchments in the form of a topographic depression (TDF, which stands for "topographic depression failure") may exhibit characteristics intermediate between that of CDF and OHL in terms of mechanism and mobility of debris movement. Through the back analysis of 46 TDFs selected from the Enhanced Natural Terrain Landslide Inventory using a range of rheological parameters, recommendations on the generic parameters to be adopted in assessing the mobility of TDF have been made.
- Clarification of the 'react-to-known-hazard' (RTKH) principle - Under the LPMitP, a Study Area typically comprises one or more HLCs, which are taken as satisfying the RTKH principle, and the adjoining natural hillside catchments with similar geological and geomorphological settings, which are denoted as Related Catchments but may not meet the RTKH principle. The enhanced approach provides a framework for screening out catchments that do not satisfy the RTKH principle from detailed study.
- Rationalization of the design event assessment (DEA) - The differentiation of 'Worst Credible Event' and 'Conservative Event' is no longer made in the revised DEA framework as the terms have caused confusion to some practitioners in the past. In addition, the revised framework allows the use of either analytical design or empirical design depending on the types of hazards arising from the catchments under consideration as well as the facilities affected by the hazards.
- Development of prescribed flexible barriers - LPMitP's experience indicates that the cost of mitigation works designed by analysis for OHL is much higher than that for CDF, which is not commensurate with the relative levels of landslide risk arising from OHL and CDF. This is largely due to the linear nature of many OHL catchments that calls for spatially extensive mitigation works. Limited knowledge of OHL hazards may also lead to over-conservative design that may not be practicable to construct and could give rise to environmental concerns and public complaints. Therefore, it is more practicable to adopt empirical design in general based on the use of prescribed flexible barriers instead of analytical design for mitigation of OHL hazards (GEO, 2014).

3.2 Hillside pockets

Given the history of infrastructure and building development on Hong Kong's foothills, small tracts of hillsides within developed areas are common. Hillside pockets are a form of natural hillside catchments that have been affected by human disturbance to varying degrees (e.g. construction of roads or building platforms) in the past. The occurrence of landslides on some hillside pockets during the June 2008 rainstorm indicates that the landslide risk posed by hillside pockets was not insignificant. A review of landslides that occurred within hillside pockets suggests that the presence of loose fill, inadequate drainage provision, presence of disturbed ground and poor slope surface protection are the probable contributing factors to these landslides. Given that the site setting of hillside pockets is different from typical natural hillsides, significant landslide risk may be posed by certain hillside pockets that do not meet the HLC selection criteria.

GEO has recently identified the deserving and vulnerable hillside pockets, which affect toe facilities of consequence-to-life Category 1 (i.e. buildings, important transport corridors and infrastructure) and

have a history of landslides and/or disturbance, for inclusion in a combined priority ranking list (i.e. HLC and hillside pockets) for action under LPMitP. Detailed technical guidelines on natural terrain hazard studies for hillside pockets are given in GEO (2016) and Ho & Robert (2016).

3.3 Enhancement of corrosion protection of flexible barriers

Steel flexible barriers have been widely used in Hong Kong as natural terrain hazard mitigation (NTHM) measures. Given the sub-tropical location of Hong Kong characterized by the hot and humid weather, the steel components of the flexible barrier system are highly susceptible to corrosion unless they are adequately protected. GEO has conducted a review of the condition of flexible barriers constructed so far, and observed that some components of the flexible barriers, e.g. wire clips and shackles, appear to be more susceptible to corrosion.

Having consolidated the experience of design and construction of steel flexible barriers and following extensive consultation with the profession and the proprietary product suppliers, a unified set of particular specification (PS) of steel flexible barriers has been developed. The PS specifies the corrosion protection requirements for every component of the steel flexible barrier system. For example, the principal nets and wire ropes shall be coated with either zinc or zinc/aluminium alloy (Zn 95 / Al 5) in accordance with BS EN 10244-2:2009 – Class A or equivalent as approved by the Engineer, while hot dip galvanizing in accordance with BS EN ISO 1461:2009 shall be applied to the steel posts, ground plates, shackles, wire rope clips, bolts and nuts, and other steel components. To further reduce the chance of damages of the protective coating in the course of assembling the flexible barrier system which might not be noticeable on site, the PS also stipulates that zinc-rich priming paint shall be applied to all parts of shackles, wire rope clips, bolts and nuts after their assembly, as well as to any repairs to galvanization coating for other parts of the flexible barrier.

3.4 Loose fill slopes

Many of the old (i.e. pre-1977) fill slopes comprise loosely dumped or end-tipped fill materials without compaction. They are susceptible to static liquefaction when they become saturated. A proven method of treating such existing loose fill slopes is to excavate and re-compact the top 3 m of loose fill to a dry density of not less than 95% of the maximum dry density (Plate 1), together with provision of subsurface drainage measures (Hong Kong Government, 1977).

Plate 1: Re-compaction of an existing loose fill slope

Difficulties can arise during the course of excavation and re-compaction of fill due to lack of working space, the need to work at height and difficult access problems. In addition, the works necessitate the removal of the prevailing trees on the slopes, which has become less acceptable by the public. To minimize the disturbance to the environment and minimize the earthworks, an alternative method of upgrading loose fill slopes using soil nailing was developed by the GEO in conjunction with the Hong

Kong Institution of Engineers. The enhanced approach was summarised in CEDD & HKIE (2011). A novel design methodology was developed to take full account of the liquefaction potential of the loose fill with relative compaction values exceeding 75%. This entails the use of soil nails together with a surface reinforced concrete grillage connecting the soil nails head. A series of comprehensive numerical analyses had been carried out to model the behaviour of soil nails in loose fill slope (Cheuk et al., 2013; Figure 1). Several rows of soil nails were connected together by a structural facing on the slope surface of a uniform loose fill layer of 3 m. The numerical analysis results demonstrate that the soil nail system with a structural facing of grillage beam can effectively limit the uplifting and horizontal movement of the liquefied loose fill layer within the slope. This method is now commonly used for upgrading loose fill slopes in Hong Kong (Figure 2).

Another alternative option for upgrading loose fill slopes is the pit-by-pit re-compaction method. It is used in situations where the site constraints preclude the use of soil nailing. Examples of site constraints include close proximity of the slope to private lot boundary and existing fill with relative compaction less than 75%. Apart from using the original soil excavated in the vicinity, other materials such as soil-cement, mass concrete, lightweight concrete or no-fines concrete have been commonly used for backfilling (Chan & Chan, 2008). A layer of topsoil is usually placed on the top of the concrete backfill for vegetation growth (see Figure 3). The construction is, however, normally more time consuming.

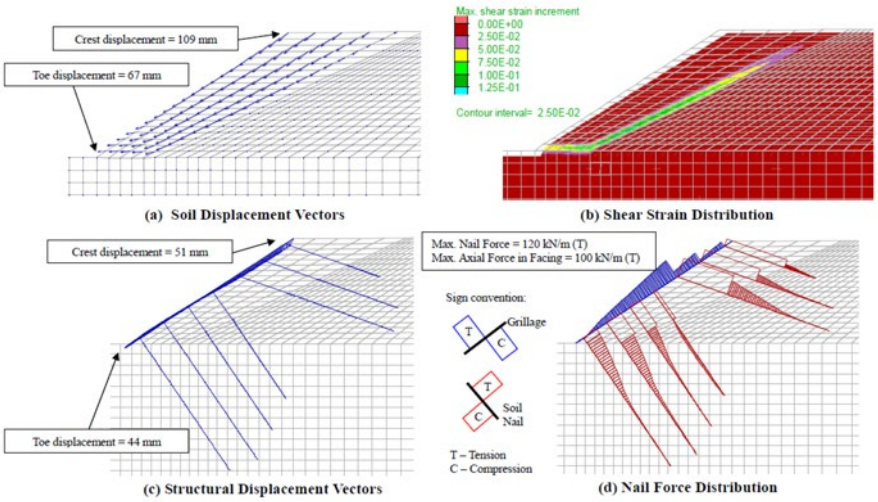

Figure 1: Typical results of numerical analysis of soil nails in loose fill slope (Cheuk et al., 2013)

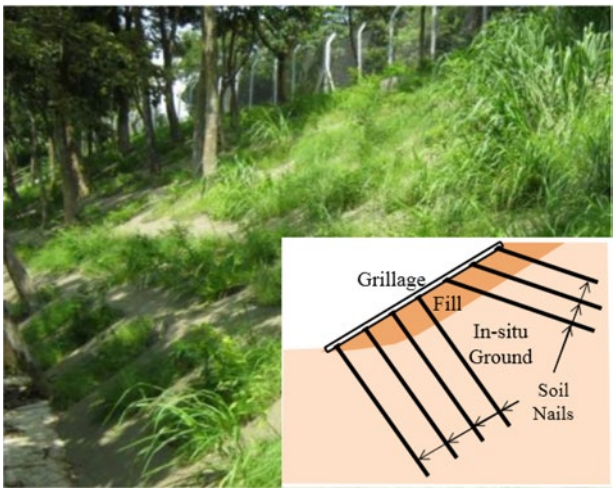

Figure 2: Upgrading of loose fill slope by means of soil nails and reinforced concrete grillage beams

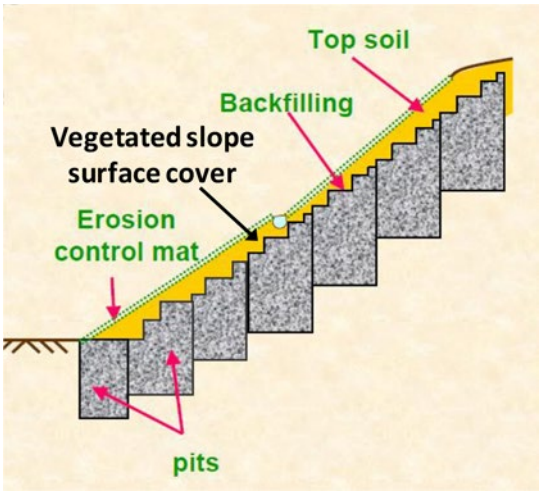

Figure 3: Typical cross-section using pit by pit method with vegetated slope surface cover

3.5 Landscaping and greening of slopes

It is Government policy to make slopes look as natural as possible, blending them with their surroundings and minimizing their visual impact on the built environment. To implement this policy, vegetation is generally used as slope surface cover in the upgrading of existing man-made slopes that are not steeper than 55°. A hard surface cover such as chunam or shotcrete may be used for steeper slopes as a last resort or gentler slopes that have a history of failures, but suitable landscaping measures such as applying subdued colour, masonry facing, providing planter holes and proprietary greening product on the slope surface for screen planting are adopted to minimize the visual impact. For natural terrain mitigation works, the extent of works is minimised as far as practicable in order to reduce disturbance to the hillside and the environment. The existing vegetation, including trees and shrubs, is also preserved where possible during the construction of landslide risk mitigation measures. Landscape treatment such as vertical greening, screen planting and toe planters would be provided to minimise the visual impact of the mitigation works and blend them with the surrounding environment (see Plate 2).

In 2000, the GEO produced technical guidelines on landscape treatment and bioengineering for man-made slopes and retaining walls (GEO, 2000). A review was carried out in 2010 with a view to promulgating the latest best practice and expanding the scope to include landscape treatments for natural terrain mitigation works and landslide repairs. The review culminated in the new GEO Publication No. 1/2011 "Technical Guidelines on Landscape Treatment on Slopes" (GEO, 2011). GEO promotes input by professional landscape architects during the early stage of the design process working along geotechnical engineers to ensure that the landscaping considerations are integrated with the geotechnical input.

Plate 2: Landscape treatment on a rigid barrier

4 CASE STUDIES OF NOTABLE SLOPE WORKS PROJECTS

A selection of recent case studies of LPMitP projects is presented below to highlight the challenge posed and the approaches adopted to add value to the design or implementation of the works.

4.1 Natural terrain mitigation works above Castle Peak Road

Flexible barriers have been commonly used to mitigate CDF and OHL in Hong Kong and other countries. A force approach for design of flexible barriers was introduced in Hong Kong by Kwan and Cheung (2012) and has been implemented under LPMitP in two pilot projects. In 2015, an enhancement of the assessment of landslide debris impact velocity was developed by GEO (2015). This improved the design of flexible barriers using the force approach by taking into account debris velocity attenuation upon impact on the barrier, hence providing a more realistic impact load.

The GEO in-house design team has recently adopted this enhanced force approach to design flexible barriers for NTHM works above Castle Peak Road near Wah King Hill Road. An advanced finite-element program NIDA-MNN developed by Professor S.L. Chan of the Hong Kong Polytechnic University (Chan et al. 2012) was adopted in this study for analysis of the flexible barriers. NIDA-MNN has been

demonstrated to be capable of analyzing large deformations of structural elements, such as ring nets and energy dissipating devices. The model setup and computer simulation of the flexible barrier using NIDA-MNN of this study are shown in Figure 4.

To further optimise the design and ensure structural adequacy of the proposed flexible barriers, Architectural Services Department provided technical support to the structural design of the barriers. In addition, a robustness check was undertaken to ensure that the overall performance of the flexible barrier was still adequate under some adverse scenarios, e.g. mal-function of any individual key structural component such as brake element.

Ongoing technical development work is in progress to refine the force approach by taking into account the dynamic effects of debris-barrier interaction.

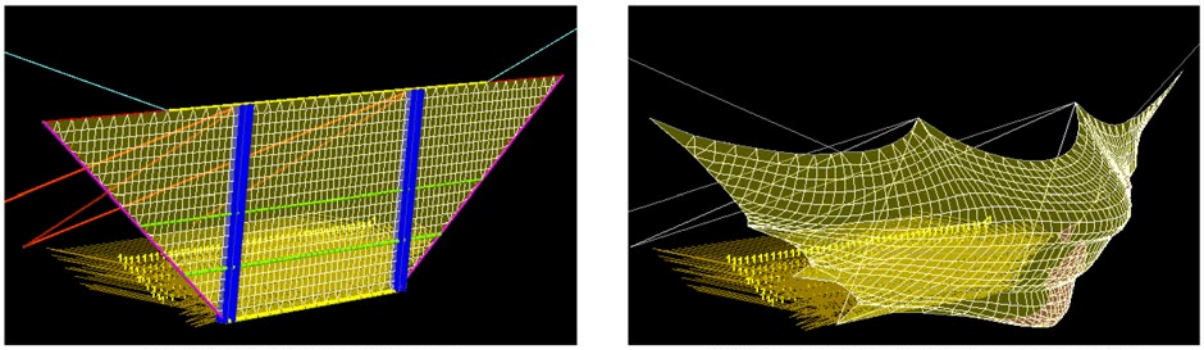

(a) NIDA-MNN model setup (b) Simulated barrier deformation profile

Figure 4: Numerical model setup and computer simulation of flexible barrier

4.2 Natural terrain mitigation works above Shek Pai Wan Road

A detailed study of NTHM works for the natural hillside above Shek Pai Wan Road was carried out by the GEO in-house design team. The proposed NTHM works included construction of a reinforced concrete debris-resisting rigid barrier. The design followed the latest technical guidelines based on recent technical development (Kwan, 2012), and was reviewed by an international expert.

Recently, the use of Building Information Modelling (BIM) is promoted. BIM is not just a 3-dimensional (3D) tool but a new tool to holistically manage information relating to construction projects from planning stage to design, construction and operational stages. GEO adopted BIM tool in this study and applied the advanced 3D geometric information. The use of BIM enhanced the design information for the project team to minimise the disturbance to the environment by optimising the design layout. The client and local residents can easily visualise the final mitigation works with the proposed restoration scheme of the landscaping works (see Figure 5).

A pilot use of geophysics survey using the resistivity method for determination of rockhead level within the study area was undertaken as part of the natural terrain hazard study to supplement the information obtained from conventional ground investigation works.

Figure 5: Computer simulation of a rigid barrier using BIM

4.3 Fill slope below junction of Fortress Hill Road and Tin Hau Temple Road

Figure 6 and Plate 3 show a 17 m high, 35° fill slope. The slope was located at the downhill side of the junction of Fortress Hill Road and Tin Hau Temple Road with an old 900 mm diameter stormwater drain pipe which carried surface runoff from the hillside catchment above Tin Hau Temple Road straddling across the slope. Despite the engineering input in the past, the slope has a history of repeated landslides, which were largely attributed to the persistent leakage problem of the stormwater drain pipe. During the slope stability assessment, an investigation by the Drainage Services Department concluded that the pipe needed to be upgraded. The drainage improvement works within the slope were subsequently entrusted to CEDD for construction.

Considering cost-effectiveness, future maintenance and construction difficulties, upgrading works comprising replacement of existing fill with compacted rock fill, and strengthening of the existing toe wall were proposed. The upgrading works enhanced the sub-surface drainage in order to avoid excessive build-up of transient groundwater pressure. Furthermore, a concrete trough for housing the diverted stormwater drain pipe was constructed as an integral part of the slope upgrading works. The merits of the concrete trough are easy to maintain and good protection against potential leakage from the pipeline that would adversely affect the stability of the fill embankment (ETWB, 2006).

As the alignment of the stormwater drain pipe inevitably traversed across the slope with a 15 m level difference, extensive temporary excavation with a maximum retained height of approximately 7.5 m was required. Considering the history of repeated landslides and the concern of the public safety during construction, a temporary pipe pile wall with tie-backs as the temporary works was designed to facilitate the construction of the proposed stabilization works. The works were completed without any adverse effect to the surrounding foundations and undue ground movement

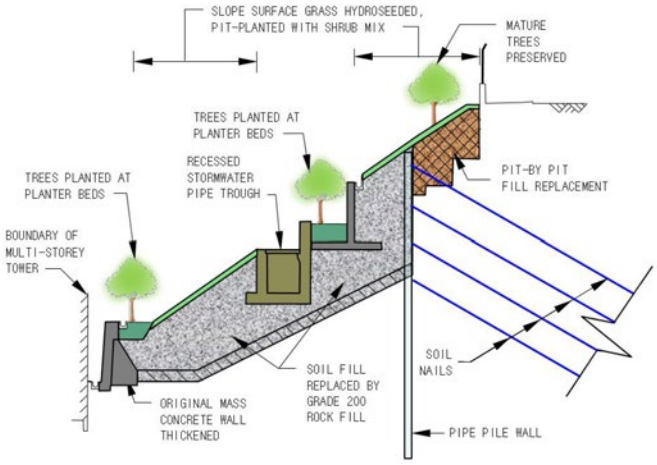

Figure 6: Cross-section of the site

Plate 3: General view of the slope after establishment period

4.4 Fill slope at Bowen Road

Standing at an average angle of 40° with a maximum height of almost 70 m, this fill slope is located downslope of Bowen Road overlooking a number of high-rise residential blocks. It was registered after a major landslip in 2005 that involved a failure mass of almost 1000 m^3. The upgrading works adopted a 300 mm thick reinforced concrete slab tied back by soil nails. Reinforced concrete planter-walls were constructed monolithically with the reinforced concrete slabs to facilitate planting (Figure 7). The greatest challenge of implementing the upgrading works was the access problem and the associated traffic arrangements (Figure 8). Due to the site constraints, access to the slope through its crest via Bowen Road was needed.

A section of Bowen Road with 21 spans of arches was granted the status of Declared Monument under the Antiques and Monuments Ordinance in 2009. At its narrowest section, Bowen Road measures only 2.5 m wide at most with no lay-by or verge. In order to gain vehicular access to the works site

through Bowen Road, application for a separate permit for each construction vehicle using Bowen Road east of Bowen Drive was made to Transport Department (TD). At the peak, there were in total six active construction sites at different locations along that section of road (Figure 8). Besides vehicular traffic, Bowen Road is a favourite spot for morning-walkers, holiday-makers and tourists alike. After close liaison with different stakeholders including the Police, TD, project teams of all the projects concerned, the District Councillors and members from the public, consensus was reached on the conditions to be imposed with the objective of ensuring the safety of all road-users. These included, inter alia, the implementation of a gyratory traffic flow scheme restricting traffic flow to one direction only with priority given to pedestrians. Also, vehicular access, with a speed limit of 10 km/hr, was restricted between 10:00 and 16:00, and only one vehicle was allowed to access the prohibited zone at any one time.

The slope is situated at a very prominent location above Wan Chai. It could be viewed from far away. In the landscaping design, the majority of species selected for planting was native species with a view to promoting development of sustainable ecological habitats. In total, 2 types of whips, 4 types of shrubs, 3 types of groundcovers, 7 types of climbers and 3 types of small trees were planted. The landscaping design of this slope won the 2015 Sustainable Slope Landscaping Award under the category of man-made slope / retaining wall. Photographs showing the establishment of vegetation after completion of upgrading works are shown in Plate 4.

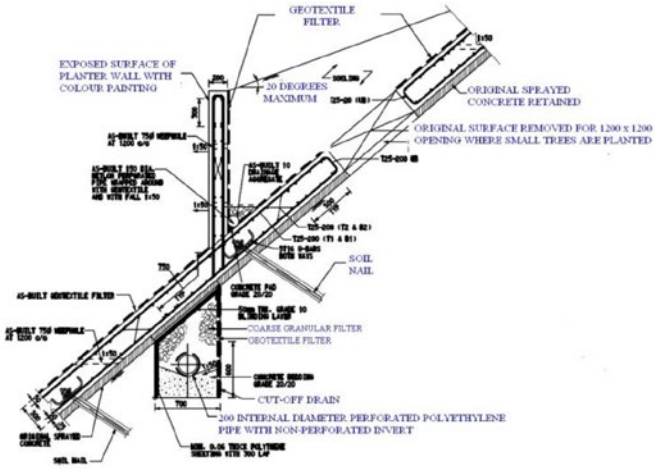

Figure 7: Typical Details of Planter Wall

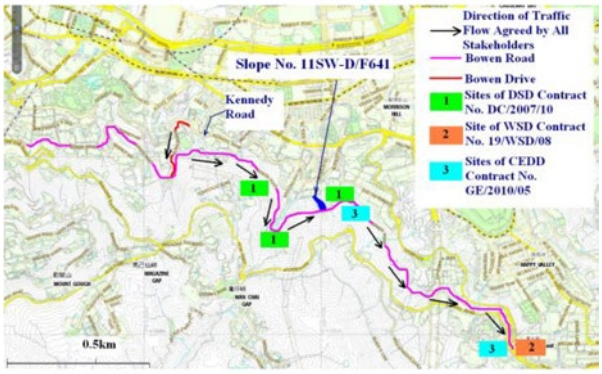

Figure 8: Temporary Traffic Arrangement

Plate 4: Establishment of vegetation after completion of upgrading works in 2011 (left) and 2015 (right)

5 CONCLUSIONS

The concerted effort of the Hong Kong Government in the past 40 years has brought about substantial improvement in slope safety and a significant reduction in landslide fatalities. The LPMP and the subsequent LPMitP have evolved progressively with time to address the slope safety needs of the community. In the past ten years, the scope of the slope retrofitting programme has been expanded to cover natural terrain, which has brought about many new challenges and constraints. Innovative technical development work has been completed to enhance the reliability, cost effectiveness and buildability of slope works. This has been achieved through partnership with the geotechnical profession.

ACKNOWLEDGEMENTS

This paper is published with the permission of the Head of the Geotechnical Engineering Office and the Director of Civil Engineering and Development, Hong Kong SAR Government. The authors would like to acknowledge the contributions to this paper by Ms H.W.M. Li, Dr E.H.Y. Sze, Mr D.Y.W. Chan and Ms C.W.K. Lin.

REFERENCES

CEDD & HKIE. 2011. *Design of Soil Nails for Upgrading Loose Fill Slopes.* Civil Engineering and Development Department, HKSAR Government and the Geotechnical Division of the Hong Kong Institution of Engineers, Hong Kong.

Chan, S.L., Zhou, Z.H. & Liu, Y.P. 2012. Numerical analysis and design of flexible barriers allowing for sliding nodes and large deflection effects. *Proceedings of Seminar on Natural Terrain Hazard Mitigation Measures, Hong Kong,* 29-43.

Chan, T.C.F. & Chan, D.C. 2008. A glimpse of the new technology applications in the landslip preventive measures programme. *Proceedings of the HKIE Geotechnical Division 28th Annual Seminar* (published under the title Applications of Innovation Technologies in Geotechnical Works), Hong Kong, 73-81.

Cheng, P.F.K. 2013. *The New Priority Ranking Systems for Man-made Slopes and Retaining Walls,* GEO Report No. 284. Geotechnical Engineering Office, Civil Engineering and Development Department, HKSAR Government, Hong Kong.

Cheuk, C.Y., Ho, K.K.S. & Lam, A.Y.T. 2013. Influence of soil nail orientations on stabilizing mechanisms of loose fill slopes. *Canadian Geotechnical Journal*, 50(12): 1236-1249.

ETWB. 2006. *Code of Practice on Monitoring and Maintenance of Water Carrying Services Affecting Slopes (2nd edition)*. Environment, Transport and Works Bureau, Government of Hong Kong, Hong Kong.

GEO. 2000. *Technical Guidelines on Landscape Treatment and Bio-engineering for Man-made Slopes and Retaining Walls,* GEO Publication No. 1/2000. Geotechnical Engineering Office, Civil Engineering and Development Department, HKSAR Government, Hong Kong.

GEO. 2011. *Technical Guidelines on Landscape Treatment for Slopes,* GEO Publication No. 1/2011. Geotechnical Engineering Office, Civil Engineering and Development Department, HKSAR Government, Hong Kong.

GEO. 2013. *Guidelines on the Assessment of Debris Mobility for Failures within Topographic Depression Catchments,* GEO Technical Guidance Note TGN No. 38. Geotechnical Engineering Office, Civil Engineering and Development Department, HKSAR Government, Hong Kong.

GEO. 2014. *Empirical Design of Flexible Barriers for Mitigating Natural Terrain Open Hillslope Landslide Hazard,* GEO Technical Guidance Note TGN No. 37. Geotechnical Engineering Office, Civil Engineering and Development Department, HKSAR Government, Hong Kong.

GEO. 2015. *Assessment of Landslide Debris Impact Velocity for Design of Debris-resisting Barriers,* GEO Technical Guidance Note TGN No. 44. Geotechnical Engineering Office, Civil Engineering and Development Department, HKSAR Government, Hong Kong.

GEO. 2016. *Supplementary Guidelines on Natural Terrain Hazard Studies for Hillside Pockets,* GEO Technical Guidance Note TGN No. 46. Geotechnical Engineering Office, Civil Engineering and Development Department, HKSAR Government, Hong Kong.

Ho, H.Y. & Roberts, K.J. 2016. *Guidelines for Natural Terrain Hazard Studies,* GEO Report No. 138 (2nd edition). Geotechnical Engineering Office, Civil Engineering and Development Department, HKSAR Government, Hong Kong.

Hong Kong Government. 1977. *Report on the slope failures at Sau Mau Ping, August 1977*. Hong Kong Government, 104.

Kwan, J.S.H. 2012. *Supplementary technical guidance on design of rigid debris-resisting barriers*, GEO Report No. 270. Geotechnical Engineering Office, Civil Engineering and Development Department, HKSAR Government, Hong Kong.

Kwan, J.S.H. & Cheung, R.W.M. 2012. *Suggestions on Design Approaches for Flexible Debris-resisting Barriers,* GEO Discussion Note No. DN 1/2012. Geotechnical Engineering Office, Civil Engineering and Development Department, HKSAR Government, Hong Kong.

Ng, K.C., Parry, S., King, J.P., Franks, C.A.M. & Shaw, R, 2003. *Guidelines for Natural Terrain Hazard Studies,* GEO Report No. 138. Geotechnical Engineering Office, Civil Engineering and Development Department, HKSAR Government, Hong Kong.

Tang, M.C., Ho, K.K.S., Chan, T.C.F. & Chan, N.F. 2007. The landslip preventive measures programme of the Hong Kong SAR Government - reflections on achievements, advancement and lessons learnt in past 30 years. *A Commemorative Volume Published in Conjunction with the 40th Anniversary of the Southeast Asian Geotechnical Society*, Kuala Lumpur, 337-359.

Wong, H.N. & Ho, K.K.S. 1997. The 23 July 1994 landslide at Kwun Lung Lau, Hong Kong. *Canadian Geotechnical Journal*, 34(6): 825-840.

Wong, H.N. 2005. Landslide risk assessment for individual facilities, In *Proceedings of International Conference on Landslide Risk Management*, Vancouver, Canada, 237-296.

Wong, H.N. 2009. *Holistic urban landslide risk management – challenges and practice.* Keynote lecture at the 7th Asian Regional Conference of the International Association for Engineering Geology and the Environment, Chengdu, China.

Recent Advances in Debris Mobility Modelling for Assessing Natural Terrain Landslide Hazards in Hong Kong

Raymond P.H. Law, Florence W.Y. Ko, Julian S.H. Kwan & H.W. Sun
Geotechnical Engineering Office, Civil Engineering and Development Department, The Government of Hong Kong Special Administrative Region

ABSTRACT

Debris mobility modelling has made major advances in the past decade in the Geotechnical Engineering Office. The advances are two-fold. Firstly, there are improvements in numerical tools for both two- and three-dimensional debris mobility analyses. Two-dimensional debris mobility modelling has changed its computing engine from Microsoft Excel using the programming language Visual Basic to a stand-alone calculation module using the multi-paradigm programming language C# that coupled with ArcGIS. Three-dimensional debris mobility modelling has gained the benefits of advances in computer technology to couple Smoothed Particle Hydrodynamics, a numerical method used for simulating the dynamics of continuum media, with ArcGIS. Secondly, there are technical developments on the choice of basal resistance models and use of mobility parameters for assessing the mobility of different landslide hazards, such as those within channelised debris catchments with adverse site settings that are prone to the development of sizeable channelised debris flows with high mobility and those within topographic depression catchments. This paper presents the background to the technical advances in debris mobility modelling in the past decade and summarises details of the individual developments.

1 INTRODUCTION

Hong Kong is characterised by its dense population fringing the hilly terrain, which inevitably expose the city to a high risk of landslide hazards, such as natural terrain landslides. Amid the presence of such risk, the Geotechnical Engineering Office (GEO) has been taking a leading role in Hong Kong in advancing the understanding of landslides, and enhancing the techniques, knowledge and expertise in the management of natural terrain landslide risk in the past decades.

In particular, strategic and continuous efforts have been made to enhance the capability of the profession to carry out forward prediction of the mobility and runout distance of natural terrain landslides by means of numerical simulation, with notable progress in the past two decades. A detailed account of the work done in the period from 1997 to 2007 has already been documented in Kwan et al. (2007). As for the past decade, major advances in debris mobility modelling have been achieved in Hong Kong, especially under the impetus of the launch of the Landslip Prevention and Mitigation Programme (LPMitP) in 2010 to systematically mitigate and contain landslide risk from both man-made slopes and natural hillsides.

The advances of this subject area in the past decade are two-fold. Firstly, there are improvements in numerical tools for both two- and three-dimensional debris mobility analyses. Two-dimensional (2D) debris mobility modelling has changed its computing engine from Microsoft Excel using the programming language Visual Basic to a stand-alone calculation module using the multi-paradigm

programming language C# that coupled with ArcGIS, a Geographic Information System (GIS) desktop software. Three-dimensional (3D) debris mobility modelling has gained the benefits of advances in computer technology to couple Smoothed Particle Hydrodynamics (SPH), a numerical method used for simulating the dynamics of continuum media, with ArcGIS. A summary of the use of SPH and other numerical modelling techniques in simulating landslide motion is presented in Soga et al. (2016). Both advances have enhanced the computational capability and efficiency of the modelling tools, streamlined the work process of natural terrain hazard studies and improved output visualisation that have, in overall, provided better results and efficiency in the study and mitigation of natural terrain landslide risk. Secondly, there are technical developments to support the selection of appropriate basal resistance models and use of mobility parameters for assessing the mobility of different types of landslide hazards, such as those within channelised debris catchments with adverse site settings that are prone to the development of sizeable channelised debris flows with high mobility and those within topographic depression catchments. This paper presents the background to the technical advances in debris mobility modelling in the past decade and summarises details of the individual developments.

2 ENHANCEMENTS OF NUMERICAL TECHNIQUES

2.1 Two-dimensional debris mobility modelling

In light of the simplicity of 2D modelling over its 3D counterpart, 2D debris mobility modelling tools have been widely adopted in daily practice for natural terrain hazard studies and detailed design of natural terrain mitigation measures in the last decade. Among the 2D debris mobility modelling tools, "2d-DMM" (which stands for two-dimensional debris mobility modelling) which was developed by the GEO (Kwan & Sun 2006) has been one of the most popular tools in Hong Kong. It was coded initially using Visual Basic for Applications on Microsoft Excel, and thus providing a basic, easily-understandable platform for analysis and plotting of numerical results. Nonetheless, with the increasing demand of both computational and graphical performance of 2D debris modelling by the geotechnical profession in recent years, particular under the context of the LPMitP, the computation architecture of 2d-DMM needs to be upgraded to enhance the analytical capability, visualisation, user friendliness, as well as possible integration of the debris mobility modelling package with the GIS, which is frequently used by the geotechnical profession to carry out assignments ranging from desk study of natural terrain hazards to detailed design of natural terrain hazard mitigation measures.

In 2014, the GEO undertook the initiative to revamp 2d-DMM from a program embedded in a spreadsheet to a stand-alone Microsoft Windows application, by means of the modern multi-paradigm programming language C#. Brought by the change of the programming architecture, the revamped 2d-DMM (Version 2.0) is more extensible to additional features and compatible with third-party programs. With these advantages, new customisations were made on the revamped 2d-DMM (Version 2.0) to suit the need of routine geotechnical study and design, such as to enable specification of any number of "block" (an element which represents landslide debris) to represent the landslide debris, resulting in more precise computation results. Also, new graphical post-processing features such as on-the-run generation of various hydrographs, (i.e. the time history of an attribute, velocity for example, of the landslide debris over stationary reference locations, e.g. the proposed location of structural measures to contain landslide debris) are provided. The user interface of the revamped 2d-DMM (Version 2.0) is given in Figure 1.

The GEO continued its effort to enhance the user experience of 2d-DMM (Version 2.0) by incorporating 2d-DMM (Version 2.0) in ArcGIS Desktop. As GIS technology is becoming more popular in Hong Kong, the geotechnical professionals rely increasingly on the capability of GIS to display and analyse spatial data in relation to the study and design of natural terrain hazards and their mitigation measures. Recently, ArcGIS has been widely adopted in the geotechnical industry to analyse and exchange spatial data for planning, investigation and design purposes. Typically, the topography of a study area of natural terrain based on Light Detection and Ranging (LiDAR) data is stored in the digital elevation model (DEM) on the ArcGIS platform. With the ArcGIS application for 2d-DMM, the vertical profile of the flow path, which is an essential input for the debris mobility analysis, can be generated automatically and more accurately based on the DEM. In addition, a batch of numerical runs along various prescribed flow paths may be

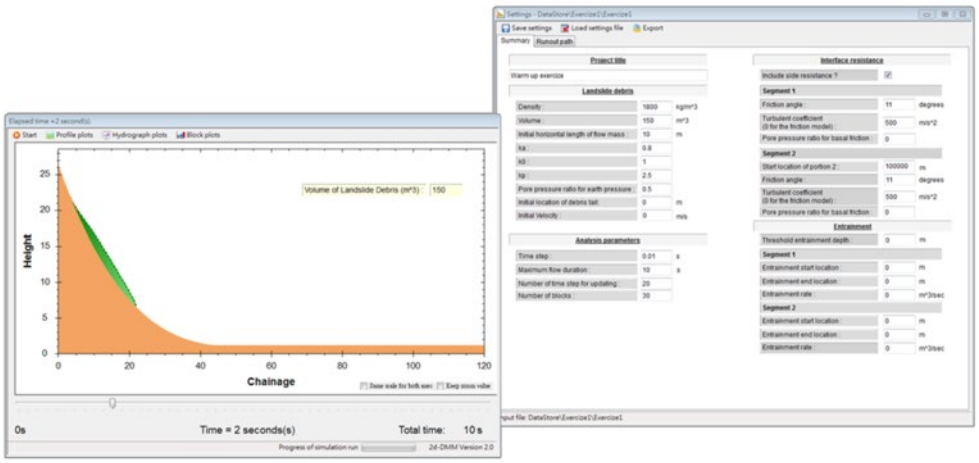

Figure 1: Graphical user interface of 2d-DMM (Version 2.0)

specified using the ArcGIS application for 2d-DMM calculations, thus eliminating the manual effort in carrying out 2D simulation for each flow path one-by-one. In addition, numerical results, such as the runout distance and the hydrographs, may be shown on the ArcGIS platform directly. With such integration, 2D debris mobility modelling may now be carried out directly on ArcGIS in a more accurate and efficient manner, bringing values at different design stages of natural terrain hazard mitigation measures.

In order to ascertain that the revamped 2d-DMM (Version 2.0) is capable of producing reliable numerical results, the program was validated against the field observations of historical natural terrain landslides in Hong Kong, as well as against the previous version of 2d-DMM which has already been well-validated before. The validation work indicated that the revamped 2d-DMM (Version 2.0) is consistently capable of producing results that match closely the field observations and results produced by the previous version of 2d-DMM. The 2d-DMM (Version 2.0) is now one of the standard software packages for geotechnical study of natural terrain hazards and design of mitigation measures in Hong Kong.

2.2 Three-dimensional debris mobility modelling

While 2D simulation strikes a good balance between computation efficiency and modelling capacity, it has its own limitations. For example, 2D simulation cannot explicitly calculate the change of landslide motion due to the presence of transverse bends, nor be able to model the splitting of landslide debris passing through a bifurcation of drainage lines. In these cases, 3D debris mobility modelling is preferred. In 2004, the GEO has pioneered the development of 3D debris mobility modelling by adopting the concept of Particle in Cell (PIC). Details of the PIC numerical model is documented in Kwan & Sun (2007). An extra step was made in 2009 to develop a new debris mobility modelling module which made use of the numerical scheme of SPH to simulate the motion of landslide debris in a more computationally cost-effective manner. The SPH model is one of the rapidly evolving, well-recognised by the literature and popular tools to calculate the motion of deformable materials. The formulation principle of the SPH module, in general, followed McDougall & Hungr (2004). The fundamental concept of SPH is to split the landslide debris into smoothed particles which, by means of spatial interpolation, enables a meshless particulate numerical scheme to solve continuum governing equations. The SPH simulation is undertaken in a time-stepping finite difference framework with an initial condition that all the particles are at rest. Formulation of the underlying governing equations of the 3D debris mobility modelling is given in Law et al. (2016).

The SPH module was coded as a stand-alone Microsoft Windows application, and designed to be computationally efficient and extensible in order to allow for easy integration with third-party applications. Nonetheless, labour-intensive pre- and post-processing are the major drawbacks of any 3D analysis. Some tedious steps involved are conversion of the DEM to the coordinates of the topography, calculation of the geometry of the landslide source, import and export of data for simulations and post-processing, as well as generation of engineering plots based on the raw textual outputs. These procedures

may be error-prone and time-consuming, requiring experience to diagnose problems encountered and thus creating a major hurdle to the practical use of the SPH module for day-to-day applications.

In order to tackle such a bottleneck, a one-stop GIS solution has been developed which integrates the SPH module with ArcGIS, through an ArcGIS application that comprises three modules, viz. input module, SPH module and post-processing module. The modules are connected seamlessly such that there is no need to export data from one module to another manually. The input module is responsible for guiding the user to set up the SPH model on the ArcGIS platform in a step-by-step manner. In particular, the module converts raw topography data (e.g. LiDAR point clouds) to the grid-based topography input data for SPH analysis. The module offers an option to trim the topography at the source location considering the detachment of debris material at its basal sliding surface. After the user has entered all the input data, the SPH module is turned on which is capable of running on multiple processors. Based on the computed attributes of the SPH points (e.g. debris thickness, location, velocity), the SPH module prepares the data files for the post-processing module to display the results on the ArcGIS platform. Important engineering plots such as the velocity profile of landslide debris along the flow path, and the time history of the velocity and thickness of the landslide debris passing through a user-specified location in the flow path are available. Export of data to Microsoft Excel format for other analysis is also enabled. Furthermore, landslide animation in three dimensions can be generated in order to facilitate a review of the simulated flow process (Figure 2). The ArcGIS application, bundled with the input module, SPH module and post-processing module, is called the 3d-DMM (Version 2.0). Similar to the 2d-DMM (Version 2.0), validation work was undertaken to confirm that the computer program is capable of producing reliable numerical results. Historical landslides in Hong Kong were back-analysed in the validation work which showed that the 3d-DMM is consistently capable of producing results that match closely the field observations. Details of the validation exercise are given in Law et al. (2016).

Figure 2: Simulated landslide motion in three-dimension using 3d-DMM (Version 2.0)

3 ENHANCED GUIDELINES ON ASSESSMENT OF DEBRIS MOBILITY

3.1 Channelised debris flows

Lo (2000) summarised the findings of back analyses and gave recommendations on the basal resistance model and the associated model parameters for natural terrain landslide simulations in Hong Kong. Lo (2000) suggested to adopt an apparent basal friction angle (ϕ) of 20° when the friction model is used, whereas ϕ = 11° and a turbulence coefficient (ξ) = 500m/s^2 (which have been found to be appropriate by Hungr (1998) and Ayotte & Hungr (1998)), were recommended when the Voellmy model is used to assess the mobility of channelised debris flows. Since the publication of Lo (2000), additional data on natural terrain landslides in Hong Kong have become available and more cases have been back analysed by the GEO.

A systematic back analysis of the known long-runout (i.e. >200 m) historical channelised debris flows in Hong Kong was completed in 2011 using 2d-DMM (Version 1.1). Based on the results, the Voellmy

model would provide a better prediction of the spatial distribution of debris deposition along the runout path, as well as velocity profile where the velocity might be cross-checked against that deduced from the available information, as compared with the friction model. Also, the friction model tends to give a higher predicted velocity profile along the runout path of a channelised debris flow. Similar observations were made by Ayotte & Hungr (1998). In fact, the friction model suffers the defect of being unable to raise the basal resistance under high debris travelling velocity, which does not make physical sense in view of the presence of increased dissipative interactions such as particle collision and turbulence drag anticipated during rapid debris motion. As such, it was concluded that the Voellmy model is a better rheological model for channelised debris flows and that the recommendations of Lo (2000) on the use of friction model for channelised debris flows are no longer applicable (GEO 2011).

In addition to the choice of basal resistance model, the recommended value of input parameters for the Voellmy model for forward prediction of the mobility of channelised debris flows were reviewed with reference to the newly available field records. In particular, back analyses of selected June 2008 channelised debris flows of high mobility were carried out using 2d-DMM (Version 1.1). Based on the results of the back analyses, it is projected that approximately 99% of the June 2008 channelised debris flows were less mobile than that predicted using the recommended Voellmy parameters given in Lo (2000). Thus the recommendations given in Lo (2000) were considered to be robust for forward prediction purposes. As for the approximately 1% of the June 2008 channelised debris flows that were more mobile than that predicted using the recommended Voellmy parameters given in Lo (2000), most of these landslides involved adverse site settings and watery debris (i.e. debris mass with a very high water content) of high mobility. Adverse site settings that are prone to the development of sizeable channelised debris flows with watery debris of high mobility have been diagnosed by Wong (2009). These include the following:

- Sizeable debris flow at a major drainage line (e.g. site with a large catchment and a long flow path where a large amount of storm water and entrainable materials may be available for mixing with the landslide debris).
- Sizeable debris flow along a major drainage line into which many tributaries are feeding (i.e. possible sudden increase in the water content of the moving debris whenever the debris passes through a confluence point).
- Discharge of debris onto a pool of water on the drainage line or debris from a small drainage line onto a major drainage line, where there is a potential for a large amount of running storm water.

For forward prediction of channelised debris flow catchments that are deemed to be prone to watery debris (e.g. with any of the above adverse site settings), the following Voellmy parameters are recommended: $\phi = 8°$ and $\xi = 500$ m/s^2. Further details of the review of the mobility modelling of channelised debris flows are given in GEO (2011).

3.2 Failures within topographic depressions

Ho & Roberts (2016) described two main types of natural terrain landslide hazards in Hong Kong, viz. channelised debris flows and open hillslope landslides. However, there are occasions where a natural terrain landslide does not fit in neither the classification of channelised debris flow nor open hillslope landslide. With continuous and focused effort in landslide study, Wong et at. (2006) introduced an additional hazard type to deal with the intermediate situation between channelised debris flow and open hillslope landslide. The new hazard type is associated with failures occurring within topographic depression catchments (TDF). Following the identification of TDF, systematic back analyses were carried out to study the runout characteristics of TDF in order to identify the suitable set of model parameters for forward prediction of TDF in Hong Kong. Historical landslides in Hong Kong were selectively reviewed, with emphasis on mobile landslides (runout distance exceeding 100 m) that occurred within topographic depressions. The site settings of these cases were reviewed using the 1:1000-scale topographic maps and aerial photographs to ensure that they are genuine TDF. The actual runout distances of the selected TDF

were critically examined based on site-specific aerial photograph interpretation to discard uncertain runout measurement, such as debris runout due to secondary washout.

The turbulent action involved in the debris motion of TDF is expected to be present, though less than that of CDF. The basal resistance may, therefore, be modelled using the Voellmy model. As discussed above, when using the Voellmy model to assess the mobility of CDF, a turbulence coefficient = 500 m/s^2, is considered appropriate. Based on the numerical formulation of the Voellmy model (Hungr 1995), mobility analyses using a high turbulence coefficient, e.g. 5000 m/s^2 or more, would render the turbulence effect negligible and thus produce results comparable to those derived from the friction model with the use of the same apparent friction angle. Based on the above argument, the back analyses adopted the Voellmy model as the basal resistance model, with the turbulence coefficient within the range of 500 m/s^2 to 5000 m/s^2, by using the computer program 2d-DMM (Version 1.2).

A matrix of probable Voellmy runout parameters (Figure 3) was considered in order to identify the most appropriate set of rheological parameters for forward prediction of the debris mobility of TDF in Hong Kong. Among the rheological parameters considered, the one with apparent basal friction angle (ϕ) = 18°, turbulence coefficient (ξ) = 1000 m/s^2, give runout distances larger than the actual distances analysed for majority of the cases. Having regard to the nature of the dataset, results of the above sensitivity analyses, uncertainties involved and dependence of runout distance on the severity of rainfall, the rheological parameters, ϕ = 18°, ξ = 1000 m/s^2, are recommended for forward prediction of the debris mobility of TDF in general. Nonetheless, case-by-case assessments of the suitable input parameters are still necessary when more mobile historical landslides in the TD catchments are identified.

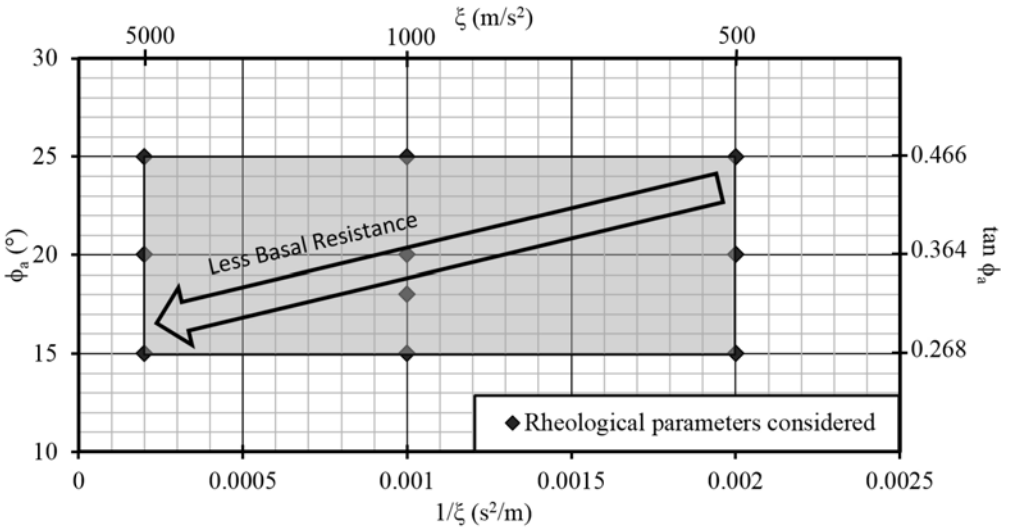

Figure 3: Range of Voellmy parameters considered (GEO 2013)

The recommended Voellmy parameters (ϕ = 18°, ξ = 1000 m/s^2) was tested against a TDF in Kau Lung Hang Shan, Tai Po, which was mapped in detail and super-elevation data were available (GEO 2006). Debris velocity at different points along the runout path were deduced from the super-elevation data, which were compared with the predicted debris velocity profile. Figure 4 shows that the suggested rheological parameters provide a reasonably good fit to both the velocity data and runout distance (within about 10%). Further details of the review of the mobility modelling of TDF are given in GEO (2013).

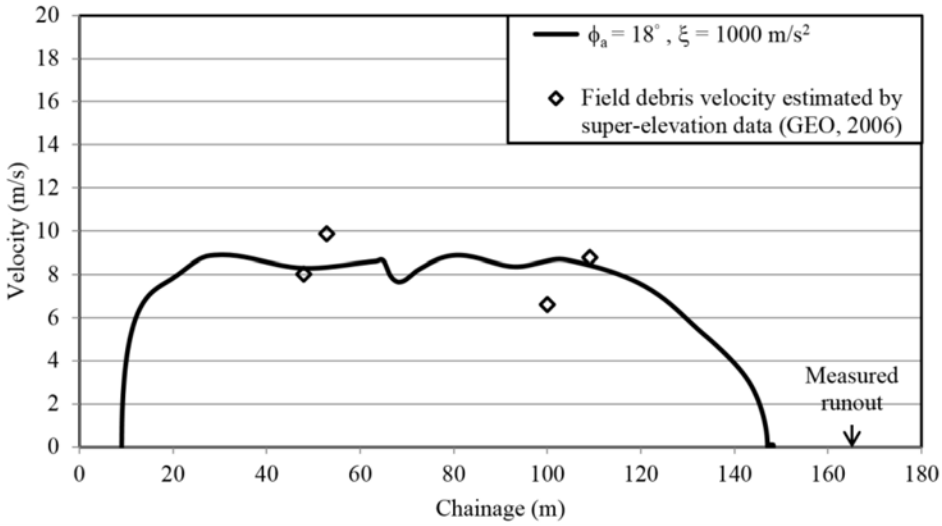

Figure 4: Comparison of predicted debris velocity profile using ϕ_a = 18°, ξ = 1000 m/s² and field debris velocity (GEO 2013)

4 DISCUSSIONS

GEO (2011) recommended to consider 3D debris mobility models to simulate debris flows over irregular and complex terrain profiles (e.g. without a well-defined channel alignment, drainage lines with abrupt bends, splitting of debris at bifurcation of drainage lines etc.), and estimate the lateral spread of debris at the outlets of drainage lines. With the launch of 3d-DMM (Version 2.0), the practical deployment of 3D debris mobility modelling in geotechnical study and design becomes more convenient, and thus practitioners are encouraged to use more frequently 3d-DMM (Version 2.0) or subsequent updates in their geotechnical studies and designs.

On the other hand, GEO (2011) recommended to use DEM derived from multi-return air-borne LiDAR to develop debris mobility models. Experience has been gained recently in relation to the choice of appropriate grid size of DEM for 3D debris mobility simulations. For a standard desktop computer with 8 GB of Random-access Memory (RAM), 3d-DMM (Version 2.0) handles in general DEM of about 2,500,000 pixels without encountering computational problems. This is equivalent to the use of a 2 m x 2 m DEM for most of the hillside catchments in Hong Kong. A 2 m x 2 m DEM is considered sufficiently fine to realistically represent the topography of most of the natural terrain and its surrounding features. Figure 5 shows the results of 3D debris mobility modelling in which a 2 m x 2 m DEM was adopted to simulate a number of natural terrain landslides moving along the drainage line and overflowing onto the adjoining man-made features, a dual single-lane road, and a nullah of about 6.5 m wide and 4.5 m deep. The results that the effect of the topography using the 2 m x 2 m DEM to the landslide mobility could have been duly accounted for in the simulations. A 2 m x 2 m DEM seems to provide results that strike a good balance between calculation accuracy and efficiency. Nonetheless, attention shall be paid to certain geometrical characteristics of flow paths (e.g. very narrow flow path) which may demand finer DEM grid than 2 m x 2 m.

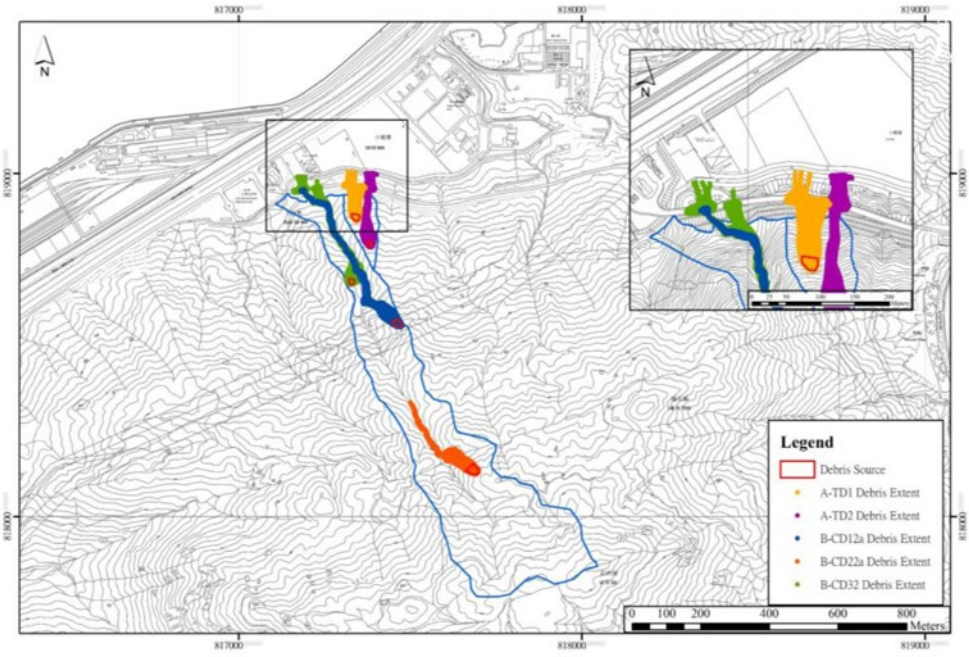

Figure 5: Example of 3d-DMM (Version 2.0) simulations using a 2 m x 2 m DEM

5 CONCLUSIONS

Debris mobility modelling has made major advances in the past decade. With the continuous improvements in computer technology and understanding of behaviour of natural terrain landslides through field observations and physical tests, more major developments in debris mobility modelling and applications are anticipated in the future.

ACKNOWLEDGEMENTS

This paper is published with the permission of the Head of the Geotechnical Engineering Office and the Director of Civil Engineering and Development, Government of the Hong Kong Special Administrative Region.

REFERENCES

Ayotte, D. & Hungr, O. 1998. *Runout Analysis of Debris Flows and Debris Avalanches in Hong Kong.* A Report for the Geotechnical Engineering Office, Hong Kong. University of British Columbia, Canada, 90 p.

GEO 2006. *The 5 May 2003 Debris Flow at Kau Lung Hang Shan, Tai Po (GEO Report No. 196)*. Geotechnical Engineering Office, Hong Kong, 84 p.

GEO 2011. *Guidelines on the Assessment of Debris Mobility for Channelized Debris Flows (Technical Guidance Note No. 29)*. Geotechnical Engineering Office, Hong Kong, 6 p.

GEO 2013. *Guidelines on the Assessment of Debris Mobility for Failures within Topographic Depression Catchments (Technical Guidance Note No. 38)*. Geotechnical Engineering Office, Hong Kong, 8 p.

Ho, H.Y. & Roberts, K.J. 2016. *Guidelines for Natural Terrain Hazard Studies (GEO Report No. 138 (Second Edition))*. Geotechnical Engineering Office, Hong Kong, 173 p.

Hungr, O. 1995. A model for the runout analysis of rapid flow slides, debris flows and avalanches. *Canadian Geotechnical Journal*, 32: 610-623.

Hungr, O. 1998. *Mobility of Landslides in Hong Kong: Pilot Analysis Using a Numerical Model*. A Report for the Geotechnical Engineering Office, Hong Kong. O. Hungr Geotechnical Research Inc., Canada, 52 p.

Kwan, J.S.H. & Sun, H.W. 2006. An improved landslide mobility model. *Canadian Geotechnical Journal*, 43(5): 531–539.

Kwan, J.S.H. & Sun, H.W. 2007. Benchmarking exercise on landslide mobility modelling - runout analyses using 3dDMM. *Proceedings of the International Forum on Landslide Disaster Managemen*t. Hong Kong, vol. II: 945-966.

Kwan, J.S.H., Wong, T.K.C. & Ko, F.W.Y. 2007. Development and applications of debris mobility modelling in assessment of natural terrain landslide hazards. *Proceedings of the HKIE Geotechnical Division 27th Annual Seminar on Geotechnical Achievements in Hong Kong since 1970s*. Hong Kong Institution of Engineers (HKIE): 241-247.

Law, R.P.H., Kwan, J.S.H. & Ko, F.W.Y. 2016. *Validation of Geotechnical Computer Program "3d-DMM (SPH Version 2.0)". (Technical Note No. 3/2016)*. Geotechnical Engineering Office, Hong Kong, 57 p.

Lo, D.O.K. 2000. *Review of Natural Terrain Landslide Debris-resisting Barrier Design (GEO Report No. 104)*. Geotechnical Engineering Office, Hong Kong, 91 p.

McDougall, S. & Hungr, O. 2004. A model for the analysis of rapid landslide motion across three-dimensional terrain. *Canadian Geotechnical Journal*, 41: 1084–1097.

Soga, K., Alonso, E., Yerro, A., Kumar, K. & Bandara, S. 2016. Trends in large-deformation analysis of landslide mass movements with particular emphasis on the material point method. *Géotechnique*, 66(3): 248–273.

Wong, H.N. 2009. Rising to the Challenges of Natural Terrain Landslides. *Proceedings of the HKIE Geotechnical Division Annual Seminar on Natural Hillsides: Study and Risk Management Measures*. Hong Kong Institution of Engineers: 15-53.

Wong, H.N., Ko, F.W.Y. & Hui, T.H.H. 2006. *Assessment of Landslide Risk of Natural Hillsides in Hong Kong (GEO Report No. 191)*. Geotechnical Engineering Office, Hong Kong, 117 p.

Minimizing Traffic Impact Arising from Upgrading of a Roadside Man-made Slope: from Ideas to Implementation

Keith P.W. Leung
Arcadis Design & Engineering Limited
Alfred Y.C. Wong
Hyder-ESA Joint Venture
Rupert K.Y. Leung
Arcadis Design & Engineering Limited

ABSTRACT

Upgrading works for steep roadside man-made features along heavily trafficked roads in Hong Kong has long been a problem to slope engineering practice due to the potential impact to the road users caused by temporary closure of traffic lanes. This problem is especially more acute for slopes along busy roads along hillside at the south of Hong Kong Island, where pedestrian footpath along slope toe is often not provided. Under such circumstances, temporary traffic arrangement measures with 24-hours road closure or detour would be extremely difficult as it is often the case that the road is the only route in the traffic network. Hence, success of slope upgrading works along heavily trafficked roads is much dependent on having a temporary traffic arrangement scheme with minimal traffic impacts. A roadside slope along one of the major roads at the south of Hong Kong Island, Tai Tam Road, was selected for upgrading under CEDD Agreement No. CE29/2012(GE), one of the first government consultancies to adopt the Innovation and Creativity Proposal for consultant selection. Various ideas were put into the proposal to minimize the need for traffic lane closure, among them was the use of an excavator-mounted drilling rig for rock dowel and soil nail installation. The use of the excavator-mounted drilling rig has allowed upgrading of slope successfully carried out within a limited time frame from November 2016 to March 2017. This paper discusses how the ideas were brought forward from proposal stage to actual implementation. Comparison with other construction methods for roadside soil nail installation also shows the advantages of the excavator-mounted mobile drilling rig in terms of flexibility and safety.

1 INTRODUCTION

Slope upgrading works along heavily trafficked roads, especially for roads at the south of Hong Kong Island where pedestrian footpath is not provided, is one of the major challenges for slope engineering practice in Hong Kong. Major difficulties of upgrading roadside slopes were well documented (Lee et al. 2011; Ho et al. 2011; Wong et al. 2011). Commonly encountered ones include (i) traffic impact, (ii) limited work space, (iii) tree felling and landscaping treatment, (iv) public concerns. Apart from the

* "Hyder Consulting Limited" is currently known as "Arcadis Design & Engineering Limited"

conventional method of using scaffolding, other methods have been developed and tried for upgrading of roadside slopes within the limitation of the constraints, as further elaborated in Section 3. The subject of this paper is a steep roadside cut slope, Feature No. 11SE-D/C143 (referred as "the Feature" hereinafter), which was selected for studying and upgrading under CEDD Agreement No. CE29/2012(GE) as a pilot case of adopting the "Innovation and Creativity Proposal (ICP)" approach for consultant selection. The awarded consultants (i.e., Hyder*-ESA Joint Venture) proposed, in their ICP, to use a mobile drilling rig for installation of soil nails and rock dowels as an alternative to conventional construction method using scaffolding. Coupled with the adoption of prescriptive design approach to avoid the need of ground investigation, the combination of ideas served to mitigate the need of 24-hours lane closure and, in turn, minimize the traffic impacts induced by the slope upgrading works. This paper outlines the development of the above ideas from proposal stage to actual implementation and, in particular, how the use of excavator-mounted mobile drilling rig was put into practice. Advantages and limitations of the mobile drilling rig, as compared to other methods, are also presented. Upgrading of the Feature, comprising installation of 80 soil nails, 49 rock dowels and shotcreting of approximately 500m^2 of slope surface was commenced in November 2016 and completed in March 2017 before the rainy season.

2 SITE DESCRIPTION

The Feature is located at the junction of Tai Tam Road and Shek O Road, which is the main route to the bathing beaches at Shek O. At this location, the road is an approximately 7m wide single 2-lane carriageway with no pedestrian footpath at slope toe. The Feature is approximately 10m high and 50m long with an average slope gradient of 80^0. Location plan and general view of the Feature are shown in Figure 1 and Plate 1 below.

Figure 1: Location plan of the Feature

Plate 1: General view of the Feature

3 IDEAS PRESENTED IN INNOVATION AND CREATIVITY PROPOSAL

Key ideas presented in the ICP submitted by the Consultant are as follows:

i. Use of prescriptive design approach to avoid ground investigation;

ii. Use of a excavator-mounted drilling rig for soil nail and rock dowel installation to avoid 24-hour road closure; and

iii. Temporary Traffic Arrangement Scheme to maintain traffic flow at the roundabout during lane closure.

3.1 Prescriptive Design Approach

In order to minimize the traffic impacts caused by the slope upgrading works, prescriptive design approach was proposed in the ICP to mitigate the need of road closure for ground investigation works. A detailed review of the history and performance of the Feature was carried out to ensure the qualifying criteria for prescriptive design as recommended in GEO Publication No. 1/2009 (GEO, 2009) were met. Photographs of the Feature before shotcreting (Plate 2) and the previous ground investigation carried out at an adjoining slope were also reviewed to gain a better insight into the geology of the Feature. The Feature was revealed to have its upper portion composed of highly to completely decomposed tuff and its lower portion of moderately decomposed tuff.

Plate 2: View of exposed surface of the Feature

3.2 Excavator-mounted Mobile Drilling Rig

Apart from the conventional method of using scaffolding, contractors in the past have tried different methods to provide temporary working platform for installation of soil nails and rock dowels at roadside slopes. They are shown in Figure 2.

There are various limitations associated with the above-mentioned methods. The conventional method of scaffolding, while working well for gentler slopes, will encroach into the carriageway if the slope is steep, as will be the case here, that either 24-hour road closure is required or the scaffolding needs to be dismantled and re-erected the next day to allow unrestricted traffic flow after the working hours. The three options of raising a working platform from a vehicle, while allowing mobility, presents higher risk to workers in particular when required to reach a great height.

The idea of excavator-mounted mobile drilling rig was borrowed from drilling jumbos widely used in tunneling projects for drilling blast holes and holes for rock bolts in hard rock tunneling. The Project Team had studied and reviewed the operational mechanism of drilling jumbo and proposed to mount the drill for soil nail and rock dowel on an excavator such that the mobility of the soil nail/rock dowel drilling operation could be greatly enhanced. With the aid of excavator-mounted mobile drilling rig, 24-hours lane closure would no longer be necessary such that arrangement of the slope upgrading works could become more feasible. In addition, with the drill mounted directly to the excavator, the system offers much better stability as compared to previous methods involving mounting the drill on an elevated or hanged working platform proposed by others. The risks associated with workers on the

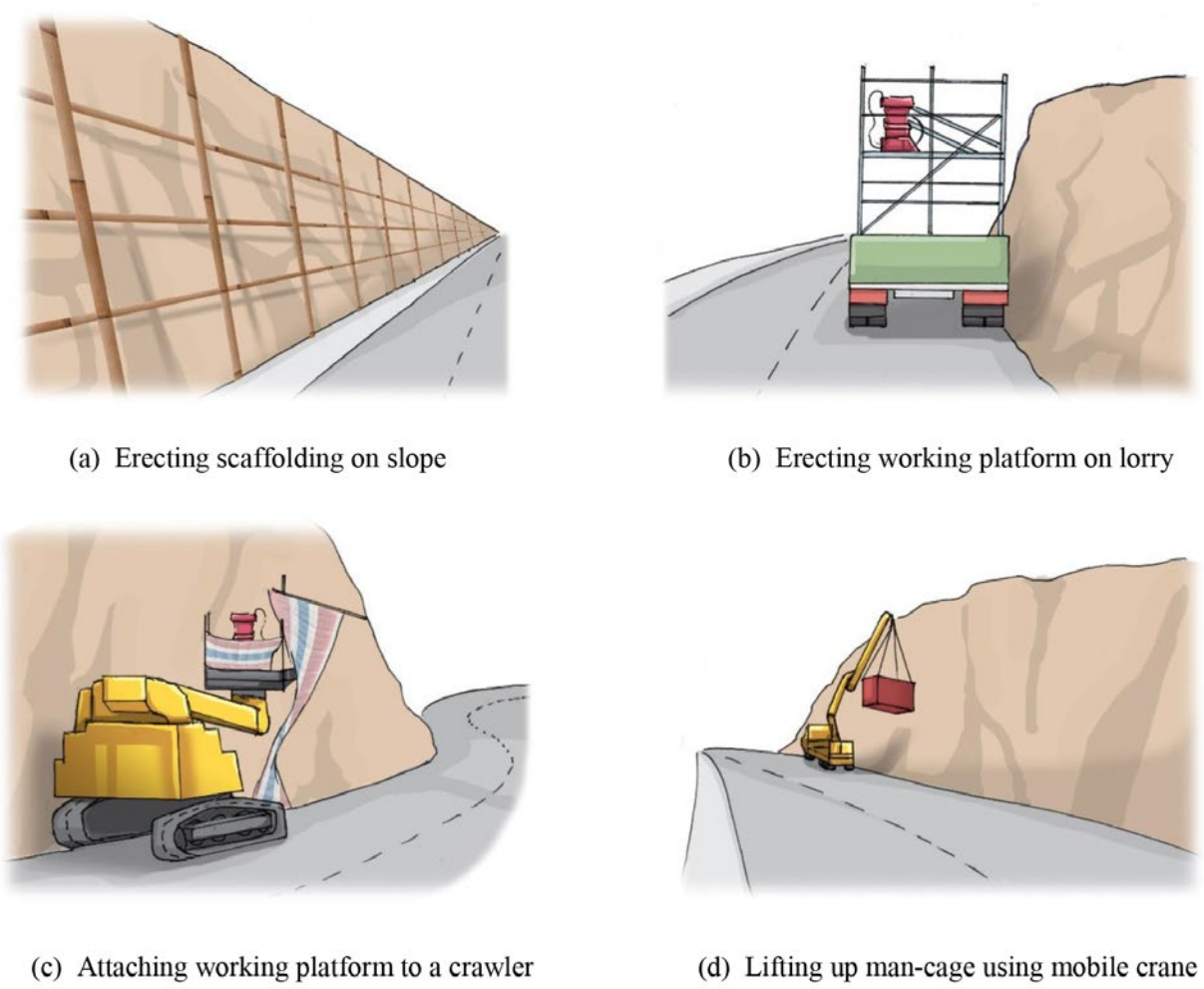

(a) Erecting scaffolding on slope

(b) Erecting working platform on lorry

(c) Attaching working platform to a crawler

(d) Lifting up man-cage using mobile crane

Figure 2: Tried methods for providing working platform for upgrading roadside slopes

working platform for drilling are also be mitigated. This is of particular importance in the consideration that the risk of overall failure of the working platform may be overlooked as revealed in recent fatal accidents related to falling from height. Conceptual figure of the proposed excavator-mounted mobile drilling rig is presented below.

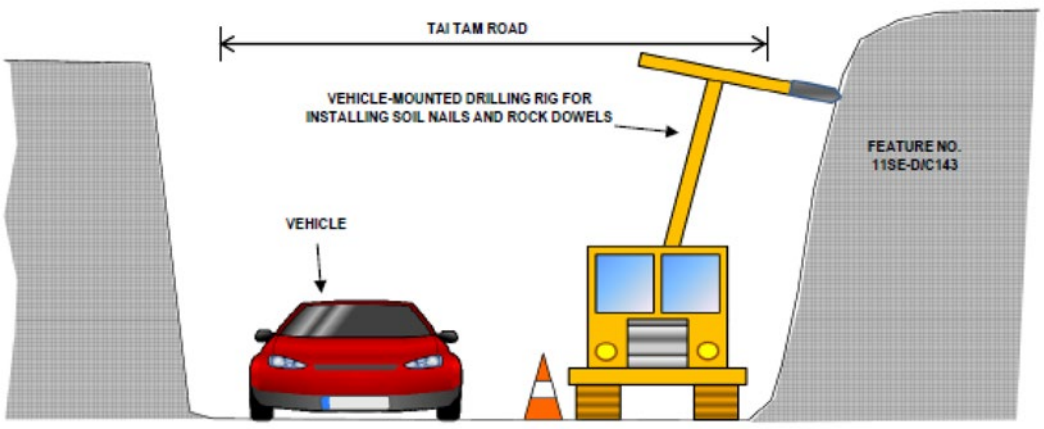

Figure 3: Conceptual figure of mobile drilling rig

3.3 Preliminary Design of Temporary Traffic Arrangement Scheme

As the Feature is located at the junction of Tai Tam Road and Shek O Road, 24-hour road closure was not practicable in consideration of the safety of road users, especially at night when no traffic controller would be available and the vision would be limited. Taking cognizance of the characteristic of Tai Tam Road and Shek O Road, as well as the need to maintain full-time road access to Shek O and other parts of the Southern District, especially for emergency services, a TTA scheme with daytime-only (from 10:00 to 16:00 hours) closure of the lane in front of the slope (i.e. eastbound traffic lane), as shown in Figure 4, was proposed.

Shek O Road is the main access route to the bathing beaches at Shek O. It was anticipated that the volume of traffic during the swimming seasons would increase substantially. Meanwhile, the Feature is also located in close proximity to the Cape Collison Columbarium where special traffic measures would be implemented around Ching Ming Festival (normally in April) and Chung Yeung Festival (normally in September/October) during which the area would be crowded with grave-sweepers. Hence, it was considered necessary to further minimize the traffic impact to the public by restricting the temporary lane closure to the period after Chung Yeung Festival and before Ching Ming Festival, i.e. from October to March.

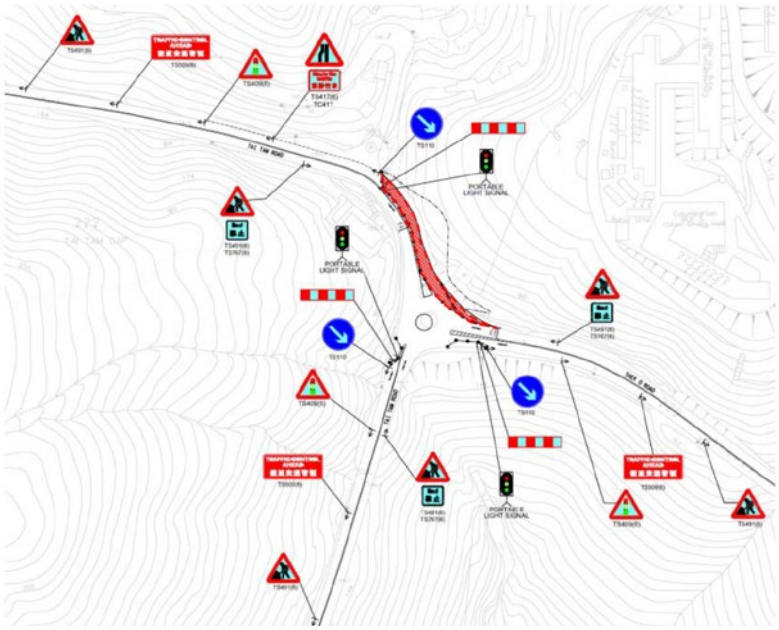

Figure 4: Preliminary temporary traffic arrangement scheme

4 DETAILED DESIGN DEVELOPMENT

4.1 Prescriptive Design of Slope Upgrading Works

As mentioned in Section 3.1, prescriptive design approach was adopted in the detailed design of the slope upgrading works. Based on the prescriptive design, 80 nos. of 6m long 25mm diameter soil nails with double corrosion protection at 1.5m c/c horizontal spacing installed at 20° inclined to horizontal and patterned 4m and 6m long 32mm diameter rock dowels (49 nos. in total) at 2m c/c horizontal spacing were proposed. The final design of the slope upgrading works is presented in Figure 5 below.

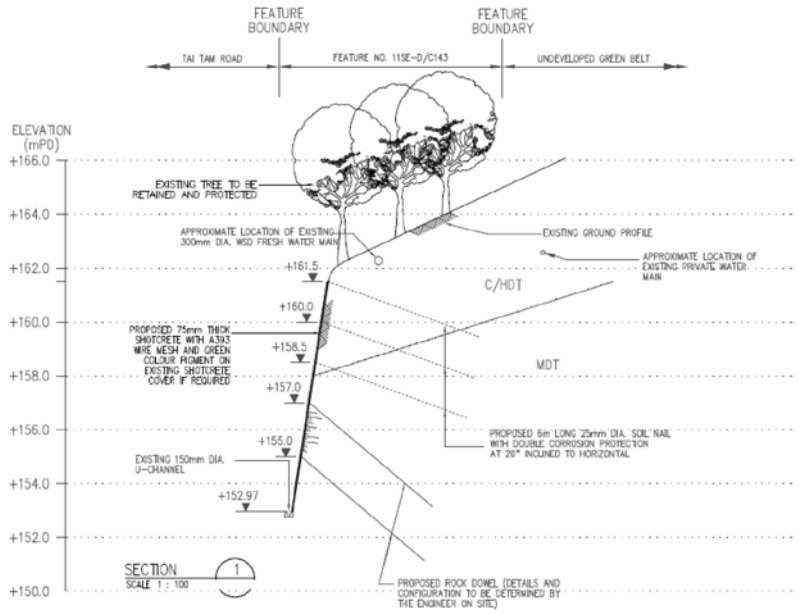

Figure 5: Final design of slope upgrading works

4.2 Assessment of the Method of Implementation of Using Excavator-mounted Mobile Drilling Rig

In order to gain a more in-depth understanding of the latest drilling technology, the Project Team carried out discussion with local and overseas suppliers, tapping their experience on the manufacturing and supply of excavator-mounted mobile drilling rigs, or the like. Product catalogues and quotations of such drilling rigs previously used in other projects were collected and reviewed in detail to facilitate the assessment of the cost implication and method of procuring the excavator-mounted mobile drilling rig for use in the upgrading works.

4.3 Detailed Design of Temporary Traffic Arrangement Scheme

Site inspections were carried out to review if the operational dimension of the proposed excavator-mounted mobile drilling rig is compatible with the temporary traffic arrangement scheme. The operational width of the excavator-mounted mobile drilling rig was thus set to 3m. The proposed temporary traffic arrangement scheme was submitted to Transport Department (TD) and Hong Kong Police Force (HKPF) for approval prior to the award of the works contract to ensure timely commencement of the work.

5 CONTRACT PROVISIONS

The subject Feature was one of the man-made slope features upgraded under a Schedule of Rates (SoR) contract. To ensure that the developed methodology of using an excavator-mounted mobile drilling rig would be used for installation of soil nails / rock dowels, it was essential to make the corresponding provisions in the contract documents. The provision of an excavator-mounted drilling rig was set as an extra-over item for the soil-nailing / rock-doweling works in the SoR. Specification of the excavator-mounted mobile drilling rig was provided in the Particular Specification, making reference to the information gathered during the detailed design stage.

6 IMPLEMENTATION

6.1 Procurement / fabrication of Mobile Drilling Rig

Prior to the commencement of works, the Contractor had been seeking suitable machineries to procure / fabricate the excavator-mounted mobile drilling rig being capable to carry out the drilling works at the Feature. Different types of drilling rigs and excavators from overseas, Mainland China and Hong Kong had been evaluated to cope with the limited space in the cordoned zone and to reach the required drilling height. After considering essential factors including the cost and time in purchasing, delivery and maintenance, the Contractor eventually decided to appoint a Mechanical Engineer to custom-made a mount for the drill to allow the drill to be attached to excavators of different sizes to suit working space limitation and height requirement. Site trials were carried out at the site depot, using a concrete block to simulate a rock slope surface, under the supervision of the Consultants' supervisory staff. The performance of the excavator-mounted mobile drilling rig system in terms of buildability, stability and workability was considered satisfactory during the site trials.

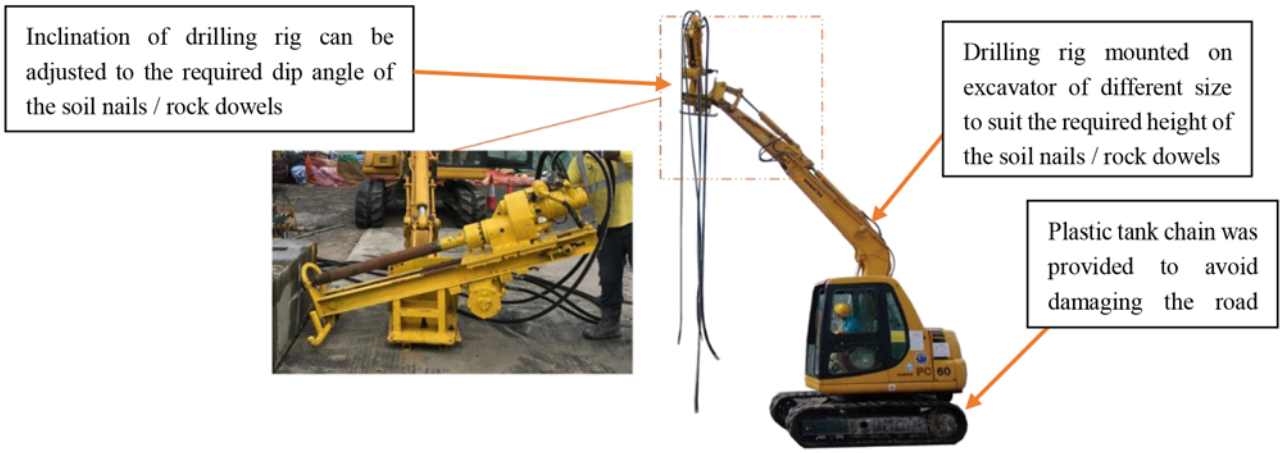

Plate 3: Excavator-mounted mobile drilling rig fabricated by the Contractor

Plate 4: Site trial at the Site Depot

6.2 Development of Temporary Traffic Arrangement (TTA)

The Contractor submitted a TTA Scheme to the TD in August 2016 for approval. Two trial runs were conducted in September 2016 and November 2016 respectively. Representatives from the bus operator and the HKPF were invited to assess the practicability of the scheme, taking into account the traffic volume, maneuverability of long vehicles and the adequacy of traffic signage on site. Arising from the trials, the road closure area was allowed to be enlarged as shown in Figure 6.

As stipulated by TD's approval, the TTA should only be implemented from 10:00 to 16:00 on Monday to Friday from mid-November 2016 to end-March 2017.

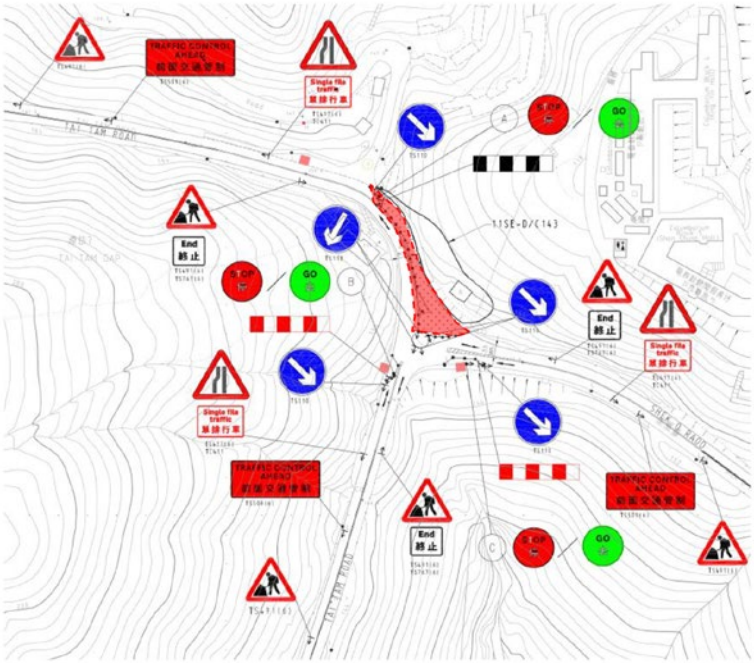

Figure 6: Final temporary traffic arrangement scheme

6.3 Construction Stage

The mobile drilling rig mounted on a 6-ton excavator and the auxiliary mobile scissors platform were transported to the storage area near the Feature in end November 2016. It could undertake drilling up to 6m height. The mobile scissors platform served as a working platform for worker to facilitate the drilling and rebar installation works at height. The drilling for rock dowels and soil nails at the lower portion of the Feature was commenced in early December 2016.

The excavator-mounted mobile drilling rig could maneuver to the rock dowel and soil nail setting-out position easily and the inclination of the drilling rig was adjusted to the designated angle by the worker at position. Checking of the specified inclination of the drilling rig was carried out by the Consultants' supervisory staff before the drilling and periodically during the drilling work. If the rock dowel and soil nail were located at height, the use of mobile aerial platform would be required for the worker for adjusting and the supervisory staff for checking the inclination angle of the drilling rig to ensure the requirement was complied. The grouting work for the soil nails and the rock dowels was a separate operation and was carried out concurrently during the drilling operation by the excavator-mounted mobile drilling rig.

Upon completion of all rock dowels and soil nails works up to 6m, the Contractor changed the 6-ton excavator to a 13-ton excavator. The mobile drilling rig mounted on a 13-ton excavator could undertake drilling of the top row of soil nails at 9m height. An additional mobile aerial platform was used as a working platform for the drilling rig operator to control the drilling works at height. As mentioned in Section 3.2 above, due consideration of the safety of working on elevated working platform was well

recognized and, therefore, an independent lifeline with fall arresting device anchoring to secure point at slope crest was provided as a contingency measures for fall of person due to collapse of the working platform.

The allowable working hours was limited to six hours per day under the TTA requirement. Having allowed the time for daily TTA and site setup as well as road cleaning after completion of works, the actual working hours per day was approximately 4½ hours. The average daily drilling production rates of the excavator-mounted mobile drilling rig for the rock dowels and soil nails were 15m and 25m respectively.

All drilling works at Feature No. 11SE-D/C143 by the excavator-mounted mobile drilling rig were completed in mid-February 2017 and the upgrading works for this feature were substantially completed by end-March 2017. The drilling operation by the 13-ton excavator-mounted drilling rig in conjunction with a mobile scissors platform and a mobile aerial platform at the Feature is shown in Plate 5 below.

Plate 5: Implementation of excavator-mounted mobile drilling rig

7 COMPARISON WITH OTHER METHODS

7.1 Advantages of Excavator-mounted Mobile Drilling Rig

Excavator-mounted mobile drilling rig enables drilling operation at locations where conventional scaffolding erection is not feasible and full closure of road lane is not permitted. It can maneuver easily and swiftly to the designated drilling locations and the rig can be adjusted to the specified angles without great difficulties. Comparing with the traditional methods for upgrading roadside slopes as mentioned in Section 3.2 above, drilling operation by the excavator-mounted mobile drilling rig with the support of auxiliary mobile platforms as described above offers several advantages, including: (i) scalability – making use of excavators with different reaches allows great flexibility for installation of soil nails / rock dowels at various height of steep slopes; (ii) enhanced Safety – independent aerial platforms provided for workers, instead of confining the workers and the drilling rig within a man-cage which could jeopardize the workers' safety in case of failure of the moveable parts of the drilling equipment; (iii) ease of application – fabrication / repair of the excavator-mounted mobile drilling rig does not require unique parts, and all the components of the excavator-mounted mobile drilling rig are readily available in Hong Kong, and (iv) theoretically, average production rate would be higher. A tabulated summary and comparison between excavator-mounted mobile drilling rig and other traditional methods for upgrading roadside slopes with limited 1-lane day-time closure only, e.g. from 1000 to 1600 hours, is shown below:

Table 1: Comparison with other common existing methods for upgrading roadside slopes

	Meet Height Requirement?	Meet TTA Requirement?	Daily Labour Requirement	Estimated Daily Production Rate		Remarks
				Soil Nail	Rock Dowel	
Erecting scaffolding on slope	✓	✗	5 x Scaffolders 1 x Operator 1 x Worker 3 x Signal man	12m	5m	Full time scaffolding erection is not allowed for steep slopes as the scaffolding would be occupying Tai Tam Road. Daily erection and dismantling of scaffolding is not practicable considering the limited working hour (from 10:00 to 16:00) for erecting and dismantling an 8m high scaffolding.
Erecting working platform on lorry	Max 3.5m	✓	1 x Driver 1 x Operator 1 x Worker 3 x Signal man	25m	15m	Approximately 15 minutes for drilling soil nails / rock dowels of the same row horizontally (~4 hours for customize the scaffolding to reach required level of soil nails/rock dowels).
Attaching working platform to a crawler	Max 6m	✓	1 x Driver 1 x Operator 1 x Worker 3 x Signal man	25m	15m	Approximately 10 minutes moving time and 30 minutes for setup and secure the mobile platform. Limited working space with the drilling rig may pose safety risk.
Lifting up man-cage using mobile crane	✓	✓	1 x Driver 1 x Operator 1 x Worker 3 x Signal man	25m	15m	Approximately 10 minutes moving time and 30 minutes for setup and secure the man-cage. Limited working space with the drilling rig may pose safety risk.
Excavator-mounted mobile drilling rig	✓	✓	1 x Driver 1 x Operator 1 x Worker 3 x Signal man	25m	15m	Approximately 15 minutes moving time and setup

7.2 Limitations of Mobile Drilling Rig

The maximum drilling height of the excavator-mounted mobile drilling rig is largely dependent on the size and reach of the excavator. Normally the bigger size the excavator, the higher the reach. However, the allowed width of lane closure or any permitted space at toe would limit the size of the excavator that can be used. Although the costs of using the excavator-mounted mobile drilling rig system as described in this paper would be higher due to the initial set up costs, it is believed that with more usage of this new system, the cost would become comparable with that adopting the common existing drilling methods for upgrading roadside slopes.

8 CONCLUSIONS

Slope upgrading works along heavily trafficked roads in Hong Kong, especially in Hong Kong Island, has long been a problem in slope engineering practices due to the traffic impacts induced by road/lane closure. The scheme of slope upgrading works of Feature No. 11SE-D/C143, as studied under CEDD

Agreement No. CE29/2012(GE), has provided an engineering solution that could minimize the traffic impacts induced by temporary road closure.

With the strong support of, the Client's Project Team, and in collaboration with the Contractor, Fraser Construction Company Ltd., the innovative idea of adopting excavator-mounted mobile drilling rig for installation of soil nails and rock dowels was brought into reality. The satisfactory completion of the slope upgrading works demonstrates the feasibility of using excavator-mounted mobile drilling rig in upgrading steep roadside slopes overlooking busy road with very limited working space. The method is also proven effective in enhancing safety of workers and road users. While there is an initial cost for fabrication, the excavator-mounted mobile drilling rig set-up shall prove itself a good investment as it can used again for upgrading similar roadside slopes. It is also illustrated that innovative ideas could be adopted and implemented with a careful and thorough planning of works.

ACKNOWLEDGEMENTS

This paper is published with the permission of the Head of the Geotechnical Engineering Office and the Director of Civil Engineering and Development, the Government of the Hong Kong Special Administrative Region.

REFERENCES

Geotechnical Engineering Office. (2009). *GEO Publication No. 1/2009 - Prescriptive Measures for Man-made Slopes and Retaining Walls.* Hong Kong.

Ho, N. L., & Wright, M. J. (2011). Construction of Slope Upgrading Works Along Busy Road in Hong Kong. *HKIE Geotechnical Division Annual Seminar 2011 - Landslide Risk Reduction through Works: 35 Years of Landslip Preventive Measures Programme and Beyond* (pp. 82-89). The Hong Kong Institution of Engineers.

Lee, F. Y., Chu, B. S., & Wong, T. K. (2011). Challenges of Landslip Preventive Measures Works with Complex Site Constraints: Case Study - Four Slope Features at Coombe Road. *HKIE Geotechnical Division Annual Seminar 2011 - Landslide Risk Reduction through Works: 35 Years of Landslip Preventive Measures Programme and Beyond* (pp. 90-98). The Hong Kong Institution of Engineers.

Wong, V., Kok, T., & Chan, J. (2011). Characteristics of Highways Department Roadside Slope Upgrading. *HKIE Geotechnical Division Annual Seminar 2011 - Landslide Risk Reduction through Works: 35 Years of Landslip Preventive Measures Programme and Beyond* (pp. 130-136). The Hong Kong Institution of Engineers.

Adopting Advanced Technology for Terrain Evaluation

Samson K.H. Leung & Geoffrey G. Pook
Meinhardt Infrastructure and Environment Ltd., Hong Kong

ABSTRACT

Global climate changes have resulted in more frequent occurrence of extreme weather conditions worldwide. In Hong Kong, the torrential rainfall event that occurred in June, 2008 caused widespread natural terrain landslides in the western part of Lantau, and resulted in both Government and public concern on the potential for increasingly severe rain-induced natural terrain geo-hazards. In response to this, various state-of-the-art technologies have been adopted by the Hong Kong geotechnical engineering practitioners over the past decade to facilitate the enhanced evaluation of the natural terrain hazards.

Air Borne LiDAR data have been widely adopted for terrain classification in recent years. The use of UAV and Geomatics can further assist the surveying of terrain characteristics, anthropogenic activities and geomorphological features which were previously inaccessible and obscured by vegetation. This paper presents how the developments of the above advanced technologies is enhancing the evaluation of natural terrain.

1 INTRODUCTION

The susceptibility of an area to landslides is affected by its geological, geomorphological and hydrological setting and terrain evaluation is therefore considered the first step in landslide investigation and evaluation. Aerial photo and satellite image interpretation are widely adopted as data collection methods to assist in terrain evaluation. However, the limitation of the above methods has restricted their ability to increase the accuracy of the terrain evaluation in civil use. Over the last two decades, the use of air-borne LiDAR and high resolution satellite image have become more common in both commercial and civil sectors around the world with LiDAR, in particular, commonplace in Hong Kong. Unfortunately, these technologies are still hindered by high cost and limited frequency. Therefore, new technology such as unmanned aerial vehicle (UVA) LiDAR and Photogrammetry are introduced. These new technologies may be able to overcome some, or even all, of the limitations of current available technologies.

2 AERIAL PHOTO AND SATELLITE IMAGE INTERPRETATION

Aerial photography and space-borne remote systems have long been considered a significant aid to the more traditional terrestrial data collecting techniques. The increase in data sources provides greater flexibility for resolution of observations and verification. With at least 10 civilian satellites currently in orbit and around 10 additional upcoming in the next few years, the potential for available data at higher resolutions is increasing (Zhang, 2017).

The methods of air- and space-borne remote sensing possess numerous advantages of ground based methods (Gilvear and Bryant, 2005):

- enhanced spatial and temporal resolution of data collection
- improved storage of data in digital format allowing for shorter turnover time for interpretation and providing access to a larger and more dynamic sample population

- increased scope of data collection including electromagnetic radiation (EMR) emitted or reflected from land and water

Tangible positive effects of remote sensing data can only achieve their potential if field-based methods are used to support remotely sensed data. By way of an example, geomorphological data obtained from mapping traverses coupled with an assessment of GI to produce geological cross-sections in catchments can be extended to inaccessible areas. Additionally, the scale of observed features can be increased with support from remotely sensed data. Image analysis can be applied to remotely sensed data to provide information, such as temporal changes or surface material, on catchments and land-use into a landscape scale which can then be verified through site inspection.

Considerations for use of remote sensing techniques (adapted from Gilvear and Bryant, 2005):

- Size of site and accessibility of data:
  - Drones/UAVs for scale of less than 0.5km
  - Airborne for 0.1-1km
  - Satellite for >1km
- Spatial resolution required:
  - image format/size can hinder identification of small isolated features
  - catchments may have elongated shape which requires multiple images fixed together
- Nature of land cover or sub-surface properties to be detected
- Degree of precision and accuracy acceptable
- Frequency with which changes might need to be detected

Image analysis of aerial photographs using correlation between light reflectance and terrain features such as exposed rock, boulders and water bodies (Gilvear and Bryant, 2005) is a commonly adopted technique. These observations can be verified through ground data collected contemporaneously with the image. Colour photography is particularly useful in that subtle differences in land cover that relate to topography and geology are more easily seen. Cloud cover can be a problem in mapping by aerial photography and as such the all-weather capability of radar is generally considered more attractive. Offsetting this is that fact that aerial photographs can feasibly be scheduled and carried out upon request depending on size and scale of project with subsequently a lower cost incurred for air-borne photography as opposed to air multi-spectral scanners.

Space-borne remote sensing techniques include both electromagnetic radiation (EMR) and synthetic aperture radar (SAR). EMR reflections are dependent on location, time, geometry of observation and waveband. While SAR interferometry has been used to assess erosion and deformation/settlement using sequential DEMs and phase coherence to record relative changes in the condition of a surface (Gilvear and Bryant, 2005, Zhang, 2017). Deformation and ground movement can be detected using phase shift algorithms, with the highest resolution currently achieveable in the order of 1m with the resultant measurable deformation at the mm scale (Zhang, 2017). These techniques are limited due to temporal resolution, currently around 11 days, which means the actual benefits from using satellite techniques are maximised if used in conjunction with ground monitoring points. This can achieve a balance between temporal and spatial limitations of the both satellite and terrestrial methods but serves to underline the limitations of both methods used in isolation. The integration of global positioning systems with image capture on a variety of satellite platforms allows for the identification of absolute location. This can also allow measurements taken on the ground to be linked to individual pixels on imagery allowing for more accurate calibration and validation (Gilvear and Bryant, 2005). The use of space-borne multi-spectral scanners allows the identification of the following features from spectral response curves: water and shadow; trees and vegetation; exposed sediment e.g. broken ground, boulder/outcrop or anthropogenic activity. In detection of terrain, however, vegetation will likely result in noise if the wave length is insufficient to penetrate the ground cover. This results in DEM models rather than DTM which have limited application to the detection of natural terrain instability concerns.

A strong understanding of the factors affecting the interaction with the surface and capturing by the sensor are required in order to fully utilize the data. Fundamentally, most features can only be differentiated if the reflectance of the measured wavelengths is different from that of adjacent features. Literature, spectral libraries or field collection of image/spectra reflectance data can be used to aid in the identification of the captured data (Gilvear and Bryant, 2005). The technique of space-borne remote sensing is often limited to producing only a DEM which does not isolate topography and also includes trees and building heights (Nico et al., 2005). This limits the applicability to small scale sites where local, subtle changes are more influential. Space-borne image analysis is dependent on the following factors when differentiating between terrain features:

- Radiometric resolution of the sensor
- Atmospheric scatter
- Surface roughness of features
- Spatial variability of reflectance within wider field of view
- Uneven radiation capture due to variations in illumination

With the remote sensing techniques providing large, dynamic sample populations, it is useful to consider the implications and potential costs of adopting such methods to facilitate terrain analysis. With regards to aerial photographs (see Figure 1), high purchase costs and significant procurement time are required for acquiring photos covering large areas. Regarding the use of satellite imagery for a particular site temporal flexibility is reduced in the use of satellite platform/sensor combinations due to the fixed nature of satellites paths. Other limitations include inability to target site-specific data collection, atmospheric influences, and vegetation interference; which, due to the nature of space-borne multi-spectral scanning, are out of the control of the geologist. In many cases the data obtained is limited to that available, which may be of an insufficient wavelength to penetrate the vegetation or a resolution not high enough for the site scale.

Figure 1: Sample of Aerial Photo Interpretation

3 AERIAL PHOTOGRAMMETRY AND AIR-BORNE LIDAR

In aerial photogrammetry the key considerations are the angle and scale of the obtained photographs. For the purposes of terrain analysis, only vertical aerial photographs are of sufficient value. An overlap of 60% is generally required to provide a stereoscopic view of the area. By using the effect of parallax, viewing an object from two different angles using stereo pairs of photographs through a stereoscope, it is possible to measure and observe the height of features. Computer-based photogrammetry

programmes can produce digital terrain models from point clouds generated from captured images but cannot displace the observation stage carried out by a trained professional observing the stereo pairs in parallax.

Analysis of a series of aerial photographs and remotely sensed data over a defined time period has wide applications in mapping terrain, measuring temporal changes in slopes features and detecting/assessing catchment processes. The options include the use of space-borne sensors for large scale topographical information using DEMs, whilst air-borne remote sensors can provide LiDAR information for geomorphology and DTMs. The direct suitability of LiDAR data to 3D modelling has proved an enormous advantage to 3D interpretation of natural terrain and associated features. Data, in the form of geospatial image files, is obtained and can be read by a variety of spatial software, such as ArcGIS, and used to generate interpretative data (see Figure 2).

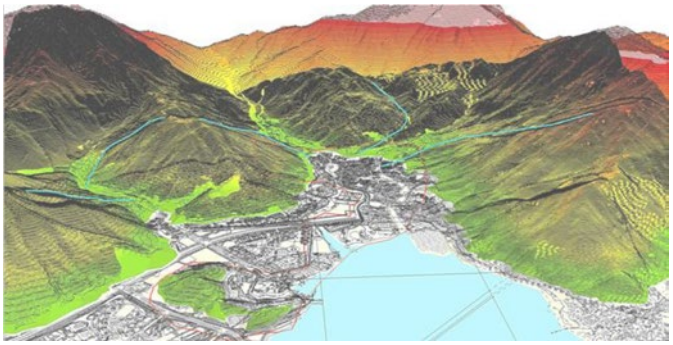

Figure 2: Terrain interpretation from DTM

In order to maximize the potential of the analysis of aerial photogrammetry and other remotely sensed data to study terrain a solid understanding of the following is crucial: spatial and temporal capabilities of different sensors; the range and usefulness of a variety of image analysis techniques; the spectral characteristics of a natural terrain site; and the nature and scale of geomorphic processes and features under investigation.

These techniques allow the visualization, description and classification of a multitude of geomorphic attributes of natural terrain and slope features over a wide range of spatial scales and the detection of change over timescales from days to decades. Such information is crucial in the planning and assessment of infrastructure and mitigation with regards to terrain analysis.

4 THREE-DIMENSIONAL TERRESTRIAL LASER SCANNING (3DTLS)

Three-dimensional terrestrial laser scanning uses the principles of scan stations and fixed objects (e.g. spheres) to generate point clouds from superposition of the fixed spheres. Large data files are produced and require powerful workstations to manipulate the images. High resolution images from high-density point clouds can be achieved using instruments with high measuring rates. Occlusions, blank regions within the point clouds, can generate low quality point clouds if occurring in large numbers. These can be reduced when considering line of sight orientation and also by the alignment of subsequent scans (Cacciari and Futai, 2016). UAV and TLS are still susceptible to the influence of vegetation when used in the determination of terrain relief (Gruszczynski et al., 2017)

5 UAV PHOTOGRAMMETRY AND LIDAR

The use of UAV Photogrammetry and LiDAR is similar to Aerial photogrammetry and air-borne LiDAR but using alternative platform to acquire data. However, the use of UAV has opened various new applications in the close range domain with a lower cost in comparison to hiring an aircraft. A laser scanning device or high resolution digital camera is mounted on the UVA using a Global Navigation Satellite System (GNSS) and this enables high precision surveying with accuracy down to 1 to 2 cm (see Figure 3).

Figure 3: Example of UAV with mounted camera

5.1 UAV Photogrammetry

UAV photogrammetry should be understood as using a remotely controlled semi-automated or automated flight to acquire photogrammetric data for processing. For terrain evaluation, close range UAV photogrammetry allows the user to collect high accuracy data and overcome physical obstructions in the field (such as dense boulder clusters, vegetation or unstable ground) to provide visual inspection where other systems cannot. These advantages are due to the rapid advance of the hardware and software of UAVs over the last decade. The image collection capabilities, flight planning capability and flight stability of UAV have significantly improved including the introduction of the Inertia Navigation System (INS) for stability of image capturing (see Figure 4). The system continuously detects the position, orientation and velocity of the UAV as well as the change of surrounding by its accelerometers, gyroscopes and computers. The system itself is autonomous and does not rely on visibility condition. These technological advances allow the UAV to operate in various environments where the user is capable of capturing high quality images whilst stationed from distance and maintaining a line of sight to the UAV, Besides the image capability, the use of INS and GNSS on an UAV also provide a safe alternative to high risk situations at low altitudes that conventional aerial strategies are unlikely to access. It is important to note that the accuracy of the UAV photogrammetry is still controlled by the mounted camera. Currently, the cameras currently used are able to adjust its position to capture high-accuracy work on a per-image basis. In light of this, UAV photogrammetry can provide a real-time, low cost, project specific capability to survey the concerned area where satellite or traditional aerial images may not be able to provide the detail or visibility.

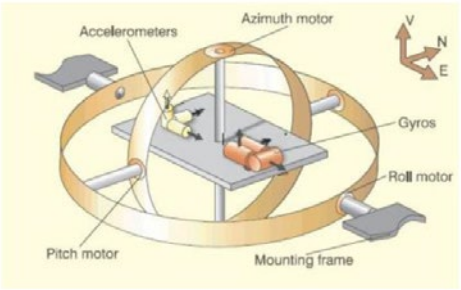

Figure 4: Details of Inertia Navigation System

However, despite the versatility of this method, for large spatial extents it is likely more efficient to use conventional aerial photogrammetry strategies even though UAV photogrammetry is able to provide higher accuracy and overcome local obstructions. Conventional strategies can act as a basis to identify whether additional focussed UAV photogrammetry is needed.

5.2 UAV LIDAR

Similar to the UAV photogrammetry, the UAV LiDAR also includes an inertia navigation system to conduct the aerial surveying. The system is essential to ensure the scanner of UAV LiDAR can capture hundreds of square meters in a single day. The combination of these systems allows the positioning and orientation of the footprint of a laser beam as it hits an object which ensures the high degree of accuracy. Tens to hundreds of points will be measured in every square meter in order to create a detailed digital

model of the mapped area. This model is even capable to illustrate sharp-edged features narrow and/or small objects which conventional technology such as Structure from Motion (SfM) algorithms and Dense Image Matching (DIM) do not correspond very well. Objects like transmission line, pipelines and boulders can be illustrated on the model because the point cloud of UAV LiDAR is measured by a single ray from the scanner providing better approximations of objects. Additionally, as the scanner is mounted on the UAV the set-up is affordable for the majority of commercial and/or civil users.

Table 1 refers to a comparison of the UAV methods with other aerial and satellite technologies:

Table 1. Comparison of different technology

	Aerial Photo/Satellite Image Interpretation	Aerial Photogrammetry/ Air-Borne LiDAR	UAV Photogrammetry/ LiDAR
Planning	automatic/manual	automatic (manual configuration)	automatic (manual configuration)
Data acquisition	manual	automatic/manual	automatic
Size of the area	km^2	km^2	m^2-km^2
Image resolution/GSD	m	cm-m	mm-m
Distance to object	km	100m-10km	m-km
Accuracy	m	cm-m	cm-m
Area Coverage	Small to Large scale	Large scale	Small scale

6 CONCLUSION

An assessment of the existing, traditional methods of terrain evaluation and those adopting newer technologies currently being explored has been presented. The pros and cons of traditional aerial and satellite methods demonstrate the current limitations of the use of technology to assist in terrain evaluation. It has been shown that techniques incorporating compact and lightweight versions of traditional techniques possess valuable advantages over their more traditional counterparts albeit with some inherent limitations due to the nature of data collection or the sample population obtained. In this way, technological innovations such as UAVs, a prime example of the stream lining and miniaturisation of the equipment used in the processes of photogrammetry and LiDAR, will naturally help to bridge the gap between the technological capabilities of traditional aerial and satellite remote sensing techniques and the direct approach of site-specific data collection. It is hoped that further reductions in costs and perfecting techniques through successful utilisation of these advanced technologies in projects in Hong Kong will result in a wider suite of enhanced options available for terrain evaluation which ultimately aid in the detection and assessment of potential geo-hazards.

REFERENCES

Cacciari, P. P. and Futai, M. M. Mapping and characterization of rock discontinuities in a tunnel using 3D terrestrial laser scanning. *Bulletin of Engineering Geology and the Environment*. 2016. Vol. 75 (1) pp. 223-237.

Eisenbeib, H. UAV Photogrammetry. *Dissertation*. University of Technology Dresden. 2009.

James M.R., Robson, S. d'Oleire-Oltmanns, S. and Niethammer, U. Optimising UAV topographic surveys processed with structure-from-motion: Ground control quality, quantity and bundle adjustment. *Geomorphology*. 2017. Vol.80 pp. 51-66.

Gilvear, D. and Bryant, R. G. Analysis of Aerial Photography and Other Remotely Sensed Data. *Tools in Fluvial Geomorphology*. 2005. John Wiley & Sons, Ltd, pp.135-170.

Gruszczynski, W, Matwij, W, and Cwiakala, P. Comparison of low-altitue UAV photogrammetry with terrestrial laser scanning as data-source for terrain covered in low vegetation. *ISPRS Journal of Photogrammetry and Remote Sensing*. 2017. Vol. 126 pp. 168-179.

Nico, G., Rutigliano, P. Benedetto, C. and Vespe, F. Terrain modelling by kinematical GPS survey. *Natural Hazards and Earth System Sciences*. 2005. Vol. 5 pp. 293-299.

Woodman, O.J. An introduction to inertial navigation. *Technical Report published by University of Cambridge Computer Laboratory*. 2007 Number 696.

Zhang, L. Urban land and infrastructure deformation monitoring by satellite radar interferometry. New advances in Instrumentation Monitoring and Remote Sensing, *IOM3 Technical Seminar*. 2017. Hong Kong Polytechnic University, Hong Kong.

Overall strength evaluation of a soil-cement column under axial compression

Y. Liu
Department of Civil & Environmental Engineering, National University of Singapore, Singapore
A.L. Saw
Golder Associates (HK) Limited, Hong Kong

ABSTRACT

Deep mixing or jet grouting methods are widely used technique for soft ground stabilization. These techniques involve mixing admixtures, usually cementitous, into soft soils. It is well-known that this process of chemical improvement can introduce significant heterogeneity into the improved ground. Generally, a relatively small diameter core (50mm to 100mm) is sampled from a 1m to 2m diameter deep mixing column/cluster. The unconfined compressive strength from core samples is often highly variable, ranging from around 0.5MPa to 5MPa. The coefficient of variation of the strength is typically as high as 0.4 to 0.6, which is about twice that of natural soils. Due to the existence of the heterogeneity in strength, it is necessary to evaluate the behavior of the deep mixing column from a perspective of full-scale column instead of from small core test results. As a result, a 3-D finite element method was used in this paper to examine the overall performance of a deep mixing column. The strength of the column is described as a random field, where weak and strong regions concurrently exist. The statistical parameters of the random field are determined from the typical site experience. The numerical results were also compared with test results of full scale columns based on literature. The strength acceptance criterion of cement-treated columns under axial compression was discussed in detail.

1 INTRODUCTION

Deep mixing and jet grouting are widely used techniques for soft ground stabilization. These techniques involve mixing admixtures, usually cementitous, into soft soils by mechanical mixing process. In deep mixing, the mechanical mixing system consists of hollow rotating shafts with cutting tools, mixing paddles and/or augers mounted at various locations along the shafts (e.g. Chew et al. 1997). In jet grouting, a high-pressure pump is used to convey the binder through a set of nozzles located above the drill bit. The high-pressure fluids or binders are injected into the soil to break up the soil structure and subsequently mix the soil particles in situ. It is well known that this process of chemical improvement can introduce significant heterogeneity into the improved ground. Many instances of spatial variability in the properties of cement-treated soil have been reported. For instance, Chew et al. (1997) reported a wide strength distribution in jet-grouted marine clay in the Singapore River Widening Contracts C1 to C3. The unconfined compressive strength (UCS, denoted as q_u) of the core samples varied from 0.5MPa to about 4MPa. In deep mixing, Kawasaki et al. (1984) also reported variation in direct shear strength of core samples, from about 0.5MPa to about 2.5MPa. Recently, Chen et al. (2011) also reported variation in UCS of core samples varying from about 1MPa and 5MPa. Similar range of UCS was observed by Liu et al. (2015), as indicated in Figure 1. Lately, Liu et al. (2017a) extensively reviewed the main statistical

characteristics of cement-treated soils from deep mixing projects, and they noted that the variations in UCS and the sample size of core strength data should be both taken into account in determination a representative strength for a full scale column. Because of the non-uniformity observed in UCS, assessing the overall strength of a soil-cement column becomes very challenging. In this paper, the overall strength of a soil-cement column refers to its stress level at the ultimate bearing capacity. In practical design procedures, the average and coefficient of variation (COV) in UCS are normally used; however, this design methodology ignores the spatial correlation that measures the similarity in UCS at two spatially lagged points. To fill in this gap, the concept of the random field can be applied. This approach considers a probability distribution as well as the spatial dependence between different points. Namikawa and Koseki (2013) examined the effect of spatial correlation on the overall behavior of an axially loaded column by finite element analysis, where the strength and modulus of the material were considered to be random fields. This method was able to readily obtain the mean and standard deviation of the overall strength of a full-scale column. Therefore, these results are likely to be more scientific in determining design values. Liu et al. (2017b) examined the spatial variability as well as the mean trend of cement-treated soils of a 2m-length soil-cement column, and the statistical characteristics of the overall strength of the column was investigated.

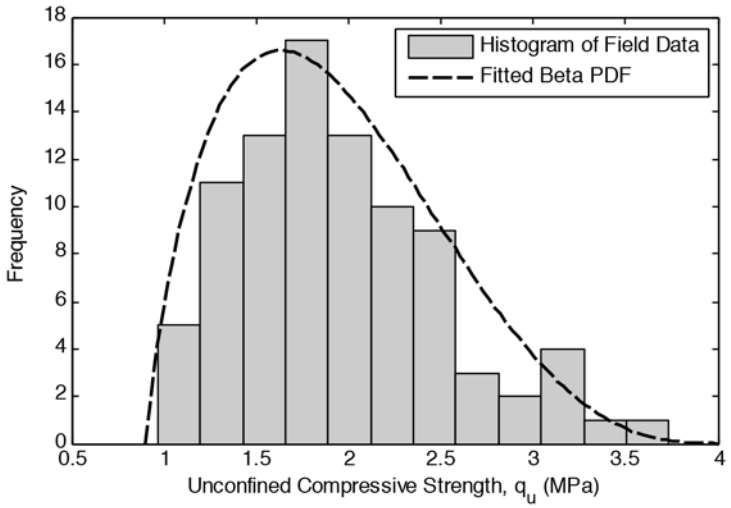

Figure 1: Histogram and fitted probability density function of unconfined compressive strength of cement-admixed soils based on field data. (After Liu et al., 2015).

As an extension of the work by Liu et al. (2017b), this study examines the randomness in UCS of a 20m-length soil-cement column subjected to axial compression. The background of this study is the ground treatment in the center of an embankment or reclaimed ground, where the soft clay is often treated by isolated soil-cement clusters (e.g. 4 overlapped deep mixing columns form a cluster) and subjected to vertical loads. The overall performance of such a soil-cement column cluster is examined by numerical simulations. The anisotropy of heterogeneity in UCS is considered by adopting different scales of fluctuation (SOFs) in the cross-section plane and along the axial direction. The SOF refers to the similarity degree in UCS between two points. The aim of this study is to evaluate the overall strength of a column/cluster in a more scientific manner.

2 Random field finite-element analysis

As shown in Figure 2(a), a soil-cement column of 2.4m in diameter and 20m in length is considered in this study. 3-D finite element software ABAQUS was employed to perform the analyses. The mesh size is set approximately the same size of the field test measurement (i.e. 100mm diameter core sample) so that the variation in UCS can be consistent between the numerical simulation and field data. As a result, the model consists of 131,600 8-noded brick elements as shown in Figure 2(a).

The key controlling parameters of a random field are the SOF and the marginal distribution. Liu et al. (2015, 2017a) extensively examined the marginal distribution of the UCS of cement-treated soils. As

suggested in Fig. 1, the UCS data is slightly skewed. After a comparison among the normal, lognormal, Weibull and beta distributions, Liu et al. (2017a) observed that the beta distribution shows superior performance over other distributions in fitting the UCS data. The SOFs of UCS are generally anisotropic; the horizontal SOF is less than vertical SOF. The statistical parameters used in this study were based on the data listed Table 1. Figure 2(a) illustrates one of the realizations of the UCS. In this study, the cement-treated clay is modelled in a total stress framework, as a Tresca material with a stress strain behaviour shown in Figure 3. According to Kitazume and Terashi (2013), in the case of small confining pressure, the residual strength of cement-treated soil is about 80% of the UCS. In order to closely simulate a constructed soil-cement column below the embankment or reclaimed land, 20% reduction in UCS was considered to account for the observed strain-softening effect of cement-treated soils as reported by Kitazume and Terashi (2013).

Table 1: Statistical characteristics of cement-admixed soils (after Liu et al., 2015)

References	Mixing method	Test	COV	Scale of fluctuation * (m)	
				Vertical	Horizontal
Honjo (1982)	Wet method	Unconfined compressive test	0.21-0.36 (clay) 0.32-0.40 (sandy soils)	0.8-0.8	–
Navin (2005)	Wet Method	Unconfined compressive test	0.34-0.74#	–	Approximate 24.0
Larsson et al. (2005)	Dry Method	Hand-operated penetrometer test	<0.60	–	Radial: <0.13 Orthogonal: <0.32
Larsson and Hilsson (2009)	Dry Method	Cone penetration test	0.20-0.60	–	1.8-3.6
Chen et al. (2011)+	Wet Method	Unconfined compressive test	0.43 (Phase 2) 0.46 (Phase 3A) 0.41 (Phase 3B) 0.41 (Phase 3C) 0.29 (Phase 4)	–	–
Chen et al. (2011)	Combination of wet method and jet grouting	Unconfined compressive test	0.23	–	–
Al-Naqshabandy et al. (2012)	Dry method	Cone penetration test	0.22-0.67	0.2-0.7	2.0-3.0

Notes: * The concept "auto-correlation distance" was used in some literature, which was converted to "scale of fluctuation" in this table. + Data were from different phases of Marina Bay Financial Cenre project in Singapore. # This range was adopted by the Federal Highway Administration Design Manual (see Bruce et al. 2013).

Four different cases of UCS were considered in this study.

- Case 1: mean strength = 2.07MPa, COV = 0.4;
- Case 2: mean strength = 2.94MPa, COV = 0.4;
- Case 3: mean strength = 2.82MPa, COV = 0.5;
- Case 4: mean strength = 5.71MPa, COV = 0.5;

The parameters in Cases 1 and 3 were determined so that the lower 10^{th} percentile was around 1MPa, and the parameters in Cases 2 and 4 were determined so that the lower 5^{th} percentile was around 1MPa.

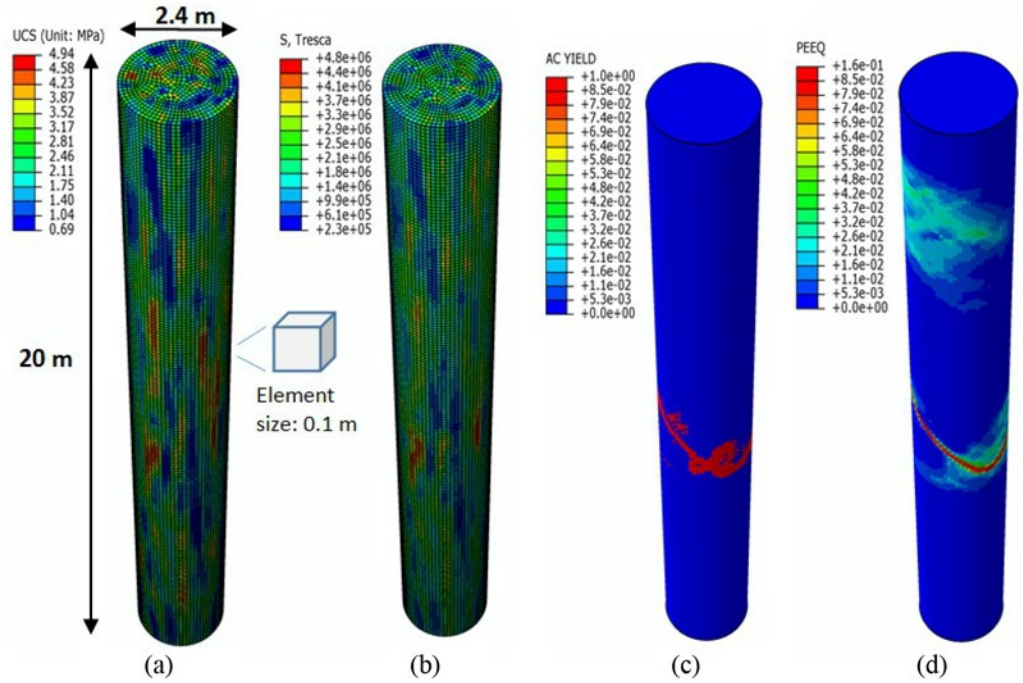

Figure 2: Different state variables of a random analysis of Case 1. (a) unconfined compression strength (UCS), (b) Tresca stress contour, (c) yield zone, (d) plastic strain contour.
Boundary conditions: (axial) displacement control with unconfined condition.

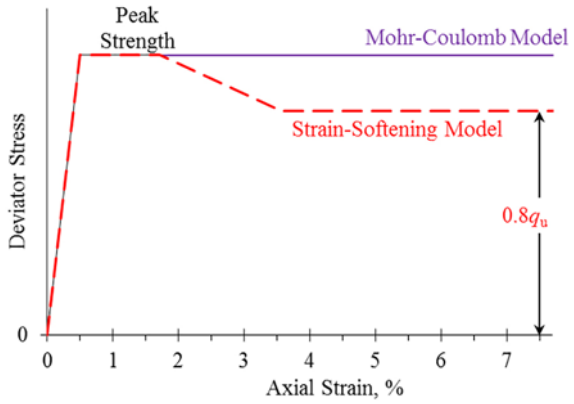

Figure 3: A strain-softening model used in numerical analysis of cement-admixed soils.

Each of four cases was repetitively simulated for 100 times (i.e. Monte Carlo simulations), and the stress-strain curves for full scale soil-cement column are plotted in Figure 4. The lowest overall strengths are also indicated in Figure 4; as the results show, the ratio of the lowest overall strength over the mean core UCS is about 0.7 for all four cases. This finding is generally consistent with the full scale test, as reported by Kitazume and Terashi (2013). They observed that the overall strength of a soil-cement column was about 0.7 times of the mean core UCS; the latter was based on core strength data (small scale tests). Similar problem was also analysed by probabilistic deductions using the Gaussian distribution for the strength variation (e.g. Honjo 1982; Liu et al. 2008); however, those studies did not take the SOF into account. By contrast, the random field used in this study considers both the SOF and variation of the strength. As Figures 2(b) – 2(d) show, the stress contour, yield zones and the high strain regions do not form regular patterns when the soil-cement column approaches failure.

On the other hand, the COVs in the overall strength for full scale column of all cases are generally less than 0.1, which is much lower than the COVs in UCS of core samples. This finding implies that the overall strength possesses a much smaller variation than that in core UCS. The Building Center of Japan (1997) proposed the following equation for cement-admixed soil strength design:

$$Q_d = u - 1.33\sigma \quad (1)$$

where Q_d, u and σ are the design strength of a full scale soil-cement column, mean core UCS and standard deviation of core UCS, respectively. According to Equation (1), the corresponding design strength values of Cases 1-4 are 0.97MPa, 1.37MPa, 0.94MPa and 1.91MPa, respectively. Those values are smaller than the lower bound of the corresponding numerical results, as shown in Figure 4. The numerical results obtained in this study indicate that Equation (1) could yield safe design.

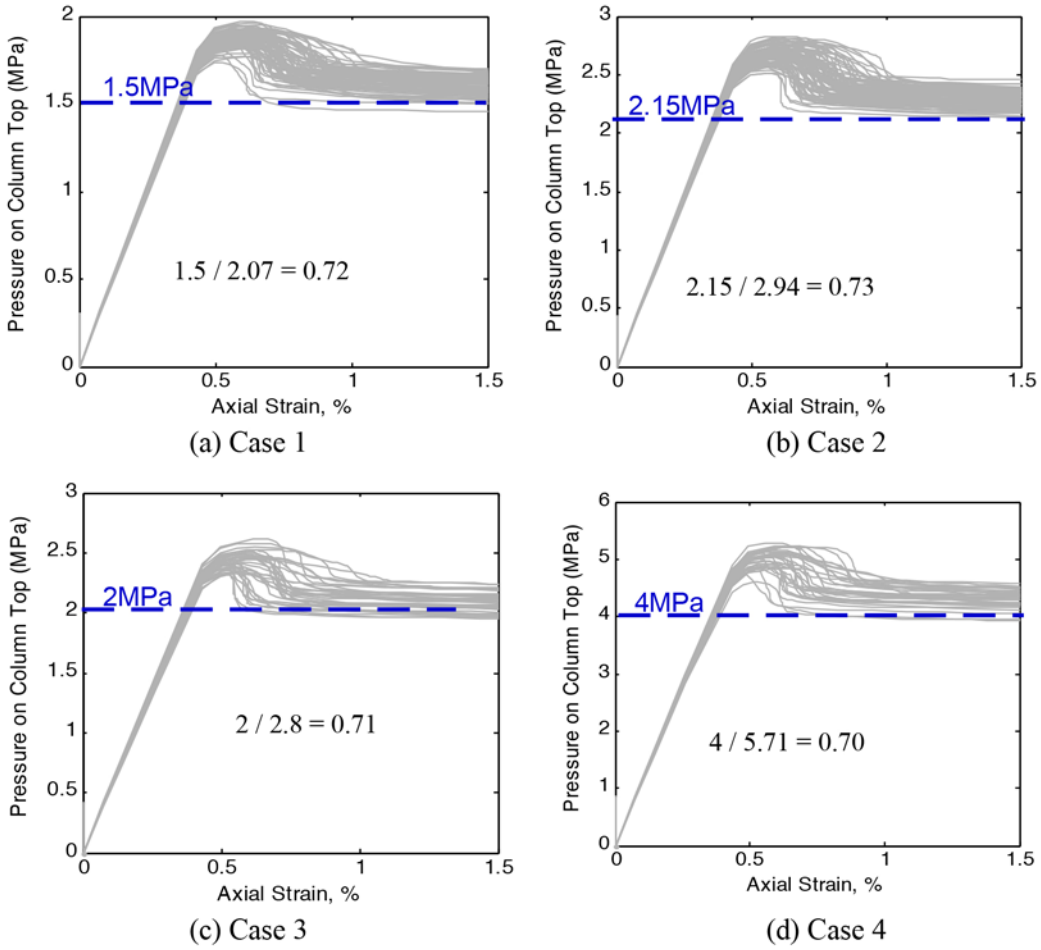

Figure 4: Stress-strain curves of overall strength of a soil-cement column for different cases.

3 CONCLUSIONS

This study considers the heterogeneity in the strength of a soil-cement column under axial compression. The heterogeneity was simulated as a 3-D random field that was controlled by a marginal beta distribution and a scale of fluctuation. The random field finite element method was used to analyze the soil-cement column, and these results were used to conduct a series of parametric studies. The analyses results show that the overall strength of a full scale soil-cement column possesses a much smaller variation than that in core UCS. The ratio of the lowest overall strength for a full scale soil-cement column over the mean core UCS is about 0.7. The design strength formula proposed by the Building Center of Japan (1997) is likely to yield safe design values.

REFERENCES

Chen, J. Lee, F.H. & Ng C. C. (2011) Statistical analysis for strength variation of deep cement mixing columns in Singapore. *ASCE Geotechnical Special Publication* 211 (GeoFrontiers 211 on Advances in Geotechnical Engineering): 576 – 584.

Chew, S. H., Lee, F. H., Lee, Y. & Yogarajah, I. (1997) Jet grouting in Singapore Marine Clay, *Proceedings of 3rd Young Geotechnical Engineers' Conference*, ed. TS Tan, SH Chew, KK Phoon and TG Ng, pp231-238. Singapore.

Honjo Y. A probabilistic approach to evaluate shear strength of heterogeneous stabilized ground by deep mixing method. *Soils and Foundations*, 1982; 22(1): 23-38.

Kawasaki, T., S. Saitoh, Y. Suzuki & R. Babasaki. (1984) Deep mixing method using cement slurry as hardening agent. In Seminar on Soil Improvement and Construction Techniques in Soft Ground, pp17-38, Singapore, JSSMFE, NUS, AIT.

Kitazume, M., Terashi, M., (2013). *The deep mixing method*. CRC Press, Taylor & Francis Group, New York.Liu Y., Zheng J. J. & Guo J. 2008. Statistical evaluation for strength of pile by deep mixing method. *Proceedings of the Second International Conference on Geotechnical Engineering for Disaster Mitigation and Rehabilitation*, Nanjing, China. pp: 195 – 201.

Liu, Y., Lee, F. H., Quek, S. T., Chen, J. E. & Yi, J. T. (2015). Effect of spatial variation of strength and modulus on the lateral compression response of cement-admixed clay slab. *Géotechnique* 65, No. 10, 851-865.

Liu, Y., Jiang, Y. J., Xiao, H. & Lee, F. H. (2017a). Determination of representative strength of deep cement-mixed clay from core strength data. *Géotechnique* 67, No. 4, 350-364.

Liu, Y., Hu, J., Li, Y. P. & Li, L. H. (2017b). Statistical evaluation of the overall strength of a soil-cement column under axial compression. *Construction and Building Materials* 132, 51-60.

Namikawa T, Koseki J. Effects of spatial correlation on compression behavior of cement-treated column. *J. Geotech. Geoenviron. Eng.*, 2013; 139(8): 1346-1359.

The Building Center of Japan (1997). *Design and quality control guideline of improved ground of building*. (in Japanese).

Evolution of Landslide Susceptibility Mapping for Natural Hillsides in Hong Kong

F.L.C. Lo & F.W.Y. Ko

Geotechnical Engineering Office, Civil Engineering and Development Department, The Government of Hong Kong Special Administrative Region

ABSTRACT

Landslide susceptibility mapping has evolved taking advantage of the emerging computer technology. Previous studies related to terrain evaluation and relationship between rainfall and natural terrain landslides have identified rainfall, slope angles, and geology as some key territory-wide attributes affecting natural terrain landslides in Hong Kong. It is understood that there are other causal factors affecting the mass wasting process, such as structural, hydrogeological and morphological features. It is, however, not possible to study statistically their relationships with landsliding in a territory-wide scale due to a lack of data covering the entire Hong Kong. Without the support of advanced computer technology at the time of the previous studies, relating all relevant data to achieve a meaningful territory-wide correlation of natural terrain landslides and their attributes was hardly possible. The novel digital technologies and remote sensing techniques that have emerged, such as the Geographic Information System and Light Detection and Ranging, coupled with the unprecedented computation power available in the last decade, allow the collection and geographic-based analysis of large amount of spatial data in relation to terrain characteristics, landslides, and their attributes. It opens up the opportunity for digital landslide susceptibility mapping that considers high-resolution multi-variants rainfall and terrain input. This paper presents a few relevant studies related to landslide susceptibility mapping and demonstrates how technological advances in the past decades help consolidate and enhance the past efforts in landslide susceptibility mapping to the current state-of-the-art capability.

1 INTRODUCTION

It is indisputable that over the past 40 years, computer technology has evolved to become more readily accessible and more easily manageable, with unprecedented computation power and at affordable cost all the time. Hong Kong is one of the parties taking the lead to leverage whenever the latest computer technology to advance geotechnical practice and enhance the capability and efficiency of a wide range of geotechnical work. This has been achieved through applying novel digital technologies in geotechnical work and developing advanced numerical models for geotechnical analyses (Wong 2001; Wong 2005). Landslide susceptibility mapping is one of the technical development work that has gained the benefits of advances in computer technology to achieve the current state-of-the-art capability.

Previous studies related to terrain evaluation and relationship between rainfall and natural terrain landslides have identified rainfall, slope angles, and geology as some key territory-wide attributes affecting natural terrain landslides in Hong Kong. It is understood that there are other causal factors affecting the mass wasting process, such as structural, hydrogeological and morphological features. It is, however, not possible to study statistically their relationships with landsliding in a territory-wide scale due to a lack of data covering the entire Hong Kong. Without the support of advanced computer

technology at the time of the previous studies, relating all relevant data to achieve a meaningful territory-wide correlation of natural terrain landslides and their attributes was hardly possible. This paper presents a few relevant studies related to landslide susceptibility mapping undertaken in the 1980s, 1990s, 2000s, and post-2010s and demonstrates how the application of novel digital technologies and remote sensing techniques that have emerged, such as the Geographic Information System (GIS) and Light Detection and Ranging (LiDAR), coupled with the unprecedented computation power, has allowed the collection and geographic-based analysis of large amount of spatial data in relation to terrain characteristics, landslides, and their attributes to consolidate and enhance the past efforts in landslide susceptibility mapping to the current state-of-the-art capability.

2 THE 1980s: GEOTECHNICAL AREA STUDIES PROGRAMME

It is the period when work by hand still dominated people's life. Hand drawings and calculations, assisted by handheld electronic scientific calculators, were the mainstream in the engineering sector. Computer technology in the period was not in pace with the need of engineers. Personal computers have just started to emerge in the commercial market in the early 1980s, for example, IBM introduced their first personal computer in 1981 operating on MS-DOS 1.0. By the end of the decade, personal computers operating on 80286 and 80486 processors had been introduced. Some historic software introduced during the period are: Microsoft Word and Lotus 1-2-3 (both released in 1983) and Adobe Photoshop software in 1988. Work by hand was found to be the most cost-effective and efficient means of delivering work output in the period.

In terms of landslide susceptibility mapping, the Geotechnical Control Office (GCO) (renamed Geotechnical Engineering Office (GEO) in 1991) has recognised the major importance of effective land use planning in which terrain stability consideration is prominent, due to the scarcity of readily usable land, combined with the geological and climatic conditions, since its establishment in 1977. It initiated the Geotechnical Area Studies Programme (GASP) in 1978 to provide information for land use planning and management purposes in Hong Kong (Burnett et al 1985). These studies were based largely on systematic terrain classification mapping on both territory-wide (1:20,000) and site-specific (1:2,500) scales based on aerial photography interpretation, site reconnaissance, and existing geotechnical information from borehole logs, technical reports, etc. Six attributes were considered in the terrain classification: slope gradient, terrain component, terrain morphology, erosion, slope condition, and hydrology. The studies were sufficiently detailed to facilitate recognition, delineation and documentation of the majority of landslides within the areas concerned, which enabled the creation of a systematic landslide inventory of their local distribution and characteristics. The GASP and the methodology used were described by Brand et al (1982a, 1982b) and Styles et al (1982) respectively.

It was found from the studies that slope gradient and landslide activities were statistically correlated. The terrain classification maps were the first generation of landslide susceptibility map in Hong Kong based on terrain classification mapping. Systematic terrain classification mapping by hand on paper maps was undoubtedly the state-of-the-art method of studying and understanding the terrain evolution in Hong Kong during the period that provided useful outcomes for reference in strategic land use planning and/or site-specific land development.

3 THE 1990s: TERRITORY-WIDE NATURAL TERRAIN LANDSLIDE SUSCEPTIBILITY MAP

3.1 Computer Technology in the 1990s

According to the GIS history, commercial GIS software was first released in 1991 that provided access to GIS for a wider group of users of the technology. By the end of the decade, the software has been improved to provide even more full-featured GIS functionality, including full support of extensions for raster and three-dimensional processing and advanced spatial analysis. This has been supported by a parallel advance in computer technology. Some of the key computer products introduced at the end of the decade were the Intel Pentium II in 1998 and Pentium III in 1999 and Microsoft Windows 98.

As soon as the GIS technology has become readily available in the market, the GEO has recognised the importance of spatial data and spatial analysis to driving advances in geotechnical practice and

enhancing the capability and efficiency of a wide range of geotechnical work. Since early 1990s, the GEO, with support from practitioners, has been developing geotechnical spatial datasets and GIS capability and promoting GIS application to geotechnical work in Hong Kong (Wong 2005). Towards the end of the decade, the enhanced GIS technology has opened up an opportunity to adopt more advanced GIS functionality to deal with geotechnical issues in Hong Kong. This has been possible as a result of the building up of GIS capability among the geotechnical profession over the years as well as an increased demand for use of GIS in solving geotechnical problems.

3.2 First Natural Terrain Landslide Susceptibility Map

The GEO, at the support of the latest GIS technology during the decade, developed the first territory-wide landslide susceptibility map in Hong Kong (Figure 1) in 1998. The territory-wide landslide susceptibility map was prepared using GIS spatial analysis that correlates landslide density (landslides/km^2) and landslide frequency (landslides/km2/year) with slope angle and geology (Evans & King 1998). Five susceptibility classes were defined: very low, low, moderate, high and very high with landslide densities varying from < 10 to > 100 landslides per km2 corresponding to frequencies varying from 0.1 to > 1 landslide/km^2/year. Nevertheless, the broad categorisation has not been used for direct application due to the following limitations:

(a) The resolution achieved in terms of landslide frequency, which spans about one order of magnitude between the least and most susceptible zones, is very limited for practical use. As a comparison, it is not difficult to achieve resolution better than three to four orders of magnitude in consequence assessment with the use of a generic consequence model.

(b) Natural terrain landslides are far sensitive to short-duration, intense rainfall than terrain characteristics, such as slope angle. If rainfall is not considered, the outcome would not be very accurate. For example, in year 2000, many landslides were found on hillsides of "medium" and "low" susceptibility classes but few landslides occurred on hillsides of "very high" and "high" susceptibility classes, when the heavy rainstorm mainly hit natural terrain areas of "medium" and "low" susceptibility classes.

(c) The susceptibility analysis considers both recent and relict landslides at equal weight. However, recent and relict landslides are different types of landslide features. Recent landslides are those landslides that are visible landslide incidents identified from aerial photographs since 1924. The year of occurrence of these landslides can be confirmed by reference to earlier aerial photographs. Relict landslides are those that occurred earlier than the time scale of the available aerial photographs. They were identified in aerial photographs as morphological features (e.g. degraded landslide scarps), which are often covered with vegetation, that give an indication of past landslide activities. The number of relict landslides observed does not give a full picture of the number of past landslides. Combining them together for quantitative analysis may be misleading.

(d) But if only recent landslides are taken into consideration, the observation period of recent landslide activities would be too short as compared with the long-term landslide triggering period. The observation period of the recent landslides is about 35 years. This is far too short as compared with the landslide triggering period that is more than hundreds and thousands of years long. As natural terrain landslides are very sensitive to short-duration intense rainfall, the short observation period of recent landslide activities would not be adequate to average out rainfall effect.

To overcome the limitations, a new territory-wide rainfall-based landslide susceptibility analysis was developed in 2014 that correlates rainfall and landslide density with slope angle and bedrock geology. This is discussed in Section 5.

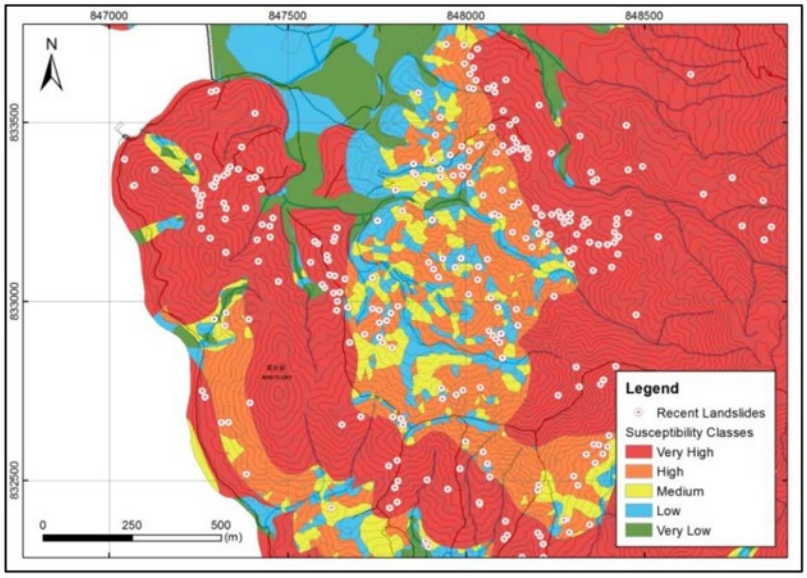

Figure 1: An extract of the first territory-wide landslide susceptibility map in Hong Kong (Evans & King 1998)

4 THE 2000s: RAINFALL-NATURAL TERRAIN LANDSLIDE CORRELATIONS AND SMALL-SCALE LANDSLIDE SUSCEPTIBILITY ANALYSES

The computer technology in both hardware and software has continued to expand and advance in the 2000s. In particular, the unique capability of GIS analysis in geotechnical research and development work involving spatial analysis of geotechnical data has become more mature and comprehensive. Taking advantage of the technology, the GEO has used GIS spatial analysis together with GIS-based geo-statistics to establish the first year-based and storm-based correlations between natural terrain landslide density and rainfall intensity in Hong Kong (Ko 2005). Figure 2 shows an example where the correlation between natural terrain landslide density and rainfall intensity in Hong Kong has been established using GIS analysis together with GIS-based geo-statistics. The correlation was updated in 2010 that covered more rainfall and landslide data over an extended observation period and adopted a more rigorous approach in deriving the storm-based correlation (Chan et al 2010). Figure 3 compares the first year-based rainfall-natural terrain landslide density correlation and the updated year-based correlation.

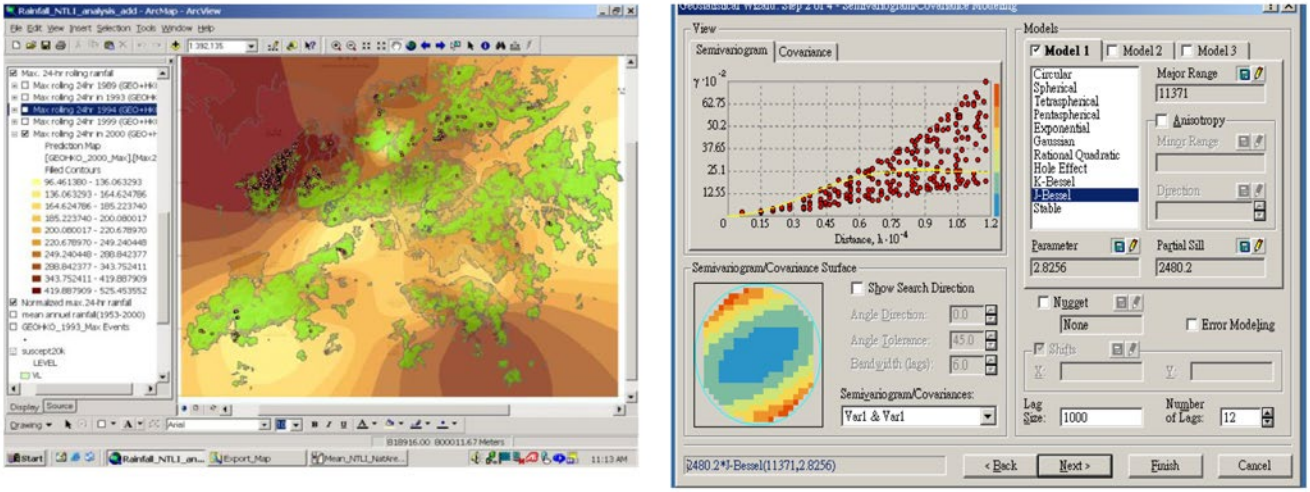

(a) Year 2000 maximum rolling 24-hr rainfall and natural terrain landslide locations

(b) GIS-based geo-statistical analysis

Figure 2: GIS analysis of natural terrain landslide-rainfall correlation

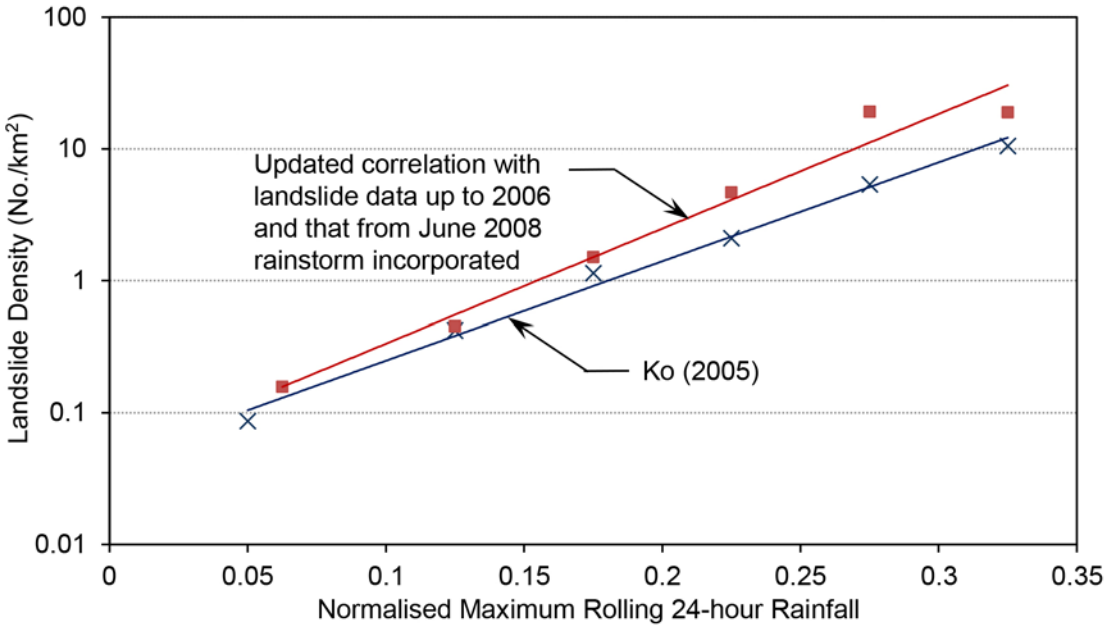

Figure 3: The first year-based rainfall-natural terrain landslide density correlation and the updated year-based correlation (Chan et al 2010)

Susceptibility analyses to different scales and levels of details have been carried out in the early 2000s to examine the practicality and reliability of susceptibility and hazard zoning. Notable work completed include: 1:5,000 regional susceptibility analysis using logistic regression (Dai & Lee 2002; Dai 2002), 1:5,000 regional susceptibility analysis using Artificial Neural Network (ANN) techniques (Lee et al 2002), and 1:2,000 area-based susceptibility analysis using additional field mapping data (Maunsell Fugro Joint Venture 2003). Wong (2003) summarised the key observations arising from Hong Kong's experience. They include the following:

(a) Where data are available, it is practical to carry out susceptibility analysis to obtain insight on correlation of landslide susceptibility with different terrain attributes, and to give broad categorisation of landslide frequency and susceptibility zoning.

(b) Use of GIS technology greatly improves the capability and efficiency of susceptibility analysis and reduces human error. Statistical, probabilistic and ANN methodologies provide useful tools to analyse the data and develop susceptibility models.

(c) Hong Kong is rich in data at 1:20,000 to 5,000 scale. Regional analyses carried out at this scale give reasonable statistical correlation and reasonable susceptibility categorisation. However, the bandwidth achieved in terms of landslide frequency (in the unit of number per year), which spans about one order of magnitude between the least and most susceptible zones, is limited. These susceptibility analyses form an important part of the continued technical development work. But in practice, given the overall low resolution, the zoning derived has not been directly applied in the management of natural terrain landslide risk under Hong Kong's slope safety system.

(d) The resolution and reliability of the susceptibility zoning can be improved in site-specific studies at 1:2,000 to 1:1,000 scale, together with collation of supplementary data. This requires considerable additional resources, which are costly particularly if a large area is covered. The work completed in Hong Kong to date shows that the resolution may be improved to covering about two orders of magnitude in respect of landslide frequency. This improvement enhances hazard zoning and quantitative risk assessment work. However, susceptibility zoning at this resolution is still of limited use for direct application. As a comparison, it is not difficult to achieve resolution better than three to four orders of magnitude in consequence assessment with the use of a generic consequence model (e.g. Wong et al 1997).

5 THE POST-2010s: RAINFALL-BASED LANDSLIDE SUSCEPTIBILITY MAP

5.1 Consideration of Rainfall Effect

Knowledge and experience gained from the past efforts in the study of landslide susceptibility for natural terrain in Hong Kong and the building up of GIS capability among the professional and technical staff of the GEO have laid down a concrete foundation and provided an opportunity for achieving a breakthrough in landslide susceptibility analysis in the early 2010s.

The breakthrough involves decoupling rainfall from the contribution of terrain attributes as was previously considered in the 1998 analysis to duly account for their extrinsic and intrinsic roles in causing landslides respectively (Ko & Lo 2016). When a hillside on which landslides occur is considered, rainfall is external to the ground system and is time-dependent (extrinsic), while terrain attributes are inherent and relatively time independent (intrinsic). Rainfall effect needs to be separately and systematically considered in a landslide susceptibility analysis such that its temporal variability is duly accounted for in developing a predictive model to response to different rainfall events in the future. Hong Kong is in a unique position to undertake this decoupled analysis given the abundant high quality rainfall data.

5.2 Geotechnical Spatial Datasets

The essential spatial datasets associated with landslide susceptibility mapping that was available in digital format on the GIS platform are discussed in Ko & Lo (2016). They are year-on-year rainfall contours, Enhanced Natural Terrain Landslide Inventory (ENTLI), slope angle map and bedrock geology map. It is worthwhile to highlight that in the early 2010s, the GEO completed a multi-return airborne LiDAR survey for the whole territory of Hong Kong. Wong (2007) summarised the capability of using multi-return airborne LiDAR for high-precision and virtual-deforestation over-ground survey. In essence, the technique allows landslide geomorphology to be interpreted and landslide maps to be produced to a resolution that cannot otherwise be achieved by using conventional aerial photographs. The technical requirements of the airborne LiDAR survey in Hong Kong were: sampling interval at 1.3 m, and horizontal and vertical data accuracies at 0.3 m and 0.13 m respectively. The survey results were used to develop a 0.5 m-grid digital elevation model (DEM) for the whole territory of Hong Kong. For global assessments, a 5 m-grid DEM was prepared by resampling from the 0.5 m-grid DEM. The 5 m-grid DEM were later converted into a 5 m-grid slope angle model for undertaking the landslide susceptibility analysis.

5.3 Rainfall-based Landslide Susceptibility Analysis

Ko & Lo (2016) documents the technical details of the new rainfall-based landslide susceptibility analysis. Figure 4 shows the year-based landslide susceptibility model (for all geological types). The development work started in end 2013 and was substantially completed in 2014. On hearing the key findings of the landslide susceptibility analysis in the 2014 meeting, the Slope Safety Technical Review Board (SSTRB) remarked that *"... The model is one of the few substantial attempts to introduce rainfall intensity as a predictor in a statistical manner ... the new GEO model is possibly the most advanced tool currently available world-wide for the prediction of the susceptibility to rainfall-triggered landslides. This is a remarkable scientific achievement with important practical utility ..."* (SSTRB 2014). Hungr (2016) also commented that the new landslide susceptibility model produced excellent results that were well validated using Hong Kong data. For the time being, the new susceptibility model can be applied in predicting number of natural terrain landslides in a rainstorm and undertaking global analysis, for example, global quantitative risk assessment and priority ranking of vulnerable hillside catchments. However, the resolution and reliability of the model are not yet sufficient to support direct application for site-specific hazard assessments and risk-based decision making at this stage.

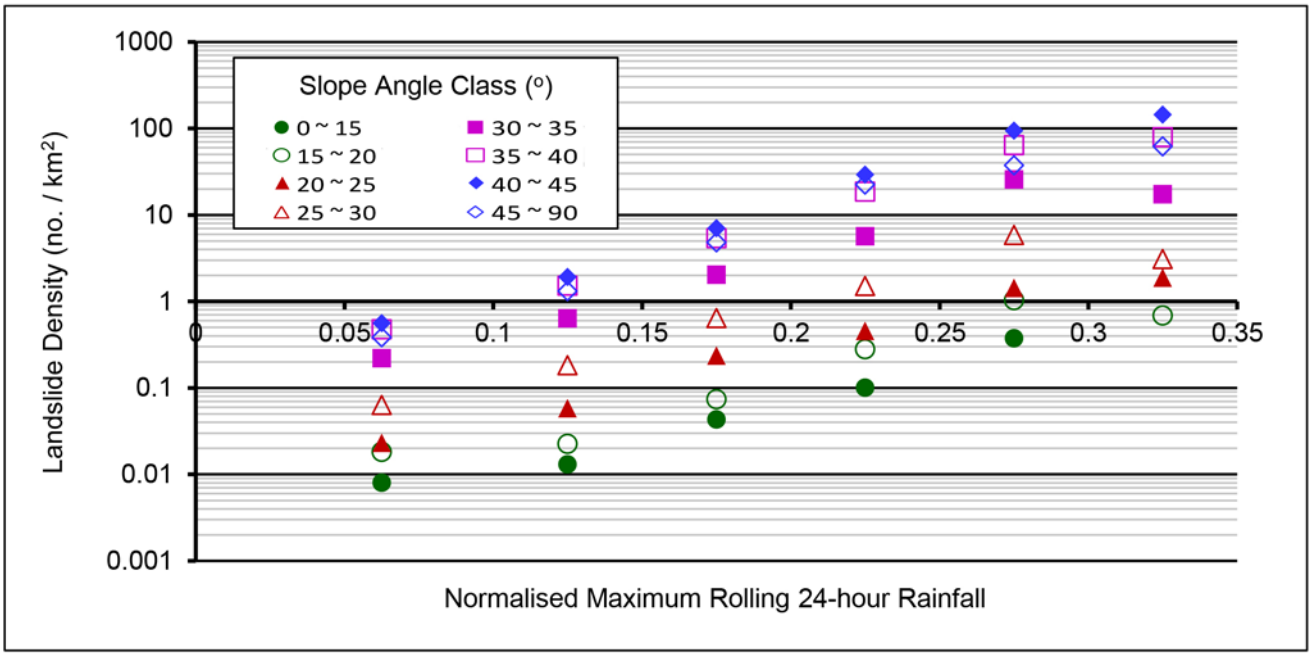

Figure 4: Year-based rainfall-landslide correlation for combined intrusive and volcanic areas

5.3 Territory-wide Landslide Frequency Map

In 2015, the rainfall-based landslide susceptibility model was applied to produce a terrain-based landslide frequency map for natural terrain in Hong Kong. The technical details involved in developing the map are presented in Ko (2015). The terrain-based landslide frequency map is a digital map produced using GIS technology and shows, for every grid of 5 m x 5 m on the natural terrain, annual theoretical landslide frequency. An annual theoretical landslide frequency (in the unit of no./year) is the expected number of landslides that would likely occur in a year given the mean annual frequency of occurrence of rainfall. It was first adopted in Wong et al (2006) as one of the components considered in calculating the hazard frequency in the global landslide risk assessment for natural terrain in Hong Kong. The same methodology, with the incorporation of the rainfall-based landslide susceptibility model (Ko & Lo, 2016), was used in deriving the annual theoretical landslide frequency in the natural terrain landslide frequency map. In the map, the annual theoretical landslide frequencies of the 5 m x 5 m grids are shown in five different colours that represent their relative levels of susceptibility to landslide. Yellow and light blue grids represent terrain with above-average susceptibility (Classes I and II respectively). Dark blue grids represent terrain with average susceptibility (Class III). Light green and dark green grids represent terrain with below-average susceptibility (Classes IV and V respectively). Figure 5 shows a typical map layout.

A preliminary validation of the map was carried out qualitatively through visual comparison of locations of actual recent landslides and the corresponding susceptibility classes. It was observed that for natural terrain areas such as Shek Pik, Tai O, Tung Chung, Mid-levels and Pat Sin Leng, most of the recent landslide crowns fall within susceptibility Classes I and II of the map. Recently, validation of the landslide frequency map has been carried out in a quantitative manner following the international practice. A few techniques commonly used by international peers have been adopted to evaluate the landslide frequency map. The major work done and key findings are presented in Lo & Ko (2017a). The validation shows that the map is highly consistent with the observed data for both presence and absence of landslides.

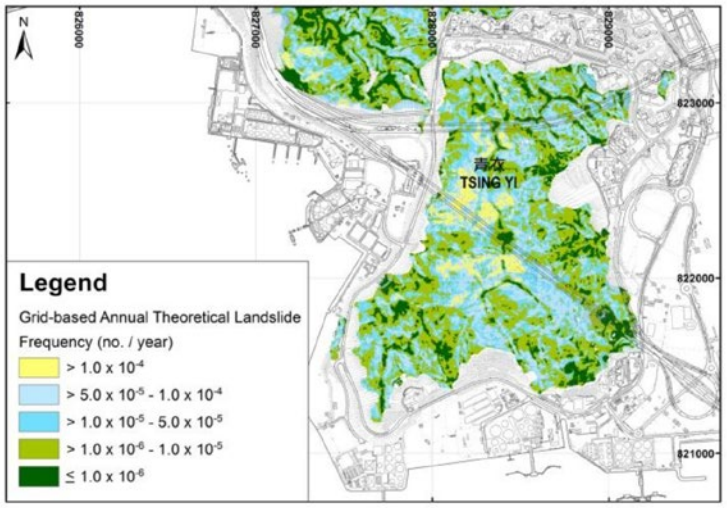

Figure 5: Part print of the natural terrain landslide frequency map

5.4 Relationship with Clusters of Relict Landslides

Despite the establishment of the rainfall-based landslide susceptibility model in 2014 that correlates rainfall, slope angle and bedrock geology with recent landslide activities, it is understood that there are other causal factors affecting the mass wasting process, such as geological, hydrogeological and morphological features. It is, however, not possible to study statistically their relationships with landsliding in a territory-wide scale due to a lack of their spatial data covering the entire Hong Kong.

Notwithstanding, it is noted from the ENTLI that at many locations, there are clusters of relict landslides. Recent and relict landslides are different types of landslide features. While recent landslides are visible landslide incidents identified from aerial photographs since 1924, relict landslides are morphological features that give an indication of past landslide activities. Clusters of relict landslides in an area may be a proxy to the presence of adverse geological and/or morphological features that have been affecting slope movement in the area. To test the validity of this observation, the rainfall-based landslide susceptibility model was updated in 2016 to include clusters of relict landslides as an additional predictor parameter and examine how they relate to recent landslides statistically.

Lo & Ko (2017b) provides the technical details of the analysis. Figure 6 shows the year-based correlations for both intrusive and volcanic terrain within and outside the cluster unit of relict landslides for slope angle from 30∞ to 45∞. The corresponding territory-wide year-based correlation (denoted as "Mean" in the legend of Figure 6) is also presented in Figure 6 for reference. Landslide data in other slope angle classes are not shown for simplicity and clarity. It is noted that on average, the terrain within the cluster unit is five times more susceptible to landslides than the terrain outside the cluster unit. For some locations within the cluster area, their landslide susceptibility is even higher, for example, a hillside catchment at Keung Shan Road, Lantau. These locations have been identified on a catchment basis by considering, for each catchment, (a) percentage of relict landslides and (b) percentage of recent landslides within the cluster unit.

The study shows that clusters of relict landslides and recent landslide activities are statistically correlated. The next step is to investigate the underlying physical, geological and morphological factors that may potentially control the mass wasting process in an area. The findings will provide insight to explore the relevance of the geomorphological features to rainfall-based landslide susceptibility.

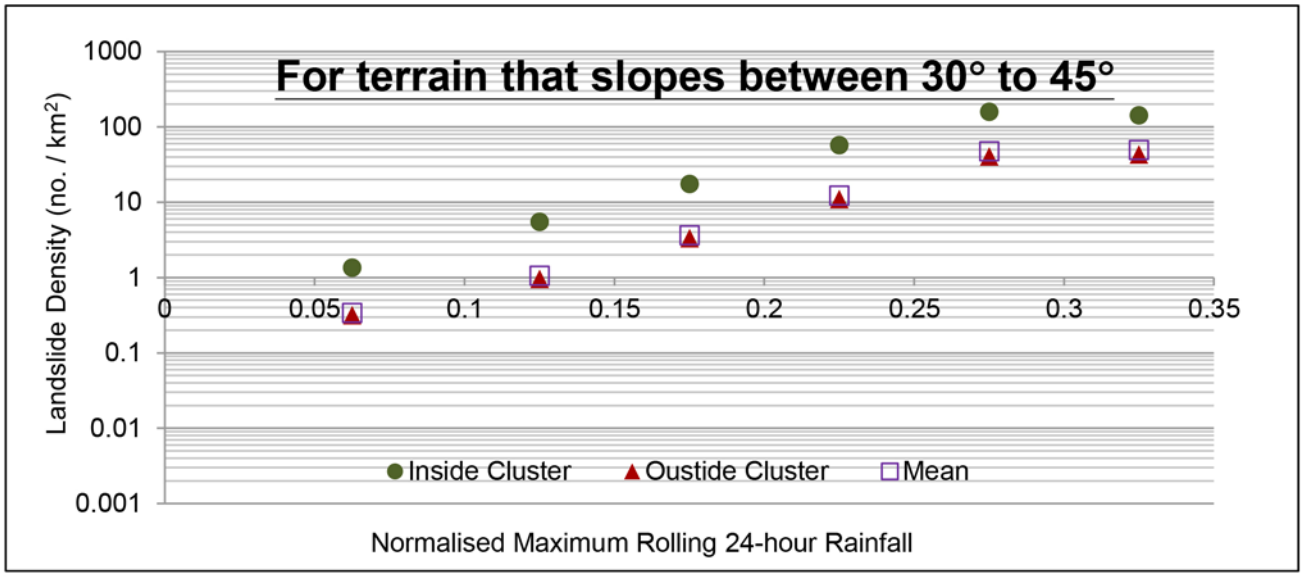

Figure 6: Year-based correlations for terrain within and outside cluster unit of relict landslides

6 STUDY OF LANDSLIDE SUSCEPTIBILTIY - EXPERIENCE ELSEWHERE

It is widely agreed that study of landslide susceptibiltiy is core and instrumental to effective landslide risk management and there has been vast variety of research and development work in the subject area over the past 30 years elsewhere outside Hong Kong. While different approaches have been proposed, the landslide susceptibility assessments mainly involve subdividing hillsides into different zones or pixels (if GIS technology is deployed) that have different likelihood for landslides of a particular type to occur in future through the use of predictive analytics or other advanced methods to correlate available landslide, terrain and rainfall data to make spatial prediction about future landslide activities. Inventory based, event-inventory based, heuristic approach, statistical approach, and deterministic approach are some common approaches to undertaking landslide susceptibiltiy assessments, in particular by our counterparts in other parts of the world (Dai & Lee 2002; Cascini et al 2005; Cascini 2008; Lee et al 2008). Their wide popularity is achieved for their ability to define a range of landslide susceptibility zones even on the basis of very limited, both in terms of number and resolution, landslide, terrain and rainfall data, at both regional and site-specific scales. As in most of the cases, only a small pool of landside data and coarse resolution of terrain and rainfall data are available for analyses, the resolution of the hazard/susceptibility zones as derived is usually very coarse (i.e. within about one order of magnitude between the least and most susceptible zones). The reliability of the landslide hazard/susceptibility maps thus developed for direct application and practical use, for example, in land use planning, is therefore doubtful.

Decoupled analysis is rarely undertaken elsewhere and rainfall effect is usually considered in the following ways:

(a) Effect of transient groundwater response as a result of rainfall is simulated by transient hydrogeological models (e.g. dynamic infinite slope modelling with rainfall trigger (Baum et al 2002; Simonie et al 2008)). Their use in regional susceptibility analyses are often constrained by the impracticality in obtaining necessary data (e.g. soil layers, shear strength parameters of soils, hydrogeological responses) over an extensive area with sufficient reliability and spatial resolution.

(b) For heuristics and data-driven approaches, while much of the focus of the previous work was on correlating past landslides activity with relevant terrain attributes (e.g. Van Westen et al 2008; Evans & King 1998; Dai & Lee 2002), the attention given to rainfall as the main causal factor is relatively limited. Arguably the main reason behind is that the practicality of establishing the correlation between rainfall and landslides is often limited by the spatial and temporal resolution of rainfall data.

(c) Some practitioners have attempted to consider rainfall effect by lumping it with other terrain attributes in the landslide susceptibility analyses (e.g. Bui et al 2016). To this extent, unless rainfall is largely uniform across the area and across time, it is deceptive to claim predictive capability of any landslide susceptibility map thus developed.

7 CONCLUSIONS

Advances in computer technology, together with the continual efforts in the past in landslide susceptibility mapping, building of GIS capability in both hardware and software and strengthening of staff in manipulating GIS, have allowed the current generation to undertake the state-of-the-art landslide susceptibility analysis. This is also possible due to the availability of abundant high-resolution rainfall data, which is unique worldwide. Further validation of the model by means of comparing landslide predictions against data from large rainstorms in the recent past and the near future will be undertaken. In addition, areas for improvement are constantly identified with a view to further improving the predictability of the model. More studies will also be carried out to investigate the underlying physical, geological and morphological factors that may potentially control the mass wasting process in an area, with a view to providing insight to explore the relevance of the geomorphological features to rainfall-based landslide susceptibility.

ACKNOWLEDGEMENTS

This paper is published with the permission of the Head of the Geotechnical Engineering Office and the Director of Civil Engineering and Development, Government of the Hong Kong Special Administrative Region.

REFERENCES

Baum, R.L., Savage, W.Z. & Godt, J.W. 2002. *TRIGRS - A Fortran Program for Transient Rainfall Infiltration and Grid Based Regional Slope Stability Analysis.* Open file report 02-424: Colorado, USA, U.S. Department of the Interior and U.S. Geological Survey.

Burnett A.D., Brand, E.W. & Styles, K.A. 1985. Terrain classification mapping for a landslide inventory in Hong Kong. *Proceedings of the IVth International Conference and Field Workshop on Landslides*. Tokyo, 63-68.

Brand, E.W., Burnett, A.D. & Styles, K.A. (1982a). The Geotechnical Area Studies Programme in Hong Kong. *Proceedings of the 7th Southeast Asian Geotechnical Conference*. Hong Kong, Vol. 1, 107-123.

Brand, E.W., Styles, K.A. & Burnett, A.D. (1982b). Geotechnical land use maps for planning in Hong Kong. *Proceedings of the 4th Congress International Association of Engineering Geology.* New Delhi, Vol. 1, 145-153.

Bui, D.T., Tuan, T.A., Hoang, N.D., Thanh, N.Q., Hguyen, D.B., Liem, N.V. & Pradhan, B. 2016. Spatial prediction of rainfall-induced landslides for the Lao Cai area (Vietnam) using a hybrid intelligent approach of least squares support vector machines inference model and artificial bee colony optimization. *Landslides*, doi:10.1007/s10346-016-0711-9.

Cascini, L., Bonnard, Ch., Corominas, J., Jibson, R. & Montero-Olarte, J. 2005. Landslide hazard and risk zoning for urban planning and development. *Landslide Risk Management* (Hungr, O., Fell, R., Couture, R., Eberthardt, E. (Eds.), Taylor and Francis, London, 199-235.

Cascini, L. 2008. Applicability of landslide susceptibility and hazard zoning at different scales. *Engineering Geology,* 102 (3-4), 164-177.

Chan, C.H.W., Ting, S.M. & Wong, A.C.W. 2012. *Development of Natural Terrain Landslip Alert Criteria. (Special Project Report No. SPR 1/2012).* Geotechnical Engineering Office, Hong Kong, 68 p.

Dai, F.C. 2002. *A Spatial-temporal Approach to Landslide Hazard Modeling Using Multi-temporal Aerial Photographs and GIS Technology.* Research Project Report, The Jockey Club Research and Information Centre for Landslip Prevention and Land Development, University of Hong Kong, 75 p.

Dai, F.C. & Lee, C.F. 2002. Terrain-based mapping of landslide susceptibility using a geographic information system: a case study. *Canadian Geotechnical Journal,* Vol. 38, 911-923.

Evans, N.C. & King, J.P. 1998. *The Natural Terrain Landslide Study: Debris Avalanche Susceptibility (Technical Note No. TN 1/98)*. Geotechnical Engineering Office, Hong Kong, 96 p.

Hungr, O. 2016. A review of landslide hazard and risk assessment methodology. *Proceedings of the 12th International Symposium on Landslides.* Naples, Italy, 3-27.

Ko, F.W.Y. 2005. *Correlation between Rainfall and Natural Terrain Landslide Occurrence in Hong Kong* (GEO Report No. 168). Geotechnical Engineering Office, Hong Kong, 77 p.

Ko, F.W.Y. & Lo, F.L.C. 2016. Rainfall-based landslide susceptibility analysis for natural terrain in Hong Kong - a direct stock-taking approach. *Engineering Geology,* 215, 95-107.

Ko, F.W.Y. 2015. *Terrain-based Landslide Frequency Map for Natural Terrain in Hong Kong (Technical Note No. 4/2015).* Geotechnical Engineering Office,16 p.

Lee, C.F., Ye, H., Yeung, M.R., Chan, X. & Chen, G. 2002. Application of Artificial Intelligence to natural terrain landslide susceptibility mapping in Hong Kong. *Proceedings of the Conference Natural Terrain - A Constraint to Development.* Institution of Mining and Metallurgy - Hong Kong Branch, 223-237.

Lee, C.T., Huang, C.C., Lee, J.F., Pan, K.L., Lin, M.L. & Dong, J.J. 2008. Statistical approach to storm event-induced 467 landslides susceptibility. *Natural Hazards and Earth System Sciences,* 8, 941-960.

Lo, F.L.C. & Ko, F.W.Y 2017a. *Validation of Natural Terrain Landslide Frequency Map (Technical Note No. 1/2017)*. Geotechnical Engineering Office, 36 p.

Lo, F.L.C. & Ko, F.W.Y 2017b. *Rainfall-based Correlation of Recent Landslides with Clusters of Relict Landslides (Discussion Note No. 2/2017).* Geotechnical Engineering Office, 9 p.

Maunsell Fugro Joint Venture 2003. *Natural Terrain hazard Study for Tsing Shan Foothill Area - Landslide Susceptibility Analysis.* Report to Geotechnical Engineering Office, Hong Kong, 71 p, plus 2 Appendices.

Simonie, S., Zanotti, F., Bertoldi, G. & Rigon, R. 2008. Modelling the probability of occurrence of shallow landslides and channelised debris flows using GEOtop-FS. *Hydrological Processes,* 22 (4), 532-545.

Slope Safety Technical Review Board 2014. *Report No. 24 to the Director of Civil Engineering and Development Department.* Government of the HKSAR, 38 p. (Internal).

Styles, K.A., Burnett, A.D. & Cox, D.C. (1982). Geotechnical assessment of the terrain for land management and planning purposes in Hong Kong. *Proceedings of the Symposium in Soil, Geology and Landforms: Impact on Land Use Planning in Developing Countries.* Bangkok, F.16.1-F.16.9.

Van Westen, C.J., Soeters, R. & Sijmons, K. 2000. Digital geomorphological landslide hazard mapping of the Alpago area, Italy. *International Journal of Applied Earth Observation and Geoinformation,* 2 (2000) 1, 51-60.

Wong, H.N. 2001. Recent advances in slope engineering in Hong Kong. *Proceedings of the 14th Southeast Asian Geotechnical Conference.* Hong Kong, Vol. 1, 641-659.

Wong, H. N. 2003. Natural terrain management criteria - Hong Kong practice and experience. *Proceedings of the International Conference on Fast Slope Movements: Prediction and Prevention for Risk Mitigation*. Naples, Italy, Vol. 2.

Wong, H.N. 2005. Digitial technology in geotechnical engineering. *Proceedings of the HKIE Geotechnical Division Annual Seminar.* Hong Kong.

Wong, H.N., Ho, K.K.S. & Chan, Y.C. 1997. Assessment of consequence of landslides. (Theme Paper). *Proceedings of the International Workshop on Landslide Risk Assessment*. Honolulu, 111-149.

Wong, H.N., Ko, F.W.Y. and Hui, T.H.H. 2006. *Assessment of Landslide Risk of Natural Hillsides in Hong Kong (GEO Report No. 191)*. Geotechnical Engineering Office, Hong Kong, 117 p.

Advancements in Ground Improvement Techniques for Non-dredged Reclamation Solutions in Hong Kong

A.D. Mackay
HSS Integrated, Kuala Lumpur, Malaysia

ABSTRACT

Reducing settlement to acceptable limits within an acceptable time period has significant uncertainties for reclamation formation. In the Hong Kong Special Administrative Region (HKSAR) pressure has increased to use non-dredged construction solutions to reduce environmental disturbance and to form larger scale reclamations further offshore. A major effect of placing reclamations further offshore is the presence of an increased thickness of the underlying weaker superficial deposits. This is due to the greater depth of deposition during past increased sea levels, and an increase in the proportion of finer grained constituents from deposition in a less energetic marine environment. The result is a greater period needed to reduce settlement to acceptable limits. This paper outlines uncertainties assessing geotechnical parameters of the superficial deposits due to the variability of the deposition environment, which can have particles ranging from clay to sand sizes. Specific past case histories are referenced for the geotechnical parameters, particularly the rate of primary and long-term consolidation for non-dredged reclamations. An overview of ground improvement techniques is provided from case histories of wick drain installation and vibro-replacement.

1 INTRODUCTION

The HKSAR requires level space for development, leading to large scale reclamation construction being located further offshore with limitations on dredging to avoid environmental disturbance. The challenges associated with this are placement on uneven sea-bed topography with variable water currents and erosive effects and challenges controlling stability and settlement of the underlying ground conditions.

For non-dredged reclamations placed on weak superficial deposits, variations in the particle size, thickness and deposition surface, influenced by past reduction in sea-bed level, are common. Particular attention is needed during design and construction for the provision of representative geotechnical parameters to reasonably predict the magnitude, rate and differential settlement. This is typically based on site investigation (SI) data supplemented by geotechnical parameters gained from past back analyses and test records from similar reclamation works placed on similar ground conditions.

Settlement can be reduced by either strength improvement or acceleration to allow the subsequent construction works to proceed. Experience of settlement acceleration using wick drain installation with sand blanket placement and geotextile separators been gained and experience of both settlement acceleration and strength increase has been gained using vibro-replacement techniques (Mackay & Wightman, 2016). Deep-cement mixing used to strengthen the ground is presently being considered for HKSAR projects, however long term records of its success in the HKSAR has not been obtained to date. Selected case studies from the Sai Wan Ho Depot and Macau Waste Re-use facility have been used to present the ground improvement techniques.

2 UNDERSTANDING THE GEOTECHNICAL PARAMETERS

2.1 Variability of the Superficial Deposits

Offshore superficial deposits in the Pearl River delta region, including both HKSAR and Macau, comprise marine deposits, which include recently placed soft marine silt and clay, typically placed in horizontal layers, overlying Alluvial deposits. The marine deposits were placed following the recent glacial period after 10,000 years rising to the current sea-levels about 6000 years ago (Fyfe et al, 2000), with deposition continuing until present. During this period the environment has been stable leading to a more consistent silt and clay deposition in horizontal layers with more consistent geotechnical parameters (Yeung & So, 2001). This deposition becomes coarser grained in more active environments closer to the shoreline and more constricted offshore channels with increased water flow (GEO, 2007). The deposits can range from structure-less, grey, silty clay (see Figure 1) to laminated silt and clay with sand lenses (see Figure 2). An example of marine deposits (clay) overlying alluvium (medium sand) is provided in Figure 3 (Fletcher, 2004).

Figures 1 & 2 – Marine Deposit

Figure 3 – Marine Clay Overlying Alluvium

Figure 4 – Alluvium; variable deposition

Figure 5 – Alluvium; medium sand

Figure 5 – Alluvium; sub-aerial weatherin

Alluvial deposition took place in a water-borne environment, typically along stream courses, which are linear and, due to the variable erosive nature, comprise lenses and laminae of silts and sands. These allow preferential drainage paths to form with a large variation in geotechnical parameters, particularly permeability, coefficient of compressibility (C_c) and coefficient of consolidation (c_v) which influence the rate of settlement (GEO, 2007). Sub-aerial deposition has also occurred, forming weathered crusts, which have an increased strength and can prevent penetration into the underlying weaker material. The variability in alluvial deposits is presented in Figures 4 to 6; this includes small scale variability,

ranging from silty clay to sand over about 300mm length of a sample (Figure 4, GEO, 2007), consistent medium grained sized sand deposition (Figure 5, Fletcher, 2004) and grey, silty clay deposition with orange brown mottling from sub-aerial weathering effects (Figure 6, Fletcher, 2004).

The coarser grained constituents can form drainage paths allowing release of excess pore-water pressure and acceleration of settlement during reclamation. For the settlement to be assessed properly during design or subsequent stages of construction and maintenance, judgement is needed whether individual layers have sufficient thickness and persistence for the parameters to be represented separately. The total amount of settlement depends on the thickness of the deposit, which is greater in areas of irregular basal drainage channels.

2.3 Geotechnical Parameter Ranges

2.3.1 Marine Deposits

As the Marine Deposits were place recently they have not experienced a past stress history and are therefore classified as normally consolidated. Given the different deposition environments in the HKSAR the geotechnical parameters are dependent upon the deposition location, which have consistent geotechnical parameters. As referenced in Ho & Chan, 1994, variations are present across the HKSAR as shown by test results and case study records, including (Fung et al, 1984, Siu & Chow, 1988 and Bramall & Raybould, 1993) at different locations. References Beggs & Tonks, 1985 and Plant et al, 1998 show more consistent results taken from specific locations at the North West New Territories (NWNT) and the Chek Lap Kok (CLK) test embankment, with records upon commencement of the settlement back analysis. The ranges in values for plasticity indices (PI), liquid limit (LL); effective angle of internal friction (Φ'); undrained shear strength (s_u), permeability (k), compression indices and compressibility moduli (m_v; m^2/kN) are shown in Table 1. The Compression indices are defined as the variation of void ratio (Δe) divided by the variation of the effective stress, ($\Delta \log \sigma_{ef}$); the Unit Weight (ϒ) had a consistent value of $1.45 Mg/m^3$ for all case studies.

Table 1 – Marine Deposit Geotechnical Parameters

Parameter	Beggs & Tonks, 1985	Ho & Chan, 1994	Chao et al, 1998	Plant et al, 1998
PI (%)	20 – 35	10 – 60		
LL (%)	38 – 60	20 – 100		
Φ' (°)	24			
s_u (kPa)	30			
k (ms^{-1})		10^{-8} - 10^{-10}		
c_v; m^2/year	1.0 - 20.0; av. 10	0.3 – 3.5	1	1.3
$C_r / (1+e_0)$	0.08 - 0.24; av. 0.14	0.4 – 1	0.36	0.4
m_v x 10^{-4} ; m^2/kN	1.6 - 6.0; av. 3.5		1	1.5 – 4

During the back analyses of the CLK trial embankment reclamation (Plant et al, 1998) the c_v values showed changes with an increase in ϒ, see Figure 7.

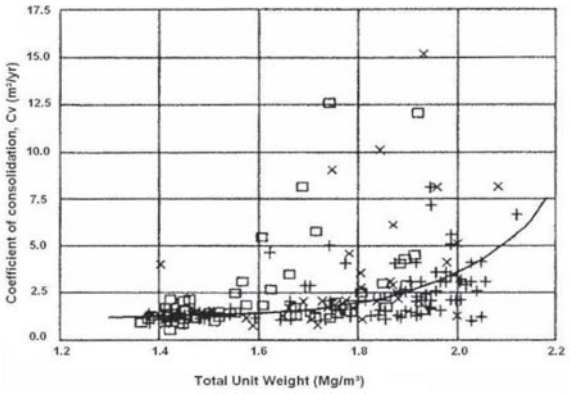

Figure 7 – Cv against unit weight

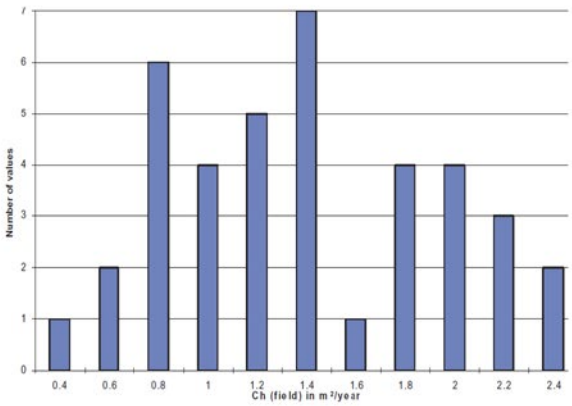

Figure 8 – Ch (field) values (Sai Ho Wan)

2.3.2 Alluvial Deposits

These were deposited when the sea levels were considerably lower than present. The increase in sea-level and effects of terrestrial weathering have given the alluvium a variable stress history and physical characteristics at each deposition location.

The geotechnical parameter ranges for deposits with different particle size distributions, categorized into different clay, silt and sand ranges for sand (0-20, 10-30 and 50-95%); silt (5-20, 30-70 and 15-55%) and clay (20-50, 40-70 and 0-50%) respectively for the NWNT are shown in Table 2 (Beggs & Tonks, 1985).

Table 2 – Alluvial Parameters; variability with particle size

Parameter	Clay	Silt	Sand
PI, %	20 - 55	15 - 33	10 – 22
LL, %	40 - 80	32 - 60	22 - 38
c' (kPa)	5	5	0
Φ,°	28	30	36
S_u, kPa	30		
cv (m^2/year)	1 - 10	8 - 40	
Cc ($1+e_0$)	0.05 - 0.15	0.05 - 0.28	
mv $x10^{-4}$; m^2/kN	0.9 - 4.1	0.9 - 7.5	

Geotechnical parameters were determined by Lo et al, 1998, for laboratory tests carried out on high quality "piston" samples from the CLK formation west of Lam Chau, beneath the CLK southern runway. The deposit was generally described as a very silty clay with particle size distribution ranges from sand (0-3%), silt (49-73%) and clay (24-51%) and parameters ranges for ϒ (1.67–2.06 Mg/m^3), PI (19-35%) and LL (39-68%).

Similar to the marine deposits the Cc, ($1+e_0$) and cv vary with different ϒ. The records from the CLK Airport back analysis are presented in Table 3 (Choa et al, 1990).

Table 3 – Alluvial Parameters; variability with ϒ

ϒ; Mg/m^3	1.7	1.8	1.9	2
cv; m^2/year	0.5 – 1.5	0.5 – 1.5	0.5 – 1.5	0.5 – 1.5
Cc; $1+e_0$	0.2 - 0.35	0.15 – 0.3	0.12 – 0.27	0.1 – 0.25

2.4 Rate of Consolidation

Permeable horizontal layers are often present in superficial deposits with horizontal pore water dissipation and coefficient of horizontal consolidation (c_h) increasing accordingly. This typically occurs closer to shore and near channels with more granular deposition. For the CLK embankment, the c_h value from field test data showed 4.3m^2/year for soft marine clay deposits (Plant et al, 1998), giving a factor of about 3 increase from the coefficient of consolidation in the vertical direction (c_v), see Table 1. At the Sai Ho Wan Depot reclamation c_h values were assessed from back-analysis of the reclamation records and averaged 1.3m^2/year, refer to Figure 8 for the range in ch values back analysed (De Silva et al, 1998).

The time for primary settlement is defined as the period required for the excess pore water pressure to dissipate. A further uncertainty for reclamation settlement is the period and magnitude required for secondary settlement, defined by the coefficient of secondary compression index (c_a) presented graphically as a constant rate of change in void ratio against log time period following completion of the primary consolidation. The c_a typically increases with an increased compression index (c_c), defined as a constant rate of change in void ratio against log effective pressure index. Characteristics are an increased clay sensitivity, defined as increased compressibility index below the A line in the plasticity chart (Lo & Premchitt, 1999 and Walker L.K. 1969), and a high organic content. The long term settlement within the stiff CLK formation was found to vary with the magnitude of loading ranging from 0.025 to 0.003 with a c_a / c_c ratio of 0.044 (Lo & Chan, 2004).

3 IMPROVEMENT USING DIFFERENT GROUND TREATMENT METHODS

3.1 Siu Ho Wan Depot, Lantau (Surcharging and band drain installation)

The Siu Ho Wan Reclamation covers about 150 Hectares and accommodates the Mass Transit Railway Corporation (MTRC) Airport Express Link Railway Depot, North Lantau. It was placed on Marine Deposits, mainly comprising soft to very soft sandy silty clay, with localized marine sand up to 5m thick; overlying Alluvium, ranging from 3 to 12m thick further offshore. The Alluvium comprised inter-bedded layers of medium stiff to hard sandy clay ranging to dense to medium dense sand (De Silva et al, 1998).

The majority of the marine deposits were improved using prefabricated vertical band drains (PVBD) installations placed in a triangular pattern from a fill level of +2.5m Principal Datum (mPD) to the base of the marine deposits. Surcharging raised to different levels was placed to further accelerate settlement. Instability, from mud wave failure occurred locally and needed enhanced treatment using vibro-floatation methods and additional PVBD installation. A summary of selected settlement and settlement rates for different surcharges for PVBD installed into varying thicknesses of underlying Marine Deposits is given in Table 4 (De Silva et al, 1998). The records are provided for stable portions of the reclamation, the settlement rate was recorded immediately prior to surcharge removal and records taken from plates placed at the base of the marine deposits, installed from +2.1 to -1.9mPD.

Table 4 – Consolidation and Settlement Behaviour during Ground Treatment with PVDS

Thickness (m)	Settlement (m)	Level (mPD)	Settlement period	PVBD space(m)	Degree of Consol.	Settle. Rate (mm/ day)
8	1.25	10.5	11/93 - 5/95	1.7	80 - 85%	0.8
5,5	2.0	10.5	11/93 -12/95	1.2	95%	1.2
7.3	1.15	10.75	11/93 - 11/95	1.2	80 - 85%	0.4
3.5	0.45	10	9/93 - 5/95	1.7	85%	0.3
6	0.95	12	10/93 - 5/95	1.7	85%	0.3
18	1.75	12	10/93 - 5/95	1.2	80%	0.3
6	2.2	12	10/93 - 5/95	1.2	80%	2.3
5.5	2.0	12.5 - 12	7/93 - 2/95	1.7	100%	0.7
3	1.52	12	10/93 - 10/95	1.7	80%	1.2
7.5	1.7 - 1.35	9.5	10/93 - 10/95	1.6	80%	0.3

The subsequent building construction was placed on pad foundations. Despite the degree of consolidation achieved further settlement occurred, ranging from 3 to 389mm and angular distortion ranging from 1 to 250 to 1 in 2500. The increased settlements occurred from pre-existing failures and placement over areas with different ground improvement types. Refer to Figure 9 for the settlement records (De Silva et al, 1998).

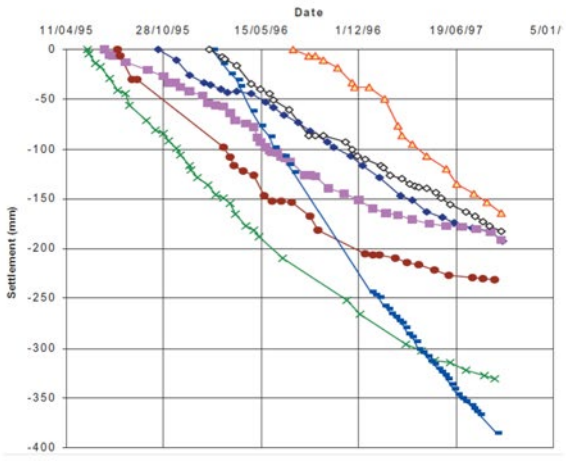

Figure 9 – Foundation settlement, Sai Ho Wan Ho

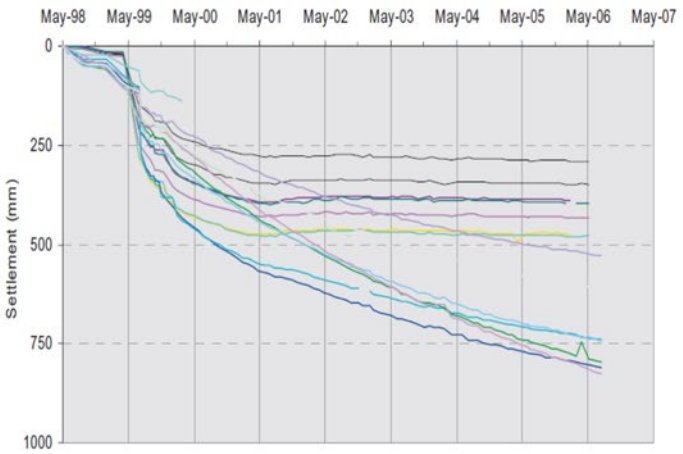

Figure 10 – Settlement records (TKO, Zone B)

Reclamations with vertical band drain installations have accelerated the primary consolidation, however longer term settlement from secondary consolidation has typically continued. Examples are presented from records taken from the Tseung Kwan O (TKO) and Ma On Shan reclamations (Ng & De Silva, 2007), see Figures 10 to 12.

Suggested mitigation to limit future long term settlement is to achieve 100% consolidation under the anticipated working loads by applying a degree of over-consolidation, say 1.2, typically allowing an economic construction to continue (De Silva et al, 1998).

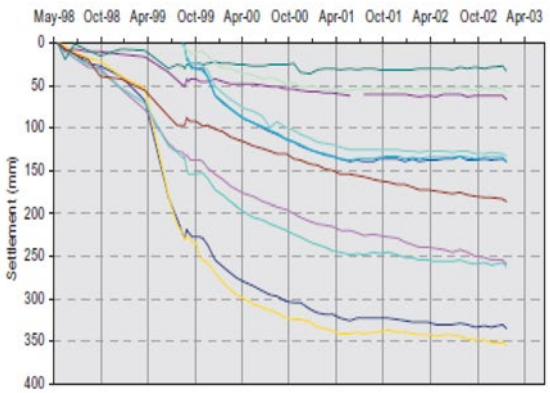

Figure 11 – Settlement records, TKO Ind. Estate

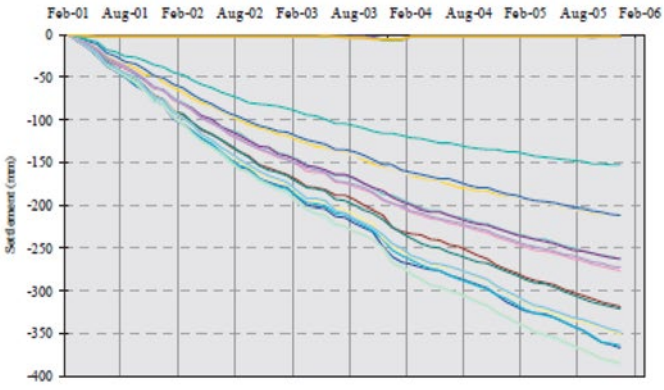

Figure 12 – Settlement records, Ma On Shan

Cotai Waste Receiving Facility, Macau (Vibro-replacement)

The Cotai Waste receiving facility is located on reclaimed land placed on superficial deposits between the Taipa and Coloane islands west of the Macau International Airport Southern Taxiway Bridge (STB) and the Cooling water intake plant, Coloane Island. During recent decades the volume of waste taken to the receiving facility increased to levels greater than anticipated; instability of the underlying superficial deposits occurred from the additional loading forming mud waves extending significant distances beyond the facility perimeter (De Silva & Fong, 2013). Refer to Figures 13 and 14 for the locations.

Figure 13 – Mudwave location

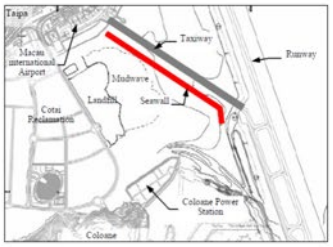

Figure 14 – Stone column bund, "Seawall", location

To allow continued operation of the waste Receiving Facilities and prevent impact to the STB, and other facilities, vibro-replacement stone columns were installed. The superficial deposits underlying the installation comprised 13 to 28m of soft to very soft clay to silty clay and sandy silty clay Marine Deposits, underlain by Alluvium with interbedded soft to stiff clay, silty clay and silt and sand. The stone columns comprised 1.2m diameter, 2.5m c/c triangular spaced stone columns which were installed beneath a 50 m wide bund to increase the strength of the underlying Marine Deposits. The installation provided a 21% replacement of the Marine Deposit with granular fill with a sufficient strength increase to mitigate instability and increase permeability to allow release of excess pore water pressure (De Silva & Fong, 2013 and Barksdale & Bachus, 1983).

6 CONCLUSIONS

Reclamations in the HKSAR are being placed onto non-dredged soft superficial deposits with increased uncertainties for settlement periods required prior to construction. To address this issue representative geotechnical parameters need to be ascertained using comparisons with parameters determined from long term settlement records from past projects. An understanding has been gained of the limitations using wick drain installation, which needs a suitable over-consolidation, of say 1.2, to address long term settlement, and vibro-replacement techniques which can be used to improve both strength and accelerate settlement. Both ground improvement techniques require careful installation techniques to limit instability. For the vibro-replacement longer term settlement monitoring to verify success in accelerating settlement in typical HKSAR ground conditions is required.

ACKNOWLEDGEMENTS

The contents of this paper do not necessarily reflect the views and policies of these supporting organizations, nor does the mention of trade names and commercial products constitute endorsement or recommendation for use.

REFERENCES

Barksdale, R.D. & Bachus, R.C. 1983. *Design and Construction of Stone Columns;* Vol. 1, US Dept of Transport.

Beggs, C.J. & Tonks, D.M. 1985. *Engineering Geology of the Yuen Long basin.* Hong Kong Engineer, Vol. 13, No. 3: 33-41.

Bramall, R.H. & Raybould, M.J. 1993. *Lai Chi Kok Marine Reclamation,* Case Study. Int. Conf. on Soft Soil Engineering, Guangzhou: 58-67.

Choa V., Wong K.S. & Low B.K. 1990. *Airport at CLK,* Geotechnical Review Assessment.

De Silva, S., Sekula, J., & Endicott, L.J., 1998. *LAR Depot Construction on Reclamation at Siu Ho Wan. HK,* Inst. Engineers (HKIE), Geot. Div., 18th Ann. Sem., 29 May, 1998. Geotech Aspects Airport Core Projects: 155- 169.

De Silva & Fong, L.T.T. Fong, 2013. *Design Construction of Landfill Containment Supported on Stone Columns Installed in Very Soft Marine Mud in Cotai, Macau.* Hong Kong Institution of Engineers, Geotechnical Division, 37th Ann. Sem., 29 May, 2013: 111-118.

Fletcher, C.J.N. 2004. *The Geology of Site Investigation Boreholes from Hong Kong. 2000.* Association of Geotechnical and Environmental Specialists.

Fung, A.K.L., Foot, R., Cheung, R.K.H., & Koutsoftas, D.C. 1984. *Practical Conclusions from Geotechnical Studies on Offshore Reclamation for proposed CCLK Airport*. Hong Kong Engineer, Vol. 12, No. 6: 17 – 26.

Fyfe, J.A., Shaw, R., Campbell, S.D.G., Lai, K.W., & Kirk, P.A. 2000. *The Quaternary Geology of HK.* HK Geological Survey, Geotechnical Engineering Office, Civil Engineering Department. The Government of the Hong Kong Special Administrative Region.

GEO. 2007. *Engineering Geological Practice in Hong Kong*. GEO Publication 1/2007.

Ho, K.S & Chan, Y.C. 1994. *Ground Improvement Marine Mud,* Proc. Ground Improvement, 1994, Hong Kong Institution of Engineers, Geotechnical Division, pp85 - 102.

Hunt, T., Kemp, W. R. & Koo, Y.C. 1982. *Castle Peak Bay reclamation, Hong Kong.* Proc. of 7th SE Asian Geot Conf., Hong Kong.

Lo, D.O.K. & Chan, Y.C. 2004. *Secondary compression of soils under the CLK Airport.* Proc. of Int Conf. Coastal Infrastructure Development–Challenges in 21st Cent, HK.

Lo, D.O.K. & Premchitt, J. 1999. *Long term consolidation tests on soils from the CLK.* Hong Kong Institution of Engineers, Transactions HKIE, Vol. 6, No. 3: 8-14.

Mackay, A.D & Wightman, N.R. 2016. *Design and Construction Reclamations & use of Vibro-Compaction.* Hong Kong Institution of Engineers, Geotechnical Division. 36th Ann. Sem., Recl: Challenges & Beyond.

Ng, F.H.Y & De Silva, S. 2007. *Geotechnical Practice of Reclamations in Hong Kong.* Hong Kong Institution of Engineers, Geotechnical Division, Ann. Sem., 2007, Geotechnical Advancements Hong Kong since 1970s: 69-83.

Plant, G.W. Covil, C.S & Hughes, R.A. 1998. *Site Preparation New Hong Kong International Airport.* Thomas Telford Publishers.

Siu, M.P., & Chow, K.C., 1988. *Use of vertical drains construction of Island Eastern Corridor Road.* Hong Kong Engineer, Vol. 16, No. 2: 13-18.

Ng, H.Y. 1991. *Case Histories of Reclamation Techniques.* Proceedings of the Hong Kong Institution of Engineers, Geotechnical Division.

Siu, M.P. & Chow, R.C. 1988. *The Use of Vertical Drains in Construction of the Island Eastern Corridor Road.* HK Engineer 16: 13-18.

Yeung, A.T. & So, S.T.C. 2001. *Geotechnical Engineering Properties of Hong Kong Marine Clay.* Proc of Third Int Conf on Soft Soil Engineering, HK, 6-8 Dec, pp 695-700., 2001.

Walker L.K. 1969. *Secondary Settlement in Sensitive Clays.* Canadian Geotechnical Journal, vol. 6, 2: 219-222.

Artificial Ground Freezing Hong Kong Case Histories: Lessons Learnt

A.D. Mackay
HSS Integrated, Kuala Lumpur, Malaysia

ABSTRACT

Artificial Ground Freezing (AGF) was established 1862 as a robust ground support and groundwater cut-off technique for sub-surface excavations. In the Hong Kong Special Administrative Region (HKSAR) it was initially used for a pipe jacking launch for the Harbour Area Treatment Scheme (HATS) during 2001. Since then it was used for cross passage (CP) construction for the Lok Ma Chau, Sheung Shui to Chau Tau Tunnel, 2004, and for Tunnel Boring Machine (TBM) launches and retrieval for the HATS Stonecutters Island Sewage Treatment connecting tunnels, 2011 and the Mass Transit Railway Corporation (MTRC), West Island Line (WIL), 2012. The use of AGF in the HKSAR culminated in the MTRC, WIL adit construction between the Sai Yin Pun Station and Des Vouex Road entrance, 2014; currently the longest excavation using the AGF in Asia. Although this technique requires a greater time and cost compared to other ground improvement for excavations in soils with variable particle sizes. This paper provides an overview of the use of the AGF internationally and typical design and construction methods used. A review of the use of AGF in the HKSAR and a summary past case histories in the HKSAR provided.

1 INTRODUCTION

AGF techniques have been used as a robust ground support and groundwater cut off for subsurface excavation for over a century internationally and during the last two decades in the HKSAR. It provides greater security against settlement and instability for variable ground conditions compared to other support methods, however, there are cost and time implications, particularly the time required to gain the soil strength needed and the energy required. The most recent use of the AGF has been the Sai Ying Pun (SYP) Station to Des Voeux Road West adit connections, comprising an inside diameter (ID) of 6.5m, lengths of 20 and 83m.

AGF has been used in the HKSAR for a ground conditions ranging from Marine Deposits, Alluvium, volcanic and granitic saprolites and partially weathered, "mixed" ground conditions (GCO,1988 and GEO, 2007) and for civil engineering applications for CPs, TBM launches and retrievals, mined excavation between shafts and ultimately for larger scale adit construction.

This paper provides an overview of the use of AGF design and construction and a history of its use in the HKSAR, summarizing the challenges faced. A summary of published case histories is provided for the use of AGF in the HKSAR from published information for the HATS Stage 1, Contract DC/93/10, 2001; the Lok Ma Chau Spur Line, Sheung Shui to Chau Tau Tunnel, Contract LDB 201, 2004; the HATS Stage 2A Pumping Station, Stonecutters Island Sewage Treatment Works and connecting tunnels, Contract DC/2009/05, 2011; the MTRC, WIL, Sheung Wan to Sai Yin Pun Tunnels, Contract No. 703, 2012 and the WIL, Contract 704 adits, 2014. The lessons learnt from the range of civil engineering applications used and ground conditions encountered is given, including the program constraints, equipment set-up, and the time required for the AGF to reach design thickness and the excavation techniques.

2 BACKGROUND TO THE USE OF THE ARTIFICIAL GROUND FREEZING TECHNIQUE

2.1 Overview

AGF is an internationally established, robust ground support and groundwater cut-off technique. The AGF is achieved through refrigeration of a cooling fluid, which is pumped along freezing tubes installed into the ground needing support and groundwater cut off surrounding the excavation. The main freezing stages are the freezing commencement around the tubes; closure of the gaps between frozen sections and completion of the freezing block or annulus upon reaching the design thickness and temperature. The two available cooling fluids are liquid nitrogen or brine. Brine is cooled in a refrigeration unit to -28 to -35°C and liquid nitrogen to a condensation temperature of -196°C prior to circulation through freezing pipes surrounding the excavation. Following circulation, the brine is returned to the refrigeration unit for cooling and recirculation; the liquid nitrogen is released to the atmosphere. As the brine operates at a higher temperature it has lower operating costs and reduced refrigeration power; however it has the disadvantages of a more complicated installation, operation and management for the refrigeration set up and increased ground freezing periods and limited scope in the presence of moving groundwater.

2.2 International use of AGF and history

AGF was initially used 1862 to support shaft construction for coal mining access in South Wales. Shortly after F. Hermann Poetsch patented the "Method of and Apparatus for Sinking Shafts through Quicksand", 1883, it became frequently used for mining operations throughout Europe thereafter and in Russia for mining operations, 1928 (AGS, 2013). In the United States of America (USA) AGF was used about 80 years ago by the Chapin Mine Company, Iron Mountain, Montana for a 100 feet deep; 33m below ground level (m bgl) shaft excavation. 60 years later it was used to sink the 765-feet deep; 250m bgl, shaft for the Potash Company of America's Carlsbad, NM mine (Moretrench). In the Peoples Republic of China (PRC) its initial was used for shaft construction during 1955 and used with increased frequency for railway construction after 1992 (AGS, 2013). More recently it was used for the Chong Ming Tunnel CP construction between the 7.5 m I.D twin tunnels formed by TBM construction beneath the Yangzi River Shanghai, 2011. The CPs were 2 m I.D. located about 65 m bgl and constructed through silty alluvium.

2.3 Advantages and limitations of the AGF

The AGF can be used in variable ground conditions and ranges of soil particle sizes, from Clay <0.001mm diameter (dia.) to Cobbles, >60mm dia. (GCO, 1988). Alternative ground improvement techniques, such as dewatering, grouting and compressed air, are limited to selected soil particle size ranges as summarized in Table 1 (AGS, 2013).

Table 1: Grain Size Limitation Range and Other Disadvantages of Alternative Ground Improvement Techniques

Method	Grain Size (GCO, 1988)	Other Disadvantages
Dewatering	C. silt (>0.05mm) – f. gravel (<2mm)	potential settlement effects areas away from the dewatering location
Grouting (cement – bentonite)	F. sand (>0.1mm) – c. gravel (<60mm)	
Grouting (chemical)	M. silt (>0.05mm) – c. gravel (<60mm)	
Compressed air	F. silt (>0.01mm) – c. sand (<1mm)	associated health hazards

Further advantages of the AGF is that the equipment assembly can be remote from the construction location and environmental advantages such as use of non-toxic and non-intrusive constituents and potential re-circulation of the cooling agent. The dis-advantages for the AGF are the time required to achieve the design strength and freezing thickness, freeze – thaw effects causing expansion and contraction, weakening effects after thawing, the need for a fully saturated medium, associated used of grout injection and relative time and cost compared to other techniques.

2.4 Design and Testing Considerations

Laboratory testing used to determine the design parameters for AGF includes Unconfined Compressive Strength (UCS), creep, frost heave / thaw, consolidation, thermal conductivity and heat capacity testing, as outlined in the Ministry of Coal Industry, PRC (MCI, 1996, a&b) and the American Society of Standard Testing (ASTM), both of which have been used as standards for AGF laboratory testing in the HKSAR.

The strength and deformation of the frozen annulus depends upon the saturation, air content and volume of ice formed between the soil particles, the original soil structure and groundwater flow rate. Figure 1 presents variations in UCS against water content and temperature for river sand (Kuribayashi et al; 1985).

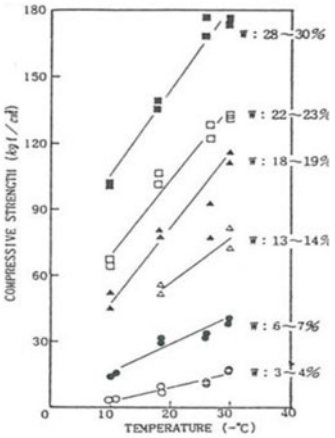

Figure 1 – sand variations

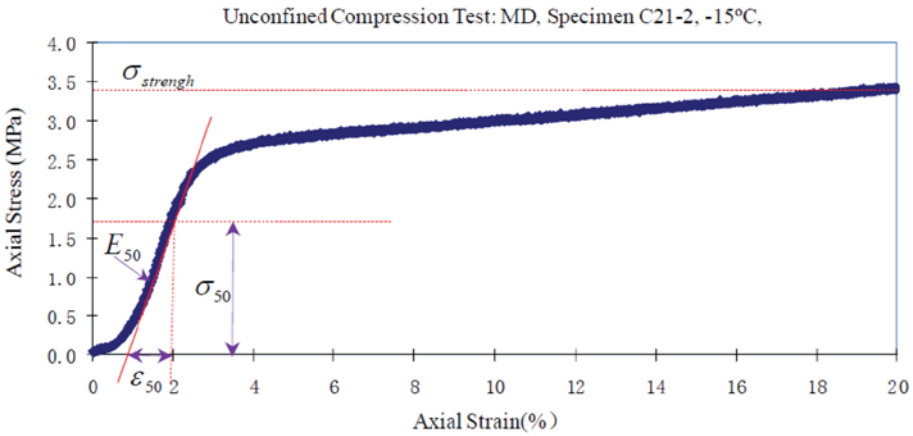

Figure 2 – axial stress - strain; -15°C; Marine Deposits

UCS tests carried out at different temperatures are used to establish a strength to frozen temperature sensitivity. The stress is typically applied at a constant strain rate of 1% per minute, up to a 20% axial strain, to obtain the UCS (qi) at the "instantaneous strain rate". Examples of the testing from the HATS 2A Contract DC/2009/05 revealed that the qi for Marine Deposits (GCO, 1988 and GEO, 2007) typically occurred at strain rates less than 20%. The specimens, frozen at -10 and -15°C presented in Figures 2 and 3, showed the axial stress to increase with a constant rate up to qi values of 2 and 2.8MPa, the strain rate increased with a reduced stress increase thereafter.

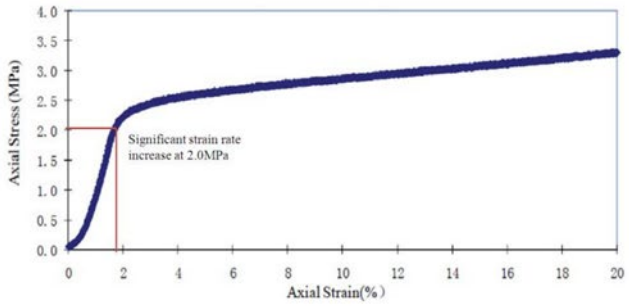

Figure 3 – axial stress - strain; -10°C; Marine Deposits

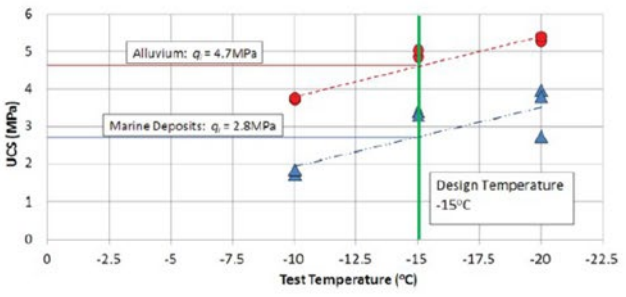

Figure 4 – axial stress - strain; -10°C; Marine Deposits

The variation of q_i for Marine Deposits and Alluvium are presented in Figure 4 (Tsang et al, 2012a); the q_i values were taken to be 2.8 and 4.7MPa respectively for the design temperature of -15°C.

As ice and frozen soil can creep under loading, the creep strength and strain needs to be determined; in general, the long term strength of frozen soil is approximately 40% to 60% of the instantaneous strength (Schultz & Hass, 2011). Testing is typically carried out at constant load applications of 0.7, 0.5, 0.4 and 0.3q_i. The creep curve typically passes through the primary, secondary and tertiary stages representing a decrease, constant and increase in strain rates accordingly. The termination criteria is

typically after 24 hours with creep strains less than 5%. Examples of tests carried out at constant and variable strain rates at $0.7q_i$ on Marine Deposits from the HATS 2A, Contract DC/2009/05 are shown on Figures 5 and 6 (Tsang et al, 2012a).

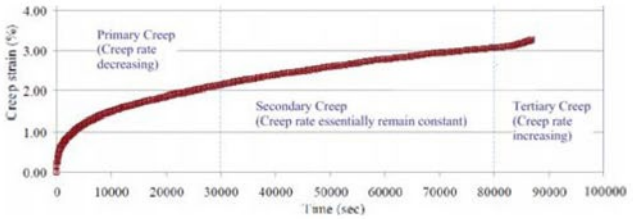

Figure 5 – Creep strain; time (variable strain rate)

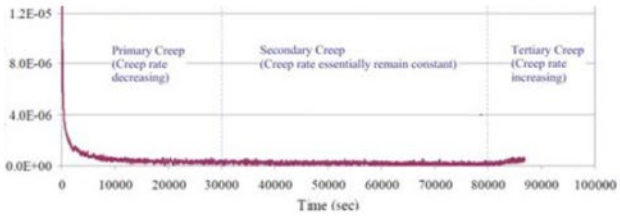

Figure 6 – Creep strain; time (constant strain rate)

2.3 General Requirements

To ensure the safe operation of the AGF a back-up generator and refrigeration unit is generally used. The freezing pipe spacing is assessed based on either past case history experience or a thermal analyses carried out during the design and verification stages of the freezing operation. Grout is used to backfill voids surrounding freezing pipe to allow connection with the ground. Thermocouples and digital thermometer installations monitor the ground temperatures (AGS, 2013).

3 PAST USE OF THE ARTIFICIAL GROUND FREEZING TECHNIQUE IN THE HKSAR

3.1 Overview

AGF techniques have been used in the HKSAR for the HATS Stage 1 Sewage Conveyance tunnel (Contract. DC/93/10; 2001); the Lok Ma Chau Spur Line, Lok Ma Chau, Sheung Shui to Chau Tau Tunnels (Contract LDB 201; 2004); the HATS Stage 2A Pumping Station, Stonecutters Island Sewage Treatment Works and connecting tunnels (Contract DC/2009/05, 2011), the MTRC, WIL, Sheung Wan to Sai Yin Pun Tunnels (Contract 703, 2011) and the MTRC, WIL adit connections from Des Voueux Road to the Sai Ying Pun Station (Contract 704, 2014). The locations of the AGF is presented in Figure 7.

Figure 7 – Locations of AGF Case Histories

A summary of the application of the AGF technique in the HKSAR in chronological order is provided in Table 2 (Mackay et al, 2014):

Table 2: The use of AGF techniques in the HKSAR

Date used	Contract	Excavation details	Purpose and AGF summary	Reference
2001	HATS Stage 1, DC/93/10.	1.8 m internal diameter (I.D.); 22 m bgl; 6m length.	Pipe jacking launch from Kwun Tong shaft. Vertical freezing pipes advanced from ground level.	Pakianathan. et al, 2002a.
2004	LDB 201.	3No. CPs, 3 by 2m I.D, 17 m bgl crown level, 7 m max. length.	Restricted access from the surface. Horizontal freezing pipes advanced from main tunnel.	Storry et al, 2006
2011	HATS Stage 2A, DC/2009/05.	4m I.D., 28 m bgl crown level, 2.5m length.	TBM launch. Vertical freezing pipes advanced from ground level.	Leung et al, 2012; Tsang et al, 2012a
2011		2m I.D., 28 m bgl crown level, 14m length.	Connection tunnel between rising main and TBM launch shaft. Horizontal freezing pipes advanced from TBM launch shaft.	Tsang et al, 2012b.
2012	MTRC, WIL, 703.	4m I.D., 30 m bgl crown level, total 33m length.	Excavation gallery and TBM recovery beneath congested area. Horizontal ground freezing tubes, max. length 20m.	Polycarpe et al, 2012
2014	MTRC, WIL, 704.	2No. adits of 6.5m I.D., 25 – 30 m bgl to crown level, 20 and 83 m length.	2No. adits beneath congested area. Vertical freezing pipes advanced from ground level; horizontal freezing pipes from the adit access.	Mackay et al, 2014 & Chan et al, 2015

The HATS Stage 1 Sewage Conveyance tunnel, Contract. DC/93/10, used Liquid Nitrogen Coolant; all other Contracts used brine cooling fluids.

The ground conditions encountered included Marine Deposits for the HATS Stage 1; volcanic saprolites and partial weathered, "mixed" ground for the Lok Ma Chau Spur Line (LDB 201); inter-bedded granular and cohesive bedded Alluvium (Chan et al, 2015), overlain by Marine Deposits (HATS Stage 2A; DC/2009/05) and granitic saprolite and "mixed" ground (GCO, 1988 & GEO, 2007) for the MTRC, WIL contracts. The AGF was amenable to soils, particularly with increased porosity and moisture content; however difficulties were encountered within "mixed" ground for providing accurate freezing pipe alignment; connection between the pipe and the rock constituents and variable thermal properties between the rock and soil, increasing the freezing periods (Storry et al, 2006 & Mackay et al, 2014).

3.2 HATS Stage 1 Contract. DC/93/10

During the formation of the junction between the shaft and the tunnel adit for the Kwun Tong pumping station difficulties were encountered from a sudden in-rush of sand and groundwater (Pakianathan. et al, 2002b). Due to the potential increase in groundwater flow at this location AGF with liquid nitrogen coolant was used to provide an impermeable plug and support for the pipe jack launch through the diaphragm wall at this location.

3.2 Lok Ma Chau, Sheung Shui to Chau Tau Tunnel, Contract LDB 201

The MTRC, Lok Ma Chau Spurline connects the East Rail Line to the PRC Lok Ma Chau Border crossing. 3.2 km of the alignment were formed using twin TBM excavations with 7.625 m I.D tunnels. The fire safety evacuation requirements needed CPs to be located every 240 m along the running tunnels. Due to restricted access from the surface within the environmentally sensitive Long Valley wetlands area, 3No. CPs, referenced 2, 3 and 4, required AGF support and groundwater cut off installed from within the tunnel.

The design and construction challenges included a target 4 week freezing program; efficient connection of the freeze envelope to the running tunnels; and minimal impact on adjacent sensitive receivers, such as running tunnel lining and on-going tunneling operations. Design parameters; q_i

of 2.4MPa and initial secant modulus (E_{50}) of 200MPa were adopted and a thermal analysis used to estimate the time required to form the frozen annulus to achieve sufficient strength to support the overburden pressure whilst minimizing imposed stresses imposed on the tunnel lining. 32 No. freezing pipe installations were designed for the CP excavations.

The freezing pipes had an inner tube dia. of 40mm and outer dia. of 60mm installed after the 2nd TBM drive had passed the CP location. 3 No. 94kW refrigeration units were used to circulate brine with target temperatures ranging between -30 to -35°C. Thermocouples were installed to measure temperatures within the tubes and tunnel lining. Temperature measurements were also taken for the supply and return of the brine coolant; plant operations and ambient air temperature. Piezometric pressures inside and outside the frozen annulus were taken to verify closure of the frozen annulus and deformation and induced stress monitoring taken for the CP support frames. The piezometric pressures and changes in temperature mid-way along the CP invert is presented in Figure 2 and temperature distribution along the CP presented in Figure 8.

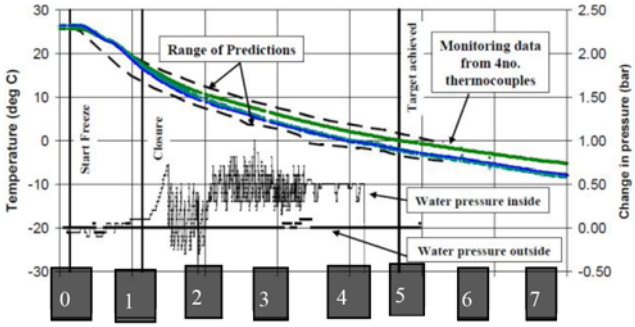

Figure 8 – Piezometric pressure; freezing period; weeks*

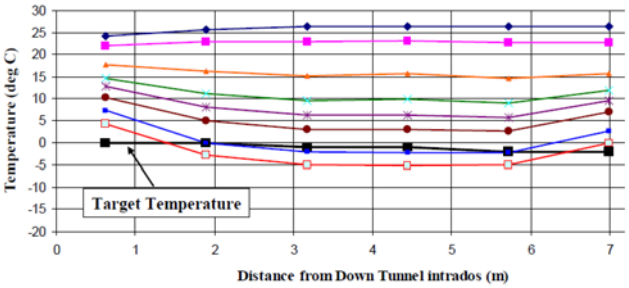

Figure 9 - freezing period along CP*

* Figures cover the 7 weeks from 8 December 2004 to 26 January 2005.

Figure 8 shows the piezometric pressure outside the frozen annulus did not vary after closure of the frozen annulus following 7 days of freezing. The piezometric pressure within the annulus revealed fluctuations from pressure variations during freezing. The temperature measurements showed that freezing occurred after about 4 to 4.5 weeks. Figure 9 shows temperature increases towards the tunnel and CP junctions.

Mixed ground conditions were encountered in the upper levels of CP4. This resulted in an increased period to reach freezing compared with the other CPs and the lower levels of CP4; refer to Figure 10 for the periods required to reach freezing. The thermal analysis for CP4 is presented in Figure 11, as shown the decrease in temperature was recorded in rock conditions located towards the upper levels.

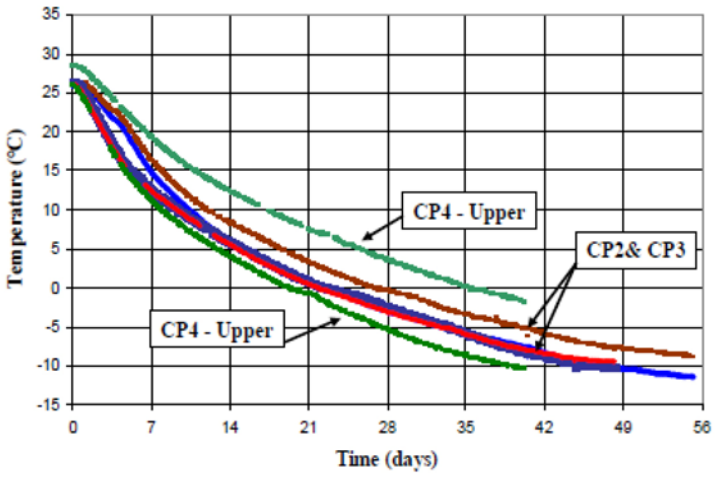

Figure 10 – Freezing period mid-way along the CPs

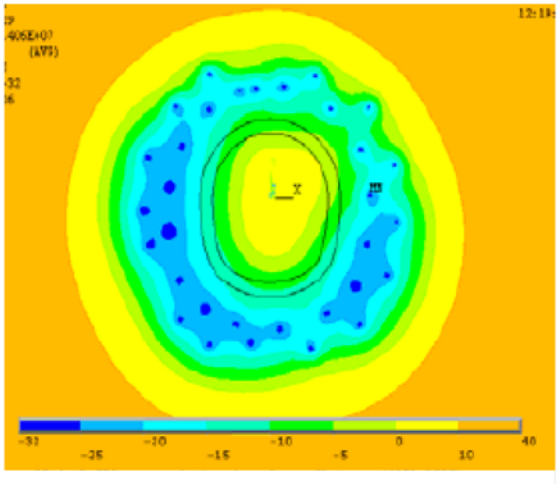

Figure 11 – CP4 freezing after 28 days

Handheld pneumatic tools were used to excavate the CPs and temporary support provided by circular arch ribs and sprayed shotcrete. The permanent lining was provided by 300mm thick sprayed shotcrete over the waterproofing membrane. The sequence used for the CP ground freezing pipe installation and excavation works, typical of CP excavation using AGF is presented in Figures 12 to 15 and AGF installation and CP excavation sequence summarized in Table 3 (AGS, 2013).

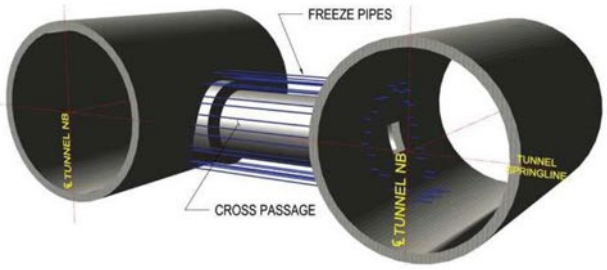

Figure 12 - Freezing Pipe drilling; double ring

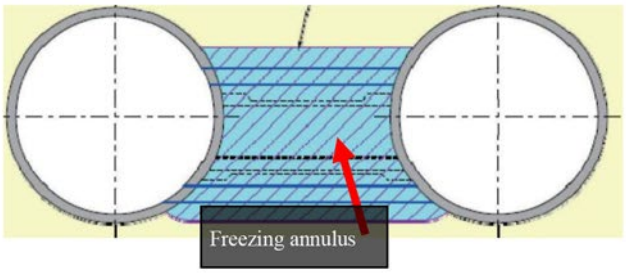

Figure 13 – Completion of freezing annulus

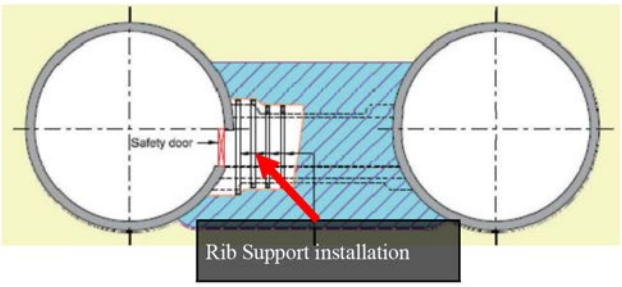

Figure 14 – Excavation and Temporary Rib Support

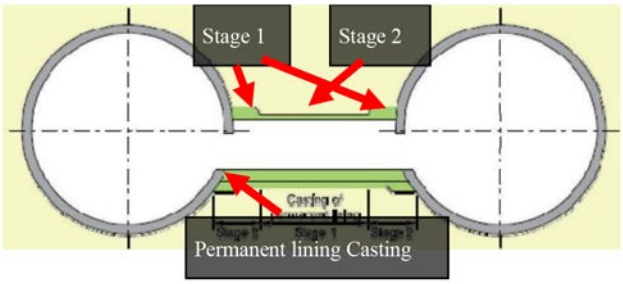

Figure 15 – Construction of Permanent Lining

Table 3: CP construction stages (AGS, 2013)

Stage	Works
Stage 1; Figure 12	Drill through the lining from one or both sides of the tunnel; a blow-out preventer is used to prevent inflow through the drill-rod. A double ring is typically form for the freezing annulus.
Stage 2; Figure 13	Set up the condenser, brine tank, pump, clean water pump, coolant, power support control and keep active freezing for about 45 to 60 days. The ground freezing annulus thickness is typically 1.5 to 2 m. The system is then tested and monitored until the required temperature and thickness is achieved
Stage 3; Figure 14	Probe to ensure minimal water ingress prior to excavation; install safety door and steel rib support; spray shotcrete as excavation proceeds. Apply thermal insulation layer between frozen soil and temporary support
Stage 1; Figure 15	Concrete is cast from mid-way along the CP until reaching the tunnel lining connection

The scaffold set up and Blow out Preventor used for the CP construction are shown in Plates 1 and 2.

Plate 1 – Scaffold for CP Access

Plate 2 – Blow out Preventor

The CP works and AGF construction program comprised approximately 5 to 7 weeks primary freezing, 6 weeks maintenance phase (excavation and construction) and 8 weeks thaw period.

3.3 Harbour Area Treatment Scheme, Stage 2A, Drainage Service Department Contract DC/2009/05

Contract DC/2009/05 involved the construction of a Pumping Station connecting to the Existing Riser Shaft via a TBM launch shaft. The Launch shaft connected to the New Pumping Station through a 236m length tunnel formed by TBM, referenced "Tunnel A", and to the Existing Riser Shaft, through a 14m length mined tunnel, referenced "Tunnel B". AGF techniques were required to support the ground and provide groundwater cut off for the entire length of Tunnel B and for the TBM launch into Tunnel A. Refer to Figures 16 and 17 for the AGF locations and Tunnel B configuration between shafts supported by Diaphragm Walls.

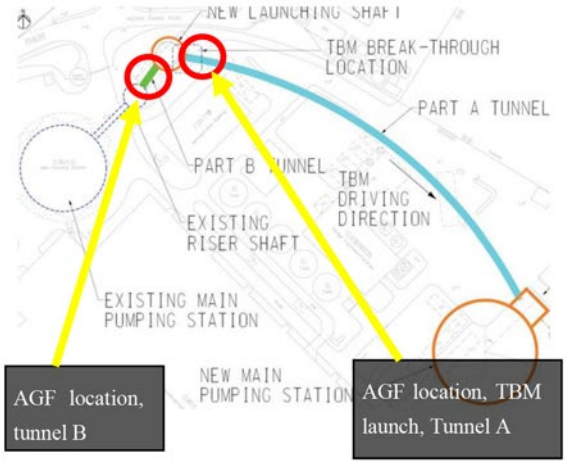

Figure 16 – Tunnels A and B locations

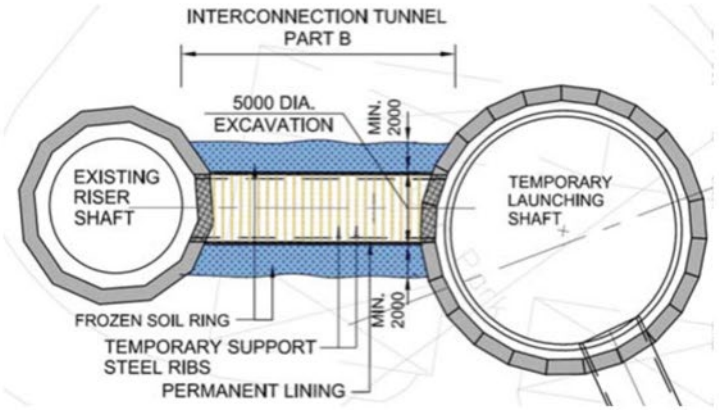

Figure 17 – Tunnel B configurations

The design strength parameters included q_i values of 2.8 MPa for Marine Deposit and 4.7 MPa for Alluvium. As excessive deformation was anticipated the design creep strength was taken to be 40% of the qi values (Tsang et al, 2012a). Other mechanical properties determined from the laboratory testing and adopted for the design, included the Creep Modulus and the Frost Heave and Thaw Consolidation Ratios for the Marine Deposits and Alluvium. The design parameters are summarized in Table 5 (Leung et al, 2012).

Table 5: Design Mechanical Properties for Marine Deposits and Alluvium

Frozen Ground	Creep Modulus (MPa)	Frost Heave Ratio (%)	Thaw Consolidation Ratio (%)
Marine Deposits	21	1.18	13
Alluvium	36	5.1	8.65

Two dimensional thermal analyses were carried out to determine the freezing pipe configurations and the time, energy and temperature required to form the frozen block and annulus. The input parameters for the analyses included the geometry, thermal conductivity at different temperatures. For the TBM launch the initial temperature was set at 25°C, reduced progressively to -28°C. The analysis showed that the design temperature of -15°C for the launch could be achieved within 20 days using a refrigeration system with a heat exchange of rate of 435 kJ / hour / m^2, multiplied by the launch face area. Immediately prior to the TBM launch the freezing pipes required extraction. A thermal analysis was there carried out to verify the heat loss within the 24 hours TBM launch period. (Leung et al, 2012). Refer to Figures 18 and 19 for the thermal analyses prior to launch (AGS, 2013).

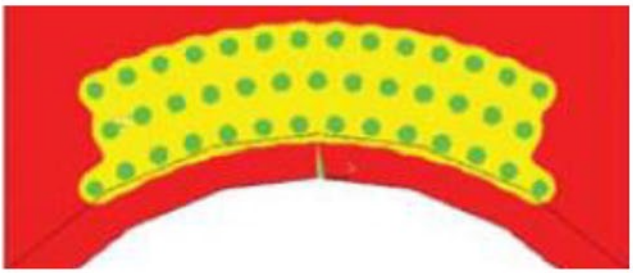

Figure 18 – Plan, thermal Analysis, 10 days freezing

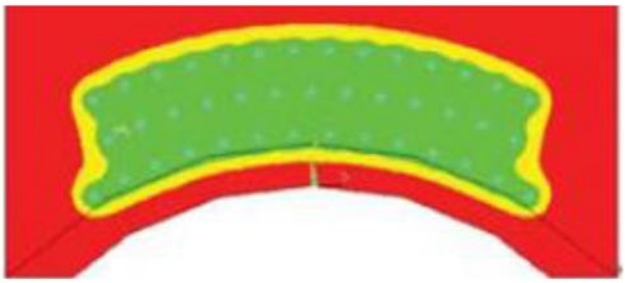

Figure 19 – Plan, thermal Analysis, 20 days freezing

* Green signifies the design temperature of-15°C.

The freezing pipe installations comprised two inner tubes of 0.38 m O.D. installed within an outer tube used to circulate the cooling agent within the outer tube, installed vertically from the ground surface for the TBM launch into Tunnel A, and horizontally from the TBM launch shaft, terminated "as close as possible" to the Existing Riser Pipe Diaphragm Wall, for Tunnel B (Tsang et al, 2012b). Refer to Figure 20 and Plate 3 for the freezing tube circulation and the installation configuration at the ground surface (Tsang et al, 2012a).

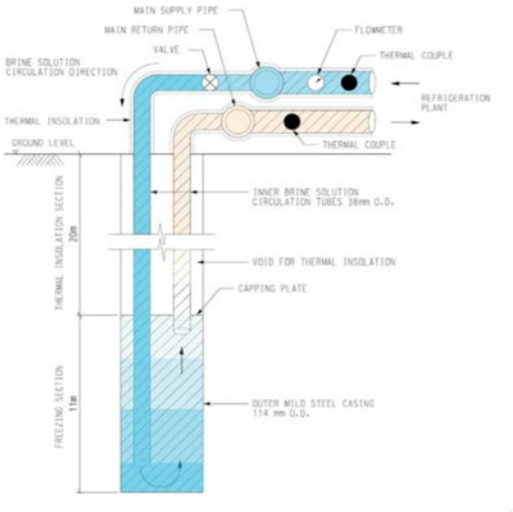

Figure 20 – Freezing pipe circulation system

Plate 3 – Freezing pipe installation; ground surface

38 No. freezing pipes installed in 2 rings were used to form a 2m thick annulus surrounding the excavation were installed to provide the AGF for Tunnel B. The freezing pipe installation had a maximum 0.2m deviation tolerance to ensure the frozen annulus formation. The estimated freezing duration was 60 days and excavation commenced after the required design temperature was achieved. Steel ribs at every 0.6 m advancement with intermediate steel plate insulation were installed as temporary support during excavation (see Figure 17).

The TBM launch into Tunnel A followed removal of the diaphragm wall and exposure of the frozen block. The frozen block had dimensions of 11 by 11m area with a thickness of 2.5m formed by 3 layers of freezing tubes. The freezing pipe configuration is shown in Figures 21 and 22 and frozen soil after diaphragm wall (D-wall) removal in Plate 4 (Tsang et al, 2012a). A TBM launch and AGF installation sequence is provided in Table 6 (AGS, 2013).

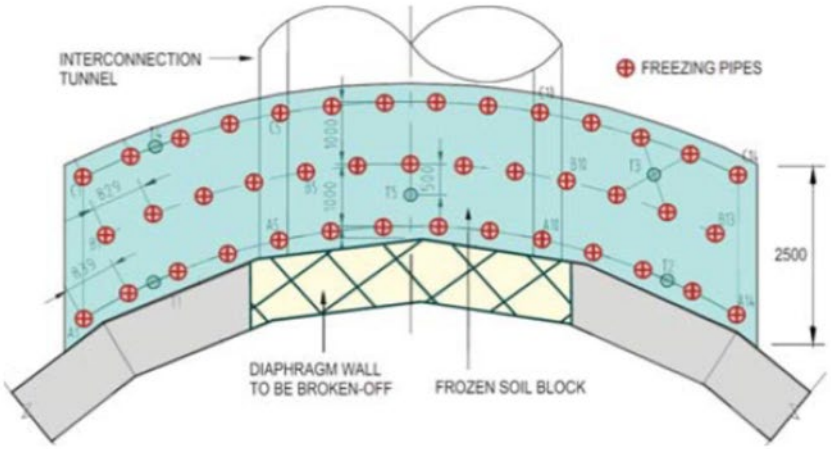

Figure 21 – Plan, freezing pipe configuration

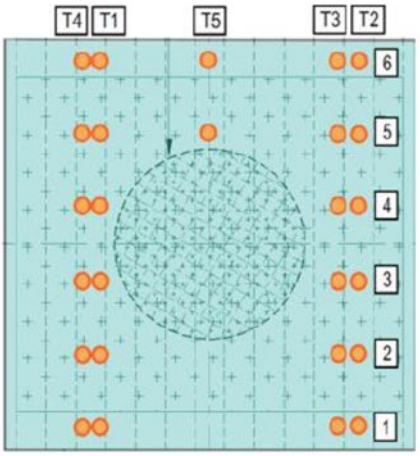

Figure 22 – Elevation, freezing pipes

Table 6: TBM CP construction stages (AGS, 2013)

1	Vertical ground freezing pipes are installed and ground freezing commences and TBM assembled
2	The Diaphragm Wall is opened, the TBM is advanced into position and water stop encases TBM as a safety precaution
3	Withdraw the ground freezing pipes to the tunnel crown level and restart freezing to ensure watertightness, possibly destroyed by the freezing pipe lifting operation. The frozen soil shall be maintained throughout the TBM breakout process
4	TBM breaks though the frozen block, the segmental lining is installed and annulus grouting installed as the TBM moves forward. Remove ground freezing pipes and carry out permeation grouting as contingency measures against thaw settlement if required.

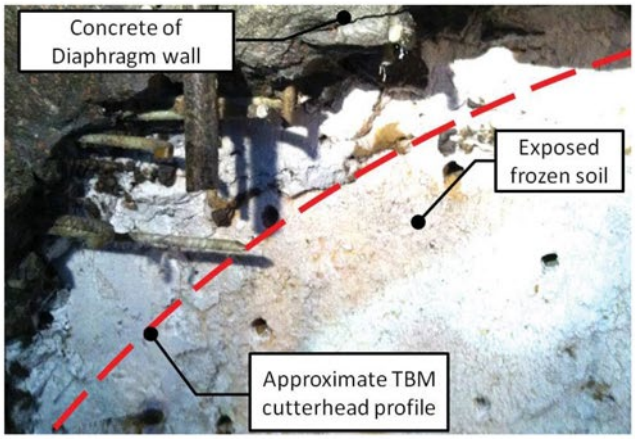

Plate 4 – frozen soil after diaphragm wall removal

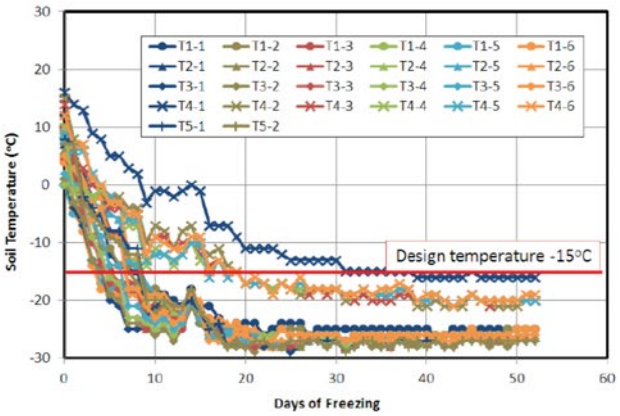

Figure 23 – temperature monitoring

The temperature was monitored by 26 thermal couples, referenced T1-1 to T5-2, as located in Figure 22. The design temperature of -15°C was reached after a 30 day active freezing period as shown by the monitoring results in Figure 23 (Tsang et al, 2012).

3.4 AGF for the MTRC, WIL.

The MTRC, WIL extends for 3.3 km from the existing Island Line (ISL), Sheung Wan Station (SHW) to the new Kennedy Town Station (KET) through the new Sai Ying Pun (SYP) and Hong Kong University (UNV) Stations. Contract No. 703 forms the connection between the existing SHW to the new SYP Station and involved the construction of the SHW to SYP Station connection tunnels and the ISL Cross Over Box (COB). Contract No. 704 comprised the construction of the new SYP and UNV Stations, connection tunnels between the KET, UNV and SYP Stations and associated adits. Refer to Figure 24 for the MTRC, WIL alignment.

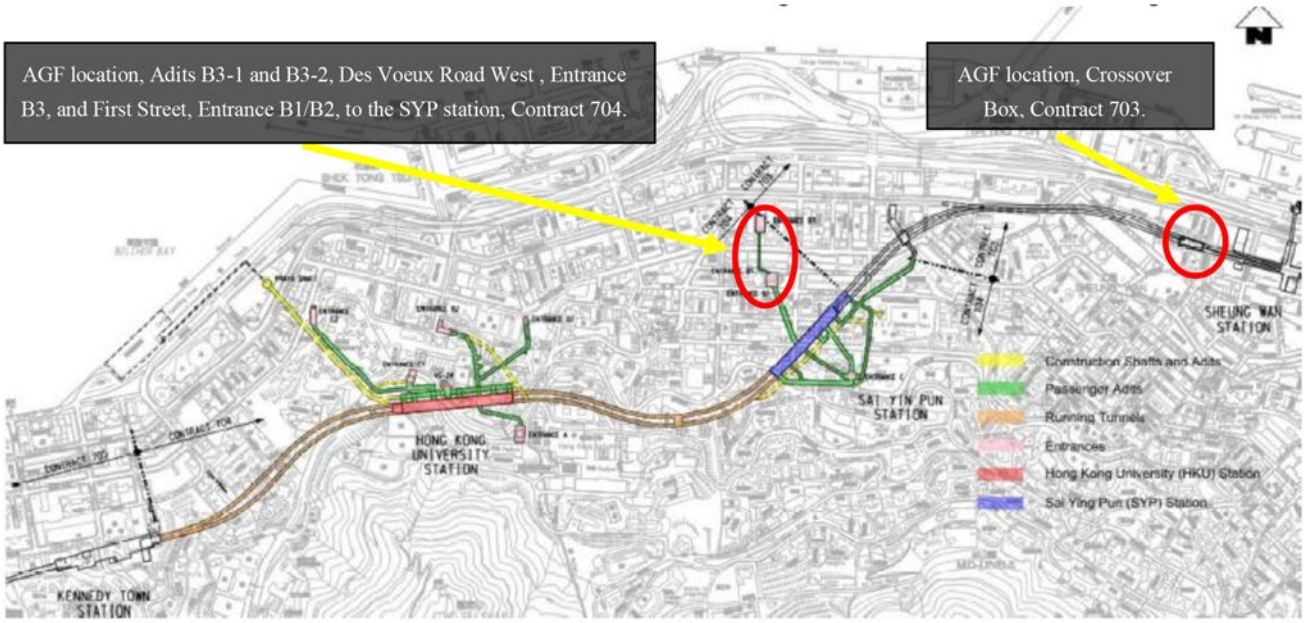

Figure 24 – AGF locations for MTRC WIL, Contracts 703 and 704.

3.4.1 Sheung Wan to Sai Yin Pun Tunnels, Contract No. 703.

The AGF for Contract No. 703 was used for an excavation gallery to allow access for removal of in-situ steel sets installed as temporary rock support for caisson foundation excavations for the Western Market development, Sheung Wan. The steel sets imposed a risk to the TBM advancement of the Up Track tunnel connection to the existing ISL. The gallery used to access the steel sets was 4 m I.D. and 33 m long; refer to Figure 24 for the location. Following the steel set removal the AGF was used to improve poor ground conditions present in the upper levels of the TBM break-in to the existing ISL, COB. Mechanical, thermal, and hydrological parameters were used for the PLAXIS, FLAC, TEMP/W and SEEP/W computer program input (Wong et al, 2012) and thermal analysis used to estimate the time to achieve the -10°C design temperature.

The DH deviation tolerance was limited to 1.5% to 2% for the freezing tube installation and were formed using a conventional Wassara W100 down-the-hole water hammer system, replaced by coring equipment when obstructions were encountered. The 33m long sub-horizontal and inclined freezing holes (22 nos.) and monitoring holes (5 nos.) were drilled through the mixed ground conditions and the as-built alignment records provided by a "Deviflex" system, used to generate 3D DH configurations. Due to DH deviations during drilling an additional 6No. compensatory freeze holes required installation. The frozen annulus comprised 2No. freezing ring installations and each freezing tube a high density polyethylene (HDPE) to avoid obstruction to the TBM drive. The freezing tube installation dimensions comprised a 90mm O.D outer tube and 50mm O.D; 41mm I.D. inner tube to allow brine flow circulation, refer to Figure 25. Voids surrounding the outer tube were backfilled using bentonite-cement mix grout.

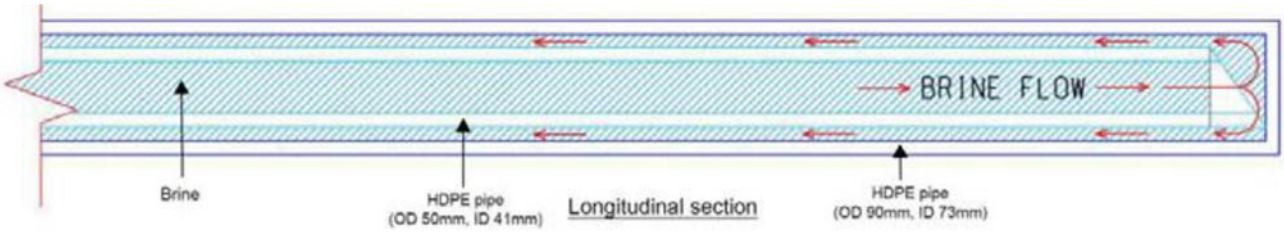

Figure 25 – Freezing tube configuration.

Temperature sensors were installed at 1 m spacing along each freezing tube and records taken in real time over a 24 hour periods. Piezometric records were taken within and outside the frozen annulus to record pore-water pressure increases during the freezing annulus formation. It took 8 weeks to achieve the designed frozen annulus, varying in thickness from 0.5 m in rock to 1.7 m in the saprolitic soils.

The TBM break-in through the permanent D-wall into the COB required AGF support and groundwater cut for the uppermost levels of the final 2m of the TBM advancement. The ground comprised moderately decomposed granite (MDG) rock overlain by completely / highly decomposed granite (C/HDG) saprolite; refer to Figure 26.

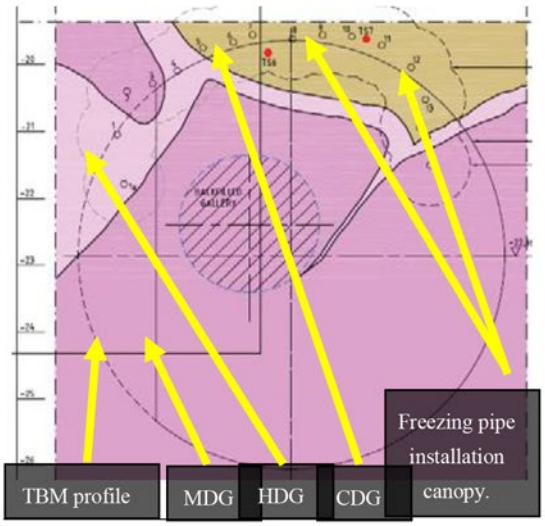

Figure 26 – Ground Conditions, TBM face

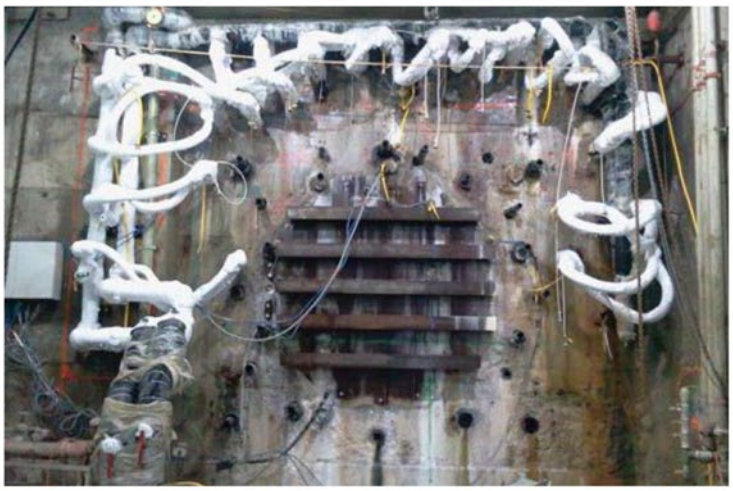

Plate 5 – Freezing Tube installation canopy

The AGF support canopy was formed by the installation of 15 freezing pipes above the excavation profile. Refer to Plate 5 for the freezing pipe installations from the COB.

3.4.2 Sheung Wan to Sai Yin Pun Tunnels, Contract No. 704.

AGF was required to provide ground support and groundwater cut off for Adits, referenced B3-1 and B3-2, providing passenger access between the SYP Station and Des Voeux Road West through SYP Entrances B3 and B1/B2, beneath First Street; refer to Figures 24 and 27 for the adit locations. The excavation lengths were 83m for Adit B3-1 and 20m for Adit B3-2; the O.Ds were 6.5m and final I.Ds, 5.9m and the depth to Adit B3-1 invert level increased from 20 to 40 m bgl from north to south respectively.

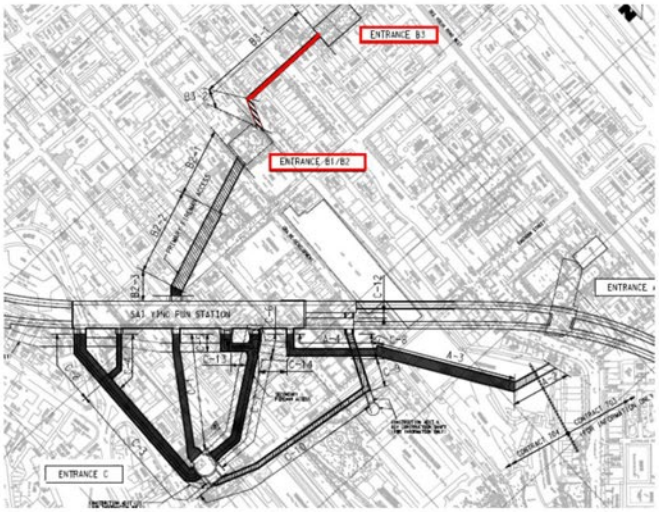

Figure 27 - SYP Adits B3–1 and B3–2 located between the First Street and Des Voeux Road West Entrances.

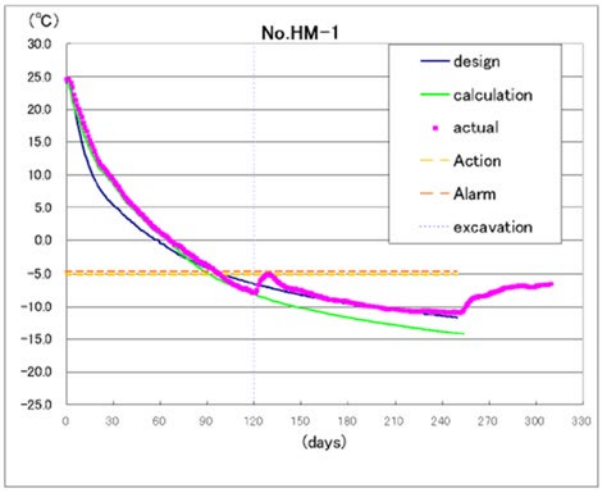

Figure 28 - Geological Plan, Adit B3–1 (GCO, 1986).

Both adits were located beneath old buildings sensitive to ground displacement and vibration, supported by a variety of foundations including rafts and driven friction piles extending to variable depths above bedrock. Given the risk to the sensitive buildings and excavation through highly variable ground conditions, AGF was selected to provide temporary ground support and groundwater cut-off.

Laboratory tests carried out to determine the strength and thermal properties of the CDG included UCS tests at temperatures of -5, -10 and -20°C; UCS tests at different strain rates and Creep tests, involving UCS tests with constant stress application. Refer to Figures 29 to 31 for the findings (Chan et al, 2015).

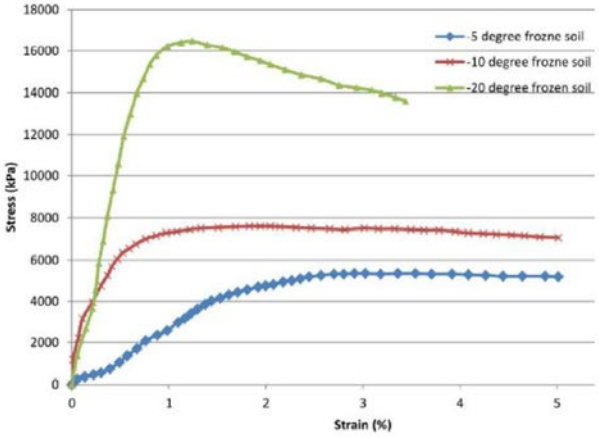

Figure 29 - UCS tests at -5, -10 and -20°C

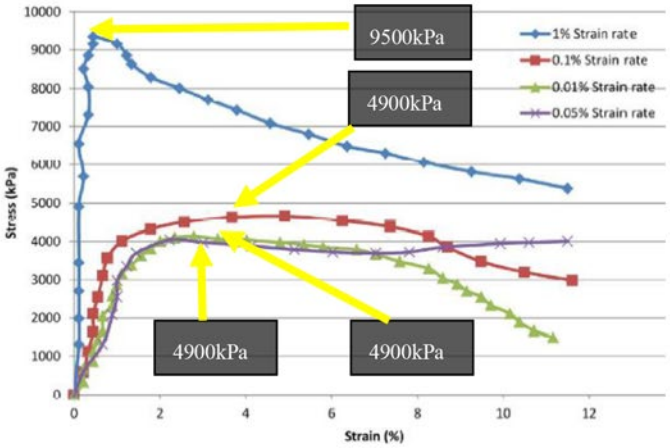

Figure 30 – Peak UCS, 0.05 – 1% strain rates at -10°C

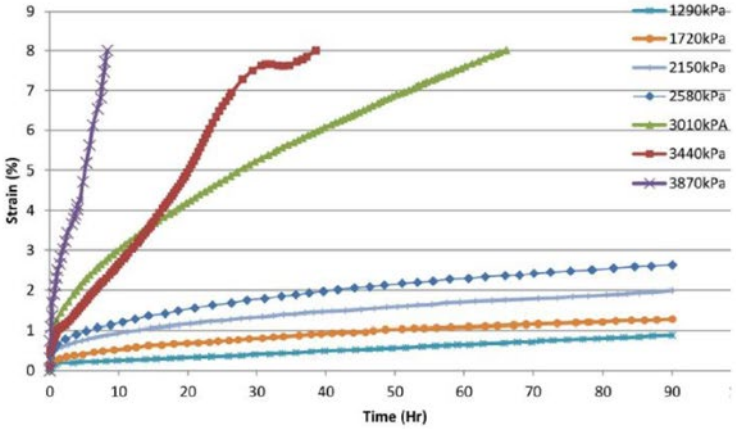

Figure 31 – Creep tests (strain / time), CDG specimens, -10°C

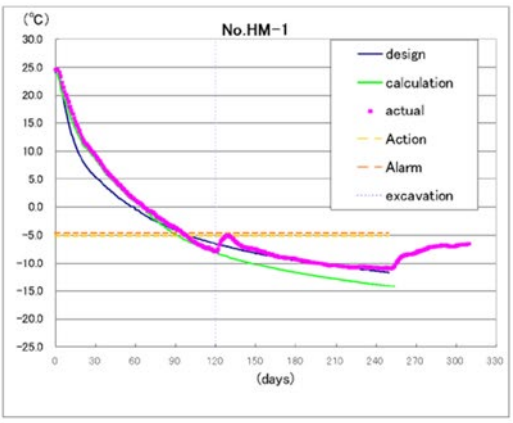

Figure 32 - temperature monitoring with time

The UCS tests revealed that an average temperature of -10°C could provide temporary support whilst maintaining suitable levels of stiffness and ductile failure mode. The UCS carried out at different strain rates (Figure 30) revealed that increased strain rates increase the peak strength, which occurs at reduced strain levels and for the Creep tests at -10°C (Figure 31) deformations increase significantly with time for axial loads greater than 2150kPa. Based on the results a min. 1.3m thick frozen soil ring with an average temperature of -10°C within the AGF annulus core was adopted with a 3m frozen end wall for Adit B3-1 to maintain longitudinal compression of the AGF annulus. The frozen soil ring and temporary composite lining (steel rib with shotcrete) area, were designed independently; both temporary supports accounted for the anticipated ground deformation, existing building impact, the lining structural capacity and deformation. The estimated period for the AGF annulus formation and end wall development was 89 days based on the assumption that the ambient ground and groundwater temperatures at these depths remained consistent at around 25°C. Refer to Figure 32 for an example of comparison of the designed and actual temperature monitoring results.

The freezing tube dimensions, and coolant flow and were selected based on the design thickness for the AGF annulus and required soil temperature and were similar to Contract 703, refer to Figure 25. The O.Ds for the freezing tubes ranges between 150 to 250mm for the O.D. and tube spacing installed

at 992mm c/c with a maximum deviation tolerance of 100mm. 25 No. ground freezing holes with 5 No. additional holes were installed to form the annulus and 6No. thermo-couple (temperature) monitoring installations were required around the periphery of both adits. A temporary composite lining was installed within the frozen soil annulus within two weeks after excavation and comprised a temporary steel arch ribs and shotcrete with an overall thickness of minimum 293mm, accounting for the additional shotcrete application. This provided an approximate 5.9 m I.D. adit following the temporary lining installation; see Figure 33 (Mackay et al, 2014).

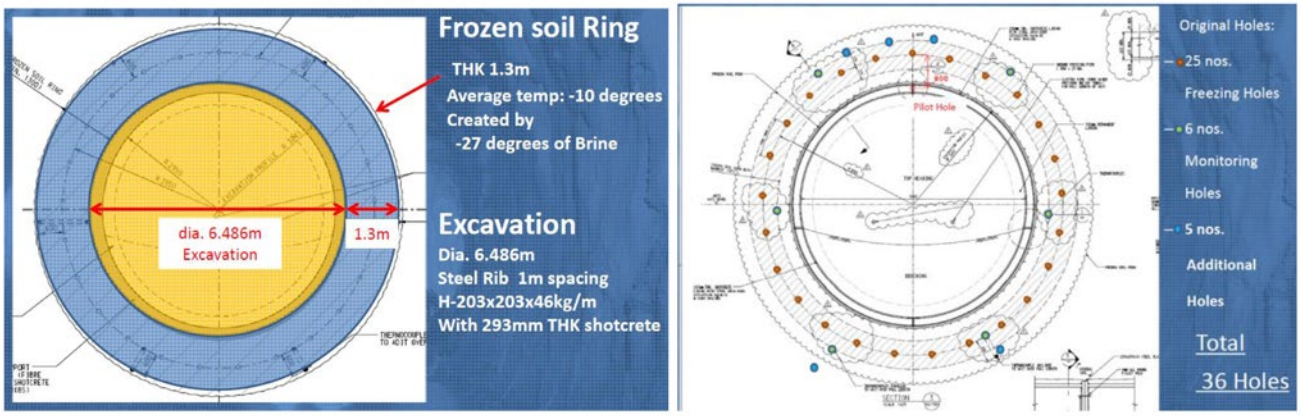

Figure 33 Design for the frozen soil ring and freezing pipes

6 No. thermo-couple holes were installed around the AGF periphery to record the temperature and 40m long water relief pipes installed within the AGF annulus to measure pore water pressure, provide pressure relief and verify the extent of closure of the frozen AGF annulus. To ensure the DH alignment was maintained the DHs were formed using a Horizontal Directional Drilling (HDD) techniques with a steerable mud motor and a tricone bit to cope with the variable ground conditions (Mackay et al, 2016). The freezing period was a longer duration than the anticipated design freezing period of 89 days, due to the over-freeze required to achieve the average temperature of -10°C, the freezing annulus extending a greater distance than anticipated at design stage; and deviation of the HDD beyond the 100mm c/c limit. The progressive AGF development is presented in Figure 34.

After the pile pipe wall breakthrough, initial excavation commenced within the top heading advanced 4m ahead of the bench, see Figures 35 and 36. Composite steel arch rib and fibre-reinforced shotcrete lining was installed as the excavation progressed, see Figures 37 and 38. An additional 40 mm sacrificial shotcrete layer was placed to ensure better curing over the 293 mm composite shotcrete and steel arch installation within the top and lower benches. A max. one week time limit was allocated to achieve the 25MPa strength criteria.

The increase in volume of frozen ground within the excavation, and associated increase in strength, reduced the rate of excavation to approximately one full rib installation per day. Upon reaching the end of the adit and installation of the final steel arch set, the excavation continued a further 1.4m to install a fibre reinforced shotcrete end plug placement with 3 layers of wire mesh to allow de-freezing of the AGF annulus and the end wall plug to take place. Commencement of the waterproofing membrane placement and permanent lining installation was then carried out. Refer to Figures 39 and 40 for the final lining installation.

4 CONCLUSIONS

Some of the lessons learnt and thoughts for improvement for the use of AGF include improvements in locating and controlling the DH direction; ensuring sufficient distance between the freezing pipes and the excavation periphery and the AGF does not extend too far into the excavation zone causing excavation difficulties. To control the AGF consideration could be given to reducing the average temperature and using a sprayed insulation layer (if available) immediately after excavation. The use of the AGF in mixed ground conditions also raises challenges to ensure drilling operations and freezing tube installation can achieve an accurate alignment, providing adequate connection between rock components and the

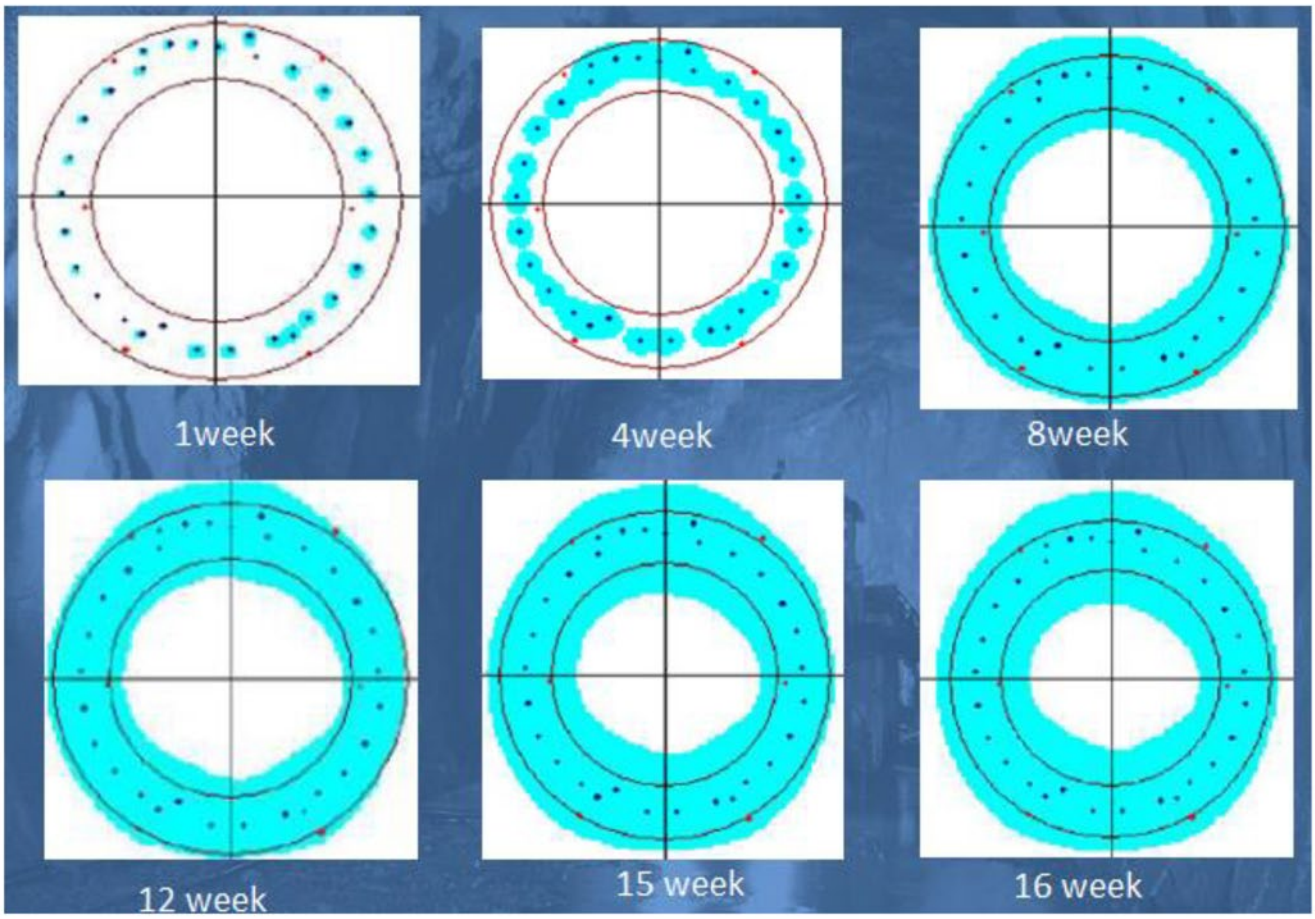

Figure 34 – Progressive freezing of the AGF

Figure 35 – Breaking bored pipe wall

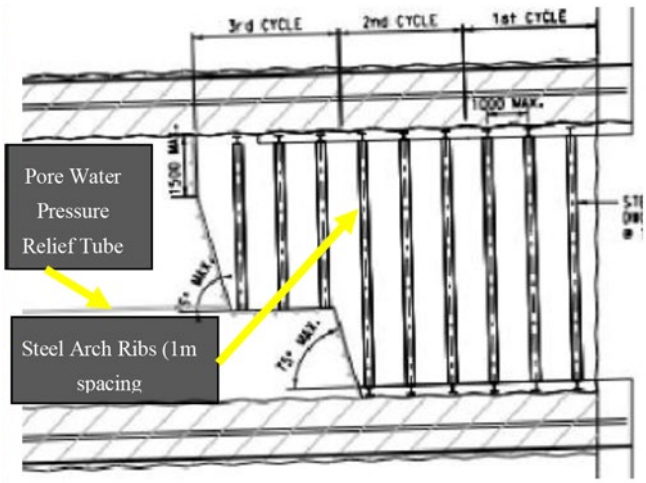

Figure 36 - Heading and Bench Excavation

Figure 37 – Steel rib installation

Figure 38 – Shotcrete application

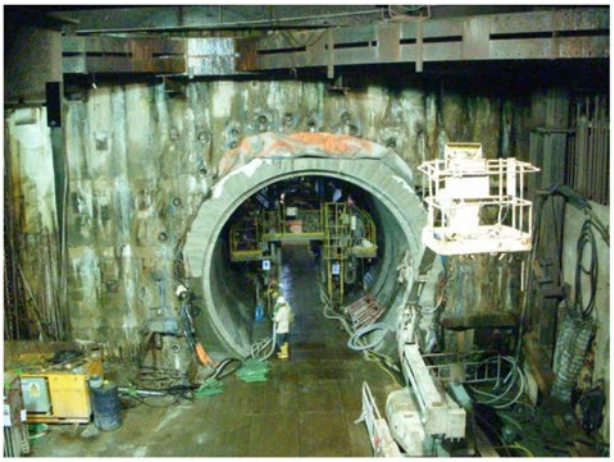

Figure 39 – Final Lining installation with ELS

Figure 40 – Final; lining installation

freezing tubes and the highly variable thermal properties within the ground. Other challenges include overcoming the program constraints, the excavation rate and the AGF set up. However in the HKSAR the AGF has been successful in overcoming challenges imposed by supporting the variable, soft ground conditions and minimizing impacts induced from settlement and vibration to the overlying sensitive structures. The use of the AGF in the HKSAR has culminated in Adit B3-1, Contract 704, MTRC, WIL, being the longest adit construction using AGF in Asia and provided a safe technique for ground support and groundwater cut off preventing disturbance to sensitive structures in an urban environment.

ACKNOWLEDGEMENTS

Any opinions expressed in this paper are those solely of the authors and not of any other party. The author would like to thank past authors for publishing details for the use of the AGF in HKSAR. The author was employed as the Contractor and Independent Checking Engineer on the more recent projects using AGF techniques, including HATS Stage 2A, Contract DC/2009/05; the MTRC, WIL, Contract 703 and the MTRC, WIL, Contract 704.

REFERENCES

Association of Geotechnical and Geo-Environmetal specialists (AGS), Hong Kong, 2013. *Guidance Notes on Ground Freezing Construction*, Tunnel Construction Guidelines No. 04.

Chan W.K.A, Mackay, A.D. & Wightman N.R., 2015. *The Effects of the Undrained Triaxial Tests on Saprolite Shear Strength,* 35th Annual Seminar, 2015, Soil-structure Interaction: From Modelling - Observations. Hong Kong Institute of Engineers (HKIE), Geotechnical Division (GD), pp 151 – 160.

Chan, Y.Y., Swales M.J., Cheung, W.M. & Chu, K.H., 2015. *Design Considerations for Artificial Ground Freezing for Passenger Adit Tunnel for Hong Kong MTR West Island Line.* Proceedings of the Institute of Civil Engineer, Hong Kong Association Annual Conference, Thinking out of the box in infrastructure development and retrofitting.

Geotechnical Control Office, 1988. *Guide to Rock and Soil Descriptions (Geoguide 3)*, GCO, HKSAR, 195 p. (Reprinted in 1994).

Geotechnical Engineering Office (GEO), 2007. *Engineering Geology Practice in Hong Kong.* The Hong Kong Government Publication.

Harris, J.S., 1995. Chapter 4, *Ground Freezing in Practice,* Thomas Telford.

Kuribayashi, E., Kawamura, M. & Yui, Y. 1985. *Stress-strain characteristics of an Artificially Frozen sand in Uniaxially Compressive tests*. In Kinosita, S. & Fukuda (Eds.), Proc. 4th International Symposium on Ground Freezing, Sapporo, 2: 177-182.

Leung, R.K.Y., Ko, K.K.Y., Hu, H.B., Cheung, A.K.K. & Chan, W.L., 2012. *Artificial Ground Freezing for TBM break-through - Design considerations.* Proceedings of the HKIE Geotechnical Division Annual Seminar, 119-124.

Mackay, A.D., Chan W.K.A & Wong, J., 2016. *An overview of the Horizontal Drilling Coring technique during Site Investigation*, 15th World Conf. of Associated Research Centres for the Urban underground Space (ACUUS), 2016, St Petersburg.

Mackay, A.D., Shimizu, T. Saito, T., Tam, C, Lee, M., Cook, R.J, Gunning, P. & Tang, A., 2014. *Artificial Ground Freezing for an Adit Construction for Hong Kong Mass Transit Railway Corporation West Island Line.* TUCSS & NUS. Underground Singapore 2014 Conf; pp 349-364.

Ministry of Coal Industry (MCI), 1996a. *Artificial Ground Freezing Uniaxial Compressive Strength Testing Method,* MT/T 593.4-1996, MCI, Peoples Republic of China (PRC).

MCI, 1996b. *Artificial Ground Freezing Uniaxial Creep Testing Method*, MT/T 593.6-1996, MCI, PRC.

Pakianathan L. J., Kwong A. K. L., McLearie D.D., & Chan W. L., 2002. *Pipe Jacking: Case Study on. Overcoming Ground Difficulties in the Hong Kong SAR Harbour Area Treatment Scheme,* Trenchless Asia 2002, 12-14 November 2002, Hong Kong.

Polycarpe, S., Ng, P.L., Barrett, T.N.D.R., 2012. *Construction Risk Mitigation of the Tunnel to Station connection Using Artificial Ground Freezing in the MTRCL West Island Line Contract 703.* Proc. of the HKIE GD Annual Seminar, 131-136.

Schultz, M. & Hass, H. 2011. *A cooler approach.* North American Tunneling Journal, February 2011, 18-21.

Story, R.B., Kitzis, B., Martin, O., Harris, D. & Stenning, A., 2006. *Ground Freezing for Cross Passage Construction beneath an environmentally sensitive Area,* Proceedings of the HKIE, GD, 26th Annual seminar, pp 161-168.

Tsang, L., Cheung, A., Leung, C. and Chan, W.L., 2012. *Mined Tunnel Construction using Artificial Ground Freezing Technique for HATS 2A Project*. Proc. of the HKIE, GD Annual Seminar, 131-136.

Tsang, L., Cheung, A., Leung, C. and Chan, W.L. (2012). Artificial ground freezing for TBM break-through - Construction. Proc. of the HKIE, GD, pp 125-130.

T.S.K. Lam & P.L.R. Pang (2014). *Geotechnical control for artificial ground freezing works in tunnel projects in Hong Kong. Geotechnical Aspects of Underground Construction in Soft Ground*, Yoo, Park, Kim & Ban (Eds).

Wong, E.K.F., Ng, O.N.T., Zhou, R.Z.B., Polycarpe, S., Ng, P.L. & Salisbury, C.D. 2012. *Ground freezing for removal of underground steel obstructions,* Proc. World Tunnel Congress 2012, Bangkok, Thailand.

Rock Mass In-Situ Stress in Hong Kong Determined by Hydraulic Fracturing Testing

A.D. Mackay
HSS Integrated, Kuala Lumpur, Malaysia
G. Klee
MeSy-Solexperts GmbH, Bochum, Germany
J. Wong
Lam Geotechnics Limited, Hong Kong

ABSTRACT

Hydraulic-fracturing, or Hydro-fracture, stress tests are used to define the rock mass stress magnitude and its orientation. The test is fundamental for ground investigations (GIs) for rock masses where subsurface excavations are proposed. The test can be carried out in both, massive (unfractured) rock and rocks containing pre-existing fractures. Publications prior to 2000, established a maximum horizontal stress orientation trending west north-west (WNW) to east south-east (ESE); since then numerous tests have been completed as part of the infrastructure boom in the Hong Kong Special Administrative Region (HKSAR) during the last decade and generally revealed that major stress orientations to correspond with the proximity of the main fault zones, trending north-west (NW) to south-east (SE) and perpendicular to this throughout the HKSAR. Local changes in orientation were observed based on the local tectonic influences, such as those present at Tsing Yi Island, and the presence of persistent discontinuities. This paper summarises the findings of tests completed since 2000 and updates the understanding of the rock mass stress magnitude and orientation. Whilst a trend in rock mass stress magnitude and orientation is identified it does not replace the need for site specific hydraulic fracture testing to provide greater certainty and accuracy.

1 INTRODUCTION

Determining the in situ rock mass stress is fundamental for subsurface design and construction. Although a range of tests are available to determine in-situ stresses (ISRM, 2003), the Hydro-fracture test is preferred due to the relative ease of mobilization, set up and straight-forward test conduction. It is also referenced in the HKSAR Government publications for good practice, such as GEO, 1992 & 2009 and has the availability of numerous past test results to provide a comparison with the findings. Past publications up to 2000 (Free et al, 2000 and Klee et al, 1999) provide test records from over a decade previously. Since then numerous Hydro-fracture tests have been completed for infrastructure development during the last 15 years.

The Hydro-fracture test is carried out by exerting pressure onto intact rock to initiate a fracture to define the magnitude and orientation of the maximum, intermediate and minimum stress tensors. The test needs to be carried out over a sufficient depth range to ensure the in-situ stresses influencing the excavation are recorded. The shut-in pressure during testing is a direct measure of the normal

stress acting across the induced fracture plane and is usually influenced by the presence of persistent discontinuity sets and tectonic influences in the area.

Past publications established that the orientation of the maximum horizontal stress S_H was aligned west north-west (WNW) to east south-east (ESE, Free et al, 2000) at Tsing Yi Island and was influenced by the tectonic settings of the locations tested (GEO, 2007). The orientation of the intermediate horizontal stress S_h was aligned perpendicular to S_H and the minimum stress component was vertical (S_v) at depths less than 150 m. Below 150 m, S_v increased sufficiently to become the intermediate principal stress.

This paper provides an overview of the test method, data analysis for the Hydro-fracture test, provides the finding of the stress measurements at site specific locations at the Nam Wan Tunnel, Shatin Central Link and Shatin Sub-surface Sewage works and provides updates for the magnitude and direction of in situ stress acting in the rock mass throughout the HKSAR based on previously published and recent test records.

The Hydro-fracture test records in this paper were carried out by MeSy-Solexperts GmbH, Bochum, Germany, who are the specialist sub-contractor used by Lam Geotechnics Limited, HKSAR for this work and have experience spanning more than 25 years in the HKSAR.

2 IN SITU STRESS MEASUREMENTS AND THE HYDRAULIC FRACTURE TEST

2.1 Overview of In-situ Rock Mass Stress Testing

The magnitude and direction of in situ stress is vital for the design of underground structures in rock. For example, sub-surface excavations with a high horizontal stress normal to the axis of excavation can increase the crown stability by increasing the horizontal stress relative to the vertical stress, they can also increase the capacity to resist pull-out for a bridge anchorage (GEO, 2007). The in-situ rock mass stress can be determined using Over-coring, Flat-jack and Hydro-fracture techniques (ISRM, 2003; GCO, 1987 & GEO, 1992). The Over-coring test typically has a wide variation in results leading to inaccuracies; it also requires the test location to be free of fractures, which are commonly encountered in rock masses in the HKSAR (GCO, 1988). A large number of tests may also be required, perhaps 20 or more, to obtain statistically significant results. The Flat-jack requires exposure of a rock surface at depth to provide a test set up which limits the test to post subsurface excavation stages, which is often too late for design input. Although the Hydro-fracture test has similar drawbacks to the Over-coring method, being prone to inaccuracy in the presence of intense fracturing, the inaccuracy is relatively limited. The Hydro-fracture test has also been used frequently during GIs throughout the HKSAR which can be used to validate the test findings.

2.2 The Hydro-fracture Test

High quality drilling methods are required to minimize drillhole (DH) disruption and limit fracture initiation. This can include triple barrel coring (GCO, 1988) at shallower depths, and wireline drilling to increase DH advancement and limit periods with the DH left open with potential collapse (Mackay & Chan, 2010). The Hydro-fracture test is carried out by sealing off a test section, of typical length in the order of 1 m, by packer installation. Refer to Figures 1 and 2.

The test follows the procedure set out in ISRM, 2003 as follows:

- Rock core is inspected to identify suitable test sections; ideally without fractures;
- The packers are placed and inflated to seal off the test section;
- Water is injected into the test section and pressurized to between 2 to 5 MPa, the test section is then shut-in for several minutes to check if the test section is sealed and impermeable;
- If the section is sufficiently impermeable the water pressure is increased to failure, termed P_f.
- Once a fracture is induced, or pre-existing fracture opened, the water inflow is stopped and the hydraulic system sealed to determine the “shut-in” pressure (P_{si}).

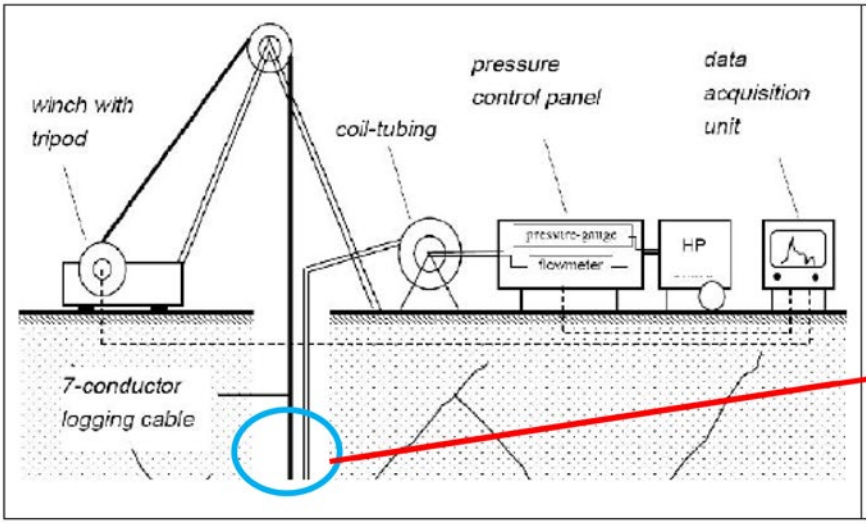

Figure 1 – Wire-line Hydro-fracture test set up (surface).

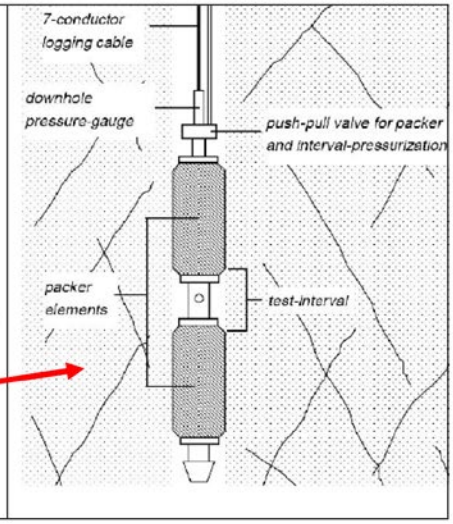

Figure 2 – Wire-line Hydro-fracture test set up (sub-surface).

- The test is then re-pressurised in three cycles to obtain the re-opening (P_r) and verify P_{si} pressures;
- Following the P_r and P_{si} tests a step rate test is carried out;
- The test assembly is then removed and an oriented impression packer imprint taken to identify induced fracture locations.

Each test cycle to obtain P_{si} and P_r pressures takes about 30 to 60 minutes; refer to Figure 3.

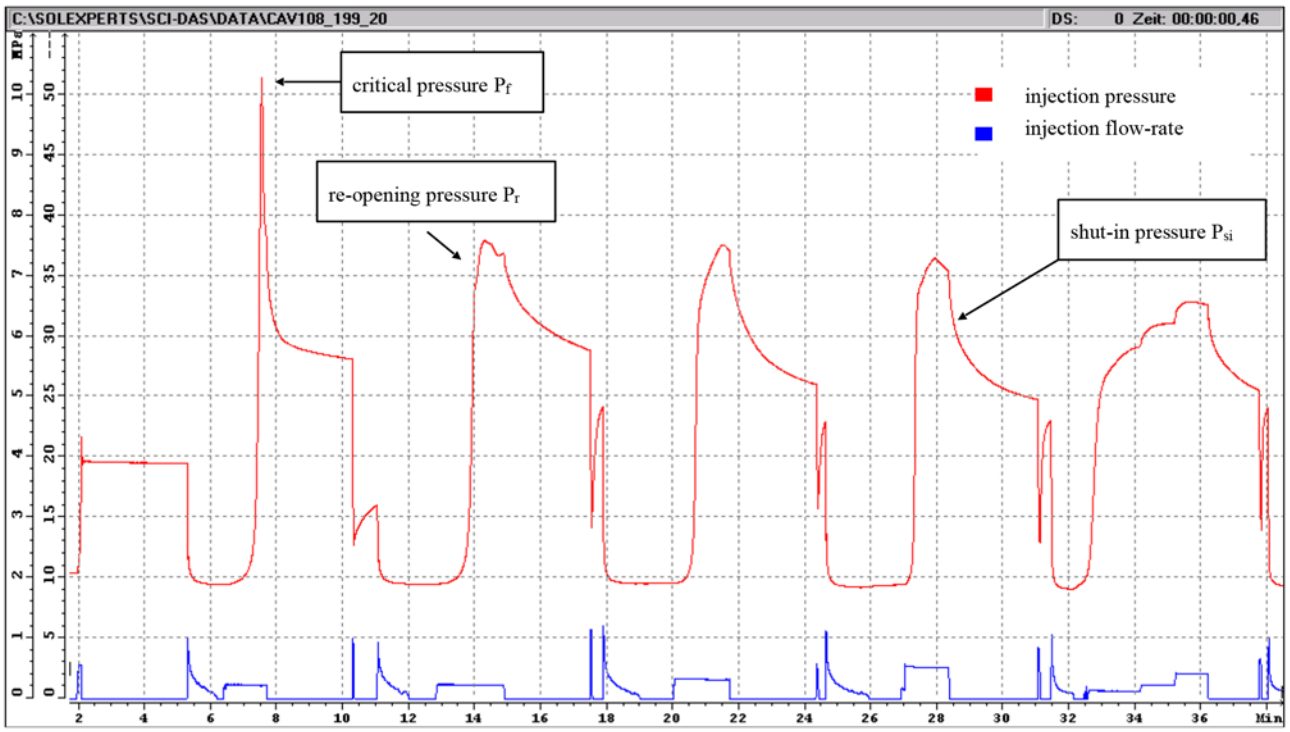

Figure 3 – Example of test results, taken from 199.0m depth, BH-CAV108, Shatin, HKSAR.

2.3 Data Analysis

It is assumed that the stress distribution is within an elastic, homogeneous and isotropic material surrounding a vertical, circular opening formed by a DH that does not deviate more than 15° from the vertical. For vertically to sub-vertically induced fractures the horizontal principal stresses, minimum, S_h and maximum, S_H, can be determined from the following formulae (Hubbert & Willis, 1957):

$$S_h = P_{si} \quad (1)$$

$$S_H = T + 3P_{si} - P_f - P_o \quad (2)$$

$$T = P_f - P_r -- P_o \quad (3)$$

$$S_v = \rho \cdot g \cdot z \quad (4)$$

where S_H = maximum horizontal stresses; S_h = minimum horizontal stress; T = in-situ rock tensile strength; S_v = vertical stresses; P_{si} = shut in pressure; P_r = fracture re-opening pressure; P_o = rock mass pore pressure (should be zero); P_f = fracture initiation or critical pressure; ρ = average overburden rock mass density; g = acceleration due to gravity and z = depth (m) below ground level (m bgl).

In cases where fractures are initiated with different spatial orientations, it is assumed that the P_{si} keeps the pre-existing fracture open and is equal to the normal stress acting on the fracture plane; the vertical stress is a principal stress, and the stress regime varies linearly with depth. Based on this the magnitude and orientation of the horizontal principal stresses can be obtained by resolving six measurements of the normal stress acting on fractures of different orientations and different depths (Cornet & Valette, 1984; Cornet, 1986 and Baumgärtner & Rummel, 1989). In fissured rock conditions; interpretation of the triaxial stress state can still be carried out where fissures are opened (Cornet, 1986).

3 HYDRO-FRACTURE TEST CASE HISTORIES

3.1 Route 9, Nam Wan Tunnel, Tsing Yi, HKSAR (Free et al, 2000)

The Nam Wan Tunnel was completed 2004 to provide a Link beneath Nam Wan Hill, Tsing Yi Island between the Stonecutters Bridge to the SE to Sai Tsoi Wan to the NW for the Route 9 highway link (see Figure 5). The tunnel is 1.3 krn long, and provides a 3-lane carriageway, of approximately 9 m height and 12 m span, at a maximum depth of about 250 m bgl, 275 metres Principal Datum (mPD), beneath the Nam Wan Hill (See Figure 7).

Figure 5 – Nam Wan Tunnel location, Tsing Yi

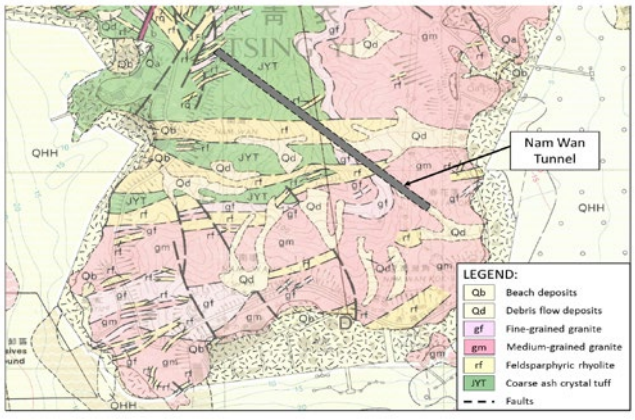

Figure 6 – Geology, Tsing Yi Island

The solid geology comprises medium to coarse granite to the east and coarse ash crystal tuff in the west. Both rock types vary in strength and degrees of weathering (GCO, 1988 and Free et al, 2000) and were intruded by dykes and traversed by faults. Refer to Figure 6 (Fletcher, 2004 & GEO, 1991) and Figure 7 for a general geological section along the tunnel alignment. Different types of dyke are present in south Tsing Yi, as summarized in Table 1.

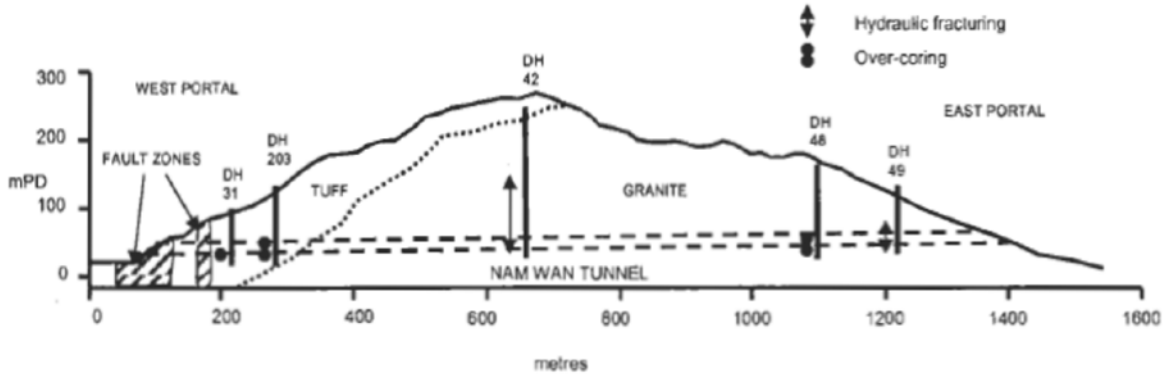

Figure 7 – General Geological Section along alignment showing the Hydro-fracture test locations (Free et al, 2000)

Table 1: Dyke characteristics, south Tsing Yi Island, HKSAR.

Dyke	Orientation	Thickness range	Characteristics
Feldsparphyric	ENE – WSW	10 – 100m	Trend parallel & perpendicular to the major faults in the region
Fine grained Granite	ENE - WSW & NNW – SSE	variable	Trending parallel to the major faults in the region. Also located along the margin between the coarse ash tuff and medium to coarse grained granite
Basalt	NE – SW	up to 10m	Relatively minor and impersistent basalt dykes

The GI comprised 5No. DHs with 8No. Hydro-fracture tests carried out in DH42, between 98.3 to 204.3 m bgl, and 9No. tests in DH 49 between 42.5 and 83.5m bgl. DH42 was advanced through granite and DH 49 through feldsparphyric rhyolite. The depths, characteristic hydrofracture pressure records, P_f, P_r, P_o and P_{si}, and fracture orientation for each test result are presented in Free et al., 2000. The analysis present ing the findings of the 3 principal stresses, S_H, S_h and S_v are summarized in Table 2 (Free et al, 2000). The S_v results were calculated from the overburden pressure and S_H, S_h and S_v values against depth plotted in Figure 8 (Free et al, 2000).

DH	depth (m bgl)	S_H (MPa)	S_h (MPa)	S_v (MPa)	S_H orientation/ gradient
42	98.3	5.67	3.43	2.60	095 / 16
42	151.5	6.85	3.89	4.01	097 / 06
42	171.3	6.62	3.5	4.54	103 / 06
42	194	6.79	3.64	5.14	110 / 04
42	196	5.81	3.52	5.19	119 / 00
42	199	5.41	3.32	5.27	127 / 00
42	202.7	6.37	3.71	5.37	128 / 10
49	42.5	3.09	2.13	1.13	095 / 07
49	48.3	3.1	1.55	1.28	103 / 07
49	54.6	3.3	2.25	1.45	107 / 00
49	66	3.8	2.12	1.75	098 / 00
49	83.5	4.24	2.45	2.21	120 / 08

Table 2: Hydro-fracture test summary

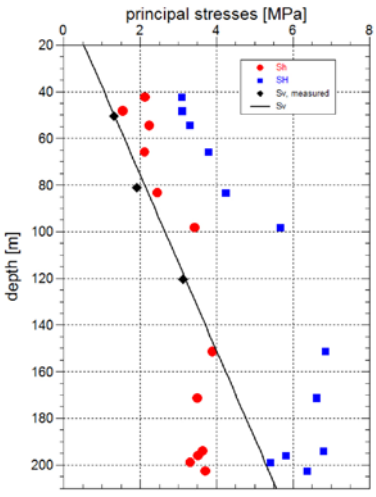

Figure 8 – Principal stresses vs depth

Hydro-fracture tests with a horizontal induced fracture were recorded at 120 m bgl in DH42 and 50.5 and 81.1 m bgl in DH49. The hydro-fracture test results generally revealed a WNW - ESE orientation (see Table 1), trending sub-parallel to the feldsparphyric rhyolite and fine grained dykes and regional faults in that area (See Figure 6). The tests at greater depths in DH42 revealed a greater consistency in stress records with increased depth. Two no. sub-horizontal induced fractures were recorded in the tests at 42.5 and 66 m bgl (DH49). The difference between the calculated and recorded values did not vary with depth with differences ranging from 1 to 10%.

3.2 Shatin Central Link Scheme Design Ground Investigation

The Shatin Central Link (SCL) original scheme design alignment (2002 to 2004) ran between the East Rail Tai Wai and the Island Line Central Stations, see Figure 9 (Wallis, 2008). The GI for the Scheme design was awarded as 2 contracts, SAW120, north of Victoria Harbour, and SAW620 to Lam Geotechnics, including Victoria Harbour and Hong Kong Island (Ng & Wardall, 2003). Both Contracts were carried out from late 2002 to 2004, for an approximate total cost of HK$ 64 million. The works comprised 437 land and marine drillholes, extending to a maximum depth of 375 m bgl. A total of 16 No. Hydro-fracture tests were carried in the Central District under Contract SAW620 in DH47, between 51 to 77.5 m bgl, and DH35, between 20.5 to 53m bgl. Refer to Figure 10 for the test set up at DH35, Queensway, Central.

Figure 9 – SCL original Scheme design alignment 2002 - 2004

Figure 10 – Test set up, Queensway, Central

The solid geology and locations of DH47 and 35 are presented in Figure 11 (Strange & Shaw, 1986).

The DHs were advanced through medium grained granite; major sub-vertical faults dipping sub-vertically trending NE to SW and NW to SE and NNW to SSE. The 3 principal stresses, S_H, S_h and the calculated S_v for DHs 35 and 47, are shown in Figures 12 and 13.

For DH47 generally more than one fracture was induced during each test and the dips for each fracture greater than 60°, with the shallowest (50 – 55 m bgl) and deepest (78 m bgl) dipping between

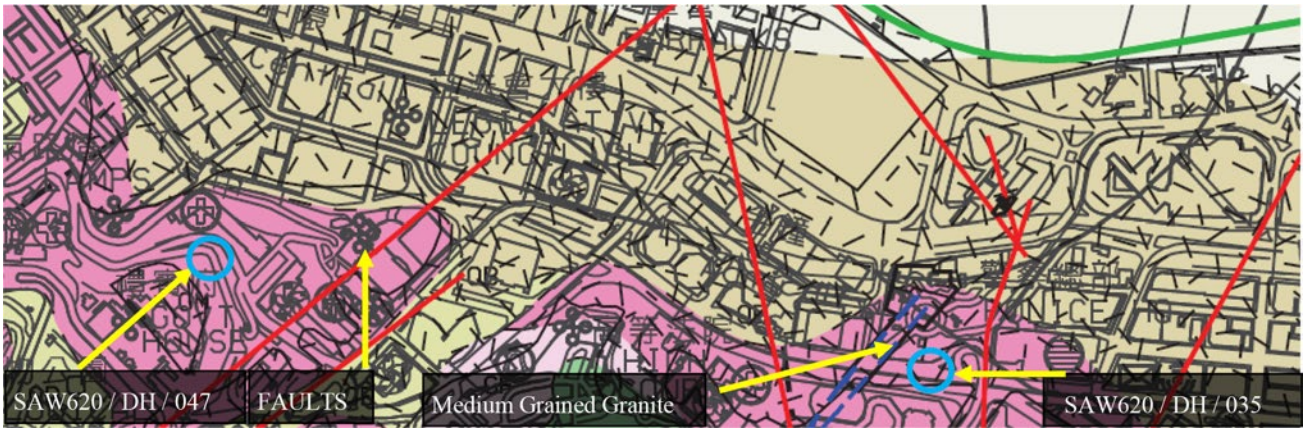

Figure 11 – General Geology of Hong Kong Island showing faults and granite locations

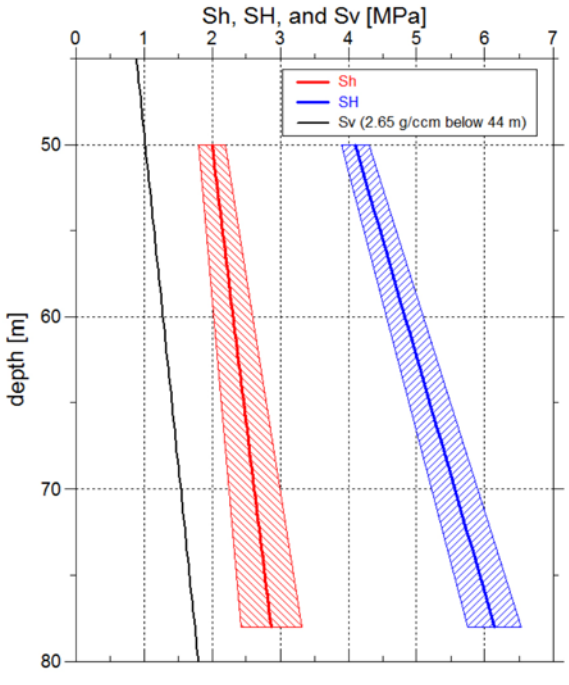

Figure 12 – Principal stress vs depth, DH47

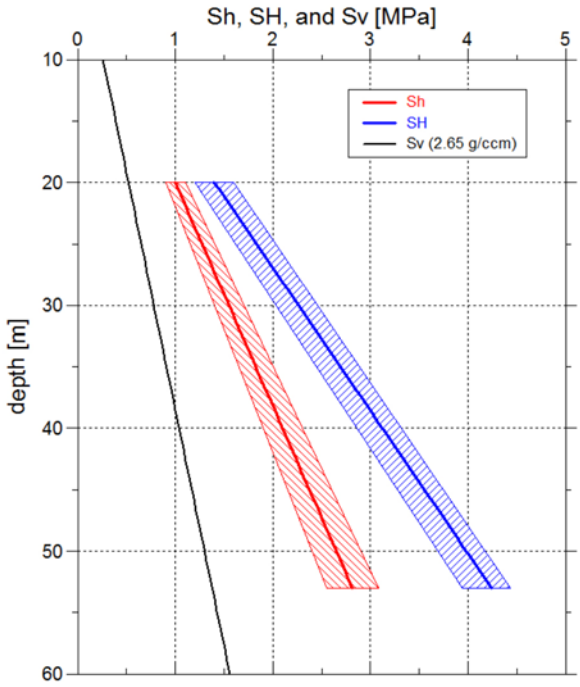

Figure 13 – Principal stress vs depth, DH35

15 - 40°. The fracture orientations ranged from 098 ± 4°, sub-parallel to the regional faults, the results became more scattered with depth possibly due to the greater influence of the overburden pressure.

For DH35 the tests were carried out at a shallower depth with generally one or 2 fractures dipping steeply, 75° or greater. The fractures within the uppermost levels were generally perpendicular to the trend of the faults becoming aligned with the fault, trending N 112° ± 6°, with depth.

3.3 Shatin Cavern

The Shatin Cavern will be located beneath the hillside located alongside Mui Tsz Lam Road, Shatin, and will be used to relocate the existing Shatin Sewage Treatment works located west of Mui Tsz Lam Road. The GI works are being carried out by the Drainage Services Department of the HKSAR Government under Contract DC/2015/01. The solid geology comprises medium grained granite with widely spaced joints with a major fault running NE to SW along the footprint of the Nullah. The GI for the cavern comprised 48No. Hydro-fracture tests carried out in 4 vertical DHs and 1 DH inclined 29° from the vertical, referenced BH CAV108, 109, 115, 120i and 126. Refer to Figure 14 for the DH, general cavern and nullah locations, Shatin.

Figure 14 – DH locations above Mui Tsz Lam Road, Shatin

The depth ranges, principal horizontal stresses (S_H & S_h) and dip and angle and orientation of the induced fractures from the test records are summarized in Table 3 and the ratio of the horizontal principal stresses (S_H & S_h), divided of the calculated or measured vertical principal stresses (S_v) are presented graphically for each DH in Figure 15.

DH-CAV	Depth (m bgl)	Sh (MPa)	SH (MPa)	Strike° N
115	81.6 – 94	4.5 ± 0.3	8.15 ± 0.2	124° ± 6°
115	104.5 – 130	3.65 ± 0.4	6.4 ± 0.4	124° ± 6°
120i	55 – 112	3.1 + 0.017·(z-55)	6.9 + 0.040·(z-55)	118° ± 5°
109	77 – 141	2.4 + 0.003·(z-77)	5.7 + 0.025·(z -77)	105° ± 4°
126	133 – 142.5	4.3	8.4 ± 0.1	71° ± 11°
126	151.5 – 183	3.25 ± 0.4	5.85 ± 0.5	71° ± 11°
108	151 – 219	4.6 + 0.019·(z-151)	9.6 + 0.034·(z -151)	86° ± 2°

Table 3: Summary Hydraulic Fracture test results for the DHs above Mui Tsz Lam Road, Shatin

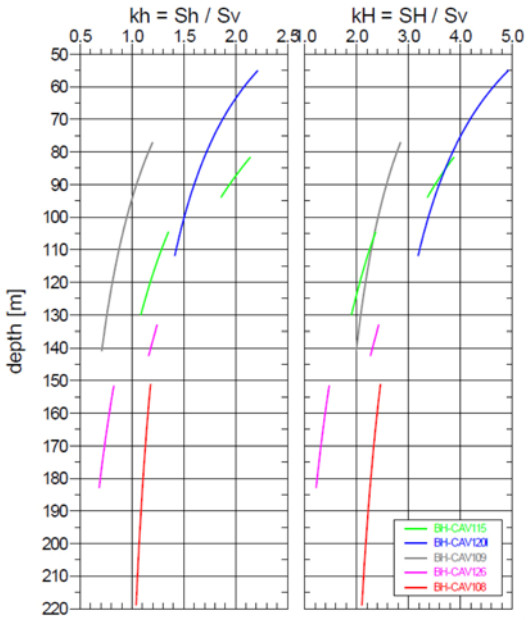

Figure 15 – Principal horizontal stress ratios

The induced fractures were generally vertical to sub-vertical in all DHs with the main horizontal stress orientation (S_H) approximately aligned parallel to the main fault trending NE to SW. The ratio of the principal horizontal stresses (S_H & S_h) against S_v for DH CAV126 confirmed the findings in Free et al, 2000 that K_h is greater than unity up to 150 m bgl and less than unity below this depth, and K_H

is greater than unity up to 250 m bgl. Although there was a decrease in stress ratio in BH CAV108 the horizontal principal stresses were maximum to 220 m bgl. In addition to the increase in vertical stress, this was possibly due to the DH being advanced from a relatively greater level surrounded by steep terrain, reducing the magnitude of the horizontal principal stress.

4 IN SITU STRESS MEASUREMENTS IN THE HKSAR

4.1 Findings of the Hydro-fracture test results up to 2000

A total of 167No. Hydro-fracture in-situ stress measurements taken at Hong Kong Island, Kowloon Peninsula and the New Territories were summarized by Klee et al, 1999 and Free et al, 2000. The test locations, referenced in chronological order and colored blue and orientations of the test results for the Route 3 – Cheung Ching Tunnel (1), Strategic Sewage Disposal System (SSDS), Mount Davis Cavern Facilities (2), SSDS Tunnel Alignment North Point (3), Tsing Ma Bridge Anchorage (4), MTR Quarry Bay Extension (5), MTR Chiu Keng Wan Shan (6), Additional Water Treatment Facility (7), Kowloon Canton Railway Corporation (KCRC) West Rail (8), MTR Pak Shing Kok Tunnel (9), Central Kowloon Route (10) and Route 9 (11) projects are presented in Figure 16.

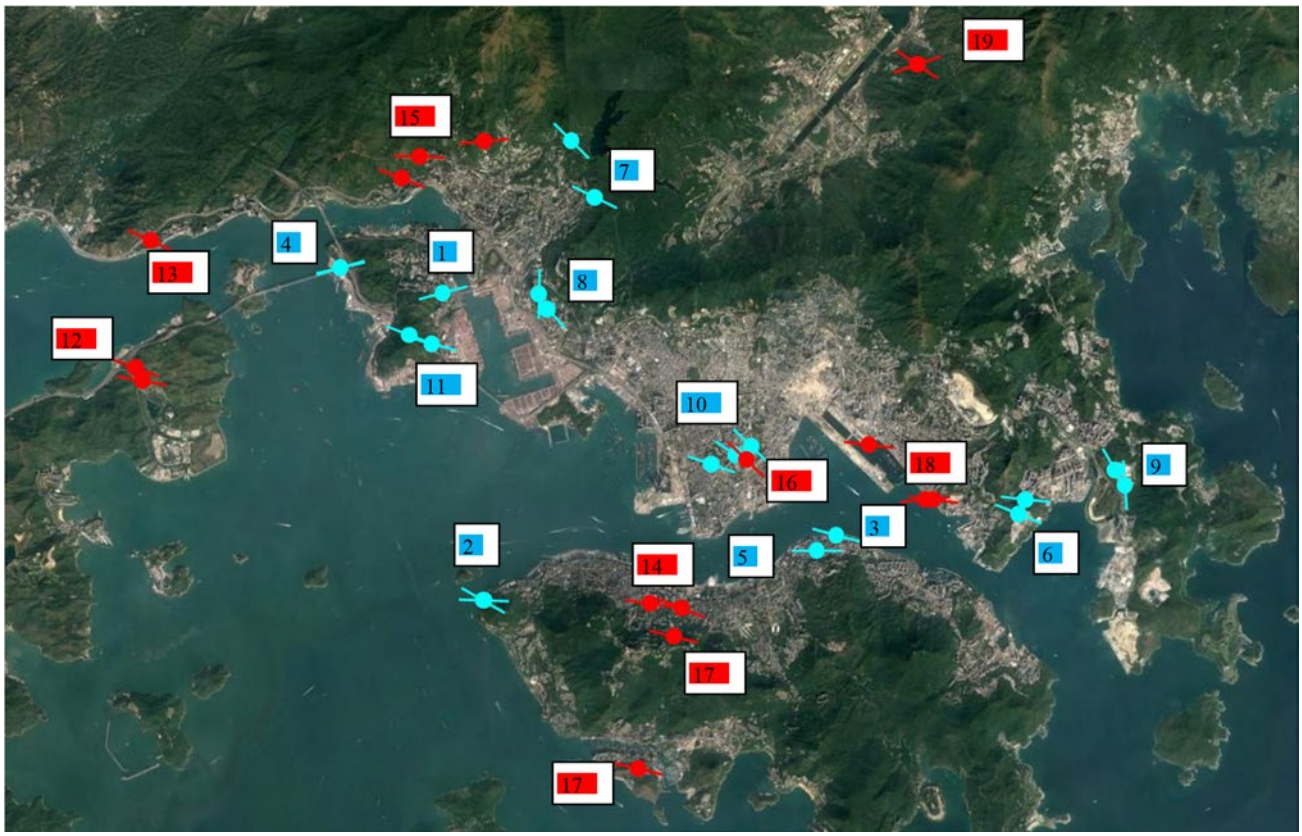

Figure 16 – Hydro-fracture test locations and orientations of maximum horizontal stresses.

The test results from each of the projects showed that the vertical principal stress (S_v) becomes greater than the intermediate horizontal stress (S_h) at depths greater than 150 m and the maximum horizontal stress (S_H) increases to twice the vertical stress S_v at depths of less than 50 m. The regional variation in the major horizontal stress varied from N 075° ± 25° on Tsing Yi Island to N 102° ± 11° on Hong Kong Island and N 130° ± 30° in Kowloon and the New Territories. Although the principal horizontal stresses appear to have a consistent trend with the regional tectonics, the measurements taken at Tsing Yi, showed a preferred E-W orientation of the maximum horizontal stress (S_H), perpendicular to the N-S extension superimposed on the NE-trending faults; the strong E-W trend of the rock mass structure coincided with opening of the rock mass allowing the intrusion of the E-W-trending dykes (GEO, 2007).

4.2 Findings of the Hydro-fracture test results post 2000

Since 2000, the number of available records from MeSy-Solexperts GmbH, and Lam Geotechnics Limited has increased. The test locations, coloured in red, carried out in chronological order since 2000 for the MTR Penny's Bay Rail Link (12), Route 10, Tsing Lung Tan Section (13), KCRC SCL (14), Tsuen Wan Drainage Tunnel (15), MTR Kwun Tong Line Extension (16), MTR South Island Line Extension (17), Trunk Road T2 at South Apron (18) and Sha Tin Sewage Treatment cavern (19) are shown in Figure 16.

The graphical plots for all kH and kh results carried out prior to and after 2000 are presented in Figure 17. The plots reveal that Sv becomes greater than Sh at depths greater than 150 m, with the exception the results taken from the Shatin Sewage Cavern which showed the increase to occur below 200 m, due to the abrupt topographic changes in the terrain surrounding the GI location in this area. Notwithstanding at shallower depths, less than 50m bgl, the scatter increases possible due to the range of influences such as weathering effects on the in-situ stresses towards the ground surface.

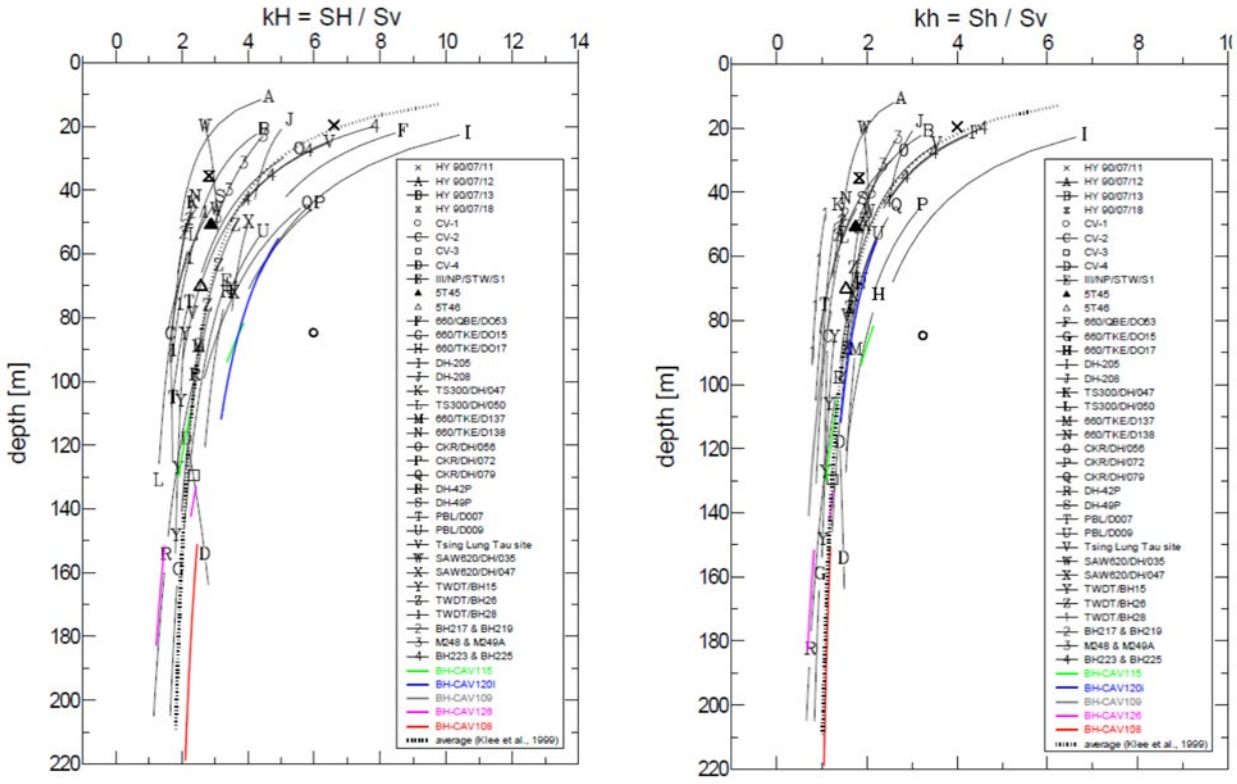

Figure 17 – Stress Ratios, K_H & K_h, updated to include test locations post 2000.

The location of all test locations and the regional geology, including the major fault locations, is presented in Figure 18 (Fyfe et al, 2000) and a summary of the test orientations against the trend of the major tectonic influences is summarized in Table 4.

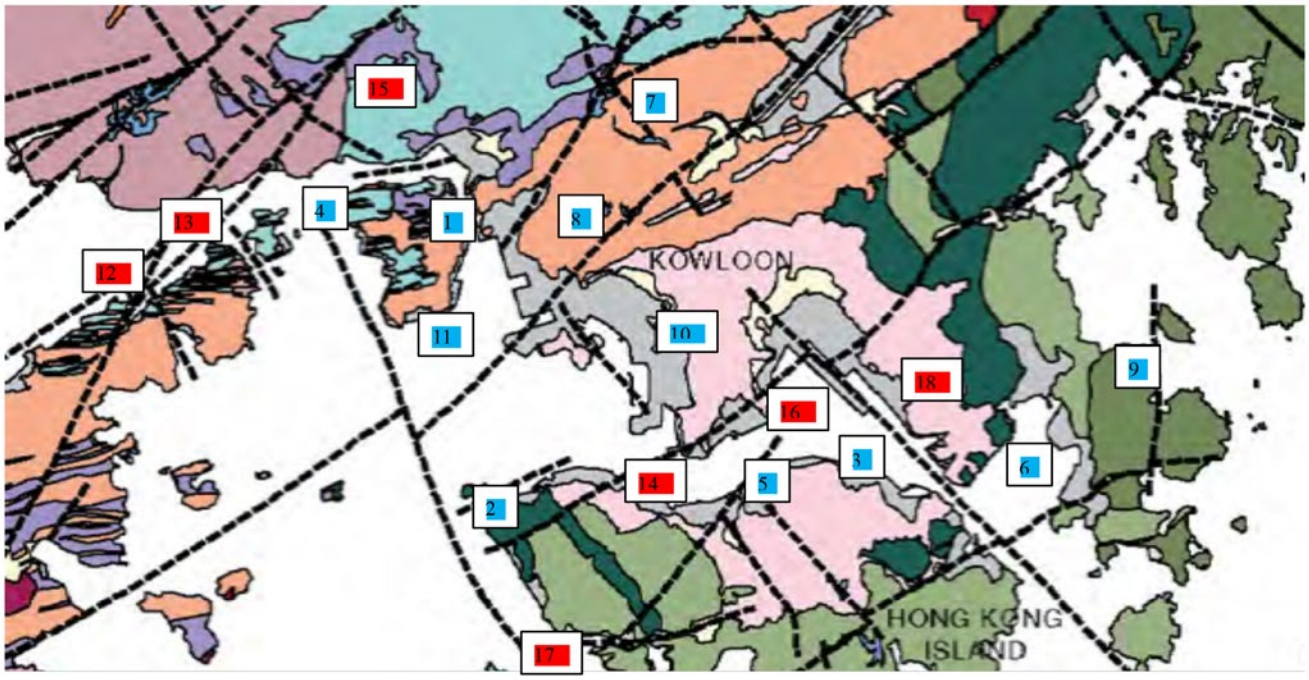

Figure 18 – General geology of Hong Kong (Fyfe et al, 2000).

Table 4: Summary of the hydro-fracture test locations, orientations local tectonic influences.

Ref.	Project	Test Orientation	Likely Tectonic influence	Orientation
1	Route 3 – Cheung Ching Tunnel	85°±? - 135° ±?	Fault / Dykes	E-W (85°±?)
2	SSDS Mount Davis Cavern Facilities	120° ±?	Anticlinal folding	NW – SE (135° ±??)
3	SSDS Tunnel Alignment North Point	100° ±?	Fault	NW – SE (135° ±??)
4	Tsing Ma Bridge Anchorage	80° ±?	Fault / Dykes	E-W (85°±?)
5	MTR Quarry Bay Extension	100°±?	Geol. boundary	E-W (90°±?)
6	MTR Chiu Keng Wan Shan	100°±? - 120°±?	Geol. boundary	E-W
7	Additional Water Treatment Facility	120°±? - 145°±?	Fault	NW – SE (135° ±??)
8	KCRC West Rail	000°±? - 145°±?	Topography	N-S (000°±?)
9	MTR Pak Shing Kok Tunnel	000°±? - 145°±?	Geol. boundary	N-S (000° ±??)
10	Central Kowloon Route	120°±? - 145°±?	Fault	NW–SE (135° ±??)
11	Route 9	120°±?	Fault / Dykes	NW – SE (135° ±??)
12	Penny's Bay Rail Link	100°±? - 110°±?	Dykes	WNW- ESE(135° ±?)
13	Route 10, Tsing Lung Tan Section	110°±?	Fault	NW – SE (135° ±??)
14	KCRC SCL	098±4°	Geol boundary	E-W (95°±?)
15	Tsuen Wan Drainage Tunnel	80°±? - 110°±?	Fault / Dykes	E-W (85°±?)
16	MTR, Kwun Tong Line Extension	135°±?	Fault	NW–SE (135° ±??)
17	MTR South Island Line Extension	100°±?	Geol boundary	E-W (95°±?)
18	Trunk Road T2 at South Apron	95°±? - 105°±?	unknown	
19	Sha Tin Sewage Treatment cavern	124°±6° - 71°±11°	Faults	NW – SE / - SW

The results generally corresponded with the regional trend influencing the location, typically faults and also dykes, geological boundaries, abrupt topographical changes and anticlinal folding towards Mount Davis.

5 CONCLUSIONS

The increased number of Hydro-fracture test results over the last 15 years have increased our understanding of in-situ stresses of rock masses since 2000. It is confirmed that the vertical stress (S_v) is greater than the intermediate horizontal stress (S_h) at depths greater than 150 m, and the orientation of the S_H generally trends parallel to the main tectonic influences, such as the ENE to WSW trending dykes at Tsing Yi Island. Despite a better understanding the horizontal stress ratio and orientation can be influenced by topography at relatively shallow depths, locked-in stress from different stress regimes over geological time, and proximity to major geological fabrics and structures. These influences can lead to scatter over relatively short horizontal and vertical distances.

ACKNOWLEDGEMENTS

The authors would like to thank the contribution from the MeSy-Solexperts GmbH, and Lam Geotechnics Limited staff for assistance in preparing this paper. Any opinions expressed in this paper are those solely of the authors and not of any other party.

REFERENCES

Baumgärtner, J. & Rummel, F. (1989). Experience with "Fracture Pressurization Tests" as a Stress Measuring Technique Jointed Rock Mass. Int. J. Rock Mech., Min. Sci. & Geom. Ab; 26-6:661-671.

Cornet, F.H. & B. Valette (1984). In situ stress determination from hydraulic injection test data. J. Geophys. Res. 89, 11,527-1 1,537.

Cornet, F. H. (1986). Stress Determination from Hydraulic Tests Pre-existing Fractures; HTPF Method. Proc. of the Int. Symp. on Rock Stress Measurements, Stockholm, CENTEK Publishers: 301-312.

Fletcher, C.J.N. (2004). The Geology of Site Investigation Boreholes from Hong Kong. Association of Geotechnical and Environmental Specialists.

Free, M.W, Haley, J, Klee, G & Rummel (2000), F. Determination of in-situ stress in Jointed Rock in Hong Kong using Hydraulic Fracturing and Over-coring Methods, The Institution of Mining and Metallurgy – Hong Kong Branch, Engineering Geology, HK, November 31-46.

Fyfe, J.A., Shaw, R., Campbell, S.D.G., Lai, K.W. & Kirk, P.A. (2000). The Quaternary Geology of Hong Kong. Geotechnical Engineering Office (GEO), HKSAR, 209 p.

Geotechnical Control Office (GCO, 1987). Guide to Site Investigation (Geoguide 2). GCO, HKSAR, 362 p.

GCO (1988). Guide to Rock and Soil Descriptions (Geoguide 3). GCO, HKSAR, 195 p. (Reprinted in 1994).

Geotechnical Engineering Office (GEO, 1991). Silvermine Bay. Hong Kong Geological Survey Sheet 10, Solid and Superficial Geology, 1:20,000 Series HGM20, HKSAR.

GEO (1992). Guide to Cavern Engineering (Geoguide 4). GEO, Civil Engineering Development Department (CEDD), HKSAR.

GEO (2007), Engineering Geological Practice in Hong Kong, GEO Publ. No. 1/2007, HKSAR Government.

GEO (2009). Site Investigation, Tunnel Works. Technical Guidance Note (TGN) 24, GEO, CEDD, HKSAR.

Hubbert, M. K. and D. K. Willis (1957). Mechanics of Hydraulic Fracturing. Trans AIME; 210: 153-163.

ISRM (2003). Suggested Methods for Rock Stress Determination. International Journal of Rock Mech., Min. Sci. & Geomech. Abstr., 24 (1), 5 3-73.

Klee, G., F. Rummel & A. Williams (1999). Hydraulic Fracturing Stress Measurements in Hong Kong. Int. J. Rock Mech., Min. Sci. and Geomech. Abstr., 36, 73 1-741.

Mackay, A.D & Chan W.K.A. (2010). Hydraulic Fracture Testing to Determine In-situ test Parameters, Shatin-Central Link Scheme Design. World Tunnel Congress, 36th General Assembly. Montreal, Canada.

Ng, N. & Wardall, R. Site Investigation for the Shatin Central Link in Hong Kong. Proceedings of the Int. Symp. on Design, Construction and Operation of Long Tunnels, Taipei, Taiwan, Vol 1 (2006) 107–118

Strange, P.J. & Shaw, R. (1986). Geological Memoir No. 2. Geology of Hong Kong & Kowloon. HKSAR Geological Survey, GEO, HKSAR

Wallis, K (2008). Heralding a New Era in Hong Kong, Tunnels & Tunneling International, British Tunneling Society.

4D Passive Seismic Imaging for soil monitoring during TBM excavation, Paris Metro

C. Mogenier
SIXENSE Ltd., Hong Kong
S. Robert
SIXENSE Geophysics, Nanterre

ABSTRACT

The ambitious Grand Paris Express project is part of a more extensive project, the New Grand Paris, which includes the development and modernization of the existing network. The extension of four metro lines prefigures the Grand Paris project by linking Paris with its neighboring towns and enhancing the mobility between suburbs. We report the first application of passive seismic technique to monitor the underground during tunneling excavation works of one of this new metro lines, in Paris in 2016. The technology allowed us to image and monitor the subsurface solely by processing continuous seismic records from ambient seismic noise in an urban setting, where conventional active seismic techniques are precisely constrained by this ambient noise and vibrations affecting the quality of the results. A 4D passive seismic imaging, carried out for several weeks in a very dense urban zone affected by subsidence during excavation works, allowed us to monitor ground stiffness beneath a building along the tunnel alignment after the crossing of the TBM, during grouting works, and finally over few weeks after grouting to follow ground conditions in terms of stiffness (stress changes). It helped the contractor in preventing and mitigating the risks during works.

1 INTRODUCTION

The construction of a new metro line requires the implementation of invasive excavation equipment. Despite the deployment of risk mitigation measures, such works can severely disturb the stability of the surrounding ground, and through a domino effect damage the infrastructures and superstructures located nearby.

Main risks come from the occurrence of phenomena like sinkholes and ground surface settlements, water seepages within the tunnel could also affect hydrogeological regime at surface. Such risks are well known but was always dreaded by tunnel contractors, as illustrated by recent cases shown on Figure 1. To counter such event, numerous ground treatment techniques can be used to ensure the completion of underground projects.

While monitoring and quantifying the effect of such remedial ground treatment works, risks of schedule delaying and costs going under control can be mitigated. Safety risks become mitigated as well, by verifying the actual positive effect of ground treatments, their completeness in space, and by comparing their effect to the predictions made by calculation at earlier design stage.

Figure 1: Recent sinkholes resulting from TBM excavations (a. Fukuoka – 08/11/2016, b. Seattle – 12/01/2016)

2 GEOPHYSICAL MONITORING: A SUSTAINABLE NON INVASIVE METHODOLOGY

2.1 Urban areas:

Applied Geophysics is a non destructive way to investigate the underground. It is the suitable tool to follow its evolution, more precisely to monitor its response to a solicitation, like its electrical resistivity when injecting electrical current into it, or its seismic velocity when creating shocks and measuring seismic waves transiting time.

One of its main limitation lies in its difficulty to be implemented in a dense urbanized area. Indeed, most of the surface based geophysical techniques are of limited use in urban environment because of the difficulty to obtain a good signal-to-noise ratio, due to electromagnetic interferences or vibrations for instance. This is the reason why borehole geophysics is generally preferred to surface based methods while working in such environment, but it requires to have available boreholes, and area of investigation is still limited to the vicinity of the boreholes, or the space between them.

All these limitations and facts led to an alternative method which does not require boreholes, and the reliability of the alternative method is not affected by ambient noise, while keeping a good resolution and accuracy in depth, especially in a dense urbanized area. This method would have to be repeatable along time to allow 4D monitoring applications:

1. Before works: it gives the possibility to anticipate geotechnical risks while highlighting weak zones (voids, weathered zones, dissolution zones, etc.), and define areas which may require preliminary ground treatment. It also allows to image areas beneath buildings, where conventional site investigations cannot access,
2. During works: it gives the possibility to follow the evolution of soil characteristics (impact from works, impact from water pumping, impacts from blasting, etc.), before eventually observing settlement at surface with surface instrumentation and monitoring means, if the phenomena finally reaches the surface,
3. After works: to evaluate the final impact of ground treatment works, or to check whether negative long term impacts remain at an acceptable level or not, like for settlements or gypsum dissolution issues.

3 THE BIRTH OF AN INNOVATIVE SOLUTION

3.1 A need from a renown French authority

Current monitoring solution of underground soil, through inclinometer, extensometer and the like are appropriate during the construction period but not so much during the long life time of a structure, as they would require maintenance, re-installation or the like.

It appeared that a technique which was formerly used for Seismology, could image seismic velocities with a high resolution, using ambient seismic noise. The fact that it did not necessarily require boreholes and active seismic sources was also a key advantage when working in urban areas. It uses the ambient

noise and vibration to solicit the underground and to know its constitution. More the noise there is, and more the investigation works.

Moreover, this technique was based on the interpretation of short time period phenomena (one to a few hours), and was repeatable as many times as needed. It offered the possibility to carry out a 4D monitoring of seismic velocities changing in depth.

3.2 Original applications and History

Main original applications are the study of deep earthquake and fault zones (Roux et al. 2011), the study of main faults like San Andrea fault in USA (Roux et al. 2011), and the study of magmatic chambers evolution as a predictive tool to mitigate risks linked with volcano eruption (Brenguier et al. 2007).

It was then applied at a smaller scale and at shallower depths, for monitoring of a blast effect on geo-mechanical properties of a rock mass (Olivier et al. 2015), or for dykes internal erosion and channeling surveillance (VIBRIS Project, Figure 2):

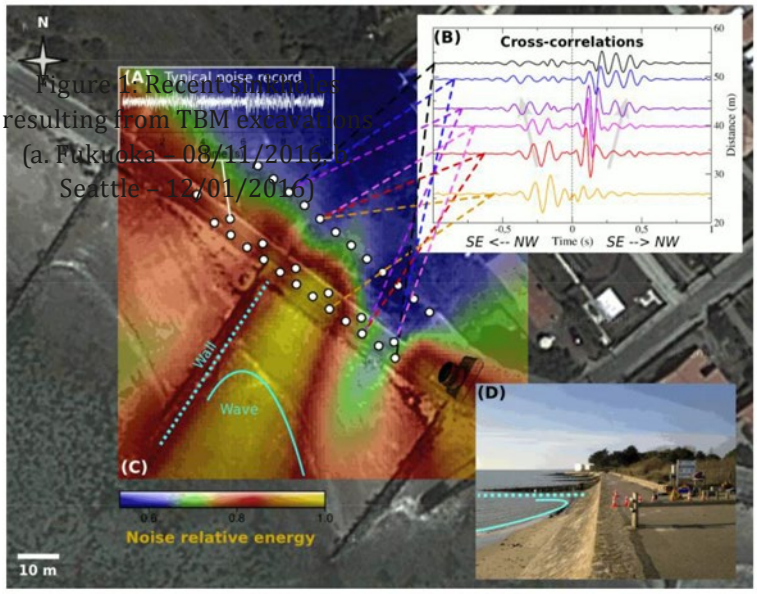

Figure 1: Recent structures resulting from TBM excavations (a. Fukuoka – 08/11/2016; Seattle – 12/01/2016)

Figure 2: Experimentation of the method on a dyke - Les Moutiers-en-Retz, Loire Atlantique, France – project VIBRIS - OSUNA laboratory (France)

Following the very promising results of those trials, which confirmed the potential of this monitoring method, a partnership between Sixense and ISTERRE laboratory was sealed in order to further develop this method. ISTERRRE, world renown laboratory in passive seismic, would provide their intensive knowledge in the interpretation of those complex results.

This methodology was then presented to the key players (owners, contractors, consultants) of the Grand Paris projects, in order to prove the advantages it can bring, and to find a possible location that could host trials.

3.3 The Grand Paris project, a reality check for the 4D Passive Seismic Imaging method

In October 2016, SIXENSE was solicited for the extension to an existing line, in the Northern area of Paris, where unexpected settlements were measured by SIXENSE Soldata at surface (cf. Figure 3), following the excavation.

It was decided by the client to carry out a Passive Seismic survey at this location, to test this innovative solution in real site conditions, to image the underground and follow its evolution over several months, especially after the end of decided ground treatment.

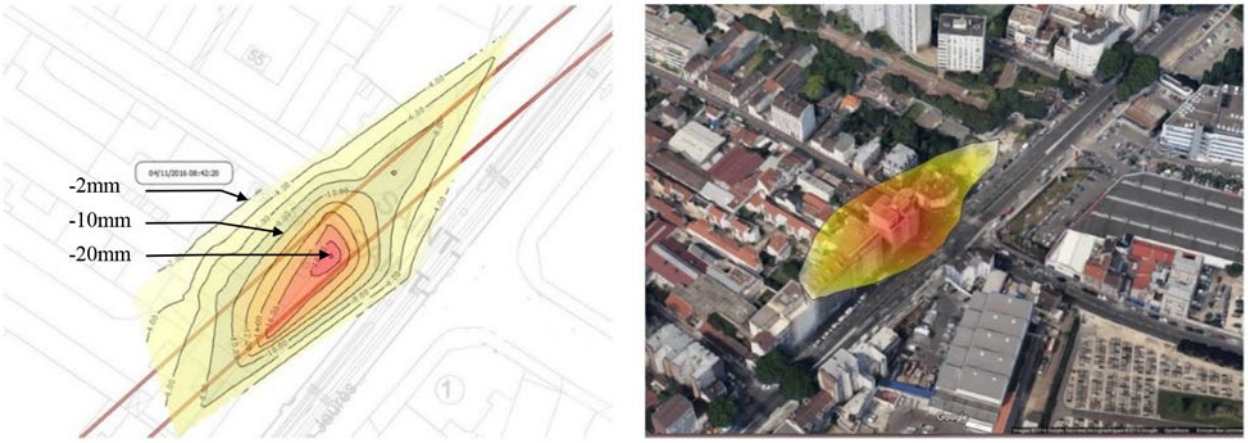

Figure 3: Settlements observed at surface (SIXENSE Soldata, 2016)

The survey carried out by SIXENSE had two purposes:

1. Imaging the underground where surface settlements were observed by automatic deformation monitoring system. The idea was to bring a volumetric information on the affected area, and quantify ground treatment effect.
2. Carry out a seismic monitoring of this area in order to verify the evolution of underground motion, generally de-correlated or de-synchronized from surface settlements, and finally to observe, evaluate and validate the positive effect of ground treatment works.

4 IMPLEMENTATION OF 4D PASSIVE SEISMIC IMAGING

4.1 Some technical considerations

Some technical terms should be explained first, in order to better understand the rest of the article:

Ambient noise: any vibrations coming from human activities (traffic, plants, jobsites, etc.) and telluric activity (waves, earthquakes, etc.). These vibrations are recorded by seismographs and are made of volume waves, surface waves, and other derived complex effects.

Surface waves: these are seismic waves which propagate along a free surface, in this case at the contact between air and soil. They transit slower than volume waves but their amplitude is higher, and decreases while the distance to the surface increases (ie. the depth in our case).

Seismic velocity: it is the velocity at which the seismic waves propagate through the considered medium. It depends on the nature of the crossed material, and more specifically its density and it elastic properties (Lamé, μ and λ coefficients).

Tomography: principle of imaging a structure or a volume through one of its physical properties. In this case, for the passive seismic surveys based on the analysis of ambient noise, the velocity of surface waves is used as the parameter to image the underground.

Monitoring: surveillance activity of a physical parameter or of an activity. The monitored parameter in our case is the variation of the seismic velocity (dV/V, in %), obtained by a signal process which is different from the one used for tomography: the cross-correlation of ambient seismic noise.

4.2 Scope of works carried out for the Grand Paris Express metro project

In the context of the Grand Paris Express metro project, following works had to be carried out:

1. A 3D Tomography of the survey zone before ground treatment works (TAM grouting), which should constitute the initial state tomography.
2. A 3D Tomography of the survey area after ground treatment works, which would constitute the final state tomography.

3. A following 4D monitoring of the seismic velocities by ambient noise cross-correlation, from 26/11/2016 to 06/01/2017.

The ambient noise was recorded with a network of 25 remote operating seismic sensors (Figure 4). These sensors are capable of recording signals during 2 weeks to 1 month before recharging the batteries. Each sensor integrates an internal hard drive to store data, a Wifi antenna to transfer it, and a GPS clock to synchronize the signals.

The distance between geophones around the settlement depends on the required depth of investigation, that was about 30m here. Having never been installed before in such urban context, the team of SIXENSE had to be smart enough to place them in safe and adapted locations. Some were installed beneath central reservations, in condos garden, or even in cemetery shrubberies!

Despite this unusual kind of installation, it revealed itself perfectly operational, without any disturbances or damages to the third parties such as happening when excavating trial pits or when drilling boreholes. It is perfectly enclosed within the urban environment, hidden or buried as often as possible.

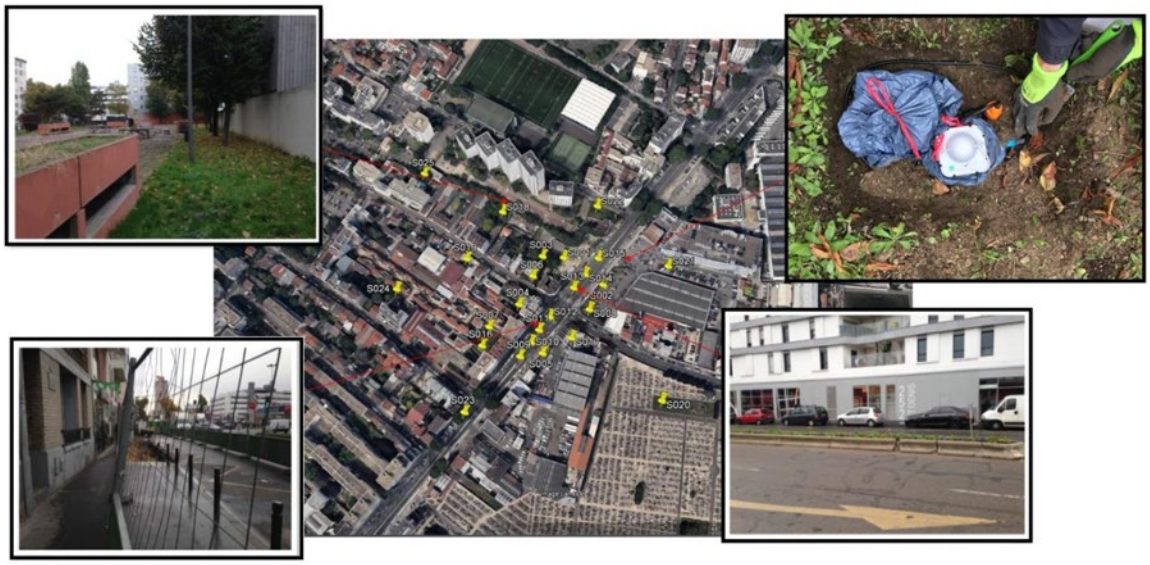

Figure 4: Network of autonomous seismic sensors, and discreetly hidden installation

4.3 Interpretation of initial state tomography results

Figure 5 presents an extract from the initial tomography results, before grouting. The shown slice is for the depth 10.0 to 12.5m below ground level. The color scale indicates Shear waves velocity in m/s. The well solved zone is at the center, between sensors. Outside of this zone, the average speed can be estimated, but the structures are not well resolved because of the poor sensor coverage.

Seismic shear waves velocity is a characteristic which is directly linked to the stiffness of the material (Shear modulus). A geological layer is supposed to present a constant seismic velocity as long as its constitution remains homogeneous. Thus it is possible to build a geological layered model with this solution. A weak or weathered area will appear as a zone of lower velocity (lower velocity = less stiff).

This initial state can be compared to the settlement layout of Figure 2: important settlements are correlated with lower velocities.

This zone of lower velocity, i.e. of lower geotechnical characteristics, is located just beneath the building affected by actual settlements. The area requiring grouting works was perfectly known from the geophysical seismic survey, in 3 dimensions.

This imaging technique also brings the key to explain the settlements observed at surface. Indeed, the velocity observed within the Sands of Beauchamp presents important lateral variations.

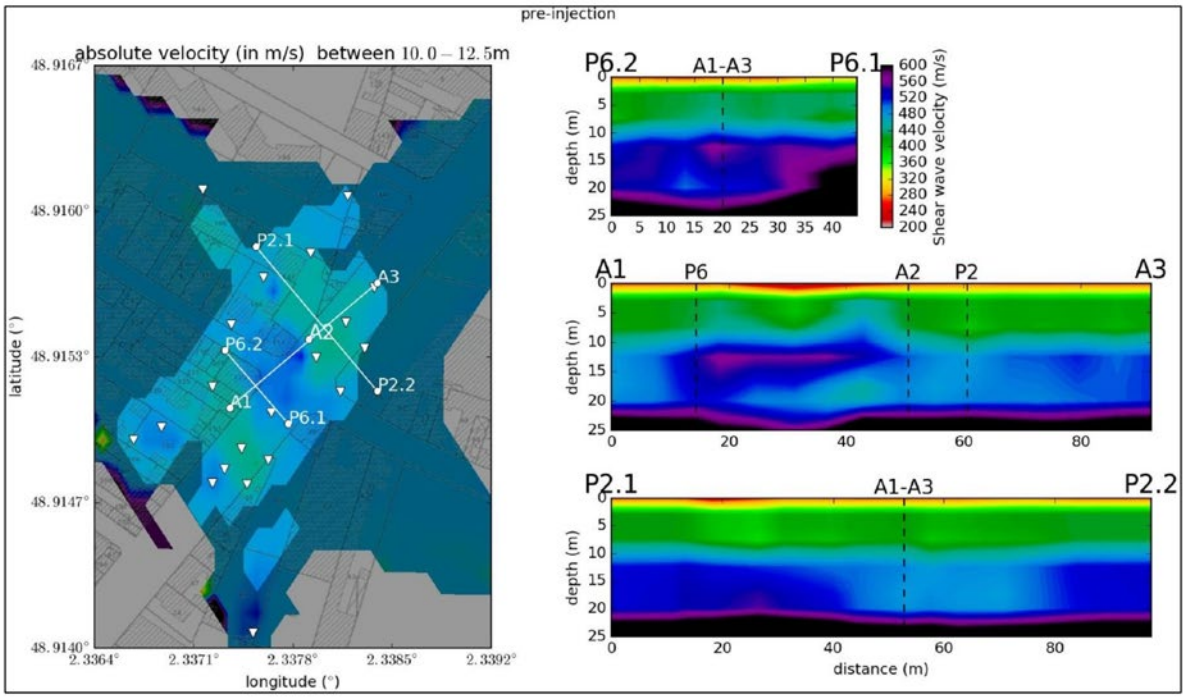

Figure 5: initial state tomography, slice 12.5 to 15m below ground level

4.4 Interpretation of tomography results one week after grouting

A second tomography, processed with the data recorded one week after grouting, allowed us to establish a comparison between velocities observed before and after grouting works. (Figure 6)

The expected effect was the increase in the measured velocity, at the locations where the ground had been previously grouted.

This increase, although restrained by the spatial distribution of grouting works, is significant, especially when comparing sections P6.2-P6.1 before and after grouting. Seismic velocities were increased up to values comparable to those observed within surrounding Sands of Beauchamp, considered of good geotechnical characteristic.

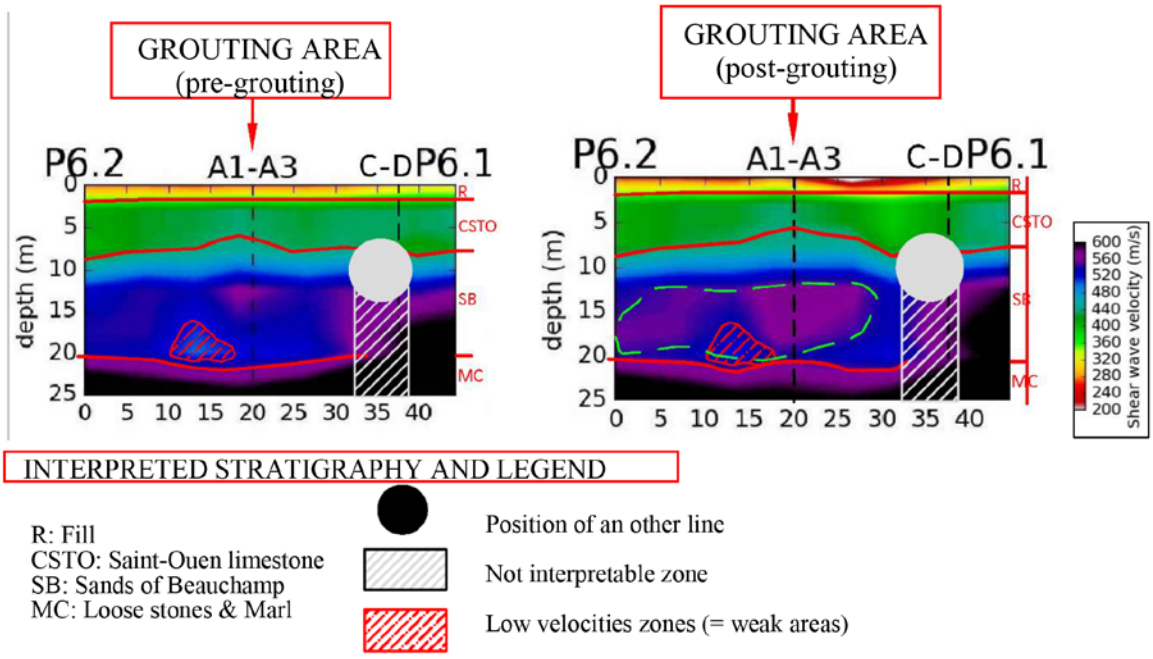

Figure 6: pre- and post-grouting tomographies, with interpreted stratigraphy

4.5 Interpretation of long term monitoring results

4.5.1 Principle of cross-correlation

The monitoring of seismic wave propagation parameters conduct in 1984 to the discovery of repeating events (doublets) allowed natural seismicity to be used again as a source for waves, with virtually all of the unwanted path effects eliminated from the measurement. During the 1990's controlled source experiments have found that measurable velocity variations do occur in the crust (experiments from the San Andreas Fault Observatory at Depth). In the 2000's appeared the evidence that ambient seismic noise correlations were sensitive to changes in the medium along the path between two stations as presented in Figure 7.

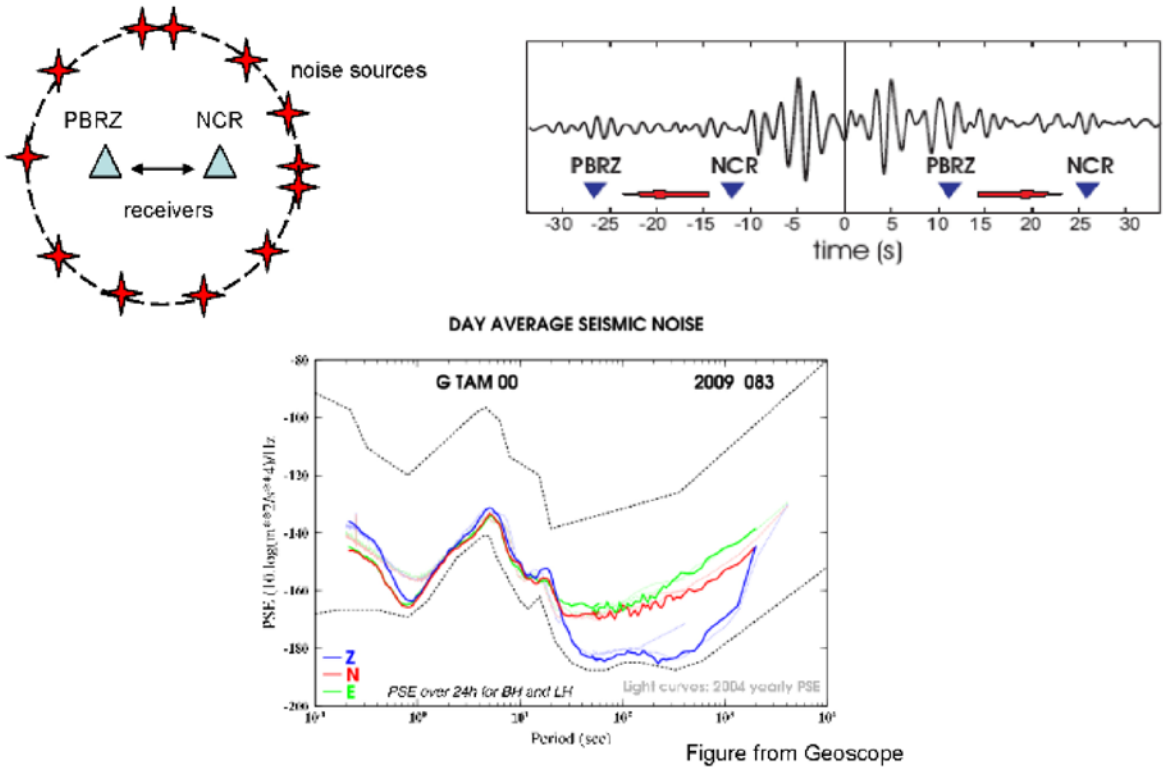

Figure 7: Ambient noise cross-correlations as seismic doublets

The link between seismic velocity changes and stress-strain changes was established.

$$V_p^2 = \frac{(\lambda + 2\mu)}{\rho} \quad (1)$$

$$V_S^2 = \frac{\mu}{\rho} \quad (2)$$

Where λ and μ are the Lamé coefficients

For all cases, both seismic wave velocities decrease with increasing crack density. The velocity ratio $\frac{V_p}{V_S}$ decreases for dry cracks and increases for saturated cracks.

If stress change induces a crack density increase, velocity decreases.
If stress change induces a crack density decrease, velocity increases.

4.5.2 Application to monitoring of extension to Grand Paris metro line:

This means that from the same network of sensors, a second type of signal processing has been applied to the data set, in order to obtain a 4D seismic monitoring.

This latter is based on the study of cross-correlations of ambient seismic noise (contrary to tomography, which is based on the inversion process of the dispersion of surface waves) and allows to obtain seismic velocities variations (dV/V) with an accuracy up to 0.01%.

The network of sensors (Figure 8) was implemented by SIXENSE 2 months after the first surface settlements were observed. Thus, the sudden movement of 2cm (net breaking over a short period), that can be observed on surface settlement monitoring graphs, was not covered by this technique. Only the more stabilized phase happening after has been monitored by seismic cross correlations.

The aim was to observe any evolutions still happening in the underground, because these evolutions can be desynchronized from the ground settlements.

Data recording covered a period from November 2016 to January 2017. Among the notable events that happened during this period, 15th and 16th correspond to the grouting works beneath the existing affected building.

Velocity curve presented in Figure 8 characterizes the averaged velocity variations of the surveyed area as a whole. These results are totally decorrelated from external variations like the temperature and other environmental variables.

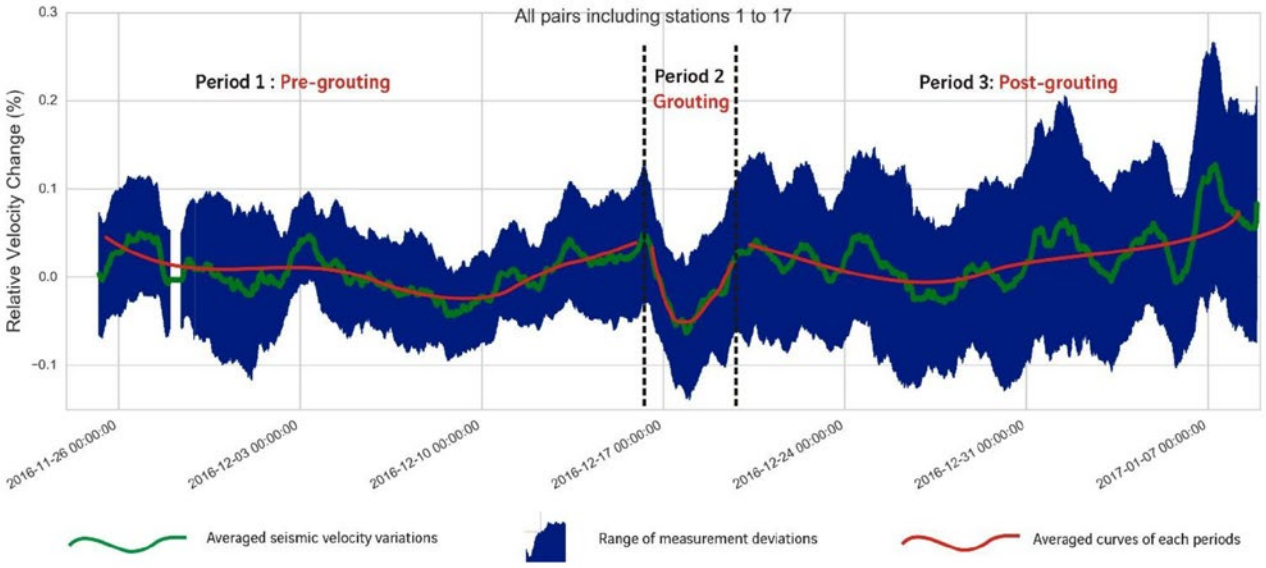

Figure 8: Passive seismic monitoring, evolution of velocities before, during and after grouting works

The curve was interpreted as 3 distinct periods:

Period 1: from the beginning of the survey till the day before grouting works (from 26/11 until 15/12/2016), a relative stability in the seismic velocities variations was observed. These oscillations are lower than +/-0.05%. These weak variations, without any significant tendencies, indicate a balanced system within the survey area, over this period.

Period 2: from 15/12 until 21/12/2016, a generalized decrease of about 0.1% of the seismic velocities. This decrease quickly returns to the initial range previously observed. This variation is concomitant with the grouting works, which were still "fresh" at that time, i.e. unconsolidated.

Period 3: from 21/12 till the end of the surveillance, a two-stage evolution of the seismic velocities. A first stage is relatively stable until 29/12/2016, and then constant increase to reach 0.1% at the end of the surveillance. These evolutions are likely explained by the grouting works effect: although the treated zone was very restrained in space (400m^2, for a surveyed area of 14 000m^2, for a depth of 20m), variations have been measured through the extreme sensitivity of the technique. The increase of the average seismic velocity at the end of the surveillance constitutes a significant tendency that can be linked with ground treatment works.

5 CONCLUSIONS

This methodology, originally used for academic research, is totally innovating at the scale of urban excavation works and more generally for civil works purposes.

Following this first modest but successful experiment, many opportunities have been opened up:

The system can be implemented before a TBM crossing to establish a proper initial state of the undisturbed underground, and to enlighten about the risks to encounter any geological issues that may have been missed by the conventional ground investigations. It would be used to highlight potentially hazardous areas, and thus to limit any future unexpected intervention at the location, which would probably become more expensive and time consuming.

This system may be densified where geotechnical issues are expected to cause severe damages when the TBM will cross. By knowing the evolution of seismic velocities before and after TBM crossing, the return to an acceptable and stable state would be assessed through the monitoring.

As observed during this experiment, the system also allows to evaluate and eventually validate – after several bench trials – ground treatment works. This solution would offer to contractors some arguments towards their clients to prove the efficiency of their work, or to suggest more appropriate works if needed.

Finally, an owner or a concessionaire could envisage to deploy this system at a larger scale over its network and thus to monitor the evolution of the underground over his asset area, over a long period like the time of his concession. That constitutes the initial reason why SIXENSE has been challenged by the Grand Paris authority. The benefits are perspicuous, in terms of insurance towards environment and third parties integrity, in terms of responsibility, and in terms of maintenance works optimization and efficient scheduling.

This innovation is an answer to an emerging specific need of owners and concessionaires: managing all aspects of theirs assets on long terms.

REFERENCES

O'Connell, R. J., and B. Budiansky (1974), Seismic Velocities in Dry and Saturated Cracked Solids, *J. Geophys. Res.*, 79(35), 5412–5426.

Brenguier F., Monitoring the earth interiors using seismic noise, Doctoral class, *IPGP,* March 31 2009.

Shapiro N.M., Campillo M., Stehly L., Ritzwoller M.H., (2005), High-Resolution Surface-Wave Tomography from Ambient Seismic Noise, *Science* Vol 307 11 march 2005 p1615.

Brenguier F., Campillo M., Hadziioannou C., Shapiro N.M., Nadeau R.M., Larose E. (2008), Postseismic Relaxation Along the San Andreas Fault at Parkfield from Continuous Seismological Observations, *Science* Vol 321 12 September 2008, p1479.

Effect of Multiple Rainstorms on Landslides – A Case Study

A.K.L. Ng
AECOM Asia Co. Ltd., Hong Kong

ABSTRACT

Many landslides in Hong Kong were triggered by short and intense rainstorms. However, it is not uncommon that there were also rainstorms occurred prior to the rainstorm that triggered the landslide. These preceding rainstorms could have contributed to the failure by increasing water content in the slope, leading to reduction in soil suction and promoting development of transient perched groundwater table in the subsequent triggering rainstorm.

Among other approaches, analytical approach to study the subject is possible, using modern-day transient seepage analysis with finite element method. However, this approach faces its own challenges, for example, the complex boundary conditions and the interplay of permeability/water content and soil suction of the near-surface unsaturated soils.

This paper is intended to shed some light on the subject by presenting a case study where probably the landslide had been contributed by the preceding rainstorm. The slope was studied with transient seepage analyses, experiencing the multiple rainstorms. The changes in the pore water pressures in the slope, from suction to become positive as these rainstorms progressed are of particular interest and the phenomena was presented and discussed in this paper. Factors of safety using the estimated pore water pressures from the transient seepage analyses were also calculated for different stages in order to understand the impact to the stability.

1 INTRODUCTION

The landslides in Hong Kong often involve shallow failures of slopes, whether man-made or natural. The rapid change in groundwater conditions in the near-surface soils during heavy rainfall has been known as the triggering factor of many landslides.

While many landslides occurred during a particular rainstorm, would the preceding rainstorms have any contribution to the landslide? And if yes, to what extent? The historic frequency of intense rainstorms, say, he Amber, Red and Black Rainstorm Warnings may be relevant. For example, the average interval of all the above Rainstorm Warnings between May and July 2016 was about 4.7 days, where 2016 was not a particular wet year. However, if a very wet year is considered, say 2008, the average interval of all the Rainstorm Warnings between May and July 2008 reduced to 2 days only. For such a short interval, there was a great possibility that some preceding rainstorms had an adverse accumulated effect to the groundwater conditions and contributed to the subsequent landsides.

To study the subject, one of the approaches can be the direct measurement of groundwater responses in piezometers installed on the slopes. However, the instrumentation can be challenging in terms of finding the right slopes to instrument and the cost incurred.

An alternative is to carry out numerical analysis. This paper attempts to provide a better understanding of the subject by developing and testing a numerical model for a local landslide occurred in 2008, to study the response of groundwater, or to be more specific, the pore water pressures when the

slope was subject to multiple rainstorms. The transient 2-D seepage analysis adopts the finite element method (computer software SEEP/W). The results of testing this model provide some insight on how rainstorm affects the pore water pressures in the slope and some understanding on the mechanism by which a transient perched groundwater table is developed. The pore water pressures estimated by the transient seepage analyses using SEEP/W for any particular time can be imported to another software SLOPE/W, a limit equilibrium analysis to calculate the respective factor of safety.

2 CASE STUDY

2.1 Landslide at the University of Hong Kong on 7 June 2008

On the morning of 7 June 2008, a landside occurred on a natural hillside behind Chow Yei Ching Building at the University of Hong Kong (HKU) (Plate 1). The landslide comprised a larger primary and a smaller secondary source area, involving a total displaced volume of about 2,740 m^3. 2,340 m^3 of the volume came from the primary source area. The crown of the primary source area was located at approximately 190 mPD, on a natural hillside inclined at about 34° in a broad topographic depression. At the maximum, the primary source area is about 60 m long and 42 m wide, with a maximum depth of 3 m. Given the dominant size of the primary source area, the primary source area is selected for this study.

The detached material from the primary and secondary source areas entered an ephemeral drainage line in the lower hillside where the debris became confined and channelized. The landslide debris travelled a total distance of 210 m before coming to rest at the side of Chow Yei Ching Building (Figure 1).

The landside was studied by Maunsell Geotechnical Services Limited (MGSL) and based on which, GEO Report No.276 was published (MGSL 2013).

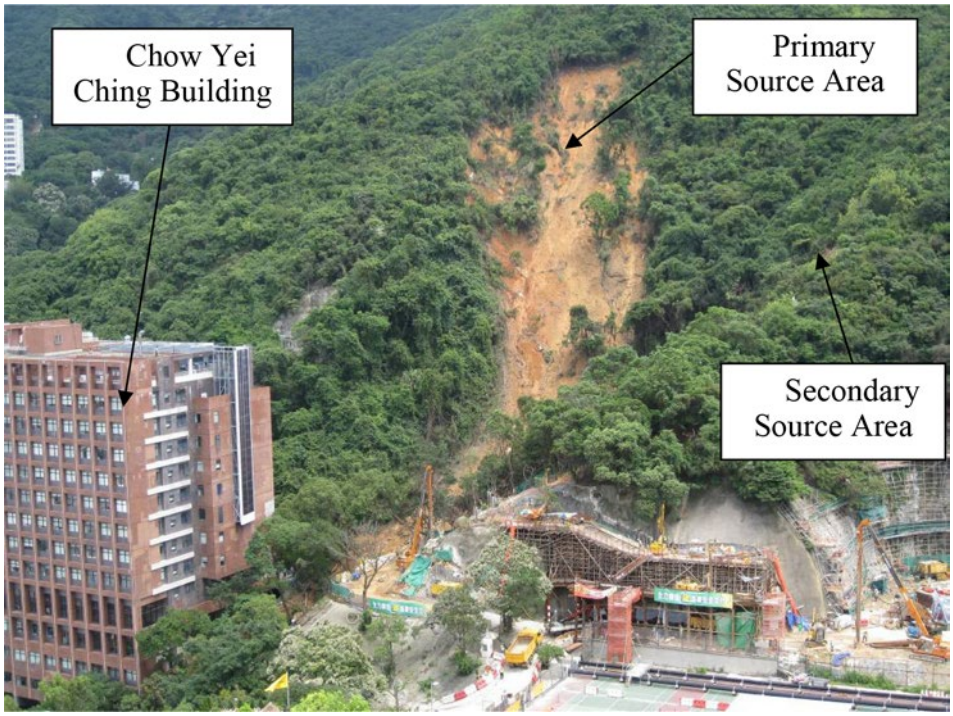

Plate 1: General view of 7 June 2008 landslide at HKU (MGSL, 2013)

2.2 Geology, Groundwater and Failure Modes at Primary Source Area

From the report (MGSL 2013), at the primary source area, young colluvium of up to 2.5 m thick was encountered at the ground surface, which generally comprises a firm, yellowish to orange brown, slightly sandy silt/clay with some/occasional gravel-, cobble- and boulder-sized tuff fragments. The young colluvium appears to be associated with relatively recent local landslide activity from the relict

landslide scars immediately uphill. Below the young colluvium was a layer of old colluvium of up to 3.2 m thick. The old colluvium typically comprises firm to stiff, reddish brown, yellowish brown and purplish red, sandy silt/clay with some to many cobble- and boulder-sized tuff fragments. A thin layer of residual soil of up to 1.5 m thick underlay the old colluvium, which was typically a firm reddish brown to greyish brown clayey silt. The residual soil was underlain by highly to completely decomposed tuff (C/HDT) and further down, by highly to completely decomposed granite (C/HDG).

Subsequent to the incident, the groundwater was monitored and the base groundwater table was about 15_m or more near the crest of the primary source. The report (MGSL 2013) opined that the 7 June 2008 landslide was triggered by development of transient perched ground above the old colluvium/ residual soil interface rather than a rise in the much deeper base groundwater table.

Two failure modes at the primary source area were considered in the report (MGSL 2013); failure mode 1 involving 2 stages of failure and failure mode 2 involving a single failure only. The failure 1 was reported by eye-witness and the first stage of failure (slip surface no. 1 in Figure 2) has been selected for this study.

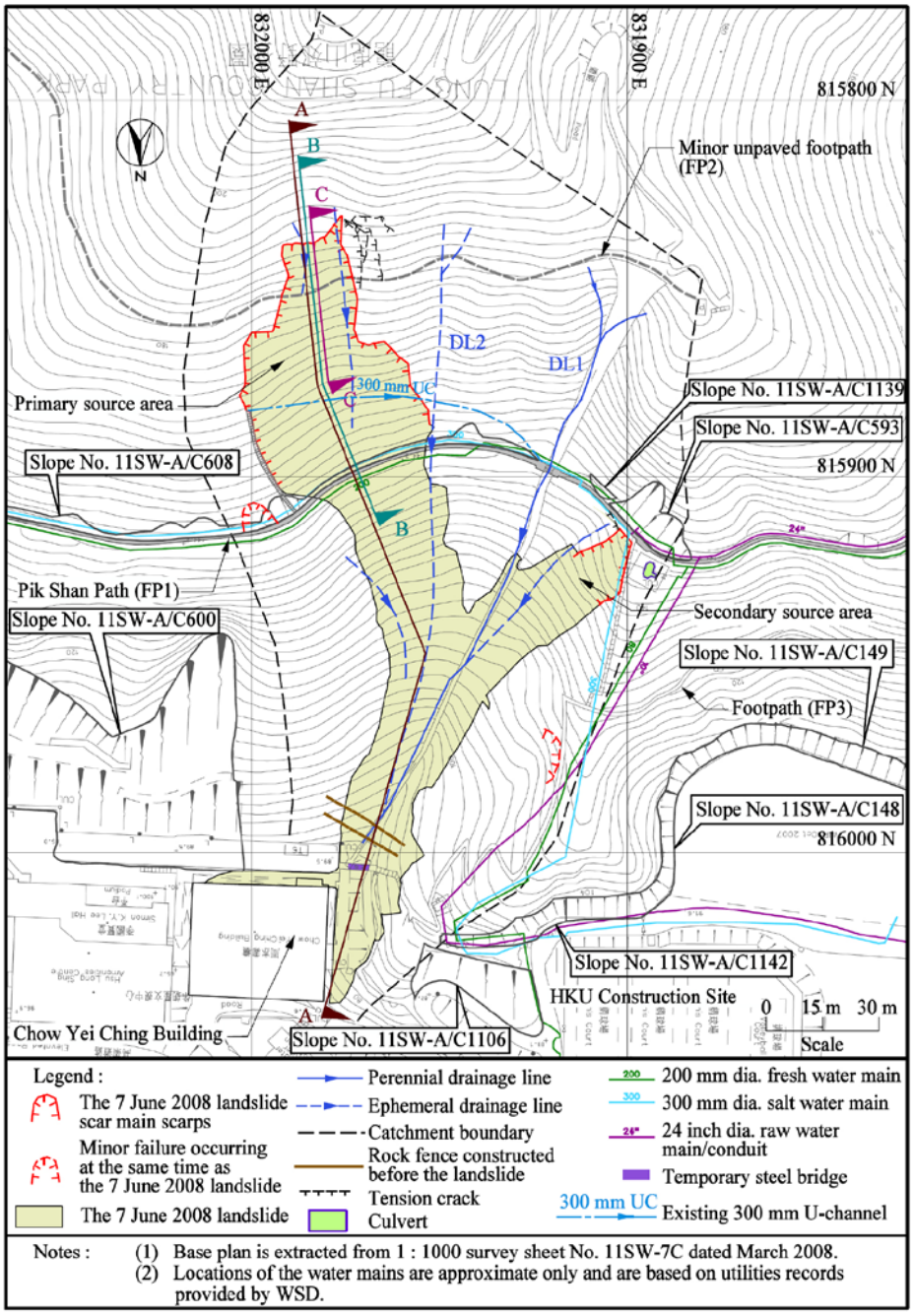

Figure 1: Site layout plan (MGSL 2013)

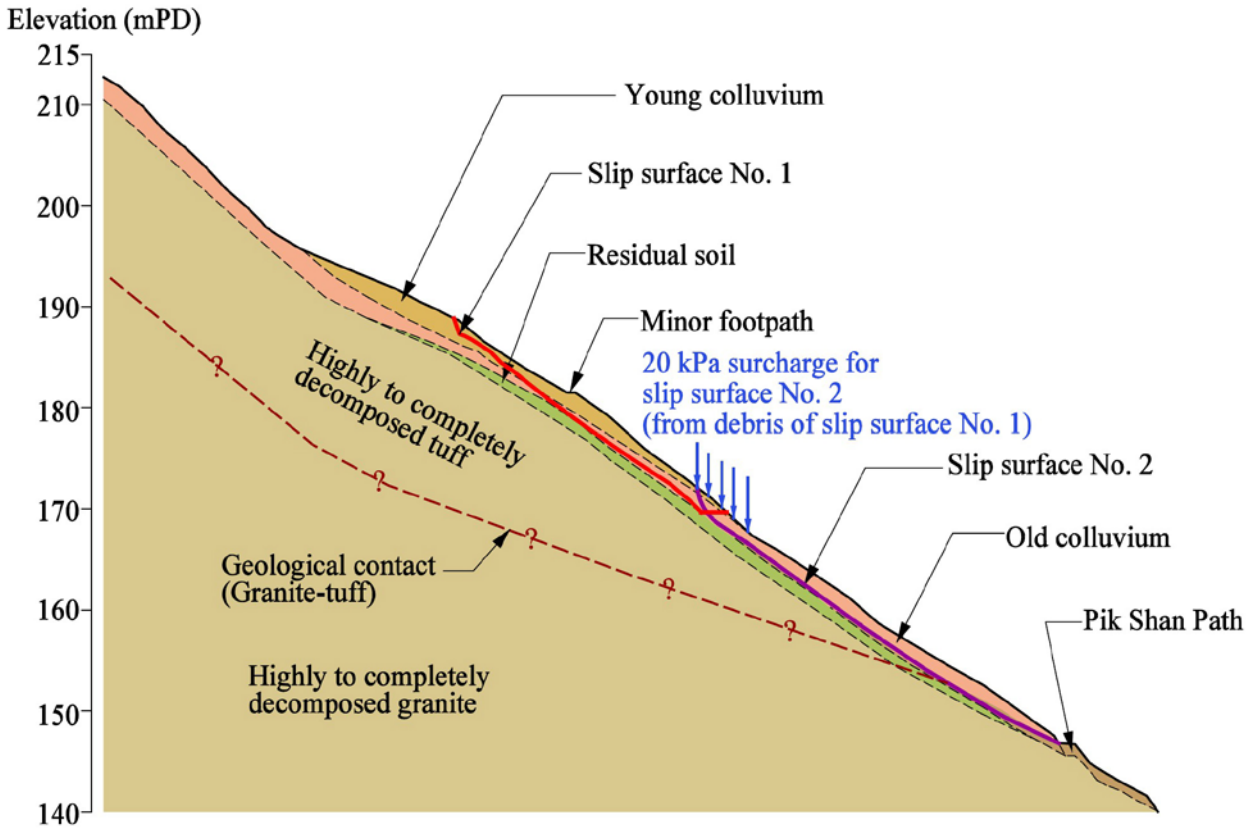

Figure 2: Failure at primary source area (Section B-B in Figure 1) - failure mode 1 (MGSL 2013)

2.3 The Numerical Model

2.3.1 Introduction

A number of numerical analyses on the hydrogeology of slopes in Hong Kong had been performed in the past. For example, Leach and Herbert (1982) examined the overall hydrogeology of a Hong Kong natural hillside using finite difference method. Ho (1982) developed finite element models and calibrated the models against the groundwater tables measured in the field. Ng et al. (2001) performed 3-D transient analysis on a man-made slope subject to different scenarios of rainfall patterns, durations and return periods.

In this paper, a numerical model was developed for the primary source area at the HKU landslide in 2008 to investigate the impact of the multiple rainstorms to the pore water pressures in the natural hillside. The numerical model has been developed based on the geological cross-section in the report (MGSL 2013). The finite element mesh can be seen in Figure 3.

The calculated pore water pressures at different stages were then imported into another computer software SLOPE/W which adopts the limit equilibrium method, in order to estimate the respective Factors of Safety.

2.3.2 Rainfall Records

The HKU landslide occurred at about 9 a.m. on 7 June 2008 when the Black Rainstorm Warning was in effect. The rainfall records in May 2008 and those in June but prior to 9 a.m. of 7 June 2008 from two nearby rainfall gauges, H02 and H04 (MGSL 2013) were examined in order to select the appropriate rainstorms for the case study.

There were three less severe rainstorms in May 2008, with daily rainfall between about 50 mm and 70 mm. In June and prior to the landslide, there were rainstorms on 1 to 4 June 2008 and 6 June 2008. The daily rainfall on 1 to 4 June 2008 was about 50 mm. On the other hand, the 6 June 2008 rainstorm has a much higher daily rainfall of 150 mm and was only less than a day from the landslide. It was

considered the 6 June 2008 was appropriate to be selected as the preceding rainstorm in this case study. Table 1 summarizes the rainstorm data.

Table 1: Rainfall of Selected Preceding Rainstorm and Triggering Rainstorm

Date	Time	Duration (Hours)	Average rainfall (m/s)
6 June 2008 (preceding)	8:00 a.m. – 7:00 p.m.	11	3.79×10^{-6}
7 June 2008 (triggering)	5:00 a.m. – 9:00 a.m.	4	1.11×10^{-5}

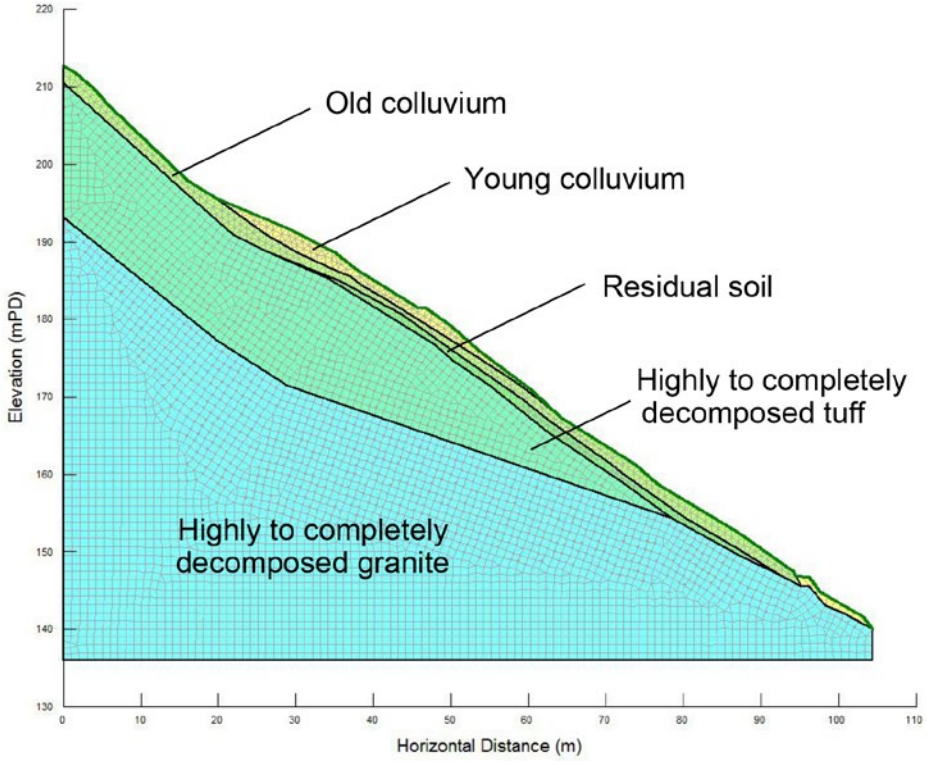

Figure 3: Finite element mesh in transient analysis

2.3.3 Permeability and Volumetric Water Content

The water flow within unsaturated soil has been a challenging subject given that unsaturated soil actually contains three phases; soil particle, water and air. Some researchers developed useful correlations between suction (negative pore water pressure) and permeability, and between suction and volumetric water content, assuming that the air flow within the unsaturated soil in slopes was secondary in the water flow. The computer program SEEP/W used here adopts such correlations and the program algorithm becomes relatively simple as the only key unknown is the water head.

For this paper, the saturated permeability (pore water pressure equal to 0 kPa) is taken as the permeability measured by constant head permeability tests (MGSL 2013), except for the residual soil and C/HDG where no field data was available and requires own estimation. From the literature, the permeability in the suction range can reduce by few orders when the suction reaches 100 kPa (Ng 2016). However, little data was available for local soils. The drop in number of orders in permeability in the suction range was therefore based on the typical values in the literature. For the volumetric water content, the value at saturated state was based on the ballpark figure on the void ratio, but the drop of the volumetric water content would have to be based on typical value from the literature. Table 2 and Table 3 show the values at the saturated state and at suction of 100 kPa, for the permeability and volumetric water content respectively.

The permeability and volumetric water content of all the soils were assumed to be constant in the positive range of pore water pressure and equal to the saturated value.

It should be noted that the permeability of some soils needed to be adjusted in the calibration exercise as described in the later section.

Table 2: Permeability Soil

Soil	Saturated permeability (m/s)	Permeability at suction of 100 kPa (m/s)
Young colluvium	1.02×10^{-5}	1.02×10^{-8} #
Old colluvium	5.53×10^{-7}	5.53×10^{-10} #
Residual soil	2.5×10^{-6}*	2.5×10^{-10} #
C/HDT	2.5×10^{-7}	2.5×10^{-11} #
C/HDG	2.5×10^{-7}*	2.5×10^{-11} #

* Own estimation
# Reduction of values (in orders) based on literature

Table 3: Volumetric Water Content

Soil	Saturated volumetric water content*	Volumetric Water content at suction of 100 kPa #
Young colluvium	0.45	0.18
Old colluvium	0.45	0.18
Residual soil	0.38	0.095
C/HDT	0.38	0.095
C/HDG	0.38	0.095

* Ballpark figures
# Reduction of values based on literature

2.3.4 Shear Strengths

The concerned slip surface (Slip surface No. 1 in Figure 2) only passed through the young and old colluvium. The respective shear strength parameters were measured in triaxial tests (MGSL 2013) and they have been taken for this paper (Table 4):

Table 4: Shear Strength Parameters

Soil	Effective cohesion c' (kPa)	Effective friction angle φ' (°)
Young colluvium	2	35
Old colluvium	2	35

2.3.5 Infiltration and Boundary Conditions

In order to estimate the rate of infiltration into the primary source areas, it is necessary to consider the various hydrogeology components in play:

a) Tree canopy runoff;

b) Tree intake and evaporation;

c) Direct evaporation from ground surface;

d) Direct infiltration; and

e) Surface runoff.

The two rainstorms 6 and 7 June 2008 to be studied in this paper occurred within 2 days. Thus it was considered that items a) to c) above was secondary and could be ignored. However, these components play an important role in a longer term, for example, the overall conditions for the dry season. The effect of these components would eventually affect the suction of the near-surface soils. Post-landslide ground investigation indicated the suction towards the dry season after the landslide, increased from about 7 kPa to 40 kPa (MGSL 2013).

Based on this measurement, it was assumed that the suction in the near-surface soils was about 20 kPa for the conditions in the dry season prior to the preceding rainstorm, given few less severe rainstorms occurred in May and 1-4 June 2008 (Section 2.3.2). For the boundary conditions during rainstorms, the direct infiltration and surface runoff (items d and e above) are more relevant. Under gravity flow, the rate of infiltration cannot exceed the permeability of the soil and the remaining rainfall reaching the ground will become surface runoff. Therefore in this study, for rainfall (Table 1) larger than the soil permeability, a zero pore water pressure boundary was applied. However, for rainfall smaller than the soil permeability, the infiltration rate should be applied on the surface. As the permeability at the surface also changed during the rainstorms (according to the permeability and suction correlation), the boundary conditions were reviewed with the results of each time step, to make sure that the boundary conditions applied were appropriate. The analysis would be re-run with the corrected boundary conditions if necessary.

2.3.6 Calibration of Numerical Models

The whole numerical process started with the parameters described above. However, the model needed to be calibrated to match the fact that the primary source area at HKU failed on 9 a.m. 7 June 2008, i.e. the factor of safety at that particular time should be 1. There were many possibilities in changing the various parameters to achieve this scenario.

The permeability of the near-surface soil strata, namely, the young and old colluviums was considered as the most control parameters. Thus in the calibration exercise, the permeability of young and old colluviums (from saturated state to suction of 100 kPa) was factored by the same amount until the landslide scenario occurred. And it was found that when the permeability of the young and old colluviums was 4 times the field measured value (Table 2), the landslide scenario could be modelled. As in many calibration exercises, there are many ways to adjust different parameters to model the same field observations. The factor of 4 applied to the permeability in this case study does not necessary mean the actual permeability should be 4 times the field measured values, as the calibrated permeability also absorbed the uncertainty from other aspects in the complex analysis. Nonetheless, from past experience, permeability measured in the field or laboratory for the same soil can vary significantly, between orders. In this aspect, a factor of 4 does not seems to be totally out of range.

2.3.7 Results of Numerical Models and Observation

Immediately prior to the 6 June 2008 rainstorm (preceding rainstorm) the pore water pressures in the vicinity of the slip surface was mainly controlled by the assumed soil suction of 20 kPa (Section 2.3.5).

Figure 4 shows the corresponding contours of the pore water pressures from SEEP/W. The pore water pressures were imported to SLOPE/W for stability assessment and the estimated factor of safety was 2.29 (Table 5).

At the end of preceding rainstorm, it can be seen from the contour of pore water pressures (Figure 5) that the suction within the young and old colluviums had been reduced and a saturated zone with positive pore water pressure developed directly above the lower part of the slip surface. The slip surface typically passed through soils with suction between 5 kPa and 10 kPa. The reduction in soil suction due to the preceding rainstorm had reduced the factor safety to 1.48 (Table 5).

At the outset of the 7 June 2008 rainstorm (triggering rainstorm), which was also the end of the no rain period, the water previously entered in the near-surface soil during the preceding rainstorm had travelled further downstream and the saturated zone developed then had disappeared (Figure 6). The factor of safety increased slightly back to 1.75 (Table 5).

By the time of the landside (9:00 a.m. 7 June 2008), the triggering rainstorm had significantly increased water content in the near-surface young and old colluviums. A substantial saturated zone had been developed, embracing the entire slip surface (Figure 7). Positive pore water pressures or transient perched water tables were found at the young and old colluviums interface at two locations. The maximum positive pore water pressures there were about 10 kPa to 15 kPa. The factor of safety was 1.01 (close to 1, Table 5 & Figure 8) as it was calibrated to.

Table 5: Factors of safety at different times

Immediately prior to preceding rainstorm (8:00 a.m. 6 June 2008)	At the end of the preceding rainstorm (7:00 p.m. 6 June 2008)	At the outset of triggering rainstorm (end of no rain period) (5:00 a.m. 7 June 2008)	At the time of landslide (9:00 a.m. 7 June 2008)
2.29	1.48	1.75	1.01

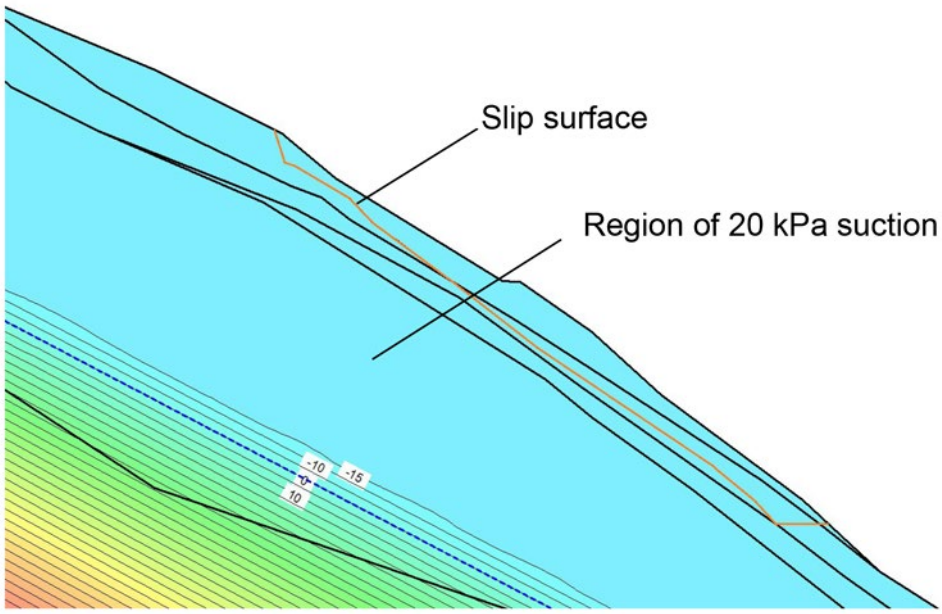

Figure 4: Pore water pressure immediately prior to the preceding rainstorm (8:00 a.m. on 6 June 2008)

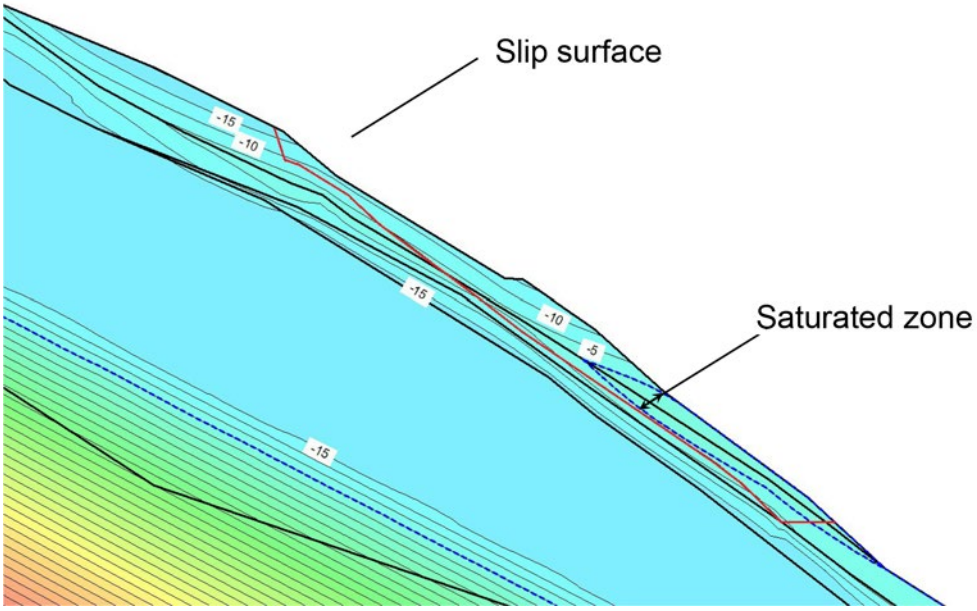

Figure 5: Pore water pressure at the end of the preceding rainstorm (7:00 p.m. on 6 June 2008)

3 The effect of multiple rainstorms on landslides

The numerical results of this case study indicate there were effects to the landslide due to the multiple (preceding and triggering) rainstorms. The preceding rainstorm dropped the factor of safety of the primary source area moderately prior to the triggering rainstorm. This implies without the preceding rainstorm, the landslide on 7 June 2008 might not have occurred or would only occur at a later time when source area was more saturated by the triggering rainstorm. The case study also demonstrates similar approach can be adopted to study other landslides, whether potential or historical, providing a more quantitative mean to assess the effect of multiple rainstorms on landslides.

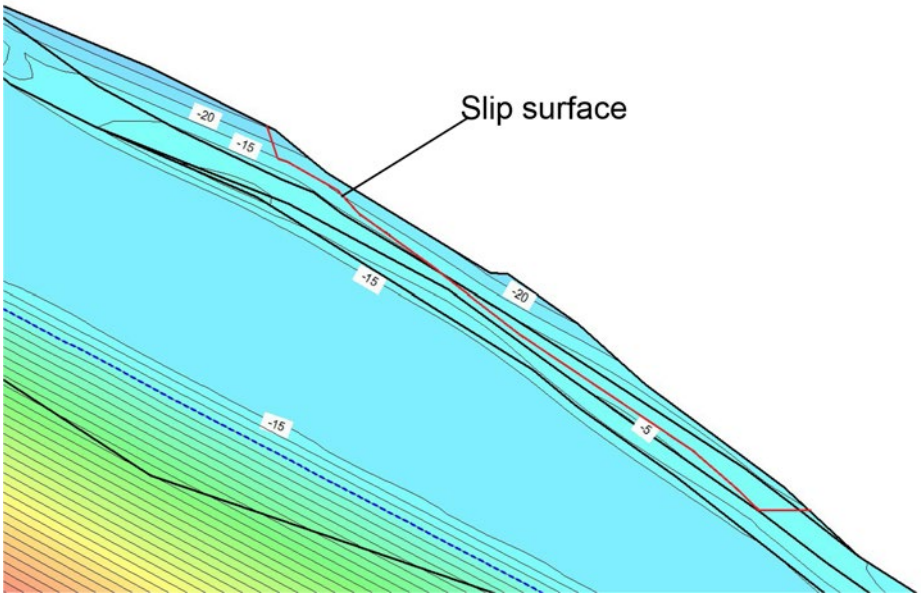

Figure 6: Pore water pressure at the outset of the triggering rainstorm (5:00 a.m. on 7 June 2008)

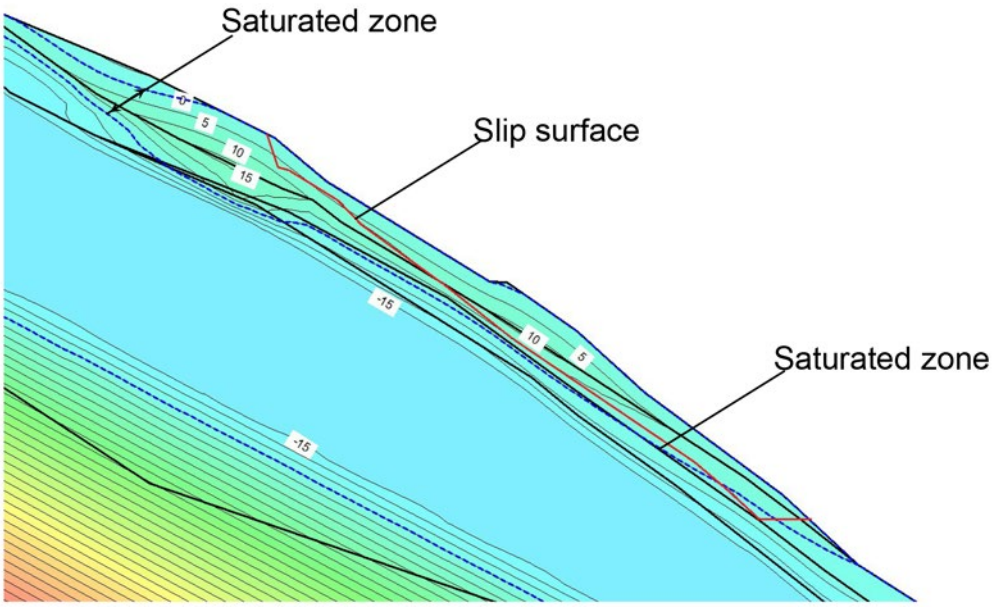

Figure 7: Pore water pressure at time of the landslide (9:00 a.m. on 7 June 2008)

In addition, at the time of landslide, the C/HGT layer still remained in suction (Figure 7). The saturation in this layer was much slower than that in the near-surface soils, probably due to the greater thickness of the C/HGT layer and the impedance of flow by the overlaying old colluvium.

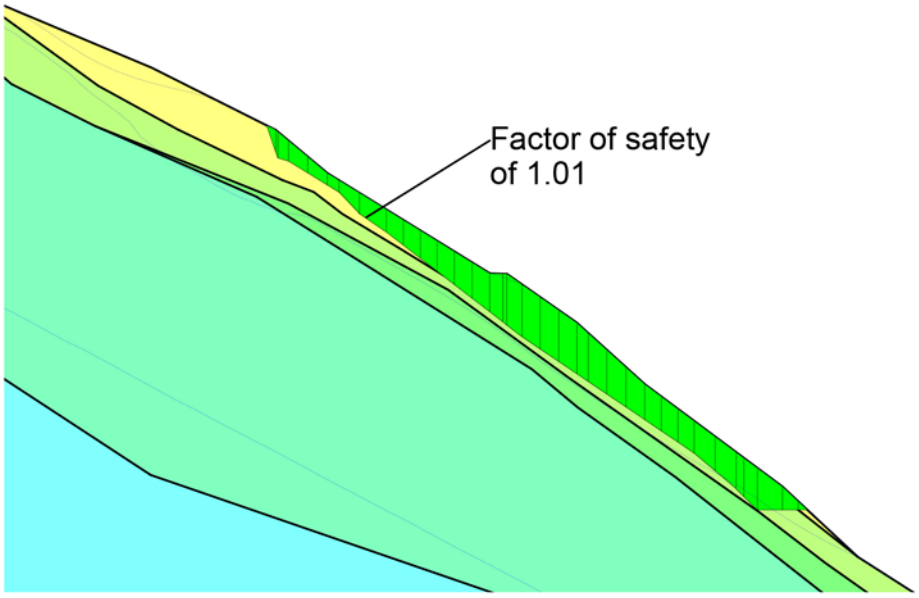

Figure 8: SLOPE/W plot of slip surface for the time of landslide (9:00 a.m. on 7 June 2008)

4 CONCLUSIONS

This paper presents an approach to study the effect of multiple rainstorms to landslide based on numerical modelling. A local case study was carried out and presented. While there are limitations in the numerical models, it is considered that the models have generally captured the effect of multiple rainstorms (preceding and triggering) on the selected landslide, using which the changes in groundwater conditions and factor of safety as the rainstorms progressed were assessed and better understood.

ACKNOWLEDGEMENTS

This paper is published with the permission of the Head of Geotechnical Engineering Office and the Director of Civil Engineering and Development of the Government of the Hong Kong Special Administrative Region.

REFERENCES

Ho, K.Y. 1982. Finite element modelling and its calibrations as applied to the prediction of groundwater table movements. *MPhil Thesis*. University of Hong Kong.

Leach, B. & Herbert, R. 1982. The genesis of a numerical model for the study of the hydrogeology of a steep hillside in Hong Kong, *Q J. Eng. Geol. London,* 15, 243-259.

Maunsell Geotechnical Services Limited. 2013. Detailed Study of the 7 June 2008 Landslide on the Natural Hillside behind Chow Yei Ching Building at the University of Hong Kong, Pok Fu Lam, *GEO Report No. 276,* Civil Engineering and Development Department, HKSAR.

Ng, A. & Small, J.C. 2000. Use of coupled finite element analysis in unsaturated soil problems, *International Journal for Numerical and Analytical Methods in Geomechanics,* 24, 7394.

Ng, A.K.L. 2016. Numerical modelling of groundwater response in slopes in Hong Kong. *Proc of the 15th Asian Regional Conference on Soil Mechanics and Geotechnical Engineering, 986-989. Fukuoka, 9-13 November 2015.* Japanese Geotechnical Society Special Publication.

Ng, C.W.W., Wang, B & Tung, Y.K. 2001. Three-dimensional numerical investigations of groundwater responses in an unsaturated slope subjected to various rainfall patterns. *Canadian Geotechnical Journal,* 38(5), 1049-1062.

Design and Construction of a Rigid Steel Boulder-resisting Barrier in a Drainage Line, Lantau

Leslie H. Swann, Malcolm J. Lorimer, Stanley Chung,
Paco Tsang & Felix Cham
Jacobs China Limited, Hong Kong

ABSTRACT

During detailed natural terrain hazard study (NTHS) of a 270,000m^2 hillside catchment above a village on Lantau, a debris flood hazard was identified in a drainage line. Boulder impact from debris flood hazard was determined to pose a risk to residential facilities and thus hazard mitigation works were recommended to mitigate the risk. Various barrier design options were examined to arrest moving boulders at the remote site. A steel rigid barrier option was selected for detailed design which minimized restricting drainage line water flow. The steel boulder-resisting barrier was designed to retain up to 25 nos. of 1.5m diameter boulders and to withstand boulders moving at a velocity up to 5.1m/s. Construction involved fabrication, transport and welding of large steel members and was challenged by the remote drainage line site but was successfully completed on time and on budget.

1 INTRODUCTION

1.1 Background

Jacobs China Limited was appointed by the Geotechnical Engineering Office (GEO) of Civil Engineering and Development Department (CEDD) to carry out investigation and design of natural terrain hazard mitigation works to natural terrain hillside catchments, as part of the Landslip Prevention and Mitigation Programme (LPMit Programme). Hillside Catchment 9SW-B/DF2 located at Sham Shek Tsuen, Lantau is one of the hillside catchments investigated under the LPMitP. Hillside Catchment 9SW-B/DF2 is a large northwest facing hillside catchment which has a maximum elevation of +504mPD with an average slope gradient of 22° and an approximate area of 270,000m^2. Three drainage lines (DLs) descend the hillside catchment and intersect at the lower part of the Hillside Catchment to form a single DL. The hillside catchment generally comprises a broad open depression. Residential buildings are located below the hillside catchment adjacent to the DL. Based on the results of ground investigation, this hillside catchment comprises Colluvium overlying Completely Decomposed Sandstone (CDS) and Moderately Decomposed Sandstone (MDS) of undivided Mai Po Member, which belongs to the Lok Ma Chau Formation of the San Tin Group. Boulders were mapped along the DL during site inspection. The boulders are typically 0.2 m to 1.5 m in diameter. Boulders larger than 0.5 m in size were typically fine ash tuff/rhyolite. Natural terrain hazard study (NTHS) was conducted for Hillside Catchment 9SW-B/DF2 in May 2013.

The natural terrain hazard study (NTHS) based on Design Event Approach has been carried out on the Study Area to examine the natural terrain landslide hazards affecting the facilities and formulate appropriate hazard mitigation strategies to mitigate landslide risk. Based on the geomorphological setting and the engineering geological model, debris flood was an identified hazard which could affect the facilities below Hillside Catchment 9SW-B/DF2. Boulders in the DL may be picked up from bedload, moved and impact the residential facilities in the event of debris flood. Boulder impact from debris flood

hazard was considered the principal hazard for the hillside catchment which would pose a potential risk to the occupants of the residential buildings at the toe of this hillside catchment. Hazard mitigation measures are therefore required for Hillside Catchment 9SW-B/DF2.

2 DESIGN STAGE

2.1 Design options for natural terrain hazard mitigation works

The S2(H) Study report comprising a NTHS and a Design Options Assessment was submitted to GEO in May 2013. Three design options, which are rigid steel boulder-resisting barrier, flexible barrier system and a reinforced concrete check dam in the DL at the lower part of the hillside catchment, were proposed as the natural terrain hazard mitigation works.

Flexible barrier systems are commonly used for mitigation of natural terrain boulder fall hazards from hillside catchment in Hong Kong. A flexible barrier system is a cost-effective means for protecting the facilities below from boulder fall and the adverse visual impact of a flexible barrier system is low. However, the water flow of the DL may be large during storms. A large amount of water and bedload flow continuously passing through a flexible barrier may adversely affect the performance of the system and damage the corrosion protective coating (typically zinc or zinc/aluminum alloy coating), hence the durability of the flexible barrier may be reduced. Repainting of corrosion protective coating, especially for the principal net of the flexible barrier, is difficult and costly. Therefore, frequent inspection and high maintenance cost would be required if a flexible barrier system is used for Hillside Catchment 9SW-B/DF2.

Significant excavation, casting of reinforced concrete and tree felling are required for construction of a check dam. Hence a third option of a steel boulder-resisting barrier was formulated which allows the storm water to pass through, as a result, the force acting on the steel boulder-resisting barrier by debris flood is comparably less. Repainting of corrosion protective coating for structural steel and the steel components are required for maintenance of the steel boulder-resisting barrier. However, it is easier to repaint the corrosion protective coating for structural steel member of steel boulder-resisting barrier when compared with ring net of steel flexible barrier system.

After consideration of cost, duration of construction period, maintenance requirement, environmental impact, construction problems and constraints of construction of steel boulder-resisting barrier, construction of flexible barrier system and construction of check dams, construction of steel boulder-resisting barrier was selected as the natural terrain hazard mitigation works for Hillside Catchment 9SW-B/DF2 in July 2013.

Plate 1: Large water flow of the drainage line after a rainy day

2.2 Detailed design of steel boulder-resisting barrier

The design alignment for the steel boulder-resisting barrier was at the mid-portion of Hillside Catchment 9SW-B/DF2 in the stream course, 10m upstream of the residential buildings. Based on the boulder mapping record, numerous boulders with diameter of maximum 1.5m are identified along the DL. Based on the results of Colorado Rockfall Simulation Program (CRSP) and Debris Mobility Assessment, the maximum velocity of boulder is 5.1 m/s. The steel boulder-resisting barrier is therefore designed to resist the impact of boulders of diameter 1.5m travelling at a velocity of 5.1 m/s. The estimated boulder impact load is 2,427 kN calculated using the Hertz Equation (Zhang et al, 1996) in Appendix B of GEO Report No. 270 and the equation is shown below:

$$F = K_c n \alpha^{1.5} \quad (1)$$

where

$$n = 4 r_b^{0.5} / 3\pi(k_b + k_B) \quad (2)$$

$$\alpha = (5 m_b v_b^2 / 4n)^{0.4} \quad (3)$$

$$k_b = (1 - \mu_b^2)/(\pi E_b) \quad (4)$$

$$k_B = (1 - \mu_B^2)/(\pi E_B) \quad (5)$$

and where K_c = load reduction factor = 0.1 (recommended in GEO Report No. 270), r_b = radius of boulder, m_b = mass of boulder, v_b = velocity of boulder normal to barrier wall, E_b = elastic modulus of boulder, E_B = elastic modulus of barrier, μ_b = Poisson ratio of boulder and μ_B = Poisson ratio of barrier.

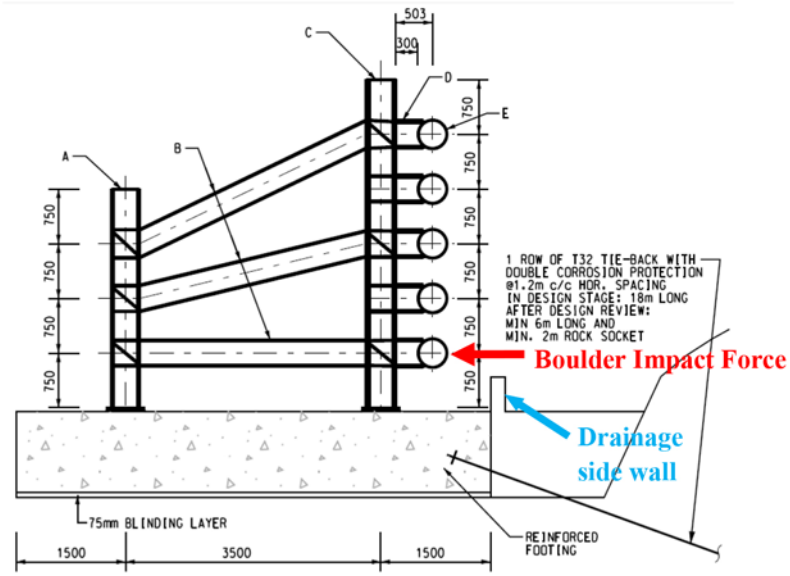

Figure 1: Typical section of steel boulder-resisting barrier

The design addressed the steel members, reinforced concrete footing, tie-backs and surface drainages. Based on the results of Colorado Rockfall Simulation Program (CRSP), the maximum bounce height of the boulder is 2.8m. The height of the barrier was designed to provide adequate retention capacity and avoid boulder from spilling over whereas the length of the barrier was designed to protect the residential building from all possible boulder impact track. The barrier is therefore 4.5m in height and 22 m in length. Five rows of circular hollow sections (CHS) (Member E shown in Figure 1) placed

horizontally at 0.75m c/c vertical spacing were designed to resist the impact load of boulders. Two rows of universal columns (Members A and C shown in Figure 1) were designed as the posts of the steel boulder-resisting barrier to support the CHS and transfer the boulder impact load to the reinforced concrete footing. The structural steel posts are placed at 2m c/c horizontal spacing. Three structural steel members (Member B shown in Figure 1) were designed to connect the Members A and C and transfer the boulder impact load from Member C to Member A in order to minimize the shear force at Member C. In the event of a boulder directly impacting the CHS (Member E), the force will distribute between the steel members and transfer to the reinforced concrete footing via the columns (Members A and C). The boulder impact force is finally resisted by the resistance force of the tie-backs, the friction and the bearing pressure from the soil beneath the reinforced concrete footing. A 3D model developed at the design stage is shown in Figure 2 and a typical cross section of the steel boulder-resisting barrier is shown in Figure 1. Zinc coating and painting are provided to improve corrosion protection for the structural steel members in order to enhance durability and reduce frequency of maintenance.

As the location of the steel boulder-resisting barrier is surrounded by Lantau North (Extension) Country Park and Government Land License (as shown in Figure 3 and Plate 2), the area for construction of reinforced concrete footing is constrained. It is necessary to minimize the size of steel boulder-resisting barrier and volume of excavation. The reinforced concrete footing has a width of 6.5m, depth of 1.5m and length of 22m. The reinforced concrete footing was designed to found on Colluvium. A temporary cut slope is required for construction of the reinforced concrete footing and temporary soil nails were designed for the temporary cut slope.

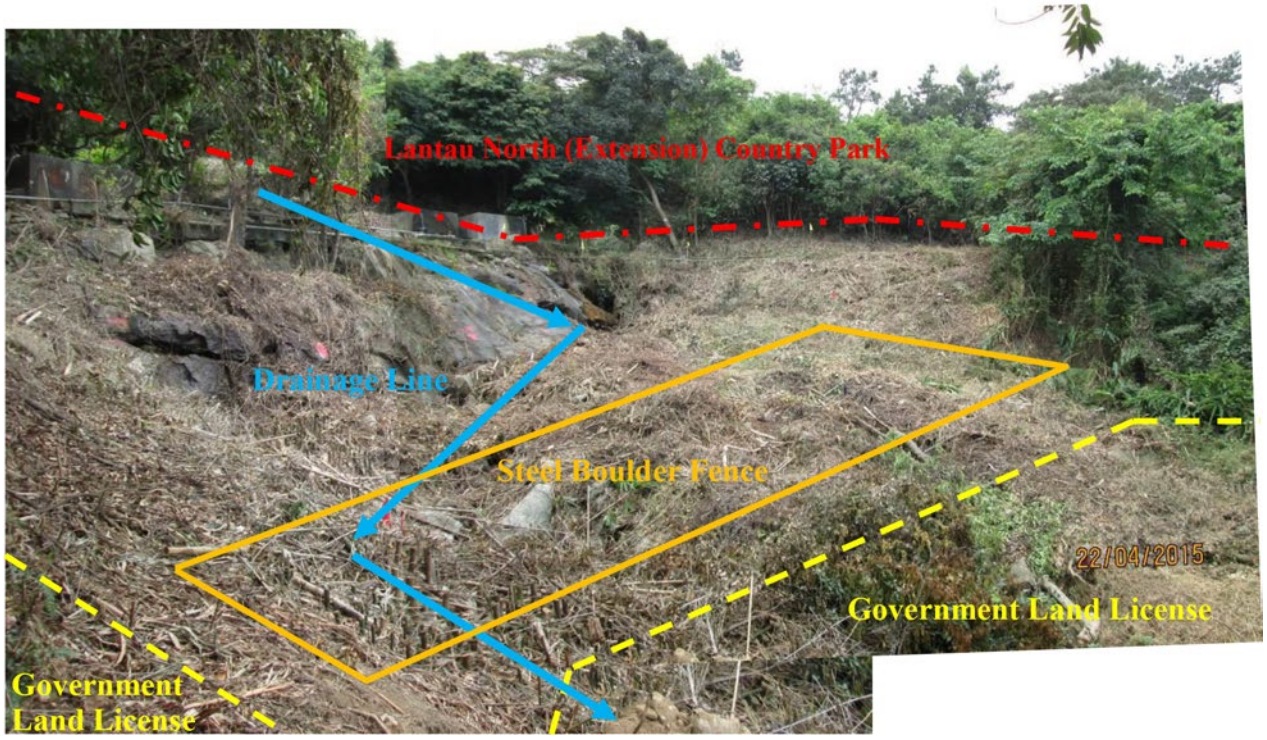

Plate 2: General view of the construction site of steel boulder-resisting barrier

A row of permanent 18m long T32 high yield steel bar tie-back at 1.2m c/c was specified to anchor the reinforced concrete footing to the ground in front of the streamline against the sliding forces and overturning forces induced by the impact load of boulder as well as the groundwater uplift force. The tie-back was designed to be bonded in CDS or better material. As the tie-backs were designed to be installed under the DL and the tie-backs are one of the main components of the steel boulder-resisting barrier transferring part of boulder impact force to the ground, it is necessary to ensure the durability of the tie-backs. Soil aggressivity assessment was carried out based on the laboratory test results of the soil samples collected from site-specific ground investigation. The result of the assessment indicated that the surrounding soil was aggressive. Therefore, corrugated plastic sheathing was provided as additional corrosion protection measures to the tie-backs.

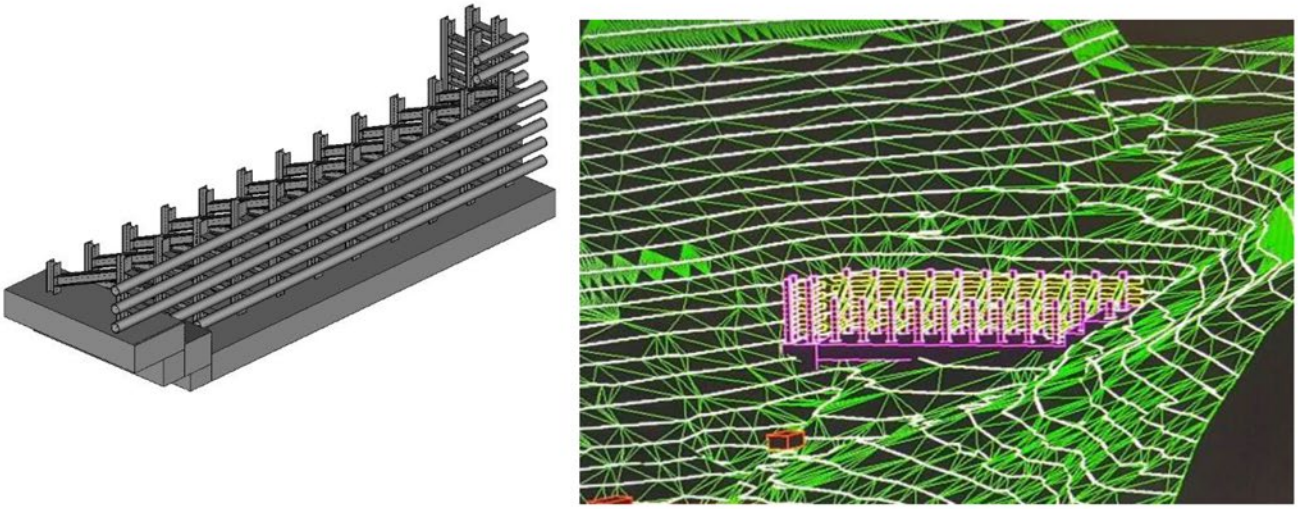

Figure 2: 3D Model for design of Steel boulder-resisting barrier

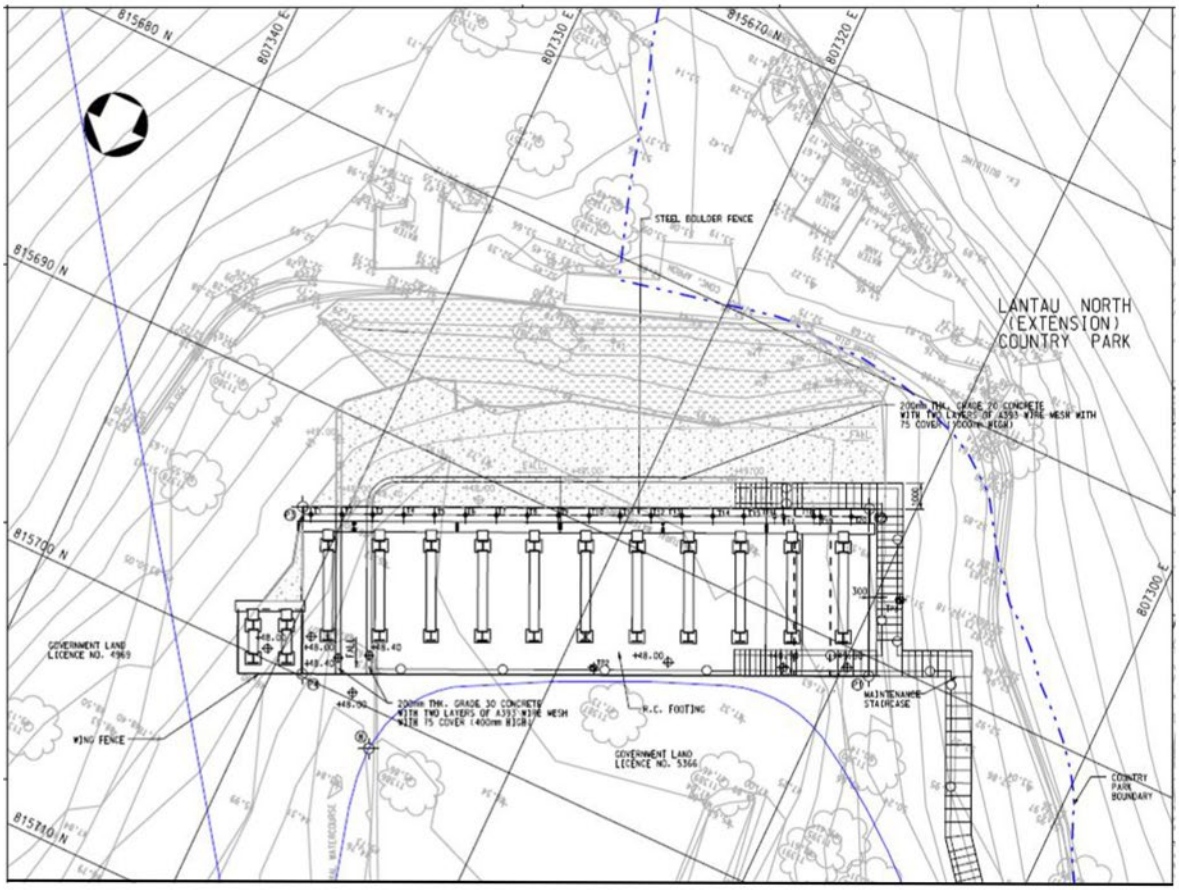

Figure 3: Plan of steel boulder-resisting barrier

1m width of concrete maintenance access and stairway was designed in order to provide enough space to carry out routine maintenance, such as removal of boulders trapped by the steel boulder-resisting barrier and replacement of structural steel members if necessary. The detailed design of the steel boulder-resisting barrier was completed in December 2014.

3 CONSTRUCTION STAGE

The construction of the steel boulder-resisting barrier was commenced in February 2015. The construction included general site clearance, excavation for foundation, construction of reinforced concrete footing, installation of tie-backs, erection of structural steel members, welding and painting for the structural steel members and construction of surface drainage system and maintenance access. The design of the steel boulder-resisting barrier was reviewed during the construction stage and minor design changes were made to suit the actual site condition, minimize the environmental impact and reduce the construction difficulty.

The construction site is located at Sham Shek Tsuen. However, the practical access point for loading and unloading is located at the northern end of Sham Wat Road which is about 1.5 km away from the construction site. A relatively large amount of structural steel members, steel reinforcement and concrete was required to be transported to the construction site for erection of steel boulder-resisting barrier and construction and demolition (C and D) materials generated by excavation needed to be removed and disposed of from the site. Transportation of materials was the main difficulty for the construction.

As the construction site was located at a DL, a drainage diversion was required before any construction works. A temporary steel structure certified by an Independent Checking Engineer was erected to divert the water from the DL. A temporary concrete drainage inlet was constructed at the end of the temporary steel structure to collect the water into a large diameter PVC pipe for drainage diversion. The drainage diversion was commenced immediately after commencement of the works and was completed before the wet season, therefore the excavation works and construction of the reinforced concrete footing was able to be carried out smoothly without major obstruction. After the completion of the drainage diversion, the excavation for the reinforced concrete footing was carried out.

At the design stage, temporary cut slope with temporary soil nails were designed for construction of the reinforced concrete footing and erection of steel boulder-resisting barrier. After site clearance, design reviews had been carried out to minimize the excavation. Stepped reinforced concrete footing and specially designed wing shaped fence had been considered and provided at the western end and the eastern end of the steel boulder-resisting barrier respectively in order to minimize the excavation and the environmental impact to the existing DL and the adjacent country park. No temporary cut slope was required as stepped reinforcement concrete footing was provided. Hence, temporary soil nails proposed at the design stage were no longer required. C and D materials generated by excavation were reduced and relieved stress of transportation of materials away from the remote site. The loose material at the ground surface was removed exposing CDS and the reinforced concrete footing was founded on CDS which is stronger than the formation of Colluvium assumed in the design.

Plates 3 and 4: Temporary steel structure for drainage diversion

A row of permanent 18m long T32 high yield steel bar tie-backs at 1.2m c/c was designed at the design stage to anchor the reinforced concrete footing to the ground. The tie-back was originally designed to be bonded in CDS or better material. After site clearance, it was found that the rock mass in front of the proposed location of the steel boulder-resisting barrier was MDS and good material. It was possible to reduce the length of tie-back. 2 pullout tests with 6m long test soil nails with 2m bond length were carried out for determining the pullout capacity of the MDS. Based on the result of the pullout test, the allowable pullout resistance provided by the 2m bond length bonded in the MDS is larger than the required working load of the tie-back. In other words, 2m rock socket length in MDS is enough to mobilize the required working load of each tie-back. Hence, the length of permanent tie-back was revised to 6m with at least 2m rock socket length in order to reduce the material and the transport and the construction cost. The tie-backs were installed with corrugated plastic sheathing as corrosion protection measures and the plate of the tie-backs were placed at the specified location within the reinforced concrete footing.

Concreting of the reinforced concrete footing was carried out followed by installation of tie-backs. T40 high yield steel bar was designed as the reinforcement of the reinforced concrete footing of the steel boulder-resisting barrier. However, the weight of a single steel bar is high which caused transportation difficulty. After discussion with the contractor, the T40 high yield steel bar was revised to T32 high yield steel bar arranged at a closer spacing. The weight of each single steel bar was reduced so that transportation of the steel bar to the remote site is easier.

Erection of structural steel members was carried out after completion of concreting of the reinforced concrete footing. Butt weld and fillet weld were applied to connect the structural steel members. The structural steelworks were painted to enhance the corrosion protection and to blend with the surrounding in order to minimize visual impact. In order to ensure the performance and durability of the steel boulder-resisting barrier, the condition of welding of the structural steelworks, the corrosion protective coating and the painting are important. All welds were visually examined with the aid of optical instrument and checked by magnetic particle inspection in order to ensure the quality of welding. Non-destructive tests were carried out by ultrasonic examination to all weld joints at the support of all cantilevered structural elements to verify the integrity and adequacy of the welds. The structural steelworks including structural steel member, bolts, nuts and washer were hot-dip galvanized in order to protect the structural steelworks from corrosion. Visual inspection was carried out in order to ensure that the painting for the steelworks was successfully completed.

Plates 5: Front view of steel boulder-resisting barrier

Plate 6: Non-destructive test on welding quality with ultrasonic examination

Plates 7 and 8: Rear view of steel boulder-resisting barrier (after general site clearance, during excavation of reinforced concrete footing)

Plates 9 and 10: Rear view of steel boulder-resisting barrier (one week before completion of works, one year after completion of works)

A surface drainage system was provided in front of the steel boulder-resisting barrier. The drainage system was specially designed and comprised a half-round channel and a drainage side wall. When the water flow is normal, the area between the drainage side wall and the rock mass will act as the drainage channel. If the water flow is small, the water will be collected by the half-round channel in order to maintain flow velocity thus assuring self-cleaning action. When the water flow is extremely large, the water will overflow from the drainage side wall and flow between the posts of the steel boulder-resisting barrier and finally return to the original downslope DL. This drainage system design can protect the steel boulder-resisting barrier from the water in the event of small and normal amount of water flow in the DL in order to enhance the durability of the steel boulder-resisting barrier.

The construction of the steel boulder-resisting barrier was completed in March 2016. Although the construction was constrained by the remote location of the site which is situated in a DL, the construction difficulties were eliminated by close cooperation between the contractor, the resident site staff and the design engineer. The design was reviewed and revised during the construction period to make the construction easier. The construction was successfully completed on time and on budget.

A site inspection was carried out in March 2017 to check the condition of the steel boulder-resisting barrier, especially the coating and painting of structural steel member. It was found that the painting and corrosion protective coating of the structural steel member was in good condition one year after completion of works even though the steel boulder-resisting barrier was constructed in a DL. Hence, the required routine maintenance should be minimal. Hydroseeding was applied to reinstate the area adjacent to the construction site after completion of construction works. Plates 9 and 10 show the difference between the area before and one year after application of hydroseeding. The condition of the plants on the hydroseeded area is good and the area is fully reinstated and blended with the surroundings. The drainage system in front of the steel boulder-resisting barrier is working well with normal water flow along the DL. No debris was found in the drainage system.

4 CONCLUSIONS

A steel boulder-resisting barrier was constructed as the natural terrain hazard mitigation measures for Hillside Catchment 9SW-B/DF2 which has principal hazards of boulder impact from debris flood in the hillside catchment. The steel boulder-resisting barrier is a non-standardized design and was designed on a case-by-case basis to suit the actual site condition. The construction was challenged by the remote, drainage line site but was successfully completed on time and on budget. It is found that the steel boulder-resisting barrier is generally in good condition and no debris was found behind the barrier as well as in the associated drainage system, the painting and corrosion protective coating of the structural steel member is in good condition one year after completion of works even though the steel boulder-resisting barrier is located on an active drainage line. Hence, the required routine maintenance should be minimal.

It is suggested to monitor the condition of steel boulder-resisting barrier to review its performance in the future. Further testing, for instance, full scale field test, was recommended to be conducted to verify its structural performance. It would help to facilitate the future development in adoption of a steel boulder-resisting barrier for natural terrain hazard mitigation works.

ACKNOWLEDGEMENTS

This paper is published with the permission of the Head of Geotechnical Engineering Office and the Director of Civil Engineering & Development, The Government of Hong Kong Special Administrative Region.

REFERENCES

Geotechnical Engineering Office. 2012. *GEO Report No. 270 – Supplementary Technical Guidance on Design of Rigid Debris-resisting Barriers.* Geotechnical Engineering Office, Hong Kong.

Geotechnical Engineering Office. 2013. *Stage 2(H) Study Report (No. S2(H)R 21/2013) for Study Area 9SW-B/SA1 behind Sham Shek Tsuen, Lantau.* Geotechnical Engineering Office, Hong Kong.

Geotechnical Engineering Office. 2015. *Stage 3(H) Study Report (No. S3(H)R 005/2014) for Study Area 9SW-B/SA1 behind Sham Shek Tsuen, Lantau.* Geotechnical Engineering Office, Hong Kong.

Zhang, S., Hungr, O. & Slaymaker, O. 1996. The calculation of impact force of boulders in debris flow. *Debris Flow Observation and Research*, edited by R. Du, Science Press, 67-72.

Finite Element Analysis of Deep Excavations in Soft Ground

Leslie H. Swann & Ci Wang
Jacobs China Ltd.

ABSTRACT

Excavations in reclaimed ground in urbans need to be designed to control ground settlement to limit damage to adjacent structures. As 3D finite element models become more user friendly, the benefits of using 3D models to design excavation and lateral support can be significant. This paper describes how 3D analysis can be used to produce economic design solutions which are impossible with conventional 2D analysis.

1 INTRODUCTION

Evaluating the magnitude and distribution of ground movement adjacent to a deep excavation is an important part of the design process when excavating in an urban environment. The magnitude of ground movement introduced by a deep excavation depend on numerous factors, such as the soil and groundwater conditions, excavation geometry, surcharge loads, existence of adjacent structures, construction method, stiffness and penetration of the retaining walls, type and installation method of the props, etc. Furthermore, in certain excavations, the distance from the evaluated section to the corner of the excavation also affects the magnitude and distribution of ground movement. The effect of the section's position on the displacement is known as the "three-dimensional" effect or the "corner effect", whereby ground movement decreases near the corners of the excavation due to the stiffening effects of the corners. This corner effect of ground displacement may not correspond to that found in conventional plane stain (2D) simulation of excavation.

This paper presents a design development of a particular section of a cut and cover tunnel at tender design stage from the numerical modeling aspect, concentrating on demonstrating the benefit of adopting 3D finite element analysis to mobilizing the most of corner effect of ground movement assessment, and comparing it to the 2D finite element analysis proving the benefits of the 3D modeling for potential economical engineering design.

2 Project Background

The Government of the Hong Kong SAR was proposing to build a new highway, known as Route 6, to connect West Kowloon with Tseung Kwan O via a series of tunnels, viaducts and at-grade roads. A short section of Route 6 will be constructed as advance works as an underground supporting structure (SUS) in Shing Cheong Road in the former South Apron of the old Kai Tak airport, this short section as part of the Route 6 is known as Trunk Road T2. The proposed Trunk Road T2 alignment is presented in Figure 1.

The Conforming scheme of the Supporting Underground Structure (SUS) is approximately 409m in length, 30m in width and 13m in height. It is formed as a twin cell box structure founded on external diaphragm walls and central barrettes bearing on rock. The diaphragm walls also form the permanent external walls of the box structure and the barrettes also form, in part, the central dividing wall and roof support. The thickness of diaphragm walls varies from 1.2m to 1.5m. The thickness of cast in situ base

slabs, roof slabs, and central walls were up to 1.5m. The proposed tunnel box was found on diaphragm walls and H piles beneath the center wall. A typical section of the proposed SUS structure is presented in Figure 2.

The excavation and lateral support system for the proposed T2 tunnel box includes propped permanent diaphragm walls with water cut-off. The Public Works Central Laboratory (Lab) is located adjacent to the proposed East end of the tunnel. To confine the settlement limit to 6mm, ground treatment is proposed. The location of the proposed T2 tunnel to the Lab can also be found in Figure 1.

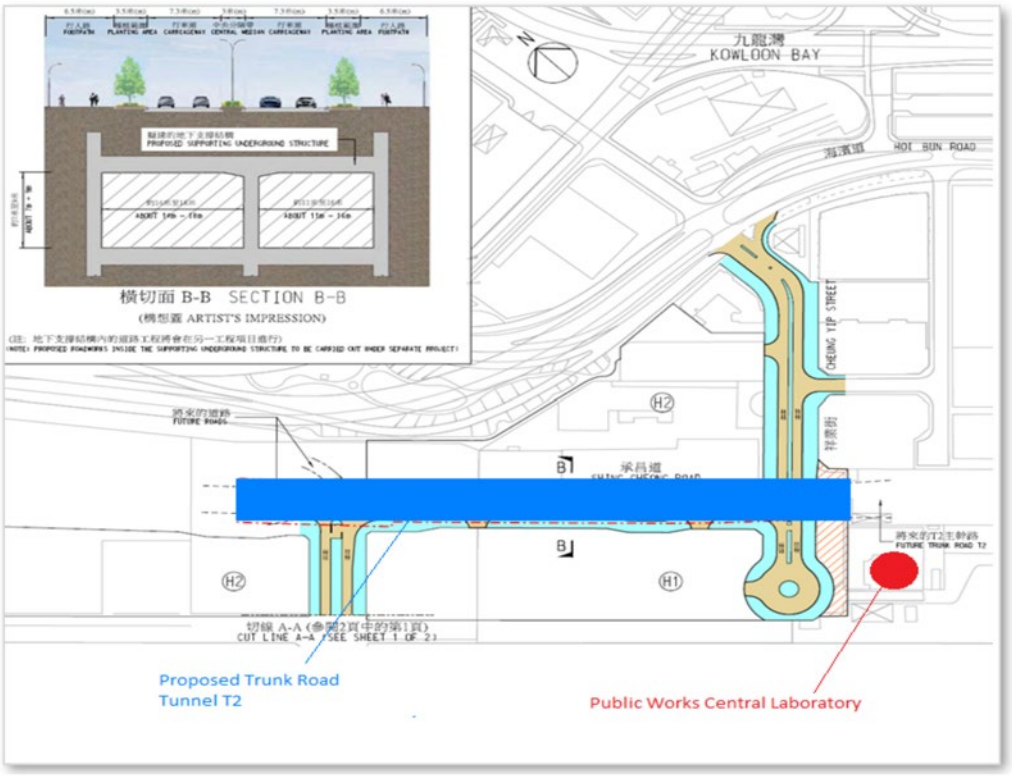

Figure 1 – Proposed Trunk Road T2 Tunnel Alignment

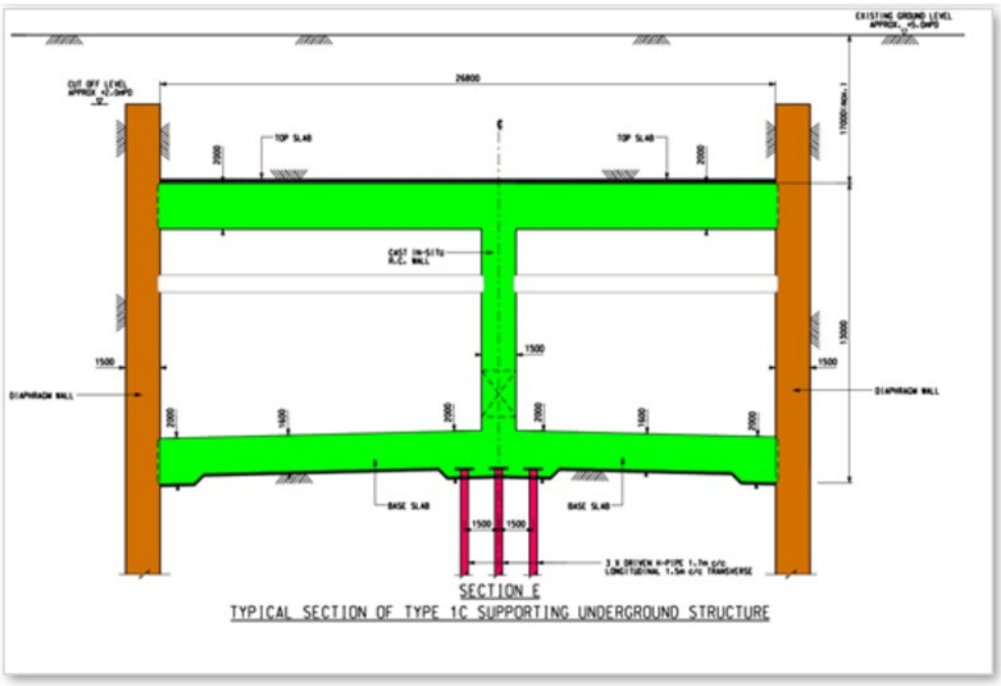

Figure 2 – Typical Cross Sections of the Proposed T2 Tunnel Box

This paper is focused on design development of the temporary lateral support system and ground treatment at the east end of the proposed T2 tunnel alignment, in order to control the maximum design settlement at within the Lab within the settlement limit.

3 Site Description and Geology

3.1 Site location and topography

The site was formed by reclamation in the 1970s for the South Apron of the former Kai Tak Airport. It is generally flat with ground level at approximately +5.0mPD. It is bounded to the north and east by Kwun Tong Bypass; south by Cheung Yip Street and Public Works Central Laboratory Building; and west by Kai Tak approach channel and former Kai Tak runway.

3.2 Ground condition

The site is underlain by Fill, marine deposits, alluvium, and localized colluvium overlying completely weathered granite. Fill is encountered in every borehole with thickness varying from 6m to 25m. It is generally composed of medium dense to dense, occasionally loose, silty gravelly SAND with occasional cobbles and small boulders. Marine clay deposits underlying fill are encountered in some boreholes with approximately 1m to 10m in thickness. Lenses of marine sand are observed in few boreholes. The stratum beneath is alluvium, which is encountered in all boreholes and blankets the underlying in-situ material. Its thickness varies between 5m and 27m. The alluvial deposits on site consist mainly of medium dense to dense, clayey silty medium to coarse SAND. In some locations, it has lenses or/and is interbedded with alluvial clay and occasionally alluvial gravel/cobble of various thickness. Colluvium, underlying alluvium, is observed in 2 boreholes at the SE end of the east bound of tunnel alignment. Beneath is a stratum of completely decomposed granite (CDG) and highly decomposed granite (HDG) with moderately strong to strong corestones. The CDG/HDG layer is approximately 5m to 35m thick. Bedrock is typically medium-grained granite with undulating rock head level in the range of approximately -40mPD to -60mPD, which is 45m to 65m below ground level.

Groundwater levels were measured in piezometers and standpipes that were installed in boreholes during previous GI at or near the site. It is noted that the available monitoring data is limited for analysing seasonal or anomalous variations at the site. According to the limited monitoring records, the groundwater level surrounding the site varies from 2.2m to 4.5m below existing ground level.

Based on the existing borehole information and the interpreted geology, the adopted geological profile at the east end of the T2 tunnel alignment (focus area for this study) is presented in Figure 3.

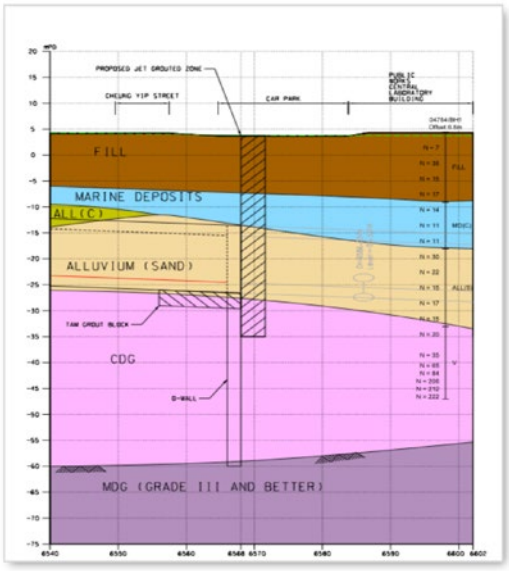

Figure 3 – Interpreted Typical Geological Profile at East End of the Proposed Trunk Road T2 Tunnel Alignment

4 Adopted Design Parameters

4.1 Adopted Geotechnical Parameters

Based on the borehole information in the vicinity along the T2 tunnel alignment, the adopted design parameters are presented in Table 1. The selected values of E' are determined based on the derived correlations of SPT N values with depths. The values are also considered as representative values typically used in Hong Kong. It should be noted that a constant SPT N value has been adopted for increasing depth of CDG although the SPT N values for CDG generally increase with depths based on the available data.

Due to lack of sufficient monitoring data, the design groundwater level is taken to coincide with the existing ground level for the worst case condition consideration.

Table 1 – Adopted Geotechnical Design Parameters for Each Strata Layer

Material	Unit Weight (kN/m^3)	Correlated SPT Result (N values)	Young's Modulus E' (kN/m^2)	Undrained Strength Cu (kN/m^2)	Effective Shear Strength		Permeability K (m/s)	Poisson's Ratio (v')
					Cohesion C' (kPa)	Shear Angle ϕ' (deg)		
Fill	18.5	10	15,000	–	0	33	2E-05	0.3
Marine Deposits	18.0	–	–	2.5x D*	–	–	1E-06	0.3
Alluvium	18.5	25	37,500	–	0	35	5E-06	0.3
CDG	19.0	N=2.7x D*–33 (D* <50m)	2x(2.7 x D* –33)	–	5	36	1E-06 to 1E-07	0.3
		N = 100 (D*>50m)	200,000					

*Note: * D – depth below existing ground level (m).*

4.2 Adopted Structural material properties

4.2.1 Concrete

Grade 45D/20 concrete will be used for the tunnel external walls, centre wall, base slab and top slab structures of the proposed tunnel box. This concrete grade is used to meet the 120 years design life and durability requirement. The properties of concrete are listed below.

- Concrete Grade (fcu) 45 MPa
- Young's Modulus, E short term 26.4 kN/mm^2
- Young's Modulus, E long term 13.2 kN/mm^2
- Poisson's Ratio 0.2
- Unit Weight of Structural Concrete 24.5 kN/m^3

4.2.1 Structural Steel

Structural steel properties for piles, props, walers and king posts are listed below.

- Steel Grade (fy) 430MPa
- Young's Modulus 205 KN/mm^2
- Poisson's Ratio 0.3

5 Excavation and Lateral Support (ELS) System Design Development

Based on the proposed tunnel design and the existing ground condition, the proposed tunnel box at the East end of the T2 tunnel alignment is founded approximately 30m below the existing ground level. The majority of the tunnel box is located within the Alluvium layer, above the CDG layer.

Three rounds of the design assessment were undertaken for getting the settlement within the required limit at the foot print of the Lab. The logistic of the developing the design assessment is presented in Figure 4.

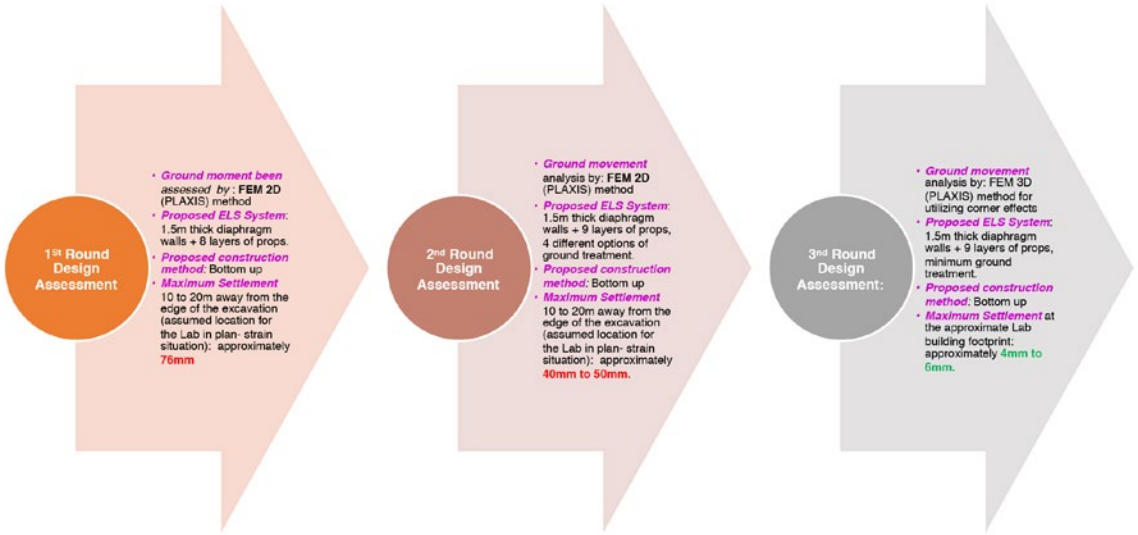

Figure 4 – Overall ELS Design Development for Settlement Control

5.1 1st Round Design Assessment

First round assessment was focused on the natural ground's response based on the proposed ELS design scheme, using PLAXIS 2D software to assess sections along and across the proposed T2 tunnel alignment at the East end. The sections indication is shown in Figure 5.

The proposed ELS system for this round of the design assessment comprised 1.5m thick diaphragm walls, with eight layers of corner struts. The sizes and levels of the proposed H section props are can be found in Table 2.

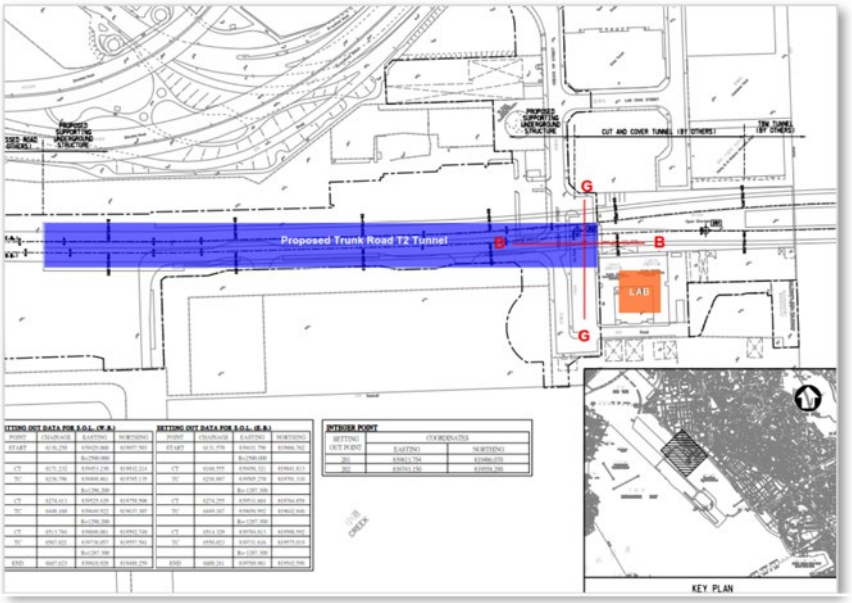

Figure 5 – Section Indication for 1st and 2nd round Design Assessment

Table 2 – 1st Round Design Assessment – Details of Props

Strut ID	Level (mPD)	Size	Pre-stress load (KN/m)	Twin Section Propping (Y/N)
S1	3.4	356x406x551	0	N
S2	-0.6	914x305x253	300	Y
S3	-4.6	914x305x289	500	Y
S4	-8.6	914x305x289	600	Y
S5	-12.6	914x419x388	800	Y
S6	-16.6	914x419x343	800	Y
S7	-20.6	914x419x343	1000	Y
S8	-23.6	914x419x343	1000	Y

The material properties for each soil layers used in the PLAXIS 2D analysis for are presented in Table 3. The Mohr-Coulomb Soil Model is used for all strata layers.

Table 3 – PLAXIS 2D Soil Model and Drainage Condition

Soil Layer	FEM Material Model	Drainage Type
Fill	Mohr-Coulomb	Drained
Marine Deposits	Mohr-Coulomb	Undrained Type B
Alluvium	Mohr-Coulomb	Drained
CDG	Mohr-Coulomb	Drained

The proposed construction sequence at this stage of the design is comprised 30 stages to model each stage of excavation, strut installation, tunnel construction and back filling / reinstatement.

Based on the PLAXIS 2D analysis result, settlement increases as construction stages increases. The maximum ground settlement occurred at the final stage (back filling to the road level), and the magnitude of the maximum settlement outside the tunnel box footprint is approximately 75mm. The ground movement results from the PLAXIS 2D analysis far exceeded the design limit of 6mm. The maximum settlement resulted from Section G is presented in Figure 6.

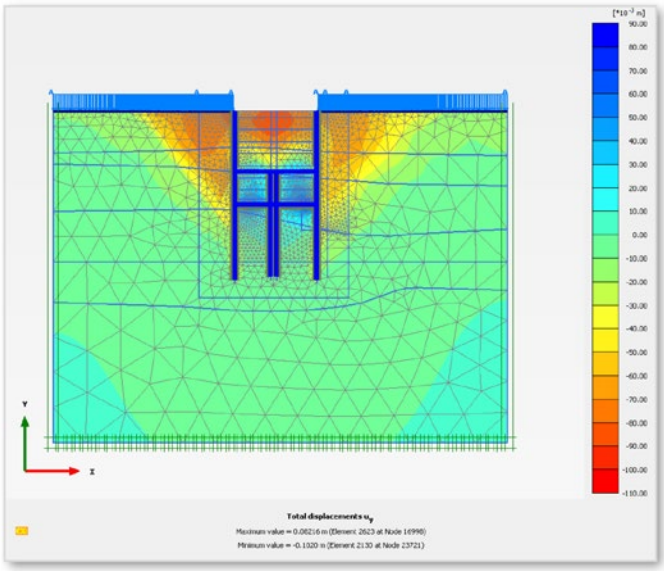

Figure 6 – Settlement result from 1st round of the design assessment

5.2 2nd Round Design Assessment

Based on the result from the 1st round design assessment, and four ground treatment options with an additional layer of strut at -13.6mPD was proposed and tested by PLAXIS 2D analysis at the same sections showing in Figure 5. The indications of each ground treatment options are shown in Figure 7 to Figure 10. The Results of maximum ground settlement 10m to 20m outside of the excavation are summarized in Table 4.

The adopted stiffness parameters for the jet grouping were E = 200MPa and Su = 2000kPa. The proposed ground treatment options are summarized below:

Option 1 – Jet grout the entire MD layer inside excavation with 3m wide jet grouting strips, 5m apart center to center (2m apart edge to edge); leave the struts in when back filling to the top;

Option 2 – Jet grouting the entire MD layer inside excavation with 3m wide jet grouting strips, 5m apart center to center (2m apart edge to edge); 3 rows of 1.2m jet grout at MD layer outside excavation (jet grouting properties same as inside excavation, 3m wide, 2m edge to edge distance);

Option 3 – Jet grouting the entire MD layer inside excavation with 3m wide jet grouting strips, 5m apart center to center (2m apart edge to edge); 5m wide jet grout through MD layer from -5mPD to -20mPD (outside excavation, jet grouting properties same as inside excavation, 3m wide, 2m edge to edge distance). An additional layer of struts was required at -13.6mRL; and

Option 4 – Jet grout the entire MD layer inside excavation with 3m wide jet grouting strips, 5m apart center to center (2m apart edge to edge); 10m wide jet grout through MD layer from -5mPD to -20mPD (outside excavation, jet grouting properties same as inside excavation, 3m wide, 2m edge to edge distance)

An additional layer of struts was required at -13.6mRL.

Table 4 – 2nd Round Design Assessment Settlement Results

Ground Treatment Options	Maximum Settlement (10m to 20m outside of the excavation) at Back Filling Stage (mm)
Option 1	49.2
Option 2	45.0
Option 3	39.0
Option 4	34.0

Based on the settlement results from this round of PLAXIS 2D analysis, the settlement was controlled significantly by adopting ground treatment and an additional layer of strut. Understanding the ground should have greater stiffness due to the corner effect at the proposed design target location. However, due to the limit of 2D analysis, the amount of ground moment due to excavation at the corner was still unknown at this stage of the project. Furthermore, adopting jet grouting ground treatment was an expensive construction activity, whether it was necessary to grout this much (as in option 3 and option 4) to control the ground movement was unknown at this stage.

5.3 3rd Round Design Assessment-3D FEM analysis

In order to access the settlement at outside at the corner of the T2 trunk road excavation, incorporate with the proposed ground treatment options, 3D FEM analysis was undertaken by using PLAXIS 3D, 2013 version.

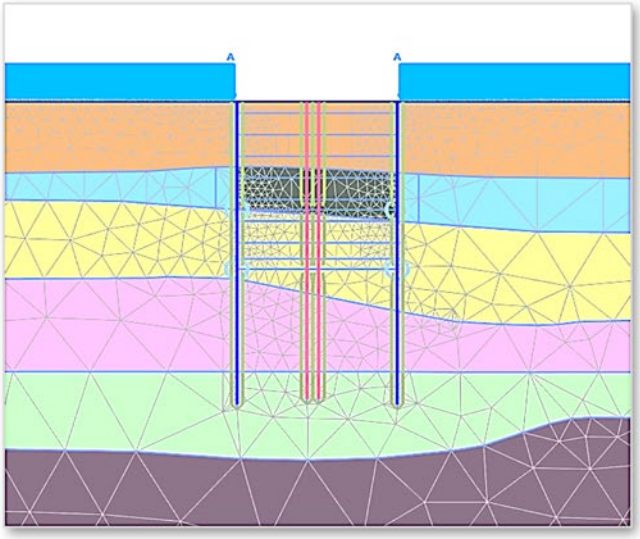

Figure 7 – Ground Treatment Option 1

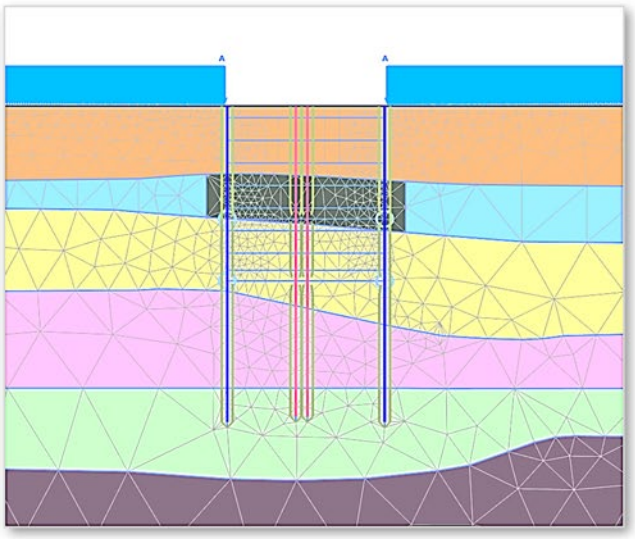

Figure 8 – Ground Treatment Option 2

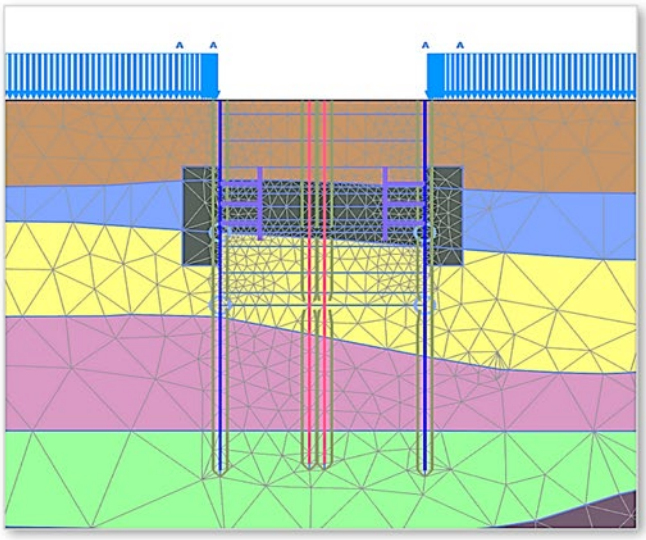

Figure 9 – Ground Treatment Option 3

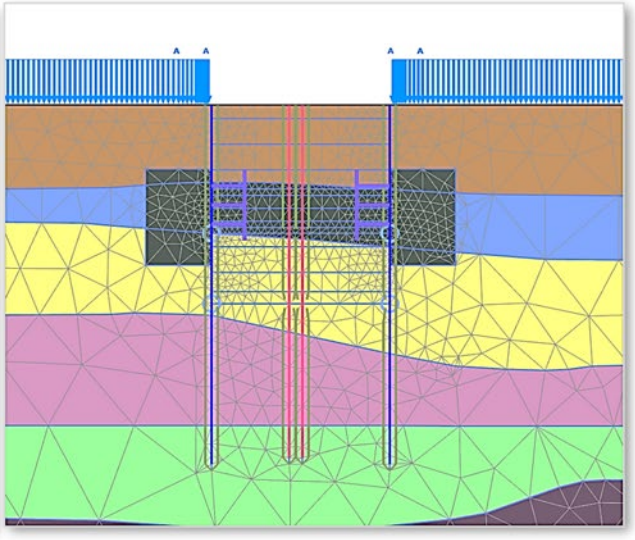

Figure 10 – Ground Treatment Option 4

The 3D model was developed in a 150m long x 90m wide x 100m deep rectangular block, representing a 90m long x 28m wide x 32m deep tunnel excavation section, supported by 9 layers of struts (including corner struts) for the temporary stage. Tunnel permanent stage (i.e., Tunnel box and back filling to the road level) is also simulated in the 3D model. The 3D model comprised approximately 96,000 soil elements. A general view of the 3D model is presented in Figure 11 and Figure 12.

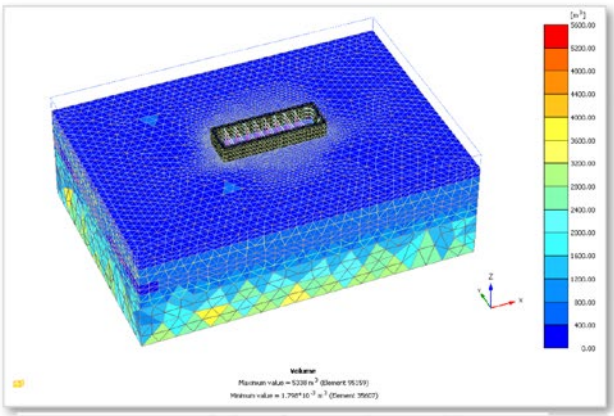

Figure 11 – General View of T2 Tunnel 3D Model

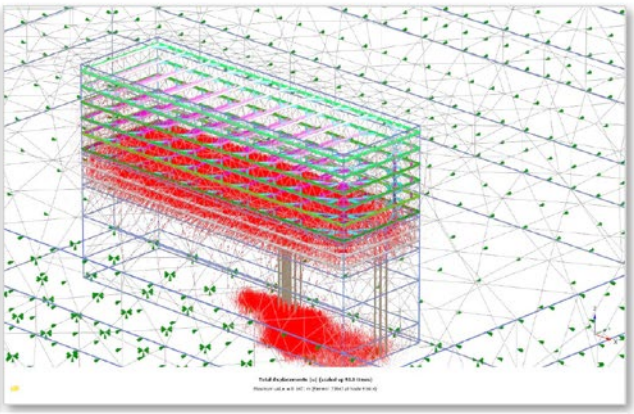

Figure 12 – General View of T2 Tunnel 3D Model Structural Elements

The soil parameters, material properties and drainage types in the 3D model remain the same from 2D models. In PLAXIS 3D model, the diaphragm wall and the tunnel boxes (base slab, roof slab and the middle wall) were modeled as "plates"; struts (including corner struts, and minor struts) were modeled as "anchors"; the walings were modeled as "beams"; tension piles were modeled as "embedded piles". Groundwater and groundwater boundary condition in 3D model remain the same from 2D models. Construction sequence in 3D model kept the same as the 2D model.

Ground treatment in the 3D model only considered grouting inside of the excavation from -6.0mPD to -15.0mPD (the marine clay layer), similar to Option 1 from 2nd round design assessment.

The result of the PLAXIS 3D analysis showed the maximum ground settlement at the Lab footprint was within the design limit of 6mm. From the 3D analysis, a trend of the corner effect was indicated from the ground movement plot. The settlement results from PLAXIS 3D analysis are presented in Figure 13 and Figure 14. An indication of the trend of corner effect is presented in Figure 15.

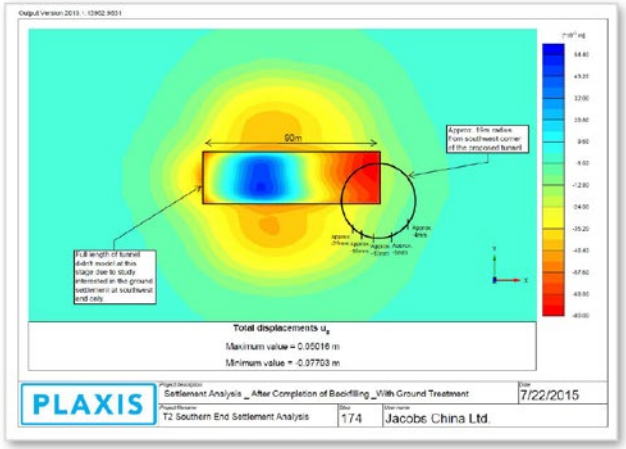

Figure 13 – PLAXIS 3D Result – Settlement due to T2 Tunnel Excavation (Plan View)

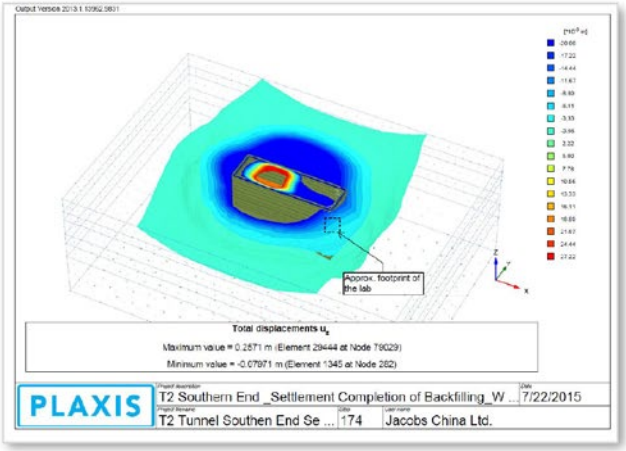

Figure 14 – PLAXIS 3D Result – Settlement due to T2 Tunnel Excavation (3D View)

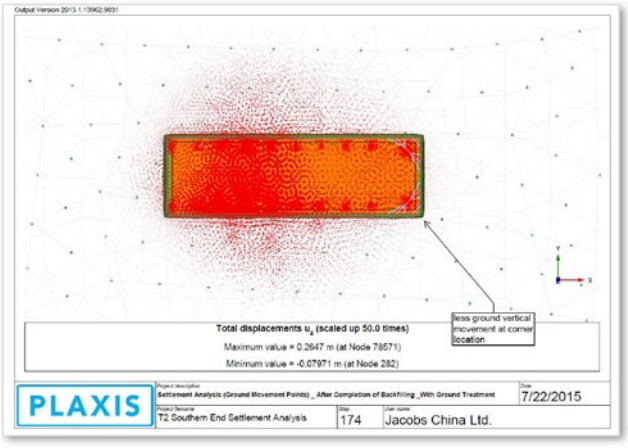

Figure 15 – PLAXIS 3D Result Indication of Corner Effect in terms of Ground Movement due to Excavation

6 Conclusion

Numerical analyses of deep excavations are commonly simplified by assuming plane strain conditions when designing support systems and making estimates of associated ground movements. However, in reality excavations behave in a manner more accurately described as three-dimensional, as a result of the differences in boundary conditions due to the stiffening effects at corners. This paper was using a design development as an example by comparing three rounds of design assessment; ground settlement

was reduced by ground treatment and corner stiffening effects. It is appears engineers can adopt a more economical solution by reviewing the design development from plane strain FEM analysis to 3D analysis as it accounts for the corner effect benefits.

References

PLAXIS 2D 2015, Reference Manual.

PLAXIS 3D 2013, Reference Manual.

Bin-Chen Benson Hsiung, Kuo-Hsin Yang, Wahyuning Aila, Ching Hung, 2016. Three-dimensional effect of a deep excavation on wall deflection in loose to medium dens sand, Computers and Geotechnics.

Application of an Automated LiDAR-based Mapping System in Natural Terrain Hazard Studies in Hong Kong

Jesse H.T. Tam, Colin K.W. Yeung, Jason P. Yu,
Rolan S.L. Hu & Kevin A. Styles
Fugro (Hong Kong) Limited

ABSTRACT

Over the last 10 years, natural terrain landslide hazard studies have become an essential part of the slope safety system in Hong Kong. Consideration of the geomorphological and geological characteristics of undeveloped and often landslide prone terrain is now a prerequisite for public and private development. Hong Kong is an *innovative* world leader in the development and implementation of natural terrain landslide hazard assessment ranging from public policy creation, terrain characterisation techniques, through design and to construction of mitigation works.

Since 2011 there has been growing use of LiDAR survey data across a spectrum of applications. This data can assist in site characterisation and has enabled improvements to conventional methods of terrain classification, many of which were pioneered in Hong Kong during the late 1970s and 1980s. This paper outlines a LiDAR-based DEM terrain classification system developed primarily to create preliminary *conceptual* landform models. The technique known as AIMS (Automated Integrated Mapping System) is based essentially on slope gradient and Topographic Position Index (TPI) to provide a simple, turn-key *first-pass framework* classification to assist in geomorphological, geological field mapping and modelling. The benefits are in automated, consistent and systematic terrain classification at a range of scales, particularly on remote and inaccessible terrain, in a form amenable for *change analysis*. Innovative AIMS Solutions developed in Hong Kong can be designed for a range of user requirements anywhere.

1 INTRODUCTION

Natural terrain hazard studies (NTHS) have become an essential part of the slope safety system in Hong Kong, and a prerequisite for public and private development near landslide prone terrain. Hong Kong is an innovative leader in public policy creation, development of terrain characterisation techniques, through design and to construction of mitigation works.

Over the last 5 years, there has been a growing use of airborne and terrestrial Light Detection and Ranging (LiDAR) survey data across a spectrum of applications, and in particular for NTHS in Hong Kong. Advantages of airborne-LiDAR include comparatively penetrative methods to identify ground surface, ease of survey both in time and cost, and the volume and type of data collected during a single survey. High resolution Digital Elevation Model (DEM) generated from LiDAR point cloud data can provide more detailed ground surface information than conventional photogrammetric methods in vegetated terrain, and enables derivation of topographic attributes such as slope gradient, aspect and morphology for terrain analysis. Parry & Jonas (2007) described the use of LiDAR data in natural terrain hazard

assessment in Hong Kong. Lai et al. (2012) illustrated the advantages of LiDAR data in 3D visualisation, landform identification and detection of landform change. The DEM also provides opportunities for indirect mapping and analysis in computer models and Geographic Information System (GIS). Sas et al. (2012) evaluated the use of LiDAR-derived DEM using different processing techniques for detection of old agricultural terraces. Sas (2014) demonstrated the application of LiDAR-derived DEM for terrain mapping using Topographic Position Index (TPI) and for landslide susceptibility mapping using PISA-m (Haneberg, 2007).

Systematic terrain classification in Hong Kong was pioneered during the late 1970s and 1980s at scales from 1:2 500 to 1:20 000 as a Territory-wide physical land resource inventory known as the Geotechnical Area Studies Programme (GASP) (Styles & Hansen, 1989). In recent decades, systematic terrain classification has become feasible on a DEM in an automated manner. MacMillan et al. (2000) discussed the concepts of automated landform classification based on DEM, which could be enhanced by advances in LiDAR data collection and improvement in resolution. Such approaches generally involve generation of data layers of morphometric variables from DEM, followed by classification in GIS (e.g. Dragut & Blaschke, 2006; Samodra et al., 2014). Since development by Weiss (2001), TPI has gained popularity as a tool for morphometric data manipulation for terrain classification (e.g. Jenness, 2006; Tagil & Jenness, 2008).

This paper illustrates an automated LiDAR DEM-based mapping system, known as AIMS (Automated Integrated Mapping System), which integrates TPI and slope gradient data systematically in GIS to assist geomorphological mapping in Hong Kong. Two NTHS areas at different scales across a variety of terrain are presented as simple case studies for AIMS application.

2 METHODOLOGY

Slope gradient is a major driver of slope processes and is often a primary input in terrain classification. Surface morphology, quantitatively described by TPI, is ultimately related to geology, geomorphological processes, weathering and types of denudation. As slope gradient data and TPI are derived from elevation data, an effective and fit-for-purpose DEM is fundamental for interrogating spatial information at the scale of interest. The Territory-wide LiDAR survey conducted by the GEO in 2010 (Lai et al., 2012) provided airborne-LiDAR point cloud data suitable to generate high resolution DEM for most areas of Hong Kong.

Based on experience using different spatial interpolation algorithms (e.g. Inverse Distance Weighted (IDW), Kriging, Triangulated Irregular Network (TIN) and ANUDEM), IDW is considered to be the most capable for generating natural terrain landscape DEM in many cases. The other techniques can be applied on a case by case basis. For example, if there are significant artifects on IDW-derived DEM due to low point cloud density, Kriging could be used instead to reduce these artifects, though a much longer processing time is required compared with IDW. Other interpolation methods may produce usable DEMs provided very dense point cloud coverage is available. The choice of DEM cell size should be based on the general quality of point cloud data and purpose of the study. A cell size from 2 to 5 m is considered appropriate for the range of scales used in landslide hazard assessment in Hong Kong.

Slope gradient is calculated for each grid cell as the first derivative of elevation. TPI is calculated for individual grid cell by comparing the elevation of a grid to the elevations of the neighbourhood grid cells of the targeted cell. Positive TPI values indicate the cell is higher in elevation than the neighbourhood cells while negative indicate it is lower. The size of the neighbourhood controls the landform features discovered by TPI. The smaller the neighbourhood chosen, the smaller landform feature it can identify. Therefore, landform mapping can be carried out using TPI at different scales through adjustment of the neighbourhood size.

Systematic integration of TPI and slope gradient is achieved in GIS, with output files in raster or vector form. Smoothed segmentation of terrain classes is produced through iterative filtering procedures.

3 APPLICATION IN NTHS

3.1 Case Study I: Site-specific NTHS

The Study Area (about 7 ha) is a natural hillside with a prominent rock cliff in the upper terrain. The Study Area is underlain by Volcanic Tuff of the Ap Lei Chau Formation and Mt. Butler Granite in the upper and lower portions respectively. The terrain is covered by dense vegetation as shown in aerial photographs since 1963, except for the rock cliff areas (Figures 1A & 1B). LiDAR data is particularly useful in revealing the details of exposed ground surface and beneath all but the most-dense vegetation. AIMS is applied to provide a first-pass derivative map.

For the *conceptual* model, three TPI classes were defined, which could be correlated to surface morphology and tied to Breaks-in-Slope (i.e., convex, planar and concave respectively), generated by AIMS. Three slope angle classes (<25°, 25°-45° and >45°) are defined together with three morphological classes, forming nine terrain classes. The nine-unit classification and major breaks-in-slope in this example (Figure 2A) serves as a starting point for API integrated with field survey or for more complex classification, depending on user requirements.

Figure 1A: 1963 orthophoto over DEM

Figure 1B: 2015 orthophoto over DEM

Based on Fugro's best practice procedures, less than a man-day was required for the processing of AIMS. The results are presented in 3D models to enhance visualisation (Figure 2B).

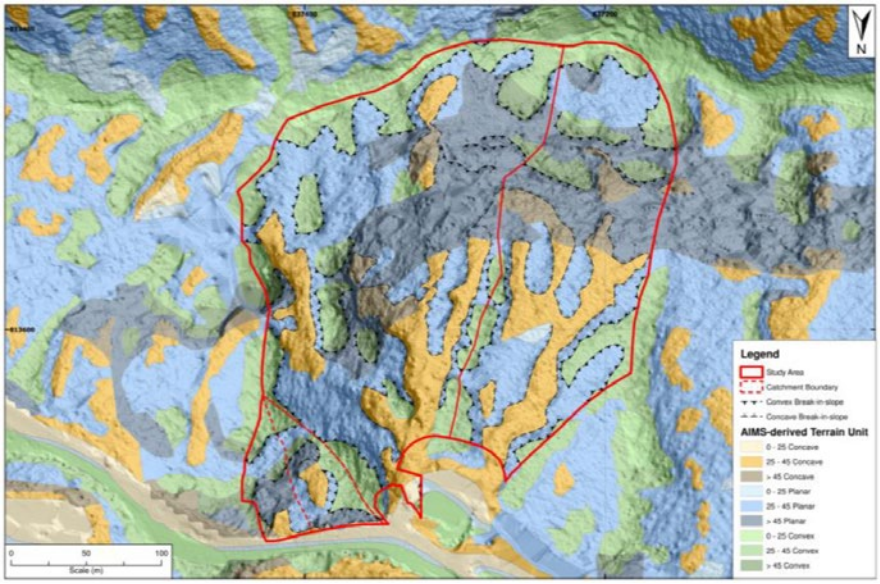

Figure 2A: AIMS-derived Terrain Classification Map with Major Breaks-in-Slope

Visual examination shows that AIMS is able to delineate major morphological units without over-segmentation and with minimal noise. It creates a distinctive landform pattern using a consistent mapping approach. This provides a preliminary systematic framework for terrain characterisation. In this instance, the purpose is a first-pass *conceptual* terrain model which provides a guide for field mapping and also a systematic general treatment of steep, remote and inaccessible areas. Subsequent API and field mapping used the results of AIMS. A basemap overlain with AIMS was used during API and field mapping for terrain evaluation and engineering geomorphological mapping. When integrated with API, it also helped highlight features consistently and identified key target areas of interest for field mapping and design of ground investigations. Attention can be drawn to features that may not be obvious on a simple topographic map. AIMS is a morphological mapping technique that enables subsequent terrain unit mapping to be refined by a combination of morphological, morphographical, morphogenetic and morphochronological mapping (GEO, 2004). The refined site-specific terrain unit map shows AIMS classes can be broadly correlated with landform features such as rock cliffs, topographic depressions and spurlines (Figure 2C).

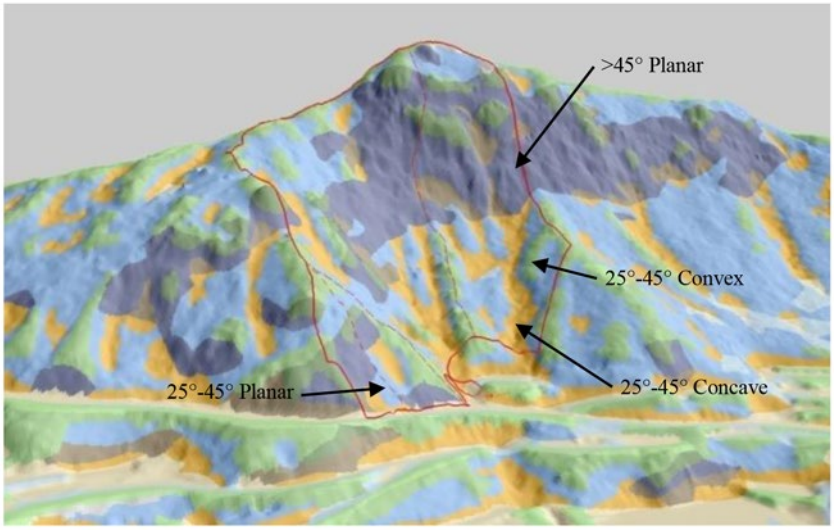

Figure 2B: AIMS-derived Terrain Classification

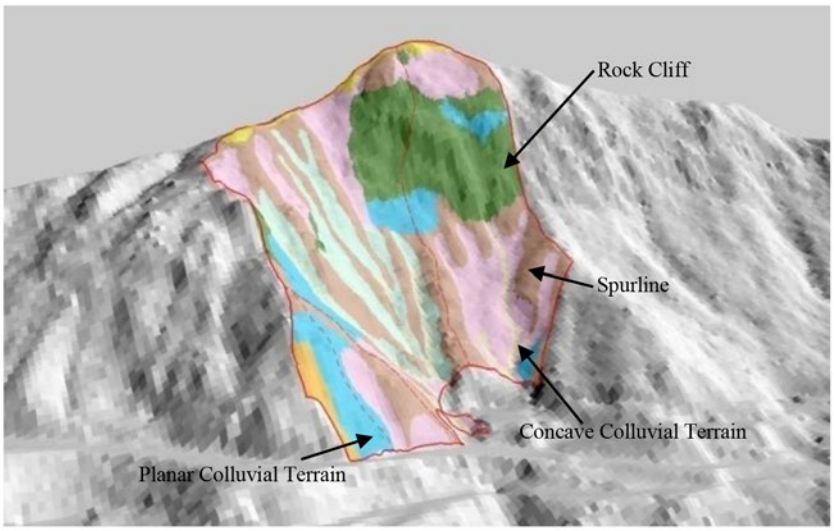

Figure 2C: Site-specific Terrain Units

The case study indicates that in the first instance, AIMS can be applied as a conceptual landform model for preliminary site characterisation i.e., desk study in NTHS and as a preliminary field map for more detailed field mapping integrated with API. It provides a fast, uniform, systematic and consistent approach for terrain classification. Used as conceptual model inputs, AIMS can enhance the appreciation of any Study Area within the overall regional geomorphological setting.

3.2 Case Study II: Regional NTHS

AIMS classification can also be applied on a regional scale. Figures 3A & 3B present the AIMS-derived terrain classification across an area of about 18 km^2 (18 000 ha) of Western Lantau using small and large neighbourhood size respectively. AIMS with a broad-scale TPI performs better at this regional scale (1:20 000) in capturing the terrain pattern than fine-scale TPI, which results in more segmented terrain units at a regional scale. Major landforms such as spurlines, cliff areas and gentle slopes are distinctive. It is envisaged that detailed landform features e.g. upland valleys, saddles and other terrain elements can be differentiated by AIMS with the following techniques.

1. Finer breakdown of TPI classes and/or slope gradient;
2. Use multi-scale TPI classification; and/or
3. Incorporate additional slope attributes, such as elevation, slope aspect and surface roughness into classification.

Geological and pedological units may also be allocated to AIMS classes for landslide susceptibility mapping e.g. using PISA-m, such that preliminary hazard maps can be generated at an early stage of NTHS or as part of a broader physical land resource inventory.

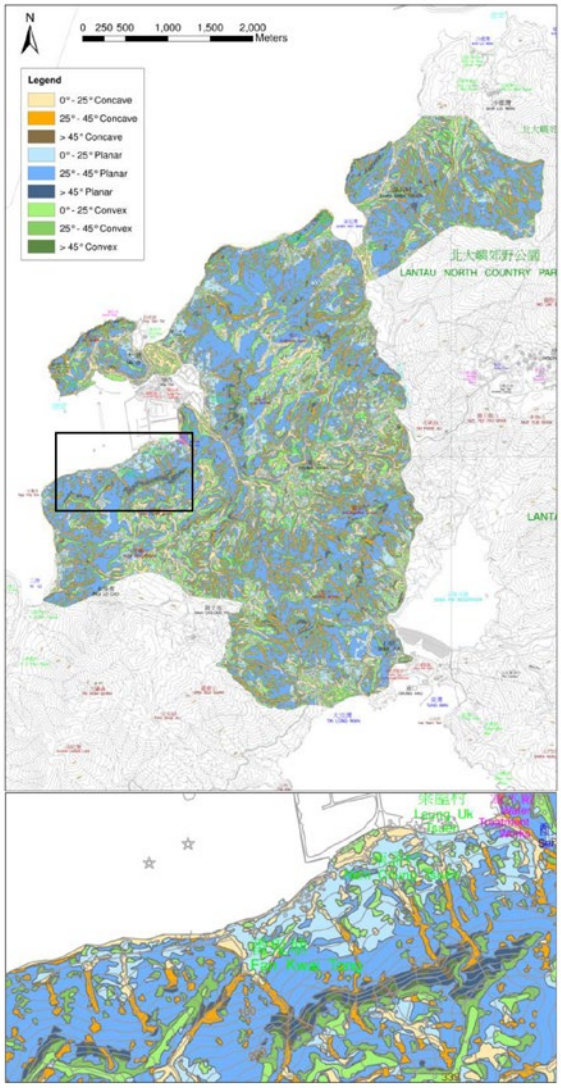

Figure 3A: AIMS-derived Terrain Classification using Fine-scale TPI

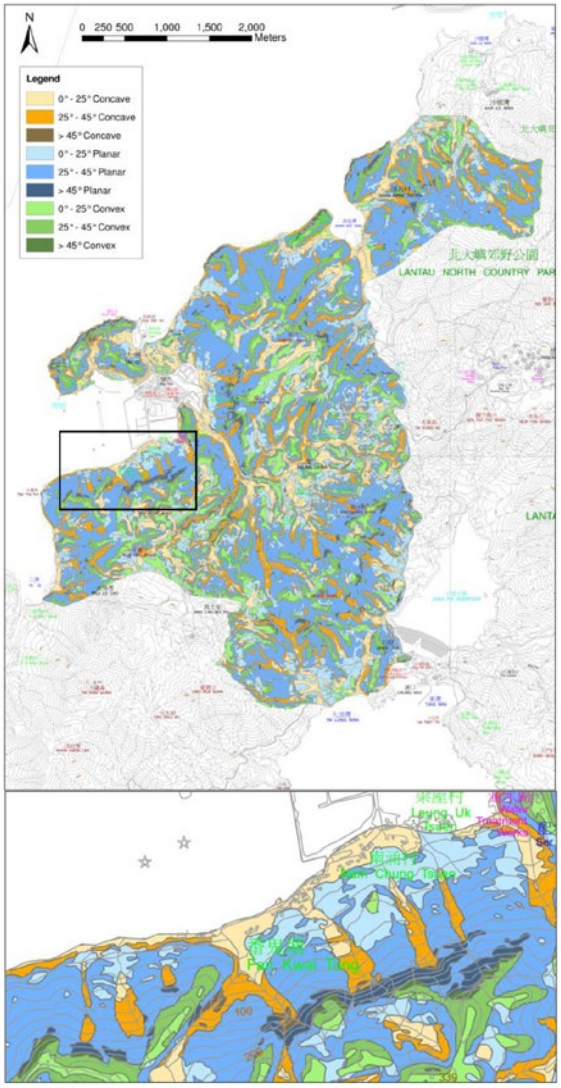

Figure 3B: AIMS-derived Terrain Classification using Broad-scale TPI

4 CONCLUSIONS AND PROSPECTS

AIMS (Automated Integrated Mapping System) utilises the advantages of LiDAR-derived high-resolution DEM to develop simple morphologically-based terrain models that are systematic and repeatable across the terrain at a range of scales from site-specific to more regional (e.g. 1:1 000 – 1:20 000). Both airborne and terrestrial LiDAR can be employed for AIMS application with great flexibility in the selection of attributes. The case studies demonstrate that AIMS, currently based on TPI and slope gradient, is effective in producing rapid terrain classification that can be applied as a simple, turn-key first-pass framework to assist in geomorphological and geological field mapping and modelling. The benefits are in automation, consistency and systematic terrain classification particularly on remote and inaccessible terrain.

AIMS provides an innovative concept for site characterisation that can be manipulated upon, layer by layer, flexibly targeted at a range of potential problems or user requirements. It can be applied from broad scale physical land resource inventory to detailed site assessment for landslide investigation. Further applications of AIMS could relate to site characterisation along route corridors through challenging and inaccessible terrain or marine environment where seabed morphology may be a concern. With regular updates of LiDAR survey and DEM data, "change analysis" is possible for better asset management of our landscape. Examples of applications include, tree interactions, landslide analysis, flood plain mapping and mine spoil management.

ACKNOWLEDGEMENTS

This paper is published with the permission of the Head of the Geotechnical Engineering Office and the Director of Civil Engineering and Development Department, the Government of Hong Kong Special Administrative Region. Also, gratefully acknowledged is the contribution of R.J. Sas during his time in Fugro (Hong Kong) Ltd. Many thanks to colleagues from Fugro (Hong Kong) Ltd. for their advice and inspiration.

REFERENCES

Dragut, L. & Blaschke, T. (2006). Automated Classification of Landform Elements Using Object-Based Image Analysis. Geomorphology, 81, 330-344. http://dx.doi.org/10.1016/j.geomorph.2006.04.013

GEO (2004). Guidelines on Geomorphological Mapping for Natural Terrain Hazard Studies. GEO Technical Guidance Note No. 22 (TGN 22). Geotechnical Engineering Office, Civil Engineering Department, Hong Kong, 8 p.

Haneberg, W.C. (2007). PISA-m: Map-based probabilistic infinite slope analysis, version 1.0.1 user manual: http://www.haneberg.com/downloadables/manual_1_0_1.pdf.

Jenness, J. (2006). Topographic Position Index (tpi_jen.avx) Extension for ArcView 3.x, v. 1.3a. Jenness Enterprises.

Lai, A.C.S., So, A.C.T., Ng, S.K.C. & Jonas, D. (2012). The territory-wide airborne light detection and ranging survey for the Hong Kong Special Administrative Region. The 33rd Asian Conference on Remote Sensing, Pattaya, Thailand.

MacMillan, R.A., McNabb, D.H. & Jones, R.K. (2000). Automated landform classification using DEMs: A conceptual framework for a multilevel, hierarchy of hydrologically and geomorphologically oriented physiographic mapping units. Proceedings from the 4th International Conference on Integrating GIS and Environmental Modeling (GIS/EM4): Problems, Prospects and Research Needs. Banff, Alberta, Canada. September 2-8, 2000.

Parry, S. & Jonas, D. A. (2007). The use of LiDAR for landslide hazard assessments: Hong Kong case studies. Conference on Engineering Geology in Geotechnical Risk Management, pp 155-161. Hong Kong Regional Group of the Geological Society of London.

Samodra, G., Chen, G., Sartohadi, J., Hadmoko, D. S. & Kasama, K. (2014). Automated Landform Classification in a Rockfall Prone Area, Gunung Kelir Java. Earth Surface Dynamic, Vol 2, 339-348.

Sas Jr., F.J., Yu, J.P., Pau, Y.Y. & Styles, K.A. (2012). Detection of Old Agricultural Terraces in Steep, Vegetated Terrain Using Airborne LiDAR: Case Studies from Hong Kong. 33rd Asian Conference on Remote Sensing (ACRS 2012) Pattaya, Thailand. 10p.

Sas Jr., R.J. (2014). Some Applications of Airborne LiDAR for Mapping and Analysis in Landslide Hazard Assessment. Proceedings of Advances in Terrain Mapping and Analysis for Landslide Hazard Assessment Conference. The Hong Kong Regional Group of the Geological Society of London, 9 p.

Styles, K.A. & Hansen, A. (1989). Geotechnical Area Studies Programme GASP XII - The Territory of Hong Kong. Geotechnical Control Office, Civil Engineering Services Department, Hong Kong Government, Government Printer HK ISBN 962-02-0072, pp 251-306.

Tagil, S & Jenness, J. (2008). GIS-Based Automated Landform Classification and Topographic, Landcover and Geologic Attributes of Landforms Around the Yazoren Polje, Turkey. Journal of Applied Sciences, 8, pp 910-921.
Weiss, A. (2001). Topographic Position and Landforms Analysis. Poster presentation, ESRI User Conference, San Diego, CA.

Back analysis of temporary piles in alluvium using Plaxis 3D

M.R. Thompson
The University of Hong Kong, Master Student
G.S.H. Toh
Lambeth Associates Limited

ABSTRACT

The Chek Lap Kok Formation is highly variable in nature meaning that selecting an appropriate value for the shaft resistance coefficient (β) is problematic. Current practice for the design of temporary tubular steel piles relies upon local experience and the methods described in GEO publication No. 1/2006. Although these methods are largely applied with success they do have short comings dependent upon the site ground conditions. This paper outlines the results of back analysis carried out on selected temporary tubular steel piles using Plaxis 3D. The numerical results are compared with post construction settlement data from the site. General observations and results are presented along with a summary of relationships that may be applied to future design problems.

1 INTRODUCTION

The evolution of geotechnical design in Hong Kong and elsewhere has been greatly affected by advances in analytical software and how they might be applied to design problems. It has been shown that Plaxis 3D can be adopted to back analyse the coefficient of resistance in temporary piles constructed offshore (Toh and Li, 2015). This paper develops the idea of using Plaxis 3D in this way by undertaking a more thorough analysis of temporary piles constructed at site in order to derive design relationships for use in future design problems.

2 BACKGROUND

2.1 Problem

The piles used in the analysis are 1.2 m diameter tubular steel piles constructed at the Tuen Mun Chek Lap Kok Link Road site to support temporary offshore platforms. The piles are set in the alluvium of the Chek Lap Kok formation. The contractor found that when constructing temporary tubular steel piles in alluvium and saprolite that the construction depth differs greatly from the tentative design depth. This resulted in piles being set significantly shallower than they were designed to be. It was deemed unsafe and impractical to carry out conventional load tests on the short piles so finite element analysis was adopted to determine the capacity of these piles.

Piles in sand are designed using β-method. Equation 1 is used for calculating the mobilized shaft resistance of the pile.

$$\tau_s = \beta \sigma_v \quad (1)$$

Where τ_s = Shaft Resistance (kPa), β = Shaft Resistance Coefficient, τ_s = Shaft Resistance (kPa)

The engineer must select an appropriate value for the coefficient of shaft resistance β using past experience. The current guidance for pile design in Hong Kong, GEO Publication 1/2006, gives typical values for the β. GEO (2006, page 96) gives a range of 0.2 to 1.5 for large displacement piles and 0.1 to 0.5 for small displacement piles in loose to medium dense sand. This large range creates uncertainty in the design and leads to uneconomical design solutions.

2.2 Ground conditions

The ground conditions on site comprise a relatively thick layer of superficial deposits overlying weathered granite. The superficial deposits include a layer of marine silt and clay over alluvial sand, silt, and clay. Summary descriptions of the geology have been included in Table 1.

Table 1: Summary of geology encountered at site

	Formation Name	Description
Superficial	Hang Hau Formation	Marine deposits comprising very soft to soft dark grey silty clay with laminations of sand and occasional shells.
	Chek Lap Kok Formation	Alluvium comprising brown and grey clay, silt and sand. Occasional gravel and organic content.
Bedrock	Lantau Granite	Fine to medium grained, inequigranular acidic igneous rock. Common megacrysts of Alkali feldspar.

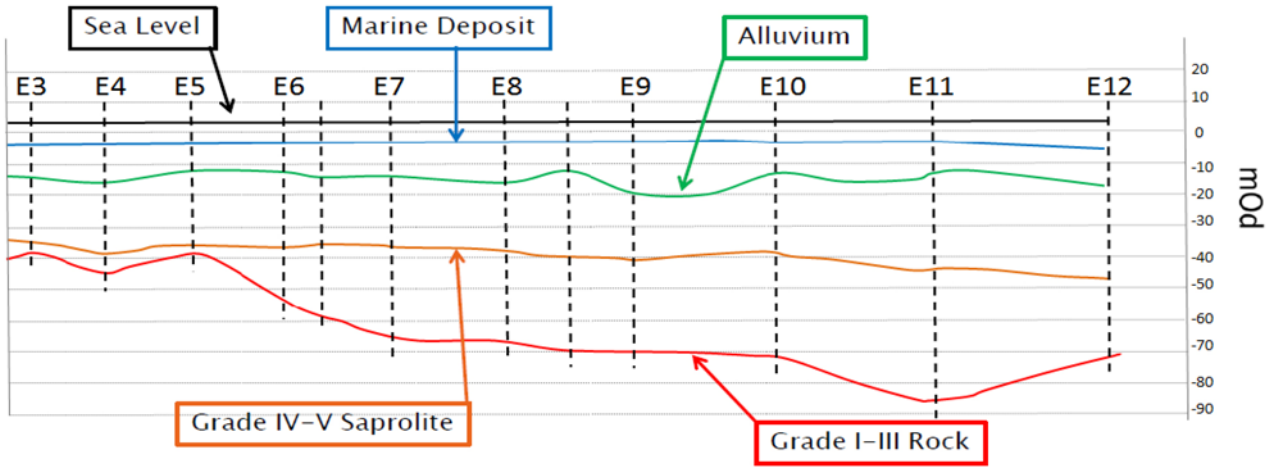

Figure 1: Geological cross section

3 METHOD

3.1 Selection of data

The ground investigation included a single borehole at each pier location. The data from this borehole was used to define the tentative design depth of each pile driven at that location. For the purposes of this study the worst case pile at each location was selected for analysis.

As it is assumed that the ground conditions are the same at for each pile at a single location it follows that the shortest pile would be the worst case. This pile would be utilizing the least shaft resistance from the soil meaning it has the lowest ultimate capacity.

3.2 Model geometry

The model geometry has three components to it; the boundaries, soil elements, and structural elements.

The boundaries were set at such a distance to ensure the boundary conditions did not influence the

behaviour of the pile. The x and y boundaries were each set at positive and negative 20m from the center of the pile, the pile being at the center of the model. The z boundaries are set as the top of the pile and 5m into the rock head as described in the corresponding borehole log. The boundary conditions were set as free draining. They were completely fixed at the x and y boundaries however, the z boundary allowed movement in the z direction.

The structural elements include the pile and loading plate. These were both modeled as plates. The full length of the pile was modeled from nominal sea level.

The strata thicknesses are derived from the borehole record closest to the pile being modeled. Within each model it is assumed that the strata are horizontal.

3.4 Mesh

The mesh is automatically created in Plaxis 3D. The coarseness of the mesh was set to "medium" with all other settings kept as default. A medium mesh was used as the model geometry is simple. This kept the computing time low while not sacrificing accuracy.

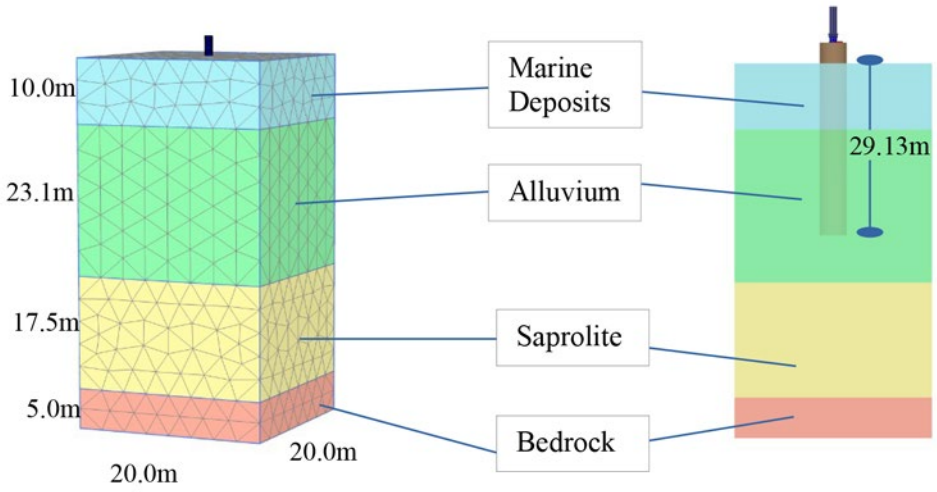

Figure 2: An example of the model geometry

3.5 Interfaces

Interfaces were included in the model to allow some flexibility however the focus of this study was not on the interface effects between the pile and soil. Therefore R_{int} = 1.0 meaning no interface effects were being considered.

3.6 Failure criteria

The soils were modeled using the Mohr-Coulomb failure criterion. This is a linear relationship between shear stress and normal stress, the equation for which follows:

$$\tau = c + \sigma_n \tan\phi \quad (2)$$

Where: τ = shear stress, φ = friction angle of soil, σ_n = normal stress

3.7 Material properties

The material properties adopted for this study were derived from the ground investigation undertaken for this project. These are summarized in Table 2.

Table 2: Soil shear strength parameters

Soil Type	Unit Weight (KN/m^3)	Friction Angle (°)	Cohesion (kPa)	Undrained Shear Strength (kPa)
Marine Deposit	15	–	–	5
Alluvium	19	30	4	–
Saprolite	19	30	4	–

In order to model the soil behaviour using Mohr-Coulomb failure criteria the material stiffness (E) and stiffness increase (E_{inc}) must be defined in the model.

The SPT N value of the alluvium were used to estimate the stiffness of the soil to be input. A number of studies have back analysed the relationship between the stiffness and N.

Table 3: Summary of E/N relationships

Source	E (MPa)
GEO (2006) a	3.5N – 5.5N
GEO (2006) b	0.2N – 3.0N
Chan (2003)	2.0N
Littlechild et al. (2000)	1.4N

As Table 3 shows, the E may be anywhere between 0.2N and 5.5N. For this study a reasonably conservative relationship of E=1N was used.

$$E = 1N \quad (3)$$

Where E = stiffness, N = Uncorrected SPT N

3.8 Pile properties

A total of eight open-ended tubular steel piles were analysed in this study. The geometry and material characteristics of the modeled piles has been included below:

- Pile diameter – 1.2 m
- Wall thickness – 16 mm
- Material – Steel
- E – 205 Gpa
- v – 0.2

3.9 Groundwater flow

The groundwater table is set as the nominal sea level, zero, within the model. The soil is assumed to be fully saturated and all strata horizontal. For these reasons there is no groundwater flow considered in the analysis.

3.10 Calculation phases

The General Specification for Civil Engineering Works (HKG, 1992) states that piles should be tested to not less than twice the working load ie. $Q_{max} \geq 2WL$. There should be three cycles of loading at $0.25Q_{max}$, $0.50Q_{max}$, and $1.0Q_{max}$. In this case the working load is taken as 3000 kN therefore Q_{max} = 6000 kN. In order to ensure the pile is failed in this model a further loading cycle of $1.5Q_{max}$ will be used.

The calculation will include four loading phases to incrementally increase the axial load applied to the loading plate of the pile. These will be multiples of the assumed working load, 3000 kN. The load increments used in the model were; 1326 kPa, 2653 kPa, 5305 kPa, and 7958 kPa.

3.11 Assumptions

The model assumes the pile is under static axial loading. The pile driving and related stress changes will not be considered in the analysis. This means the analysis is a reference for the medium to long term stability of the pile, in effect modeling a load test carried out after the induced stresses from pile driving have dissipated.

The working load is assumed to be 3000 kN. This is an estimate made by the contractor as to the maximum loading that will exerted on each pile. During construction the loads may not be applied equally or continuously to 3000 kN.

The load distribution derived from the analysis is curvilinear as the stiffness of the soil increases with depth. When calculating the mean shaft resistance mobilized within the alluvium this is simplified to a bilinear distribution.

Toh and Li (2015) found piles modeled in plugged and unplugged mode had similar behaviour at the loads applied in the model. As the pile is large diameter it is less likely to achieve plugged condition, however it cannot be ruled out.

Each soil stratum is assumed to be uniform and horizontal. This means that the shear strength parameters and drainage characteristics remain the same throughout. The alluvium will be modeled as a drained material as it has relatively high permeability compared to the marine deposits. This allows the β-method to be used to design the piles. The grade 3 and higher rock will be modeled as a free draining linear elastic material as the rock is not being explicitly examined in this project.

3.12 Back calculation of the coefficient of shaft resistance

Several outputs are required from the analysis in order to back calculate the shaft resistance coefficient. The load-displacement curves are used to determine the ultimate capacity of the pile being analysed. The load distribution curves for each load increment are generated and the load displacement for the estimated ultimate capacity is interpolated. The mean shaft resistance and effective stress within the alluvium are then calculated, enabling the shaft resistance coefficient to be calculated.

The ultimate load may be determined from the load-displacement curve as the lower of the point at which: the deformation becomes perfectly plastic, or axial displacement is greater than 10% of the pile diameter (ISSFME, 1985).

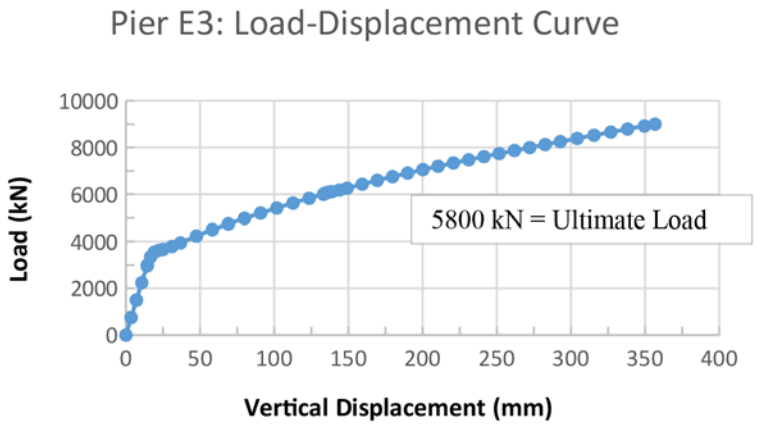

Figure 3: Load – Displacement curve for Pier E3

The ultimate load is then plotted on the load distribution graph using interpolation to define the end points of each section of the line.

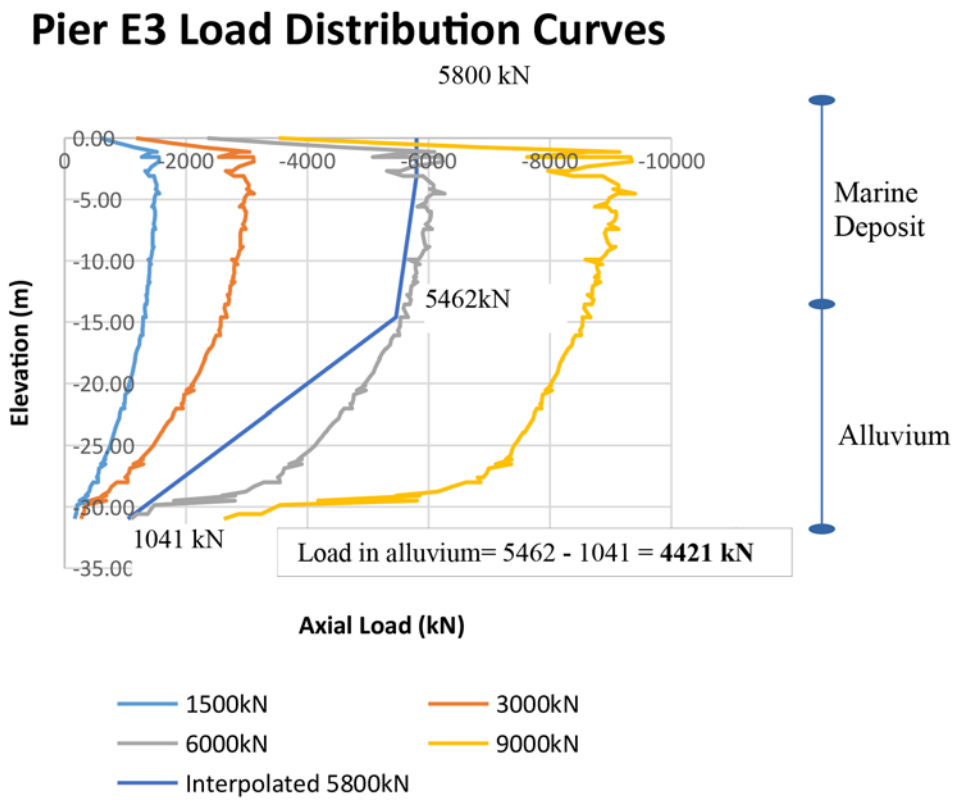

Figure 4: Load distribution curves showing the interpolated curve

The magnitude of mobilized shaft resistance across the alluvium is now known. Rearranging equation 1 allows β to be calculated.

$$\beta = \frac{71.55}{205} = 0.35$$

4 RESULTS

All the piles analysed failed by the 10% diameter displacement criteria. The ultimate loads for the piles analysed fall within the range 3900 kN to 6100 kN. End bearing resistance is mobilized at displacements between 14% and 20% of the pile diameter.

The shaft resistance within the alluvium accounts for between 64% and 81% of the loading at ultimate capacity. The end resistance for all piles analysed is less than 25% of the total resistance.

Table 4: Distribution of pile loading as a percentage of ultimate load

Pile Reference	Ultimate Capacity (kN)	End Resistance (%)	Shaft Resistance in Marine Deposit (%)	Shaft Resistance in Alluvium (%)
E3	5800	18	6	76
E5	6100	15	4	81
E6	4300	16	6	78
E7	3900	19	9	72
E8	5500	14	5	81
E10	5300	25	8	67
E11	4000	16	6	78
E13	5900	20	16	64

The vertical displacements calculated at each pile location subjected to the assumed 3000 kN working load are summarized in Table 5. The displacements range from -12.2mm to -44.8mm.

Table 5: Total vertical displacement calculated at each pile location

Pile Reference	Maximum Calculated Displacement (mm)	Maximum Measured Displacement (mm)	Difference (mm)
E3	-14.3	-7	7.3
E5	-12.2	-6	6.2
E6	-22.6	-10	12.6
E7	-23.9	-10	13.9
E8	-16.1	-7	9.1
E10	-16.7	-18	-1.3
E11	-44.8	-16	38.8
E13	-15.1	-15	-0.1

The β values back calculated for the alluvium range from 0.24 to 0.35.

Table 6: Summary of pile construction and results

Pile Ref.	Ultimate Load (kN)	Length of Pile in Soils (m)	Length of Pile in Alluvium (m)	Depth to Rock Head from Pile Toe (m)	Mean Uncorrected SPT N Value along the length of the shaft	Mean Shaft Resistance in Alluvium (kPa)	Mean Effective stress in Alluvium (kPa)	Back calculated β
E3	5700	27.89	16.39	6.89	19	35.77	103	0.35
E5	6100	27.91	17.91	8.04	24	36.50	106	0.35
E6	4300	26.03	16.03	24.42	15	27.93	97	0.29
E7	3900	26.41	14.91	35.79	13	24.84	96	0.26
E8	5500	30.69	19.19	33.29	18	30.66	115	0.27
E10	5300	28.33	18.33	40.57	19	25.75	107	0.24
E11	4000	24.06	14.06	57.49	18	29.48	88	0.33
E13	5900	31.42	14.42	34.67	18	34.66	107	0.32

5 DISCUSSION

5.1 Load distribution

It was found that the end bearing resistance is mobilized at displacements of between 1.4% and 2.0% of the pile diameter.

In terms of distribution the piles behave as friction piles. The end resistance accounts for approximately 15% to 20% of the total mobilized resistance with the exception of Pier E10 where it accounts for 25%. The majority of shaft resistance is mobilized within the alluvium. This is typically 75% to 80% of the total resistance. The marine deposit of Pier E13 accounts for a larger proportion of the total resistance than in the other piles because the marine deposit is approximately twice as thick at this location.

5.3 Vertical displacement

As shown in Table 5 the vertical displacement calculated in the model for most of the pile locations is overestimated when compared with the measured displacement. The exceptions to this are at Pier E10 and Pier E13 which closely match the measured displacement on site.

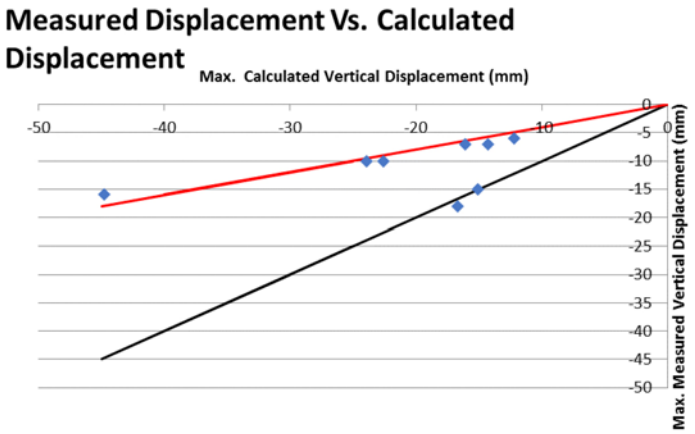

Figure 5: Graph showing the relationship between calculated and measured displacements

Figure 5 shows that there is a relationship between the measured and calculated displacements. The calculated displacement is approximately 2.5 times the measured displacement.

The underestimation of displacement may be due to differences between the assumed working load and actual working load on site. It may also be that the value for stiffness (E) used in the model is too conservative and therefore the displacements larger than expected. This study assumed E=1N as a conservative relationship for E however a less conservative value may be more appropriate to create a more accurate model. It is also likely that the use of Mohr Coulomb model in the analysis has resulted in some error regarding the stiffness of the soil. The simple nature of the Mohr Coulomb model cannot accurately simulate the true complexity of the soil. A more suitable E-N relationship may defined using a parametric study.

GEO (2006) has a number of suggestions for E values in saprolite but not for alluvial silt and sand. For driven piles constructed in saprolite it is suggested to use E=3.5N to 5.5N. This follows research published by Vesic (1969) in which a suitable value for E in sands should be approximately 4N. This value may be optimistic as there are a number of papers that suggest more conservative values for E in saprolite.

For the alluvium it may be suitable to use the relationship E=1.5N as suggested by Chan (2003). However this relationship is based upon back analysis of retaining wall deflection in excavations so is not necessarily applicable to driven piles.

An alternative relationship could be determined using a parametric study focusing on the effects of changing E in the model. In this way a suitable relationship for determining E to be used in future Plaxis 3D modeling of driven piles can be found

5.4 Shaft resistance coefficient β

The back calculated values for shaft resistance coefficient are in the range of 0.24 to 0.35. The mean β found for the piles in the main study is 0.30.

This is higher than what would be predicted using the Paulos and Davies (1980) method however it is within the range for small displacement piles in medium and dense sand as given by GEO (2006). The range is also at the lower end of that given for large displacement piles.

The values of β found in this study are lower than those found by Toh and Li (2015). This may be due to different interpretations of the SPT results. There may also be other discrepancies in the modeling process that had an impact on the results.

5.5 Relationships

A number of design relationships have been found that may be useful in the future design of temporary steel tubular piles constructed in the alluvium.

The mean shaft resistance throughout the alluvium is well correlated with both the mean effective stress σ_v' and the mean SPT N value. The relationship with SPT N value is consistent with GEO (2006)

that states, from limited test data, the shaft resistance in small displacement piles can be defined as 1.5N to 2.0N.

The relationships found for β generally have a larger scatter than those for shaft resistance. However, it is possible to define some useful relationships for depth to rock head and mean N value.

There is a positive correlation between the mean N value and β. This is as expected for driven piles and shares a similar trend to the relationship for driven piles in CDG as published in GEO (2006).

A relationship between β and the depth to rock head beneath the pile toe has been observed. Figure 9 shows a negative correlation between the depth to rock head beneath the pile toe and β. This means that as the rock head gets further away from the pile toe the shaft resistance coefficient falls.

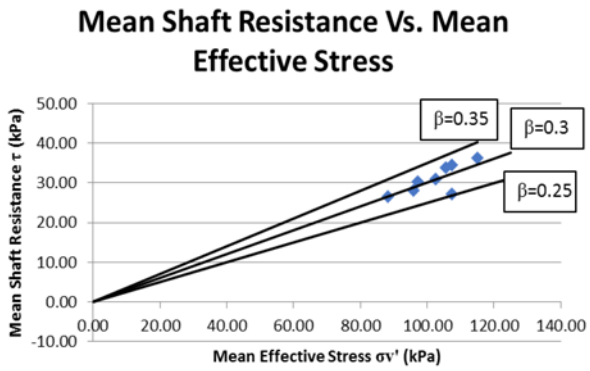

Figure 6: Mean τ Vs. Mean σ_v'

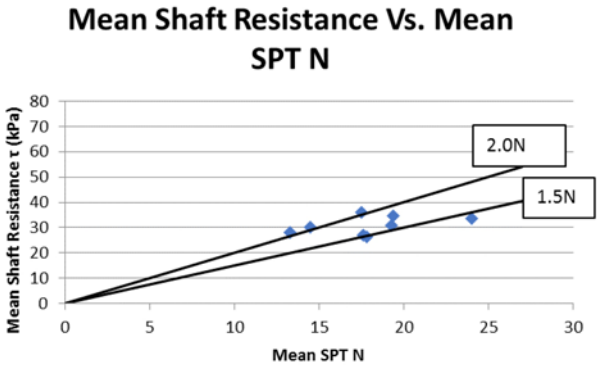

Figure 7: Mean τ Vs. Mean SPT N

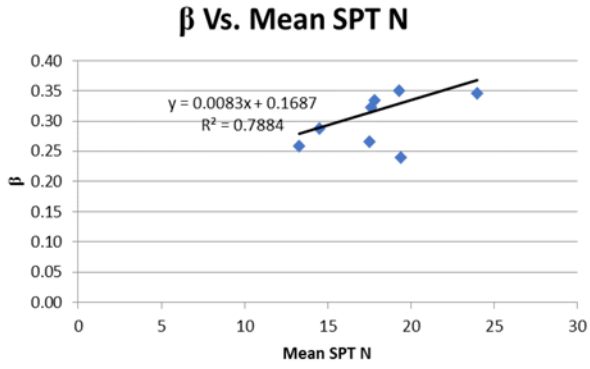

Figure 8: β Vs. Mean N

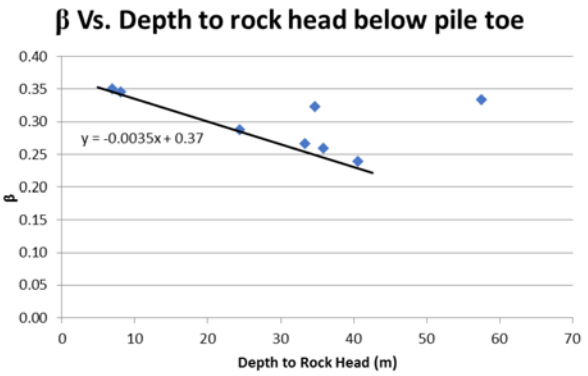

Figure 9: β Vs Depth to rock head beneath pile toe

These relationships will be useful in the initial design of driven piles in alluvium as they give a good estimation of β based on in situ testing. However, caution should be taken as the results are sensitive to the interpretation of SPT results.

6 CONCLUSION

This paper has demonstrated how the design of foundations is evolving as numerical modeling programmes become more refined and engineers accustomed to their application for design and research applications.

A number of design relationships for deriving the coefficient of shaft resistance β have been described and compared with previous research. This relationship applies to tubular steel piles driven in the alluvium of the Chek Lap Kok Formation.

Future work may include a study into how pile groups, pile construction method and diameter affect β. A parametric study focused on the relationship between SPT N value and stiffness would help to refine the model.

REFERENCES

Buildings Department. (2004). Code of Practice for Foundations. Hong Kong SAR.

Chan, A. (2003). Observations from excavations – A reflection. Proceedings of the seminar on case histories in geotechnical engineering in Hong Kong. HKIE Geotechnical Division.

Geotechnical Engineering Office, (2007). Engineering Geological Practice in Hong Kong. GEO Publication No. 1/2007. CEDD, Hong Kong SAR.

Geotechnical Engineering Office, (2006). Foundation Design and Construction. GEO Publication No. 1/2006. CEDD, Hong Kong SAR.

Geotechnical Engineering Office., (1988). Geoguide 3 – Guide to Soil and Rock Descriptions. CEDD, Hong Kong.

HKG (1992). General Specification for Civil Engineering Works. (1992 edition). Hong Kong Government, vol. 1.

ISSFME. (1985). Axial Pile Loading Test Part 1: Static Loading. ASTM Subcommittee on Field and Laboratory Testing, Geotech. Journal GTODJ, vol.8, no.2. pp 79 – 89.

Littlechild, B.D., Hill, S.J., Statham, I., Plumbridge, G.D. And Lee, S.C. (2000) Stiffness of Hong Kong Rocks for Foundation Design. Proceedings of the 19th Annual Seminar - Geotechnical Division of the Hong Kong Institution of Engineers, pp. 179 - 190.

Lumb, P., (1977). Geotechnical Aspects of Soft Clays – The Marine Soils of Hong Kong and Macau. Edited by Brenner, R.P. and Brand, E.W. Proceedings of the International Symposium on Soft Clay, Asian Institute of Technology, Bangkok, Thailand. Ch.1, pp45-59.

Toh, G.S.H., and Li, C. (2015). Does 3D Finite Element Analysis Allow Better Design of Piles? – A Case Study for Temporary Marine Pile Design. Proceedings of the 35th Annual Seminar – Geotechnical Division, The Hong Kong Institute of Engineers, pp 57 – 64.

Langford, R.L., (1994). Sheet Report No. 2 – Geology of Chek Lap Kok. Geotechnical Engineering Office, CEDD, Hong Kong SAR.

Poulos, H.G. and Davis, E.H. (1980). Pile Foundation Analysis and Design. John Wiley & Sons, New York, p. 397.

Vesic, A.S. (1969). Experiments with instrumented pile groups in sand. ASTM Special Technical Publication No. 444, Performance of Deep Foundations, American Society for Testing and Materials, pp 177-222.

Machine Learning Study on Man-made Features in Hong Kong – A Data Driven Approach to Feature Classification

Kevin C.H. Tse, Addy C.K. Chan & Kenny K.F. Yau
AECOM Asia Company Limited, Hong Kong

ABSTRACT

Machine Learning (ML) methods are applied on a sample multivariate dataset of 1,275 man-made features in Hong Kong to uncover any naturally occurring data structures without a priori information. Traditional methods to classify the man-made slopes and retaining walls in the territory are based on deterministic rule-based systems devised with expert domain knowledge. In many fields of science and engineering, ML methods have been introduced to cope with the rapidly increasing volume and variety of incoming data. In this study, unsupervised learning algorithms, an increasingly popular genre of ML methods, have revealed previously unknown data clusters on the sample datasets. The data structures discovered provide objective insights in the relative importance of parameters which can maximize the inter-cluster variance between groups of man-made features in the datasets. The study sets a pioneering example on the application of unsupervised learning methods in slope engineering by exploring innovative ways of classification of features.

Keywords: Machine Learning, Man-made Features, Classification

1 INTRODUCTION

The Slope Information System (SIS) which contains detailed information about over 60,000 registered man-made slopes and retaining walls is one of the largest of its kind in the world. It is managed and updated by the Geotechnical Engineering Office (GEO), Civil Engineering and Development Department (CEDD) to provide comprehensive and up-to-date slope information in the planning and implementation of the government slope safety work. The existing dataset collected and updated for the man-made features in Hong Kong has been developing for four decades and its primary purpose is for the prioritization of maintenance and upgrading work of the large number of man-made features in Hong Kong (Cheng, 2013).

In this study, a new approach based on machine learning (ML) methods will be adopted on multivariate datasets collected for 1,275 man-made features over eight Landslip Prevention and Mitigation (LPMit) agreements in the past three years. ML methods have become popular in many areas of science and engineering, including prediction of landslides (Yao, 2008), classification of sediments (Insua, 2015) and study of ocean drill data (Tse, 2017). ML methods can process a large amount of data and capable of uncovering interesting structures within the data. The goal of the study is to conduct data mining experiment on these existing data to explore alternative ways of classifying the features in Hong Kong.

2 METHOD

2.1 Dataset

The raw data used in this study originated from data collection information on 1,275 man-made features accumulated over 3 years. A selected 18 attributes are extracted from the raw data and a synthetic dataset (1,275 × 18 matrix) is prepared for analysis. The data is pre-processed to remove missing values and categorical data are converted into numerical data for use by ML algorithms.

2.2 Unsupervised Learning

Unsupervised learning (UL) is a type of ML methods which does not require *a priori* information in the dataset. In other words, no presumptions or labelling of the input data are required and the algorithm behaves like a "black box" that simply takes data and outputs a function $f: R^N \rightarrow R^K$ that maps an input vector x to a new feature vector of K features (Way, 2012). This is in contrast to supervised learning, a common form of ML methods widely used in sciences and engineering fields in the last decade, in which the main objective of the algorithm is to perform prediction based on a set of training data. UL has become more and more popular in recent years due to the explosive growth of data and advancement in deep learning algorithms (Murphy, 2013). Clustering is a common method of UL in which data is classified into homogeneous groups (clusters) according to a chosen criteria and algorithm (Hennig, 2015).

2.3 Principal Component Analysis (PCA)

Principal Component Analysis (PCA) is a widely used UL method to reduce the dimensions of multivariate data onto principal axes (Murphy, 2013). It summarises the whole of available data via eigenvalue decomposition and transforms them into principal components corresponding to the largest variance. The data expressed in the principal components are often easier to visualize and most of the variance can be expressed by the first and second principal components. The principal components are orthogonal to each other, meaning that they are statistically uncorrelated to each other (Way, 2012).

2.4 K-means

K-means is a widely used partitional clustering method in which data are decomposed into non-overlapping clusters and each data point is not in more than one cluster, also known as disjoint clusters (Jain, 2010). The method is capable of handling large datasets with continuous data and the absence of non-convex clusters (Kabacoff, 2015).

Given a set of m-dimensional vector X of n points, and specified integer k, the objective is to assign the n data points into k disjoint clusters $\pi_k = (\pi_1, \ldots, \pi_k)$, where $\pi_k \cap \pi_{k'} = \phi$, centered at cluster means μ_j for j = (1,...,k), based on the initial conditions, the goal is to seek clustering results where within-cluster variance is a minimum (Murphy, 2013):

$$D(\{\pi_c\}_{c=1}^{k}) = \sum_{c=1}^{k} \sum_{x_i \in \pi_c} ||x_i - \mu_c||^2, \text{where } \mu_c = \frac{\sum_{x_i \in \pi_c} x_i}{|\pi_c|}$$

In the equation above, π_c denotes the c-th cluster, $\{\pi_c\}$ denotes the clustering and μ_c represents the centroid or mean of cluster π_c. The iterative algorithm starts at a randomized centroid and improve its fit with the observed data along the way. Each data point is associated with each cluster π_c by its distance from the centroid μ_c under the chosen distance metric D.

2.5 Random Forest

Random Forest (RF) is an ensemble classification algorithm based on tree classifiers. An ensemble learning method is basically a general framework primarily for supervised data mining where the same base learner is used to learn multiple models (Murphy, 2013). It creates bootstrap samples to re-simulate the sampling procedure and randomly split on a subset of M features. In other words, it re-simulates the entire experiment by bootstrapping with replacement. The process is termed bagging (Breiman, 1996) (which stands for bootstrap aggregating) and is capable of taking repeated samples from the training data set randomly and rapidly improving the performance of the algorithm (Breiman, 2001; Hastie, 2009).

$$\hat{f}_{bag}(x) = \frac{1}{B}\sum_{b=1}^{B}\hat{f}^{*b}(x)$$

B different bootstrap samples are constructed accordingly and used to train the same number of decision trees. Decision trees are increasingly common for various ML tasks. Tree learning is non-robust and even though a tree classifier can grow very deep to learn highly irregular patterns, the fact that they have low bias and high variance can cause overfitting on the trained datasets. In other words, a minor variation in the input would change the entire decision tree model. RF provides a means of taking an average on the decision trees trained on the re-simulated training data and reduce the variance significantly (Murphy, 2013).

3 RESULTS

A synthetic dataset consisting of 18 attributes extracted from 1,275 existing man-made features have been input in the Random Forest algorithm. The 18 selected attributes originated from data collection information and include type of toe facility, type of crest facility, height of rock slope, height of soil slope, height of toe wall, height of crest wall, total height of feature, slope angle, distance of toe facility from the feature, distance of crest facility from the feature, consequence-to-life (CTL) category, SIFT category, formation year, geotechnical input, old technology, squatter slope, past incident and feature type.

Figure 1 shows the four clusters identified by RF and presented on the principal component plane. The biggest cluster (blue) spans the widest range of First Principal Component (PC1) and Second Principal Component (PC2) and appears to be the most scattered with a tail of high principal components. The smallest cluster (red) appear to be the most concentrated as well, around the origin of the principal component plane. The other two clusters (cyan and green) appear to be located along similar values of PC1 and split into positive and negative values of PC2.

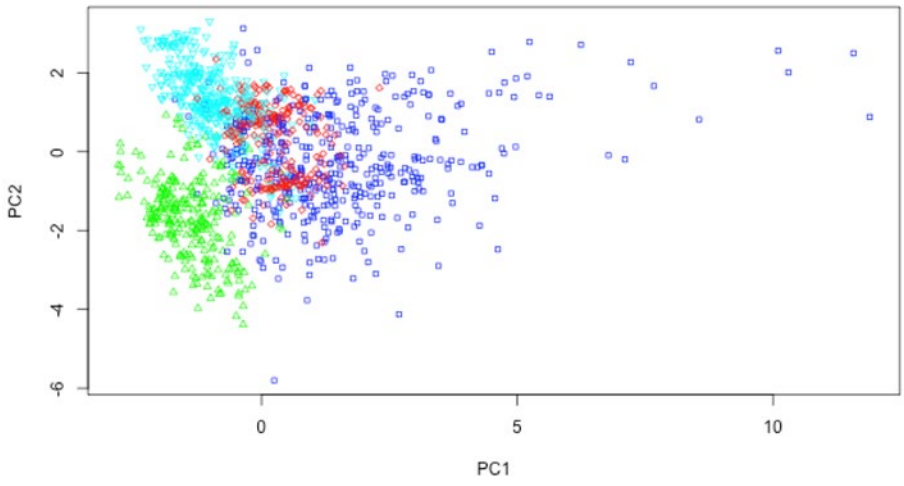

Figure 1: Biplot of the two principal components (PC1 and PC2) from the 18 selected variables. Different colors indicate different clusters determined by Random Forest method.

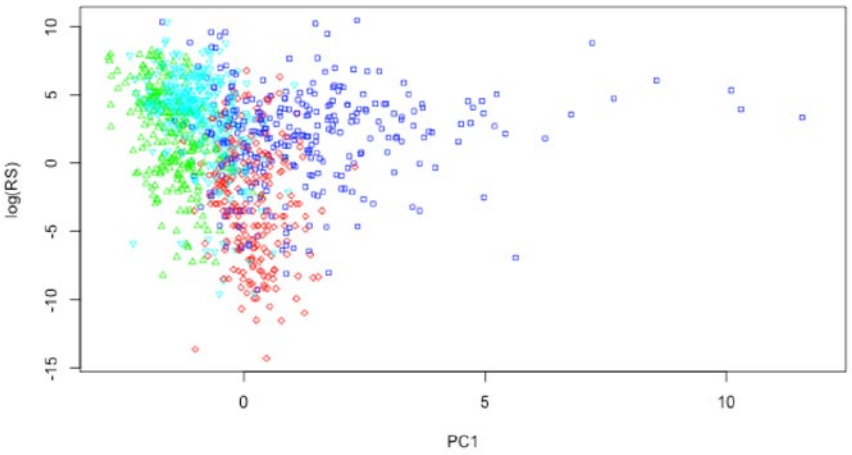

Figure 2: Plot of RS (Ranking Score) against PC1 and same colors correspond to the same clusters shown in Figure 1.

Figure 2 shows the plot of ranking score (RS) against PC1 with the colors indicating the same clusters shown in Figure 1. RS is calculated under the New Priority Ranking System (NPRS) currently in use to prioritize slope upgrading work in Hong Kong. Differences in the distributions of RS for the four clusters are observed. Clusters 1 (blue) and 4 (cyan) are more concentrated on the higher RS. Cluster 2 (red) is positioned at a lower RS portion among the four clusters.

The number of clusters was chosen to be 4 as a balance between minimizing within-cluster variance and ease of interpretation of cluster results (Figure 3).

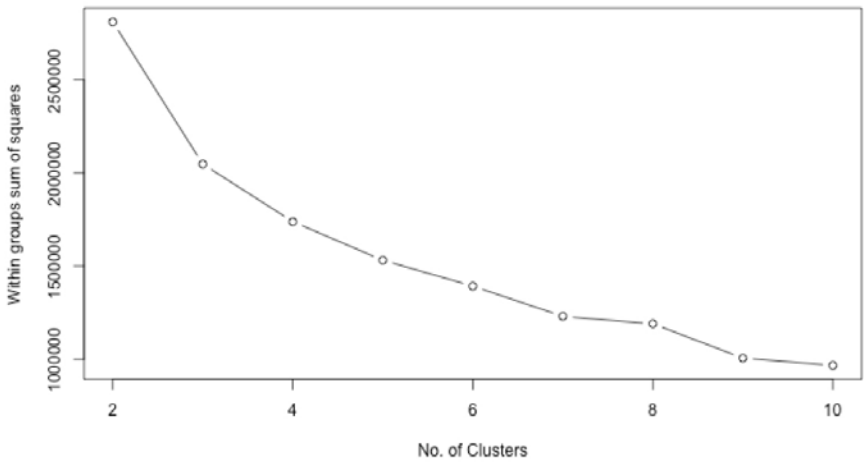

Figure 3: The within-cluster sum of squares (WSS) (Macqueen, 1967) is plotted against number of clusters. A balance is struck between minimizing WSS and maintaining a comprehensibility of the clustering results.

Table 1 shows the percentage contribution of each of the 18 chosen attributes in the first and second principal components. The most important contributing attributes for PC1 are soil height (15.3%), total height (15.2%) and slope angle (9.7%), and for PC2 they are toe wall height (13.4%), SIFT (12.6%) and feature type (14.8%).

Attribute	PC1	PC2
Toe Code	3.93	5.00
Crest Code	2.98	6.46
Rock Height	2.56	0.87
Soil Height	15.3	3.82
Toe Wall Height	3.87	13.4
Crest Wall Height	0.26	1.58
Total Height	15.2	0.54
Slope / Face Angle	9.67	4.94
Toe Distance	6.10	0.77
Crest Distance	3.28	3.21
CTL	4.87	1.05
SIFT	4.78	12.6
Formation Yr	3.94	3.74
Geotechnical Input	7.95	8.34
Old Technology	5.68	8.59
Squatter	3.18	2.21
Past Incident	2.05	8.13
Feature Type	4.36	14.8

Table 1: Percentage contributions of PCA loadings for the first two principal components of the 18 attributes of the dataset. Categorical and text variables (toe code, crest code, SIFT, geotechnical input, old technology, squatter, past incident) are converted into integers. Feature type is defined as: 1 for cut slope, 2 for cut slope with wall, 3 for wall, 4 for fill slope, 5 for rock slope. SIFT is defined as: 1 for B1, 2 for B2, 3 for C1, 4 for C2. Geotechnical Input: 1 for (i), 2 for (ii), 3 for (iii), 4 for (iv). For old technology, squatter and past incident: 1 for N, 2 for Y. Top 5 contributors for PC1 are namely soil height, total height, slope angle, geotechnical input and toe distance. Top 5 contributors for PC2 are toe wall height, SIFT, feature type, old technology and geotechnical input.

	Cluster 1 (blue)	Cluster 2 (red)	Cluster 3 (green)	Cluster 4 (cyan)
No. of Features	442	247	267	339
Toe Code	16.7	31.1	15.6	6.7
Crest Code	15.4	22.5	11.9	19.5
Rock Height	0.71	0.14	0.01	0.03
Soil Height	15.9	6.76	0.48	4.21
Toe Wall Height	1.23	0.21	4.33	0.25
Crest Wall Height	0.19	0.03	0.13	0.06
Total Height	18.0	7.10	4.94	4.57
Slope / Face Angle	43.8	49.2	82.9	59.3
Toe Distance	3.56	0.57	1.44	1.17
Crest Distance	1.24	0.35	0.96	0.28
CTL	1.45	2.45	1.31	1.06
SIFT	2.77	2.60	1.70	3.06
Formation Yr	1976.2	1968.2	1973.9	1969.3
Geotechnical Input	2.52	1.30	1.93	1.33
Old Technology	1.03	1.03	1.07	1.33
Squatter	1.05	1.00	1.01	1.04
Past Incident	1.30	1.23	1.17	1.85
Feature Type	3.42	2.39	3.46	1.24

Table 2: Mean values of all 18 attributes of the four clusters identified by Random Forest in the study.

	Cluster 1 (blue)	Cluster 2 (red)	Cluster 3 (green)	Cluster 4 (cyan)
Ranking Score	370.1	9.20	328.0	411.7

Table 3: Mean ranking score of the four clusters identified by Random Forest in the study.

4 ANALYSES AND DISCUSSIONS

Rule based systems such as the currently used New Priority Ranking System (NPRS) is an advanced slope ranking system which has been developing in the past decades. Hong Kong is regarded as one of the few cities in the world where much updated data are collected for man-made features for stability risk ranking purpose. Study on these data via ML methods provide the objective insights into the data structures and provide an alternative way of classification of features based solely on ranking scores.

Table 2 summarizes the four resulting clusters by the average values of all 18 attributes of the features in each cluster. The number of features are quite even since no cluster is too big or too small. The Random Forest algorithm decided that the features in each of these clusters are similar to each other by considering all the 18 selected attributes at the same time. Cluster 1, for instance, has a medium class of consequence-to-life (CTL) category, a high feature type number (meaning fewer soil cut slopes), longer toe distance, etc, while for cluster 4, features with a higher class of CTL category, low feature type number (more soil cut slopes), medium toe distance, etc. are considered similar and placed in the same group. The physical reasons behind these objective choices of features to be assigned to the same group by the RF method are not immediately obvious since the human mind cannot comprehend 18 attributes at the same time. However, through further comprehensive analyses of the selected attributes in each cluster, the selected features in each cluster may possess similar characteristics and relationships.

A comparison of the clustering results is also made for the average ranking scores of features placed by the ML algorithm in each cluster (Table 3 and Figure 2). It is observed that even though ranking scores are not included in the 18 selected attributes input into the ML algorithm, the resulting clusters display a clear differentiation in their mean ranking scores. Cluster 2, for instance, has very low average ranking score compared with the other 3 clusters.

ML methods have been successful in processing high dimensional data in different fields of science and engineering and is capable of classification tasks by considering a large number of attributes simultaneously. While a typical rule based classification system aims to compute a single value such as the ranking score to provide the rankings of different slopes and retaining walls, this study shows that ML methods can consider multiple parameters at the same time.

It should be noted that, however, ML methods explored in this study would not replace the existing classification systems which have been successfully in use for decades, at least in the short term. However, the results indicate that there could be some unknown relationship for the features being classified into the same cluster. Such relationship may not be of direct relevance to the prioritization of features based on their stability risks at present, but it could not be ruled out that further study could reveal useful knowledge in the future.

5 CONCLUSIONS

Machine learning methods have uncovered data patterns from datasets collected for the purpose of prioritization of features for carrying out upgrading works. The results would potentially provide new insights into the classifications of man-made features in Hong Kong.

Similar approach can also be applied to datasets obtained in other fields of slope engineering such as landslide studies, natural terrain hazard studies, etc. and new data patterns uncovered could lead to new discovery of knowledge.

ACKNOWLEDGEMENTS

This paper is published with the permission of the Head of the Geotechnical Engineering Office and the Director of the Civil Engineering and Development Department, the Hong Kong SAR Government to the use of the information concerned.

REFERENCES

P. Cheng, 2013, “The new priority ranking systems for man-made slopes and retaining walls”, tech. rep., Geotechnical Engineering Office.

X. Yao, 2008, “Landslide susceptibility mapping based on Support Vector Machine: A case study on natural slopes of Hong Kong, China”, Geomorphology 101, 4, 572-582.

T. L. Insua, 2015, “Advanced classification of carbonate sediments based on physical properties”, Sedimentology 62, 590-606.

K. Tse 2017, “Unsupervised Learning on Scientific Drill Data of South China Sea”, University of Hong Kong.

M. J. Way, J. D. Scargle, K. M. Ali, et al., 2012, Advances in Machine Learning and Data Mining for Astronomy, CRC Press.

C. Hennig, 2015, “What are the true clusters ?”, Pattern Recognition Letters 64, 53-62.

A. K. Jain, 2010, “Data clustering: 50 years beyond k-means,” Pattern Recognition Letters 31, 651–666.

R. I. Kabacoff, 2015, R in Action - Data analysis and graphics with R, Manning.

K. P. Murphy, 2012, Machine Learning A Probabilistic Perspective, The MIT Press.

L. Breiman, 1996, “Bagging predictors,” Machine Learning 24, 123–140.

L. Breiman, 2001, “Random forests,” Machine Learning 45, 5–32 (2001).

T. Hastie, R. Tibshirani, and J. Friedman, 2009, The Elements of Statistical Learning, ch. Random Forests,

587–604. Springer New York, New York.

B. Lowe and A. Kulkarni, 2015, “Multispectral image analysis using random forest,” International Journal on Soft Computing 6, 1–14.

J. Quinlan, 1993, Programs for Machine Learning, Morgan Kaurmann.

L. Breiman, 1984, Classification and Regression Trees, Chapman & Hall.

J. Mingers, 1989, “An empirical comparison of selection measures for decision-tree induction.,” Machine Learning 3, 319–342.

A. M. Reading, M. Cracknell, and T. Chalke, 2015, "Combining machine learning and geophysical inversion for applied geophysics.," in 24th International Geophysical Conference and Exhibition.

J. MacQueen, 1967, "Some methods for classification and analysis of multivariate observations," in Proceedings of the Fifth Berkeley Symposium on Mathematical Statistics and Probability, L. M. Le Cam and J. Neyman, Eds., 281–297, University of California.

Practical Use of PLAXIS 2D for Tunnel Support in Variable Ground Conditions in Hong Kong

Calvin H.P. Wong
Sambo E&C Co. Ltd. HKIA 3203 (formerly Jacobs China Ltd.)
Leslie H. Swann & Richard G. Hinchliffe
Jacobs China Ltd.

ABSTRACT

The detailed design of tunnel supports in mixed soil/rock conditions for the Mass Transit Railway Corporation (MTRC) Kwun Tong Line Extension (KTE) Contact 1001 project was undertaken by Soil-structure interaction modellings (i.e. PLAXIS 2D) throughout the construction period of tunnel excavation and support works from 2011 to 2013.

This paper discusses the use of PLAXIS 2D numerical modelling. Practical tunneling design experiences gained from the modeling of weathered ground-structure interaction in drained condition for the design of temporary tunnel supports using pre-installed grouted canopy tubes, composite steel arches and shotcrete lining where the weathered rock properties are derived to be considered as a "soil mass" based on the generalised Hoek-Brown failure criterion (2002).

Two locations of deep weathering have been selected to demonstrate the practical use of PLAXIS 2D numerical modelling for tunnel supports design. At each location, several ground models were adopted to simulate possible variable conditions in mixed ground. In soft ground condition, methods of preventing soil failure were also demonstrated.

The use of PLAXIS 2D numerical modelling also demonstrated that the soil stiffness can be derived from a comparison of the predicted original surface settlements in the model to the observed ground settlements in order to assess the impact of tunnel construction on adjacent buildings.

1 INTRODUCTION

1.1 Background

The Kwun Tong Line Extension (KTE) project is a 2.5km long wholly underground extension of the existing MTR Kwun Tong Line (KTL) running from the current terminus at Yau Ma Tei (YMT) station to a new terminus at Whampoa (WHA). An intermediate station at Ho Man Tin (HOM) will serve as an interchange station with KTE and the future Shatin to Central Link (SCL). KTE Contract 1001 project comprises construction of the new station at Ho Man Tin (HOM), a 120m section of twin single track tunnels connecting with the YMT existing over-run tunnels, a 1200m section of twin track tunnel connecting with the HOM West Cavern, a section of 580m long twin track tunnels and 90m long single track tunnel extending from HOM East Cavern to WHA. In addition, two access shafts were also constructed, one at Fat Kwong Street Playground (FKSP) and one for the Wylie Road Ancillary Building (WAB).

1.2 Ground condition of the deep weathering areas inferred by the Geotechnical Engineering Report

In between YMT and HOM as well as between HOM and WHA, the inferred geological sections in the Geotechnical Engineer Report (GER) showed sufficient rock cover right above the tunnels with an indication of inferred fault or photo lineaments at or adjacent to the actual deep weathering areas. In particular, between HOM and WHA initial investigations indicated that there may be less than 0.5 times the tunnel diameter of rock above the tunnel crown. Anticipated ground conditions are indicated in Figures 1a and 1b.

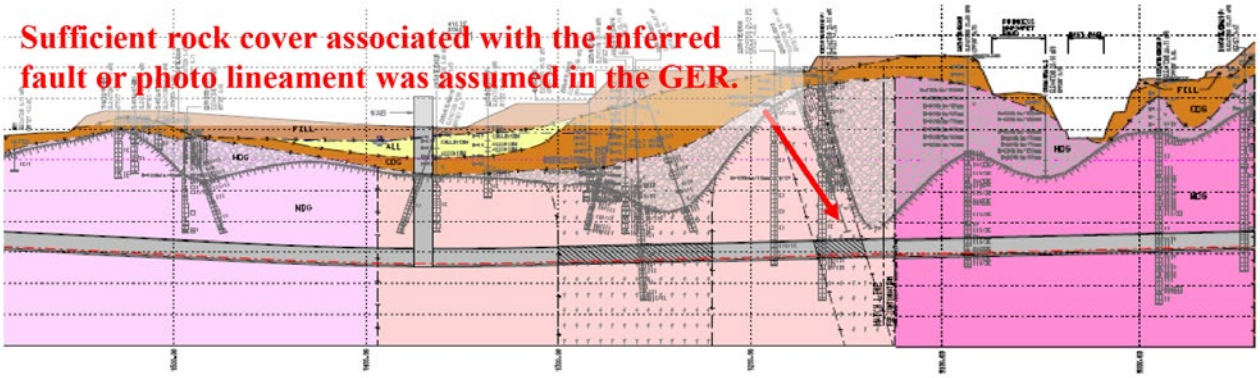

Figure 1a: Inferred geological section showing the sufficient rock cover with inferred fault zone before tunneling.

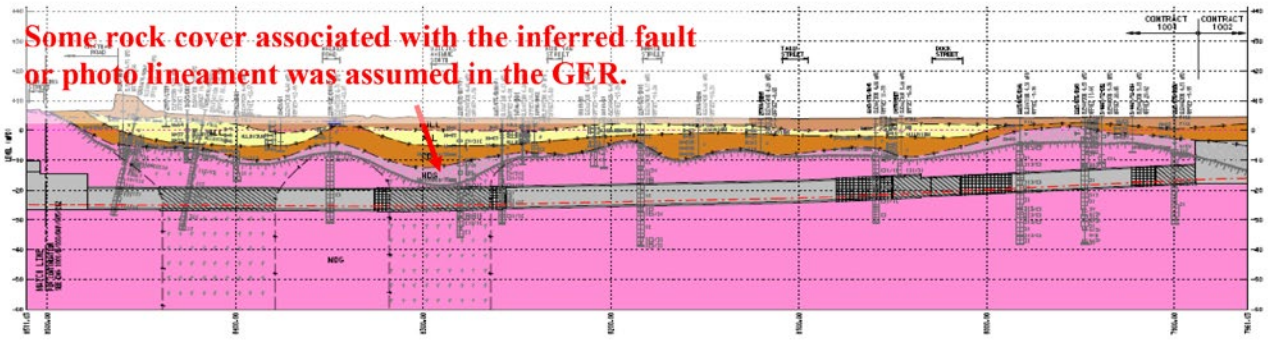

Figure 1b: Inferred geological section showing the sufficient rock cover with inferred fault zone before tunnelling.

1.3 Deep weathering encountered beneath King's Park in YMT to HOM Tunnel

The twin track tunnels between YMT and HOM were excavated through rock by blasting in both directions from WAB shaft. When the tunnel from WAB towards HOM reached Downtrack Chainage (CH) 9112, full face Completely Decomposed to Highly Decomposed Granite (CDG/HDG) was encountered (Plate 1), which resulted in a loss of ground. This location lies 60m below the sports field at King's Park, as shown in Figure 2a. The method of tunneling was then amended to mechanical excavation of the top heading and bench and the installation of stiff steel arch supports and sprayed concrete linings designed using PLAXIS 2D. Canopy tubes (114.3mm dia. with 6mm thick walls) were adopted to support the ground above the tunnel face by bridging the roof between the face and the previously installed ribs as recommended by John and Mattle (2002).

1.4 Deep weathering encountered at Wuhu Street in HOM to WHA Tunnel

The tunnels between HOM and WHA were excavated in generally good quality rock mass conditions, with some zones of deep weathering encountered at the tunnel level. At CH8318 beneath the intersection of Wuhu Street and Gillies Avenue South, CDG was encountered at the tunnel crown, as shown in Figure 2b. Three 50m-long horizontal boreholes were drilled into the tunnel face at CH8318 in the

Plate 1: Mixed ground tunnel face at CH9112 and CH8312 where deep weathering ground conditions encountered.

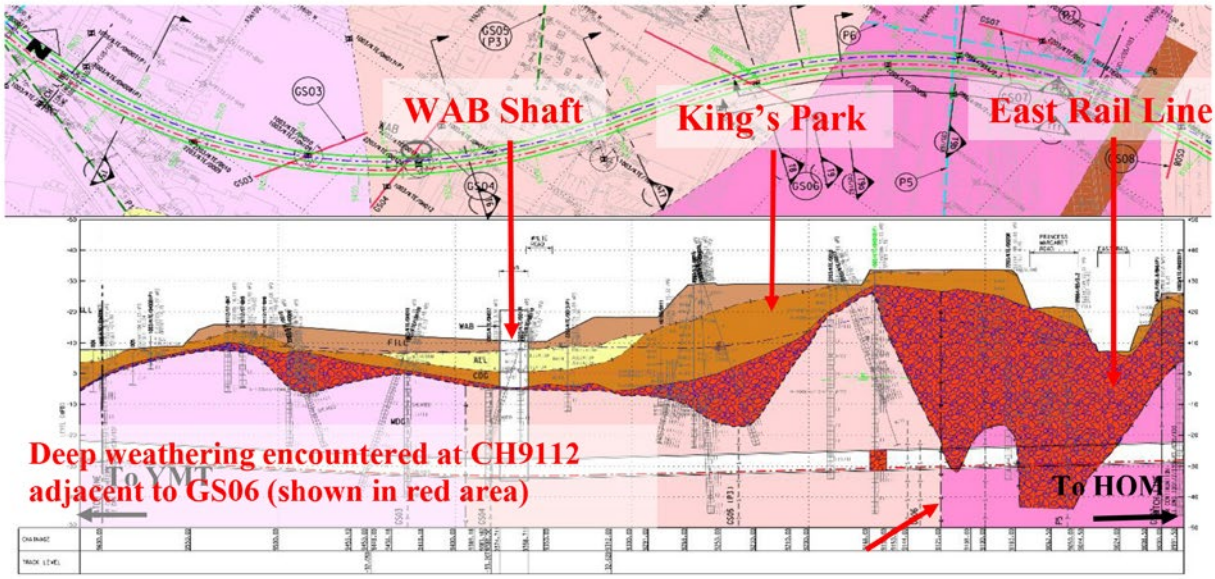

Figure 2a: As-built Layout plan and section showing the deep weathering encountered beneath King's Park.

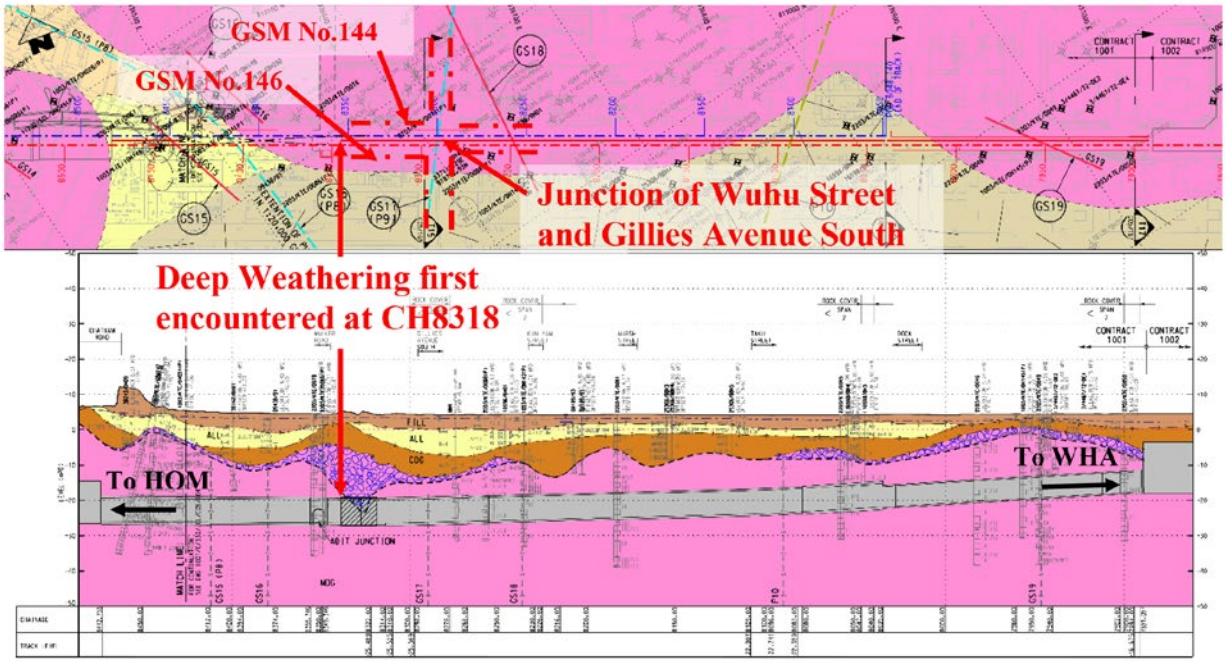

Figure 2b: As-built Layout plan and section showing deep weathering beneath Wuhu Street near Gillies Avenue South.

direction of WHA. The borehole cores indicated a zone of CDG dipping and striking across the tunnel horizon, suggesting that the CDG would extend below the tunnel crown within a 20m long section where the tunnel was to be excavated in part rock and part mixed ground conditions. The tunnel was then advanced through this initial 20m section by mechanical excavation with steel arch ribs installed and sprayed shotcrete lining, designed using PLAXIS 2D. An AGF canopy tube umbrella system with 3m overlaps was installed to support the ground above the tunnel face and to limit ground convergence ahead of the face.

2 DESIGN SCHEME FOR DEEP WEATHERING ENCOUNTERED IN TUNNELS

2.1 Synopsis

The KTE running tunnels between YMT to HOM and HOM to WHA generally run through consistent, good quality rock mass conditions. Drill and blast was used and the tunnel support in rock was designed based on the NGI Q-system Barton et al, (1974). The running tunnels at rock sections were supported by swellex dowels and fibre-reinforced shotcrete according to the determined Q-values and the corresponding support categories in the Q-system design charts. However, the Q-system does not cover the geological conditions where mapped Q-values are lower than 0.001 (i.e. lower bound of value of the Q-system charts) or where the thickness of rock cover is less than half of the tunnel span, regardless of Q-value (i.e. rockhead level below half of tunnel span above the tunnel crown). Therefore, the deep weathering, which was associated with geological structures comprising lineaments, shear zones and faulting, encountered along the KTE tunnels, represent geological conditions that are not covered by the Q-system. A numerical design approach using PLAXIS 2D was adopted to cover the design tunnel support in highly to completely decomposed granites. To demonstrate that the tunnelling works would not result in adverse ground movement that may cause damage to existing buildings, utilities, existing slopes/earth-retaining features or public roads, an extensive instrumentation and monitoring program was established by the Contractor. Instrumentation and survey stations, including ground settlement markers (GSM), utility monitoring points (UMP), tilting markers (TM) and standpipes/piezometers (SP/P) were installed and monitored along the whole tunnel alignment prior to commencement of tunnel excavation to establish consistent and reliable baseline readings. Those readings were continuously monitored and no significant movement was recorded when tunnelling through the deep weathering zones.

2.2 Site Geology

The 1:20,000 and 1:100,000 scale geological maps of Hong Kong (Strange and Shaw,1986 and Sewell et al, 2000) published by Geotechnical Engineering Office (GEO), suggest that the entire KTE alignment is within the Kowloon Granite, which comprises fine and medium grained granites. It was noted that deep weathering was likely to be found at CH9140-9144 below King's Park due to the presence of a geological structure (GS06), as shown in Figure 1. A deep corestone layer (HDG) was interpreted from GI data to overlie MDG bedrock, with a minimum of 7 to 8m rock cover anticipated above the tunnel crown.

2.3 Geotechnical design parameters for numerical analysis

The geotechnical parameters for the soil mass and the rock mass used in the analysis are shown in Table 1. The rock mass equivalent friction and cohesion were derived using RocLab, based on the generalised Hoek-Brown failure criterion (2002). The groundwater levels used were taken from the highest groundwater monitoring data from piezometers in boreholes installed for this Contract. To prevent excessive groundwater drawdown, pre-excavation face grouting up to 2m thick around the extrados of the tunnel was undertaken where groundwater inflow rates exceeded 10L/min/100m of tunnel, to decrease the permeability of the soil and rock mass. Seepage analysis using PLAXIS 2D was undertaken to check the tunnel section where pre-excavation grouting was required to reduce the permeability of ground materials and hence reduce the groundwater inflow rates. The permeability parameters for the soil and rock mass used in the numerical analysis are also shown in Table 1.

Table 1: Summary of geotechnical parameters for numerical analysis

Material	Bulk Unit Weight (kN/m^3)	Q	GSI	Modulus E' (MPa)	C'(kPa)	Friction, φ'(°)	Poisson's Ratio	Permeability k (m/s)
Fill	19.0	–	–	^1.5(0.5z+9.7)	0	37	0.3	5.0×10^{-6}
CDG	19.0	–	–	^2(4.29z+20)	5	39	0.25	2.5×10^{-6} / $*1.0 \times 10^{-8}$
MDG	26.0	0.01	11	1182	144	53.9	0.2	5.0×10^{-8} / $*5.0 \times 10^{-9}$
MDG	26.0	0.28	41	5903	374	64.9	0.2	5.0×10^{-8} / $*5.0 \times 10^{-9}$

^z is depth in meters. *The permeability of the grouted material.

In-situ stress testing using hydro-fracturing and impression packer tests indicated a very variable horizontal stress ratio (K) of between 1 and 2 at shallow depths, decreasing along sub-vertical weathered faults and shear zones. Therefore, a horizontal stress ratio of 2 was adopted for MDG properties in the numerical model.

Hoek (2006) suggests a method to determine ground relaxation around an excavation area, which is equivalent to the stress relief. Using the Longitudinal Displacement Profile with the assumption of weak rock, a ground relaxation of 30% was initially evaluated. However, to ensure greater control of potential ground movements in an urban environment (i.e. King's Park sports field and Wuhu Street), a ground relaxation of 10% was adopted for the PLAXIS 2D numerical modelling analyses. Hence, heavier support was proposed to control these ground movements.

2.4 Design Approach

The PLAXIS 2D axial force and bending moment outputs induced by ground loading and groundwater pressure from steady-state seepage were adopted for the tunnel structural support designs. Plain sprayed concrete support was designed as a short column equivalent and subjected to axial loads with uniaxial bending at an ultimate limit state. The steel arch ribs were designed as composite columns encased in shotcrete lining in order to sustain the ground loading and groundwater pressures. PLAXIS 2D was also used to evaluate the ground movements caused by tunneling.

2.5 Blasting load check for tunnel support in numerical models

Due to the irregularity of the rock head level along the deep weathering zones, excavation of running tunnels in such deep weathering zones was undertaken using both mechanical and drill & blast methods to allow maximum construction flexibility. Blasting was undertaken where rock had a sufficient separation distance from soft ground. A non-blasting zone equal to half of the tunnel span (i.e. 6m) was adopted as a minimum separation distance between the blasting and rockhead levels. The potential rock wedges in immediate contact with the tunnel support were assumed to be driven by the blasting vibration to exert an additional blasting load to the tunnel supports. The blasting load was calculated based on Equation (1) using the pseudo-static method by H.N. Wong (1992). The additional blasting load exerted to the mixed ground tunnel support was then checked using the PLAXIS 2D numerical models.

$$K_c = \omega \times K_a \times \frac{PPV}{g} \quad (1)$$

Where $\omega = 2\pi f$, f = frequency, K_a = Magnification factor refers to H.N. Wong (1992), and PPV = peak particle velocity (mm/s). The PPV (peak particle velocity in mm/s) was calculated by equation (2):

$$PPV = K(R/\sqrt{W})^{-B} \quad (2)$$

Where K = rock transmission constant, R = distance between blast and measuring point (m), W = max. charge weight per delay interval (kg) and B = attenuation exponent.

2.6 Design scenarios in variable ground condition

To check the design of the tunnel supports with varying depths of weathering, four hypothetical ground models were selected for PLAXIS 2D analyses. The four models were:

Case 1: Full face rock with minimum 3m rock cover with 0.14 min. Q_{mapped} value.
Case 2: Full face rock with minimum 1m rock cover with 0.01 min. Q_{mapped} value.
Case 3: Half-face rock with 0.01 min. Q_{mapped} value and CDG extending down to the invert level
Case 4: Full face CDG to below the invert level. (Not used in HOM to WHA tunnel).

Cases	Hypothetical Cases	Q-value	Tunnel Support Type
CASE 1 (Shallow rock cover, optimized to omit steel ribs)	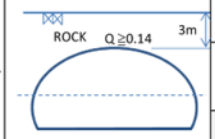	0.28 ≦ Q	1. Steel Fibre Reinforced Shotcrete 200mm thick with spot dowels
		0.14 ≦ Q < 0.28	1. Steel Fibre Reinforced Shotcrete 300mm thick with spot dowels 2. Splies T40 at 300mm c/c
		0.01 ≦ Q < 0.14	Refer to Case 2
		Q < 0.01	Refer to Case 3 or Case 4
CASE 2 (Shallow rock cover)	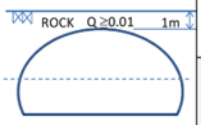	0.01 ≦ Q	1. Steel Rib UC-254x254x73kg/m at 1m c/c with Steel Fibre Reinforced Shotcrete 350mm thick 2. T40 Spiles at 300mm c/c
		Q < 0.01	Refer to Case 3 or Case 4

Cases	Hypothetical Cases	Q-value	Tunnel Support Type
CASE 3 (Rock level between crown to invert level)	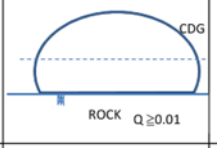	N/A	1. Steel Rib UC-254x254x73kg/m at 1.0m c/c with Steel Fibre Reinforced Shotcrete 350mm thick 2. AGF pipe O.D. 114mm 12m long@9m longitudinal spacing, 350mm c/c
CASE 4 (Full face CDG)	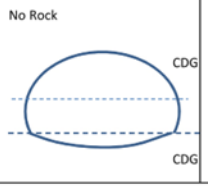	N/A	1. Steel Rib UC-254x254x73kg/m at 0.8m c/c with Steel Fibre Reinforced Shotcrete 350mm thick 2. AGF pipe O.D. 114mm 12m long@9m longitudinal spacing, 350mm c/c 3. Mass concrete with wire mesh at invert concrete

Figure 3: Criteria for adoption of PLAXIS 2D numerical analysis for mixed ground tunnel support.

2.7 Difficulties and experience gained in designing deep weathering tunnel support

Design for the four hypothetical cases of mixed ground support was carried out by PLAXIS 2D numerical modelling.

The baseline case represents the lower bound Q_{mapped} value of 0.14 with at least half tunnel span (i.e. 6m) of rock cover above tunnel crown. The tunnel support for this case is systematic dowels with the addition of 50mm to 200mm shotcrete as specified in Q-system support categories. *Case 1* represents the lower bound Q_{mapped} value of 0.14 and a minimum rock cover of 3m applying a plain shotcrete lining. Case 3 was defined as the rock head level at exactly or above the invert level with a min. of 0.01 Q_{mapped}. Composite steel rib UC 254x254x73kg/m with 1000mm spacing and 350mm thick shotcrete tunnel support and 2m thick pre-excavation grouting around the extrados, was used for the numerical analysis. A canopy tube umbrella system AGF 114.3mm dia. was proposed to support the tunnel advance of the tunnel face. In *Case 2*, similar tunnel support as per Case 3 was proposed, which means composite steel ribs UC 254x254x73kg/m with 1000mm spacing and 350mm thick shotcrete tunnel support for the rock head level between 3m above tunnel crown and invert level. However, the canopy tube umbrella system was replaced by prescriptive 4m long T40 spiles at 300mm centers perpendicular to the tunnel face and 1000mm centers longitudinally spaced, so as to accelerate the construction programme.

The extent of deep weathering was uncertain in particular areas due to inaccessibility for further GI boreholes. Therefore, full face CDG tunnel support was proposed to cover the worst case scenario of deep weathering extending below the tunnel invert level. The numerical analysis was carried out for the full face CDG tunnel support (Case 4 tunnel support) and was assumed to be composite steel ribs UC 254x254x73kg/m at 800mm spacing with 350mm thick shotcrete and 2m thick pre-excavation grouting around the extrados as per Case 3 tunnel support. Unlike other cases where the MDG is present at or above the tunnel invert, the CDG material is assumed to be found at or below the tunnel invert. Since, the Young's Modulus E' values for CDG are much lower than MDG E' values (E' values of CDG being between 2 to 30 times smaller than MDG from ground surface to tunnel invert level), insufficient bearing capacity resulted in theoretical instability of the tunnel support and subsequent soil failure. This instability of tunnel support was due to shear failure occurring along two shear zones that extend upwards from the outer boundaries of the tunnel invert towards the ground surface (i.e. lines of soil arching: Terzaghi, 1943), which resulted in severe settlement at the tunnel crown and ground heave at the invert level. The

numerical model detected soil failure, which led to the ground loading (ΣMstage) not being able to attain the value of 1 (approx. 85%), as shown in Figure 4. The Mohr-Coulomb points represent shear failure and are concentrated at the tunnel crown and along the lines of soil arching up from both sides of the tunnel, resulting in soil body collapse.

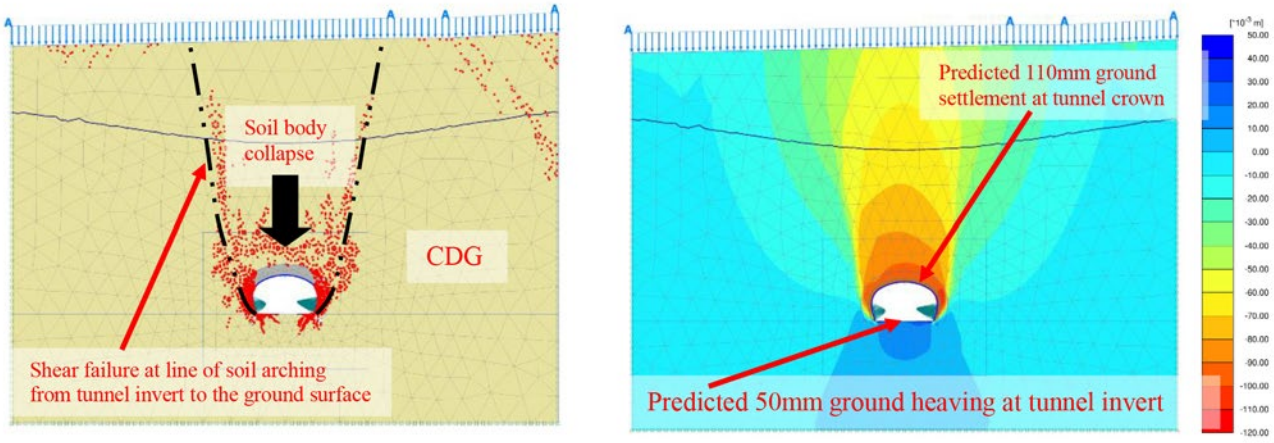

Figure 4: Soil failure detected in the numerical analysis output for full CDG tunnel profile without a firm base support (i.e. ΣMstage could not reach 1.0 during analysis). Predicted Mohr-coulomb point (shear failure) shown in red dots in the right hand image and predicted ground movement shown in the left hand image.

To avoid shear failure occurring along two shear zones rising from the outer boundaries of the tunnel invert towards ground surface leading to the development of soil arching, a 3m deep excavation below the original tunnel invert to form a round tunnel form was proposed. Upon modelling the round shaped tunnel support, the bearing area was enlarged from two tunnel "toes" to a full rounded tunnel, which resulted in an increase of bearing capacity. Following numerical analyses, ΣMstage in the calculation process of the PLAXIS 2D model reached 1. Hence, the shear failure could not extend to the ground surface and the ground movement around the tunnel was greatly reduced. Therefore, the tunnel became geotechnically stable without exceeding the structural capacities of the composite steel ribs and shotcrete tunnel support in the numerical analysis. Therefore, a round shaped composite steel rib UC 254x254x73kg/m at 800mm spacing with 350mm thick shotcrete with a canopy tube umbrella system to support the tunnel crown during excavation was proposed for full face CDG (Case 4) tunnel support (Figure 5).

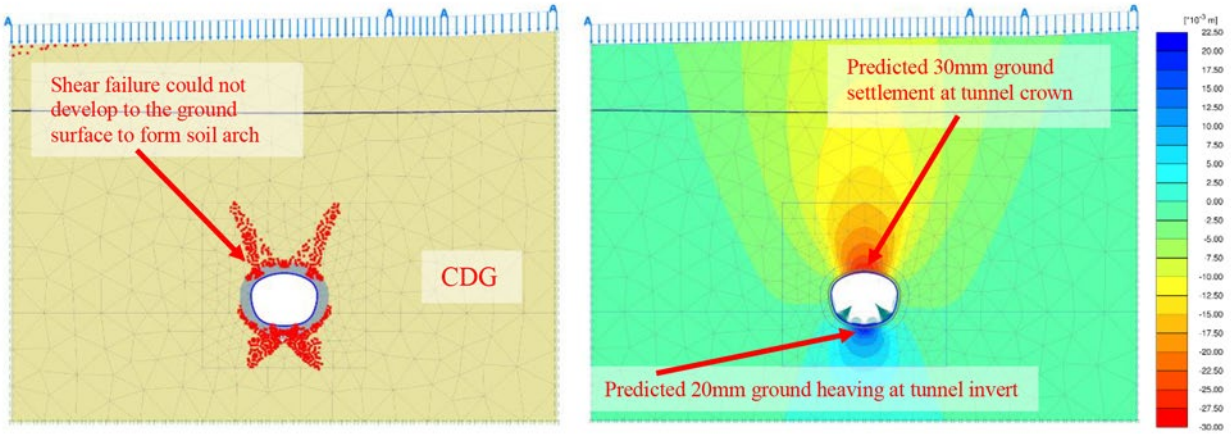

Figure 5: Numerical analysis output for full CDG tunnel profile with round shaped tunnel support. Predicted Mohr-coulomb point (shear failure) shown in red dots in the right hand image and predicted ground movement shown in the left hand image.

2.8 Predicted Ground Movement and Impact Assessment

The risk of ground movement caused by bulk excavation and groundwater drawdown in the mixed ground tunnel beneath the King's Park Sports Field and East Rail was relatively low compared to the tunnel beneath Wuhu Street. This is because the ground cover under the King's Park Sports Field is three times greater than above the mixed ground tunnel running beneath Wuhu Street. Greater silo pressures occurred above the tunnel with greater ground cover, resulting in less surface settlement. Also, there are no buildings located at the King's Park Sport Field within 50m of the tunnel excavation influence zone. However, potential ground movement at Wuhu Street was critical owing to the presence of adjacent buildings, which were mainly residential and included some founded on raft footings with some aged low-rise residential buildings also present. Alert-Action-Alarm response levels for ground movement were set at 12mm, 18mm and 25mm, respectively. Surcharge loadings for the carriageway, footpath and the buildings beside Wuhu Street were taken into consideration in the numerical models. Loss of geotechnical pile capacity for buildings sitting on friction piles was checked according to the method proposed by Poulos and Deng (2004). A concern was that additional negative skin friction could be mobilised due to the ground loss induced by tunnel excavation. Ground loss would induce an increase of pile axial load, which could result in the existing pile capacity being exceeded.. Pile P1 of the Hop Yee Building, which is the closest pile to the tunnel (Figure 6), was checked for loss of capacity by carrying out numerical analysis based on ground settlement observations.

2.9 Soil stiffness derived from observed settlement due to tunneling works in Wuhu Street

In the investigation, it was found that when CDG was encountered in the tunnel face, the observed surface settlement at the nearest GSM located on nearby footpaths (Figures 2 and 6), was 2mm. This settlement was observed prior to the installation of steel ribs at the beginning of the mixed ground zone and before the injection of grout around the tunnel annulus ahead of the tunnel face. The predicted settlements from numerical analyses for a ground model with CDG above the tunnel invert were between 4mm and 5.7mm. The observed settlement inferred that the ground is stiffer than had been assumed in the original analysis. Based on the observed settlement, the stiffness of the CDG was increased by a factor of 2.5 in the numerical model. This factor is on the conservative side as three 50m-long horizontal boreholes drilled into the tunnel face from CH8318 showed a variable zone of CDG, HDG and MDG extending across the tunnel alignment and down to the springline in the worst case. The numerical model at Section CH8318 was re-run with a CDG stiffness value E'CDG 2.5 times higher than the original and predicted ground movements were reduced to between 2.3mm and 3.2mm, close to the measured value.

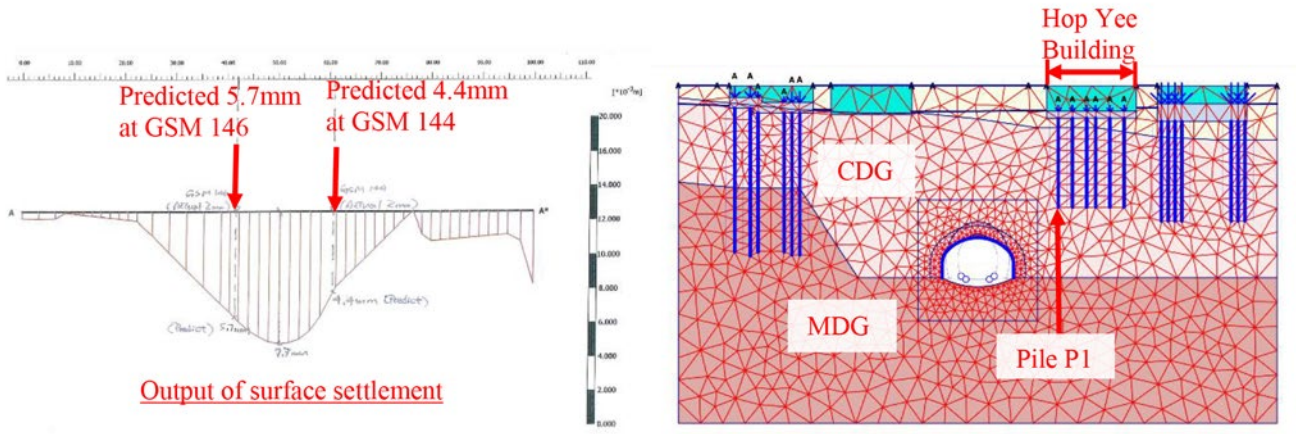

Figure 6: Numerical model output of surface settlement under original E'CDG and the Numerical model section CH8318 layout showing the relationship of tunnel excavation and Hop Yee Building piles.

It was agreed that the increased soil stiffness, E'CDG, be adopted to check the existing Hop Yee Building's pile capacity due to the ground loss from tunnel excavation. The predicted relative movement of the soil and the Hop Yee building pile P1 was calculated to be 0.13mm in the updated numerical model,

at Section CH8318. This relative movement prediction was much less than the allowable 0.5% of pile diameter (305x305mm H- pile of P1) and was insufficient to fully mobilise negative skin friction, Poulos (1990). Hence, the additional axial loads due to tunnel excavation were negligible and it was agreed the tunnel excavation works did not have any adverse impact to the Hop Yee Building piles.

3 CONCLUSIONS AND RECOMMENDATIONS

The stability of the tunnel excavation support as determined from the numerical modelling of various deep weathering scenarios was found to be satisfactory when taking into account the stress relief induced by the tunnel excavation. Since the numerical modelling was analysed using the Mohr-Coulomb parameters as suggested by the Hoek Brown Failure Criterion (2002), which conservatively assume the MDG as a rock mass, regardless of rock joints and discontinuities to find the equivalent frictional angle and cohesive strength, the specific localised adverse rock joints/discontinuities in the numerical model were addressed separately on site by spot dowels and shotcrete. The methodology as described in this paper for the practical use of PLAXIS 2D numerical models to determine the tunnel supports in mixed ground conditions (i.e. deep weathering) is considered valid as the tunnels were successfully excavated, supported and the lining completed. There was no distress observed at the tunnel crown or sidewalls during excavation works and all the monitoring did not record any significant movement. During the tunnelling works, the soil was found to behave differently than was expected as in the case beneath the Wuhu Street adjacent to the Hop Yee Building, where the observations from the monitoring data showed that the soil was stiffer than in the numerical model. Hence, the soil stiffness was revised based on back analysis to review the building pile capacity.

In order to gain greater confidence of the soil behaviour during future tunnel excavations, comprehensive monitoring systems are recommended to be installed adopting a safe baseline envelope of AAA trigger levels. The monitoring data should be collected daily from the monitoring points and reported to the designer for calibration or back analyses of the soil-structure interaction numerical model to minimise the risks during tunneling works.

ACKNOWLEDGEMENTS

The authors are grateful to Dr. Alan K. L. Kwong, Mr. Andrew Houghton, Mr. Chi Ng, and Mr. Leo K. H. Lee their professional contribution and discussion throughout the mixed ground tunnel issue in the KTE Contract. The contents of this paper are not liable to any commercial use of the discussed ground geology or to the product trade names mentioned.

REFERENCES

Evert Hoek, Itasca Carranza-Torres & Brent Corkum. 2002. Hoek-Brown Failure Criterion. Rocsicence Inc.

Evert Hoek. 2006. Tunnel in weak rock. Practical Rock Engineering. Evert Hoek Consulting Engineer Inc.

Geotechnical Engineering Report. 2010. Kwun Tong Line Extension Consultancy Agreement No. C1001 Detailed Design for Yau Ma Tei to Whampoa Tunnels and Ho Man Tin Station. MTRC.

H.N. Wong. 1992. Geotechnical Engineering Office Report No. 15 Section 2: Pseudo-Static Assessment of Stability of Soil Slopes Subjected to Blasting Vibration. Geotechnical Engineering Office.

Karl Terzaghi. 1943. Arching in Ideal Soil (P.66-76). Theoretical Soil Mechanics. John Wiley And Son, Inc.

Max John and Bruno Mattle. 2002. Design of Tube Umbrella. ILF Consulting Engineers.

N. Barton, R. Lien and J. Lunde. 1974. Engineering Classification of Rock Masses for the Design of Tunnel Support. Norwegian Geotechnical Institute, Norway.

Nick Barton and Eystein Grimstad. 1993. Updating of the Q System for NMT. Norwegian Geotechnical Institute, Norway.

Nick Barton and Eystein Grimstad. 1994. The Q-System Following Twenty Years of Application in NMT Support Selection. Norwegian Geotechnical Institute, Norway.

Poulos, H.G. 1990. Design of piles for negative friction. Proceedings of the Conference Piletalk International '90, Jakarta, pp 123-129.

Poulos H.G. and D. Wang. 2004. An Investigation on Tunnelling-Induced Reduction of Pile Geotechnical Capacity, 9th Australia New Zealand Conference on Geomechanics, Auckland, Auckland: New Zealand Geotechnical Society and the Australian Geomechanics Society.

Numerical Analysis of Bored Piles in Sandstones

L.W. Wong
SMEC Asia Ltd, Hong Kong

ABSTRACT

Numerical analyses on two test piles using the Hardening Soil model have been conducted for estimating the settlements of the piles. The nonlinear stiffness parameters adopted for the analysis are assessed from the t-z curves obtained from the instrumented pile load tests. Close agreement between the observed and calculated pile head displacements validates the non-linear Hardening Soil model.

1 INTRODUCTION

Pile settlements have been one of the criteria for designing pile foundations. Due to variation on the supporting ground conditions and the non-linearity of the ground stiffness, pile settlement prediction has been one of the major challenges for design engineers.

Numerical analyses on the performance of piles have become popular. Toh and Chao (2015) presented the results on 3-D analyses on driven piles in marine deposits and alluvium using the Mohr-Coulomb (MC) model. Since the ground stiffness is non-linear in nature, the use of the linear elastic-perfectly plastic MC soil model would have limitations. Extrapolating the load-settlement curve beyond the maximum test load would be uncertain due to the non-linearity of the ground stiffness. The non-linear hyperbolic Hardening Soil (HS) model would be applicable for predicting the pile performance under the full range of loading. On the other hand, determination on the Young's moduli for the ground supporting the piles has been another challenge. The medium-strain secant moduli are normally obtained from the triaxial tests conducted in the laboratory. The best method for estimating the Young's moduli is by back-calculating the results of the pile load tests.

This paper presents the results of numerical analysis using the software PLAXIS 2-D and the HS model. Two case histories on pile load tests have been collected. The inputting Young's moduli of the supporting ground are assessed from the pile load test results. The calculated pile head displacements under various applied loads are compared with those observed. Close agreement between the observed and the calculated pile head displacements has been obtained and thus the non-linear Hardening Soil model is validated.

2 ESTIMATION OF ELASTIC MODULI

2.1 Hyperbolic t-z curves

The Young's moduli for the ground surrounding the piles could be determined by conducting compression tests on soil and rock specimens. Wong (2010a) reported the application of in-situ tests including the pressuremeter tests and the P-S logging for shear wave velocity measurements to assess the medium-strain and the small- strain ground stiffness values respectively. The most reliable method would however be by conducting back-analysis on the pile load tests.

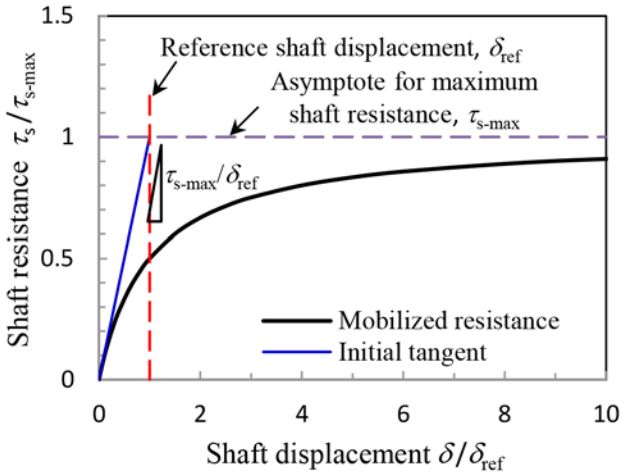

Figure 1: Mobilization of pile shaft resistances

Wong (2010b) assessed the initial stiffnesses of the ground surrounding the piles from the load-displacement relationships of the pile shaft, the t-z curves. The t-z curves interpreted from the instrumented pile load tests are idealized to the hyperbolic curves that have the expression:

$$\tau_s = \tau_{s\text{-}max} / (1 + \delta_{ref} / \delta) \quad (1)$$

where $\tau_{s\text{-}max}$ is the maximum shaft resistance, δ_{ref} is the reference shaft displacement, τ_s is the shaft resistance mobilized at the shaft displacement δ. The relationship between the pile shaft resistance and the shaft displacement is depicted in Fig. 1. The ratio $\tau_{s\text{-}max} / \delta_{ref}$ is the initial stiffness of the hyperbolic t-z curve.

2.2 Estimating elastic moduli from t-z curves

The elastic moduli of the surrounding ground supporting the pile shaft can be estimated from the $\tau_{s\text{-}max} / \delta_{ref}$ ratios of the hyperbolic t-z curves expressed in Eq. 1. Based on the elastic solution on the load-displacement relationship of a single pile presented by Randolph and Wroth (1978), Wong (2010b) established that the initial shear modulus, G_i, of the surrounding ground is represented by the following expression:

$$G_i = \tau_{s\text{-}max} \, r_o \ln (r_m / r_o) / \delta_{ref} \quad (2)$$

$$r_m = 2.5 \, L \, \rho (1 - \nu) \quad (3)$$

where r_o is the radius of the pile, r_m is the radius of the influence zone, L is the pile length, ν is the Poisson's ratio of the surrounding ground and ρ is the ratio of the shear moduli at the depths of L/2 and at L. Wong and Yong (2011) applied Eqs. 2 and 3 to establish the theoretical t-z curves for predicting the performance of the bored piles.

3 CASE HISTORY ON BORED PILES - CASE 1

The test pile for the Case 1 study is located in Manila where an expressway of 40 km in length has been constructed. In order to refine the design of bored piles supporting the viaducts, seven instrumented pile load tests were conducted. The test piles are 780 mm in diameter and ranging from 10 m to 25 m in lengths.

Majority of the instrumented test piles are embedded in highly weathered to moderately weathered fine-grained sandstones. The N values of the Standard Penetration Tests for the weathered sandstones range from 16 to 78. Based on very limited numbers of uniaxial compression tests conducted on the

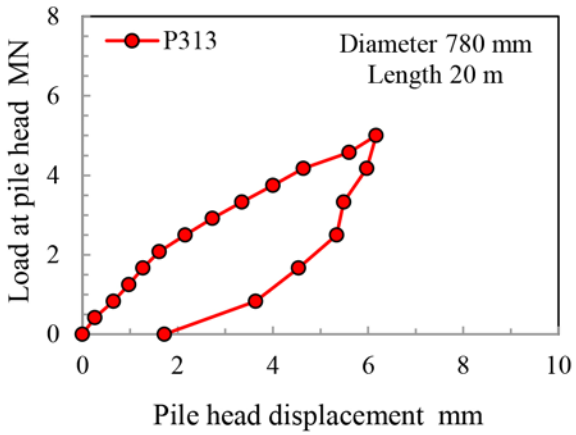

Figure 2: Pile head dispalcements for test piles P313

cored specimens, the uniaxial compressive strengths for the moderately weathered sandstones ranged from 1.7 MPa to 7.4 MPa, with an average of 3.8 MPa.

Test pile no. P313 is 20 m in length. The maximum compression load is 5 MN. The groundwater level is 6 m below surface. Figure 2 presents the pile head displacements versus various applied loads for this test pile. The pile head settlement observed at the maximum load and the residual settlement after releasing the maximum load are summarized in Table 1. The load distribution profiles interpreted from the strain gauge readings for test pile P313 are presented in Fig. 3.

Table 1: Summary of instrumented test piles

Case no.	Pile no.	Pile diameter D, mm	Pile length L, m	Maximum axial load MN	Pile head settlement, mm	
					At maximum load	Residual
1	P313	780	20	5.0	6.17	1.72
2	3C3	1500	22	35.0	52.19	37.49

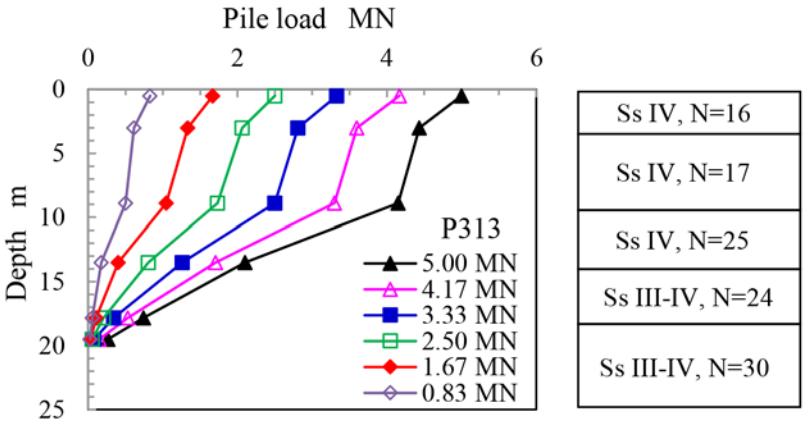

Figure 3: Load distribution curves for test pile P313

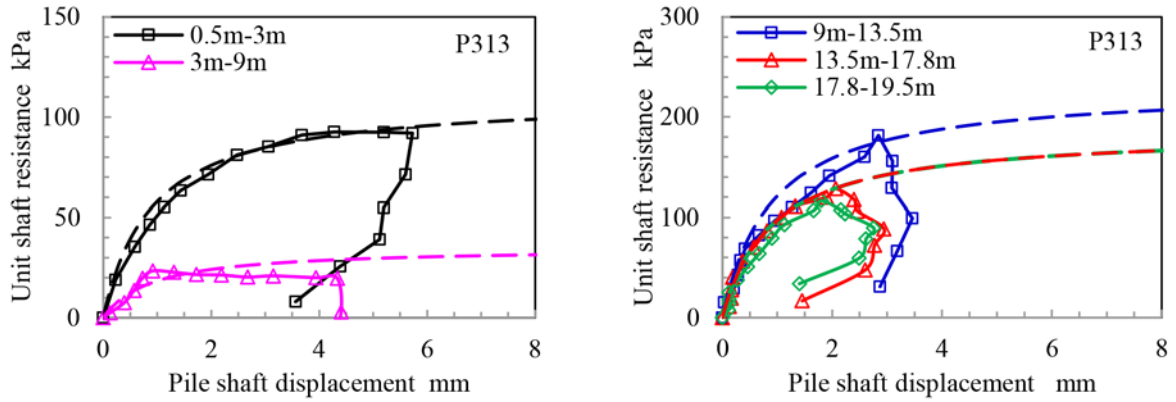

Figure 4: T-z curves for various segments of test pile P313

Table 2: Hyperbolic parameters and elastic moduli along pile shaft - test pile P313

Soil/rock	Depth m	N value	Maximum shaft resistance $\tau_{s\text{-}max}$, kPa	Reference shaft displacement δ_{ref}, mm	Initial Shear modulus G_i, MPa	Initial Young's modulus E_i, MPa
Sandstone IV	0.5 ~ 3.0	16	110	0.9	200	520
Sandstone IV	3.0 ~ 8.9	17	35	0.9	65	165
Sandstone IV	8.9 ~ 13.5	25	230	0.9	415	1080
Sandstone III-IV	13.5 ~ 17.8	24	190	0.9	335	870
Sandstone III-IV	17.8 ~ 19.5	30	180	0.9	335	870

The t-z curves for the five segments of test pile no. P313 are presented in Fig. 4. These curves are fitted into hyperbolic curves and the sets of parameters, the $\tau_{s\text{-}max}$ and δ_{ref} values, are summarized in Table 2. Inputting the $\tau_{s\text{-}max}$ and the δ_{ref} values into Eq. 2 and using $r_o = D/2$, where D is the diameter of the test pile, the calculated initial shear moduli surrounding the pile segments are summarized in Table 2.

Figure 3 shows that the load transferred to the pile base is about 3 % of that applied at the pile head. Apparently the test load was not large enough to mobilize the base resistance. The pile base resistances versus the pile toe displacements, the q-z curves, could not be reliably interpreted from this test pile.

4 CASE HISTORY ON BORED PILES – CASE 2

The northern section of the Taiwan High Speed Rail, constructed under Contracts C230 and C240, has the route length of 48 km. The viaducts were supported on bored piles embedded mainly in sandstones and mudstones. Wong et al. (2004) reported the performance of 10 instrumented compression pile load tests conducted for this section of high speed rail. The test piles are 1.5 m in diameter and ranging from 7 m to 33 m in length.

Test pile no. 3C3 for the Case 2 study is 22 m in length. The supporting ground comprises alluvial sand and gravel of 12 m in thickness underlain by slightly weathered to fresh sandstones and mudstones. The groundwater level is located at 3 m below surface. In addition to the strain gauges installed at 7 levels along the pile shaft, extensometers were installed at the toe of the bored pile. The compression loads were applied in 4 unload-reload cycles to the maximum of 35 MN. Figure 5 presents the observed pile head and pile toe displacements under various applied loads. The pile head settlement observed at the maximum load and the residual settlement after releasing the maximum load are summarized in Table 1.

The load distribution curves interpreted from the strain gauge readings are presented in Fig. 6. The t-z curves for the six segments of test pile no. 3C3 are presented in Fig.7. These curves are fitted into hyperbolic curves and the sets of parameters, the $\tau_{s\text{-}max}$ and δ_{ref} values, are summarized in Table 3. The elastic moduli calculated by Eq. 2 are presented in Table 3.

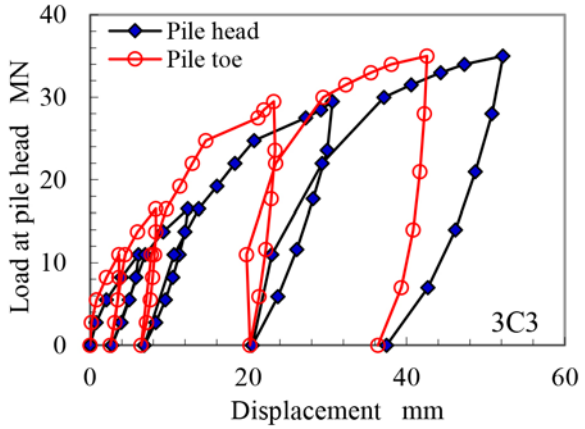

Figure 5: Pile head dispalcements for test pile 3C3

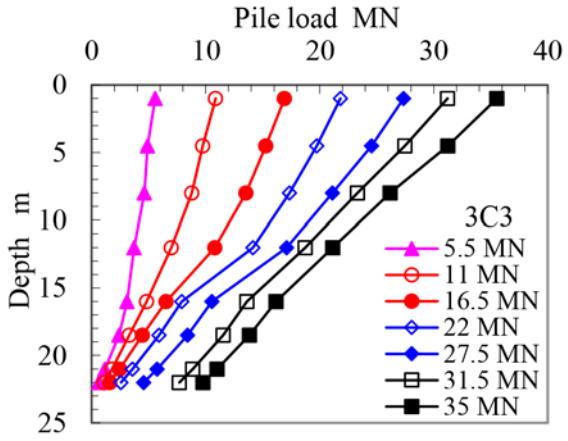

Figure 6: Load distribution curves for test pile 3C3

Table 3: Hyperbolic parameters and elastic moduli along pile shaft - test pile 3C3

Soil/rock	Depth m	N value	Maximum shaft resistance $\tau_{s\text{-}max}$, kPa	Reference shaft displacement δ_{ref}, mm	Initial Shear modulus G_i, MPa	Initial Young's modulus E_i, MPa
Sand & gravel	0 ~ 4.5	80	330	20	25	65
Sand & gravel	4.5 ~ 8.0	69	340	15	35	90
Sand & gravel	8.0 ~ 12.0	119	340	9	58	150
Ss/Ms I-II	12.0 ~ 16.0	161	340	5	105	270
Ss/Ms I-II	16.0 ~ 18.5	107	200	1	308	800
Ss/Ms I-II	18.5~ 21.0	115	240	1	370	960

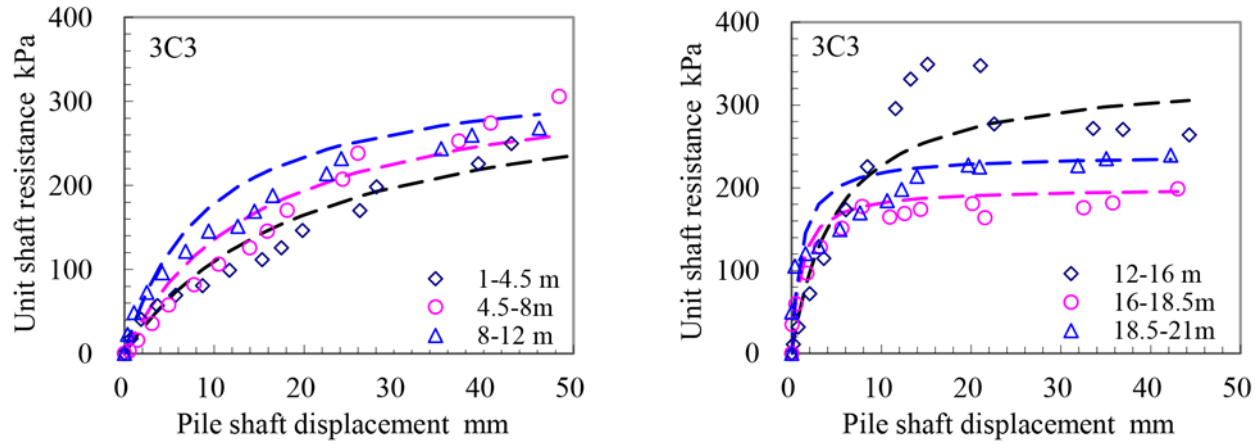

Figure 7: T-z curves for various segments of test pile 3C3

Figure 6 shows that at the maximum applied load of 35 MN, the load transmitted to the pile base is 9.8 MN. The stiffness of the ground immediately beneath the pile base could also be interpreted from the loads at pile toe versus the pile toe displacements relationship. Wong (2010c) assessed the Young's moduli for the weak rocks supporting the toes of 10 test piles conducted in Case 2. For pile no. 3C3, the initial Young's modulus of 255 MPa was interpreted for the rock beneath the base. Compared with the Ei value of 960 MPa interpreted from the t-z curve for the bottom segment, that estimated from the q-z curve is only one quarter of that from the t-z curve. Such lower in stiffness would be due to softening at the pile toe caused by bored piling.

5 NUMERICAL ANALYSIS

5.1 Hardening soil model

The PLAXIS finite element software developed by PLAXIS BV (2011) has become popular in geotechnical analysis and design. The Hardening Soil (HS) model introduced in the PLAXIS programme is the Duncan-Chang hyperbolic stress-strain model (Duncan and Chang, 1970). The hyperbolic function, as given by Duncan and Chang, for the drained triaxial test can be formulated as:

$$\varepsilon_1 = q_a\, q \,/\, E_0\,(q_a - q)\,, \quad \text{for } q < q_f \tag{4}$$

$$q_f = 6 \sin\phi' \,(\sigma'_3 + c' \cot\phi') \,/\, (3 - \sin\phi') \tag{5}$$

where ε_1 is the axial strain, E_0 is the initial modulus at small strain, q is the deviatoric stress, q_a is the asymptotic value of the shear strength, qf is the ultimate deviatoric stress, in which $q_a = q_f / R_f$ and R_f is the failure ratio. Figure 8 shows the hyperbolic relationship of stress and strain in primary loading.

Different stiffness values are used in both loading and unload-reloading. The parameters for the soil stiffness are the E^{ref}_{50}, E^{ref}_{oed}, E^{ref}_{ur} and the exponential factor m. The definitions of these stiffness parameters are:

- E^{ref}_{50} is the reference secant stiffness from standard drained triaxial test,
- E^{ref}_{oed} is the reference tangent stiffness for oedometer primary loading,
- E^{ref}_{ur} is the reference unloading/reloading stiffness,
- m is the exponential factor for stress-level dependency of stiffness.

The definition for these stiffness parameters are depicted in Fig. 8. In order to simulate a logarithmic stress dependency, m is recommended to be taken as 1 in PLAXIS.

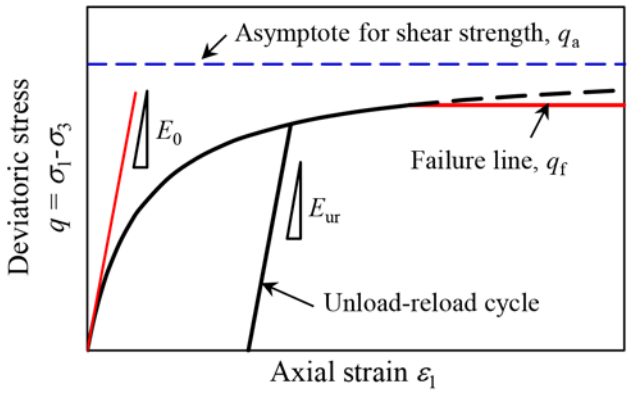

Figure 8: Hyperbolic stress-strain relationship in primary loading for the hardening soil model

Schanz et al. (1999) explained in detail the formulation and verification of the HS model. The shear strength parameters for soil in the HS model are the effective cohesion, the effective friction angle and the dilatancy angle, which are denoted by c', ϕ' and ψ' respectively.

5.2 Inputting parameters

The software PLAXIS 2-D developed by PLAXIS BV (2011) has been used for the numerical analyses for the test piles in Case 1 and Case 2. The pile structure and the ground are simulated by the axisymmetric mode. The finite element mesh for the numerical analyses on Case 1 and Case 2 are the following:

(1) Case 1: The ground model is 40 m in radius and 40 m in thickness. The pile model is 390 mm in radius and 20 m in length. The groundwater level is 6 m below ground surface.

(2) Case 2: The ground model is 40 m in radius and 40 m in thickness. The pile model is 750 mm in radius and 22 m in length. The groundwater level is 3 m below ground surface.

The finite element mesh adopted for Case 2 is shown in Fig. 9. The Hardening Soil model is used. The stiffness and the shear strength parameters adopted in the numerical analyses for Case 1 and Case 2 are summarized in Tables 4 and 5 respectively. The E^{ref}_{ur} equal to the E_i values interpreted from the hyperbolic t-z curves of the pile load tests have been adopted.

The E^{ref}_{50} value was determined by sensitivity analyses using $E^{ref}_{ur}/E^{ref}_{50}$ ratios of 2 and 3. As the $E^{ref}_{ur}/E^{ref}_{50}$ ratio of 3 gives better matching between the observed and the calculated displacements, this ratio has been adopted throughout the analyses. The E^{ref}_{oed} inputted are the default values calculated by PLAXIS. Depend on the confining pressures and the ϕ' values, the $E^{ref}_{oed}/E^{ref}_{ur}$ ratios range from 0.8 to 0.9 in this study.

Table 4: Input parameters for the hardening soil model – pile no. P313

Soil/rock	Depth m	Unit weight kN/m³	Effective shear strength			Poisson's ratio ν	Reference stiffness	
			c' kPa	ϕ' degree	ψ' degree		E^{ref}_{ur} MPa	E^{ref}_{50} MPa
Sandstone IV	4.5	19	0.5	36	3	0.3	520	155
Sandstone IV	10.5	19	0.5	36	3	0.3	165	85
Sandstone IV	16.5	19	0.5	36	3	0.3	1080	310
Sandstone III-IV	18.0	20	0.5	39	3	0.3	870	270
Sandstone III-IV	20.0	20	0.5	39	3	0.3	870	270
Sandstone III-IV	25.0	20	0.5	39	3	0.3	870	270
Sandstone III	40.0	22	0.5	39	3	0.3	870	270

Table 5: Input parameters for the hardening soil model – pile no. 3C3

Soil/rock	Depth m	Unit weight kN/m³	Effective shear strength			Poisson's ratio ν	Reference stiffness	
			c' kPa	ϕ' degree	ψ' degree		E^{ref}_{ur} MPa	E^{ref}_{50} MPa
Sand & gravel	4.5	19	0.5	42	3	0.3	65	22
Sand & gravel	8.0	19	0.5	42	3	0.3	120	40
Sand & gravel	12.0	19	0.5	42	3	0.3	270	90
Ss/Ms I-II	16.0	22	0.5	45	3	0.3	780	260
Ss/Ms I-II	18.5	22	0.5	45	3	0.3	940	315
Ss/Ms I-II	25.0	22	0.5	45	3	0.3	940	315
Ss/Ms I	40.0	22	0.5	45	3	0.3	940	315

As the ground stiffness beneath the pile base for pile no. P313 could not be reliably estimated from the q-z curve, the E_i value of 870 interpreted from the t-z curve of the bottom segment has been adopted for the ground beneath the pile base. For pile no. 3C3, the Ei value of 255 MPa estimated from the q-z curve is only 1/4 of that interpreted from the t-z curve of the bottom segment. The stiffer E_i value of 960 MPa has been adopted. The elastic modulus of 38,500 MN/m² is adopted for the reinforced concrete bored piles in Case 1 and Case 2.

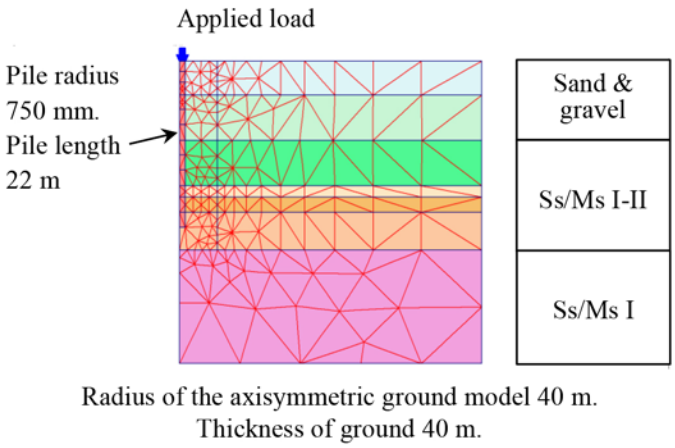

Figure 9: Finite element mesh adopted for the analyses of Case 2 – pile no. 3C3

5.3 Ultimate shear strength of ground

The shear strength parameters could be inferred from the $\tau_{s\text{-}max}$ values interpreted from the hyperbolic t-z curves using Eq. 5. The $\tau_{s\text{-}max}$ values for the various pile segments are related to the vertical effective stresses, σ'_v , in Fig. 10. Linear regression gives an average $\tau_{s\text{-}max}$ /σ'_v ratio of 0.866. Assuming c' = 0, $\sigma'_3 = K_0 \sigma'_v$ along the pile shaft and K_0 = 0.5, the ϕ' value of 43° is obtained for the weathered sandstones in Case 1. The ϕ' values ranging from 36° to 39° and from 42° to 45° for piles no. P313 and 3C3, respectively, have been adopted in the numerical analyses. The K_0 value of 0.5 and the R_f value of 0.9 have been adopted.

It is believed that sand and gravel and the weathered sandstones and mudstones have the behaviour of dense sand. The ψ' = 3° for these materials have been adopted in the analysis. In the PLAXIS analyses, the c' value of 0.5 kPa is adopted for soil and rock to avoid numerical complications.

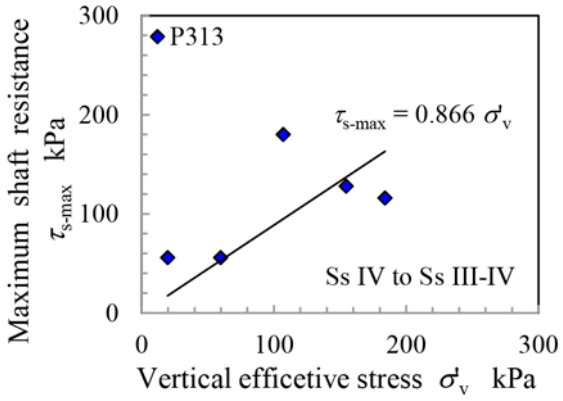

Figure 10: Relationship bewen maximum shaft resistances with vertical effective stresses for test pile P313

6 RESULTS OF ANALYSES

The computed pile head displacements under various applied loads for piles no. P313 and 3C3 are presented in Figs. 11 and 12 respectively. The calculated values are compared with the observed data. As shown in Fig. 11, at the maximum test load of 5 MN, the computed pile head displacement is 7.0 mm, which over-estimates the observed value of 6.2 mm for pile no. P313 by 11 %.

For pile no. 3C3, Figure 12 shows that the calculated and the observed pile head displacements at the maximum load of 35 MN are 38.1 mm and 52.2 mm respectively. It is noted that the 4 unload-reload cycles are not simulated in the computation. Adding the residual displacement observed at the third unloading cycle of 20.5 mm onto the computed displacement of 38.1 mm, the cumulative pile head

displacement at 35 MN applied load would be 58.6 mm. The cumulative displacement over-estimates the observed value of 52.2 mm by 12 %.

The up to 12 % difference between the observed and the calculated displacements for the Case 1 and Case 2 analyses is considered as in close agreement. The close matching not only validates the non-linear Hardening Soil model for predicting pile performance but also verifies the ground stiffness values estimated from the results of the instrumented pile load tests.

Once the non-linear Hardening Soil model has been established and the ground stiffness values are available, the response of piles with larger diameters, longer lengths and larger applied loads could be calculated. The most optimal pile design could then be selected. For example, as shown in Fig. 11, the pile response at the applied load of 9.1 MN has been simulated in the numerical analysis and the predicted pile head displacement is 27.2 mm. The Hardening Soil model could also be applicable for predicting other geotechnical works such as the performance of pile groups and the effects of excavation to the adjacent piles. Case histories on these types of geotechnical works shall however be collected for studies and for calibrating the Hardening Soil model.

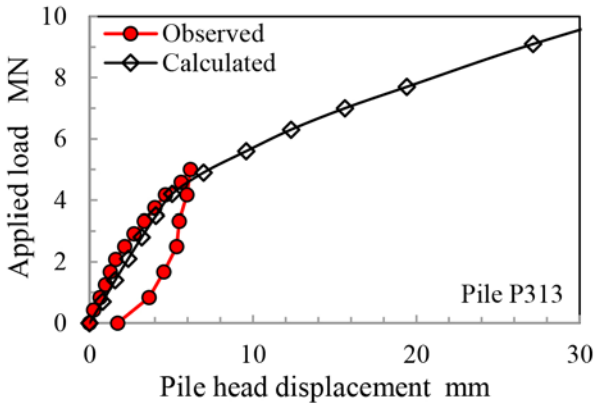

Figure 11: Calculated pile head displacements for pile no. P313

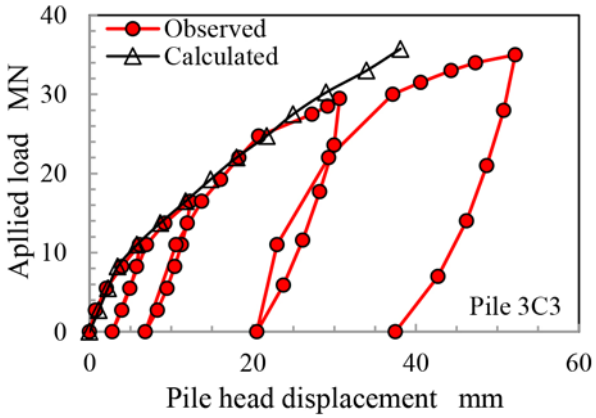

Figure 12: Calculated pile head displacements for pile no. 3C3

7 CONCLUSIONS

Numerical analyses on two case histories on axially loaded single piles have been conducted using the software PLAXIS-2D. The piles and the supporting ground are modelled by the axisymmetric mode. The non-linear hyperbolic Hardening Soil model is adopted. Based on the results of analyses, the following concluding remarks could be drawn:

(1) Close agreement between the observed and the calculated pile head displacements validates the non-linear Hardening Soil model adopted for the numerical analysis.

(2) The unload-reload stiffness values of the supporting ground to be adopted in the Hardening Soil model are equivalent to the initial tangent moduli interpreted from the t-z curves of the pile load tests.

The non-linear Hardening Soil model is an improved constitutive soil model that could simulate the non-linear stress-strain behaviour of the soil materials. Case histories on other types of geotechnical works shall be collected for studies and for calibrating the non-linear soil model. It is expected that the Hardening Soil model would replace the linear elastic-perfectly plastic Mohr-Coulomb model in the future.

REFERENCES

Duncan J.M. and Chang, C.M. 1970. Nonlinear analysis of stress and strain in soils. *Journal of Soil Mechanics and Foundations Division*, ASCE, 96(SM5), 1629-1653.

PLAXIS BV 2011. Reference Manual PLAXIS BV: Amsterdam, the Netherlands.

Randolph, M.F. and Wroth, C.P. 1978. Analysis of deformation of vertically loaded piles. *Journal of the Geotechnical Engineering Divisions*, ASCE, December, Vol. 104, No. GT12, 1465-1488.

Schanz, T., Vermeer, P.A. and Bonnier, P.G. 1999. The hardening soil model: formulation and verification. *Beyond 2000 in Computational Geotechnics*. Rotterdam, 281-296.

Toh, G.S.H and Chao, L. 2015. Does 3D finite element analysis allow better design of piles? - A case study for temporary marine pile design. *Proc HKIE Geotechnical Division Annual Seminar 2015*, 57-64.

Wong, L.W. 2010a. In-situ measurement of shear modulus of weak rocks. *Proc 17th Southeast Asian Geotechnical Conference*, Taipei, May, 141-144.

Wong, L.W. 2010b. Hyperbolic load-transfer curves for bored piles in weak rocks. *Proc 17th Southeast Asian Geotechnical Conference*, Taipei, May, 284-288.

Wong, L.W. 2010c. Base resistance of bored piles in weak rocks*. Proc Taiwan Rock Engineering Symposium 2010, KUAS, Kaohsiung*, Taiwan, October.

Wong, L.W. and Yong, C.C. 2011. Assessment of pile performance with theoretical load-transfer curves. *Proc 14th Asian Regional Conference on Soil Mechanics and Geotechnical Engineering*, May, Hong Kong, China.

Wong, L.W., Barsby, R. and Houghton, A. 2004. Load transfer characteristics of bored piles embedded in weak rocks. *Proc 15th Southeast Asian Geotechnical Conference*, November, Bangkok, Vol. 1, 217-222.

Design Suggestions on Flexible Debris-resisting Barriers

Gary Yung & Axel Ng
AECOM Asia Company Limited, Hong Kong

ABSTRACT

The use of flexible steel barriers as landslide mitigation measures for channelised debris flow in Hong Kong has gained both public and research interests in recent years. The flexible barriers have certain advantages over reinforced concrete rigid barriers, being lighter and requiring less site formation works.

The flexible barrier is a complex non-linear dynamic system which involves large deformations, energy dissipations, the plasticity of materials and dynamic loadings. With limited local experience and design guidelines available in Hong Kong, engineers require applying their engineering judgements to develop design solutions for the flexible debris-resisting barriers. This paper presents the design of flexible barrier systems as part of the landslide mitigation works on Keung Shan Road, Lantau Island, Hong Kong, using the force approach suggested in GEO Discussion Notes 1/2012.

Parametric studies were carried to review the dynamic performance of flexible barrier with various system configurations. The studies suggest that with different configurations of the barrier system, the number of wire ropes and energy dissipating devices can be optimised and the energy dissipation performance can be improved; and also the debris impact loads can be refined by reviewing the hydrograph of debris flow suggested in GEO Technical Guidance Note 44.

Key words: Channelised debris flow, Flexible Debris-resisting barriers, Dynamic analysis

1 INTRODUCTION

The flexible debris-resisting barrier has gained both public and research interests in recent years as an alternative landslide mitigation measurement to the traditional massive rigid barrier. Single or multiple flexible debris-resisting barriers installed along the expected debris flow path protect the civilian structures from the debris runoff. The key structural components of the flexible barrier system are chain wire meshes, steel ring nets, longitudinal steel wire ropes, steel posts, bracing steel wire ropes and energy dissipation devices. Plate 1 illustrates the overall view of the flexible debris-resisting system.

Plate 1: Example of flexible debris-resisting barrier

Kwan, and Cheung (2012) suggested in GEO discussion note (DN1/2012) that the flexible debris-resisting barriers can be designed by either energy approach or force approach. The energy approach is relatively simple for arresting relatively small landslides, however, it overestimates the impact energy for large scale of landslide events. The force approach considering the landslide event as a series of surges is more suitable for the large scale of landslides. Various authors, (Ng et al, 2012) (Chan et al, 2012) and (Yiu et al, 2012), used the force approach in evaluating the performance of flexible debris-resisting barriers. Individual teams from overseas have studied the numerical models with field tests and experimental results (Wendeler et al, 2006), (Canelli et al, 2012) and (Brighenti et al, 2013). Their numerical and experimental results showed that the option of using flexible debris-resisting barrier as an alternative solution for the landslide mitigation is positive. However, lack of local field test data in Hong Kong has been carried out to understand the interface behaviours between the flexible barrier and the debris impact.

With the limited understanding and guidelines developed locally in Hong Kong for the design of flexible debris-resisting barrier, engineers require applying their engineering judgements and interpretations from the numerical results to develop the design of flexible debris-resisting barriers. This paper is to share the design experience from a landslip hazard mitigation project. The functionality of the key components in the flexible debris-resisting system is discussed. Parametric studies are carried out to understand the dynamic behaviours of the flexible debris-resisting system under the impact load, which leads to the discussion of how to improve the flexible barrier system in terms of energy dissipation.

2 PROJECT BACKGROUND

This paper is written based on a selected natural terrain hazard mitigation project, as part of the Landslip Prevention and Mitigation Programme (LPMitiP), on Keung Shan road near Sham Wat road in Lantau Island, Hong Kong. Channelised debris flow (CDF) was identified as the landslide hazard. Preventing the civilian structures and the infrastructure roads from the large volume of debris runoff, a system of multiple flexible debris-resisting barriers was proposed (Figure 1). The system with two consequent flexible debris-resisting barriers was proposed to retain a single debris flow event, which requiring a total debris retention volume of 429m^3. The first layer was designed to retain 150m^3, and the second layer to retain the remaining 279m^3. The design of multiple flexible barriers is not the focus of this paper. This paper focuses on the performance of the flexible debris resisting barrier and how to improve its energy dissipation. The second layer (Flexible Barrier Type B) was chosen for the case study and its dynamic behaviours were evaluated by the force approach.

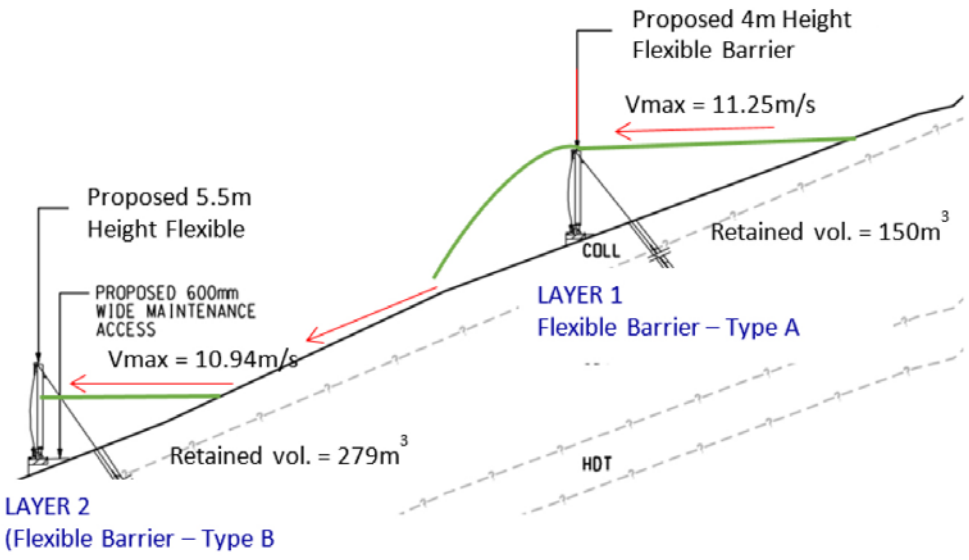

Figure 1: Maximum impact velocities and debris volumes for Keung Shan road project

3 FLEXIBLE BARRIER BEHAVIOURS AND NUMERICAL MODELS

The debris mass first hits on the chain wire meshes together with the steel ring nets, which are connected to the longitudinal wire ropes by shackles (Plate 1 and Figure 2). The steel ring net is a continuous steel wire bundled together by direct winding or spiral winding method. While the debris hits the ring net, the steel ring nets are restrained by longitudinal wire ropes at varies levels. The longitudinal steel wire ropes, metal strands twisted together, are held at different levels by the steel brackets mounted on the steel posts. The steel brackets allow the longitudinal wire ropes slide along, which transfer the internal forces to the anchor footings at each end of the barrier. The stability of steel posts is provided by diagonal bracing wire ropes that tied back to the upslope footings (Figure 2). Energy dissipating devices are connected to each wire ropes for absorbing the impact energy. It is worth to mention that the chain wire mesh and the steel ring nets are not directly connected with the steel posts, in such a way, it provides a flexible (or mouldable) steel mesh barrier to receive the impact energy and to retain the debris mass.

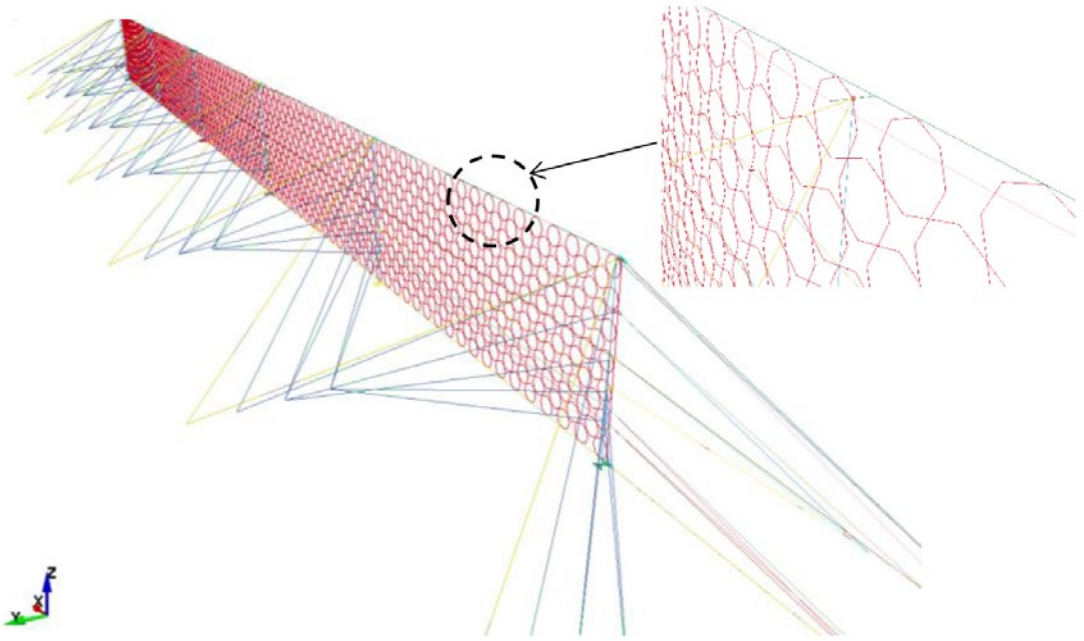

Figure 2: Numerical model of flexible debris-resisting barrier

The flexible debris-resisting barrier, a cable structure system, is a complex non-linear problem, which involves large deformations, plasticity and material hardening, contact interfaces and the load transient response. This type of nonlinear system is rather complicated to be solved analytically. LS-DYNA, a finite element program, is equipped with a wide range of non-linear material models and various types of contact definitions together with the explicit numerical solver to analyse the nonlinear response of the flexible debris-resisting barrier.

Debris mobility model (DMM) was carried out to determine the debris runout parameters such as debris travel distance, velocity, volume and predicted debris thickness. DN1/2012 suggested the debris impact load profiles be estimated as a sequence debris surges based on the parameters derived from DMM. The impact loadings were applied to the steel ring net as a series of transient loadings shown in Figure 3 to simulate the debris surges.

Two contact elements, guide nodes and pulley element, were defined in LS-DYNA for simulating the contact interfaces between the longitudinal wire ropes and other components such as the steel ring net and the steel brackets. The guide node definition allowed the steel ring net sliding along the longitudinal wire ropes. Each level of the longitudinal wire ropes consisted of two groups of ropes. Each group of wire rope(s) was only connected with half portion of the ring net in order to uniformly distribute the impact force (Figure 4). The pulley element definition was used to simulate the longitudinal wire rope sliding along at the steel post brackets, similar to a rope passing through a pulley.

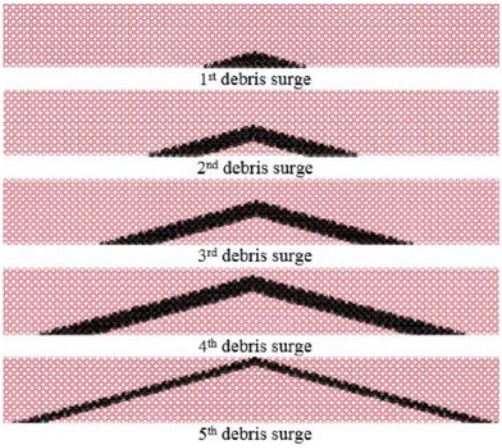

Figure 3: Load sequence of debris surges

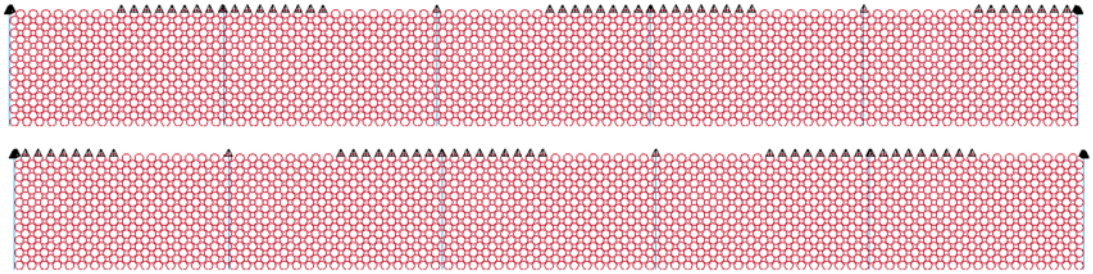

Figure 4: Each longitudinal rope group connected with only half portion of the steel ring net

In the case of debris flow impact, the steel posts were designed to form plastic hinges shown in Figure 5. The steel posts were modelled as fully integrated shell elements with the plastic kinematic material model. Unlike the longitudinal wire ropes on the steel brackets, the diagonal bracing wire ropes were directly fixed to the steel posts without sliding or pulley contact elements which provided the overall stability for the steel posts.

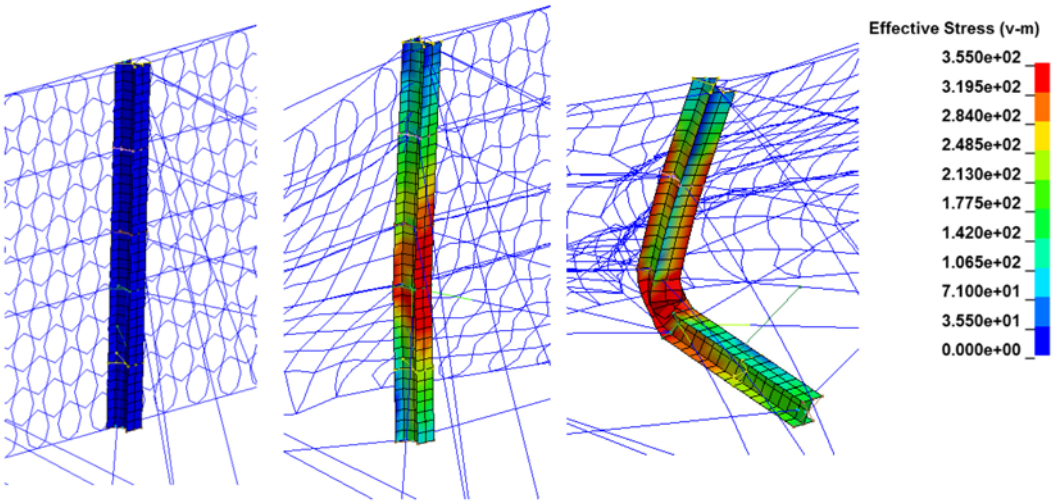

Figure 5: Plastic hinge formed in steel posts during debris impacts

Energy dissipating devices, some literature referring to the slack length of wire ropes, are the crucial components of the flexible debris-resisting barrier system. The energy dissipating devices were modelled as piecewise linear plasticity material to match with the laboratory test results. The energy dissipating devices undergo three stages to absorb the impact energy, which illustrated in Figure 6:

1. Activate stage: Energy dissipating devices are activated at a rather low applied force comparing with the yield strength of the connected wire ropes.
2. Energy dissipation stage: After the energy dissipating devices are activated, the devices then dissipate the energy by the crushing of aluminium tubes in this case study. The plastic deformation and slow hardening of devices are observed until the device reach it maximum plastic deformation at approximately 80% of the total original length. The plastic elongation of devices sometime is called as the slack length of wire ropes.
3. Hardening stage: When the energy dissipating devices reach their maximum plastic elongation, the devices re-engage the connected wire ropes, and the plastic deformation of the flexible barrier becomes limited. The connection detail between energy dissipating devices and the wire ropes are designed to have sufficient strength to withstand the ultimate strength of the connected wire ropes.

Explicit integration method was chosen over implicit integration method for the numerical solver to obtain the nonlinear dynamic response of the flexible barrier system. The implicit integration method is commonly used for most FEA software to evaluate the dynamic response of structures, however, the implicit method becomes computational expensive or difficult to obtain stable solutions for highly nonlinear or high-speed impact problems. The explicit integration, unconditionally stable if sufficiently small time step provided, is more suitable to evaluate the highly nonlinear response such as the flexible barrier system. The detail of implicit and explicit solvers can be referred to other computation literature references.

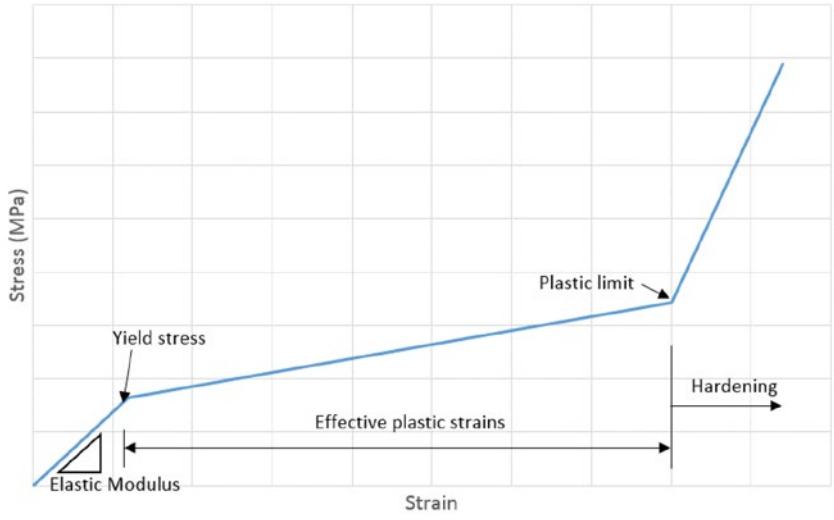

Figure 6: Piecewise linear plasticity model for energy dissipating devices

5 PARAMETRIC STUDIES AND DESIGN SUGGESTIONS

Parametric studies were carried out to provide an overall appreciation on how the flexible barrier systems perform, and to give the designer opportunities to improve and optimise the design. Various configurations of flexible barrier system and a refinement on the debris impact load were studied.

5.1 Various barrier configurations

The parametric study results showed that the stiffness flexible barrier dynamically changed during the debris impact, which mainly controlled by the nonlinear behaviours of the energy dissipating devices. The energy dissipators installed along the wire ropes were designed as fuses to dissipate the impact energy. Ideally, the energy dissipating devices are capable of being activated at low internal forces, to have high ductility capacities and to withstand the ultimate strength of the connected wire ropes without breaking. By installing the energy dissipating devices at specific locations in the flexible barrier system, it was able to control the dynamic stiffness of the system. For example, at the early stage of debris impact, the system with relatively soft stiffness allowed large plastic deformation and promoted large energy dissipation. The system then was adjusted with less energy dissipating capacity and relatively stiffer at the final stage of debris impact when the impact velocities were relatively low. This arrangement provided the overall stability of the barrier system, but also ability to receive a large volume of debris surges. Figure 7 shows the overall deformation of the flexible barrier under the debris impact load.

The studies showed that the ductility of energy dissipating devices was increased by simply connecting the devices in-series arrangement without increasing the activate force requirements. Whereas, the required activate force of energy dissipating devices was increased by connecting the devices in-parallel arrangement, which delayed the energy dissipation and limited the plastic elongation. By mixing with different arrangements of energy dissipating devices, the overall deformed shape of the barrier was controlled. For instance, the top diagonal bracing wire ropes of the steel posts were connected in parallel, which restrained the top movement of steel posts. On the other hand, the diagonal bracing wire ropes at the mid-height of steel posts were connected in series, which allowed the steel post to form a plastic hinge at mid-height shown in Figure 5. The parametric results indicated that the deformed shape of flexible barrier better matches with the debris impact surges, the better energy dissipating performance is found.

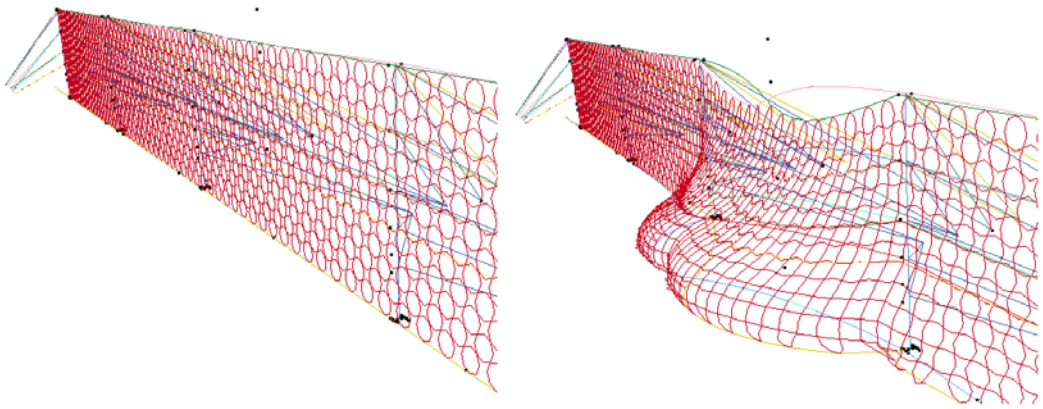

Figure 7: Large deformation of flexible debris-resisting barriers

The parametric results also showed that not only the configuration of energy dissipating devices but also the connection details of longitudinal wire ropes affected the stiffness distribution of the barrier system. Comparing with the top and bottom longitudinal wire ropes shown in Figure 7, the bottom wire ropes required to travel further to receive the debris impact load. As discussed previously, the bottom longitudinal wire ropes were split into two groups, and each group was only responsible for a half portion of the steel ring net. For the first design attempt, the bottom longitudinal wire ropes were connected to every steel post and the overall deformation of the ring net shown in Figure 8.

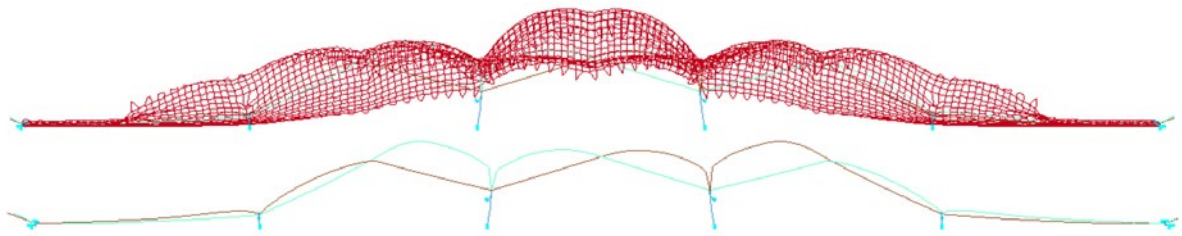

Figure 8: Plan view of bottom longitudinal wire ropes connected at every steel post (1st attempt)

Figure 8 highlighted that the out-of-plane deformation of the ring net at where the debris frontal first hit was restrained by the adjacent steel posts. As a result, relatively large internal forces in the wire ropes (both longitudinal and diagonal) and in the steel posts were observed. The base plate connections of steel posts, in particular, became very difficult to meet the design strength requirement.

To release the localise stress at the frontal of debris hit onto the barrier, the bottom longitudinal wire ropes were connected at every alternate steel post instead. A special base plate detail was proposed (Figure 9), this detail allows one group of longitudinal wire ropes to pass through the base plate but not transmitting the impact force onto the base plate.

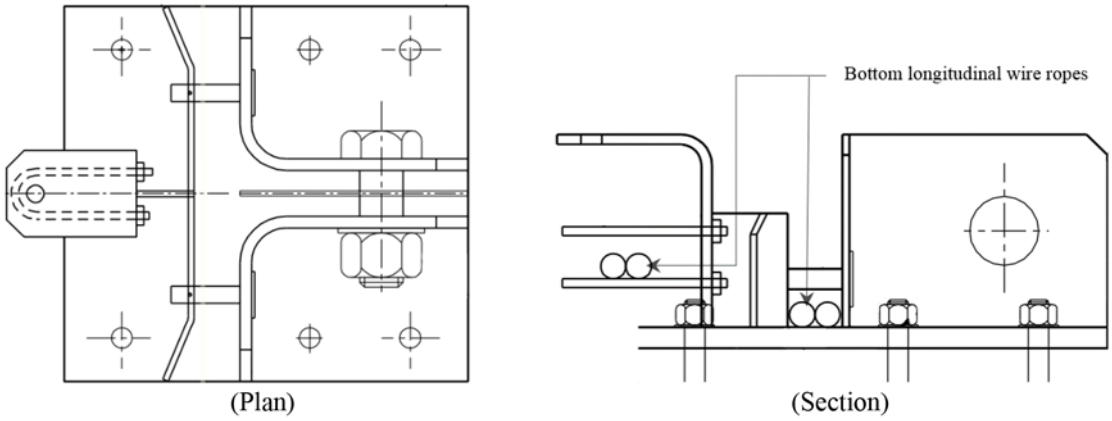

Figure 9: Base plate detail of steel posts

Figure 10 compares the deformed cross-section shapes between the first design attempt and the fine-tuned model. The first design attempt was comparatively stiffer and some restraints of ring net deformation were observed, possibly due to the energy dissipators reaching their limits too early and the bottom longitudinal wire ropes being over-restrained at the steel posts. The fine-tuned model, with optimised locations of energy dissipating devices and the special detailing in the steel post base plate, allowed the steel ring net to deform with less localise restrictions and to distribute the impact load evenly, which engaged more energy dissipating devices simultaneously to dissipate the debris impact energy in a more effective way. Figure 11 shows that the localised stresses at the adjacent steel posts have been improved with the special consideration in the base plate connection detail, and also a better load distribution throughout the barrier system has been observed.

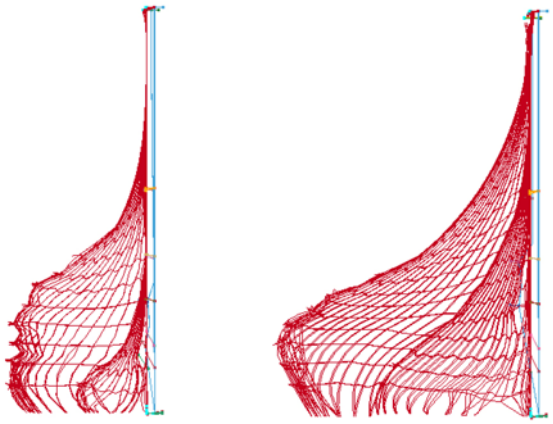

(left: 1st attempt design; right: fine-tuned design)

Figure 10: Comparison of the cross-section of deformed ring nets

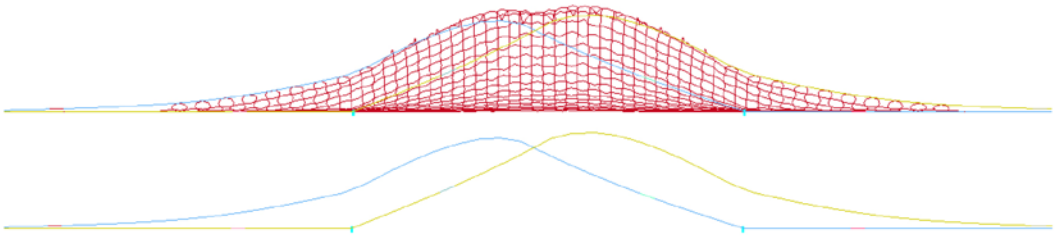

Figure 11: Plan view of bottom longitudinal wire ropes connected at every alternative steel post (fine-tuned solution)

5.2 Assessment of impact velocity

The debris impact loads were estimated by DN1/2012, and it suggested that the maximum velocity should be used to estimate the debris impact loads for each debris surge including all subsequent surges, which can be over-estimated. GEO Technical Guidance Note (TGN44) highlighted that the debris velocity varies along the length of landslide debris flow based on the observations of local landslide cases and the physical flume test results. The frontal of debris flow reaches the barrier at a maximum impact velocity, but not their subsequent surges. The impact load estimated by DN1 approach is conservative due to the fact that the subsequent debris surges are with relatively lesser impact velocities.

The studies showed that it is an opportunity to optimise the barrier design by considering the debris surges as a transient event with different impact velocities. Although, at the time of this case study, the approach with TGN44 suggestions was not adopted due to the limited design time. However, it is worthwhile to share the study findings by considering the TGN44 approach.

TGN44 suggested that the various impact velocities at different stages can be determined by hydrographs (Figure 12) which were established using landslide mobility analysis. The following assumptions were used in TGN44:

1. the maximum debris velocity in each stage should be considered to determine the design impact load of the corresponding debris flow phase;
2. the design impact velocity should not be less than 70% of the maximum debris velocity obtained from the velocity hydrograph in any stage of debris flow; and
3. the debris flow impact direction should be perpendicular to the flexible barrier system.

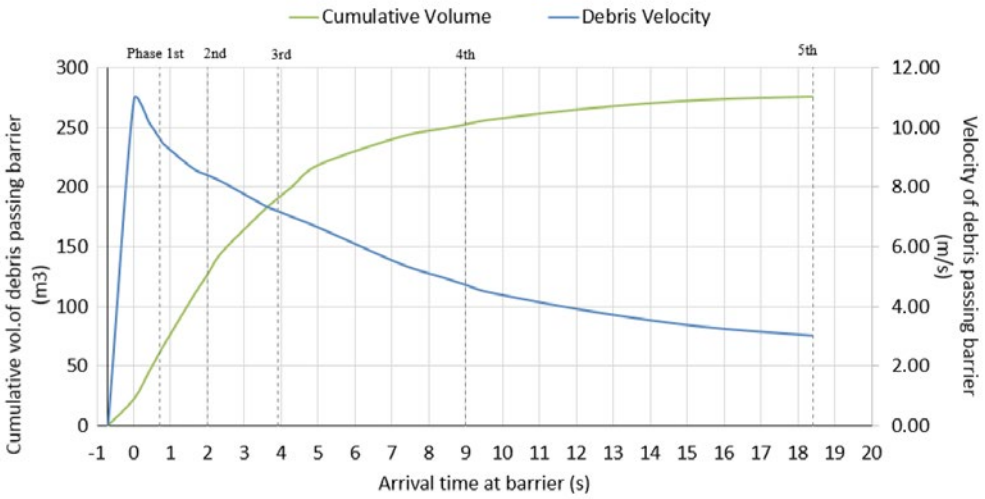

Figure 12: Hydrographs of CDF (by 2d-DMM)

By examining the 3rd debris surge with the TGN44 approach, the impact velocity and force have been reduced by about 25% and 44% respectively. Figure 14 shows that the design strength of the longitudinal wire ropes at the mid-height, at where the 3rd debris surge hit, has been reduced by approximately 40%, which means the number of wire ropes and energy dissipating devices can be reduced or optimised in the subsequent debris surges. The use of maximum impact velocity for the sequential debris surges is a conservative approach. In the future landslide projects, the estimated impact velocities are possibly refined by using TGN 44 approach or by obtaining the physical flume test results.

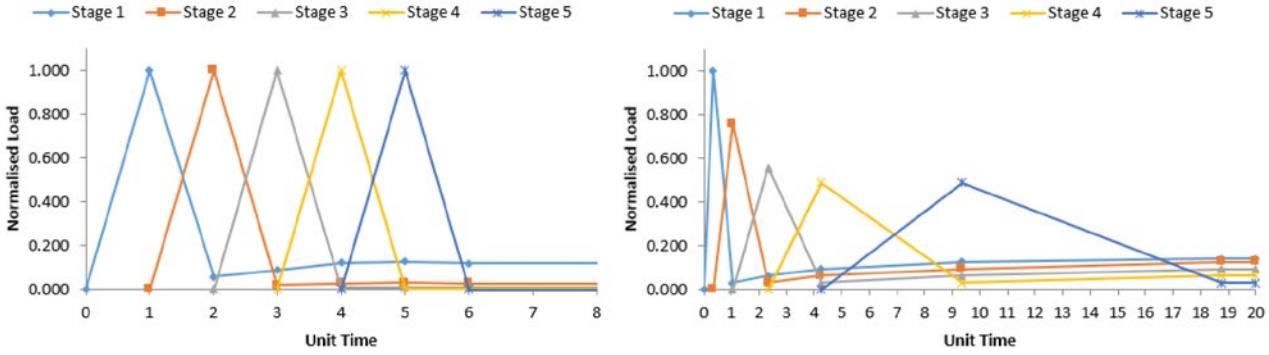

Figure 13: Normalised impact load against various debris surges (left: DN1/2012; right: TGN44)

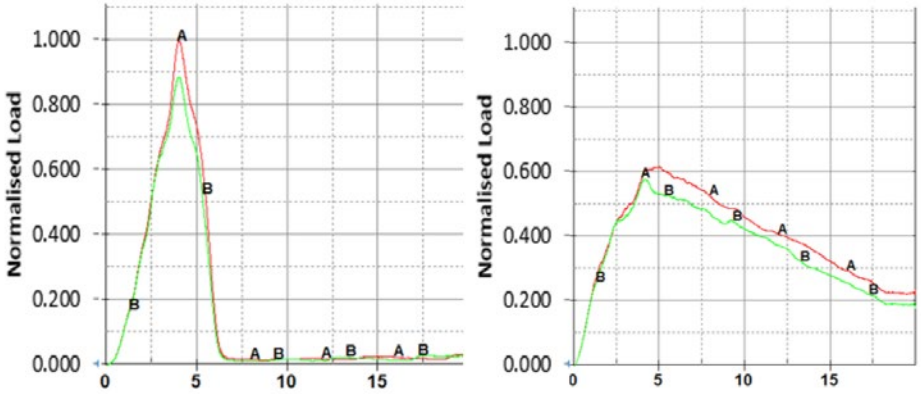

Figure 14: Normalised internal force of longitudinal wire ropes at mid-height of barrier (left: DN1/2012; right: TGN44)

6 CONCLUSIONS

The overall behaviours of the flexible debris-resisting barrier system were discussed to establish the appropriate numerical model in LS-DYNA. Parametric studies were carried out to study the flexible barrier behaviours with various configurations, and to compare the debris load assumptions estimated by DN1/2012 and TGN44.

The choice of connecting energy dissipating devices in series or in parallel have been found to provide some controls to the system stiffness during the debris flow impact, which can improve the load distribution and optimise the energy dissipation. The longitudinal wire ropes, particular for the bottom ropes, can consider being connected with every alternate steel post to provide a more flexible system for receiving the debris impact. A special base plate detail of the steel post was then suggested.

The estimated debris impact velocities by DN1/2012 appears to be conservative. A potential saving in the future design is possible to be achieved by adopting TGN44 approach or using the physical flume test results to estimate the debris impact loads.

ACKNOWLEDGEMENTS

This paper is published with the permission of the Head of Geotechnical office (GEO) and the Director of Civil Engineering & Development Department (CEDD), Government of Hong Kong Special Administrative Region. The authors would like to express our appreciation to GEO, CEDD and AECOM Asia Company Limited for the permission to publish this paper.

REFERENCES

Kwan, J.S.H. and Cheung, R.W.M., 2012. Suggestion on design approaches for flexible debris-resisting barriers. *Standard and testing division. Discussion note DN1/2012. The Government of Hong Kong Special Administrative Region*.

Ng, A.K.L., Williamson, S.J. and Chong, A.K.T., 2012. Developments in Design Considerations and Use of Flexible Barriers as Mitigation Measures for Channelised Debris Flow and Open Hillslope Failures-A Case Study. *Natural Terrain Hazard Mitigation Measures,* p.61.

Chan, S.L., Zhou, Z.H. and Liu, Y.P., 2012, October. Numerical analysis and design of flexible barriers allowing for sliding nodes and large deflection effects. In *Proceedings of the one day seminar on natural terrain hazards mitigation measures* (Vol. 16, pp. 29-43).

Yiu, J., Huang, Y., Pappin, J., Sturt, R., Kwan, J.S. and Ho, K.K., 2012. Landslide Mobility and Flexible Barrier Numerical Modelling Using LS-DYNA. *Natural Terrain Hazard Mitigation Measures,* p.67.

Wendeler, C., McArdell, B.W., Rickenmann, D., Volkwein, A., Roth, A. and Denk, M., 2006, August. Field testing and numerical modeling of flexible debris flow barriers. In *Proceedings of international conference on physical modelling in geotechnics, Hong Kong*.

Canelli, L., Ferrero, A.M., Migliazza, M. and Segalini, A., 2012. Debris flow risk mitigation by the means of rigid and flexible barriers-experimental tests and impact analysis. *Natural Hazards and Earth System Sciences,* 12(5), p.1693.

Brighenti, R., Segalini, A. and Ferrero, A.M., 2013. Debris flow hazard mitigation: a simplified analytical model for the design of flexible barriers. *Computers and Geotechnics,* 54, pp.1-15.

GEO, (2015). *Assessment of Landslide Debris Impact Velocity for Design of Debris-resisting Barriers*. Technical Guidance Note No. 44 (TGN44). Geotechnical Engineering Office, Hong Kong.